THE JOURNAL
OF
CHEMICAL PHYSICS

VOLUME 21, NUMBER 3 MARCH, 1953

Infrared and Raman Spectra of Fluorinated Ethanes. V. The Series CF_3CF_3, CF_3CF_2Cl, CF_3CFCl_2, and CF_3CCl_3†

J. RUD NIELSEN, C. Y. LIANG, AND R. M. SMITH*
Department of Physics, University of Oklahoma, Norman, Oklahoma

AND

D. C. SMITH‡
Naval Research Laboratory, Washington, D. C.

(Received September 30, 1952)

The infrared spectra of CF_3CF_2Cl, CF_3CFCl_2, and CF_3CCl_3 vapors have been obtained in the region from 2 to 38μ, and the spectra of liquid CF_3CF_2Cl and CF_3CFCl_2 in the region from 2 to 22μ, with the aid of LiF, NaCl, KBr, and KRS-5 prisms. The Raman spectra of all three compounds in the liquid state, and of gaseous CF_3CF_2Cl, were studied with a three-prism glass spectrograph of linear dispersion 15A/mm at 4358A. Depolarization ratios were determined for most of the Raman bands.

All fundamental vibration frequencies except the lowest (torsional) have been assigned for each molecule, and the observed spectra have been interpreted in detail.

INTRODUCTION

GLOCKLER and Sage[1] observed 13 bands in the Raman spectrum of liquid 1,1,1-trifluoro-2,2,2-trichloroethane and concluded that its molecules have the symmetry C_{3v}. Rank and Pace[2] studied the Raman spectrum of hexafluoroethane in the liquid state at a low temperature. The infrared spectrum of gaseous C_2F_6 was investigated in the first paper of this series,[3] as well as by Barcelo[4] who also obtained the infrared spectrum of chloropentafluoroethane gas. All fundamental vibration frequencies except the torsional have been assigned for hexafluoroethane.[2,3]

EXPERIMENTAL RESULTS

The spectra of CF_3CF_2Cl (bp−38.0°C), CF_3CFCl_2 (bp+3.0°C), and CF_3CCl_3 (bp+45.7°C) were obtained with the same instruments and in the same manner as reported in earlier papers of this series.[3,5,6,7] The infrared spectrum of gaseous CF_3CF_2Cl (at 25°C) is shown in Fig. 1, and the infrared spectrum of liquid CF_3CF_2Cl (at −45°C) is shown in Fig. 2. The KRS-5 regions are not included. In Table I are listed the wave numbers of the observed infrared absorption maxima. The Raman shifts observed for gaseous and liquid CF_3CF_2Cl are given in Table II, as well as the depolarization ratios and relative intensities of all but the weakest Raman bands. The sample§ was highly purified, and no evidence was found of impurities.

The infrared spectra of gaseous and liquid CF_3CFCl_2, obtained at 25° and −15°C, respectively, are shown in Figs. 3 and 4, and the wave numbers of the observed absorption maxima are listed in Table III. The Raman

† A part of this work has been supported by the U. S. Atomic Energy Commission under Contract No. AT-(40-1)-1074. The Raman data for CF_3CCl_3 are taken from a thesis presented by R. M. Smith to the Faculty of the Graduate College of the University of Oklahoma in partial fulfilment of the requirements for the Degree of Doctor of Philosophy.

* Present address: Minneapolis-Honeywell Regulator Company, Minneapolis, Minnesota.

‡ Present address: Phillips Petroleum Company, Bartlesville, Oklahoma.

[1] G. Glockler and C. G. Sage, J. Chem. Phys. **9**, 367 (1940).
[2] D. H. Rank and E. L. Pace, J. Chem. Phys. **15**, 39 (1947).
[3] Nielsen, Richards, and McMurry, J. Chem. Phys. **16**, 67 (1948).
[4] J. R. Barcelo, J. Research Natl. Bur. Standards **44**, 521 (1950).
[5] Nielsen, Classen, and Smith, J. Chem. Phys. **18**, 485 (1950).
[6] Smith, Brown, Nielsen, Smith, and Liang, J. Chem. Phys. **20**, 473 (1952).
[7] Smith, Saunders, Nielsen, and Ferguson, J. Chem. Phys. **20**, 847 (1952).

§ Kindly supplied by the Jackson Laboratory, Kinetic Chemicals, Inc., Wilmington, Delaware.

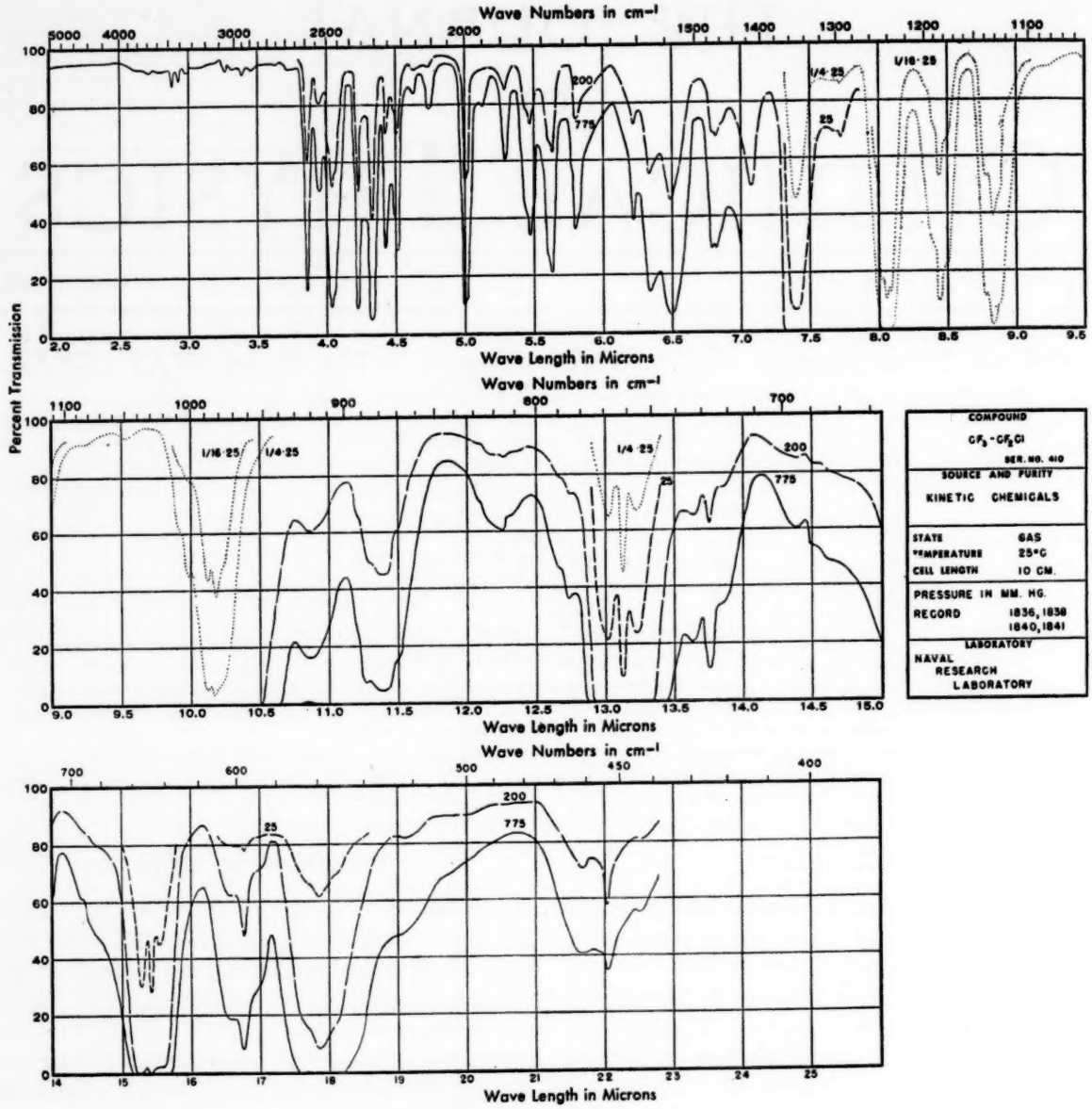

FIG. 1. Infrared spectrum of gaseous CF_3CF_2Cl. (KRS-5 region not included.)

data for liquid CF_3CFCl_2 are presented in Table IV. The sample|| contained a small amount of CO_2.

The infrared spectrum of gaseous CF_3CCl_3 is shown in Fig. 5, and the infrared bands are listed in Table V. The Raman data for this compound in the liquid state are also given in Table V. The sample¶ appears to contain a trace of an unidentified impurity.

INTERPRETATION

1. CF_3CF_3

Except for the torsional frequency, all of the fundamental vibrational frequencies for this molecule have been assigned.[2,3] The lowest E_u fundamental has not been observed directly, but has been inferred from infrared combination bands.

2. CF_3CF_2Cl

This molecule undoubtedly has the symmetry C_s, and its normal vibrations divide themselves as follows: $11\,A'+7\,A''$, where A' denotes symmetry and A'' antisymmetry with respect to a reflection in the molecular symmetry plane. All fundamentals are active both in infrared absorption and in the Raman effect. Fundamentals of species A' give rise to polarized Raman bands, those belonging to A'' to depolarized Raman bands.

The five highest Raman frequencies, observed at

|| Kindly supplied by the E. I. du Pont de Nemours and Company, Wilmington Delaware.

¶ Kindly supplied by the Jackson Laboratory, Kinetic Chemicals, Inc., Wilmington, Delaware.

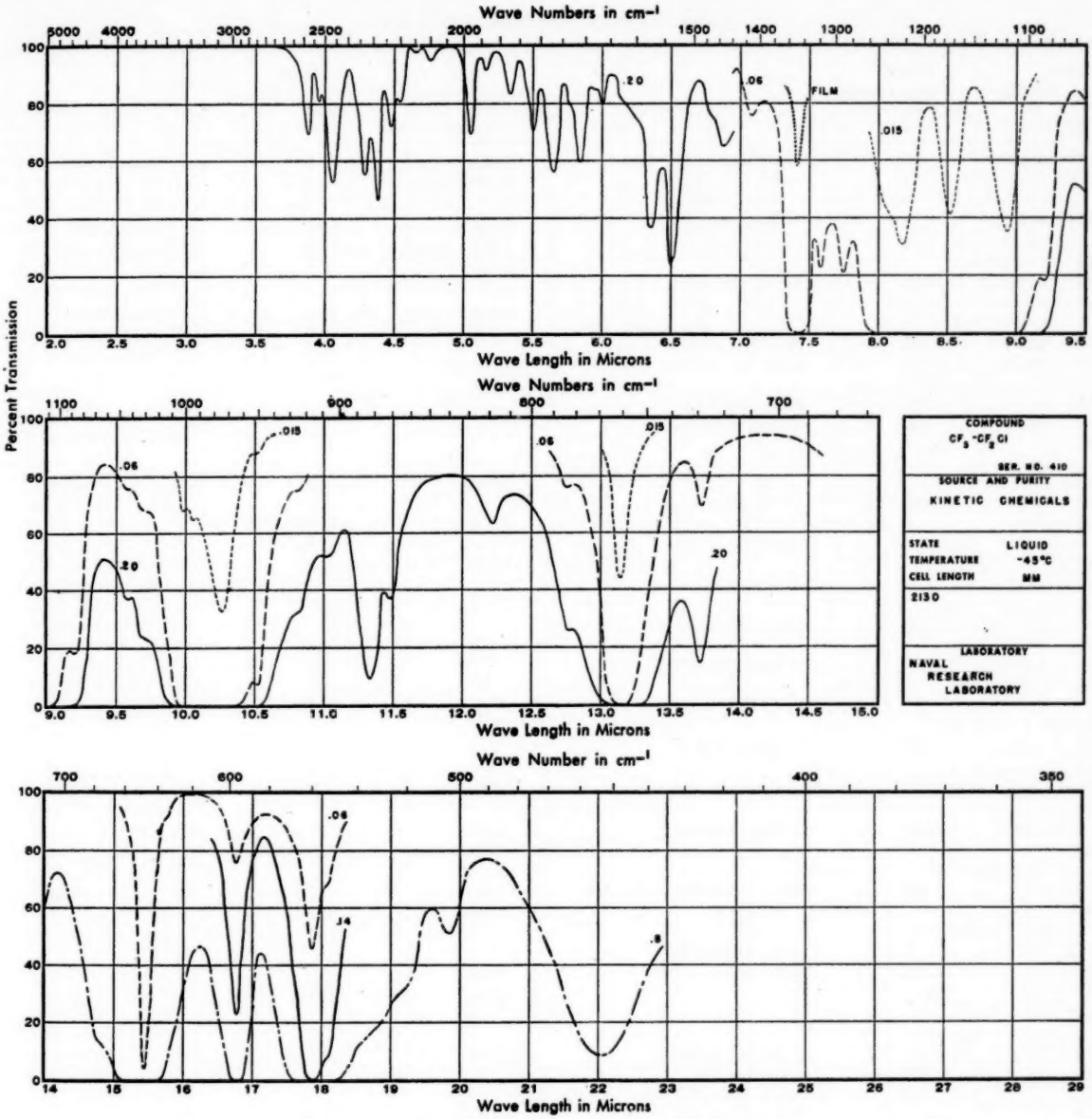

FIG. 2. Infrared spectrum of liquid CF_3CF_2Cl at −45°C. (KRS-5 region not included.)

1349, 1240, 1224, 1178, and 1124 cm^{-1} in the liquid, must represent fundamentals involving largely C−F stretching. Two of these must belong to species A'', and three to A'. Although the polarization data are not conclusive, it seems fairly certain that 1178 and either 1224 or 1240 belong to A'', and the remaining three bands to A'. In the infrared spectrum of CF_3CF_2Cl gas the second and third highest fundamentals are not resolved.

The Raman band at 977 cm^{-1} is very weak and not with certainty polarized. However, the infrared band observed at approximately this wave number is so intense that it must be assigned as a fundamental. The species must be A', and the motion must involve largely C−C stretching. The high depolarization ratio may be explained by overlapping with the combination $332+647=979$ A''.

The very intense polarized Raman band at 761 cm^{-1} must represent an A' fundamental involving largely C−Cl stretching. The bands at 647, 593, and 560 cm^{-1} are unquestionably fundamentals. That at 593 cm^{-1} must belong to A'' and the others to A'. These three fundamentals must be associated largely with CF_3 deformation.

Four A' and four A'' fundamentals may be expected to lie below 500 cm^{-1}. The polarized Raman bands at 441, 364, and 316 cm^{-1} are certainly A' fundamentals. The sharp band at 435 cm^{-1}, which has the same appearance as and about one-third the intensity of the band at 441 cm^{-1}, undoubtedly arises from molecules

TABLE I. Infrared spectrum of CF_3CF_2Cl.

Gas Wave number	Gas Description	Liquid Wave number	Liquid Description	Interpretation[a]
~307[b]				
314[b]	m sh			A' fundamental
~321[b]				
~362[b]	w b			A' fundamental
~444				
454	m sh	~455	w	A'' fundamental
~462				
~500	vw b	504	vw	186+315=501
~520	vw b	~521	vw	186+331=517
		~532	vw	
~551		~552	m	186+364=550
560	m	560	s	A' fundamental
~566				
~588				
596	m sh	596	m	A'' fundamental
~604				
		638		186+454=640
643				
648	m sh	648	s	A' fundamental
654				
		678	w	315+364=679 A'
~684				
690	vw			331+364=695 A''
~695				
~722				
727	w sh	729	m	2×364=728 A'
~733				
756				
762	s sh	761	vs	A' fundamental
768				
785	vw	784	m	186+596=782, 331+454
~790				=785 A'
~810				364+442=806 A'
~816	vw	818	w	364+454=818 A''
~822				
~828?				
~870				315+560=875 A'
877	m	877	w	2×442=884 A'
886		883	m	331+560=891 A''
~893				442+454=896 A''
		~906	w	2×454=908 A'
~922	w b	~924	w	331+595=926 A', 364+560
				=924 A'
		951	m	186+763=949
~976				
982	vs sh	974	vs	A' fundamental
988		995	s	442+560=1002 A'
1002	s	1002	s	364+648=1012 A'
~1010				454+560=1014 A''
		~1033	m	(441+594=1035 A'')
~1045	m b	~1046	m	454+595=1049 A'
~1081				315+763=1078 A'
1087	m sh	1087	s	442+648=1090 A'
~1122				
1133	vs sh	1120	vs	A' fundamental
1139				
~1176				
1185	vs sh	1178	vs	A'' fundamental
~1190				
1236		1224	vs	A' fundamental
1241	vs sh	~1240	vs	A'' fundamental
1247				
1295	w sh	1290	s	2×648=1296 A'
~1305				315+982=1297 A'
		1321	s	560+763=1323 A'
1351	s	1350	vs	A' fundamental
1414	w	1412	m	648+763=1411 A',
				442+982=1424 A'
1466	w sh	1453	vw	331+1132=1463 A'',
				(331+1122=1453 A'')
1473		~1475	vw	
		~1534		186+1350=1536
1541	w	1538	w	560+982=1542 A',
				(560+976=1536 A')
1577	w	1572	w	595+982=1577 A'',
				331+1241=1572 A''
1608	w	~1613	vw	364+1241=1605 A''
		1667	vw	315+1350=1665 A'
		~1681		331+1350=1681 A''
1724	w	1715	w	595+1132=1727 A'',
				(594+1122=1716 A'')
		~1733		(560+1176=1736 A'')
1776	w	1770	w	648+1132=1780 A',
				(648+1122=1770 A')
~1785				442+1350=1792 A'
1828	w sh	1818	vw	648+1186=1834 A'',
				(648+1176=1824 A'')
1890	w	1876	vw	648+1241=1889 A''
1949	vw	1938	vw	763+1186=1949 A'',
				(761+1176=1937 A''),
				595+1350=1945 A''
1992				648+1350=1998 A'
2000	w sh	1980	vw	763+1241=2004 A'',
				763+1236=1999 A',
				(763+1224=1987 A')
2110	vw	2101	vw	982+1132=2114 A',
				(976+1122=2098 A'),
				763+1350=2113 A'
2160	vw	2146	vw	982+1186=2168 A'',
				(976+1176=2152 A'')
2215	w	2198	vw	982+1236=2218 A',
				(976+1224=2200 A')
2220	w			982+1241=2223 A''
2257	w	2232	vw	2×1132=2264 A',
				(2×1122=2244 A')
2309	w	2283	w	1132+1186=2318 A'',
				(1122+1176=2298 A'')
2364	w	2331	w	2×1186=2372 A',
				(2×1176=2352 A')
2475	w sh	2463	w	1132+1350=2482 A',
				(1122+1350=2472 A'),
				2×1241=2482 A'
2532	vw	2525	vw	1186+1350=2536 A'',
				(1176+1350=2526 A'')
2591	w	2577	vw	1241+1350=2591 A''

[a] Wave numbers enclosed in parentheses are for the liquid state.
[b] Observed with KRS-5 prism.

having a Cl^{37} atom in the CF_2Cl group. The remaining A' fundamental is assumed to overlap with an A'' fundamental at 186 cm^{-1}.

The Raman band at 332 cm^{-1} is evidently depolarized and is assigned as an A'' fundamental. No evidence is found in the Raman spectrum for the remaining two

TABLE II. Raman spectrum of CF_3CF_2Cl.

Wave number Gas	Wave number Liquid	Relative intensity	Depolarization	Exciting Hg lines	Interpretation
186 w	186	10 d	0.73	*e*	$A'+A''$ fundamentals
315.2 m	315.8	33 sh	0.21	±*eki*	A' fundamental
331 w	332	12	0.75	±*ek*	A'' fundamental
366 w	364	11 sh	0.42	±*e*	A' fundamental
377 vw					$2\times186=372\ A'$
437 w	435	sh		±*eki*	A' fundamental $\{Cl^{37}$
441.5 m	441.3	55 sh	0.16	±*eki*	A' fundamental $\{Cl^{35}$
	552	vw	dp	*e*	186+364=550
561 w d	560	10	0.3	*e*	A' fundamental
595 vw	593	5 d	0.87	*eki*	A'' fundamental
648 m sh	647	20 sh	0.15	*eki*	A' fundamental
	678	vvw		*e*	$316+364=680\ A'$
	726	vvw		*e*	$2\times364=728\ A'$
763.3 s sh	761.3	100 sh	0.06	±*efgki*	A' fundamental
	977	vw d	0.8	*ek*	A' fundamental
					$332+647=979\ A''$
1131 vvw	1124	4	0.7	*ek*	A' fundamental
1187 vvw	1178	4	0.8	*ek*	A'' fundamental
1236 vvw	1224	4	0.7	*ek*	A' fundamental
	1240	vw d		*ek*	A'' fundamental
1348 vvw	1349	9	0.55	*ek*	A' fundamental

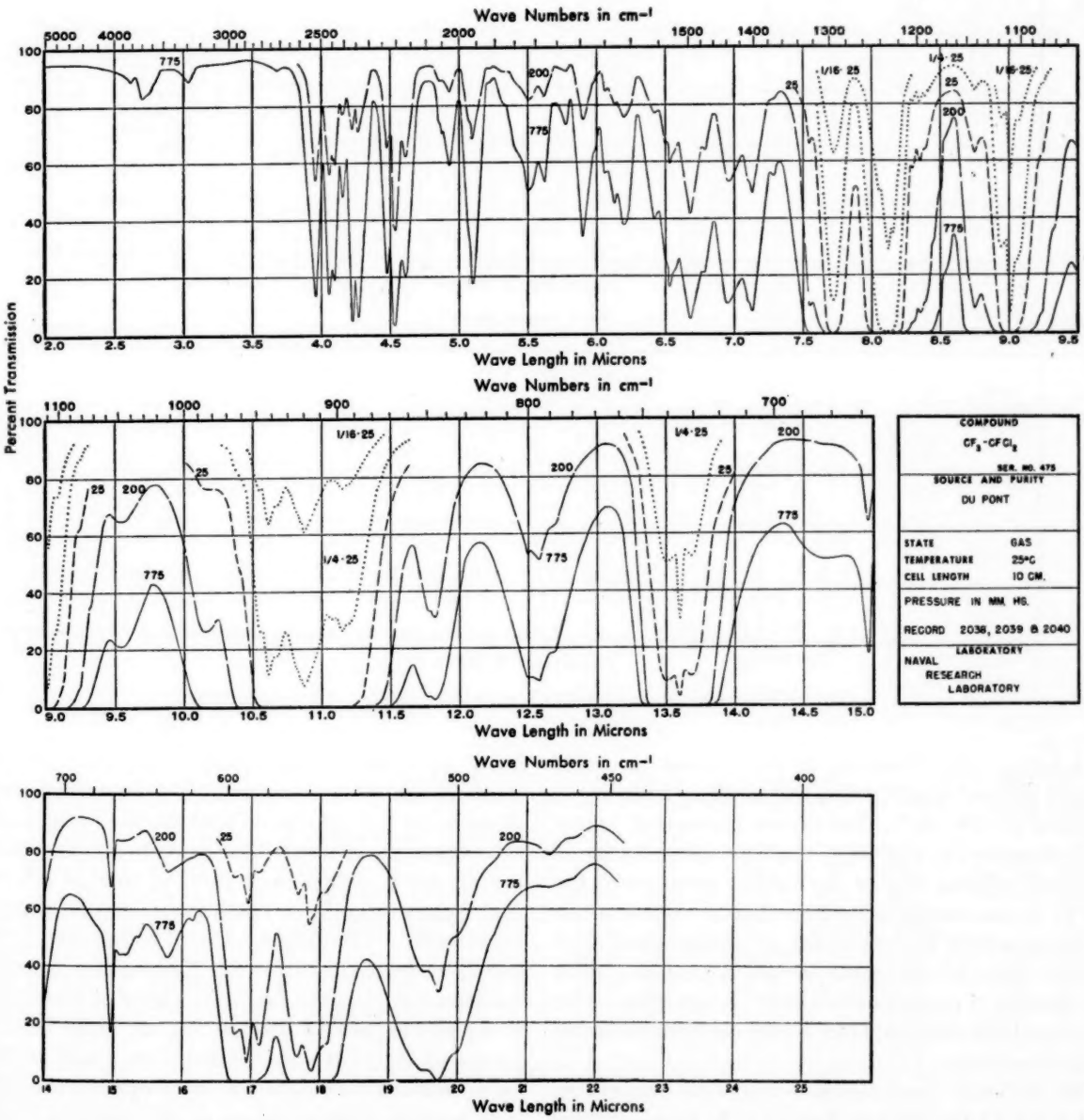

FIG. 3. Infrared spectrum of gaseous CF_3CFCl_2 (KRS-5 region not included).

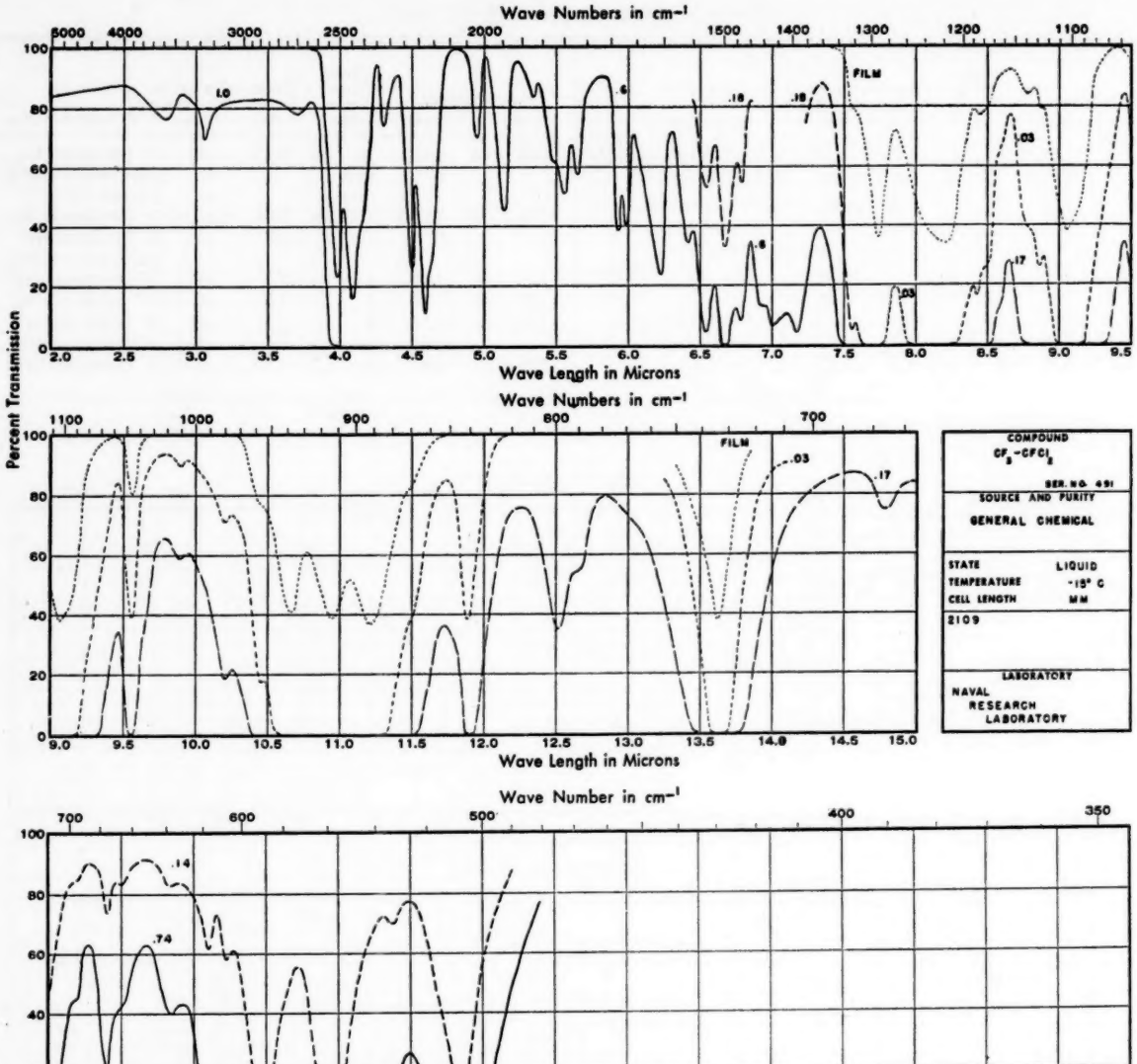

FIG. 4. Infrared spectrum of liquid CF_3CFCl_2 at −15°C. (KRS-5 region not included.)

A'' fundamentals. However, in the infrared spectrum of both gas and liquid a band of medium intensity is observed at 455 cm^{-1}. This cannot correspond to the A' fundamental at 441 cm^{-1}, since the latter occurs at this wave number also in the Raman spectrum of the gas. It is reasonable to assume that it represents an A'' fundamental. The remaining A'' fundamental must lie below 186 cm^{-1} and must be associated with torsion or a mixture of torsion and rocking. No evidence for its value has been obtained from either the infrared or the Raman spectrum.

The assigned fundamental vibrational frequencies for CF_3CF_2Cl are listed in Table VI. In terms of these frequencies all but one or two of the observed infrared bands have been satisfactorily interpreted as binary combination or overtone bands. The interpretations are given in the last column of Table I. The exceptions are the very weak infrared band at 532 cm^{-1} and the extremely faint, and possibly spurious, band at 828 cm^{-1}. The former may be a combination of the unknown (torsional) A'' fundamental with either 441 or 364, giving 91 or 168 cm^{-1} for the torsional frequency. No confirmation has been found for either of these values. It is possible that the band at 532 cm^{-1} may be a component of $186+331=517$ $(A'+A'')$, or it may be caused by an impurity. It does not seem worth while to discuss possible interpretations of the doubtful band at 828 cm^{-1}.

TABLE III. Infrared spectrum of CF_3CFCl_2.

Gas Wave number	Gas Description	Liquid Wave number	Liquid Description	Interpretation[a]
311[b]	m			A' fundamental
330[b]	s b			A'' fundamental
399[b]	m			A' & A'' fundamentals
461				
469	vw			(200+265=465 A')
~487	vw b			(181)+311=492 A''
~500				
507	m	508	m	A' fundamental
512				(200)+311=511 A', (181)+330=511 A'
		~533	w	(200)+330=530 A'', (2×265=530 A')
553				
558				
560	s sh	558	s	A'' fundamental
565				
584				
590	s sh	590	s sh	A' fundamental
596				
		608	w	(200+400=600)
619	vw	617	w	2×311=622 A'
~633	w	638	vw	311+330=641 A''
651				
658				2×330=660 A'
663				
668	w sh	~667	vw	CO_2 impurity
~680		676	w	
		~696	vw	(200+506=706 A')
730				
735	vs sh	734	s	A' fundamental
~741				
~787		~789	w	(200)+590=790 A'
795	m	798	m	2×399=798 A'
800				
846		841	s	330+507=837 A''
~850	m			(265)+590=855 A'
		~868	m	311+560=871 A''
~894				
897	vs	891	vs	A'' fundamental
903				
920	vs	914	vs	331+590=921 A''
~922				
~936				
943	vs sh	938	vs	A' fundamental
~948				
		~956	m	399+560=959
~963	w			
~984	m	981	m	399+590=989
		1010	w	2×507=1014 A'
~1049	w	1044	m	311+735=1046 A'
~1073				(181)+897=1078 A'
~1082				
~1101				
1110	vs sh	1103	vs	A' fundamental
1117				
		1127	m	2×560=1120 A', (181+939=1120 A'')
1143	m	~1139	m	(200)+943=1143 A'
~1168		~1163	m	(265)+897=1162 A''
~1176	w	~1176		
~1185	w	1186	m	2×590=1180 A'
1192				
1198	m sh			311+897=1208 A'', (265)+943=1208 A'
1205				
		~1217	vs b	A'' fundamental (liquid)
1227				
1232	vs sh			A' & A'' fundamentals (gas)
~1241				507+735=1242 A'
~1295	vs	1292	vs	A' fundamental
1325	m sh	1321	m	590+735=1325 A'
1372	vw			(265)+1110=1375 A'
1403	w sh	1393	w	507+897=1404 A''
~1408				(181)+1232=1413
		1427	w	(330+1103=1433 A'')
~1437	w	~1439	w	330+1110=1440 A'', (200+1247=1447 A'), (506+938=1444 A')
1473	w	1471	m	2×735=1470 A'
1497	w	1495	m	(200)+1295=1495 A', (265)+1232=1497
~1524				
1531	w sh	1527	m	590+943=1533 A'
1538				
1558	vw	1558	w	(265)+1295=1560 A'
~1613	w	1605	w	507+1110=1617 A', (506+1103=1609 A'), 311+1295=1606 A'
1631	vw			735+897=1632 A'', 399+1232=1631
1650	vvw			
~1667	vvw			560+1110=1670 A''
~1672	vw	1672	w	735+943=1678 A'
1695	w sh	1684	w	399+1295=1694, 590+1110=1700 A'
1730	vw			507+1232=1739
1757	vw			
1779	w	1767	w	2×897=1794 A', (2×891=1782 A')
		1795	w	507+1295=1802 A'
~1818	w			590+1232=1822
		~1825	vw	(891+939=1830 A'')
~1848	vw			735+1110=1845 A', 897+943=1840 A''
~1876	vw	1869	vw	2×943=1886 A', (2×938=1876 A')
~1912	vw			
1965	w sh	1942	w	735+1232=1967, (735+1218=1953 A'')
~1970				
2028	w	2020	w	735+1295=2030 A'
2049	vw			943+1110=2053 A'
~2062				
2165	w	~2146	w	943+1232=2175, (938+1218=2156 A'')
2169				
2203	w sh	2183	w	897+1295=2192 A'', (891+1292=2183 A'')
~2208				
2232	w sh	2222	w	943+1295=2238 A'
		2315	vw	(1103+1218=2321 A'')
2342	w sh			1110+1232=2342, or CO_2 impurity
2364	w sh			CO_2 impurity
2404	vw sh	2392	vw	1110+1295=2405 A'
2439	vw	2439	w	(2×1218=2436 A')
2445	vw			
2463	w			2×1232=2464 A'
2525	w	2513	w	1232+1295=2527

[a] Wave numbers enclosed in parentheses are for the liquid state.
[b] Observed with KRS-5 prism.

TABLE IV. Raman spectrum of CF_2CFCl_2 (liquid).

Wave number	Relative intensity	Depolarization	Exciting Hg lines	Interpretation
181	26	~0.7	±*eki*	*A″* fundamentals
200	23	0.5	±*eki*	*A′* fundamental
265	37 d	0.8	±*eki*	*A′* fundamental
312	56 sh	0.25	±*ek*	*A′* fundamental
331	20	0.85	±*ek*	*A″* fundamental
400	85 sh	0.45	±*eki*	*A′*+*A″* fundamentals
461	vvw	···	*e*	200+265=465 *A′*
505.2	87 sh	0.15	±*eki*	*A′* fundamental
559	16	0.85	*e*	*A″* fundamental
588	15 sh	0.4	±*e*	*A′* fundamental
650	vvw	···	*e*	312+331=643 *A″*
734.5	100 sh	0.15	±*efgkil*	*A′* fundamental
765	vvw	···	*e*	265+505=770 *A′*
799	vvw	···	*e*	2×399=798 *A′*
891	8 d	0.8	*ek*	*A″* fundamental
915	8 d	0.85	*ek*	734+181=915 *A″*
939	7	0.8	*ek*	*A′* fundamental
1103	9	0.7	*ek*	*A′* fundamental
1218	10 vd	0.8	*ek*	*A″* fundamental
1247	vw	···	*e*	*A′* fundamental
				505+735=1240 *A′*
1292	11	0.7	*ek*	*A′* fundamental

TABLE V. Infrared and Raman spectra of CF_3CCl_3.

Infrared (gas) Wave number	Infrared (gas) Description	Raman (liquid) Wave number	Raman (liquid) Description	Depolarization	Interpretation
		182	s	0.84	*E* fundamental
~263[a]	m	265	s	0.84	*E* fundamental
~278[a]?	vw				Impurity?
345[a]	vw				Impurity?
366[a]	m	367	m	0.80	*E* fundamental, 2×182=364 (A_1+*E*)
398[a]?	vw				
426[a]	s	429	vs	0.03	A_1 fundamental
~457	vvw				182+265=447 (A_1+A_2+*E*)
490	vw				A_1 fundamental?
~554					
561	s	561	m	0.86	*E* fundamental
~570					
~643	vw				909−265=644 *E*
~690	vvw				265+429=694 *E*
709					
714	vs sh	714	s	0.06	A_1 fundamental
719					
734	vw sh				2×367=734 (A_1+*E*)
~742					182+561=743 (A_1+A_2+*E*)
~794	m	796	vw		429+367=796 *E*
~802	w				
~832	m				265+561=826 (A_1+A_2+*E*)
859	vs	852	m	0.85	*E* fundamental
~904					
909	vs	908	w	0.7	A_1 fundamental
~917					
~927	vw				367+561=928 (A_1+A_2+*E*)
~931	vw				
992	m				429+561=990 *E*
1032	m				
1037	m				182+859=1041 (A_1+A_2+*E*)
1086	w sh				367+714=1081 *E*
~1092					182+909=1091 *E*
~1117	vw				2×561=1122 (A_1+*E*)
1124	w sh				265+859=1124 (A_1+A_2+*E*)
1129	vw				
1145	vvw				429+714=1143 A_1
1168	m sh				265+909=1174 *E*
~1172					
~1186					
1190	s sh				367+859=1226 (A_1+A_2+*E*)
1221					
1227	vs sh	1215	w	0.9	*E* fundamental
~1255	vs	1252	w	0.67	A_1 fundamental
1277	s sh				367+909=1276 *E*, 561+714=1275 *E*
1339	m				429+909=1338 A_1
1401	m				490+909=1399 A_1
1406	w				182+1227=1409 (A_1+A_2+*E*)
1418	w sh				561+859=1420 (A_1+A_2+*E*)
1431	w				182+1255=1437 *E*, 2×714=1428 A_1
1471	m				561+909=1470 *E*
1515	w sh				265+1255=1520 *E*
1575	w				714+859=1573 *E*
1595	w				367+1227=1594 (A_1+A_2+*E*)
1621	vw				367+1255=1622 *E*, 714+909=1623 A_1
1650	vvw				429+1227=1656 *E*
1710	w				2×859=1718 (A_1+*E*)
1785	w				561+1227=1788 (A_1+A_2+*E*)
1810	vvw				561+1255=1816 *E*, 2×909=1818 A_1
1930	w sh				714+1227=1941 *E*
1960	vvw sh				714+1255=1969 A_1
2075	vvw				859+1227=2086 (A_1+A_2+*E*)
2110	vw sh				859+1255=2114 *E*
2130	w sh				909+1227=2136 *E*
2155	w sh				909+1255=2164 A_1
~2365	vvw				Impurity?
2450	w				2×1227=2454 (A_1+*E*)
2480	w sh				1227+1255=2482 *E*
~2540	vvw				2×1255=2510 A_1
~2990	vvw				859+909+1227=2995 (A_1+A_2+*E*), or impurity
3360	vvw				909+2×1227=3363 (A_1+*E*)
~3610	vvw				Impurity?

[a] Observed with KRS-5 prism.

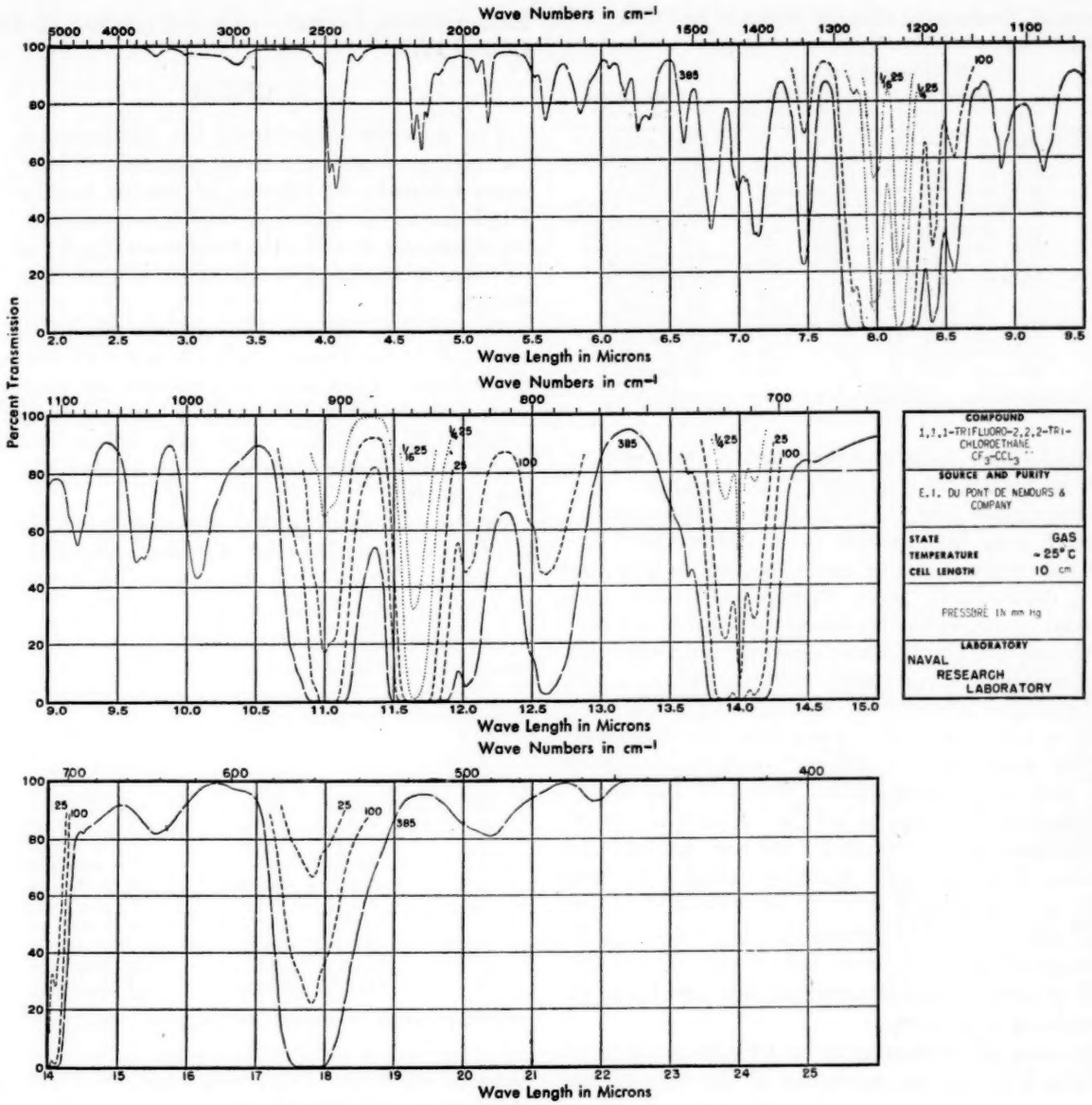

FIG. 5. Infrared spectrum of gaseous CF_3CCl_3. (KRS-5 region not included.)

3. CF_3CFCl_2

The four bands at 1292, 1247, 1218 and 1103 cm^{-1}, weak in the Raman spectrum but very strong in the infrared, must represent fundamentals involving largely C−F stretching. One of these should belong to species A'' and the others to A'. The Raman bands at 1292 and 1103 cm^{-1} are definitely polarized, that at 1218 cm^{-1} appears to be depolarized, while the band at 1247 is so weak that no polarization measurement could be made. It has been assumed therefore that 1218 belongs to A'' and 1247 to A'. In the infrared spectrum of gaseous CF_3CFCl_2 these two fundamentals seem to coincide at 1232 cm^{-1}.

Four very strong infrared bands have been observed in the region where frequencies of vibrations involving C−C and C−Cl stretching may be expected to lie. One of these, at 735 cm^{-1}, which is extremely intense and polarized in the Raman effect, must be an A' fundamental. The three other bands, at 891, 915, and 939 cm^{-1}, are very weak in the Raman spectrum and have measured depolarization ratios of ~0.8, 0.85, and ~0.8, respectively. Since that at 939 cm^{-1} appears sharper than the others, it has been assigned as an A' fundamental. Since the band at 915 cm^{-1} can be interpreted as a combination band $331+588=919\ A''$, and since the somewhat low depolarization ratio of the band at 891 cm^{-1} can be explained as resulting from overlapping with the combination $331+559=890\ A'$, the frequency 891 cm^{-1} has been assigned as an A'' fundamental.

Of the next group of bands that have high intensity in at least one of the spectra those at 588 and 505 cm^{-1} are definitely polarized, while that at 559 cm^{-1} is de-

TABLE VI. Fundamental vibration frequencies for CF_3CF_2Cl.

Symmetry species	Wave number cm^{-1} Raman (gas)	Raman (liquid)	Infrared (gas)	Infrared (liquid)	Approximate character
$A'+A''$	186 w	186 m	···	···	CF_2Cl rocking
A'	315 m	315.8 s	314 m	···	CF_2Cl deformation
A''	331 w	332 m	···	···	CF_3 rocking
A'	366 w	364 m	362 w	···	CF_3 rocking
A'	441.5 m	441.3 s	···	···	CF_2Cl deformation
A''	···	···	454 m	455 w	CF_2Cl deformation
A'	561 w	560 w	560 m	560 s	CF_3 deformation
A''	595 vw	593 w	596 m	596 m	CF_3 deformation
A'	648.4 m	647 s	648 m	648 s	CF_3 deformation
A'	763.3 s	761.3 vs	762 s	761 vs	CCl stretching
A'	···	977 vw	982 vs	974 vs	CC stretching
A'	1131 vw	1124 w	1133 vs	1120 vs	CF_2 stretching
A''	1187 vw	1178 w	1185 vs	1178 vs	CF_2 stretching
A'	1236 vw	1224 w	···	1224 vs	CF_3 stretching
A''	···	1240 w	1241 vs	1240 vs	CF_3 stretching
A'	1348 vw	1349 m	1351 s	1350 vs	CF_3 stretching

polarized. They must represent two A' and one A'' fundamental involving largely CF_3 deformation.

There remain four A' and four A'' fundamentals, all of which may be expected to lie below 500 cm^{-1}, since the motions must be largely torsion, rocking, and $CFCl_2$ deformation. Seven Raman bands have been observed in this region. However, the band at 461 cm^{-1} is extremely faint in the Raman spectrum and very weak in the infrared and can readily be interpreted as a combination $200+265=465$ A'. If this band is not interpreted as a fundamental, it seems necessary to interpret the very strong band at 400 cm^{-1}, with depolarization ratio 0.45, as a superposition of an A' and an A'' fundamental. The band at 331 cm^{-1} is certainly an A'' fundamental and the bands at 312 and 200 cm^{-1} are certainly A' fundamentals. With less certainty the band at 265 cm^{-1} is assigned as an A' fundamental and that at 181 cm^{-1} as an A'' fundamental. The remaining A'' fundamental must lie lower and involve largely torsional motion. No spectral evidence has been found for determining its frequency.

The assigned fundamentals for CF_3CFCl_2 are listed in Table VII. The interpretation of the infrared and Raman spectra is given in the last columns of Tables III and IV.

TABLE VII. The fundamental vibration frequencies for CF_3CFCl_2.

Symmetry species	Wave number cm^{-1} Raman (liquid)	Infrared (gas)	Infrared (liquid)	Approximate character
A''	181 m	···	···	$CFCl_2$ rocking
A'	200 m	···	···	$CFCl_2$ rocking
A'	265 m	···	···	$CFCl_2$ deformation
A'	312 s	311 m	···	CF_3 rocking
A''	331 m	330 s	···	CF_3 rocking
$A'+A''$	400 vs	399 m	···	$CFCl_2$ deformation
A'	505.2 vs	507 m	508 m	CF_3 deformation
A''	559 w	560 s	558 m	CF_3 deformation
A'	588 w	590 s	590 m	CF_3 deformation
A'	734.5 vvvs	735 vs	734 s	CCl stretching
A''	891 vw	897 vs	891 vs	CCl stretching
A'	939 vw	943 vs	938 vs	CC stretching
A'	1103 w	1110 vs	1103 vs	CF stretching
A''	1218 w	1232 vs	1217 vs	CF_3 stretching
A'	1247 vw	1232 vs	···	CF_3 stretching
A'	1292 w	1295 vs	1292 vs	CF_3 stretching

4. CF_3CCl_3

This molecule undoubtedly has the symmetry C_{3v}. Its normal vibrations divide themselves into symmetry species in the following manner: $5\,A_1+A_2+6\,E$. Fundamentals of species A_1 and E are active in infrared absorption as well as in the Raman effect, while the torsional fundamental of species A_2 is inactive in both spectra.

The bands at 1252 and 1215 cm^{-1} (in liquid CF_3CCl_3) are weak in the Raman spectrum but very intense in the infrared. They must be fundamentals associated largely with C−F stretching. The higher one, which is polarized in the Raman effect, must belong to species A_1, and the lower one, which is depolarized, must belong to E.

Of the next group of bands strong in one or both spectra the one at 714 cm^{-1} is strongly polarized, while the band at 852 cm^{-1} is almost certainly depolarized,

TABLE VIII. Fundamental vibration frequencies for CF_3CCl_3.

Symmetry species	Wave number (cm^{-1}) Infrared (gas)	Raman (liquid)	Approximate character
A_2	···	···	torsion
E	···	182 s	rocking
E	263 m	265 s	rocking
E	366 m	367 m	CCl_3 deformation
A_1	426 s	429 vs	CCl_3 deformation
A_1	490 vw	···	CF_3 deformation
E	561 s	561 m	CF_3 deformation
A_1	714 vs	714 s	CCl stretching
E	859 vs	852 m	CCl stretching
A_1	909 vs	908 w	CC stretching
E	1227 vs	1215 w	CF stretching
A_1	1255 vs	1252 w	CF stretching

and that at 908 cm^{-1} is probably polarized. These bands must represent fundamentals, of species A_1, E, and A_1, respectively. They must be associated with motions involving C−Cl and C−C stretching.

There remain two A_1 and four E fundamentals to assign, in addition to the inactive A_2 fundamental. The depolarized band at 561 cm^{-1} is almost certainly an E fundamental, and that at 429 cm^{-1} is certainly an A_1 fundamental. The strong bands at 367, 265, and 182 cm^{-1} appear all to be depolarized in the Raman effect (the somewhat low depolarization ratio of the band at 367 cm^{-1} can readily be explained by overlapping with the overtone $2\times182=364$ of species A_1+E) and have been interpreted as E fundamentals. That leaves one A_1 fundamental to assign. It is tentatively identified with the weak infrared band at 490 cm^{-1}.

This last A_1 fundamental together with the E fundamental at 561 cm^{-1} must involve largely CF_3 deformation. The A_1 and E fundamentals at 429 and 367 cm^{-1} must be associated largely with CCl_3 deforma-

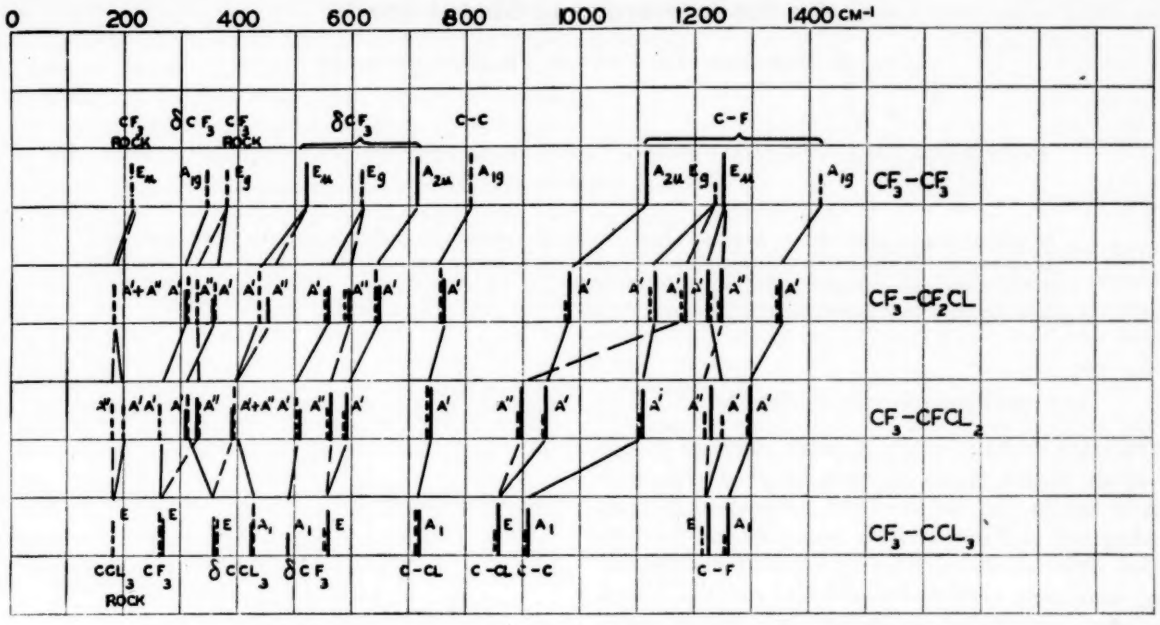

FIG. 6. Fundamental vibration frequencies for CF_3CF_3, CF_3CF_2Cl, CF_3CFCl_2, and CF_3CCl_3.

tion, and the E fundamentals at 265 and 182 cm^{-1} must involve rocking.

A strenuous attempt has been made to determine the inactive A_2 fundamental from infrared combination bands. If the weak infrared band at 345 cm^{-1} is interpreted as the overtone of the A_2 fundamental a value of 173 cm^{-1} is obtained for the latter. This serves to interpret one other weak infrared band which, however, can be fairly well interpreted otherwise. Thus, the spectral evidence for the value 173 cm^{-1} is very weak. Moreover, this value appears to be too high when it is considered that the lowest A'' fundamental in CCl_3CF_2Cl is as low as 81 cm^{-1}.

The assigned fundamentals of CF_3CCl_3 are listed in Table VIII. On the basis of these fundamentals it has been possible to interpret satisfactorily all observed bands except the two very weak infrared bands at 278 and 345 cm^{-1} and the extremely faint bands at 2365 and 3610 cm^{-1}. It is tempting to interpret 278 as a combination of 182 and the torsional frequency, giving 96 cm^{-1} for the latter. However, no evidence confirming this assumption could be found. In the absence of such evidence it appears more reasonable to ascribe the unexplained bands to a trace of impurity. The interpretation of the spectra is given in the last column of Table VII.

DISCUSSION

The assigned fundamental vibration frequencies for all four molecules of this series are correlated in Fig. 6. Solid vertical lines denote infrared bands, broken vertical lines Raman bands. A dotted line indicates a frequency inferred from overtone or combination bands but not observed directly. Coincident infrared and Raman frequencies are shown by slightly separated lines. The height of each vertical line rougly indicates the band intensity. The slanting correlation lines are drawn according to symmetry species rather than so as to join "group frequencies." Totally symmetric fundamentals are joined by solid slanting lines, and fundamentals of species E or A'' are joined by broken lines. No solid (broken) lines may cross.

The regularity of the correlation diagram is strong evidence for the correctness of the assignments made. Apart from some uncertainty with regard to the symmetry species of a few of the fundamentals, the main uncertainties in the assignments are the following. For CF_3CF_3 the E_u fundamental at 214 cm^{-1}, which has been inferred from infrared combination bands, is not quite certain. Moreover, since the Raman band at 1420 cm^{-1}, which has been identified with the highest A_{1g} fundamental, can also be interpreted as a combination, $620+809=1429\ E_g$, there is some uncertainty about this fundamental. For CF_3CF_2Cl the interpretation of the fairly weak infrared band at 454 cm^{-1} as an A'' fundamental must be regarded as tentative, as must the assumption that an A'' fundamental for CF_3CFCl_2 coincides with an A' fundamental at 399 cm^{-1}. For CF_3CCl_3 the assignment of the weak infrared band at 490 cm^{-1} as an A_1 fundamental is somewhat uncertain.

For none of the four molecules in this series has it been possible to determine the lowest fundamental, which is associated with torsion of one end of the molecule with respect to the other. For this reason calculated thermodynamic properties are not presented.

On the Interaction of Closed Shells

H. MARGENAU,* *Yale University, New Haven, Connecticut*

AND

PHILIP ROSEN, *The Johns Hopkins University, Applied Physics Laboratory,† Silver Spring, Maryland*

(Received September 19, 1952)

In calculating repulsive forces between closed shells, two essentially different methods have been used. It is shown in this paper that they should not be expected to give equal numerical results, and attention is called to some finer methodological points in the theory of exchange forces. Tables I–III give numerical results for the interaction of neutral He atoms.

STATEMENT OF THE PROBLEM

CONSIDERABLE effort is being devoted to the study of the forces between simple atoms, particularly helium, and the attention centers mainly upon the adequacy of different state functions for the task at hand. Calculations have been made with hydrogenic, Wang, and more elaborate functions, and the results have been compared. Less thought has perhaps been given to the method of calculating the forces, and to the question of whether the results obtained by different investigators have the same meaning. This note concerns the exchange interaction between atoms in nondegenerate states, such as rare gas shells. The literature contains a variety of methods for calculating repulsive atomic interactions, and it is not clear how they are related. Among these methods two seem predominant. The present paper is an appraisal of them and contains a calculation of the error implicit in one of these methods.

Slater,[1] Bleick and Mayer,[2] and Kunimune[3] are among the authors who employ a sort of perturbation procedure, the essential elements of which are as follows. The interacting atoms will be labeled a and b, and we assume in general that atom a has m and atom b has n electrons. The Hamiltonian of the total system may then be written

$$H=H_a(1\cdots m)+H_b(m+1\cdots m+n)+V(1\cdots m+n). \quad (1)$$

H_a and H_b are the unperturbed atomic Hamiltonians and V represents the interaction

$$V=-Z_ae^2\sum_{l=m+1}^{m+n} r_{al}^{-1}-Z_be^2\sum_{k=1}^{m} r_{bk}^{-1}+e^2\sum_{kl} r_{kl}^{-1}+Z_aZ_be^2/R, \quad (2)$$

the indices k and l labeling, respectively, the electrons in atoms a and b. The method under study takes atomic functions ψ_a and ψ_b, forms a Pauli determinant

$$\Psi=\sum(-1)^\lambda P_\lambda\psi_a\psi_b, \quad (3)$$

and identifies the intermolecular potential energy with

$$\tilde{V}=\frac{\sum(-1)^\lambda\int\psi_a^*\psi_b^*P_\lambda[V\psi_a\psi_b]d\tau}{\sum(-1)^\lambda\int\psi_a^*\psi_b^*P_\lambda[\psi_a\psi_b]d\tau}. \quad (4)$$

The permutations P_λ in Eqs. (3) and (4) are those among all $(m+n)$ electrons.

The peculiar form of $\tilde{V}$ comes about in this way. If one assumes ψ_a and ψ_b to be solutions of

$$H_a\psi_a=E_a\psi_a, \quad H_b\psi_b=E_b\psi_b, \quad (5)$$

then

$$H\Psi=(E_a+E_b)\Psi+\sum_\lambda(-1)^\lambda P_\lambda[V\psi_a\psi_b]$$

and

$$\bar{H}\equiv\frac{\int\Psi^*H\Psi d\tau}{\int\Psi^*\Psi d\tau}=E_a+E_b+\tilde{V}.$$

Thus the suggestion that $\tilde{V}$ be taken as the interaction energy is easily accepted.

Another procedure, however, and clearly a preferable one, is to regard as intermolecular energy the difference

$$\Delta E=\frac{\int\Psi^*H\Psi d\tau}{\int\Psi^*\Psi d\tau}-\frac{\int\psi_a^*H_a\psi_a d\tau}{\int\psi_a^*\psi_a d\tau}-\frac{\int\psi_b^*H_b\psi_b d\tau}{\int\psi_b^*\psi_b d\tau}, \quad (6)$$

provided ψ_a and ψ_b are properly antisymmetrized atomic functions. Examples of the use of Eq. (6) are found in papers by the present authors.[4,5] The quantities defined

* Assisted by the U. S. Office of Naval Research.
† Assisted by the Bureau of Ordnance, U. S. Navy.

[1] J. C. Slater, Phys. Rev. **32**, 339 (1928).
[2] W. E. Bleick and J. E. Mayer, J. Chem. Phys. **2**, 252 (1934).
[3] M. Kunimune, J. Chem. Phys. **18**, 754 (1950).
[4] P. Rosen, J. Chem. Phys. **18**, 1182 (1950).
[5] H. Margenau, Phys. Rev. **63**, 131 (1943).

in Eqs. (4) and (6) are equal only if ψ_a and ψ_b are correct atomic functions, a condition beyond fulfillment except in the case of atomic hydrogen. To be sure, $\tilde{V}$ and ΔE are both zero at infinite separation, which of course provides no justification for assuming them to be equal. Indeed they differ at finite distances by amounts comparable with their own magnitude, as will be shown. Other procedures, though outwardly different, can be reduced to one of these two. Often the use of equations like (5) is camouflaged, and the (erroneous) atomic energies do not visibly enter the scene; yet the result is that $\tilde{V}$ is being calculated. The early work of N. Rosen,[6] for example, amounts to a calculation of (4). The use of $\tilde{V}$ derives its warrant from Heitler and London, whose method leads to it at once. In the case of hydrogen there can be no question as to its correctness.

In the next section we derive a formula for the difference between ΔE and $\tilde{V}$.

GENERAL FORMULAS

The computation of quantities like $\tilde{V}$ or $\bar{H}$ with functions of the form (3) can be simplified by the use of a decomposition of the permutations P_λ into three simpler permutations. These are (1) intra-atomic or internal permutations of electrons within a, P_{λ_a}; (2) similar internal permutations within b, P_{λ_b}; (3) interatomic or external permutations between a and b, $P_{\lambda_{ab}}$. In general

$$P_\lambda = P_{\lambda_{ab}}{}^{ab} P_{\lambda_a}{}^{a} P_{\lambda_b}{}^{b}, \tag{7a}$$

where P_{λ_a} and P_{λ_b} commute. The elements of the complex P^{ab} can be enumerated as follows. There are

$$\binom{m}{0}\binom{n}{0},$$

that is to say, there is one identity permutation which does nothing. There are

$$\binom{m}{1}\binom{n}{1}$$

possible exchanges of 1 electron in a with 1 electron in b,

$$\binom{m}{2}\binom{n}{2}$$

possible exchanges of 2 electrons in a with 2 in b, and so forth. Hence the number of external permutations is

$$\sum_{\lambda=0}^{m}\binom{m}{\lambda}\binom{n}{\lambda}=\binom{m+n}{m}$$

by the addition theorem of binomial coefficients. This result can be checked by noting that the number of internal permutations is $m!n!$ and this, when multiplied by

$$\binom{m+n}{m},$$

results in

$$(m+n)!,$$

the total number of P_λ.

While each set of internal permutations forms a group, the P^{ab} do not; for it is possible to obtain an element P^aP^b by performing a sequence of external permutations. The cosets formed by combining the subgroup P^aP^b with the complex P^{ab} have the unique property of generating the entire group.

A useful result can be obtained because of the property $(P^{ab})^{-1}=P^{ab}$. Suppose that u and v are functions of the $m+n$ electron coordinates. F is a Hermitean operator. Then

$$\int u^* P^{ab} F v d\tau = \int [(P^{ab})^{-1}u^*] F v d\tau$$

$$= \int [P^{ab}u^*] F v d\tau = \int [F^* P^{ab} u^*] v d\tau.$$

In particular,

$$\int u^* P^{ab} F u d\tau = \int u F^* P^{ab} u^* d\tau. \tag{7b}$$

Changing the order of P^{ab} and F produces the complex conjugate expression.

We wish to calculate $\bar{H}=\int \Psi^* H \Psi d\tau / \int \Psi^* \Psi d\tau$, Ψ being given by Eq. (3). In the usual way, this reduces to

$$\bar{H}=\frac{\int \psi_a^* \psi_b^* H \sum_\lambda (-1)^\lambda P_\lambda \psi_a \psi_b d\tau}{\int \psi_a^* \psi_b^* \sum_\lambda (-1)^\lambda P_\lambda \psi_a \psi_b d\tau}.$$

Let us now take ψ_a and ψ_b to be antisymmetric with respect to internal permutations and assume these functions to be normalized. The operation $(-1)^{\lambda_a}P_{\lambda_a}$ will leave ψ_a unchanged. When we use the decomposition (7a), replacing $\sum_\lambda (-1)^\lambda P_\lambda$ by

$$\sum_{\lambda_{ab}} (-1)^{\lambda_{ab}} P_{\lambda_{ab}} \sum_{\lambda_a \lambda_b} (-1)^{\lambda_a+\lambda_b} P_{\lambda_a} P_{\lambda_b},$$

we obtain, on canceling a factor $m!n!$ in numerator and denominator,

$$\bar{H}=\frac{\int \psi_a^* \psi_b^* H \sum (-1)^{\lambda_{ab}} P_{\lambda_{ab}} \psi_a \psi_b d\tau}{\int \psi_a^* \psi_b^* \sum (-1)^{\lambda_{ab}} P_{\lambda_{ab}} \psi_a \psi_b d\tau}.$$

[6] N. Rosen, Phys. Rev. **38**, 255 (1931).

TABLE I. Comparison of ΔE and $\bar{V}$ computed with the use of Eq. (17).

R/a_0	$\frac{\Delta E-\bar{V}}{Rhc}$	$\frac{\Delta E}{Rhc}$
3.00	-3.19×10^{-3}	3.47×10^{-2}
4.79	-3.70×10^{-4}	6.36×10^{-4}
6.00	-4.80×10^{-5}	3.46×10^{-5}

As was pointed out, P^{ab} includes the identity operation. For convenience we split this off and denote the remaining

$$\binom{m+n}{m}-1$$

elements of P^{ab} by π_λ. Thus

$$\sum(-1)^{\lambda_{ab}}P_{\lambda_{ab}}=1+\sum(-1)^{\lambda}\pi_\lambda;$$

the π_λ are then true exchanges.

We now use Eq. (1) and abbreviate

$$\Sigma=\int\psi_a^*\psi_b^*\sum(-1)^\lambda\pi_\lambda\psi_a\psi_b d\tau,$$
$$\bar{V}=\int\psi_a^*\psi_b^*V\psi_a\psi_b d\tau, \tag{8}$$

so that

$$\bar{H}=\frac{\bar{H}_a+\bar{H}_b+\bar{V}+\int\psi_a^*\psi_b^*(H_a+H_b+V)\sum_\lambda(-1)^\lambda\pi_\lambda\psi_a\psi_b d\tau}{1+\Sigma}. \tag{9}$$

If *all* exchanges, i.e., *all* quantities containing π-operators were neglected, the classical result $\bar{V}$ is obtained for $\bar{H}-\bar{H}_a-\bar{H}_b$.

Turning to $\tilde{V}$ we find from (4)

$$\tilde{V}=\frac{\bar{V}+\sum(-1)^\lambda\int\psi_a^*\psi_b^*\pi_\lambda[V\psi_a\psi_b]d\tau}{1+\Sigma}, \tag{10}$$

where only external exchanges remain in the summation. The "cancellation" of internal permutations is possible here because the atomic functions are antisymmetric and V is symmetric with respect to internal permutations. We recall also (see Eq. (7b)) that π_λ and V are permutable and conclude after comparing Eqs. (9) and (10) that

$$\bar{H}=\frac{\bar{H}_a+\bar{H}_b+C_a+C_b}{1+\Sigma}+\tilde{V}, \tag{11}$$

provided

$$C_a=\int\psi_a^*\psi_b^*H_a\sum_\lambda(-1)^\lambda\pi_\lambda\psi_a\psi_b d\tau. \tag{12}$$

If at this stage we make the assumptions expressed in Eqs. (5), C_a becomes $\bar{H}_a\Sigma$ and $\bar{H}$ is indeed $\bar{H}_a+\bar{H}_b+\tilde{V}$. But otherwise

$$\bar{H}-\bar{H}_a-\bar{H}_b=\tilde{V}+\frac{C_a+C_b-(\bar{H}_a+\bar{H}_b)\Sigma}{1+\Sigma}. \tag{13}$$

The terms in addition to $\tilde{V}$ arise from the imperfections of the atomic functions, as was already indicated. Another way to see their meaning is to follow correctly the procedure that led to Eq. (4). Instead of (5) write $H_a\psi_a=\bar{H}_a\psi_a+\varphi_a$, $H_b\psi_b=\bar{H}_b\psi_b+\varphi_b$. The functions φ_a and φ_b represent the imperfections of the atomic functions and are orthogonal to them. If again we construct (3) and form $\bar{H}$ we obtain

$$\bar{H}-\bar{H}_a-\bar{H}_b=\tilde{V}+\frac{\int\psi_a^*\psi_b^*\sum(-1)^\lambda\pi_\lambda(\varphi_a\psi_b+\psi_a\varphi_b)d\tau}{1+\Sigma}. \tag{13'}$$

Sometimes this formula is more convenient than Eq. (13).

APPLICATION TO HELIUM

If we label the electrons in atom a by 1, 2, those in atom b by 3, 4, π_λ is one of the following transpositions: (13); (14); (23); (24); (13)(24).

Had we not performed the decomposition (7) we should have to consider initially not 5, but 24 permutations. The atomic functions for He are

$$\psi_a=2^{-\frac{1}{2}}u(1,2)[\alpha(1)\beta(2)-\beta(1)\alpha(2)],$$
$$\psi_b=2^{-\frac{1}{2}}v(3,4)[\alpha(3)\beta(4)-\beta(3)\alpha(4)].$$

Here α and β are spin functions and the coordinate functions u and v are symmetric: $u(12)=u(2,1)$. It is easily seen that integrals such as $\int\psi_a^*\psi_b^*F\pi_\lambda\psi_a\psi_b d\tau$ with $\pi_\lambda=(13);(14);(23)$; and (24), and F invariant to

TABLE II. Comparison of ΔE and $\bar{V}$ computed with the use of Wang functions.

R/a_0	$\frac{\Delta E-\bar{V}}{Rhc}$	$\frac{\Delta E}{Rhc}$
1.7778	7.95×10^{-2}	4.56×10^{-1}
2.9630	1.05×10^{-2}	2.84×10^{-2}
4.7407	1.90×10^{-4}	3.10×10^{-4}
7.1111	3.41×10^{-7}	4.28×10^{-7}

internal permutations are all equal. We thus find

$$\Sigma=\int u(12)v(34)[-2(13)+(13)(24)]u(12)v(34)d\tau$$

$$=-2\int u(12)v(34)u(23)v(14)d\tau$$

$$+\int u(12)v(34)u(34)v(12)d\tau. \quad (14)$$

Similarly,

$$C_a+C_b=\int u(12)v(34)[H_a(12)+H_b(34)]$$

$$\times[-2u(23)v(14)+u(34)v(12)]d\tau, \quad (15)$$

$$\tilde{H}_a=\tilde{H}_b=\int u(12)v(34)H_a u(12)v(34)d\tau. \quad (16)$$

In a recent article,[4] one of us has calculated ΔE with the use of functions of the form[7]

$$u(12)=\left(\frac{Z_1^3}{\pi}\right)^{\frac{1}{2}}\left(\frac{Z_2^3}{\pi}\right)^{\frac{1}{2}}(2+2t_0^2)^{-\frac{1}{2}}$$

$$\times[\exp(-Z_1A_1-Z_2A_2)+\exp(-Z_1A_2-Z_2A_1)], \quad (17)$$

$$v(34)=\left(\frac{Z_1^3}{\pi}\right)^{\frac{1}{2}}\left(\frac{Z_2^3}{\pi}\right)^{\frac{1}{2}}(2+2t_0^2)^{-\frac{1}{2}}$$

$$\times[\exp(-Z_1B_3-Z_2B_4)+\exp(-Z_1B_4-Z_2B_3)],$$

and compared the results with Slater's, who computed $\tilde{V}$. It is difficult to find C_a and C_b with Slater's nonanalytic function; nor would this be particularly meaningful because of certain approximations made in his work. To judge the importance of the methodological point of this paper we therefore calculate $\Delta E-\tilde{V}$ with functions (17).

If we define $\Delta=(2+2t_0^2)^2$, we find (the Hamiltonian is written in atomic units)

$$\Delta\cdot(\tilde{H}_a+\tilde{H}_b)=8(Z_1^2+Z_2^2-4Z_1-4Z_2)$$
$$+16(Z_1+Z_2-4)(t_0^3+t_0)Z_1F_7$$
$$+16(Z_1u+20Z_1\epsilon^3/(1+\epsilon)^5)(1+t_0^2)$$
$$-8[4(Z_1+Z_2)t_0^2+(Z_1^2+Z_2^2)t_0^4],$$

$$\Delta\cdot\Sigma=-2(s^2+s_\epsilon^2+2t^2)-8tt_0(s+s_\epsilon)+4(s^2s_\epsilon^2+t^4)$$
$$-4(t_0^2t^2+t_0^2ss_\epsilon-2t^2ss_\epsilon),$$

[7] The symbols used in this and the following equations are defined in reference 4.

TABLE III. Comparison of $\tilde{V}$ computed with different functions.

R/a_0	$\tilde{V}_W$	$\tilde{V}_S$	$\tilde{V}_R$
3.0	1.75×10^{-2}	2.5×10^{-2}	3.8×10^{-2}
4.8	1.0×10^{-4}	3.1×10^{-4}	10.0×10^{-4}
6.0	2.6×10^{-6}	1.7×10^{-5}	8.3×10^{-5}

$$\Delta\cdot(C_a+C_b)=4(Z_1^2-Z_2^2)(s^2-s_\epsilon^2)$$
$$+16(Z_2s^2+Z_1s_\epsilon^2)+16(Z_1+Z_2)t^2$$
$$+16(Z_1^2+2Z_2)st_0t+16(Z_2^2+2Z_1)s_\epsilon t_0t$$
$$-8(Z_1^2+Z_2^2)[t^4+s^2s_\epsilon^2-t_0^2t^2-t_0^2ss_\epsilon+2t^2ss_\epsilon]$$
$$-8(Z_1-2)[s+2t_0t-2s_\epsilon^2s-2t^2s_\epsilon+t_0^2s_\epsilon]Z_1F_2$$
$$-8(Z_2-2)[s_\epsilon+2t_0t-2s^2s_\epsilon-2t^2s+t_0^2s]Z_2F_2'$$
$$-8(Z_1+Z_2-4)(st+s_\epsilon t+t_0ss_\epsilon+t^2t_0)Z_1F_7$$
$$-4[t+t_0s_\epsilon+t_0s-2t^3-2tss_\epsilon+t_0^2t]$$
$$\times[(Z_2-2)(Z_1F_9+Z_2F_{10}')+(Z_1-2)$$
$$\times(Z_2F_9'+Z_1F_{10})]+16(t^2+ss_\epsilon)Z_1(F_{13}+F_{14})$$
$$-8(t+t_0s_\epsilon)(Z_1F_{15}+Z_2F_{17}')$$
$$-8(t+t_0s)(Z_2F_{15}'+Z_1F_{17})$$
$$-\frac{8(t_0t+s)\epsilon^3}{(2\epsilon-1)^{\frac{1}{2}}}Z_1F_{15}^{(2)}-\frac{8(t_0t+s_\epsilon)}{\left(\frac{1}{\epsilon}-1\right)^{\frac{1}{2}}}Z_1F_{15}^{(3)}$$
$$-8(s_\epsilon+t_0t)Z_2F_{18}'-8(s+t_0t)Z_1F_{18},$$

The symbols used here are defined in reference 4. Table I shows the error $(\Delta E-\tilde{V})$ in Rhc units for several values of the internuclear distance in units of the Bohr radius for hydrogen. Corresponding values of ΔE are also given for comparison.

Equations (14) and (15) take on a simpler form when u and v are products of one electron functions. If $u(12)=a(1)a(2)$ and $v(34)=b(3)b(4)$ and we introduce the customary overlap integral, $S=\int abd\tau$ we find

$$\Sigma=-2S^2+S^4,$$
$$C_a+C_b=-4S(aaH_aab)+2S^2(aaH_abb),$$

and the correction term becomes

$$\Delta E-\tilde{V}=\frac{2s}{(1-S^2)^2}[(aaH_aaa)(2S-S^3)$$
$$-2(aaH_aab)+S(aaH_abb)]. \quad (18)$$

Using the Wang functions, $a(1)=(Z^3/\pi)^{\frac{1}{2}}e^{-ZA_1}$, etc., with $Z=27/16$ we find for $(\Delta E-\tilde{V})$

$$\Delta E-\tilde{V}=[-4(2Z-4)SZF_2+16ZS^2-8SZF_{15}(1,\rho)$$
$$-4Z^2S^4+2(2Z-4)ZF_2S^2+4ZF_6S^2$$
$$-(4Z^2-16Z+5/2Z)(2S^2-S^4)](1-S^2)^{-2}.$$

An equation for ΔE has been derived in reference 5. Numerical values of $\Delta E - \tilde{V}$ and ΔE are given in Table II for several values of the internuclear distance.

The difference between ΔE and $\tilde{V}$ is never negligible; it is in fact comparable with ΔE itself. The magnitude of this difference is an index of the suitability of the chosen function for the purpose at hand.

The numerical values of $\tilde{V}$ for the Wang, Slater, and P. Rosen functions are given in Table III. The minimum in He comes at $5.3a_0$. The discordance of the entries strongly emphasizes the difficulties encountered in this type of work. The present calculation was carried out to see whether a comparison of similar quantities, such as $\tilde{V}$, computed with different functions, might reduce the discrepancies. The opposite, however, is the case.

THE JOURNAL OF CHEMICAL PHYSICS VOLUME 21, NUMBER 3 MARCH, 1953

The Emission Spectrum of OH from 1.4 to 1.7 μ*

W. S. Benedict,† Earle K. Plyler, and C. J. Humphreys
National Bureau of Standards, Washington, D. C.

(Received August 28, 1952)

The first overtone region of OH has been measured in emission from an oxyacetylene flame in the region of 1.6μ. The rotational structure in the P branch of the 2→0 band, from $K=4$ through $K=19$, of the 3→1 band, from $K=4$ through $K=15$, and of the 4→2 band, from $K=4$ through $K=10$, has been identified. For each K value there are four lines. These are resolved for values of $K>7$. From the intensities of the lines, a vibration-rotation temperature has been determined. For the mixture of gases burned in this work with small flames, it was found that the "temperature" was 2600±100°K.

I. INTRODUCTION

DURING the last several years there has been considerable activity in the measurement of the infrared radiation from flames. Many of the investigations have been made with prism spectrometers, and it has been possible to identify certain maxima of the emission spectrum as arising from the heated molecules of CO, CO_2, H_2O, and OH. The bands arising from these molecules have either not been resolved into their rotational structure, or only partially so, by the resolution available with the prisms used. This condition has made desirable a series of studies by the use of a high resolution grating spectrometer. The present paper reports one such study in the region 1.4–1.7μ; one other work on the emission and absorption spectrum of CO in the region 1.4–2.7μ has been published,[1] and two other studies on H_2O emission and C_2 and CN emission are in the process of publication. Abstracts of the latter two papers have appeared.[2]

In the work of Plyler and Humphreys[3] on the emission of the oxyacetylene flame the two regions of the emission spectrum at 1.5μ and 3 to 3.8μ corresponded closely with the predicted position of the OH fundamental band and its first overtone. In the region from 3 to 3.8μ, it was possible with a LiF prism to partially resolve the rotational structure, and several maxima corresponded closely in wave number with the predicted values of Dieke and Crosswhite.[4] The identification was not complete, and there was some question as to whether the emission band observed might arise from H_2O rather than OH. The purpose of this study was to measure the emission spectrum from an oxyacetylene flame in the region from 1.4 to 1.7μ and to determine if the OH vibrational band could be identified.

There is no doubt, as the result of the present work, that the vibration-rotation lines of OH are the most prominent features of flame emission in the region 1.5–1.7μ. They may be seen clearly with prism instruments in that region. Hornbeck and Herman[5] have also subsequently identified many resolved lines of the 4→0 sequence in the photographic infrared region.

II. EXPERIMENTAL METHOD

The measurements of the OH spectrum were made on a grating spectrometer which was constructed at the National Bureau of Standards. It contains a 15 000 line-per-inch grating, obtained from The Johns Hopkins University, with a ruled surface of about $4\frac{1}{2}$ inch×$7\frac{1}{2}$ inch. An off-axis paraboloidal mirror of 1-meter focus is used as the collimator and a PbS cell is used for detecting the radiation. The impulses from the detector are amplified and then fed into a high speed recorder. The instrument is able to resolve sharp lines separated

* Presented at the New York meeting of the American Physical Society, February 3, 1951.

† Present address, The Johns Hopkins University, Baltimore, Maryland.

[1] Plyler, Benedict, and Silverman, J. Chem. Phys. **20**, 175 (1952).

[2] W. S. Benedict and Earle K. Plyler, Phys. Rev. **83**, 245 (1951). Bass, Benedict, and Plyler, Symposium on Molecular Structure, Ohio State University, Columbus, Ohio, Paper No. H-4.

[3] Earle K. Plyler and C. J. Humphreys, J. Research Natl. Bur. Standards, **40**, 449 (1948).

[4] G. H. Dieke and H. M. Crosswhite, Bumblebee Report No. 87, The Johns Hopkins University, 1948.

[5] G. A. Hornbeck and R. C. Herman, J. Chem. Phys. **19**, 512 (1951).

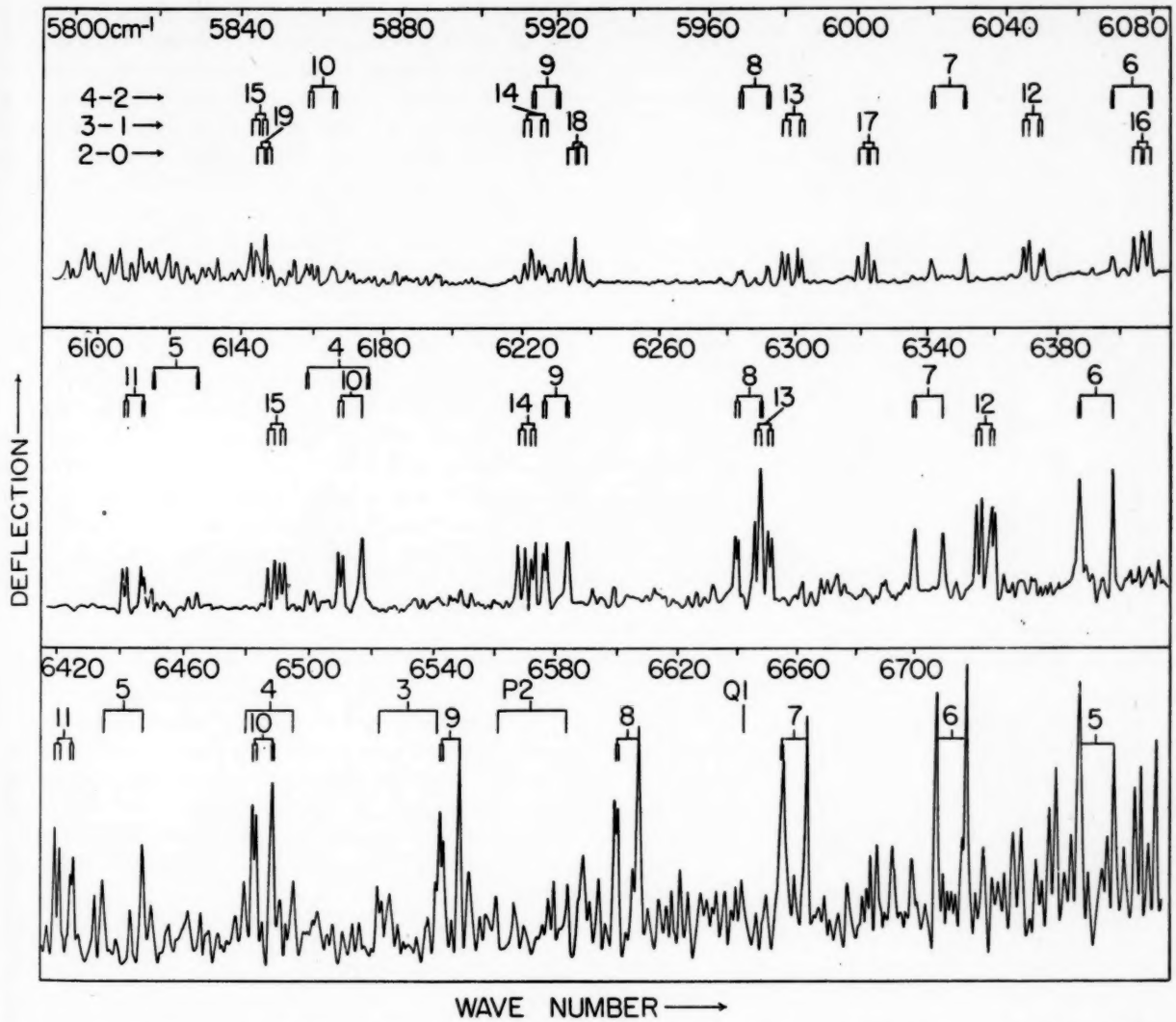

FIG. 1. The emission spectrum of an oxyacetylene flame from 5800 to 6800 cm^{-1}. The 2→0, 3→1, and 4→2 bands of OH are identified. Many of the low intensity lines in the trace are produced by H_2O molecules.

by 0.15 cm^{-1} in the region of 1.6μ. With weak sources wider spectral slits are required; and, in the recording of the spectrum of OH, the spectral slit width was 0.5 cm^{-1}.

The experimental arrangement for the source of radiation will be described briefly at this point. Since the principal objective of the work was the identification of spectra, rather than the quantitative investigation of the intensities of emitted radiation flames, the burners used, and the conditions of burning were not carefully controlled. The emission spectra of the various flames were obtained by burning premixed gases in a welding torch. The approximate relative proportions of the fuel and oxygen were metered with conventional flowmeters and the fuel-oxygen ratio could be adjusted over relatively wide limits. In general, spectra were obtained by focusing various portions of the flame upon the entrance slit of the spectrometer. A mirror was placed back of the flame so that an image was formed, inverted, and superimposed on the flame. This resulted in very nearly doubling the intensity of the emission. The particular region of the flame that was focused upon the slit and the particular fuel-oxygen ratio chosen were varied until the maximum intensity of the OH spectrum was obtained.

III. RESULTS AND DISCUSSION

It has been found that the spectrum of the first overtone sequence of OH is a very characteristic feature of the emission of H_2-O_2 and $C_2H_2-O_2$ flames in the region of 1.6μ when observed under high resolution. There is much overlapping of the spectrum of OH with that of H_2O between 6700–7189 cm^{-1} and some overlapping between 6400–6700 cm^{-1}, but between 5900–6400 cm^{-1}, the OH lines may be observed with only a weak background due to H_2O. A reproduction of an original recorder trace between 5800–6800 cm^{-1} is shown in Fig. 1. The source was an oxyacetylene flame of near-

TABLE I. Observed *P*-branch lines in overtone bands of OH.

Band K	f	2−0 ν	Int.	3−1 ν	Int.	4−2 ν	Int.
	2,2′	6818.8	*bl*	6494.4	14		
4	1,1′	803.3	*bl*	479.8	14	6159.24	*bl*
	2,2′	769.2	33	447.36	20	128.25	4
5	1,1′	756.6	44	434.74	26	115.70	5
	2,2′	717.5	47	397.3	24	(079.5)	*bl*
6	1	707.5	42	387.22	28	068.95	5.6
	1′	706.9		286.44			
	2,2′	663.6	45	345.0	20	028.81	6.6
7	1	655.45	49	336.65	22	020.39	7.1
	1′	654.43		335.52		6019.32	
	2	607.66	50	290.60	*b*1	5975.89	5.0
	2′	607.10		290.15			
8	1	600.54	53	283.46	24	968.39	4.5
	1′	599.69		282.44		967.51	
	2	549.28	45	233.81	20	920.8	4.5
	2′	548.55		233.11		920.1	
9	1	543.24	47	227.74	21.5	(914.5)	4.5
	1′	542.19		226.63		(913.5)	
	2	488.73	46.5	174.67	17	863.2	5.6?
	2′	487.82		174.09		862.6	
10	1	483.38	52	169.45	19.5	858.2	6 ?
	1′	482.32		168.35		856.8	
	2	425.74	34.5	113.53	14.5		
	2′	424.77		112.58			
11	1	421.21	41	108.99	15.3		
	1′	419.86		107.51			
	2	360.54	31	050.10	10		
	2′	359.69		049.34			
12	1	356.73	33	046.14	12.5		
	1′	355.41		6044.65			
	2	293.54	26	5984.78	10.5		
	2′	292.24		983.63			
13	1	290.17	29	981.19	10.4		
	1	288.31		979.56			
	2	224.27	18	917.06	7.6		
	2′	222.92		915.87			
14	1	221.95	21.5	914.03	9.0		
	1′	219.34		912.3			
	2	152.17		847.4	6.3		
	2′	151.39		846.0	*bl*		
15	1	150.12		844.61	*bl*		
	1′	148.16		842.72	6.3		
	2	079.51	15				
	2′	078.06					
16	1	076.98	13				
	1′	074.99					
	2	004.28	8.5				
	2′	002.52					
17	1	6002.10	*bl*				
	1′	5999.76	8.0				
	2	926.95	8.0				
	2′	925.2	*bl*				
18	1						
	1	922.78	8.0				
	2	848.19	6.0				
	2′	846.2					
19	1						
	1′	843.80	*bl*				

stoichiometric ratio observed in the region just above the tip of the inner cone. Three series of lines, each grouped in clusters of four, are observed; these are identified as the *P* branches of the 2−0, 3−1, and 4−2 bands. The number above each cluster of 4 is the *K* value of the lower state. The splitting of each *K* value into four lines is due to the $^2\Pi$ character of the electronic state. The interaction of the electronic spin and angular momentum with the rotational angular momentum of the molecule splits each level into 4, and the selection rules permit the appearance of 4 strong lines, as observed. (There are also "satellite" lines too weak to be identified.) The groups of 4 consist of pairs (spin-doublets) whose separation decreases with increasing *K*, each of which is a close pair (λ-doublets) whose separation increases with increasing *K*. The λ-doublets are clearly resolved for $K>7$, corresponding to a calculated separation of greater than 0.9 cm^{-1}. This clear resolution of the fine-structure, as well as the close agreement of the line positions with those calculated from the tables of Dieke and Crosswhite, is positive proof that the lines are due to OH.

The intensity of the OH spectrum relative to that of H_2O varies with the region of the oxyacetylene flame. In the inner cone and surrounding hot gases, it is still high, but the total OH intensity is not as great as in the region just above that point. Higher in the flame, the H_2O/OH ratio increases. In oxyhydrogen flames the same spectra can be observed, and with somewhat larger total intensity, but the H_2O/OH ratio is greater, so that the conditions are not as favorable for observing the OH.

Wavelengths of the OH lines were checked by basing a dispersion curve for the spectrometer upon second-order lines of Kr and Ne. The results, which should be good to ± 0.3 cm^{-1}, are not accurate enough to constitute an improvement upon the frequencies derived from the ultraviolet bands, but do confirm them nicely. The lines we have observed in the *P* branches of the 2−0, 3−1, and 4−2 bands are given in Table I, together with approximate values of their intensity, as averaged from several records taken under conditions similar to that of Fig. 1. The observed intensity refers to the average of the two components of the λ-doublets, which theoretically have equal intensity. When these are unresolved or partially resolved, the observed peak intensity must be correspondingly reduced. We have also been able to identify some of the lines in the *R* branches of 3−1 and 2−0, forming heads near 6845 cm^{-1} and 7189 cm^{-1}, respectively, but because of the serious overlapping with H_2O we have not tabulated them; the frequencies may be readily obtained from the energy-level table of Dieke and Crosswhite.[4] Identification of *Q*-branch lines is rather dubious, since they are relatively weak; the position of *Q*1 of 3−1 is indicated in Fig. 1, but the peak at that point may be principally due to H_2O.

As mentioned previously, the present measurements are not of sufficient accuracy to improve the determination of the energy levels and molecular constants of the $v=0$, 1, 2, and 3 states beyond the values previously reported. The $v=4$ state had, however, not been previously reported. Very recently Hornbeck and Herman[5] have observed the 4−0 band, and higher members of the $\Delta v=4$ sequence, in the photographic infrared. Our measurements yield energy levels of the $v=4$ state that are in good agreement with theirs. Since, however, their results are more extensive, and should be more accurate, we will present at this time only the following approximate values for the inertial constant and vibrational interval of this new level: $B_4=15.733$ cm^{-1}, $\Delta G_{7/2}=3077.5$ cm^{-1}.

The second-overtone sequence, 3−0 and 4−1, should also appear in flame spectra, since these bands lie in a region of relatively weak H_2O emission (R heads at 10356 cm^{-1} and 9856 cm^{-1}, respectively; P 10 at 9660 cm^{-1} and 9252 cm^{-1}, respectively). They have been observed, but in order to do so it was necessary to open the slits so wide (to 2–3 cm^{-1}) that the λ-doublets could not be resolved. Even under these conditions the lines were quite weak; it is estimated that the intensity ratio of corresponding lines in the bands 3−0 and 3−1, which have equal upper-state populations, is about 1:50. Observed features include the spin doublets in the P-branch lines of both 3−0 and 4−1 from $Q=5$ to 10, and the R-branch heads.

The 1−0 band has not been observed in the present studies with the 15 000 line grating spectrometer. The instrument might reveal a few of the lines of the R branch, whose frequencies are tabulated[4] in portions of the region 3850–3950 cm^{-1} where absorption by atmospheric H_2O is not complete. No such lines, however, could be identified, owing to the stronger emission of the higher levels in the H_2O molecules. A preliminary search of the region 3100–3500 cm^{-1} with a new grating instrument using slits about 0.5 cm^{-1} wide has, however, shown lines which definitely are the P-branch doublets of the 1−0 band, with intensities greater than the H_2O background emission in that region. Further observations will be pursued. For the present one can only say that the 1−0 band has been observed and that its intensity relative to the overtone (2−0) is somewhat lower than the relative intensity of the strong bands of H_2O (001−000 and 101−000) in the corresponding regions.

From the relative intensity of the well-resolved lines of the P branches in the 2−0 sequence, it is possible to determine a vibration-rotation temperature of the OH ground state, by a procedure exactly analogous to that described for CO.[1] For this purpose we need the rotational transition probabilities for a $^2\pi-{}^2\pi$ transition, in which both upper and lower states are intermediate between Hund's case a and case b. The formulas for this do not appear to have been previously worked out in detail, but may readily be calculated from the basic theory of Hill and Van Vleck.[6] The results are presented in Table II, where for completeness we include the unobserved satellite branches, as well as the strong P_1, P_2, R_1, and R_2 branches. Two alternative notations, those of Mulliken,[7] and Dieke and Crosswhite[4] are given. The line strengths apply strictly to only the 0−0 band, being calculated for the case in which the parameter $Y=A/B$ is the same in the upper and lower state, and has the numerical value −7.54, characteristic for $v=0$. Since $Y=-7.88$, −8.21, −8.57, and −8.96 for $v=1$, 2, 3, and 4, its variation should not lead to errors of more than 0.01 in the strengths.

In the calculation leading to the line strengths of Table II, it was also assumed that the interaction of vibration and rotation might be neglected. Oppenheimer[8] has calculated this effect for the 1−0 vibrational transition of a $^1\Sigma$ state, and Penner[9] has pointed out that its inclusion is necessary for results of the highest accuracy, particularly so when one is dealing with hydride molecules at elevated temperatures. The interaction increases the line strengths in the P branch by a factor

$$F=1+8\gamma K(1+5\gamma K/4-3\gamma/4),$$

where

$$\gamma=B_e/\omega_e=0.0051 \quad \text{for OH}$$

and correspondingly decreases the strengths in the R branch.

Inasmuch as the exact value of the "F factor" is not

TABLE II. Rotational line strengths for OH (intermediate $2\pi-2\pi$, $Y'=Y''=-7.548$).

	Branches						
$D+C$	$P_1(K)$ $R_1(K-1)$	$P_2(K)$ $R_2(K-1)$	$Q_1(K)$	$Q_2(K)$	$R_{21}(K)$ $P_{21}(K+1)$	$Q_{21}(K)$ $Q(K)$	$S_{21}(K)$ $O_{12}(K+2)$
Mull.	$P_1(K)$ $R_1(K-1)$	$P_2(K)$ $R_2(K-1)$	$Q_1(K)$	$Q_2(K)$	$R_{Q21}(K)$ $P_{Q12}(K+1)$	$Q(K)$ $Q(K)$	$S_{R21}(K)$ $O_{P12}(K+2)$
K''							
1	0	0	2.30	0.667	0.031	0.040	0.005
2	1.62	1.29	1.40	0.300	0.045	0.037	0.006
3	2.90	2.34	0.98	0.223	0.049	0.033	0.008
4	4.04	3.37	0.73	0.188	0.052	0.027	0.007
5	5.14	4.37	0.57	0.17	0.05	0.02	0.006
6	6.21	5.38	0.46	0.16	0.05	0.02	0.005
7	7.26	6.39	0.37	0.15	0.05	0.01	···
8	8.30	7.39	0.33	0.15	0.05	0.01	···
9	9.32	8.40	0.29	0.14	0.04	0.01	···
10	10.34	9.41	0.26	0.14	0.04	0.005	···
11	11.36	10.42	0.24	0.12	0.04	···	···
12	12.37	11.42	0.22	0.11	0.04	···	···
13	13.38	12.43	0.20	0.10	0.03	···	···
14	14.39	13.43	0.18	0.10	0.03	···	···
15	15.40	14.43	0.16	0.10	0.03	···	···
16	16.41	15.44	0.15	0.10	0.03	···	···
17	17.42	16.44	0.14	0.10	0.03	···	···
18	18.42	17.44	0.13	0.09	0.02	···	···
19	19.43	18.44	0.12	0.09	0.02	···	···
20	20.43	19.44	0.11	0.09	0.02	···	···

[6] E. L. Hill and J. H. Van Vleck, Phys. Rev. **32**, 250 (1928).
[7] R. S. Mulliken, Revs. Modern Phys. **3**, 89 (1931).
[8] J. R. Oppenheimer, Proc. Cambridge Phil. Soc. **23**, 327 (1926).
[9] S. S. Penner, J. Chem. Phys. **19**, 272, 1434 (1951).

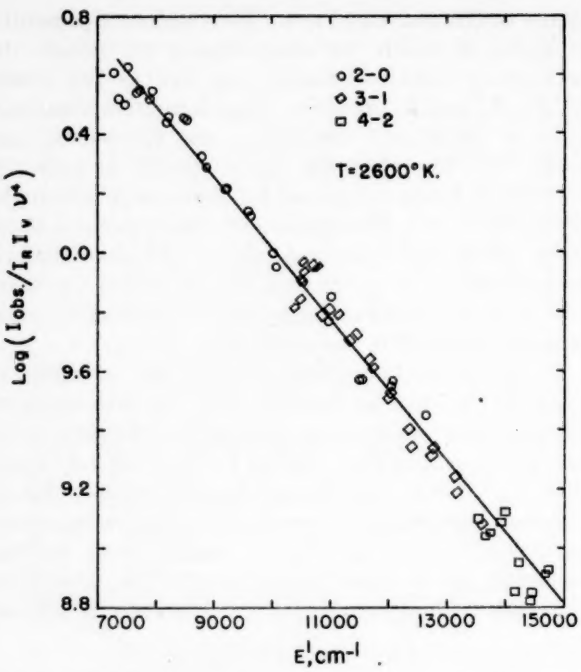

FIG. 2. The logarithm of the observed intensity, divided by ν^4 times the rotational transition probability, is plotted against the initial energy. The slope of the line corresponds to temperature of 2600±100°K.

known for overtone bands, nor for $^2\pi$ states, we have not included it in our "temperature" calculations. If the above expression were used, it would lead to a "temperature" about 300° *lower* than those found by neglecting the correction.

In Fig. 2 the logarithm (base 10) of the observed intensity, divided by ν^4 times the rotational transition probability, is plotted against the initial energy. Lines of the 2−0, 3−1, and 4−2 bands are included, the intensities of the latter two being further divided by the relative vibrational transition probabilities, 3 and 6. A single straight line falls fairly well through all points, indicating that equilibrium has been attained between the rotational and vibrational modes. The slope of the line corresponds to 2600±100°K. The 100° variation is based on reasonable limits of the position of the line in Fig. 2. This is in fairly good agreement with the "CO rotational temperature" observed for the same region of the oxyacetylene flame, but is 300–500° below the "temperatures" obtained from studies of the $^2\Sigma-^2\pi$ electronic transition of similar flames.[10]

A number of reasons can be adduced why the rotational temperatures determined from infrared vibration-rotation bands appear to be lower than those determined from electronic transitions. The principal one is undoubtedly the much longer radiative lifetime for infrared emission. For the transition in question we estimate it to be of the order of 10^{-2} sec, whereas for the electronic $^2\Sigma-^2\pi$ transition it is of the order of 10^{-6} sec. Hence, the molecules in excited states for infrared radiation must have survived many collisions before and during radiation and will be in a much closer approach to thermodynamic equilibrium than will those in electronically excited states. The OH radical, in a state of thermodynamic equilibrium with the other flame products, will be present in sufficient concentration so that there can be no doubt of the thermal origin of its infrared radiation, whereas chemiluminescence must be postulated to account for many of the characteristics of the ultraviolet radiation except in regions removed from the reaction zone. Moreover, both calculation and experiment indicate that the emissivity of the infrared OH lines is low. Hence, molecules from all regions of the flame, from the hottest ones at the center to those at the relatively cool outer fringes, will contribute to the observed radiated intensity (no "reversal" effects). The radiation laws in the infrared region are such that the cooler molecules will contribute more to the total intensity than when visible or ultraviolet radiation is observed. Finally, it may be that in the hot flame gases where the equilibrium concentration results from a balance of rapid chemical processes of formation and reaction, those molecules possessing an excess of rotational and vibrational energy over the mean Boltzmann distribution are most rapidly reacted, so that those surviving to radiate in the infrared show a low apparent temperature. In conclusion it may be stated that the temperature determination reported here is not extremely accurate, both because of experimental limitations and uncertainties in the theoretical calculation of rotation-vibration transition probabilities. However, it appears that the apparent temperatures are lower than those observed in the ultraviolet.

[10] H. P. Broida and K. E. Shuler, J. Chem. Phys. **20**, 168 (1952).

On the Existence of a Hidden Transition in Biphenyl*

ANNELIESE WENZEL
Department of Physics, Duke University, Durham, North Carolina
(Received July 7, 1952)

The 2500A transition of biphenyl is interpreted as a superposition of a strong and a weak transition corresponding to the 2100A and 2600A transitions of benzene. Evidence for the location of the weak transition near 2700A is given. The spectra of the *m*- and *p*-polyphenyls are interpreted similarly to the biphenyl spectrum. Bending has about the same effect on the intensity and the position of the first strong transition of polyphenyls with *m*- and *p*-structure as it has on the corresponding transition of cata-condensed hydrocarbons.

INTRODUCTION

THE absorption spectrum of biphenyl in the near ultraviolet taken in solution consists of a strong transition at $\lambda_{max}\sim$2500A or $\nu_{max}\sim$40 000 cm^{-1} with an extinction coefficient $\epsilon_{max}\sim$19 000. There are two other strong systems further in the ultraviolet. We are concerned here chiefly with the first long wave transition of biphenyl at 2500A. As biphenyl is composed of two coupled benzene rings, it may be expected that the spectrum of biphenyl shows some resemblance to that of benzene. Platt[1] assumes indeed that the 2500A transition of biphenyl corresponds to the strong 2100A transition of benzene, which in biphenyl is shifted towards the red. He further assumes that the weak 2600A transition of benzene is also present in the biphenyl spectrum, but is hidden by the much stronger 2500A band.

Platt's arguments for the existence of the hidden transition are based on a comparison of the absorption spectra of fluorene, α-α' bipyridyl and anthracene with that of biphenyl. In fluorene and in α-α' bipyridyl the 2500A transition of biphenyl apparently splits into two transitions. Using polarization predictions from molecular orbital considerations, Platt places the suggested hidden transition in biphenyl at 41 000 cm^{-1} (2440A) that is, a little shifted towards the ultraviolet from the observed 2500A transition. As early as 1937 Pestemer and Mayer-Pitsch[2] gave the same interpretation of the spectrum of biphenyl, and Wheland has forwarded the same ideas in 1944.[3] As will be shown, it is possible to find more arguments for the existence of the hidden transition, to locate it at approximately 2700–2750A (37 000–36 400 cm^{-1}) and also to estimate roughly its intensity.

LOCATION AND INTENSITY OF THE HIDDEN TRANSITION OF BIPHENYL

First we will compare the spectra of biphenyl, *p*-terphenyl, *p*-quaterphenyl, which have been investigated by Gillam and Hey,[4] to give additional evidence that the 2500A transition of biphenyl very probably corresponds to the 2100A transition of benzene. The first long wavelength transitions of biphenyl, *p*-terphenyl, *p*-quaterphenyl, etc., are strong systems in the region of 2500–3200A, which shift with increasing number of rings towards the red while the intensity of each increases each time. Extrapolating down to benzene as the first member of this group leads to a transition near 2100A with an extinction coefficient of ϵ_{max} about 10 000. This agrees well with the intensity and the location of the observed second benzene transition at 2100A. It should be mentioned that this transition shows structure, while the spectra of biphenyl and the polyphenyls are broad single bands.

Looking now for the analog of the first benzene transition, it apparently cannot be observed in biphenyl because of its weak intensity and its location near the strong transition. In order to reveal it, it seems advisable to study the effect of perturbation on the biphenyl spectrum by substitution. In this case 3- or 3-3′ substituted biphenyl derivatives should be used, which do not show the well-known anomalies of 4- and 2-substituted derivatives. Therefore, the spectra of the following compounds were compared with the spectrum of biphenyl:

(1) 3-3′ dihydroxybiphenyl	(alcohol solution)[5]
(2) 3-aminobiphenyl	(hexane solution)[2]
(3) 3-3′ bipyridyl	(diluted NH_3-solution)[6]
(4) 3-phenylpyridine	(diluted NH_3, diluted HCl-solution)[6]

The absorption spectra of these compounds are well known, but not all for the same solvent. However, in diluted NH_3, diluted NaOH, H_2O, and ethyl alcohol the absorption curves of these four substances should be almost the same. They are shown in Figs. 1–4 in which all have been redrawn from the original papers to the same scale. If there is in biphenyl a hidden transition which shifts upon substitution by a similar amount as do the first transitions in benzene and naphthalene, then it might be revealed by substitution. Actually the 3-3′ dihydroxybiphenyl curve shows on comparison

* This research was supported by the U. S. Office of Naval Research under Contract N6ori-107, T.O.I. with Duke University.
[1] J. R. Platt, J. Chem. Phys. **19**, 101 (1951).
[2] M. Pestemer and E. Mayer-Pitsch, Monatsh. Chem. **70**, 104 (1937).
[3] G. W. Wheland, *The Theory of Resonance* (John Wiley and Sons, Inc., New York, 1944), p. 151.
[4] A. E. Gillam and D. H. Hey, J. Chem. Soc., 1170 (1939).
[5] B. Williamson and W. H. Rodebush, J. Am. Chem. Soc. **63**, 3018 (1941).
[6] P. Krumholz, J. Am. Chem. Soc. **73**, 3487 (1951).

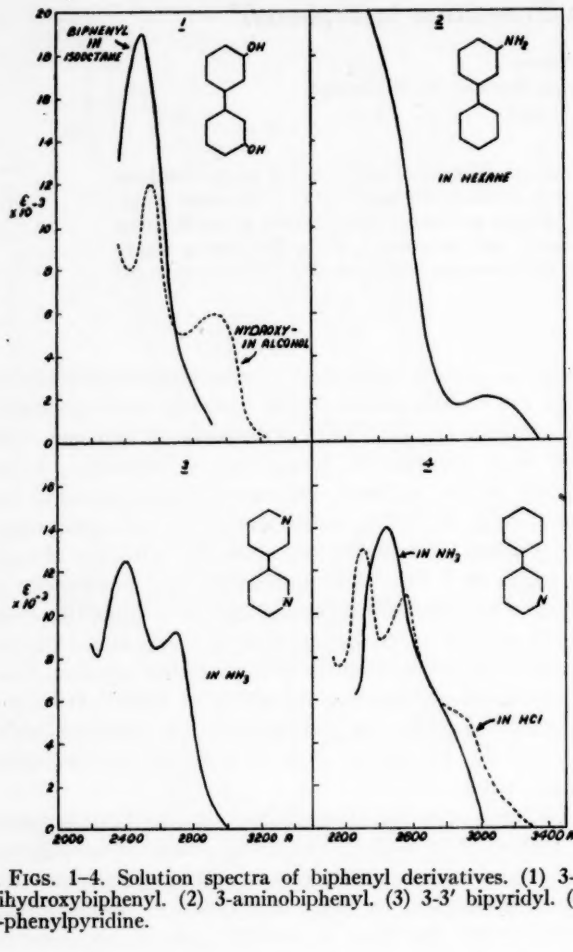

FIGS. 1–4. Solution spectra of biphenyl derivatives. (1) 3-3′ dihydroxybiphenyl. (2) 3-aminobiphenyl. (3) 3-3′ bipyridyl. (4) 3-phenylpyridine.

with the biphenyl curve a new transition appearing at $\lambda_{max}\sim$2930A (34 100 cm^{-1}) with $\epsilon_{max}\sim$6000. By comparing these results with corresponding data of the pairs benzene-phenol and naphthalene-β-hydroxynaphthalene, the location of the hidden transition may be expected at about 2750A (36 400 cm^{-1}). The curve of 3-aminobiphenyl also shows a new transition at 3030A (33 000 cm^{-1}) with $\epsilon_{max}\sim$2000. Comparison of these findings with data of the pairs benzene-aniline, naphthalene-β-aminonaphthalene places the hidden transition in biphenyl at 2710A (36 900 cm^{-1}).

Before a similar comparison is made between the spectra of biphenyl, 3-3′ bipyridyl, and 3-phenylpyridine, it is convenient to compare first the pairs benzene-pyridine and naphthalene-isoquinoline.[7–9] Isoquinoline and not quinoline was chosen for the same reasons that β-aminonaphthalene and β-hydroxynaphthalene were used. Substitution of N into the ring produces little change in the location of the π-electron spectra from the parent substance. In addition, the substitution produces in pyridine a very weak transition on the long wave upgrade part of the strong 2500 band. This transition which is not an excitation of the π-electrons, does not manifest itself as a separate peak in the absorption curve.[10,11] It is assumed that it is of similar weakness in the spectra of 3-3′ bipyridyl and 3-phenylpyridine and therefore can be neglected for our purposes. Going back to the π-electron transitions we observe that the weak first long wave transitions of benzene and naphthalene and the corresponding transitions of pyridine and iso-quinoline have almost the same location, but the intensities of the transitions of the N compounds are about 10 times higher ($\epsilon_{max}\sim$2000) in iso-octane solution than the transitions of the hydrocarbons. In contrast, the intensities of the higher $\pi-\pi$ transitions decrease about 20 percent for the next transition,† called here transition *II*, and about 50 percent for transition *III* when going from the homocyclic to the heteorcyclic compound. (Intensity of transition *III* is known only for isoquinoline).

These remarks apply to solutions in isooctane. In alcohol solution the lowest $\pi-\pi$ transition of pyridine and isoquinoline increases in intensity similarly with ϵ_{max} going from about 2000 to about 2500, and in diluted HCl-solution there is a further increase of ϵ_{max} to $\sim$6000 for pyridine and to $\sim$4500 for isoquinoline. The other two $\pi-\pi$ transitions of isoquinoline decrease in HCl solution about 50 percent as compared with iso-octane solutions and are shifted somewhat towards the red. With these remarks in mind we may now compare the absorption curves of 3-3′ bipyridyl and 3-phenyl-pyridine with that of biphenyl.

3-3′ bipyridyl in NH_3 solution shows, like 3-amino-biphenyl and 3-3′ dihydroxybiphenyl, a new transition at 2700A (37 000 cm^{-1}) with $\epsilon_{max}\sim$9000, which indicates that the hidden transition in biphenyl is at this position. The 2500A transition of biphenyl is in 3-3′ bipyridyl shifted a little towards the ultraviolet, and there is a decrease in its intensity by 35 percent as compared to biphenyl.

The curve of 3-phenylpyridine in NH_3-solution is similar to the biphenyl curve. The hidden transition is faintly revealed, which is to be expected, if the location is near 2700A as the previous curves indicate. It becomes more apparent in diluted HCl-solution by a distinct shoulder near 2800A with $\epsilon_{max}\sim$6000. Because of a red shift of the whole curve the location of the hidden transition in biphenyl will be again close to 2700A.

Platt has placed the hidden transition of biphenyl at 2440A for reasons of polarization and intensity without using the absorption curves of fluorene and $\alpha-\alpha'$ bipyridyl. Actually these curves suggest a location rather to the red from 2500A than to the violet. The 3-substituted biphenyl derivatives, which have been used here, give consistent results for the location of the

[7] H. Fischer and P. Steiner, Compt. rend. **175**, 882 (1922).
[8] G. E. Ewing and A. E. Steck, J. Am. Chem. Soc. **68**, 2181 (1946).
[9] E. F. G. Herington, Disc. Faraday Soc. **9**, 26 (1950).
[10] M. Kasha, Disc. Faraday Soc. **9**, 14 (1950).
[11] H. P. Stephenson, Ph.D. thesis, Duke University, 1952.
† For simplicity the 2600, 2100, 1900A transitions of benzene will be called here I, II and III and the same notation will be used for the corresponding transitions of naphthalene, pyridine, and isoquinoline.

hidden transition. From the intensities of the new transitions, which appear upon substitution, it may be assumed that the strength of the hidden transition in biphenyl is of the same order of magnitude as the weak benzene and naphthalene transitions. It may be mentioned in this connection that the first transitions of the monosubstituted derivatives, 3-aminobiphenyl, and 3-phenylpyridine have almost the same intensity as the corresponding spectra of the benzene and naphthalene derivatives.

SUGGESTIONS OF A HIDDEN TRANSITION IN POLYPHENYLS AND COMPARISON OF THEIR SPECTRA TO CATA CONDENSED HYDROCARBON SPECTRA

If the interpretation of the biphenyl spectrum as given here, is correct, the spectra of the *p*- and *m*-polyphenyls should be interpreted in the same way, that means, the strong first transition of these compounds in the region 2500–3000A would correspond to the 2100A transition of benzene, and a weak transition corresponding to the weak 2600 benzene transition would be hidden by the much stronger band.

The absorption of the *p*- and *m*-polyphenyls was studied by Gillam and Hey.[3] The *m*-polyphenyls show like the *p*-polyphenyls a strong first transition near 2500A, but it does not shift in the *meta* series with increasing number of rings, although these compounds have been investigated up to the sedeciphenyl, which contains 16 rings. The intensities of the spectra of the *m*-polyphenyls are apparently higher than the spectral intensities of the corresponding *p*-polyphenyls. Recently Woods, Artsdale, and Reed[12] investigated the absorption of polyphenyls, in which the benzene rings are coupled both in *m*- and *p*-position. These absorption curves give additional evidence that polyphenyls in which the benzene rings are wholly or partly coupled in *m*-position have a stronger intensity and a position farther towards the ultraviolet than the *p*-polyphenyls with the same number of benzene rings.

If the mentioned suggestion of a hidden transition and the interpretation of the polyphenyl spectra is correct, there exists a very interesting parallelism between the spectra of the polyphenyls and the spectra of the cata condensed hydrocarbons. According to Klevens and Platt,[13,14] the cata-condensed hydrocarbons show spectral resemblance, and it is possible to compare corresponding transitions. If the benzene rings are condensed in a straight line (polyacenes), transitions *I* and *II* are both moving towards the red with increasing number of rings, with transition *II* moving faster than transition *I*. If the benzene rings are not condensed in a straight line, but if there is more or less bending, the location of transition *I* is not much influenced by the bending, but transition *II* of a bent ring compound lies much more towards the ultraviolet than transition *II* of the corresponding polyacene. Bending also increases the intensity of transition *II*.

The spectra of the polyphenyls show a similar behavior. If the benzene rings are coupled in a straight line (*p*-polyphenyls), transitions *I* and *II* are also moving towards the red, transition *II* faster than transition *I*, only the rate of the shifts of both transitions is slower for the *p*-polyphenyls than for the polyacenes. If the benzene rings are not coupled in a straight line, but in *m*- and *p*-position or only in *m*-position, which possibly corresponds to the bending of the cata condensed hydrocarbons, transition *II* of a bent polyphenyl lies much more towards the ultraviolet than the transition of the corresponding *p*-polyphenyl. Bending in the polyphenyl series also increases the intensity of transition *II*. Therefore bending seems to have a similar effect on transition *II* of the polyphenyls as it has on transition *II* of the cata condensed hydrocarbons.

The mentioned influences may be seen from Tables I and II. The two series in Table II can only be compared among themselves and not with each other as different solvents have been used. Table I has already been discussed by Platt[13] in the same fashion, and has been included here for comparison only. In this Table *f* values have been included in addition to the ϵ-values since they are not proportional to each other because of the structure observed in these spectra. In Table II ϵ-values are considered sufficient since here the transitions exhibit broad structureless bands only and the proportionality may be fulfilled.

COMPARISON OF TRANSITION *I* AND *II*

It has been mentioned that the position of transition *II* of the cata-condensed hydrocarbons is more sensitive to perturbations than the position of transition *I*.[1] It is difficult to make a general statement about shifts of transition *I* and *II*, which occur on substitution in the polyacenes, since they depend very much on the position in which the substitution takes place. de Laszlo[15] has shown, that the spectra of β-substituted naphthalenes are more like the naphthalene spectrum than those of the α-derivatives. Therefore only substitution in β-position will be considered here. A comparison of transition *I* and *II* of benzene and naphthalene shows, that transition *I* of benzene and naphthalene shifts each time about the same amount towards the red, if the same substituent (CH_3, Cl, OH, COOH, NH_2) is introduced in β-position, but that transition *II* shifts differently under the same conditions. If, for example, NH_2 is substituted into benzene, transition *II* shifts from 2100A to 2350A, while on substitution in naphthalene in β-position there is practically no shift and on substitution in anthracene in β-position there is a shift towards the ultraviolet. Biphenyl behaves on substitution in 3-position like naphthalene, and this accounts

[12] Woods, van Artsdale, and Reed, J. Am. Chem. Soc. **72**, 3221 (1950).
[13] H. B. Klevens and J. R. Platt, J. Chem. Phys. **17**, 470 (1949).
[14] J. R. Platt, J. Chem. Phys. **17**, 484 (1949).
[15] H. G. de Laszlo, Proc. Roy. Soc. (London) 111, 355 (1926).

TABLE I. Influence of bending on position and intensity of transition *II* of cata-condensed hydrocarbons.

		ϵ_{max}	f	Onset of absorption λ	Onset of absorption ν	Ref.
	Benzene	6900	0.10	2080	48 050	13
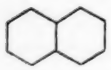	Naphthalene	9300	0.18?	2890	34 600	13
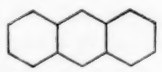	Anthracene	9000	0.10	3780	26 400	13
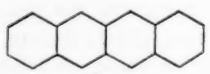	Tetracene	12 500	0.08	4730	21 100	13
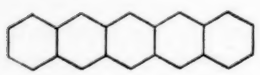	Pentacene	12 000	0.08	5850	17 100	13
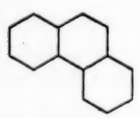	Phenanthrene	16 000	0.18	3030	33 000	13
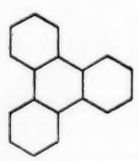	Triphenylene	20 000	0.22	3010	33 200	13
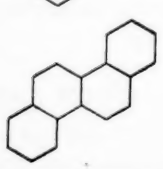	Chrysene	16 000	0.36	3310	30 200	13

for the fact that transition *I* is revealed in the curves of 3-aminobiphenyl and 3-3′ dihydroxybiphenyl.

INTERPRETATION OF THE POLYPHENYL SPECTRA BY GILLAM AND HEY

In order to explain the shift towards the red in the *p*-polyphenyls and the lack of shift in the *m*-polyphenyls, Gillam and Hey assume that in the *p*-series there exists some conjugation between all the benzene rings present while in the *m*-series the conjugation cannot extend beyond that inherent in the biphenyl structure. They further assume that the conjugation in the *p*-polyphenyls is less effective than the conjugation in the diphenylpolyenes because *p*-sexiphenyl has an absorption near 3000A, while diphenyldodecahexaene, which has an equal number of conjugated double bonds, absorbs in the region of 4000A. Gillam and Hey's first assumption is based on the statement that increase in the number of conjugated double bonds normally results in a displacement to longer wavelengths connected with an increase of intensity of absorption. This statement resulted from observations in the spectra of the polyenes and diphenylpolyenes. Whenever a comparison is made between the spectra of different compounds, only transitions of the same type should be compared; but it is not certain that this is the case here. Gillam and Hey mention that the strong transition of biphenyl may correspond either to transition *I* or *II* of benzene, but it is really transition *III* of the cata-condensed hydrocarbons which resembles to a certain extent the spectra of the polyenes. Therefore, Gillam and Hey's reasoning concerning the first assumption does not seem entirely justified. The same considerations apply to the other assumption, that the conjugation in the *p*-polyphenyls is weaker than the conjugation in the biphenylpolyenes (in this connection see also reference 12).

COMPARISON OF PRESENT CONSIDERATIONS WITH PREVIOUS INTERPRETATIONS

The interpretation of the spectrum of biphenyl, as it is given here, agrees with the interpretation of

TABLE II. Influence of bending on position and intensity of transition *II* of *m*- and *p*-polyphenyls.

	ϵ_{max}	λ_{max}	ν_{max}	Solvent	Ref.
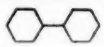	18 300	2515	39 750	Chloroform	4
	25 000	2800	35 700	Chloroform	4
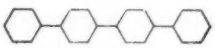	39 000	3000	33 300	Chloroform	4
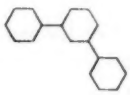	44 000	2515	39 750	Chloroform	4
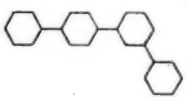	38 000	2660	37 600	Cyclohexane	12
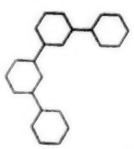	56 000	2480	40 300	Cyclohexane	12
	35 000	2820	35 500	Cyclohexane	12
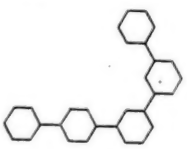	50 000	2580	38 700	Cyclohexane	12
	78 000	2480	40 300	Cyclohexane	12

Pestemer and Mayer-Pitsch, which is based on the appearance of the absorption curves of *o*-, *m*- and *p*-amino, *o*-, *m*- and *p*-nitro, and *o*- and *p*-cyanobiphenyl in different solvents, and with the interpretations given by Wheland and Platt. The interpretation does not agree with conclusions drawn from a study of absorption curves of a number of substituted biphenyl derivatives by Rodebush and co-workers.[5,16] These authors assume that the strong transition of biphenyl at 2500A corresponds to the first transition of benzene, which through the effect of conjugation is in biphenyl considerably increased in intensity. In the case of 2- and 6-methyl-substituted biphenyl derivatives they observed a strong decrease of intensity in the spectra of the new compounds on comparison with the strong biphenyl transition and explained this decrease as resulting from interference of the *o*-substituent with the coplanarity of the 2 rings, which decreases conjugation. Rodebush and co-workers did not only investigate methyl derivatives of biphenyl, but also OH-, NH_2-, and NO_2-derivatives, and they observed in the latter compounds a new transition at longer wavelengths. In the case of 3-3′-dimethoxybiphenyl (*A*) and 3-3′, *o*-*o*′-dimethyldimethoxybiphenyl (*B*) they make the statement that the spectrum of *A* shows the general absorption of biphenyl and in addition a new transition towards longer wavelengths which corresponds to the absorption of phenetol (half the molecule). On substitution of CH_3 in the *o*-*o*′ position the general absorption of biphenyl decreases considerably owing to steric inhibition, while the new transition remains almost unchanged. This interpretation of the new transition is not very convincing, as the curves of the 2- and 6-methyl-substituted biphenyls seem to indicate also the presence of a second transition.

[16] M. T. O'Shaughnessy and W. H. Rodebush, J. Am. Chem. Soc. 62, 2906 (1940).

The great difference in intensity of the weak benzene transition ($\epsilon_{max}\sim200$) and the biphenyl transition ($\epsilon_{max}\sim18\,000$) is also difficult to explain as conjugation effect alone. Therefore, the interpretation of the biphenyl band at 2500A as superposition of a strong and a weak transition is preferred here. If this interpretation is correct, the effect of steric inhibition reveals itself in biphenyl mainly in position and intensity of transition *II*.

Steric inhibition has not only been observed in *o*-methyl substituted biphenyl derivatives, but also in derivatives of nitrobenzene and dimethylaniline;[17–19] this means, the strong transition which nitrobenzene and dimethylaniline show at about 2500A decreases in intensity on *o*-methyl substitutions. In the case of dimethylaniline it is easy to connect the 2500A band with transition II and the band at 2900A with transition *I*. In the case of nitrobenzene the 2500A transition is generally considered to correspond to transition *I* of benzene, which because of increased resonance has a much larger intensity. It is not improbable that, as in the case of biphenyl, the strong transition of nitrobenzene at 2500A corresponds to transition *II* of benzene and covers the weaker transition *I*. Evidence for this assumption will be given later.

I wish to express my gratitude to Dr. H. Sponer for her help and her advice throughout this investigation and to Dr. H. P. Stephenson for many discussions.

[17] W. R. Remington, J. Am. Chem. Soc. **67**, 1838 (1945).
[18] H. B. Klevens and J. R. Platt, J. Am. Chem. Soc. **71**, 1714 (1949).
[19] W. G. Brown and H. Reagan, J. Am. Chem. Soc. **69**, 1032 (1947).

THE JOURNAL OF CHEMICAL PHYSICS VOLUME 21, NUMBER 3 MARCH, 1953

The Infrared Spectra of Tetranitromethane*†

P. H. LINDENMEYER‡ AND P. M. HARRIS
Department of Chemistry, The Ohio State University, Columbus, Ohio

(Received June 19, 1952)

Cooling curve investigations show that the transition between the two crystalline forms of tetranitromethane occurs at −99.8°C and its character suggests an order-disorder transformation. The infrared spectra of tetranitromethane were obtained at 25°C (vapor), 18°C (liquid), −40°C (solid I), −88°C (solid I), −104°C (solid II) and −126°C (solid II). The spectra of the vapor are best interpreted by a molecule with $S_4-\bar{4}$ symmetry whereas reported Raman spectra indicate $D_{2d}-\bar{4}2m$ symmetry in the liquid. Satisfactory agreement between these and the x-ray diffraction data require molecules of both symmetries. A complete lack of selection rules was observed in the spectra throughout the solid range.

INTRODUCTION

ON the basis of previous work[1] in this laboratory, it was known that there exist two forms of crystalline tetranitromethane. Just below its freezing point at 13.8°C it has a body-centered cubic lattice 7.01A on an edge, with two molecules per unit cell. X-ray powder

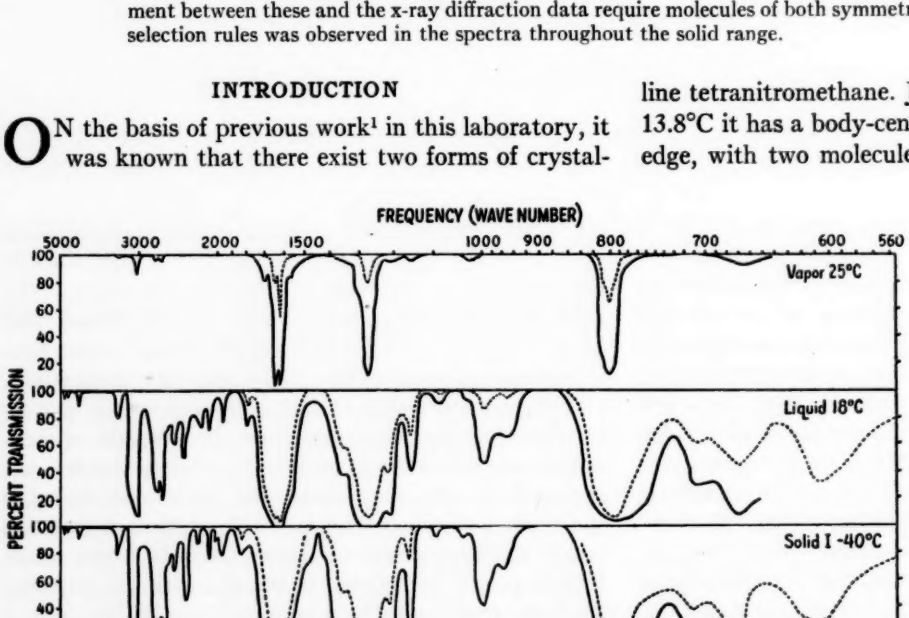

FIG. 1. Infrared spectra of tetranitromethane; Vapor: cell length 5 cm, solid line represents vapor in equilibrium with liquid, dotted line <0.5 mm Hg; Liquid and solid: solid line represents 0.15 mm cell, dotted line <0.03 mm cell.

* This work supported in part by funds from the U. S. Office of Naval Research.
† Presented in part at the Pittsburgh meeting of the American Physical Society, March 8–10, 1951. Presented by one of the authors (P. L.) in partial fulfillment of the requirements for the Ph.D. degree, Graduate School, The Ohio State University.
‡ Present address, The Visking Corporation, Chicago 38, Illinois.
[1] A. J. Mabis, dissertation, The Ohio State University, 1947.

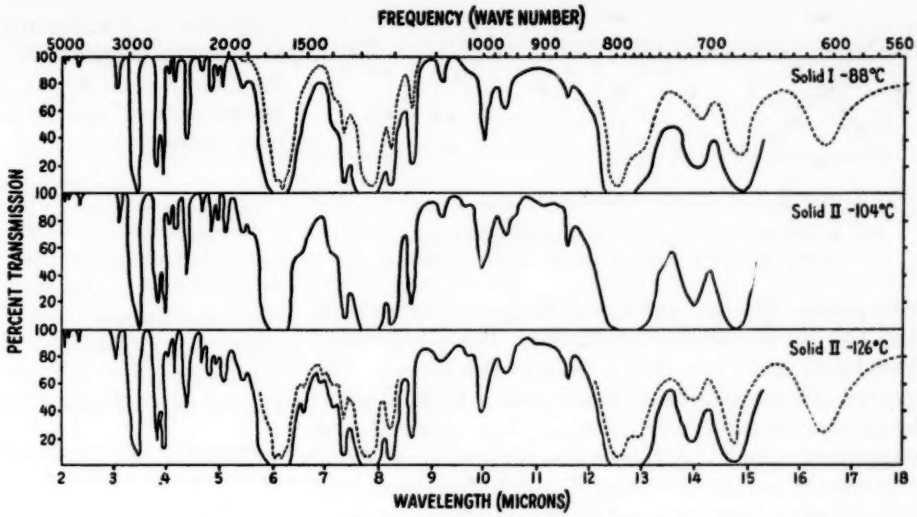

FIG. 2. Infrared spectra of solid tetranitromethane. Solid line represents 0.15 mm cell, dotted line <0.03 mm cell.

photographs taken at the temperature of liquid air, however, could not be indexed in the cubic or tetragonal systems. The transition which must exist between these two crystalline forms is shown by this investigation to occur at −98.8°C.§ Interpretation of the x-ray data for the cubic modification led to two possibilities, either (1) the nitro groups rotate about the C−N bond or (2) the whole molecule rotates about a fixed lattice point. Due to the nature of Laue-Bragg diffraction the same effect could be produced by a statistical disordering of either of these two types from one lattice point to another.‖ One cannot determine from Laue-Bragg diffraction alone the difference between a time average and a space average structure. On the other hand, the spectra of the molecules in crystals may be expected to depend upon the symmetry of the molecule and the local field which depends upon the configuration of the nearest or next nearest neighbors. Hence, as has been pointed out by Hornig,[2] the spectra may be expected to be sensitive to short range or local order and therefore may be a useful complement to the ordinary x-ray methods which are sensitive only to long range order. For this reason it seemed desirable to investigate the infrared spectra of the crystal in the hope of obtaining evidence for the type of disorder present.

Rather complete Raman spectra have been reported[3,4] for the liquid and some infrared data[3] are available. The interpretation of these data is not complete, but they indicate a molecule with $D_{2d} \equiv S_{4u} \equiv V_d \equiv \bar{4}2m$ symmetry.

EXPERIMENTAL

The tetranitromethane used was purified according to the procedure given by Nicholson.[5] The infrared spectra of the liquid and solid were obtained on a Perkin Elmer model 12*B* spectrometer using NaCl and

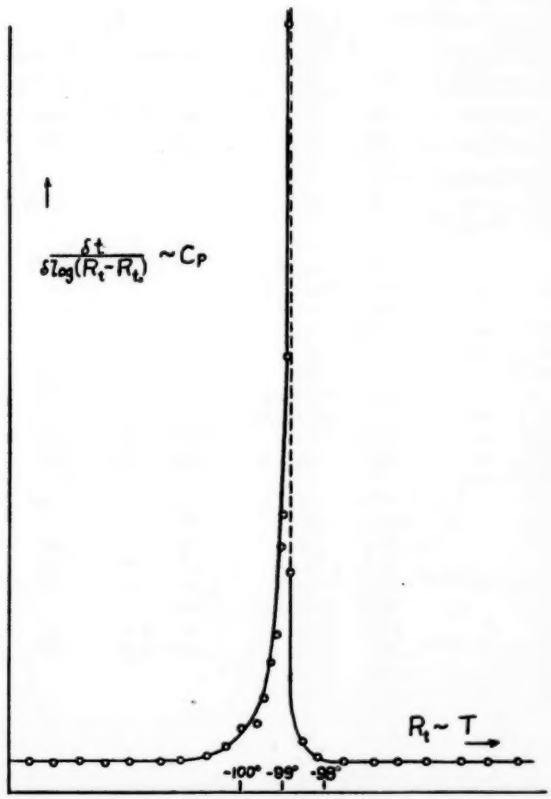

FIG. 3. The variation of the heat capacity of tetranitromethane through the transition region.

§ Recent heat capacity measurements of Dr. Jih-Heng Hu of the Cryogenic Laboratory of the Chemistry Department place this temperature at −98.21°C.

‖ A model consisting of molecules with symmetry $D_{2d}-\bar{4}2m$ (or $S_4-\bar{4}$) having the $\bar{4}$ axes lying successively along each of the 4-fold axes of the cell with equal probability has been found consistent with both Laue-Bragg and diffuse scattering of x-rays by solid I. See Oda, Iida and Nitta, J. Chem. Soc. (Japan) **64**, 616 (1943); Oda and Watanabe, *ibid.* **65**, 154 (1944); Oda and Nitta, *ibid.* **65**, 621 (1944); Oda and Matsubara, X-rays **6**, 27 (1950).

[2] D. F. Hornig, J. Chem. Phys. **17**, 1346 (1949).

[3] J. P. Mathieu and D. Massignon, Compt. rend. **211**, 323 (1940).

[4] K. W. F. Kohlrausch and H. Wittek, Z. physik. Chem. **B49**, 163-9 (1941).

[5] A. J. C. Nicholson, J. Chem. Soc. (London), **1949**, 1553.

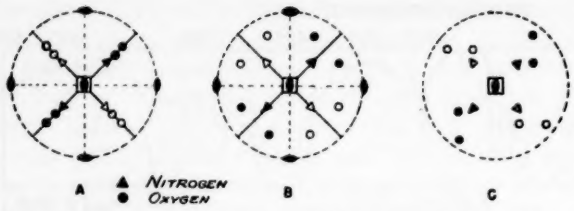

FIG. 4. Schematic projections of three proposed models of tetranitromethane showing the symmetry elements.

KBr prisms. The cell used was a variable thickness type and has been described elsewhere.[6] The sample was introduced into the cell by vacuum distillation. The spectra of the vapor were obtained on a Baird double-beam spectrophotometer using a 5-cm gas cell and tetranitromethane under its own vapor pressure at 25°C. The spectra are shown in Figs. 1 and 2. The percentage transmissions were obtained by a point-by-point division of the recorded transmission for the sample-and-cell by that of the empty cell.

The cooling curve data were taken by means of a platinum resistance thermometer and Muller-type bridge. The sample was contained in a small partially evacuated Dewar immersed in liquid air. In Fig. 3 we have plotted $\delta t/\delta \log(R_T - R_{T_0})$ which is really the derivative of the logarithmic cooling curve and should be directly proportional to the specific heat. In this function, R_T and R_{T_0} are the values of the resistance at temperatures T and T_0 of the sample and the liquid air bath, respectively.

TABLE I. Infrared and Raman frequencies of tetranitromethane.

Infrared				Raman			
Vapor		Liquid		Liquid			
				Mathieu[b]		Kohlrausch[c]	
cm^{-1}	Description[a]	cm^{-1}	Description[a]	cm^{-1}	ρ	cm^{-1}	ρ
		604	s	606	0.95	608	1.05
668	m	669	s	674	0.95	668	*dp*?
...		713	m	693	*P*	...	
797	shoulder						
802	vs	797	s, b	804	*D*	808	0.98
808	shoulder						
?		955	m	952	*D*	...	
?		996	s, sh	999	0.91	997	0.86
1022	w, d	1032	shoulder				
...		1083	w, d				
1155	w	1155	s, sh				
1217	vw	1214	s				
1278	vs	1272	vs	1274	0.92	1272	0.82
...		1361	shoulder	1348	0.07	1344	*pp*
1570	vw	?	shoulder?				
1618	vs	1618	vs	1615	0.91	1614	0.81
1648	vs	1648	vs	1648	0.90	1648	0.87
1700	vw						
...		1970	w	72	*D*?	64	*dp*?
...		2077	w	180	*D*		
...		2144	w	198	*P*?	193	1.06
...		2278	s, sh	229	0.89	228	0.87
...		2412	m	357	0.48	356	0.39
...		2480?	shoulder?	390	*D*	...	
2548	w	2550	vs	413	0.87	412	0.88
2616	w	2621	vs	862	0.05	860	*pp*
2892	m	2911	vs				
3250	vw	3252	m				
...		4255	w				
...		4695	vw				
...		4854	vw				

[a] vs very strong, s strong, m medium, w weak, vw very weak, b broad, d diffuse, and sh sharp.
[b] See reference 3.
[c] See reference 4.

[6] Holden, Taylor, and Johnston, J. Opt. Soc. Am. **40**, 757 (1950).

MOLECULAR SYMMETRY

Various structures for the tetranitromethane molecule have been suggested from time to time, but most recent workers[3,4] agree that the molecule is symmetrical with the four nitrogen atoms forming a regular tetrahedron about the carbon atom. If one makes the rather reasonable assumption that due to resonance the two oxygen atoms are equivalent, then the C$-$NO$_2$ group forms a plane. A scale model of the molecule using accepted atomic radii shows that it is not possible to rotate one nitro group very far without rotating the other nitro groups since they fit together like a set of gears.

TABLE II. Infrared frequencies in solid tetranitromethane.

−40°C		−88°C		−104°C		−126°C	
cm^{-1}	Description	cm^{-1}	Description	cm^{-1}	Description	cm^{-1}	Description
606	s	609	s			609	s
674	s	674	vs	678	vs	679	vs
710	s	710	s	716	s	716	s
...		770	shoulder			776	m
797	vs	797	vs			797	vs
...		863	w	863	m	863	m
...		...		913	vw	913	vw
956	m	951	m	957	m	958	m
997	s	996	s	1005	s	1006	s
1032	vw	1033	shoulder	1028	vw	1028	vw
1090	w	1088	w	1095	w	1092	w
1158	s, sh	1158	s, sh	1163	s, sh	1162	s, sh
1214	s	1214	s	1218	s	1217	s
1269	vs	1269	vs			1272	vs
...		...		...		1328	shoulder
1361	s	1362	s	1362	s	1364	s
?	shoulder?	?	shoulder?	?	shoulder?	1399	w
...		...		...		1444	w
?	shoulder?	?	shoulder?	?	shoulder?	1520	w
1618	vs	1618	vs			1618	vs
1648	vs	1648	vs			1648	vs
1969	m	1970	m	1970	m	1971	m
2026	vw	2026	vw	2023	w	2022	vw
2077	m	2070	m	2075	m	2076	m
2148	w	2143	w	2146	w	2147	w
2278	s	2283	s	2282	s	2282	s
2412	m	2413	m	2407	m	2407	m
?	shoulder?	2481	vw	2480	w	2478	vw
2546	vs	2550	vs	2547	vs	2546	vs
2619	vs	2619	vs	2618	vs	2626	vs
2915	vs	2899	vs	2899	vs	2899	vs
3252	m	3236	m	3236	m	3236	m
4255	w	4255	w	4219	w	4219	w
4695	vw	4651	vw	4717	vw	4652	w
4857	vw	4857	w	4857	w	4857	w

We shall consider three possible molecular symmetries. If the nitro groups rotate freely about the C$-$N bond the molecule would have the apparent symmetry T_d. In two possible static positions (Figs. 4a and 4b) the molecule would have the symmetry $D_{2d}-\bar{4}2m$ while any other simultaneous symmetrical rotation of the NO$_2$ planes reduces the symmetry to $S_4-\bar{4}$ (Fig. 4c).

The theoretical number of modes and the selection rules have been calculated for each of these molecular symmetries and are listed in Table III.¶

¶ It may be noted that the selection rules given in Table III do not agree with those given by Kohlrausch and Wittek (see reference 4) who assumed the *B* species of the model with $S_4-\bar{4}$ symmetry to be active in the Raman spectrum.

TABLE III. Symmetry relations and selection rules.

	S_4	D_{2d} (a)	T_d (a)
	8 A R(p)	5 A_1 R(p)	2 A_1 R(p)
		3 A_2	1 A_2
	9 B ir	4 B_1 R	3 E R
		5 B_2 R ir	3 F_1 R
	8 E R ir	8 E R ir	5 F_2 R ir
Total	17 ir	13 ir	5 ir
	16 R(8p)	22 R(5p)	13 R(2p)

* R—Raman active; ir—infrared active.

A set of internal valence-type coordinates was selected as shown in Fig. 5, each symbol representing an infinitesimal change in the coordinates indicated. Symmetry coordinates were obtained from these coordinates by the method of Nielsen and Berryman.[7] The coordinates obtained by this treatment were all mutually orthogonal but it was desirable to make certain linear combinations to eliminate redundancies. The final symmetry coordinates are given in Table IV.

The normal coordinate analysis was continued through the calculation of the **F** and **G** matrices for each species under $D_{2d}-\bar{4}2m$ symmetry. Since the number of force constants which could not reasonably be expected to be negligible was larger than the number of observed frequencies and the equations to be solved were of inconveniently high order, the analysis was not carried further. The symmetry coordinates were used as a basis for the assignments given in the next section.

ASSIGNMENT OF FUNDAMENTALS

A calculation of the doublet separation of parallel bands using the method of Gerhard and Dennison[8] and the molecular dimensions of Stosick[9] shows that the difference between models with $D_{2d}-\bar{4}2m$ (Fig. 4b) symmetry and $S_4-\bar{4}$ (Fig. 4c with a 60° rotation) symmetry is less than the resolving power of the instrument. Thus the band contours are of no aid in determining molecular symmetry or in assigning frequencies.

Our suggested assignments of the fundamental frequencies are given in Table V. The numbering of the fundamentals is that suggested by Herzberg[10] assuming the symmetry to be $D_{2d}-\bar{4}2m$.

The assignment of the asymmetric N—O stretching modes ν_6, ν_9, and ν_{18} is critical in determining the molecular symmetry. If the molecular symmetry is $D_{2d}-\bar{4}2m$ only ν_{18} will be active in the infrared spectrum of the vapor, whereas with $S_4-\bar{4}$ symmetry both ν_{18} and ν_9 are active. According to Smith, Pan and Nielsen[11] the asymmetric N—O stretching should have a frequency of the order of 1600 cm^{-1}. We observe two strong bands at 1648 cm^{-1} and 1618 cm^{-1} and therefore have assigned them to ν_9 and ν_{18} concluding the symmetry to be $S_4-\bar{4}$.

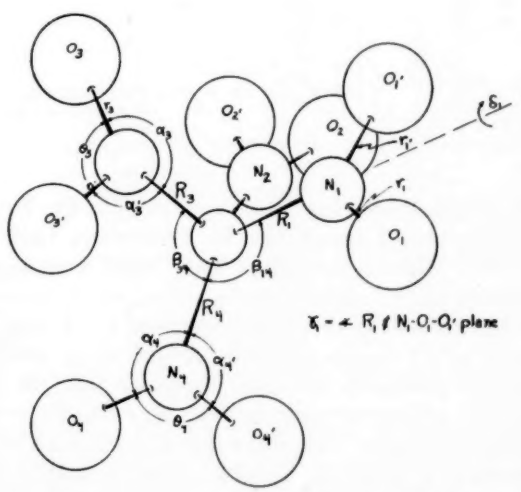

FIG. 5. Tetranitromethane model showing the choice of internal coordinates.

[7] J. Rud Nielsen and L. H. Berryman, J. Chem. Phys. **17**, 659 (1949).
[8] S. L. Gerhard and D. M. Dennison, Phys. Rev. **43**, 197 (1933).
[9] A. J. Stosick, J. Am. Chem. Soc. **61**, 1127 (1939).
[10] G. Herzberg, *Infrared and Raman Spectra of Polyatomic Molecules* (D. Van Nostrand Company, Inc., New York, 1945).
[11] Smith, Pan and Nielsen, J. Chem. Phys. **18**, 706 (1950).

TABLE IV. Symmetry coordinates.

S_4	D_{2d}	Coordinate
A	A_1	$1/2\sqrt{2}[r_1+r_2+r_3+r_4+r_1'+r_2'+r_3'+r_4']$
		$1/2\ [R_1+R_2+R_3+R_4]$
		$1/2\sqrt{3}[\alpha_1+\alpha_2+\alpha_3+\alpha_4+\alpha_1'+\alpha_2'+\alpha_3'+\alpha_4'-\theta_1-\theta_2-\theta_3-\theta_4]$
		$1/2\ [\gamma_1+\gamma_2+\gamma_3+\gamma_4]$
		$6^{-\frac{1}{2}}\ [\beta_{12}+\beta_{14}+\beta_{23}+\beta_{34}-\beta_{13}-\beta_{24}]$
		$1/2\sqrt{3}[\alpha_1+\alpha_2+\alpha_3+\alpha_4+\alpha_1'+\alpha_2'+\alpha_3'+\alpha_4'+\theta_1+\theta_2+\theta_3+\theta_4]\equiv 0$
		$6^{-\frac{1}{2}}\ [\beta_{12}+\beta_{14}+\beta_{23}+\beta_{34}+\beta_{13}+\beta_{24}]\equiv 0$
	A_2	$1/2\sqrt{2}[r_1+r_2+r_3+r_4-r_1'-r_2'-r_3'-r_4']$
		$1/2\sqrt{2}[\alpha_1+\alpha_2+\alpha_3+\alpha_4-\alpha_1'-\alpha_2'-\alpha_3'-\alpha_4']$
		$1/2\ [\delta_1-\delta_2+\delta_3-\delta_4]$
B	B_1	$1/2\sqrt{2}[r_1-r_2+r_3-r_4-r_1'+r_2'-r_3'+r_4']$
		$1/2\sqrt{2}[\alpha_1-\alpha_2+\alpha_3-\alpha_4-\alpha_1'+\alpha_2'-\alpha_3'+\alpha_4']$
		$1/2\ [\beta_{12}-\beta_{14}-\beta_{23}+\beta_{34}]$
		$1/2\ [\delta_1+\delta_2+\delta_3+\delta_4]$
	B_2	$1/2\sqrt{2}[r_1-r_2+r_3-r_4+r_1'-r_2'+r_3'-r_4']$
		$1/2\ [R_1-R_2+R_3-R_4]$
		$1/2\sqrt{3}[\alpha_1-\alpha_2+\alpha_3-\alpha_4+\alpha_1'-\alpha_2'+\alpha_3'-\alpha_4'-\theta_1+\theta_2-\theta_3+\theta_4]$
		$1/2\ [\gamma_1-\gamma_2+\gamma_3-\gamma_4]$
		$1/\sqrt{2}\ [\beta_{13}-\beta_{24}]$
		$1/2\sqrt{3}[\alpha_1-\alpha_2+\alpha_3-\alpha_4+\alpha_1'-\alpha_2'+\alpha_3'-\alpha_4'+\theta_1-\theta_2+\theta_3-\theta_4]\equiv 0$
E	E	$1/2\sqrt{2}[r_1-r_2-r_3+r_4-r_1'+r_2'+r_3'-r_4']$
		$1/2\sqrt{2}[\alpha_1-\alpha_2-\alpha_3+\alpha_4-\alpha_1'+\alpha_2'+\alpha_3'-\alpha_4']$
		$1/2\sqrt{2}[r_1+r_2-r_3-r_4+r_1'+r_2'-r_3'-r_4']$
		$1/2\sqrt{3}[\alpha_1+\alpha_2-\alpha_3-\alpha_4+\alpha_1'+\alpha_2'-\alpha_3'-\alpha_4'-\theta_1-\theta_2+\theta_3+\theta_4]$
		$1/2\ [R_1+R_2-R_3-R_4]$
		$1/2\ [\gamma_1+\gamma_2-\gamma_3-\gamma_4]$
		$1/\sqrt{2}\ [\beta_{12}-\beta_{34}]$
		$1/2\ [\delta_1+\delta_2-\delta_3-\delta_4]$
		$1/2\sqrt{3}[\alpha_1+\alpha_2-\alpha_3-\alpha_4+\alpha_1'+\alpha_2'-\alpha_3'-\alpha_4'+\theta_1+\theta_2-\theta_3-\theta_4]\equiv 0$
E	E	$1/2\sqrt{2}[r_1+r_2-r_3-r_4-r_1'-r_2'+r_3'+r_4']$
		$1/2\sqrt{2}[\alpha_1+\alpha_2-\alpha_3-\alpha_4-\alpha_1'-\alpha_2'+\alpha_3'+\alpha_4']$
		$1/2\sqrt{2}[r_1-r_2-r_3+r_4+r_1'-r_2'-r_3'+r_4']$
		$1/2\sqrt{3}[\alpha_1-\alpha_2-\alpha_3+\alpha_4+\alpha_1'-\alpha_2'-\alpha_3'+\alpha_4'-\theta_1+\theta_2+\theta_3-\theta_4]$
		$1/2\ [R_1-R_2-R_3+R_4]$
		$1/2\ [\gamma_1-\gamma_2-\gamma_3+\gamma_4]$
		$1/\sqrt{2}\ [\beta_{23}-\beta_{14}]$
		$1/2\ [\delta_1-\delta_2-\delta_3+\delta_4]$
		$1/2\sqrt{3}[\alpha_1-\alpha_2-\alpha_3+\alpha_4+\alpha_1'-\alpha_2'-\alpha_3'+\alpha_4'+\theta_1-\theta_2-\theta_3+\theta_4]\equiv 0$

Mathieu[3] observed these same two bands in the Raman spectrum of the liquid but he finds them both depolarized. This is consistent only with a molecular symmetry of $D_{2d}-\bar{4}2m$ where ν_9 and ν_{18} would be active and depolarized. If the symmetry were $S_4-\bar{4}$ then the Raman active modes would be ν_6 and ν_{18} of which ν_6 should be polarized. We must therefore conclude that either the symmetry changes from $S_4-\bar{4}$ to $D_{2d}-\bar{4}2m$ in going from vapor to liquid or that molecules with both symmetries exist in the liquid and that ν_6 and ν_9 have the same frequency through an accidental degeneracy. While it was not possible to calculate the frequencies from the **F** and **G** matrices, it was observed that the **G** matrix for the B_1 species factored into two blocks, one of which was identical with the **G** matrix for the A_2 species. The **F** matrices for these two species differ only in the signs of certain interaction force constants which are obviously negligible. Thus the assumption of accidental degeneracy seemed justified and assignments were made accordingly.

The remaining bands were assigned generally in accordance with the suggested assignment of Mathieu[3] distinguishing between B_2 species and E species on the basis of intensities, the assumption being made that the degenerate E species would have the wider and more intense band.

The assignment of the $\parallel$ wagging modes ν_7, ν_{10} and ν_{20} is open to considerable doubt. There are no unassigned frequencies in the range suggested by Smith, Pan and Nielsen,[11] (their range was admittedly uncertain). We have therefore used the only two remaining bands which are probably fundamentals due to their sharpness and intensity in the liquid and assigned ν_7 and ν_{10} to the bands at 1155 cm^{-1} and ν_{20} to 998 cm^{-1}.

THE TORSIONAL MODES

Mathieu[3] has observed a line in the Raman spectrum at 72 cm^{-1} which he suggests may be ν_{11}, an internal torsion of the whole molecule about the S_4 symmetry axis. In assigning the combination and overtone bands we found indications of two other low lying frequencies, one at 50 cm^{-1} ** and one at 97 cm^{-1}. Since these frequencies were observed principally in the solid state it is possible that they represent lattice modes. We have preferred, however, to reassign ν_{11} to 97 cm^{-1}, ν_8 and ν_{12} to 72 cm^{-1} and ν_{25} to 50 cm^{-1}. This assignment requires that the nitro groups do not rotate in the solid or liquid state.

TABLE V. Assignment of the fundamental frequencies of tetranitromethane.

	cm^{-1} [a]	Vibrational motion	D_{2d}	S_4
ν_1	1348 r	symmetrical N−O stretching	A_1 Raman (P)	A Raman (P)
ν_2	862 r	C−N stretching		
ν_3	693 r	O−N−O bending		
ν_4	357 r	wagging of NO_2		
ν_5	198 r	N−C−N bending		
ν_6	1648 r	asymmetrical N−O stretching	A_2 Inactive	
ν_7	1155 ir	wagging of NO_2		
ν_8	72 r	NO_2 twisting about C−N		
ν_9	1648 r	asymmetrical N−O stretching	B_1 Raman (D)	B Infrared
ν_{10}	1155 ir	wagging of NO_2		
ν_{11}	(97)	torsion about S_4 axis		
ν_{12}	72 r	NO_2 twisting about C−N		
ν_{13}	1217 ir	symmetrical N−O stretching	B_2 Raman (D) Infrared	
ν_{14}	958 r	C−N stretching		
ν_{15}	668 ir	O−N−O bending		
ν_{16}	398 r	wagging of NO_2		
ν_{17}	180 r	N−C−N bending		
ν_{18}	1618 ir	asymmetrical N−O stretching	E Raman (D) Infrared	
ν_{19}	1278 ir	symmetrical N−O stretching		
ν_{20}	999 r	wagging of NO_2		
ν_{21}	802 ir	C−N stretching		
ν_{22}	606 r	O−N−O bending		
ν_{23}	413 r	wagging of NO_2		
ν_{24}	229 r	N−C−N bending		
ν_{25}	(50)	NO_2 twisting about C−N		

[a] r Raman, ir Infrared vapor. ( ) Combination.

** Kohlrausch and Wittek (reference 4) report a line at 50 cm^{-1} in the Raman spectra.

TABLE VI. Suggested assignment of frequencies not interpreted as fundamentals.

Vapor 25°C	Liquid 18°C	Solid I −40°C	Solid I −88°C	Solid II −104°C	Solid II −126°C	Assignment		Symmetry
...	...	768	770	776	776	$\nu_3+\nu_{12}$	= 765	B_1
						$\nu_{23}+\nu_{24}$	= 770	E
						$\nu_3+\nu_{11}$	= 780	B_1
						$\nu_{15}+\nu_{11}$	= 765	B_1
...	...	...	...	913	913	$\nu_1+\nu_{25}$	= 913	E
						$\nu_3+\nu_{24}$	= 922	E
1022	1032	1032	1033	1028	1028	$\nu_{14}+\nu_{12}$	=1024	A_2
						$\nu_{22}+\nu_{23}$	=1019	$A_1+A_2+B_1+B_2$
						$\nu_{21}+\nu_{24}$	=1031	$A_1+A_2+B_1+B_2$
...	1083	1090	1088	1095	1092	$\nu_3+\nu_{16}$	=1091	B_2
						$\nu_2+\nu_{24}$	=1092	E
						$\nu_{15}+\nu_{23}$	=1081	$A_1+A_2+B_1+B_2$
...	...	...	...	...	1328	$\nu_{19}+\nu_{25}$	=1328	$A_1+A_2+B_1+B_2$
						$2\nu_{15}$	=1336	A_1
...	...	?	?	?	1399	$\nu_1+\nu_{25}$	=1397	E
						$\nu_{20}+\nu_{25}$	=1397	E
...	...	...	...	...	1444	$\nu_1+\nu_{11}$	=1445	B_1
						$\nu_{13}+\nu_{24}$	=1446	E
...	...	?	?	?	1520	$\nu_{18}+\nu_{11}$	=1520	E
						$\nu_1+\nu_{17}$	=1528	B_2
1570	...	...	...	...	...	$\nu_6+\nu_{12}$	=1576	B_2
						$\nu_{23}+\nu_7(\nu_{10})$	=1568	E
1700	...	...	...	...	...	$\nu_6(\nu_9)+\nu_{25}$	=1698	E
...	1970	1969	1970	1970	1971	$\nu_{18}+\nu_4$	=1974	E
						$\nu_{19}+\nu_3$	=1971	E
...	?	2026	2026	2023	2022	$\nu_7(\nu_{10})+\nu_2$	=2018	$A_2(B_1)$
						$\nu_{18}+\nu_{23}$	=2030	$A_1+A_2+B_1+B_2$
...	2077	2077	2070	2075	2076	$\nu_{19}+\nu_{21}$	=2080	$A_1+A_2+B_1+B_2$
						$\nu_{13}+\nu_2$	=2080	B_2
						$2\nu_{20}+\nu_{12}$	=2070	$A_1+A_2+B_1+B_2$
						$3\nu_3$	=2079	A_1
						$2\nu_{22}+\nu_2$	=2075	E
						$2\nu_{24}+\nu_{18}$	=2075	$3E$
...	2144	2147	2143	2146	2147	$2\nu_{10}+\nu_1$	=2144	E
						$2\nu_2+\nu_{23}$	=2139	E
						$\nu_1+\nu_{21}$	=2150	E
						$\nu_2+\nu_{19}$	=2141	E
...	2278	2278	2282	2282	2282	$\nu_{18}+\nu_{15}$	=2285	E
						$\nu_{19}+\nu_{20}$	=2277	$A_1+A_2+B_1+B_2$
...	2412	2412	2413	2407	2407	$2\nu_7(2\nu_{10})+\nu_{11}$	=2407	$B_1(A_2)$
						$2\nu_{20}+\nu_{23}$	=2411	$3E$
						$3\nu_{21}$	=2406	$3E$
...	?	?	2481	2480	2478	$\nu_{18}+\nu_2$	=2480	E
						$2\nu_{23}+\nu_9(\nu_6)$	=2474	$3E$
2548	2550	2546	2550	2544	2546	$2\nu_{19}$	=2556	$A_1+B_1+B_2$
						$2\nu_{21}+\nu_{14}$	=2556	$A_1+B_1+B_2$
						$2\nu_3+\nu_{10}$	=2543	B_1
2616	2621	2619	2618	2618	2626	$\nu_1+\nu_{19}$	=2626	E
						$2\nu_{19}+\nu_{12}$	=2628	$A_1+A_2+B_1$
						$\nu_{18}+\nu_{20}$	=2616	$A_1+A_2+B_1+B_2$
2892	2911	2915	2899	2899	2899	$\nu_{18}+\nu_{19}$	=2895	$A_1+A_2+B_1+B_2$
						$2\nu_1+\nu_5$	=2894	A_1
						$2\nu_7(2\nu_{10})+\nu_{22}$	=2916	E
						$2\nu_{14}+\nu_{20}$	=2903	E
						$2\nu_1+\nu_{24}$	=2925	E
3250	3252	3252	3236	3236	3236	$2\nu_{14}+\nu_1$	=3252	B_2
						$2\nu_{18}$	=3234	$A_1+B_1+B_2$
...	4255	4255	4255	4219	4219	$2\nu_6(2\nu_9)+\nu_{14}$	=4248	B_2
						$2\nu_{18}+\nu_{20}$	=4235	$3E$
...	4695	4695	4651	4617	4652	$2\nu_6(2\nu_9)+\nu_1$	=4644	$A_2(B_1)$
...	4854	4854	4854	4854	4854	$3\nu_{18}$	=4851	$3E$

Further evidence for the reality of the existence of the torsional modes is obtained by the following considerations. If the force constants for twisting about the C−N bond are assumed to be zero (free rotation) then the **G** matrix for the B_1 species factors into one quadratic and two linear blocks. The quadratic block consists of an asymmetric N−O stretching mode and a parallel wagging mode. Using either of the observed frequencies that must be assigned to these modes, a direct solution for the force constants yields imaginary roots. Use of the corresponding force constants for nitromethane[12] gives imaginary interaction force constants. One must assume that the twisting force constants are not zero and there

[12] A. J. Wells and E. B. Wilson, Jr., J. Chem. Phys. 9, 314 (1941).

are large interaction constants between the twisting modes and the stretching and wagging modes.

Furthermore, if the nitro groups rotate with anything that approaches free rotation, the molecular symmetry should approach T_d. In other words, the degeneracies of T_d which are split in going to $D_{2d}-\bar{4}2m$ (see Table III) should lie reasonably close together. This is not the case as can be seen by noting that the E species of T_d should split into an A_1 and a B_1 of $D_{2d}-\bar{4}2m$.

OVERTONES AND COMBINATIONS

As can be seen (Figs. 1 and 2) the spectra, particularly of the solid, are rich in overtones and combinations. This is not surprising considering (a) the large number of fundamental tones and (b) the apparent absence of selection rules in the solid. Thus it is not difficult to propose assignments for the various overtones and combinations (see Table VI), but the significance of these assignments is questionable.

LIQUID AND SOLID SPECTRA

The change in state from vapor to liquid brings a general broadening of all bands and an increase in the number of overtones and combinations. Also, two of the A_1 species, ν_1 and ν_5, show up as shoulders and ν_{14} and ν_{20}, show up strongly in the liquid.

The spectrum of the solid resembles that of the liquid with a general increase in sharpness of all bands and resolution of shoulders. The band ν_2 appears at about -60°C, increasing in intensity with decreasing temperature. The transition at -98.8°C is marked by a slight increase in frequency of a number of bands, the most pronounced being ν_{20} which changes from 997 to 1005 cm^{-1}; and by the appearance of several weak combinations.

The x-ray diffraction results show that the site symmetry in solid I is T_d, O or O_h. According to the site theory[13] the spectra should be the same as if the molecule had the symmetry of the site it occupies. Since either O_h, O or T_d symmetry would result in much more stringent selection rules than are observed we see that tetranitromethane obviously does not follow the site theory. This is to be expected in a disordered crystal[2] since the crystallographic site symmetry is only an average symmetry. Individual sites probably possess less or no symmetry but are so arranged that a space average or a time average yields the symmetry O_h, O or T_d. Tetranitromethane apparently is an example of a disordered crystal in which the local site symmetry is trivial and its spectrum approximates that of a liquid.

Since we have no information as to the site symmetry of the low temperature crystalline form we can make no predictions as to the spectra to be expected. If, however, we assume the transition at -98.8°C marks the onset of order in the crystal, then, since the spectra of solid II show no selection rules, we can predict that the site symmetry will be trivial, i.e., the molecules will occupy general positions in the crystal. Conversely, if the site symmetry turns out to be nontrivial then we must still postulate some disorder to account for the lack of selection rules in the infrared spectra.

We are pleased to acknowledge advice and suggestions from Dr. W. H. Shaffer and Dr. R. E. Kidder in setting up the normal coordinate analysis, and Dr. W. J. Taylor for interesting discussions and suggestions concerning the interpretation of the solid spectra.

SUMMARY

1. Crystalline tetranitromethane undergoes transition from a cubic lattice to one of lower symmetry at -98.8°C.

2. The infrared absorption spectra of gaseous tetranitromethane may be most reasonably explained by assuming a molecular symmetry of $S_4-\bar{4}$.

3. The reported Raman polarizabilities[3,4] require the presence of molecules with $D_{2d}-\bar{4}2m$ symmetry in the liquid.

4. The assignment of frequencies to torsional motion of the NO_2 groups about the C–N bonds requires that groups do not rotate in the solid state.

5. Although the site symmetry of solid I is at least T_d, its infrared spectra show a complete lack of selection rules. This is consistent with the spectra to be expected from a disordered crystal.[2]

[13] D. F. Hornig, J. Chem. Phys. 16, 1063 (1948).

Theoretical Considerations Concerning Hammett's Equation. IV. Calculation of ρ-Values*

H. H. JAFFÉ
Venereal Disease Experimental Laboratory, U. S. Public Health Service, School of Public Health, University of North Carolina, Chapel Hill, North Carolina

(Received June 23, 1952)

The assumption is made that the effect of a *meta* or *para* substituent X on the reactivity of a reacting center Y in a compound 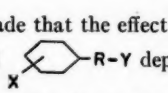 depends only on the electron density change induced by the substituent in the atom at which Y is attached to R. Using this assumption relative values of Hammett's reaction constant (ρ) are calculated for a given reaction in several series of compounds having the above formula. The calculations require the computation of the electron density changes induced by substituents in the atom at which Y is attached to R. The computations are carried out by the semiempirical LCAO MO method for several cases where R and the benzene ring form part of a single conjugated system. The resulting relative ρ-values are compared with experimental data. Reasonable agreement is found.

IN the previous papers in this series it has been shown that Hammett's σ-values[1] can be correlated with electron densities calculated by molecular orbital (MO) theory.* This correlation was made on the basis of the following hypotheses:

I. Substituents induce changes on the electron density at the *meta* and *para* position in the benzene ring which are proportional to the corresponding σ-values.[2]

II. The change of electron density induced by a substituent in a carbon atom in the benzene ring is independent of a side-chain attached to that atom.

Experimental evidence for the first hypothesis has been furnished recently by Gutowsky and co-workers from nuclear magnetic resonance measurements.[3]

On the basis of these hypotheses, σ-values can be calculated for any substituent provided the parameters (Coulomb and resonance integrals) necessary for the MO calculations are known, or the electron density changes can be evaluated in some other way.

In the present paper we shall investigate the possibility of gaining further understanding of Hammett's equation from an extension of our previous arguments.

ASSUMPTIONS

This discussion will require the comparison of series of compounds (I) differing in the nature of group R, and undergoing identical side-chain reactions at Y, under identical conditions.

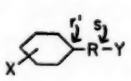

I

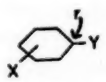

II

The atom at which the group Y is attached to R will be called s. The following further hypothesis is needed.

III. A substituent in the *meta* or *para* position of the benzene ring in (I) exerts an effect on the rate or equilibrium constants of the reaction at Y. This effect depends only on the change the substituent induces in the electron density at atom s.[2]

Dissociation constants of acids can be calculated on the basis of purely electrostatic considerations.[4] Hence, hypothesis III appears reasonable for the dissociation constants of compounds in which Y is an acid group. The general validity of Hammett's equation then suggests that this hypothesis is valid for all reactions.

Hypothesis III leads to an immediate corollary. If we are considering two series of compounds characterized by groups R_A and R_B in (I), and two series of reactions (1 and 2) at different groups Y, the ρ-values must obey the following relations:

$$\rho_{A1}:\rho_{B1}=\rho_{A2}:\rho_{B2} \tag{1}$$

where the subscripts on ρ define the series of compounds and the reaction concerned. This relation provides a test for the hypothesis III. Unfortunately, the available data are not numerous; they are summarized in Table I. Since the standard errors of most ρ-values are of the order of 10 percent, Table I shows that Eq. (1) expresses the experimental data reasonably well. The fact that different solvents are involved in the different types of reactions also may be responsible for some of the deviations.

In accordance with the previous treatment and with hypothesis III, the electron density changes at atom s in (I) will be replaced by the corresponding changes at atom s in (III), which differs from (I) only by replacement of the side-chain Y by a hydrogen atom.

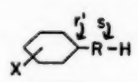

III

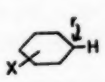

IV

* For papers I and II of this series see H. H. Jaffé, J. Chem. Phys. 20, 279, 778 (1952), hereafter referred to as papers I and II. Presented before the Division of Physical and Inorganic Chemistry, at the 121st Meeting of the American Chemical Society, Buffalo, New York, March, 1952.

[1] L. P. Hammett, *Physical Organic Chemistry* (McGraw-Hill Book Company, Inc., New York, 1940), Chapter VII.

[2] This hypothesis is based on qualitative statements made originally by Hammett, reference 1.

[3] Gutowsky, McCall, McGarvey, and Meyer, J. Chem. Phys. 19, 1328 (1951).

[4] A. Kossiakoff and D. Harker, J. Am. Chem. Soc. 60, 2047 (1938).

TABLE I. The variation of the ratios of ρ-values in series of reactions of compounds I with different groups R.

Series of compounds I $R=$	Acid dissociation of I $Y=$COOH ρ[b]	ρ/ρ_0	Ref.	Alkaline hydrolysis of I $Y=$COOEt[a] ρ[b]	ρ/ρ_0	Ref.	Average of ρ/ρ_0	Deviation from mean
···	1.000[c]	[1.000]	2	2.453	[1.000]	2		
···	1.415[d]	[1.000]	e					
$-CH_2-$	0.489[c]	0.489	2	0.824	0.336	2	0.410	0.084
$-CH_2-CH_2-$	0.212[c]	0.212	2	0.489	0.196	f	0.206	0.009
$-CH=CH-$	0.466[c]	0.466	2	1.329	0.542	2	0.508	0.038
	0.482[d]	0.341	e	0.599	0.262	g	0.303	0.040

[a] In 88 percent EtOH at 30°C.
[b] All ρ-values were recalculated by the method least squares.
[c] In H_2O at 25°C.
[d] In 50 percent butyl cellosolve at 25°C.
[e] E. Berliner and E. A. Blommers, J. Am. Chem. Soc. **73**, 2479 (1951).
[f] K. Kindler, Ann. **452**, 90 (1927), **464**, 278 (1928).
[g] E. Berliner, private communication.

CALCULATION OF ρ-VALUES

The results of the previous section show that any ρ-value may be calculated from Eq. (1) if the other three quantities appearing in the equation are known. We will now show that the above hypotheses permit calculation of ρ-values also from other data.

Let ρ_0 and ρ_1 refer to a certain reaction in the series of compounds (II) and (I) respectively, the conditions of the reaction being identical; and let k_0^0, $k_0(X)$, k_1^0 and $k_1(X)$ be the corresponding rate or equilibrium constants for the unsubstituted and substituted compounds, respectively, in the two series. Then by Hammett's equation[1] and hypothesis I,

$$\log[k_0(X)/k_0^0]=\sigma\rho_0=\kappa[q_r(X)-q_r'^0]\rho_0,$$

where κ is the proportionality constant relating σ-values and electron density changes, and $q_r(X)$ and $q_r'^0$ are the electron densities at atom r of the substituted and unsubstituted compound (IV), respectively. Also

$$\log[k_1(X)/k_1^0]=\sigma\rho_1=\kappa[q_r(X)-q_r'^0]\rho_1. \quad (2)$$

By hypothesis III

$$\log[k_1(X)/k_1^0]=\kappa[q_s(X)-q_s'^0]\rho_0, \quad (3)$$

where $q_s(X)$ and $q_s'^0$ are the electron densities at atom s in the substituted and unsubstituted compounds (III), respectively. Equating the right-hand sides of Eqs. (2) and (3) then yields

$$[q_s(X)-q_s'^0]/[q_r(X)-q_r'^0]=\rho_1/\rho_0. \quad (4)$$

This equation permits approximate calculation of the ratio of ρ-values of a single reaction of any two series of compounds (I) from the electron density changes produced by the introduction of substituents in the corresponding compounds (III). These electron density changes may be determined experimentally or calculated by some empirical or theoretical procedure.

VALIDITY OF HAMMETT'S EQUATION

Hypothesis III leads immediately to a necessary condition for the validity of Hammett's equation. Since the ratio ρ_1/ρ_0 in Eq. (4) must be independent of the nature of the substituent X, the quotient on the right-hand side of (4) must be a constant, independent of the nature of X, for any pair of series of compounds. This implies that the electron density changes induced by any substituents in atom s of (III) must be proportional to the changes induced by the same substituents in atom r in (IV).

In case of compounds in which R in (I) is not a part of the same conjugated system as the benzene ring, the electron density at s is influenced by the substituent only through an inductive effect transmitted through R. The magnitude of this inductive effect on the atom s is determined by the electron density at atom r', and is therefore proportional to the electron density change $(q_{r'}-q_{r'}'^0)$. However, the electron density change at r' will not differ appreciably from the same change $(q_r-q_r'^0)$ at atom r in (IV), since r' is identical to r except for an inductive effect due to the side-chain; this effect will be essentially identical in the substituted and unsubstituted compounds. Thus, the above condition for the validity of Hammett's equation holds in compounds in which R in (I) is not part of the same resonating system with the benzene ring.

We shall now use the MO method in the semi-empirical LCAO approximation to investigate compounds where R and the benzene ring in (I) form part of a single conjugated system. By first-order perturbation theory the electron density at atom s in a molecule is given by[5]

$$q_s=q_s^0+\sum_t \pi_{t,s}\alpha_t+\sum_{t>u}\pi_{tu,s}(\beta_{tu}-\beta_{tu}^0). \quad (5)$$

Here q_s, α_t, and β_{tu} are the electron density at atom s, Coulomb integral at atom t, and resonance integral of the bond between t and u, respectively, in the desired compound. The quantities with superscript 0 refer to a reference molecule characterized by resonance integrals β_{tu}^0 and having all Coulomb integrals $\alpha_r=0$. $\pi_{t,s}$ is the mutual polarizability of atoms s and t, and $\pi_{tu,s}$ is the atom-bond polarizability.[5]

According to hypothesis I the electron density at atom s in compound (III) is required. The substituent X will be called 0, and the carbon atom to which X is attached will be called 1. All resonance integrals in the actual compound will be the same as in the reference compound, except β_{01}. The Coulomb integrals will be treated as in papers I and II, i.e., $\alpha_t=\epsilon_t{}^n\alpha_0$, where α_0 is the Coulomb integral of the substituent X, and n_t is the number of the bonds intervening between atoms 0 and t along the shortest path. The perturbation affects all Coulomb integrals in the molecule, but only a single resonance integral. With these specific conditions (5) becomes

$$q_s-q_s^0=\alpha_0\sum_t \pi_{t,s}\epsilon^{n_t}+\pi_{01,s}(\beta_{01}-\beta_{01}^0). \quad (6)$$

[5] C. A. Coulson and H. C. Longuet-Higgins, Proc. Roy. Soc. (London) **A191**, 39 (1947).

The condition for the constancy of the left-hand side of (4) then is

$$\frac{q_s-q_s'}{q_r-q_r'^0}=\frac{q_s^0-q_s'^0+\alpha_0\sum_t \pi_{t,s}\epsilon^{n_t}+\pi_{01,s}(\beta_{01}-\beta_{01}^0)}{q_r^0-q_r'^0+\alpha_0\sum_t \pi_{t,r}\epsilon^{n_t}+\pi_{01,r}(\beta_{01}-\beta_{01}^0)}. \quad (7)$$
$$=\text{const.}$$

Unfortunately, we have not been able to show in the general case that the right-hand side of (7) is a constant independent of α_0 and β_{01}. However, the constancy of (7) may be demonstrated for several classes of molecules. If the reference compound for (III), defined in connection with Eq. (5), is an alternant hydrocarbon in the sense of Coulson and Longuet-Higgins,[6] all atom-bond polarizabilities, $\pi_{tu,s}$ and $(q_s^0-q_s'^0)$ vanish, moreover, in that case the corresponding reference compound for (IV) also is an alternant hydrocarbon, and therefore all $\pi_{tu,r}$ and $(q_r^0-q_r'^0)$ also vanish. Then (7) reduces to

$$(q_s-q_s^0)/(q_r-q_r^0)=\sum_t \pi_{t,s}\epsilon^{n_t}/\sum_t \pi_{t,r}\epsilon^{n_t}=\pi'. \quad (8)$$

This argument applies to the compounds treated in Paper II (toluene, etc.).

The situation is more complicated in molecules in which the substituent contributes one π-orbital with two p-electrons to the conjugated system, as is the case in the compounds treated in Paper I (the halobenzenes, aniline, phenol, and thiophenyl). In these compounds one must distinguish between several cases. (a) If the group R contains an even number of atoms between the benzene ring and the group Y, and if X is in the *meta* position, the bond-atom polarizabilities, and $(q_s^0-q_s'^0)$ and $(q_r^0-q_r'^0)$ again all vanish,[7] and Eq. (8) holds identically. (b) If X is a *para* substituent, or if R contains an odd number of atoms between the ring and Y, either $\pi_{01,r}$ or $\pi_{01,s}$, or both, do not vanish. We have been unable to show that (7) is constant independent of α_0 and β_{01} in these cases, but we hope that numerical calculations with actual compounds will show that Eq. (4) is a good approximation even where Eq. (8) cannot be verified.

CALCULATIONS

In order to show that hypotheses I to III lead to reasonable results, we have calculated π' for several cases

R = $-CH=CH-$, , 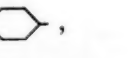 ,

for which the corresponding quantities ρ_1/ρ_0 are known. The calculations were made by first order perturbation theory as outlined by Coulson and Longuet-Higgins.[5] The alternant hydrocarbon

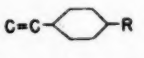

was used as the reference molecule, and the Coulomb integral of the α-carbon atom as the perturbation parameter α_0. In Paper II the Coulomb integral of the β-carbon atom was shown to exert no appreciable effect on the electron densities of the carbon atoms in the benzene ring, so that this integral may be set equal to zero. Since Eq. (8) holds for compounds of this type the calculations are relatively easy. In accordance with previous work the constant ϵ was assigned a value of $\frac{1}{3}$ and this choice will be further discussed below. All resonance integrals (β) were assumed equal, although probably bonds represented in the usual structural formulas as single bonds should have smaller resonance integrals than the nuclear C—C bonds, and bonds represented by double bonds should have larger resonance integrals. The assumption of equal resonance integrals probably does not introduce any major uncertainties.

The calculations are straightforward, and therefore details need not be given. The results are listed in Table II, and the agreement is seen to be satisfactory.

Some comment is necessary regarding the results obtained with the azo-benzene derivatives,

R = 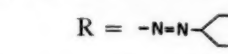 .

The reaction measured was the acid dissociation of the conjugate acids of some p-substituted p'-dimethylaminoazobenzene.[8] Two successive constants were reported, and ρ-values given for both. The authors assign $\rho_1=0.524$ to the dissociation at the azonitrogen atom farther from the dimethylamino group. Although the argument for this assignment based on the ultraviolet absorption spectra appears reasonable, the explanation of the differences in the ρ-values seems unconvincing. The pK-values corresponding to ρ_1 (for $X=H$ in 50 percent EtOH $pK=2.77$) are of the same order of magnitude as the pK's of dimethylanilinium ion

TABLE II. Calculated and observed values of π'.

$R=$	$\pi'(\epsilon=1/3)$ calc.	ρ_1/ρ_0 obs.
$-CH=CH-$	0.683	0.508[a]
	0.177	0.303[a]
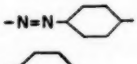	0.136	0.126[b]
	−0.013	...
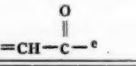	−0.010	−0.059[d]

[a] From Table I.
[b] Calculated from ρ for the acid dissociation constants of dimethylanilinium ions ($\rho=4.191$) (reference 2) at 25°, and of p'-dimethylammoniumazobenzene ions ($\rho=0.529$) (reference 7) at room temperature, both reactions in 50 percent EtOH.
[c] See *Note added in proof* at the end of this paper.
[d] From reference 12.

[6] C. A. Coulson and H. C. Longuet-Higgins, Proc. Roy. Soc. (London) **A192**, 16 (1947).
[7] H. C. Longuet-Higgins, J. Chem. Phys. **18**, 265 (1950).
[8] Rogers, Campbell, and Maatman, J. Am. Chem. Soc. **73**, 5122 (1951).

TABLE III. The dependence of π' on ϵ.

ϵ	π' for R = −CH=CH−	π' for R =	π' for R = 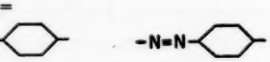
0	2.05[a]	0.467[a]	0.289[a]
0.1	0.303	0.083	0.062
0.2	0.529	0.134	0.096
0.3	0.642	0.162	0.116
0.4	0.773	0.207	0.148
0.5	0.951	0.286	0.206
0.6	1.244	0.443	0.334

[a] For these values both numerator and denominator in Eq. (8) were positive; in all other cases both were negative.

(pK=4.21 in 50 percent EtOH), whereas the pK's corresponding to ρ_2 (for $X=H$ $pK=-4.50$ in sulfuric acid) indicate a much stronger acid (weaker base), which might be expected of the azonitrogen atoms in azobenzene. Our calculations for the dimethylammonium ion in the compounds studied gave a ρ-value in close agreement with ρ_1. Unfortunately, no calculation of the ρ-value for the dissociation of the azonitrogen is possible at present. However, the nitrogen atoms in substituted anilinium and dimethylanilinium ions are in the same relative position to the substituent as the azonitrogen further from the dimethylamino group in the azobenzene derivatives. Therefore, the ρ-values for the acid dissociation constants of these three series of compounds[9] may be expected to be of the same order of magnitude. This prediction holds only if the azonitrogen in the dimethylaminobenzene is assigned the value $\rho_2=3.65$, which Rogers and co-workers had originally assigned to the dimethylammonium group.

THE VALUE OF ϵ

The assignment of $\epsilon=\frac{1}{3}$ was made in Paper I on the basis of experimental evidence there cited. No great accuracy can be attributed to this value, however, and so we have examined the effects a change in the value of ϵ would have on the present results. According to Eq. (8), π' is the ratio of two polynomials in ϵ. Each of these polynomials has a zero slightly above $\epsilon=0$, and no further zeros for $\epsilon<0.6$. Various values of ϵ were substituted in Eq. (8) and the results of these calculations are given in Table III. Although π' is not greatly affected by small changes in ϵ, the value $\epsilon=0.1$ used by most previous investigators[10] does not lead to satisfactory results. The assignment $\epsilon=\frac{1}{3}$ on the other hand, permits calculation of reasonable values of π'. A slightly larger value is suggested by the probability that a choice of better values for the resonance integrals of the nonaromatic C−C bonds would reduce the values of π'. A value of 0.4 to 0.5 has been suggested by Dewar.[11]

[9] For $ArNH_3^+$ in H_2O, $\rho=2.71$; for $ArNHMe_2^+$ in 50 percent EtOH, $\rho=4.19$, see Table II.

[10] See, e.g., G. W. Wheland and L. Pauling, J. Am. Chem. Soc. **57**, 2086 (1935).

[11] M. J. S. Dewar, J. Chem. Soc. **1950**, 2329.

PREDICTION OF ρ-VALUES

We have seen that ρ-values may be calculated in some instances. The classes of compounds in which such calculations are feasible are restricted by the condition that the electron densities can be calculated with reasonable ease and accuracy only in conjugated systems. Here we shall report a single ρ-value which has not been experimentally determined, but which seems of particular interest. In Table II a value for π' for

R=

has been included. This value permits the prediction that the ρ-values for the *m*- and *p*-substituted *m'*-biphenylcarboxylic acids will be negative, and have an absolute value less than 10 percent of the ρ-value of the *p'*-biphenylcarboxylic acids. This conclusion at first seems surprising. ρ-Values for all acid dissociation constants have long been tacitly assumed necessarily positive.[1] A small value for ρ might have been predicted on the basis of resonance between structures of types (V) to (VII). The effect of the introduction of the group *X* affects only the *ortho* and *para* position of ring *B* directly; and any inductive effect may be expected to be greatly dampened by the intervention of 6 atoms.

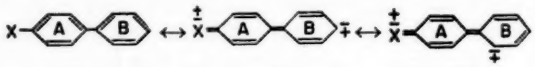

V VI VII

The difference in sign of the ρ-values of the *p'*- and *m'*-biphenylcarboxylic acids also finds a reasonable explanation. We shall write the two series of reactions as (VIII) and (IX). So far, in this paper, we have considered *Z* and ring *B* in compounds (VIII) and (IX) as substituent *X* and group *R* in compound (I), respectively. But we may equally well consider the group in (VIII) and (IX) as the substituent *X* in compounds (II), which means that we are applying Hammett's equation to ring *B* rather than ring *A*. We then have from Hammett's equation

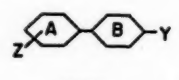

VIII

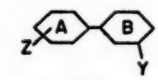

IX

$$\log(k/k^0)_p=\sigma(Z)\rho(BY)_p=\sigma(ZA)_p\rho(Y), \quad (9)$$

and

$$\log(k/k^0)_m=\sigma(Z)\rho(BY)_m=\sigma(ZA)_m\rho(Y), \quad (10)$$

where $\rho(BY)_p$, $\rho(BY)_m$, and $\rho(Y)$ are the usual ρ-values for the *p'*- and *m'*-biphenylcarboxylic acids and the benzoic acids, respectively, and $\sigma(ZA)_p$, $\sigma(ZA)_m$, and $\sigma(Z)$ are the σ-values for the ZC_6H_4-group in the *para* and *meta* position and of group *Z*, respectively. From (9) and (10) it follows that

$$\rho(BY)_p/\rho(BY)_m=\sigma(ZA)_p/\sigma(ZA)_m. \quad (11)$$

Equation (11) shows that the σ-values of the ZC_6H_4 group in the two positions must have different signs if the ρ-values of the biphenylcarboxylic acids have opposite signs, as the calculations suggest. The same result is obtained by application of our first hypothesis to the calculations, and could have been predicted from the law of alternating polarity in conjugated systems.[6]

Though the above arguments have been applied specifically to the biphenylcarboxylic acids, analogous arguments based on Eq. (1) could be applied to any other side-chain reaction of biphenyl. Moreover, the form of the various polarizabilities involved in Eq. (8) indicates that similar conclusions would be obtained if calculations were carried out for *p'*- and *m'*-azobenzene derivatives. Unfortunately, no experimental data are available to test the predictions.

Note added in proof:—Since this paper was submitted for publication, the *pK*'s of a series of benzylidenepyruvic acids in water and 50 percent methanol, and the rates of hydrolysis of their methyl ester in 50 percent dioxane have been determined.[12] The ρ-values found were -0.054 ± 0.015, $+0.165\pm0.059$, and $+0.049\pm0.038$, respectively. The value of -0.054 is the first instance of a negative ρ reported for an acid dissociation constant, although it must be pointed out that the differences between the experimentally determined *pK*-values are too small to give this ρ-value much significance. We have calculated the π' values for this series of compounds, and included it in Table II. Although this prediction was not made before the experimental value became available, the situation is quite analogous to the *m*-biphenylcarboxylic acids discussed. In the light of these additional data and the law of alternating polarity, it now seems safe to conclude that π' will have a very small, and probably negative, value whenever *R* is conjugated with the benzene ring and the number of atoms in *R* between the ring and *Y* is odd.

[12] E. D. Stecher and H. F. Ryder, J. Am. Chem. Soc. **74**, 4392 (1952).

THE JOURNAL OF CHEMICAL PHYSICS VOLUME 21, NUMBER 3 MARCH, 1953

The Entropy and Low Temperature Heat Capacity of Neptunium Dioxide

EDGAR F. WESTRUM, JR.,* J. B. HATCHER,† AND DARRELL W. OSBORNE
Argonne National Laboratory, Lemont, Illinois

(Received April 21, 1952)

The heat capacity of a two-gram sample of neptunium dioxide was determined from 10 to 315°K in an adiabatic calorimeter. At 298.16°K the molal entropy and enthalpy calculated from the heat capacity data are 19.19 ± 0.1 cal deg^{-1} and 2770 ± 15 cal, respectively. A pronounced hump was found in the heat capacity curve of neptunium dioxide at 25.3°K similar to that found by Jones, Gordon, and Long in uranium dioxide at 28.7°K. This anomaly in the heat capacity is suggestive of a cooperative phenomenon and is attributed to the incidence of antiferromagnetism below the temperature of the maximum in the heat capacity. A calorimeter for gram scale samples and a modification of the cryostat design of Ruehrwein and Huffman so as to employ only liquid helium and liquid nitrogen as refrigerants are described.

THE availability of a sample of 1.7 grams of pure Np^{237} made possible the measurement of the low temperature heat capacity of neptunium dioxide. To carry out the investigation on the limited amount of material, a small adiabatic calorimeter and a cryostat for use in the range 2 to 320°K were designed and constructed.

NEPTUNIUM DIOXIDE SAMPLE

The neptunium isotope Np^{237} was made in a chain-reacting nuclear pile by the reactions $U^{238}(n,2n)U^{237}\xrightarrow{\beta^-}Np^{237}$. This isotope decays by alpha emission with a half-life of 2.2×10^6 years.[1] It was isolated from uranium, plutonium, and fission products and was purified by Dr. Sherman Fried, Dr. J. C. Hindman, and Mr. John Malm. The neptunium dioxide was prepared by Dr. Fried by precipitating the hydroxide from a hydrochloric acid solution of neptunium (IV) with ammonia and igniting to constant weight in air in a platinum boat at 700°C. The mass of the sample was 1.9250 grams. The identity of the dioxide was established by Professor W. H. Zachariasen by x-ray analysis. The only impurities detected by spectrochemical analysis were chromium, iron, and calcium in a total concentration of less than a tenth of a percent by weight.

CRYOSTAT

The cryostat design (Fig. 1) generally followed that of several constructed by Huffman and co-workers,[2,3] with the essential differences that helium and nitrogen were used as refrigerants

* Department of Chemistry, University of Michigan, Ann Arbor, Michigan.
† Present address: Jet Propulsion Laboratory of the California Institute of Technology, Pasadena, California.

[1] L. B. Magnusson and T. J. La Chapelle, J. Am. Chem. Soc. **70**, 3534 (1948).

[2] R. A. Ruehrwein and H. M. Huffman, J. Am. Chem. Soc. **65**, 1620 (1943).

[3] H. M. Huffman, Chem. Revs. **40**, 1 (1947).

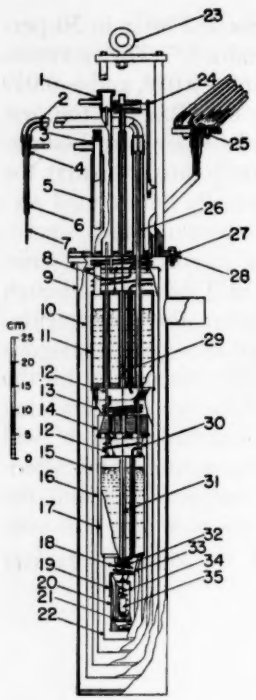

FIG. 1. The cryostat: (11) nitrogen tank; (14) "economizer;" (17) helium tank; (10), (15), (16), and (22) radiation shields; (20) and (21) adiabatic shields; (35) calorimeter; (24) windlass.

instead of hydrogen and nitrogen, and that a "helium economizer" and a second adiabatic shield were provided. The entire cryostat assembly was suspended from the cover plate (27) and was lifted from the highly evacuated outer can (9) by the ring (23) for assembly and disassembly. The cover plate was sealed with a flat neoprene gasket (28).

The outer radiation shield (10) was made of 0.8 mm-thick, chromium-plated copper. This shield was attached to the cover plate but was thermally isolated from it by means of screws with Bakelite spacers and washers. The copper nitrogen tank (11) (2.2 l volume) was supported by wire loops (8) from the outer radiation shield, as well as by its filling tube (5), and by the helium transfer tube radiation shield (26). The nitrogen inlet connection (3) was closed with a rubber stopper, and the outlet (3) was connected to a mechanical vacuum pump for operation below about 90°K.

The copper "economizer" (14) was supported from the nitrogen tank by Nylon cords (13), as well as by the helium exit tube (12), which was soldered to the helium outlet (1). The economizer was designed to use the heat capacity of the effluent helium gas to absorb part of the heat conducted down the bundle of wires and thus conserve liquid helium. It contained ten copper baffles, silver-soldered to the walls, to provide a large heat transfer surface to the gas.

The copper helium tank (17), which had 0.6-mm walls and a volume of 1.2 l, was supported from the economizer both by the helium exit tube and by nylon cords (30). The helium exit tube (12) and the helium transfer tube (7) were 3.0-mm i.d. by 0.1-mm wall monel. The latter extended to the bottom of the helium transfer Dewar vessel, entered the end of the thin-wall vacuum jacket (6), and passed through the large center holes of four star-shaped spacing washers (2), which prevented contact with the vacuum jacket or with the radiation shield. The inlet end of the helium transfer tube was closed with a plug when desired. The outlet (1) from the helium tank led to a manifold arranged for passing the effluent gas through a meter or directly to the room, for admitting helium gas from a cylinder, or for pumping.

The nitrogen (15), economizer (16), and helium (22) radiation shields were constructed of 0.8 mm-thick copper and were clamped to the bottoms of their respective tanks. Since the economizer radiation shield was found to decrease the rate of loss of liquid helium by less than ten percent, its use was discontinued. The inside and outside surfaces of the radiation shields and the accessible surfaces of the economizer and of the nitrogen and helium tanks were bright chromium plated.

The bundle of electrical leads was anchored thermally to each of the refrigerant tanks and to the economizer. The leads emerged from the cryostat through a perforated Lucite disk (25), which was covered with Apiezon wax.

The general operation of the cryostat depended on the temperature range in which it was desired to work. Above 90°K both the nitrogen and helium tanks were filled with liquid nitrogen. In the range 55 to 90°K both of these tanks were pumped to reach a temperature of about 55°K with solid nitrogen. For operation in the range 4 to 55°K the helium tank was filled with liquid helium and the nitrogen tank with solid nitrogen. Lower temperatures could be obtained by pumping on the liquid helium.

Before filling the helium tank with liquid helium it was precooled to between 55 and 60°K with small portions of liquid nitrogen. The helium tank was then filled with helium gas, the outlet (1) and inlet (7) were opened to the room, and the Dewar vessel containing liquid helium was moved up and sealed to the collar (4) with adhesive tape. Liquid helium was then forced into the helium tank with the pressure of the evaporating helium by closing the side arm on the collar (4). About 1.5 l of liquid helium were required to cool the helium tank and radiation shield from 60 to 4°K, and then enough helium was added to fill the tank. A full tank lasted 40 to 70 hours in actual runs, and the rate of loss when no electrical energy was supplied to the calorimeter and shields was about 15 cc of liquid per hour. In a test of the efficiency of the economizer, it was found that removal of the bundle of lead wires from thermal contact with the economizer approximately doubled the rate of loss of liquid helium.

Calorimeter and Adiabatic Shields

The sample was contained in the calorimeter (35) shown in detail in Fig. 2. The mass of the calorimeter was 10.4 g, and the volume of the sample chamber was 1.8 ml. It was made of 0.08 to 0.10 mm platinum sheet, with gold-soldered joints, except for the top cone (36), which was of silver-soldered copper. The platinum tube (42) extending into the sample space permitted evacuation and filling with helium gas, and the final seal was made by pinching off the gold tube (50) which extended below. The top annulus (37) was filled with a low melting indium-tin solder (Cerroseal-35). Soldering and unsoldering the top were carried out by means of an external electrically-heated coil, in an atmosphere of helium to avoid oxidation of the solder. The calorimeter heater (38) consisted of 150 ohms of double glass insulated constantan wire, bifilarly wound around a thin layer of mica (39) on the inner tube. The wire was heated bright red in air after winding to vaporize the binder in the insulation. The strain-free resistance thermometer (44) was bifilarly wound of 0.07 mm pure platinum wire. It had an ice point resistance of 83 ohms. The winding was supported in slots in six mica ribs (47) which were in turn held from outward movement by the mica end rings (48). A layer of mica (45) over the heater windings held the ribs against the end rings. A third layer of mica (43) was located just inside the outer case. The ends of the thermometer winding were spot welded to the centers of loops of 0.2 mm platinum wire which provided the four thermometer current and potential leads (49). Only two heater leads (41) (also of 0.2 mm platinum) were provided at the calorimeter, because the current-potential junctions for the heater were made midway along the helical bundle of leads (34) to the inner adiabatic shield. This bundle was 30 cm long and consisted of B. and S. No. 30 constantan wires and B. and S. No. 39 copper wires. All of the leads into the calorimeter were sealed through Corning 010 glass beads (40) in the bottom of the calorimeter. After annealing the thermometer in air, the annular space containing the heater and thermometer was evacuated, baked, filled with 0.30 atmos of helium, and then permanently sealed by pinching off the gold tube (46) welded to the outer jacket. This tube also served as a knob to

which a difference thermocouple for the shield control was secured with a measured length of copper wire.

The inner (21) and the outer (20) adiabatic shields were made of gold-plated copper and were similar except for size. The 0.25 mm-thick tubular sections and the 0.50 mm-thick removable ends were held in thermal contact with screws. Each tubular portion had a helical depression in which the leads were thermally anchored beneath the heater windings. In order to control the temperature of the shields, heaters of bifilarly wound, double glass-covered, constantan wire were cemented to the entire outer surfaces of the shields with baked Formex, and copper-constantan difference thermocouples were provided between the ends and the middle of each shield and the calorimeter. The thermocouple junctions on the shields were either cemented in place with baked Formex or were coated with baked Formex and inserted in copper tubes soldered to the ends of the shields and filled with Lubriseal grease for thermal contact.

The inner shield was supported from the outer by three loops of braided Nylon line (19) which passed through holes at the top of the outer shield. The outer shield was supported from the bottom of the helium tank by three strands of braided nylon line (33). The bundle of leads was formed into a helical shape between the inner and outer shields and between the outer shield and the helium tank.

The calorimeter was suspended on a knot at the end of a braided Nylon line (31), 0.38 mm in diameter, which was attached to the windlass (24). To cool the calorimeter and adiabatic shields, the windlass was used to bring the cones on the calorimeter, shields, and bottom of the helium tank into thermal contact. The position of the calorimeter was indicated by the pointer attached to the sprocket chain passing over a sprocket on the windlass. A spring (29) in the calorimeter suspension line prevented inadvertent excess tension.

Electrical Circuits

The copper-constantan thermocouples for controlling the adiabatic shields were connected through selector switches to two galvanometers with working sensitivities of 0.01 μv/mm. Usually one galvanometer was used to read the temperature difference between the calorimeter and the top, middle, or bottom of the inner shield, and the other was used to read the temperature difference between the middle of the inner shield and the top, middle, or bottom of the outer shield. The six shield heaters were supplied with alternating current controlled by variable voltage transformers and variable resistors.

The current and the potential drop in the resistance thermometer and in the heater were measured with an autocalibrated White double potentiometer, a galvanometer with a working sensitivity of 0.04 μv/mm, calibrated resistors, and an unsaturated Weston standard cell. Both the resistance standard and the standard cell were calibrated by the National Bureau of Standards. An electric timer operated by a calibrated tuning fork and amplifier was automatically started at the beginning of the energy input and stopped at the end. A thermometer current of 2 ma was used up to about 60°K, and 0.8 ma was used at higher temperatures.

Temperature Scale

The calorimeter thermometer was calibrated by comparing its resistance at many temperatures with that of a Leeds and Northrup 25 ohm capsule type platinum resistance thermometer (Laboratory designation A-1) inserted into the sample space of the calorimeter. Thermal contact was established with a massive copper sleeve and Apiezon stopcock grease. We gratefully acknowledge the considerable assistance of the late Dr. H. M. Huffman and Dr. G. B. Guthrie of the Thermodynamic Section, Petroleum Experiment Station, Bureau of Mines, Bartlesville, Oklahoma in the comparison of thermometer A-1 with their laboratory standard thermometer H25, which had been previously calibrated at the National Bureau of Standards over the range 14 to 717.8°K.[3,4] The calibration data for our thermometers from 90 to 373°K were used to evaluate the constants in the Callendar and the Callendar-Van Dusen equations, so that the temperature scales of our thermometers in this range should agree with the International Temperature Scale.[5] From 14 to 90°K smooth tables of R/R_0 *vs* temperature were constructed from the smoothed table for H25 and large scale deviation graphs. It is believed that the temperature scales of both the calorimeter thermometer and thermometer A-1 agree with the thermodynamic scale within 0.03° from 14 to 90°K and within 0.05° from 90 to 373°K. Below 14°K a provisional temperature scale was constructed for each thermometer by fitting the equation[4] $R=A+BT^2+CT^5$ to the resistance at the boiling point of helium and to the resistance and dR/dT at 14°K.

METHOD OF OPERATION AND RESULTS

Because of the radioactive decay of the neptunium and the small heat capacity of the calorimeter and sample, it was not convenient to operate in a strictly adiabatic fashion. The heating effect of the nuclear disintegration was 0.00047 cal/min, which produced a calorimeter temperature drift of 0.06°/min at 11°K, 0.002°/min at 50°K, and 0.0007°/min at 300°K. The thermometer current produced a temperature drift of 0.0007°/min at 11°K, 0.002°/min at 50°K, and 0.001°/min at 300°K for the loaded calorimeter and somewhat larger drifts for the empty calorimeter. To compensate for these drifts the temperature of the inner shield was maintained below that of the calorimeter at a constant galvanometer deflection chosen to give an approximately zero temperature drift at the beginning of each sequence of heat capacity measurements. The temperature drift of the calorimeter was observed for 10 to 15 minutes, then electrical energy was added for a measured period of 5 to 10 minutes, and finally the drift was observed for at least 15 minutes. Usually the drift

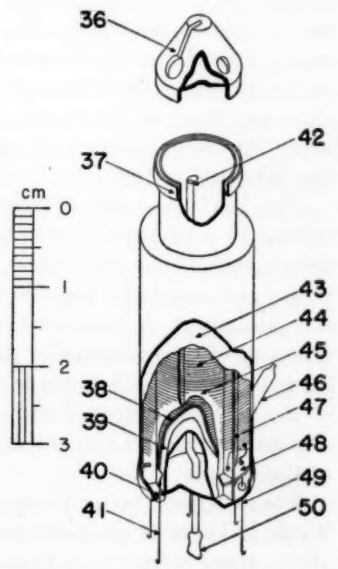

FIG. 2. The calorimeter: (36) cover; (37) annulus filled with low-melting solder; (42) tube for filling sample space with helium gas; (38) constantan heater; (44) platinum resistance thermometer; (39), (43), (45), (47), and (48) mica; (40) Corning 010 glass beads; (41) and (49) platinum leads; (46) and (50) pinched-off gold tubes.

[4] H. J. Hoge and F. G. Brickwedde, J. Research Natl. Bur. Standards 22, 351 (1939).

[5] H. F. Stimson, J. Research Natl. Bur. Standards 42, 209 (1949).

TABLE I. Molal heat capacity of neptunium dioxide.

Molecular Weight =269.07				0°C =273.16°K	
T (°K)	C_p (cal/deg)	T (°K)	C_p (cal/deg)	T (°K)	C_p (cal/deg)
Series *A*		Series *B*			
10.82	0.27	11.08	0.31	123.87	8.54
12.44	0.49	13.12	0.61	133.28	9.15
14.09	0.83	15.40	1.18	143.35	9.75
15.90	1.28	18.10	1.97	153.87	10.37
17.67	1.83	20.54	2.99	164.38	10.97
19.19	2.34	22.47	4.08	174.89	11.54
20.39	2.87	23.88	5.02	185.78	12.12
21.42	3.40	24.76	5.78	196.70	12.60
22.44	4.01	25.27	6.07	207.36	13.10
23.29	4.57	25.71	4.27	217.73	13.48
23.98	5.07	26.08	2.42	228.55	13.87
24.63	5.66	26.52	2.14	239.12	14.26
25.21	6.09	27.13	1.95	249.80	14.46
25.84	3.43	27.99	1.87	260.69	14.87
26.60	2.13	52.43	3.34	271.48	15.29
27.38	1.90	57.52	3.73	282.04	15.55
28.41	1.84	62.78	4.14	292.42	15.73
30.13	1.84	68.40	4.58	302.64	15.79
32.71	1.95	74.18	4.97	312.69	16.15
35.62	2.11	80.73	5.43		
39.07	2.36	88.10	5.96		
42.99	2.62	96.52	6.57		
47.44	2.94	104.79	7.18		
52.27	3.31	113.97	7.83		

became constant about 5 minutes after the end of the energy input. The observed drifts were used to extrapolate the initial and final temperatures to the midpoint of the energy input and thus to correct for the combined effects of heat interchange with the inner shield, nuclear disintegration, and thermometer current.

One operator observed the electromotive forces of the differential thermocouples and adjusted the current to the shield heaters to maintain the small constant temperature differential between the inner shield and the calorimeter and to maintain the outer shield several tenths of a degree colder. The temperature differential between the inner shield and the calorimeter was controlled to within 0.002° except for a few seconds at the start and finish of the energy input. A second operator made the temperature and energy measurements with the White potentiometer.

The heat capacity of the calorimeter filled with helium to a pressure of 113.6 mm at 23.7°C was first determined. Then the heat capacity of the calorimeter plus the sample and exactly the same mass of helium was measured. A correction for the slightly different quantity of Cerroseal solder used on the empty and the loaded calorimeter was made on the basis of additivity of the heat capacities of tin[6] and indium.[7] This correction amounted to 0.3 to one percent of the heat capacity of the sample.

The experimental heat capacity data are presented in Table I. Table II gives the values at rounded temperatures; these were taken from a large plot of the data. The results are expressed in terms of the defined thermochemical calorie equal to 4.1840 absolute joules. The ice point temperature was taken to be 273.16°K and the molecular weight of neptunium dioxide to be 269.07.

The first series of measurements revealed the existence of a region of high energy absorption from about 11 to 40°K with a very pronounced maximum at a temperature of 25.3°K. The subsequent measurements of Series *B* using smaller temperature increments in the region of rapid change of heat capacity satisfactorily established the shape of the curve, which rises smoothly to a value of about 6.2 cal deg^{-1} mole^{-1} at 25.3°K and then falls rapidly on the high temperature side of the maximum. The loaded calorimeter had been cooled from 77 to 4°K over a period of 12 hours before Series *A* was begun and over a period of several days before Series *B*. No evidence of hysteresis, poor thermal equilibrium, or irreproducibility was observed. The heat capacity data in the region of the anomaly are plotted in Fig. 3.

The heat capacity data were used to evaluate the molal entropy and enthalpy of neptunium dioxide at several temperatures, and the results are given in Table III. The values of these functions at 11°K were calculated from a Debye function which fits the heat capacity at 11°K. The increments above 11°K were evaluated by graphical quadrature of the heat capacity versus the logarithm of the temperature and of the heat capacity versus the temperature.

TABLE II. Molal heat capacity of neptunium dioxide at rounded temperatures.

T (°K)	C_p (cal/deg)	T (°K)	C_p (cal/deg)	T (°K)	C_p (cal/deg)
11	0.30	100	6.81	210	13.19
15	1.06	110	7.54	220	13.59
20	2.74	120	8.26	230	13.95
25	6.01	130	8.93	240	14.28
30	1.84	140	9.56	250	14.60
40	2.42	150	10.16	260	14.89
50	3.14	160	10.73	270	15.16
60	3.93	170	11.28	280	15.41
70	4.68	180	11.82	290	15.64
80	5.38	190	12.32	300	15.86
90	6.10	200	12.77	310	16.07

The precision of the individual determinations of the heat capacities of the empty calorimeter and of the loaded calorimeter was comparable to that usually obtained with larger calorimeters. It was better than 0.1 percent down to 30°K and decreased to about 1 percent at 11°K because of the decreased sensitivity of the resistance thermometer and the shorter temperature intervals used at the lower temperatures. However, because so small an amount of neptunium dioxide was available for these measurements, the ratio of the heat capacity of the sample to that of the calorimeter was smaller than normal. Thus at 11°K the heat capacity of the neptunium dioxide was about 33 percent of that of the empty calorimeter; at the peak of the anomaly it was a maximum of 89 percent, at 52°K it diminished to

[6] F. Lange, Z. physik. Chem. 110, 343 (1924).
[7] K. Clusius (private communication).

a minimum value of 13 percent, and at 300°K it was 20 percent. It is estimated that the uncertainty in the heat capacity of the sample is approximately 0.5 percent down to 20°K and increases to about 3 percent at 11°K, and that the uncertainty in the values given for the entropy and heat content at 298.16°K is about 0.5 percent.

DISCUSSION

It is of interest to note that Jones, Gordon, and Long[8] have observed a heat capacity anomaly in uranium dioxide at 28.7°K which is similar to that observed in neptunium dioxide. These heat capacity anomalies are almost certainly related to the magnetic behavior of the substances and are probably analogous to those found in other paramagnetic salts—for example, in manganous fluoride at 66.5°K[9] and in manganese dioxide at 92°K.[10] The shapes of the heat capacity curves are suggestive of cooperative phenomena and

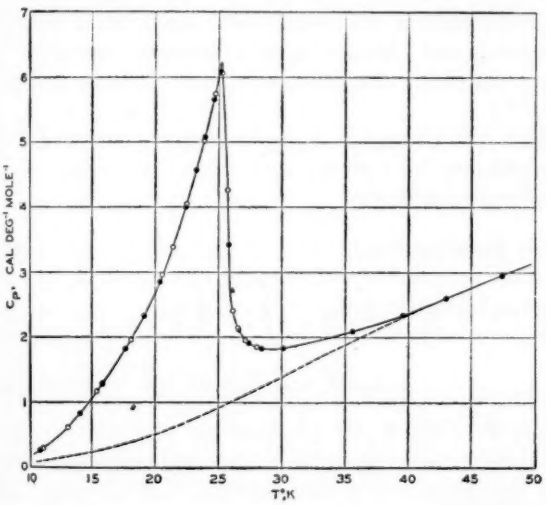

FIG. 3. The heat capacity anomaly of neptunium dioxide: series *A*, ●; series *B*, ○. The dashed curve is a Debye function which fits the observed heat capacity at 50°K.

may be due to the occurrence of antiferromagnetism below the temperatures of the maxima, as has been demonstrated in manganous fluoride[11,12] and in manganese dioxide.[13] The latter substances show maxima in their magnetic susceptibilities near the temperatures of the heat capacity maxima. Data on the magnetic susceptibilities of uranium dioxide and of neptunium dioxide over a temperature range which includes the heat capacity anomalies would aid in the interpretation of these phenomena.

TABLE III. Molal entropy and heat content of neptunium dioxide at rounded temperatures.

T (°K)	$H^\circ - H_0^\circ$ (cal)	S° (cal/deg)
11	0.8	0.10
50	94.5	3.40
100	345.3	6.73
150	773.1	10.15
200	1349	13.45
250	2036	16.51
300	2800	19.29
298.16	2770±15	19.19±0.1

A rough calculation of the extra entropy associated with the heat capacity anomaly has been made on the assumption that the heat capacity above 50°K is due solely to lattice vibrations. The lattice heat capacity of neptunium dioxide from 0 to 50°K was approximated by a Debye function which reproduced the total heat capacity in the region of 50°K. The lattice entropy at 50°K obtained from this Debye function is 1.70 cal deg^{-1} mole^{-1}. The total entropy at the same temperature (Table III) is 3.40 cal deg^{-1} mole^{-1}, and hence the entropy in excess of the estimated lattice entropy is 1.70 cal deg^{-1} mole^{-1}. This value is about 60 percent of the "spin only" value of $R \ln 4 = 2.75$ cal deg^{-1} mole^{-1} for the magnetic entropy at high temperatures. A similar calculation for uranium dioxide[8] gives an extra entropy of 0.87 cal deg^{-1} mole^{-1}, or 40 percent of the "spin only" value of $R \ln 3 = 2.18$ cal deg^{-1} mole^{-1}.

We do not believe that the difference between the extra entropy and the "spin only" value is due to the persistence of an appreciable part of the magnetic entropy below 11°K, and the entropy values in Table III are based on this assumption. The heat capacity was extrapolated smoothly from 11 to 0°K with a Debye function, and it is assumed that there are no humps in the heat capacity below 11°K which would correspond to further loss of magnetic entropy.

We consider it more probable that the estimate of the lattice heat capacity is too high and that the contribution of the electronic system is appreciable even at temperatures above 50°K. A better approximation for the lattice heat capacity of uranium dioxide and of neptunium dioxide can be obtained from the heat capacity of thorium dioxide, which is isostructural and diamagnetic. Further discussion of this matter will be given in a subsequent paper in which measurements of the heat capacity of thorium dioxide will be presented.[14]

[8] Jones, Gordon, and Long, J. Chem. Phys. **20**, 695 (1952).
[9] J. W. Stout and H. E. Adams, J. Am. Chem. Soc. **64**, 1535 (1942).
[10] K. K. Kelley and G. E. Moore, J. Am. Chem. Soc. **65**, 782 (1943).
[11] M. M. H. Bizette and T. Belling, Compt. rend. **209**, 205 (1939).
[12] de Haas, Schultz, and Koolhaas, Physica **7**, 57 (1940).
[13] M. M. H. Bizette and B. Tsai, *Les Phénomènes Cryomagnétiques* (Collège de France, Paris, 1948), page 13.
[14] D. W. Osborne and E. F. Westrum, Jr. (in preparation).

High Temperature Susceptibility of Permanent Dipole Lattices*

ROBERT ROSENBERG† AND MELVIN LAX
Physics Department, Syracuse University, Syracuse, New York

(Received August 13, 1952)

Van Vleck's exact classical treatment of dipolar materials is modified and extended. (For convenience, his expansion of the susceptibility χ in powers of T^{-1} is replaced by an expansion of the effective molecular polarizability α_s.) The present procedure exhibits the dependence of the coefficients of T^{-p} on lattice sums over certain typical interactions within "clusters" of dipoles. This feature, together with an extension to the fourth-order term, sheds light on the analytic character as well as numerical accuracy of the spherical approximation. The exact treatment also provides a standard of comparison for all other approximation methods. The fourth-order coefficient is evaluated for a simple cubic arrangement of the dipoles, and for the Onsager liquid model.

The spherical result, at least in the high temperature range, includes the most important types of interactions within clusters; it reproduces the exact series through the third-order term, and differs from the exact simple-cubic fourth-order term by only 5 percent. In addition, when evaluated for the Onsager liquid model, the spherical solution is apparently an improvement over Onsager's solution.

1. INTRODUCTION

THE treatment of interactions between permanent dipoles arranged on a lattice presents mathematical difficulties which are common to a broad class of condensed-phase problems. (The same formalism which applies to susceptibilities and specific heats also finds application in describing order-disorder transitions and cooperative phenomena, e.g., transitions to ferro and antiferro electric and magnetic states, and order-disorder in binary alloys.) The present discussion of susceptibilities, while leaving the principal difficulty unresolved, accomplishes the following:

(1) It extends Van Vleck's[1] exact high temperature expansion by one step, to include the term in T^{-4}. (The results take their most concise form when the susceptibility is expressed as a function of an effective molecular polarizability α_s, and α_s is expanded in powers of T^{-1}. All discussion of series results in this paper refers to the expansion of α_s.) Because the present method is exact, it provides a standard of comparison for all approximate results.

(2) It reorganizes Van Vleck's treatment in a manner which displays the dependence of the series coefficients on certain typical interactions within clusters of dipoles. This feature indicates what sort of interactions are included or omitted by the spherical approximation, recently applied to the problem by one of the authors.[2]

(3) It shows that the sphericalization result (a) is analytically correct to third order, (b) retains in the fourth-order coefficient the interactions which are most important for the high temperature range, and (c) is only 5 percent from the correct numerical value in the fourth-order coefficient, for the simple cubic case.

(4) It indicates that the spherical result, when adapted to the Onsager liquid model, has higher accuracy than Onsager's[3] ingenious one-body solution. (Comparison requires the fourth-order term, since both the spherical and Onsager approximations reproduce the exact series for the Onsager liquid through the term in T^{-3}.)

Van Vleck's exact many-body formulation for the suceptibility of a permanent dipolar material may be rewritten as follows:

$$\mathbf{P}=n\langle\langle\boldsymbol{\mu}_a\rangle\rangle_{E_0}; \tag{1.1}$$

$$\langle\langle\boldsymbol{\mu}_a\rangle\rangle_{E_0}=(4\pi)^{-N}[Q(\mathbf{E}_0)]^{-1}\int\cdots\int\boldsymbol{\mu}_a \times\exp[-H(\mathbf{E}_0)/kT]d\Omega_1\cdots d\Omega_N, \tag{1.2}$$

where $\mathbf{P}$ is the dipole moment per unit volume; $\boldsymbol{\mu}_a$ is the moment of a typical[4] dipole having lattice position a; n is the number of dipoles per unit volume; the double bracket $\langle\langle\ \rangle\rangle$ indicates a weighted average; the subscript E_0 indicates the presence of an applied field; $H(\mathbf{E}_0)$ is the Hamiltonian; $Q(\mathbf{E}_0)$ is the corresponding partition function; and $d\Omega_i$ is the element of solid angle which contains the direction of orientation of the ith dipole moment.

Equation (1.2) is at the heart of the mathematical difficulty, since (1.2) apparently cannot be integrated directly. Van Vleck, therefore, expanded the exponential in a power series in T^{-1}, obtaining a set of unweighted averages over orientations of the dipoles. This expansion procedure is modified in the present work, and carried to fourth order.

2. FORMULATION OF THE PROBLEM

The susceptibility $\chi=P/E$ is defined in terms of the average field $\mathbf{E}$ in the specimen rather than the field $\mathbf{E}_0$

* Supported in part by the U. S. Office of Naval Research.

† This paper is a condensed version of a thesis submitted in partial fulfillment of the requirements for the degree of Master of Science in the Graduate School, Syracuse University.

[1] J. H. Van Vleck, J. Chem. Phys. **5**, 320, 556 (1937).

[2] M. Lax, J. Chem. Phys. **20**, 1351 (1952).

[3] L. Onsager, J. Am. Chem. Soc. **58**, 1486 (1936).

[4] The dipoles are all alike only above the critical temperature T_c for the onset of order. Below T_c, (1.1) must be replaced by $\mathbf{P}=\sum_i n_i\langle\langle{}^i\boldsymbol{\mu}_a\rangle\rangle_{E_0}$, where ${}^i\boldsymbol{\mu}_a$ is typical only in the ith sublattice.

external to the specimen. **P** is given by (1.1)–(1.2). We shall confine our attention to ellipsoidal specimens with cubic structure, so that χ is a scalar, and **P** and **E** are parallel and uniform.

For cubic structures, χ can be written

$$\chi = n\alpha_s/[1-(4\pi/3)n\alpha_s], \tag{2.1}$$

where α_s, the effective molecular polarizability, is defined by

$$\langle\langle \boldsymbol{\mu}_a\rangle\rangle_{E_0} = \alpha_s \mathbf{E}_e = \alpha_s[\mathbf{E}+(4\pi/3)\mathbf{P}], \tag{2.2}$$

and chosen to agree with the notation of reference 2. $\mathbf{E}_e$ is the local field for an equivalent lattice of induced dipoles whose polarizability is α_s, i.e., $\mathbf{E}_e$ is the equivalent Lorentz field. Solution of (2.2) requires a knowledge of **P**, Eq. (1.1).

The Hamiltonian in (1.2) includes dipole-dipole and dipole-applied field interaction energies:

$$-H(\mathbf{E}_0) = n\mu^2 \sum_{i>j} w_{ij} + \mu \sum_k \boldsymbol{\epsilon}_k \cdot \mathbf{E}_0; \tag{2.3}$$

$$w_{ij} = \boldsymbol{\epsilon}_i \cdot \mathbf{G}_{ij} \cdot \boldsymbol{\epsilon}_j, \tag{2.4}$$

$$\boldsymbol{\epsilon}_i = \boldsymbol{\mu}_i/\mu, \tag{2.5}$$

$$\mathbf{G}_{ij} = r_{ij}^{-5}[3\mathbf{r}_{ij}\mathbf{r}_{ij} - r_{ij}^2\mathbf{1}], \tag{2.6}$$

$$\mathbf{r}_{ij} = \mathbf{r}_i - \mathbf{r}_j.$$

$\mathbf{G}_{ij}$ is that dyadic which, when dotted into μ_j, gives the field acting at the position of the ith dipole due to μ_j. Equation (2.6) has been made a dimensionless sum by measuring distances in units of $n^{-\frac{1}{3}}$ and inserting the factor n explicitly in (2.3).

The Boltzmann factor of (1.2) is expanded in powers of $\mathbf{E}_0$ and nonlinear terms in $\mathbf{E}_0$ are dropped, since we are not concerned with the question of saturation. The only contribution to the numerator of (1.2) then comes from the linear term of the expansion, while only the constant term contributes to the denominator Q. In the linear approximation, then, (1.2) reduces to

$$\langle\langle \boldsymbol{\mu}_a\rangle\rangle_{E_0} = (\mu^2/kT)\langle\langle \textstyle\sum_k \boldsymbol{\epsilon}_a\boldsymbol{\epsilon}_k\rangle\rangle \cdot \mathbf{E}_0; \tag{2.7}$$

$$\langle\langle \textstyle\sum_k \boldsymbol{\epsilon}_a\boldsymbol{\epsilon}_k\rangle\rangle = (4\pi)^{-N}[Q(0)]^{-1} \int\cdots\int \textstyle\sum_k \boldsymbol{\epsilon}_a\boldsymbol{\epsilon}_k \times \exp[-H(0)/kT]\, d\Omega_1 \cdots d\Omega_N, \tag{2.8}$$

$$Q(0) = \int\cdots\int \exp\left[\frac{-H(0)}{kT}\right] \frac{d\Omega_1\cdots d\Omega_N}{(4\pi)^N}, \tag{2.9}$$

where the absence of a subscript E_0 in (2.8) indicates that the averages are performed in the absence of an applied field.

The susceptibility P/E obtained from (2.7) contains the ratio E_0/E and therefore appears to be nonscalar and dependent on the shape of the specimen. These difficulties are eliminated, however, by the tensor and shape dependence of $\langle\langle \sum_k \boldsymbol{\epsilon}_a\boldsymbol{\epsilon}_k\rangle\rangle$ as discussed in Sec. 3.

The evaluation of (2.8) can be carried out after an expansion in powers of T^{-1}. Before expanding, however, the Boltzmann factor is first rearranged in accord with the Mayer and Mayer[5] cluster technique. The latter procedure has two advantages: (a) It provides a ready interpretation for the coefficients of the series; (b) it simplifies the counting of different types of terms which appear in the coefficients. The details of the expansion are given in the Appendix. The averages indicated in (2.8) are performed with the help of the following algorithms:

$$\langle \mathbf{a}_1 \cdot \boldsymbol{\epsilon}\rangle = 0, \tag{2.10}$$

$$\langle (\mathbf{a}_1 \cdot \boldsymbol{\epsilon})(\mathbf{a}_2 \cdot \boldsymbol{\epsilon})\rangle = \tfrac{1}{3}\mathbf{a}_1 \cdot \mathbf{a}_2, \tag{2.11}$$

$$\langle \prod_{m=1}^{3} (\mathbf{a}_m \cdot \boldsymbol{\epsilon})\rangle = 0, \tag{2.12}$$

$$\langle \prod_{m=1}^{4} (\mathbf{a}_m \cdot \boldsymbol{\epsilon})\rangle = \frac{1}{15}[(\mathbf{a}_1\cdot\mathbf{a}_2)(\mathbf{a}_3\cdot\mathbf{a}_4) + (\mathbf{a}_1\cdot\mathbf{a}_3)(\mathbf{a}_2\cdot\mathbf{a}_4) + (\mathbf{a}_1\cdot\mathbf{a}_4)(\mathbf{a}_2\cdot\mathbf{a}_3)], \tag{2.13}$$

where $\langle\ \rangle$ denotes an unweighted orientation average. The vectors $\mathbf{a}_1$, $\mathbf{a}_2$, $\mathbf{a}_3$, and $\mathbf{a}_4$ are arbitrary. The algorithms are also useful in computing mean values of dyadics, e.g., (2.11) yields

$$\langle \boldsymbol{\epsilon}\boldsymbol{\epsilon}\rangle = \tfrac{1}{3}\mathbf{1}. \tag{2.14}$$

3. RESULTS

The result[6] for (2.8) is

$$3\langle\langle \textstyle\sum_k \boldsymbol{\epsilon}_a\boldsymbol{\epsilon}_k\rangle\rangle = [\mathbf{1} + n\alpha\mathbf{c} + (n\alpha)^2\mathbf{c}\cdot\mathbf{c} + (n\alpha)^3\mathbf{c}\cdot\mathbf{c}\cdot\mathbf{c} + \cdots] - (n\alpha)^2\mathfrak{R}\cdot[\mathbf{1} + 2n\alpha\mathbf{c} + \cdots] + (n\alpha)^3[\mathfrak{T} + (4/25)\mathfrak{S}]\cdot[\mathbf{1} + \cdots] + \cdots, \tag{3.1}$$

where α is the abbreviation for $\mu^2/(3kT)$, and

$$\mathbf{c} = \textstyle\sum_b \mathbf{G}_{ab}, \tag{3.2}$$

$$\mathfrak{R} = \textstyle\sum_b \mathbf{G}_{ab}\cdot\mathbf{G}_{ba}, \tag{3.3}$$[7]

$$-\mathfrak{T} = \textstyle\sum_b \sum_c \mathbf{G}_{ab}\cdot\mathbf{G}_{bc}\cdot\mathbf{G}_{ca}, \tag{3.4}$$

$$\mathfrak{S} = \textstyle\sum_b \mathbf{G}_{ab}\cdot\mathbf{G}_{ba}\cdot\mathbf{G}_{ab}. \tag{3.5}$$

$\mathbf{c}\cdot\mathbf{u}$ can be interpreted as the field at a due to a set of unit dipoles $\mathbf{u}$ at all lattice sites $b \neq a$, i.e., $\mathbf{c}\cdot\mathbf{u}$ is the

---

[5] J. E. and M. G. Mayer, *Statistical Mechanics* (John Wiley and Sons, Inc., New York, 1940), Chapter 13.

[6] An intermediate result is a quotient of the form

$$\langle\langle \textstyle\sum_k \boldsymbol{\epsilon}_a\boldsymbol{\epsilon}_k\rangle\rangle = (A + BN + \cdots)/(1 + DN + \cdots), \tag{3.1}'$$

where N is the total number of dipoles in the specimen. This result apparently invalidates the expansion procedure for macroscopic specimens, for which only the highest powers of N seem to be important. As Van Vleck (see reference 1) points out, however, A, B, and D are not independent, but obey the relation $B = AD$. At least in our approximation, then, (3.1)′ is independent of N. The general relationship between the coefficients of the two series in (3.1)′ has not been investigated. [Van Vleck's symbol N = our symbol n. Nevertheless, A, B, and D are still related as indicated.]

[7] Our symbol $\mathfrak{R}$ = Van Vleck's symbol Q in reference 1.

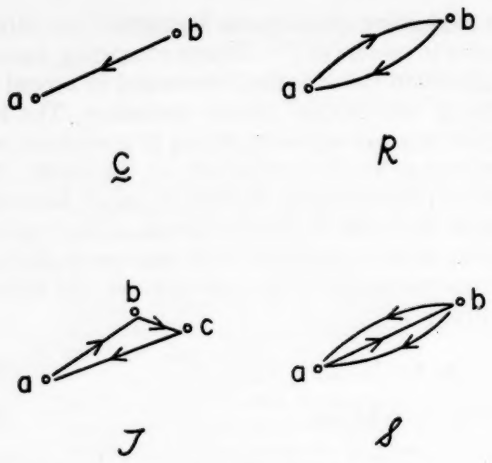

FIG. 1. The types of cluster sums appearing in the expansion of the susceptibility up to terms in T^{-4} are illustrated above. Each cluster is represented by a diagram whose vertices are located at the summation indices, e.g., $-\mathfrak{T}=\Sigma_b \Sigma_c \mathbf{G}_{ab}\cdot\mathbf{G}_{bc}\cdot\mathbf{G}_{ca}$.

Lorentz local field, so that for cubic lattices,

$$\mathbf{c}=4\pi(\tfrac{1}{3}\mathbf{1}-\mathbf{L}), \tag{3.6}$$

where $\mathbf{L}$ is the shape-dependent demagnetizing factor.

Referring to the definitions (3.2)–(3.5), and remembering that $\mathbf{G}_{ab}$ is proportional to r_{ab}^{-3}, we see that $\mathbf{c}$ has a much longer range than $\mathfrak{R}$, $\mathfrak{S}$, $\mathfrak{T}$, or any of the sums which occur in higher order terms. In macroscopic specimens, $\mathbf{c}$ carries all the shape dependence of (3.1). It is this factor which, when coupled with the factor E_0/E, preserves the scalar and shape-independent properties of the susceptibility, as discussed in Sec. 2.

Just as $\mathbf{c}$ represents the direct action of dipoles b on a, $\mathfrak{R}$ sums the $\mathfrak{R}$eactions of a on itself via one intermediate dipole at b; $\mathfrak{T}$, the $\mathfrak{T}$riangle reactions of a on itself via two intermediate dipoles at b and c; and $\mathfrak{S}$, the $\mathfrak{S}$huttling interactions of b on a, a back on b, and b back again on a. (See Fig. 1.)

The coefficients $\mathfrak{R}$, $\mathfrak{S}$, and $\mathfrak{T}$ converge rapidly by comparison with $\mathbf{c}$. For example, the overwhelming contributions to $\mathfrak{T}$ are made by those terms in the sum for which a, b, and c are within about ten lattice distances of each other. While $\mathfrak{R}$, $\mathfrak{S}$, and $\mathfrak{T}$ are therefore independent of the shape of the macroscopic specimen, they do depend on the lattice structure. For sufficiently symmetric lattices, such as the three cubic types, $\mathfrak{R}$, $\mathfrak{S}$, and $\mathfrak{T}$ are scalar sums, i.e., $\mathfrak{R}=\mathfrak{R}\mathbf{1}$, $\mathfrak{S}=\mathfrak{S}\mathbf{1}$, and $\mathfrak{T}=\mathfrak{T}\mathbf{1}$.

Finally, using (3.1) and (2.7) to solve (2.2) for α_s, we get

$$\alpha_s=\alpha\{1-\mathfrak{R}(n\alpha)^2+[\mathfrak{T}+(4/25)\mathfrak{S}](n\alpha)^3+\cdots\}. \tag{3.7}$$

Notice that all shape dependence has disappeared, since $\mathbf{c}$ does not appear in (3.7).

4. COMPARISON WITH APPROXIMATE SOLUTIONS

$\mathfrak{R}$, $\mathfrak{S}$, and $\mathfrak{T}$ have been evaluated for two arrangements of the dipoles:

(1) The dipoles conform to the Onsager liquid model.

(2) The dipoles are arranged on a simple cubic lattice.

The liquid case provides a comparison between the Onsager and spherical approximations, while case (2) checks the quantitative accuracy of the spherical approximation for the simple cubic arrangement.

The third-order coefficient $\mathfrak{R}$ has the same analytic form in the sphericalization result as in the exact expansion. In addition, the value of $\mathfrak{R}$ for case (1) is identical with Onsager's third-order coefficient. The values[1] of $\mathfrak{R}$ are listed in Table I, along with the values of $\mathfrak{S}$ and $\mathfrak{T}$, for different arrangements of the dipoles.

The fourth-order coefficients no longer agree in the different solutions, as shown in Table II.

The liquid calculations for the coefficients are accomplished by replacing the sums of (3.3)–(3.5) by integrals over the appropriate liquid distribution functions. For the sake of comparison with Onsager's results, we have chosen pair- and triple-correlation functions of the sort implied by his model. The pair-correlation function for $\mathfrak{R}$ and $\mathfrak{S}$ has the square-well shape shown in Fig. 2, where the radius of the well $b=(3/4\pi n)^{\frac{1}{3}}$. The triple-correlation function for $\mathfrak{T}$ has, in Onsager's spirit, been given the simple form of a product of such pair-correlation functions:

$$n(\mathbf{r}_1,\mathbf{r}_2,\mathbf{r}_3)=n^{-3}n(\mathbf{r}_1,\mathbf{r}_2)n(\mathbf{r}_2,\mathbf{r}_3)n(\mathbf{r}_3,\mathbf{r}_1). \tag{4.1}$$

(This is also the Kirkwood superposition approximation.)

On the basis of this choice, Table II shows that the spherical approximation agrees better with the exact solution than does the original Onsager approximation. In fact, the spherical fourth-order coefficient of α_s comes within 15 percent of the "exact" liquid result, and is only 5 percent from the exact simple cubic result.

The general form of the fourth-order coefficients, given in the first line of Table II, throws some light on the character of the spherical approximation. Whereas the complete solution includes all types of interactions $\mathfrak{R}$, $\mathfrak{S}$, $\mathfrak{T}$, etc.; the spherical approximation omits interactions of the type $\mathfrak{S}$. The implication is that the spherical model, aside from $\mathbf{c}$, involves only those interactions like $\mathfrak{R}$ and $\mathfrak{T}$ whose figures have the following property: They are closed chains which can be drawn as a succession of links without lifting the pencil from the paper; duplication of sites and links is permitted.

Examination of the fourth-order coefficients now reveals why the spherical approximation is accurate in

TABLE I. Values of the lattice sums which occur in the coefficients of the high temperature expansion for the susceptibility.

	$\mathfrak{R}$	$\mathfrak{S}$	$\mathfrak{T}$
Onsager liquid	$2(4\pi/3)^2$	$(4\pi/3)^3$	$15/16(4\pi/3)^3$
S. c. lattice	16.8	13.25	38.7
F. c. c. lattice	14.4	8.83	
B. c. c. lattice	14.5	9.03	

the high temperature range. $\mathfrak{T}$ is much larger than $(4/25)\mathfrak{S}$ for three reasons. First, the three-link closed-loop sum $\mathfrak{T}$ converges more slowly than the three-link open-figure sum $\mathfrak{S}$ as the spatial size of the figure increases. Second, the three-particle sum $\mathfrak{T}$ contains many more terms than the two-particle sum $\mathfrak{S}$. Third, the contribution of the three-link, open-figure sum $\mathfrak{S}$ is reduced by a numerical factor (4/25) introduced in performing averages over dipolar orientations. Similar considerations may be expected to apply to all higher order coefficients.

As a check on the accuracy of the result (3.7) a corresponding calculation has been carried out for the pure induced-dipole lattice by setting $\mathbf{G}_{ii}=[1/(2\alpha_0)]\mathbf{1}$, where α_0 is the real polarizability of a single dipole. Integration over dipolar magnitudes as well as orientations then produces the Lorentz-Lorenz result, i.e., (3.7) reduces to $\alpha_s=\alpha_0$.

The present formulation can be adapted to a variety of order-disorder problems by including in the Hamiltonian an interaction dyadic to account for non-dipole-dipole forces, both long and short range (see reference 2).

APPENDIX

The series expansion of the exponential in (2.8) is performed as follows: The exponential is written as a product of functions

$$1+f_{ij}=\exp[n\mu^2 w_{ij}/kT], \tag{A.1}$$

each representing a single pair of dipoles:

$$\exp[-H(0)/kT]=\prod_{i>j}(1+f_{ij}). \tag{A.2}$$

The notation $i>j$ emphasizes the fact that each pair of dipoles appears just once in the product. Equation (A.2) expands into

$$\exp\left[\frac{-H(0)}{kT}\right]=1+\sum_{c>d}f_{cd}+\frac{1}{2!}\sum_{c>d}\sum_{e>f}f_{cd}f_{ef}\times q_{ce;df}q_{cf;de}+\frac{1}{3!}\sum_{c>d}\sum_{e>f}\sum_{g>h}f_{cd}f_{ef}f_{gh}\times q_{ce;df}q_{cf;de}q_{cg;dh}q_{ch;dg}q_{eg;fh}q_{eh;fg}+\cdots; \tag{A.3}$$

$$q_{ce;df}=\tfrac{1}{2}(2-\delta_{ce}-\delta_{df})(1+\delta_{ce})(1+\delta_{df}). \tag{A.4}$$

TABLE II. Comparison of fourth-order coefficients in the effective molecular polarizability, α_s, for the solutions indicated.

	Series	Spherical	Onsager
General	$\mathfrak{T}+(4/25)\mathfrak{S}$	$\mathfrak{T}$	$2\mathfrak{S}$
Onsager liquid	$1.0975(4\pi/3)^3$	$0.9375(4\pi/3)^3$	$2(4\pi/3)^3$
S. c. lattice	40.8	38.7	Not applicable

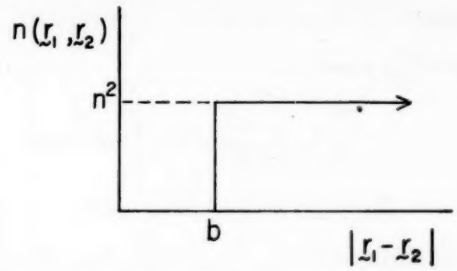

FIG. 2. The pair correlation function $n(\mathbf{r}_1, \mathbf{r}_2)$ that corresponds to the Onsager liquid model takes the form of a square well of radius $b=[3/(4\pi n)]^{\frac{1}{3}}$.

The q's are a set of operators which annihilate those terms of (A.3) containing duplicating pairs. The factorials are inserted because the notation of (A.3) permits permutations of the f's which do not occur in (A.2). The terms represented by $\cdots$ are omitted, since they only make contributions to χ of order T^{-p} with $p\geq 5$.

With the help of the expansion

$$f_{ij}=\sum_{l=1}^{\infty}\frac{1}{l!}(3n\alpha w_{ij})^l, \tag{A.5}$$

the expansion (A.3) is rearranged in powers of T^{-1}:

$$f_{cd}f_{ef}=\sum_{l=2}^{\infty}\sum_{m=1}^{l-1}\frac{(3n\alpha)^l}{m!(l-m)!}(w_{cd})^m(w_{ef})^{l-m}, \tag{A.6}$$

$$f_{cd}f_{ef}f_{gh}=\sum_{l=3}^{\infty}\sum_{m=1}^{l-2}\sum_{t=1}^{l-m-1}\frac{(3n\alpha)^l}{m!t!(l-m-t)!}\times(w_{cd})^m(w_{ef})^t(w_{gh})^{l-m-t}. \tag{A.7}$$

For our purposes, only the terms through α^3 are kept.

The final steps in obtaining (3.7) are as follows:

(1) Insert (A.5)–(A.7) into (A.3), and (A.3) into (2.8).

(2) Perform the averages indicated in (2.8).

(3) Rearrange sums over pairs into sums over particle indices.

(4) Eliminate the fields $\mathbf{E}_0$ and $\mathbf{E}$ from (2.2) by standard formulas, and solve for α_s.

As an example of steps (1)–(3), we consider that part of the quadratic term of (A.3) which corresponds to $l=2$, $m=1$ in (A.6); we designate this subterm by the symbol $II_{2,1}$:

$$II_{2,1}=\frac{1}{2!}\sum_{c>d}\sum_{e>f}(3n\alpha)^2 w_{cd}w_{ef}q_{ce;df}q_{cf;de}. \tag{A.8}$$

Inserting (A.8) into the numerator of (2.8) in place of the exponential, we get the following part of the

numerator:

$$F(II_{2,1})\equiv\langle\textstyle\sum_k \boldsymbol{\varepsilon}_a\boldsymbol{\varepsilon}_k II_{2,1}\rangle$$

$$=\frac{1}{2!}\sum_k\sum_{c>d}\sum_{e>f}(3n\alpha)^2\mathbf{Y}q_{ce;df}q_{ef;de}; \quad \text{(A.9)}$$

$$\mathbf{Y}=\langle\boldsymbol{\varepsilon}_a\boldsymbol{\varepsilon}_c\cdot\mathbf{G}_{cd}\cdot\boldsymbol{\varepsilon}_d\boldsymbol{\varepsilon}_e\cdot\mathbf{G}_{ef}\cdot\boldsymbol{\varepsilon}_f\boldsymbol{\varepsilon}_k\rangle, \quad \text{(A.10)}$$

where the single brackets, $\langle\ \rangle$, indicate that the averages are now unweighted.

Because orientational averages over odd powers of a particular $\boldsymbol{\varepsilon}_i$ vanish, the only nonvanishing form for (A.10) is

$$\mathbf{Y}=\langle\boldsymbol{\varepsilon}_a\boldsymbol{\varepsilon}_a\cdot\mathbf{G}_{aj}\cdot\boldsymbol{\varepsilon}_j\boldsymbol{\varepsilon}_j\cdot\mathbf{G}_{jk}\cdot\boldsymbol{\varepsilon}_k\boldsymbol{\varepsilon}_k\rangle. \quad \text{(A.11)}$$

This form can be obtained from (A.10) by either permutation of the pairs *cd* and *ef*; the permutations therefore cancel the 2! in (A.9).

With the help of (2.14), (A.11) reduces to

$$\mathbf{Y}=[1/(3^3)]\mathbf{G}_{aj}\cdot\mathbf{G}_{jk}. \quad \text{(A.12)}$$

We can now write in place of (A.9)

$$F(II_{2,1})=[(n\alpha)^2/3]\textstyle\sum_k\sum_j\mathbf{G}_{aj}\cdot\mathbf{G}_{jk}q_{ak;jj}. \quad \text{(A.13)}$$

The sums over pairs have been replaced by sums over particles. Other terms, which could have been obtained by permutations of the indices within each pair, are omitted because of the restrictions on the summation (A.9).

We should now like to sum k over all lattice points except j, since $\sum_k\mathbf{G}_{jk}=\mathbf{c}$. But $q_{ak;jj}$ tells us, however, that $k=a$ is forbidden. We can circumvent this difficulty by removing the q from (A.13) and adding in and subtracting off a term for which $k=a$. Equation (A.13) then becomes

$$F(II_{2,1})=[(n\alpha)^2/3](\mathbf{c}\cdot\mathbf{c}-\mathfrak{N}\mathbf{1}). \quad \text{(A.14)}$$

In a similar fashion, all the other integrations can be done using the algorithms (2.10)–(2.14).

THE JOURNAL OF CHEMICAL PHYSICS VOLUME 21, NUMBER 3 MARCH, 1953

A Detailed Formulation of Kinetic Processes. II. The Role of Collision Processes

SIDNEY W. BENSON AND ARTHUR E. AXWORTHY, JR.
Department of Chemistry, University of Southern California, Los Angeles 7, California

(Received July 7, 1952)

A detailed treatment is given of the activational processes occuring in both unimolecular and bimolecular processes. Such a treatment leads very naturally to the postulate of two critically energized species, one related to the products and one to reactants. In the case of unimolecular isomerizations it is shown that the properties of either one or both of these species may dominate the rate of the nonequilibrium reaction rate expression, and the form of the rate expression is given in terms of the Slater theory of unimolecular reactions.

In the case of unimolecular decompositions, only the complex corresponding to reactants is important, whereas in the inverse case of association reactions only that for the products is of importance. Both of these types of reactions have the same form of pressure dependence in the steady-state concentration region. The above considerations apply even when the reactions are not reversible. That is, the critically energized complex related to products is still of importance in determining the reaction rate. In the case of bimolecular and higher order processes, a detailed investigation shows that the activational processes are always maintained at their equilibrium values, and there is no region in which the rate constants will show a significant dependence on concentration of inert gas.

I. INTRODUCTION

CHEMICAL reactions having activation energies occur through the decompositions of a special group of molecules in the reacting system, namely, those of high internal energy. In the usual applications of statistical mechanics to chemical reactions, the assumption is generally made that the concentrations of these high energy (i.e., activated) molecules is substantially the same as that obtaining at equilibrium (in the absence of the reaction). Such an assumption can only be justified if it can be shown that the rate at which such molecules enter into the chemical reaction is slow compared to the rate at which they are converted back into normal, unreacted molecules.[1] While there has been a considerable amount of work devoted to the investigation of this condition in the case of unimolecular reactions[2–7] relatively little has been done concerning higher

[1] This condition is sometimes erroneously stated as "The rate at which activated molecules enter into reaction shall be small compared to their rate of formation."

[2] F. A. Lindemann, Trans. Faraday Soc. **17**, 598 (1922).

[3] H. A. Kramers, Physica **7**, 284 (1940).

[4] H. Eyring and B. Zwolinski, J. Am. Chem. Soc. **64**, 2702 (1947).

[5] J. O. Hirshfelder, J. Chem. Phys. **16**, 22 (1948).

[6] S. W. Benson, (a) J. Chem. Phys. **19**, 802 (1951); (b) **20**, 1064 (1952).

[7] I. Prigogine and E. Xhrouet, Physica **15**, 913 (1949); I. Prigogine and M. Mahieu, Physica **16**, 51 (1950).

order reactions. The recent work of Prigogine *et al.*[7] on bimolecular gas reactions while theoretically interesting is limited to considerations involving only the kinetic energies of translations of active molecules and to rather artificial expressions for the probability of reaction of an activated species.[8]

It is the purpose of the present paper to analyze in detail the activational processes involved in reactions of various molecular complexity and thus arrive at quantitative expressions for the over-all rate constants which will permit of a more critical estimate of the role of collision processes in these reactions and of the validity of the equilibrium treatments that have been made of these systems.

II. UNIMOLECULAR ISOMERIZATION REACTIONS

Let us consider in all generality a unimolecular isomerization which may reach a state of equilibrium as represented by the chemical equation[9]

$$A \rightleftarrows B. \tag{1}$$

The detailed mechanism of reaction may be represented by the following scheme:

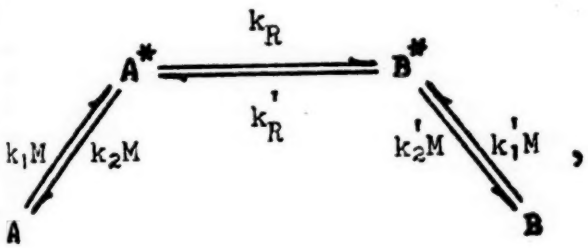

(2)

where by A^* we mean any species A with sufficient internal energy[10] to spontaneously rearrange to B^* (and similarly for the definition of B^*). M is the concentration of any species capable of exchanging energy inelastically with A and B, k_1, k_2, k_1', and k_2' are the specific rate constants for the collisional activation and deactivation of A and B, respectively, and k_R and k_R' are the specific rate constants for the spontaneous isomerization of critically activated species.

If now we make the assumption that at all time of interest $A^* \ll A$ or B and $B^* \ll A$ or B, we can apply the steady-state treatment of setting $dA^*/dt = dB^*/dt = 0$;

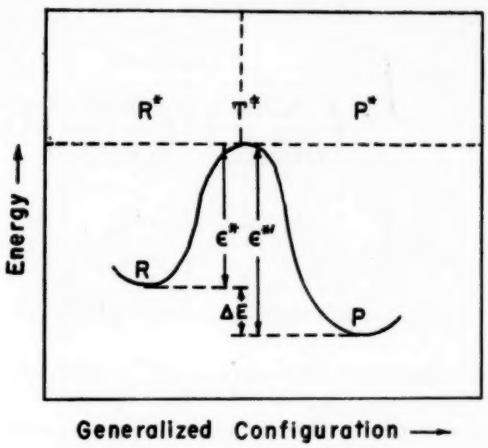

FIG. 1. Schematic comparison of the detailed theory and the equilibrium or transition state theory. For the exothermic reaction Reactants (R)→Products (P). $T^\ddagger$ is the transition state or activated complex. R^* and P^* are the critically energized complexes, not necessarily having the proper stearic configurations for reaction. All configurations to the left of $T^\ddagger$ and above the barrier belong to the set of complexes R^*, those to the right to P^*.

and we find for the net rate of reaction, expressed as $-dA/dt = dB/dt = R$,

$$R = k_2'(M)(B^*) - k_1'(M)(B) = R_A - R_B$$

$$= \frac{(A)(M)k_1k_2'k_R - (B)(M)k_2k_1'k_R'}{k_2k_R' + (M)k_2k_2' + k_2'k_R}. \tag{3}$$

The initial rate of reaction (when $B \ll A$) is then given by

$$R_A = \frac{(A)(M)k_1k_2'k_R}{k_2k_R' + (M)k_2k_2' + k_2'k_R}, \tag{4}$$

where R_A strictly represents the net rate of reaction of A by way of the intermediate species A^* with energy in the range ϵ, $\epsilon + d\epsilon$ ($\epsilon \gtrsim \epsilon^*$, the critical decomposition energy) and all the rate constants are functions of ϵ. The total rate is obtained by integrating (or summing) $R_A(\epsilon)$ in Eq. (4) over-all energy states from $\epsilon^* \lesssim \epsilon \lesssim \infty$:[11]

$$-dA/dt = \int_{\epsilon^*}^{\infty} R_A(\epsilon)d\epsilon$$

$$= (A)(M)\int_{\epsilon^*}^{\infty} \frac{k_1k_2'k_R d\epsilon}{k_2k_R' + (M)k_2k_2' + k_2'k_R}$$

[7] Prigogine's model is better suited to a study of the probability of inelastic collisions than it is to actual chemical reactions.

[9] For actual examples of such systems we may take the isomerization of *cis* or *trans* olefins (i.e., stilbenes) or the racemization of optically active biphenyls (disubstituted in *ortho* positions).

[10] The language we shall use here is that of L. Kassel, *Kinetics of Homogeneous Reactions* (Reinhold Publishing Company, New York, 1932).

[11] In the present treatment we have ignored the effect of other coupled processes such as $A^*(\epsilon_1) \rightleftarrows A^*(\epsilon_2)$ and $A(\epsilon_1) \rightleftarrows A(\epsilon_2)$ on the stationary distribution of $A^*(\epsilon)$. A completely rigorous treatment would include such processes and calculate the detailed partition function of A for all ϵ. Prigogine *et al.* (reference 7) have employed this more rigorous approach with the results that indicate that the present approximation is adequate. In this approximation the constants k_1, k_2, k_1', and k_2' may be considered to be weighted averages over all energies of A and B, respectively.

or

$$-d\ln A/dt=\int_{\epsilon^*}^{\infty}\frac{K_A(\epsilon)k_R(\epsilon)d\epsilon}{\left(\frac{k_R'(\epsilon)}{(M)k_2'(\epsilon)}\right)+\left(\frac{k_R(\epsilon)}{(M)k_2(\epsilon)}\right)+1} \quad (5)$$

$$=\int_{\epsilon^*}^{\infty}\frac{K_A(\epsilon)k_R(\epsilon)d\epsilon}{\frac{k_R(\epsilon)}{(M)k_2(\epsilon)}\left(1+\frac{k_R'(\epsilon)k_2(\epsilon)}{k_R(\epsilon)k_2'(\epsilon)}\right)+1}, \quad (6)$$

where $K_A(\epsilon)=k_1(\epsilon)/k_2(\epsilon)$ and is the equilibrium constant between species A and A^* (of energy ϵ).

We see that Eq. (5) for the rate of a unimolecular isomerization differs from the usual Lindemann expression for the rate of a unimolecular *decomposition* by the inclusion of a term $k_R'(\epsilon)/(M)k_2'(\epsilon)$ in the denominator of the integrand. This term is quite significant being in general of the order of magnitude of the ordinary term $k_R(\epsilon)/(M)k_2(\epsilon)$. It arises from the inclusion of species B^* in the reaction mechanism. The physical significance of this term is that even when an activated species A^* spontaneously rearranges to form activated species B^*, the species B^* can only lose its energy of activation by subsequent collision and failing this must itself spontaneously react to reform A^* (see Fig. 1).

Thus, for the isomerization reaction, it is not sufficient for the active complex to pass over the reaction barrier. It must then further be deactivated before it ceases to contribute to the back reaction—and this is true even when the rate of the reverse reaction $B\rightarrow A$ is negligibly slow!

At sufficiently high pressures such that $(M)k_2'(\epsilon)\gg k_R'(\epsilon)$ and $(M)k_2(\epsilon)\gg k_R(\epsilon)$ we obtain the usual high pressure rate law ("equilibrium" rate)

$$-(d\ln A/dt)_\infty=\int_{\epsilon^*}^{\infty}K_A(\epsilon)k_R(\epsilon)d\epsilon. \quad (7)$$

If we use the Slater theory[12] for the unimolecular reaction process we have

$$k_R(\epsilon)=\bar{\nu}\left(1-\frac{\epsilon^*}{\epsilon}\right)^{n-1} \quad \text{and} \quad k_R'=\bar{\nu}'\left(1-\frac{\epsilon^{*\prime}}{\epsilon'}\right)^{n-1}, \quad (8)$$

where $\bar{\nu}$ is a weighted root mean square average of the normal vibrational frequencies of A^* and $\bar{\nu}'$ is the same quantity for B^*.

Further, although ϵ is the energy of A^* measured from the lowest energy state of species A and ϵ^* is the critical energy measured from the same origin, ϵ' and ϵ'^* represent the energy and critical energy, respectively, of the complex B^* measured from the zero of energy of B. Thus, $\epsilon=\epsilon'+\Delta E$ and $\epsilon^*=\epsilon'^*+\Delta E$, where $\Delta E=$ the internal energy change in the reaction or for an ideal gas the heat of reaction (since there is no change in number of moles). It can be shown by an extension of the Slater treatment that for the model employed[13] $\bar{\nu}=\bar{\nu}'$ so that

$$\frac{k_R'(\epsilon)}{k_R(\epsilon)}=\left(\frac{\epsilon}{\epsilon'}\right)^{n-1}=\left(\frac{\epsilon}{\epsilon-\Delta E}\right)^{n-1}. \quad (9)$$

If the energy of the reaction is zero, then $k_R=k_R'$. If the reaction is exothermic ($\Delta E<0$), then $\epsilon<\epsilon-\Delta E$ (note that $\epsilon-\Delta E\geqslant 0$); and from Eq. (9), $k_R'(\epsilon)<k_R(\epsilon)$. Conversely, if the reaction is endothermic ($\Delta E>0$), then $k_R'(\epsilon)>k_R(\epsilon)$. Depending on the energetics of the overall reaction, it is thus possible for either $k_R(\epsilon)$ or $k_R'(\epsilon)$ to determine the concentration region in which such reactions will show a marked fall-off in their apparent first-order rate constants with pressure.[14] This is a result which does not seem to have been appreciated.

The net rate of the reaction under any conditions is given by Eq. (3). It can be seen that it may be decomposed into the difference of two terms representing the forward and back reactions. These are both similar in form [see Eq. (4)] and their net behavior does not give rise to any new phenomena.[15] Because the detailed analysis of the pressure dependence of the rates has been given in an earlier paper (reference 6b) it will not be further discussed here.

In the following section we shall consider a unimolecular reaction in which the reaction process is a molecular fission. This will lead us to a description of bimolecular processes and point out an essential distinction between isomerization and fission reactions.

III. UNIMOLECULAR DECOMPOSITIONS

Consider now a reversible unimolecular decomposition into two products as given by the chemical reaction

$$D\rightleftarrows A+B. \quad (10)$$

The detailed mechanism for such a scheme may be

[12] N. B. Slater, Proc. Roy. Soc. (London) **A194**, 112 (1948); see also reference 6b.

[13] This involves making a Taylor's series expansion of the internal energy of the molecule not around the equilibrium value of the lowest level but around the saddle point corresponding to the transition state. (See references 6b and 10.)

[14] An estimate of the importance of ΔE may be obtained as follows. The average species contributing to the "high pressure" rate will have energy $\epsilon=\epsilon^*+nkT$ so that

$$k_R'(\epsilon)/k_R(\epsilon)=\left(1-\frac{\Delta E}{\epsilon^*+nkT}\right)^{1-n}.$$

Thus for $\epsilon^*/kT=35$, $n=4$, and $\Delta E=\frac{1}{2}\epsilon^*$, the value is about 7, while for $n=10$ the value is about 75 (endothermic reactions).

[15] It should be observed that at equilibrium $R=R_A-R_B=0$. If the equilibrium is achieved in a pressure region in which the falling off of the rate has become pronounced, then although $R_A=R_B$, they are not equal to the high pressure rates. This makes it possible to observe the pressure dependence of the rates in such an equilibrium system by the use of tracer techniques. The rate of attainment of equilibrium distribution of the tracer will be at the prevailing low pressure rate.

represented by the following:

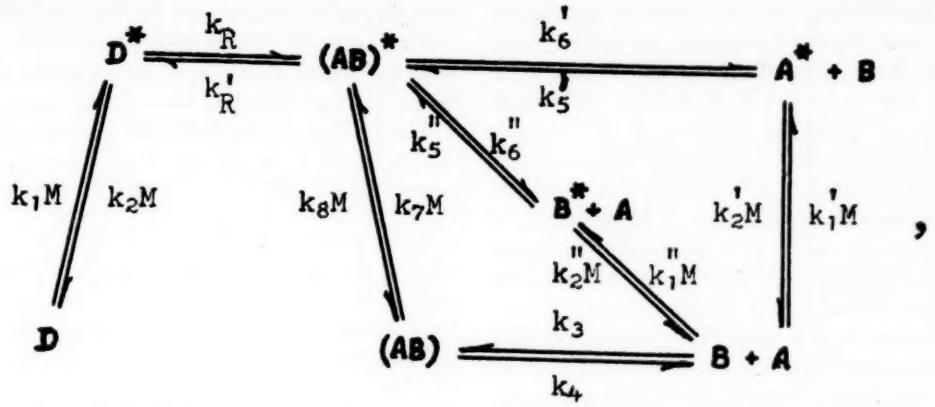

(11)

where (AB) is some loose association complex of A and B. By $(AB)^*$ we shall mean any complex of A and B which has internal energy in excess of the activation energy for the reaction, while A^* and B^* are of necessity somewhat arbitrarily defined as species having sufficiently high total energy so that a properly oriented collision with the complementary reactant (reactions 5′ and 5″) may lead to the formation of $(AB)^*$.[16]

Applying again a steady-state treatment to the intermediates D^*, $(AB)^*$, A^*, B^* and (AB), we arrive at an expression for the net rate of reaction $R=-dD/dt=dB/dt$:

$$R=\left\{\frac{(D)(M)k_Rk_1-(A)(B)(M)K_{AB}k_R'k_2}{k_R+(M)k_2}\right\}\times\left\{\frac{Z}{Z+\dfrac{(M)k_R'k_2}{k_R+(M)k_2}}\right\}, \quad (12)$$

where Z[17] is defined by

$$Z=\frac{k_2''k_6''}{k_2''+k_5''a}+\frac{k_2'k_6'}{k_2'+k_5'b}+\frac{k_4k_8(M)}{k_4+(M)k_7}, \quad (13)$$

in which $a=(A)/(M)$; $b=(B)/(M)$, the mole fractions of A and B, respectively. K_{AB} is the equilibrium constant between $(AB)^*$ and A and B.[18]

Proceeding as before, we can decompose R into two terms, $R=R_f-R_b$, where R_f is the rate of the forward reaction or the initial rate of reaction when A and B are both negligibly small. We have then

$$R_f=\left[\frac{(D)K_Dk_R}{1+\dfrac{k_R}{(M)k_2}}\right]\left[\frac{Z}{Z+k_R'\left(1+\dfrac{k_R}{(M)k_2}\right)^{-1}}\right]. \quad (14)$$

The first term in brackets in Eq. (14) represents the conventional pressure dependence to be expected of a unimolecular reaction in which $K_D=k_1/k_2$ is the equilibrium constant for the equilibrium between D and D^*. We see that the additional pressure dependence due to k_R' appears here in the second bracketed term in conjunction with the other competitive processes associated with the alternate modes of deactivation of the species $(AB)^*$.

At pressures sufficiently high so that $(M)k_2\gg\bar{k}_R$, where $\bar{k}_R$ represents the rate constant for average molecules contributing to the reaction, we have the "high pressure" or "equilibrium" limit for R_f:

$$R_{f\infty}=(D)K_Dk_R\{Z/(Z+k_R')\}, \quad (15)$$

where we must now turn our attention to Z in order to assess the importance of the remaining pressure dependence.

From Eq. (13) we see that Z depends on mole fractions (a, b) as well as total pressure (M). It can be simplified by observing that, in general, $k_4\gg k_7(M)$ since reaction 4 is a unimolecular decomposition having little or no activation energy while reaction 7 is a bimolecular reaction requiring activation energy.[19] Z can then be put in the form

$$Z=\left[\frac{k_6'}{1+(k_5'b/k_2')}+\frac{k_6''}{1+(k_5''a/k_2'')}\right]+(M)k_8 \quad (16)$$

$$=\left(\frac{k_6}{1+(k_5m/k_2)}\right)+(M)k_8=\frac{k_6}{1+K_{52}m}+(M)k_8, \quad (17)$$

[16] In a more formal calculation the reaction rates 5′, 6′, 5″, 6″ should be taken as integrated or summed over all total energies (including relative translational energy) of the pair A, B compatible with the energy range ϵ, $\epsilon+d\epsilon$ of the activated complex $(AB)^*$. This would remove the arbitrariness of defining intermediate states A^* and B^*. Such a procedure is unnecessary here, since we shall finally be concerned only with the complex $(AB)^*$, and the constants which appear in our final expression may be assumed to be the averaged, integrated rate constants for all such processes. (See reference 11.)

[17] The three terms in Eq. (13) arise from the three processes whereby $(AB)^*$ can be formed from A and B, while the terms occurring in the last denominator of Eq. (12) refer to the four processes whereby $(AB)^*$ can be destroyed.

[18] In the absence of reaction we have the equilibrium relations

$$(AB)_{eq}{}^*=\frac{k_5''}{k_6''}(A)(B^*)=\frac{k_5'}{k_6'}(A^*)(B)=\frac{k_7}{k_8}(AB)$$

$$\frac{k_1''k_5''}{k_2''k_6''}(A)(B)=\frac{k_1'k_5'}{k_2'k_6'}(A)(B)=\frac{k_3k_7}{k_4k_8}(A)(B)=K_{AB}(A)(B),$$

which relate the various rate constants to the equilibrium constant K_{AB} for the equilibrium between $(AB)^*$ and $A+B$.

[19] Under these conditions $k_4\approx\bar{\nu}\approx10^{13}$ sec^{-1} (neglecting any activation energy involved in overcoming van der Waals' attraction which will be small), while $k_7(M)$ will be of the order of magnitude of $10^{11}e^{-E/RT}$ sec^{-1} when $(M)=1$ mole/liter, which is a much smaller quantity.

where we have replaced the bracketed term in Eq. (16) by the single term in Eq. (17) in which k_6 represents some average rate for all processes whereby $(AB)^*$ dissociates with varying distributions of its energy between A and B (see footnote 16), k_5 and k_2 are similarly interpreted, and m is also some average of the mole fractions of A and B. The ratio $k_5/k_2=K_{52}$ for the specific, averaged rates of the process of "sticky" collision to collisional deactivation is difficult to evaluate. We should expect it to have an order of magnitude of about unity, but there is no good experimental evidence on this point.

Let us now consider the bracketed term in Z [Eq. (14)] which gives the effect of the back reaction (of AB^*) on the forward reaction. This term takes the form

$$\frac{[k_6/(1+K_{52}m)]+(M)k_8}{\dfrac{k_6}{1+K_{52}m}+(M)k_8+\dfrac{k_R'}{(1+[k_R/(M)k_2])}}. \tag{18}$$

Again applying the Slater theory to k_6 we see that it will have a value close to 10^{13} sec^{-1} (see footnote 19), whereas $(M)k_8$ will be less than 10^{11} sec^{-1} at any reasonable pressures. Thus, unless $K_{52}m\gg 1$, which is unlikely, we may neglect the terms $(M)k_8$ in expression 18. Now applying the Slater theory to k_R' we can write $k_6/k_R'=(1-\epsilon^{*\prime}/\epsilon')^{1-n}\geqslant 1$, so that even when the critical energy $\epsilon^{*\prime}$ of the reverse reaction is small $k_6>k_R'$, and if $K_{52}m\leqslant 1$, expression 18 will be close to unity.[20] When the critical energy $\epsilon^{*\prime}$ is large, then $k_6\gg k_R'$ and the term 18 is unity.

We observe then, the rather interesting result that the rate of the initial reaction for a fission reaction has the form [Eq. (14)]

$$R_f=\frac{(D)K_Dk_R}{1+[k_R/(M)k_2]}, \tag{19}$$

while the "high pressure" rate has the form (Eq. [15)]

$$R_{f\infty}=(D)K_Dk_R, \tag{20}$$

so that the process of reverse reaction of the activated complex is unimportant under all conditions. This is in distinct contrast to the result obtained for isomerization reactions when the same process could be as important or more important than the activation processes [Eq. (4)]. The reason for this physically is that the process of fission of an activated species into two fragments is so much faster than all other processes that once an activated complex is formed, capable of such fission, it reacts predominantly along this path.[21]

[20] Observe that when the critical energy $\epsilon^{*\prime}$ is zero (which may occur if A and B are free radicals), then B^* and B are identical (also A^* and A) so that k_2 is in essence infinitely large compared to k_5 and $K_{52}=0$. That is, every collision of A and B forms $(AB)^*$ without the intermediary stages A^* and B^*.

[21] At sufficiently high concentrations (e.g., in solution) the term $(M)k_8$ in expression 18 is no longer negligible and may dominate the expression. However, there will still be no pressure dependence since the numerator and denominator are equally affected and k_R' is still negligible.

There is one special case worthy of note in this category of reactions, and that is the case in which the critical energy of the reverse reaction $\epsilon^{*\prime}$ is zero or negative. Such a case may be expected to occur in the fission of a molecule into free radicals (e.g., $N_2O_4\rightleftarrows 2NO_2$; $C_2H_6\rightleftarrows 2CH_3$; $N_2O_2\rightleftarrows 2NO$). We would then expect that $k_6\approx k_r'$; and if we assume $K_{52}m<1$ and $Mk_8<k_6$, then term 18 reduces to

$$\frac{1+[k_R/Mk_2]}{2+[k_R/Mk_2]}. \tag{21}$$

If we substitute this back in the equation for R_f, the initial rate of reaction (Eq. (14)), we have

$$R_f=\frac{(D)K_Dk_R}{2+[k_R/Mk_2]}. \tag{22}$$

In the "high pressure" limit, $Mk_2\gg k_R$, this becomes

$$R_{f\infty}=\frac{(D)K_Dk_R}{2}, \tag{23}$$

while for the low pressure limit

$$R_{f0}=(D)(M)k_2K_D=(D)(M)k_1. \tag{24}$$

The chief difference is in the high pressure limit. We see that $R_{f\infty}$ for the fission into free radicals [Eq. (23)] has only half the value that it would normally have [Eq. (20)], while the low pressure limit is the same for both cases. The reason for this physically is that, since $k_6=k_{R'}$, every complex $(AB)^*$ that is formed has an equal chance of splitting directly into $A+B$ or of forming D^*. At high pressures the half that form D^* will be predominantly deactivated to D before reforming $(AB)^*$ and the limiting rate is half its expected value. At low pressures the converse is true, namely, activation and deactivation of D^* is so much slower than the processes for equilibrium between D^* and $(AB)^*$ and also the splitting of $(AB)^*$ that only the initial activation process k_1 is important. In the intermediate region the expression (22) must be integrated over all energies $\epsilon\geqslant\epsilon^*$ to give the over-all reaction rate.

IV. BIMOLECULAR REACTIONS

A. Associations

This case is the inverse of that just treated, namely, unimolecular decompositions and the chemical equation is given by Eq. (10), while the rate of the initial reaction is given by R_b. From Eq. (12) we have

$$R_b=\frac{(A)(B)(M)K_{AB}k_R'k_2}{k_R+(M)k_2}\times\left\{\frac{Z}{Z+[(M)k_R'k_2/k_R+(M)k_2]}\right\}. \tag{25}$$

From the preceding discussion we see that the bracketed term in Z has the value unity and so may be omitted. The result is that R_b is given by

$$R_b = R_{b\infty}\left(\frac{(M)k_2}{k_R+(M)k_2}\right), \tag{26}$$

where $R_{b\infty}=k_{AB}(A)(B)k_R'=$ the "high pressure" or "equilibrium" rate of reaction. We see that these bimolecular association reactions will have the same type of pressure dependence as that found for the unimolecular decomposition reactions, namely, that arising from the need for deactivation of the final activated product. The activation processes for formation of the initial complex $(AB)^*$ are in essential equilibrium and do not contribute to the pressure dependence for the reasons already discussed in the preceding section.[22]

B. Metatheses

These can be represented by the chemical equation

$$A+B\rightleftarrows C+D. \tag{27}$$

If we proceed to set up a symmetrical scheme analogous to the right-hand side of Eq. (11), we can carry through the stationary state calculations for the active intermediates and we arrive at an expression resembling Eq. (12)

$$R=[(A)(B)K_{AB}k_R-(C)(D)K_{CD}k_R']\times\left[\frac{ZZ'}{ZZ'+k_RZ'+k_R'Z}\right]. \tag{28}$$

It can be shown that the bracketed expression in Z and Z' [23] is essentially unity under all conditions, so that these systems of reactions are at all times independent of total pressure and the forward and back reactions follow at all times the high pressure or equilibrium rates.[24]

It can be seen by an extension of these and preceding arguments that all higher order reactions will also follow an equilibrium rate law and the rate constant will show no pressure dependence unless one of the steps in the scheme is unimolecular.

V. A COMPARISON OF THE DETAILED AND EQUILIBRIUM THEORIES

In conclusion, it is of some interest to compare the methods and nomenclature employed in the detailed (or collision) study of kinetic processes with that of the transition state or equilibrium treatment. The two approaches are best exemplified in terms of the schematic diagram shown in Fig. 1 for the chemical reaction (exothermic) of Reactants $(R)\rightarrow$Products (P).

In the transition state theory it is assumed that there is a set of configurations $T^\ddagger$ corresponding to the saddle point in the energy diagram. It is then assumed that these are in thermodynamic equilibrium with either the reactants R or products P, depending on whether the rate of forward or reverse reaction is to be calculated. The rate of reaction is then simply the concentration of these configurations $(T^\ddagger)$ times their rate of motion over the barrier. From the preceding work it is clear that such an assumption is valid only for those processes in which the motions of $T^\ddagger$ at the barrier corresponds to decomposition reactions. For reactions in which there is involved only a single species (product or reactant) such that its reaction in the system is unimolecular, the equilibrium hypothesis holds only in the region of high relative concentrations. Outside this region the theory fails badly and is incapable of representing the steady-state reaction.

The detailed theory discussed here introduces a more complex model in that it is presented in terms of two complexes, one for the reactants R^* and one for the products P^*. However, the cases of unimolecular isomerizations and association reactions which have been discussed here show the need for such a pair of complexes in presenting an adequate account of the steady state reactions. An important advantage of the detailed theory is that it presents a more complete model of the specific mechanics of a chemical reaction, and thus permits a unified approach to both stationary and equilibrium reaction processes.

VI. ACKNOWLEDGMENTS

One of the authors (S.W.B.) would like to express his indebtedness to the U. S. Office of Ordnance Research for a grant which made the present work possible.

[22] It is interesting to consider the effect of van der Waals' attractions between the separating species A and B. In this case there will be an energy requirement for the dissociation of the ground state of $(AB)^*$ complex into A and B, and this enhances the mean life time of $(AB)^*$. Unless the energy is large (which is unlikely) compared to kT, this enhancement does not contribute appreciably nor does it then affect the above arguments. Its effect may be observable in the association of free radicals, where it may show up as a negative temperature coefficient for the rate constant even in a region of no total pressure dependence. The attraction of two NO radicals has been recently measured at ~2 kcal [A. L. Smith and H. L. Johnston, J. Am. Chem. Soc. 74, 4696 (1952)], and it is this which accounts for the negative temperature coefficient of the $NO+O_2$ reaction. Dr. K. Ingold has recently described a similar result obtained in the study of methyl radical recombination (private communication).

[23] Z' is defined in symmetrical fashion to Z [see Eqs. (11) and (13)].

[24] This corrects an assertion made in a previous paper (reference 6b) that there may be a small but limited pressure dependence of bimolecular processes at sufficiently low pressures. The factor α [Eq. (19), reference 6b] included in the equation for the bimolecular rate constant had been earlier calculated to vary between 1 at high pressure to a minimum of $\frac{1}{2}$ at lowest pressures. We see the above discussion that this is not correct.

A Theory of Cooperative Phenomena. III. Detailed Discussions of the Cluster Variation Method

MICHIO KURATA, *Department of Industrial Chemistry, Kyoto University, Kyoto, Japan,*
RYOICHI KIKUCHI,* *Department of Physics, University of Tokyo, Tokyo, Japan,*

AND

TATSURO WATARI, *Faculty of Liberal Arts and Education, Yokohama National University, Kamakura, Japan*

(Received August 25, 1952)

A series of approximations for the statistical mechanics of order-disorder, proposed by Bethe, Takagi, Yang-Li-Hill, Kikuchi, and others, are investigated in detail in two ways. (1) A new interpretation of the method for constructing the combinatory factor is presented in order to give a better understanding of the nature of approximations. (2) The partition functions with approximate combinatory factors are expanded to compare with the rigorous expansion and the discrepancies between them are investigated in detail. One of the conclusions is that in order to obtain a higher approximation, it is *necessary* to use the basic figure "closed" with respect to the cluster of the preceding approximation. In appendices, an improved treatment of the body-centered cubic lattice (Ising model) is given, and Bethe's fundamental assumptions are derived from our scheme.

I. INTRODUCTION

AFTER the pioneering work of Bragg-Williams[1] and Bethe[2] concerning the problem of order-disorder, many attempts have been made to improve their approximations. Extending Takagi's[3] interpretation of Bethe's work, one of the authors[4] proposed a method of approximation which not only leads us to the Kramers-Wannier approximation[5] for the two-dimensional square lattice, but also gives us improved treatments of the three-dimensional Ising problems. The feature of the method lies in proper construction of *combinatory factors*,[6] denoted by G in TCP I, which give the entropy of the system in terms of basic figures.[7]

The idea of improving the approximation by introducing larger clusters as the basic figure was also developed independently by Yang and Li[8,9] and Hill,[10] in the method called the "generalized quasi-chemical method." These methods are extensions of the original work of Bethe[2] in the sense that they take into account correlations between elements (atoms, molecules, spins, etc.) more exactly than the latter, and also that they offer a possibility of including the interaction energies between elements farther apart than the nearest neighbors. The series of approximations mentioned so far, especially those of Takagi, Kikuchi, and Yang-Li-Hill, might be called the "cluster variation method," as the free energy is minimized with respect to variables related to clusters.

Though it seems to be an essential advantage of the cluster variation method that the approximate treatment of the three-dimensional problems can be performed in a closed form without much mathematical difficulty, it is not free from the disadvantage that the intrinsic nature of the approximation remains ambiguous. In this connection, it was pointed out by several authors[4,9,11] that the adoption of larger clusters as a basic figure does not necessarily allow us to improve the approximation. Such a case was reported in TCP I,[12] but the reason for it has been left unsolved. In view of these situations and of the fact that this method may find various fields of application,[13–15] it may be worth while to report here a different approach of constructing the combinatory factor, which contributes to clarifying the nature of the approximations. This new method is explained in sections A to E.

In order to investigate the problem more thoroughly, another approach is explained in Secs. G to I, where the partition functions with approximate combinatory factors are expanded; and by making comparison with the rigorous expansions of Oguchi,[16] the discrepancies between them are examined to reveal the nature of the approximation. All the explanations will be made on the Ising model of ferromagnetism throughout the paper, and some of the special symbolisms and idioms

* Present address: Department of Physics, Massachusetts Institute of Technology, Cambridge, Massachusetts.

[1] W. L. Bragg and E. J. Williams, Proc. Roy. Soc. (London) **A145**, 699 (1934).

[2] H. A. Bethe, Proc. Roy. Soc. (London) **A150**, 552 (1935).

[3] Y. Takagi, Proc. Phys.-Math. Soc. Japan **23**, 44 (1941).

[4] R. Kikuchi, Phys. Rev. **81**, 988 (1951). This paper will be cited as TCP I.

[5] H. A. Kramers and G. H. Wannier, Phys. Rev. **60**, 252, 263 (1941).

[6] This terminology was adopted from R. H. Fowler and E. A. Guggenheim's *Statistical Thermodynamics* (Cambridge University Press, Cambridge, England, 1939), Eq. (821.1).

[7] Some of the terminologies will be adopted from TCP I without explanation.

[8] C. N. Yang, J. Chem. Phys. **13**, 66 (1945); C. N. Yang and Y. Y. Li, Chinese J. Phys. **7**, 59 (1947); Y. Y. Li, J. Chem. Phys. **17**, 447 (1949).

[9] Y. Y. Li, Phys. Rev. **76**, 972 (1949).

[10] T. L. Hill, J. Chem. Phys. **18**, 988 (1950).

[11] See reference 6, Sec. 609.

[12] TCP I, reference 16.

[13] R. Kikuchi, J. Chem. Phys. **19**, 1230 (1951).

[14] T. Oguchi, J. Chem. Phys. **19**, 1321 (1951).

[15] It is perhaps well to point out here that the method developed in TCP I seems to give identical results as Yvon's method, though they start from different points of view. See J. Yvon, Cahiers phys. **28**, 1 (1945); G. Fournet, Phys. Rev. **85**, 692 (1952).

[16] T. Oguchi, J. Phys. Soc. Japan **6**, 27, 31 (1951).

follow those given in TCP *I*, to which reference may be made if necessary.

II. PSEUDO-ASSEMBLY METHOD

In TCP *I*, one of the authors has given a general method of constructing approximate combinatory factors. Here we give an alternative one, which will help us to understand the nature of the approximation and make it possible to rank various methods according to their own natures.

A. Linear Ising Lattice

We begin with a linear Ising lattice, shown in Fig. 1(a), composed of $N+1$ lattice points, each of which is filled by (+) or (−) spins. The probabilities of appearance of (+) and (−) spins are denoted by x_1 and x_2, and those of bonds having the configurations, (++), (+−), (−+), and (−−), by y_1, y_2, y_2, and y_3, respectively, as shown in Table I. Without loss of generality, the configurations (+−) and (−+) can be assumed to have the same probability of appearance due to their symmetry. β_i indicates the number of different configurations having the same probability. x_i's and y_i's are normalized by

$$x_1+x_2=1, \quad \text{and} \quad \sum_{i=1}^{3}\beta_i y_i=1, \tag{A.1}$$

and they are related by

$$x_1=y_1+y_2. \tag{A.2}$$

The abbreviated notations introduced in TCP *I*,

$$\begin{cases} X_N\equiv(x_1N)!(x_2N)! \\ Y_N\equiv\prod_{i=1}^{3}\{(y_iN)!\}^{\beta_i}, \end{cases} \tag{A.3}$$

will be used in the present paper. We say that the assembly of N lattice points has r.d. (right distribution) in spins when x_1N points have (+) spins and x_2N points have (−) spins. Similarly, we say that the assembly of

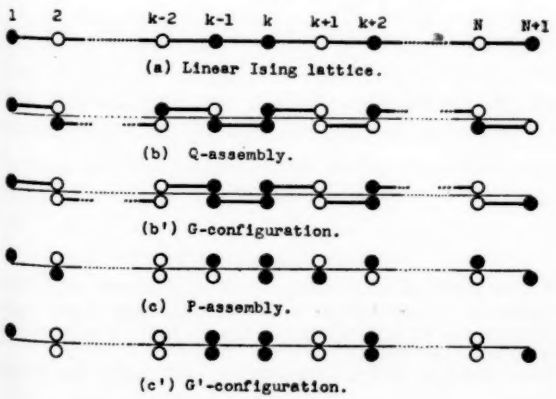

FIG. 1. Original linear Ising lattice, Q assembly, and P assembly.

TABLE I. Probabilities of appearances of spins and spin pairs. (+) spin is represented by ●, and (−) spin by ○.

Spin	Prob.	Pair	Prob.	β_i*	ε_i**
●	x_1	●—●	y_1	1	$-\varepsilon$
		●—○ ○—●	y_2	2	$+\varepsilon$
○	x_2	○—○	y_3	1	$-\varepsilon$

* β_i indicates the number of different configurations having the same probability.
** ε_i denotes the energy per spin pair.

N bonds has r.d. in pairs when y_1N bonds have (++) configurations, y_2N have (+−), y_2N have (−+), and y_3N have (−−). It should be noted that, when the assembly of N bonds has r.d. in pairs, the assembly of N right (or left) end points has r.d. in spins, because of the relation (A.2).[16a]

Now our problem is to obtain the combinatory factor G, with specified values of x_i's and of y_i's, i.e., the number of distinguishable configurations of the lattice having r.d. both in spins and in pairs. We proceed as follows.

(1) We distribute spin pairs on N bonds to make an assembly of N bonds having r.d. only in pairs as illustrated in Fig. 1(b). In this case each bond is assumed perfectly independent. Therefore such a configuration as the one shown in the figure, in which two different spins belong to the same lattice point, is included. For convenience, such an assembly is called a Q assembly. The number of distinguishable configurations of the Q assembly is denoted by the same letter Q, which is given by

$$Q=N!/(y_1N)!\{(y_2N)!\}^2(y_3N)!=N!/Y_N. \tag{A.4}$$

(2) Distribute $2N$ spins on the upper and the lower sides of the lattice to make an assembly of $2N$ spins having r.d. in spins as shown in Fig. 1(c), and call the one thus constructed a P assembly. The number of distinguishable configurations of the P assembly is denoted by the same letter P, and is given by

$$P=(2N)!/(2Nx_1)!(2Nx_2)!=[N!/X_N]^2. \tag{A.5}$$[16b]

(3) In the Q assembly, there are configurations in which two spins located on the same lattice point coincide with each other as shown in (b′). We call such a configuration a G configuration, since the number of such configurations is G itself in question. The probability of the occurrence of a G configuration in the Q assembly is denoted by Γ,

$$\Gamma=G/Q. \tag{A.6}$$

(4) Similarly, in the P assembly, there are G' configurations as shown in (c′). The probability of the occurrence, Γ', of a G' configuration in the P assembly

[16a] See the footnote 18.
[16b] As we are usually interested in assemblies with sufficiently large N, we can safely use Stirling's formula. See reference 19.

is given by

$$\Gamma' = G'/P, \tag{A.7}$$

where G' is the number of G' configurations, and is equal to the number of distinguishable configurations of the lattice having r.d. in spins only. G' is given by

$$G' = (N+1)!/X_{N+1}. \tag{A.8}$$

(5) Making a comparison of the role of Γ with that of Γ', we find an essential similarity between them: Γ selects G configurations, which have r.d. both in spins and in pairs, from the Q assembly which has been assured to have r.d. both in spins and in pairs; Γ', on the other hand, selects G' configurations, having r.d. in spins, from the P assembly which has been assured only to have r.d. in spins. Hence, we have the following identity:

$$\Gamma = \Gamma'. \tag{A.9}$$

This identity can be interpreted in more detail as follows. Suppose one constructs a Q assembly, shown in Fig. 1(b), adding bonds one by one from the left end and that one has proceeded until a certain upper bond. In the next step, when one puts a spin at the lower point opposite to the right end of the last bond, one can choose a plus or a minus spin with the probability of x_1 or x_2, respectively, independent of the sign of the upper spin. In other words one has freedom of choosing the sign of the lower spin. This freedom contributes a value, say γ, to Q. On the other hand, in a G configuration, there is no freedom of choosing the sign of the lower spin when that of the upper spin is determined. Therefore γ gives rise to a difference between G and Q. Considering that this type of freedom appears at each doubly occupied lattice point, $N-1$ times before the Q assembly is completed, and that there is no other source of difference between Q and G, as the two end points are independent of each other in G as well as in Q,[17] one obtains

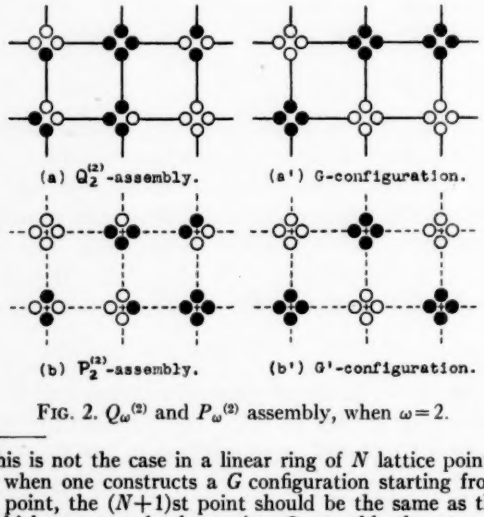

FIG. 2. $Q_\omega^{(2)}$ and $P_\omega^{(2)}$ assembly, when $\omega=2$.

the following relation:

$$1/\Gamma = Q/G = \gamma^{N-1}. \tag{A.10}$$

Similarly in a P assembly, shown in Fig. 1(c), it is recognized that the same freedom as of Q exists in choosing the sign of the lower spin when that of the upper spin is fixed, and comparing with G' in which there is no such freedom, one obtains

$$1/\Gamma' = P/G' = \gamma^{N-1}. \tag{A.11}$$

Equation (A.9) is a consequence of Eqs. (A.10) and (A.11).

(6) From Eqs. (A.4)–(A.9), using Stirling's formula, we obtain the relation

$$G = Q\Gamma' = (X_N/Y_N)(N!X_N)^{1/N}. \tag{A.12}$$

One can prove this to be rigorous by using the method of Sec. A, TCP *I* and taking into account the end effect correctly. When N is large enough, we can safely neglect the second factor in comparison to the first one in the above formula and arrive at Eq. (A.6) of TCP *I*,

$$G = X_N/Y_N. \tag{A.13}$$

We shall use the word "pseudo-assembly" in such a way that the P assembly is the pseudo-assembly of the Q assembly. As the proper construction of the P assembly plays the essential rôle in the method outlined above, it may be called the "pseudo-assembly" method.

B. Bethe's Approximation

For brevity's sake, let us hereafter call an assembly of qN points having r.d. only in spins a $Q_q^{(1)}$ assembly, and an assembly of qN bonds having r.d. in pairs a $Q_q^{(2)}$ assembly. In general, when an assembly of qN identical figures, each of which contains n points and should be properly called an n cluster, has r.d. in n clusters, it is called a $Q_q^{(n)}$ assembly.[18] The number of distinguishable configurations of a $Q_q^{(n)}$ assembly is also denoted by the same letter $Q_q^{(n)}$. For example,

$$\begin{aligned} &Q_1^{(1)} = N!/X_N, \quad Q_1^{(2)} = N!/Y_N, \\ &Q_q^{(2)} = (qN)!/Y_{qN}. \end{aligned} \tag{B.1}[19]$$

Now let us consider a lattice having N points, and denote combinatory factor by $G_q^{(n)}$ if it is constructed from $Q_q^{(n)}$ assembly. Hence, the combinatory factor corresponding to the Bragg-Williams approximation

[17] This is not the case in a linear ring of N lattice points. Because, when one constructs a G configuration starting from one lattice point, the $(N+1)$st point should be the same as the one from which one started, whereas in a Q assembly these two points may be different. This situation leaves Eq. (A.9) only approximate. Actually, though one obtains Eqs. (A.4), (A.5), and

$$G' = N!/X_N,$$

for the linear ring, the correct formula for G is

$$G = (X_N/Y_N)(y_2/x_1x_2) \neq QG'/P.$$

[18] Since relations such as Eq. (A.2) always hold between the probabilities of appearance of an n cluster and those of their subcluster, r.d. in a subcluster of the n cluster is automatically assured in a $Q_q^{(n)}$ assembly.

[19] By applying Stirling's formula, we can rewrite Eq. (B.1) as follows:

$$Q_q^{(n)} = \{Q_1^{(n)}\}^q, \quad \text{e.g.,} \quad Q_q^{(2)} = (N!/Y_N)^q. \tag{B.1'}$$

Relations of this kind will be frequently used without remarks.

(hereafter called the zeroth approximation) is written as follows:

$$G_1^{(1)}=Q_1^{(1)}=N!/X_N. \tag{B.2}$$

The purpose of the present section is to construct the combinatory factor $G_\omega^{(2)}$ of a lattice with coordination number 2ω having r.d. in ωN bonds. To do this, we make a $Q\omega^{(2)}$ assembly as shown in Fig. 2(a), from which G configurations as illustrated in (a') are selected with the probability

$$\Gamma=G_\omega^{(2)}/Q_\omega^{(2)}, \tag{B.3}$$

because the number of G configurations is $G_\omega^{(2)}$. The $P_\omega^{(2)}$ assembly, the pseudo-assembly of the $Q_\omega^{(2)}$ assembly, is constructed as shown in (b), and we have

$$P_\omega^{(2)}=Q_{2\omega}^{(1)}=(N!/X_N)^{2\omega}. \tag{B.4}$$

Hence, we can put

$$\Gamma'=G_1^{(1)}/P_\omega^{(2)}=(N!/X_N)^{1-2\omega}, \tag{B.5}$$

because the number of G' configurations, as shown in (b'), selected from a $P_\omega^{(2)}$ assembly must be equal to the combinatory factor $G_1^{(1)}$ of the zeroth approximation given above.

Following Eq. (A.9) of the one-dimensional case, it seems plausible to assume the relation

$$\Gamma=\Gamma', \tag{B.6}$$

Though there is no rigorous justification for this relation, this may be understood by the following discussion. In the process of building up a Q or a P assembly, we have freedom of putting spins of different sign at a lattice point, whereas we do not have such free choice in a G or a G' configuration. This difference in the freedom at each lattice point makes up Γ and Γ', as was the case in the previous section. But in the present section, the relation of $Q_2^{(2)}$ to G is not exactly the same as that of $P_2^{(2)}$ to G', by the reason similar to that explained for a linear ring in footnote 17.

Inserting Eqs. (B.3) and (B.5) into Eq. (B.6), one obtains

$$G_\omega^{(2)}=G_1^{(1)}[Q_\omega^{(2)}/P_\omega^{(2)}]=X_N{}^{2\omega-1}/(N!)^{\omega-1}Y_N{}^\omega, \tag{B.7}$$

which is the relation already derived by various authors, and is known to lead to Bethe's first approximation.[20] Thus the assumption (B.6) is proved to be exactly the origin of the approximation in the formula (B.7). In the following, the relation of the type (B.6) will be called, in short, the "pseudo-assembly approximation." Hereafter we shall frequently call the Bethe approximation the first approximation.

As a preparation of the next section, we consider in general an assembly of rN points connected by sN bonds. The assembly will be called a $g_r^{(1)}$ assembly when it has r.d. only in spins, and a $g_{s,r}{}^{(2)}$ assembly when it has r.d. both in spins and in pairs. An example

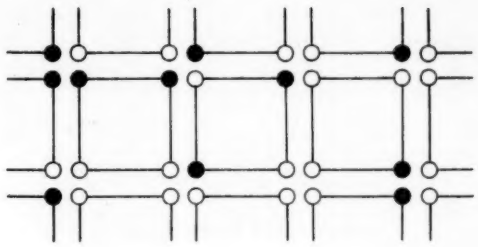

FIG. 3. $g_{4,4}{}^{(2)}$ or $g_{1,4,4}{}^{(4)}$ assembly.

of a $g_{4,4}{}^{(2)}$ assembly is shown in Fig. 3.[21] By definition,

$$g_r^{(1)}=Q_r^{(1)}=(N!/X_N)^r. \tag{B.8}$$

$g_{s,r}{}^{(2)}$ can be obtained from $Q_s^{(2)}$ and $P_s^{(2)}$ as before, and is given by

$$g_{s,r}{}^{(2)}=g_r^{(1)}[Q_s^{(2)}/P_s^{(2)}]=X_N{}^{2s-r}/(N!)^{s-r}Y_N{}^s. \tag{B.9}$$

$g_r^{(1)}$ and $g_{s,r}{}^{(2)}$ can be regarded as combinatory factors of the zeroth and the first approximations, respectively. Equation (B.9) includes Eq. (B.7), because the latter can be expressed as $g_{\omega,1}{}^{(2)}$.

C. Kramers-Wannier Approximation (Two-Dimensional Square Lattice)

A two-dimensional square lattice with N lattice points has N squares and $2N$ bonds. Our problem is to obtain combinatory factor $G_1^{(4)}$ of the assembly having r.d. in square clusters. We denote the probabilities of appearances of six kinds of square clusters by z_i's,[22] and put

$$\prod_{i=1}^{6}\{(z_iN)!\}^{\gamma_i}\equiv Z_N\equiv\{\text{Square}\}_N. \tag{C.1}$$

Now, we distribute N square clusters, one to each of the square cells to make a $Q_1^{(4)}$ assembly. The number of distinguishable configurations of the assembly is

$$Q_1^{(4)}=N!/Z_N. \tag{C.2}$$

Next we construct the $P_1^{(4)}$ assembly, i.e., the pseudo-assembly of the $Q_1^{(4)}$ assembly. As the $Q_1^{(4)}$ assembly is an assembly of N squares, $4N$ bonds, and $4N$ points, it seems natural to adopt for the $P_1^{(4)}$ assembly such an assembly of $4N$ bonds and $4N$ points as is shown in Fig. 3. Then putting $r=s=4$ in Eq. (B.9), we get

$$P_1^{(4)}=g_{4,4}{}^{(2)}=(X_N/Y_N)^4. \tag{C.3}$$

In the present case, both G and G' configurations to be selected from the $Q_1^{(4)}$ and the $P_1^{(4)}$ assembly, respectively, are those in which two pairs located on the

[20] For $\omega=1$, Eq. (B.7) reduces to Eq. (A.11). The footnote 11 of TCP *I*, which excludes the value $2\omega=3$, is not necessary. Eq. (B.7) holds also for the honeycomb net with $\omega=\frac{3}{2}$.

[21] However, it should be noted that the specification of s and r does not uniquely fix the geometrical figure of the assembly. For instance, besides the one shown in Fig. 3, a closed linear ring composed of $4N$ points, and consequently of $4N$ bonds, is also a $g_{4,4}{}^{(2)}$ assembly.

[22] TCP *I*, Table III.

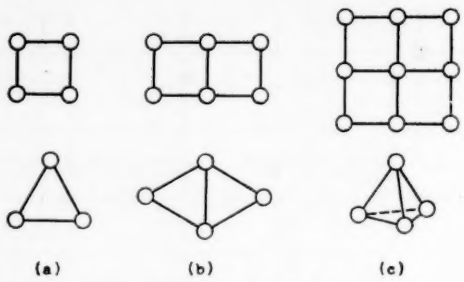

FIG. 4. Examples of *open* and *closed* clusters.

same bond coincide with each other. Hence, the number of G configurations is $G_1^{(4)}$ itself, and that of G' configurations is obviously $G_2^{(2)}$. Accordingly, we can write, with the pseudo-assembly approximation,

$$G_1^{(4)}=G_2^{(2)}[Q_1^{(4)}/P_1^{(4)}], \tag{C.4}$$

which, with Eqs. (B.7), (C.2), and (C.3), leads to Eq. (C1.5) of TCP *I*, i.e.,

$$G_1^{(4)}=Y_N^2/X_NZ_N. \tag{C.5}$$

In TCP *I*, it has been shown that the method using $G_1^{(4)}$ is equivalent to Kramers-Wannier's "variation method."[5]

We have to say a word here concerning the proper construction of the pseudo-assembly. We can postulate the following rule:

"The pseudo-assembly should be constructed in terms of the largest *closed* subcluster which is shared by any adjacent n clusters."

The words "open" and "closed" are defined in the following way. If the probabilities of appearance of a cluster B can be (cannot be) derived rigorously from those of its subcluster A, B is said to be open (closed) with respect to A. For instance, in Fig. 4, (b) is *open* and (c) is *closed* with respect to (a), if the potential energy is assumed to be contributed only from the nearest neighbor pairs. Because, the probability of appearance of, for instance, a rhombus in Fig. 4(b) is *rigorously* written as a product of the probabilities of the right and the left triangles divided by the probability of the bond in the middle. The number of independent probabilities of the configurations of (a) and (b) are equal. In the present case of the $Q_1^{(4)}$ assembly, subclusters which are shared by any adjacent squares are a point and a bond, of which the latter is the largest closed subcluster.

Again as a preparation of the following sections, we consider an assembly having tN squares, sN bonds, and rN points. The assembly having r.d. in square clusters will be called a $g_{t,s,r}^{(4)}$ assembly. In Fig. 3, a $g_{1,4,4}^{(4)}$ assembly is illustrated as an example. $g_{t,s,r}^{(4)}$ can be obtained from $Q_t^{(4)}$ and $P_t^{(4)}$ as above, and is given by

$$g_{t,s,r}^{(4)}=g_{s,r}^{(2)}[Q_t^{(4)}/P_t^{(4)}], \tag{C.6}$$

which can be written, with Eqs. (B.9), (B.1′), (C.2), and (C.3), as

$$g_{t,s,r}^{(4)}=(N!)^{t-s+r}Y_N^{4t-s}/X_N^{4t-2s+r}Z_N^t. \tag{C.7}$$

Equation (C.7) includes Eq. (C.4), which can be written as $g_{1,2,1}^{(4)}$.

D. Simple Cubic Lattice

A simple cubic lattice with N lattice points has $3N$ squares and $3N$ bonds. Hence the combinatory factor of the assembly having r.d. in square clusters, denoted by $G_3^{(4)}$, can be obtained by putting $t=s=3$ and $r=1$ into Eq. (C.7), i.e.,

$$G_3^{(4)}=g_{3,3,1}^{(4)}=N!Y_N^9/X_N^7Z_N^3, \tag{D.1}$$

which is already given in TCP *I* as Eq. (D1.1). Hereafter, the methods of approximation using combinatory factors given by Eqs. (C.5) and (D.1) are called the second approximation of the respective lattice.

A more precise picture of the simple cubic lattice is obtained by the introduction of cubic clusters each of which has eight spins. As the lattice with N points has also N cubic cells, we select $G_1^{(8)}$ from the $Q_1^{(8)}$ assembly,

$$Q_1^{(8)}=N!/\{\text{Cube}\}_N, \tag{D.2}$$

where $\{\text{Cube}\}_N$ is the abbreviated notation having the similar meaning as $\{\text{Square}\}_N$ in Eq. (C.1). For the $P_1^{(8)}$ assembly, we adopt a $g_{6,12,8}^{(4)}$ assembly, following the rule in the previous section, and because the largest *closed* subcluster shared by adjacent cubes in the simple cubic lattice is a square on a face of each cube. Hence, from Eq. (C.7), we get

$$P_1^{(8)}=g_{6,12,8}^{(4)}=(N!)^2Y_N^{12}/X_N^8Z_N^6. \tag{D.3}$$

The number of G' configurations to be selected from $P_1^{(8)}$ is obviously $G_3^{(4)}$, which is given by Eq. (D.1). Thus we obtain

$$\begin{aligned}G_1^{(8)}&=G_3^{(4)}[Q_1^{(8)}/P_1^{(8)}]\\&=X_NZ_N^3/Y_N^3\{\text{Cube}\}_N.\end{aligned} \tag{D.4}$$

The method of approximation using $G_1^{(8)}$ is regarded as the third approximation of the simple cubic lattice. Some of the improved results obtained by this approximation are already given in Sec. D7 of TCP *I*.

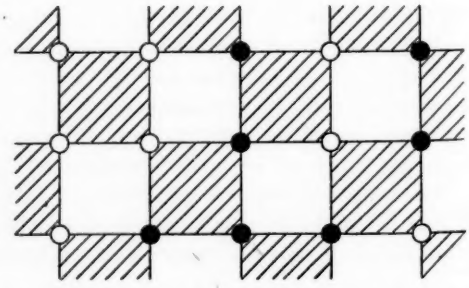

FIG. 5. Configuration of squares assured to have r.d. in square clusters in $G_1^{(4)}$.

E. Yang-Li-Hill's Approximation

Let us again treat the two-dimensional square lattice as an example. The combinatory factor of the assembly having r.d. in all of the spin pairs has been given by $G_2^{(2)}$ in Sec. B. The combinatory factor of the assembly having r.d. in all of the square clusters has been given by $G_1^{(4)}$ in Sec. C. These are the combinatory factors of the first and the second approximations, respectively, of the lattice. Now we consider a combinatory factor of the intermediate order of approximation, i.e., a combinatory factor of the assembly having r.d. in all of the pairs, but having r.d. only in some of the square clusters. Writing the number of squares which are assured of having r.d. in square clusters by qN, $(0 \leqq q \leqq 1)$, and the combinatory factor by $G_q^{(4)}$, we immediately obtain, from Eq. (C.7),

$$G_q^{(4)} = g_{q,2,1}^{(4)} = (N!)^{q-1} Y_N^{4q-2} / X_N^{4q-3} Z_N^q. \quad \text{(E.1)}$$

Putting $q=\frac{1}{2}$, we can eliminate Y_N from the above equation,

$$G_{\frac{1}{2}}^{(4)} = X_N (N!)^{-\frac{1}{2}} Z_N^{-\frac{1}{2}}, \quad \text{(E.2)}$$

which is the combinatory factor corresponding to Yang-Li-Hill's approximation.[8-10] With $G_{\frac{1}{2}}^{(4)}$, we can only assure that the assembly of squares shaded in Fig. 5 has r.d. in square clusters. In this approximation, the clusters are correlated with one another only by points. This is just the condition used in the grand partition function method of Fowler and Guggenheim[11] which leads to a set of equations of quasi-chemical equilibrium between square clusters.

Now we proceed to more general cases. We denote the number of distinguishable configurations of an assembly of qN of n clusters, each of which contains n points and p bonds, by the abbreviated notation

$$Q_q^{(n)} = [N!/\Phi(n, p)_N]^q, \quad \text{(E.3)}$$

from which a combinatory factor $G_q^{(n)}$ of a lattice having r.d. in qN of the clusters is constructed as follows. Let us assume, for simplicity's sake, that the clusters are overlapped with one another only by points or bonds. As the $Q_q^{(n)}$ assembly contains pqN bonds and nqN points, a $P_q^{(n)}$ assembly is one of $g_{pq,nq}^{(2)}$ assemblies. Hence from Eq. (B.10), we get

$$P_q^{(n)} = g_{pq,nq}^{(2)} = [X_N^{2p-n} / (N!)^{p-n} Y_N^p]^q. \quad \text{(E.4)}$$

As the number of G' configurations to be selected from the $P_q^{(n)}$ assembly having r.d. in pairs is $G_\omega^{(2)}$ itself, using Eqs. (B.7), (E.3), and (E.4), we get

$$G_q^{(n)} = G_\omega^{(2)} \frac{Q_q^{(n)}}{P_q^{(n)}} = \frac{X_N^{2\omega-1}}{(N!)^{\omega-1} Y_N^\omega} \left[\frac{(N!)^{p-n+1} Y_N^p}{\Phi(n, p)_N X_N^{2p-n}} \right]^q. \quad \text{(E.5)}$$

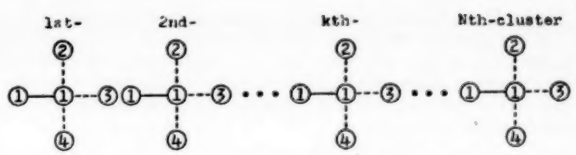

FIG. 6. Two ways of constructing $Q_1^{(2\omega+1)}$.

Putting $q=\omega/p$ to eliminate Y_N, we get

$$G_{\omega/p}^{(n)} = \left[\frac{N!}{\Phi(n, p)_N} \right]^{\omega/p} \left[\frac{X_N}{N!} \right]^{n(\omega/p)-1}. \quad \text{(E.6)}$$

Thus we obtain Eqs. (2.3) and (2.9) of Li's paper.[9]

From the above derivations, we can say that Yang-Li-Hill's approximation ranks between Bethe's one $(q=0)$ and those for which $q=1$, such as Kramers-Wannier's and some others shown in TCP *I*. Since $(\omega/p)N$ is, in usual cases, considerably smaller than the total number of n clusters in the lattice, such an approximation can hardly be expected to improve the results very much from Bethe's. However, as calculations of thermodynamic quantities become considerably simpler by the elimination of Y_N, Yang-Li-Hill's approximation may be conveniently used to take into account the interaction energies between neighbors farther apart than the nearest ones.

In connection with Eq. (E.5), here we give an example in which the constructions of the combinatory factor in terms of two types of clusters give the same result.[12] Consider a cluster composed of a point and of its first shell, i.e., a cluster having $2\omega+1$ spins and 2ω pairs.[22a] Combinatory factors in terms of the above $(2\omega+1)$ clusters are given by Eq. (E.5) as

$$G_q^{(2\omega+1)} = G_\omega^{(2)} [Y_N^{2\omega} / X_N^{2\omega-1} \Phi(2\omega+1, 2\omega)_N]^q. \quad \text{(E.7)}$$

It has already been pointed out by Li that the use of $G_{\frac{1}{2}}^{(2\omega+1)}$ leads to just the same results as those of Bethe's approximation. The reason for it can be shown for the general case of $G_q^{(2\omega+1)}$ as follows.

The number of configurations of an assembly of N clusters, each of them having $2\omega+1$ spins and 2ω pairs, is written as

$$Q_1^{(2\omega+1)} = N!/\Phi(2\omega+1, 2\omega)_N. \quad \text{(E.8)}$$

The construction of such an assembly can be analyzed in steps as follows. First we construct an assembly of N bonds marked by $1-1$ in Fig. 6, so that they have r.d. The number of ways is $N!/Y_N$. Next we add points marked 2. The number of ways is X_N/Y_N (see Sec. A of TCP *I*). Adding points $3, 4, \cdots, 2\omega$, the desired assembly is completed. Therefore we have

$$Q_1^{(2\omega+1)} = (N!/Y_N) \cdot (X_N/Y_N)^{2\omega-1}. \quad \text{(E.9)}$$

From Eqs. (E.8) and (E.9), we have the relation

$$\Phi(2\omega+1, 2\omega)_N = Y_N^{2\omega} / X_N^{2\omega-1}, \quad \text{(E.10)}$$

[22a] The two-dimensional triangular lattice and the face-centered lattice are omitted, in which the bond between two points of the first shell contributes to the energy.

TABLE II. Correlation and state figures of two-dimensional square lattice. Closed figures of white circles represent *correlation* polygons. $\Omega_{n,j}$ is the number of the jth correlation polygon with n lattice points (white circles) in the whole square lattice with N lattice points. Figures with crosses are *state* figures, a cross representing a lattice point of a reversed spin. $g_{c,j}$ is the number of the jth state figures with c reversed spins. It should be noted that the lattice for the white circles and the one for the crosses are shifted with each other by a half-lattice constant both in horizontal and vertical directions. E_c-E_0 is the increase of energy at a state $g_{j,c}$ above the state of maximum multiplicity.

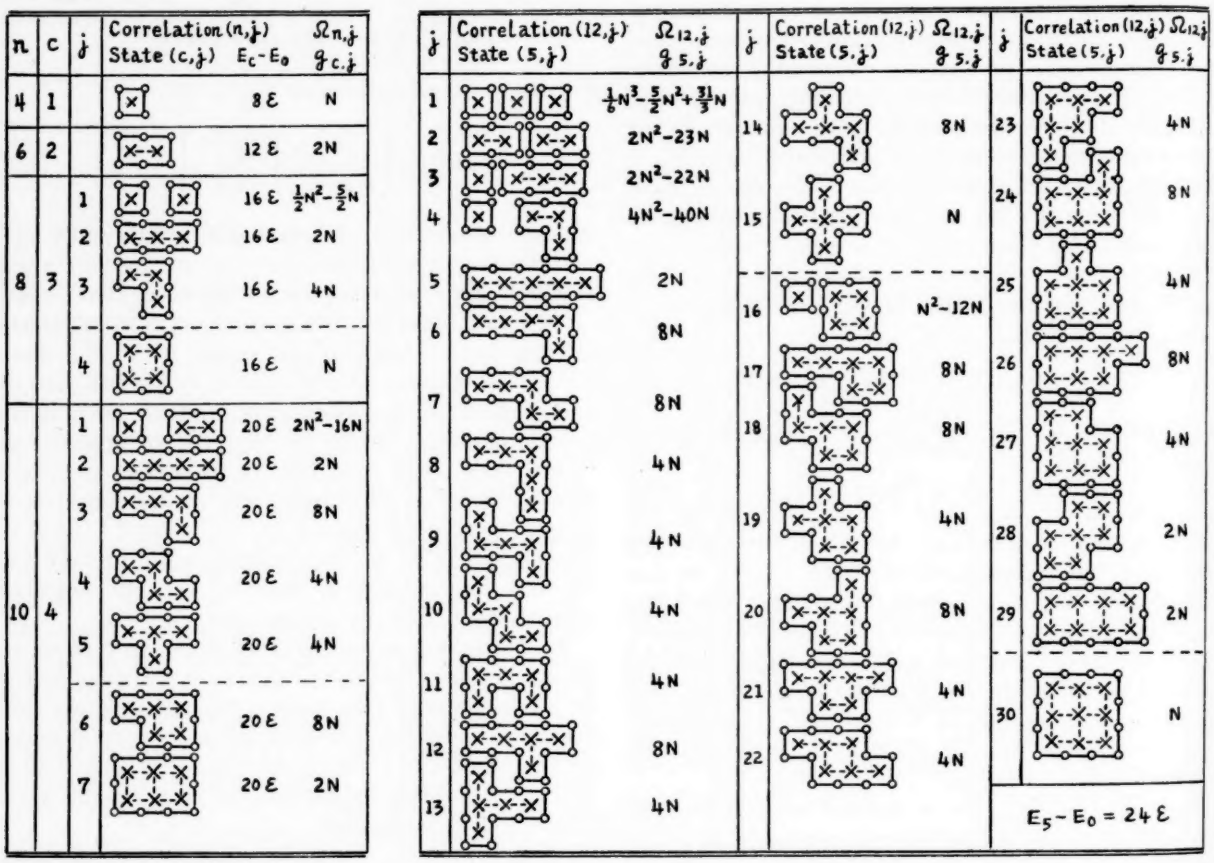

which transforms Eq. (E.7) into

$$G_q^{(2\omega+1)}=G_\omega^{(2)}, \tag{E.11}$$

for every value of q. As for the energy, when we assume that it is contributed only from the nearest neighbor pairs, the energy is written correctly as a function of y_i's both in the pair approximation and the center-and-the-first-shell approximation. From this fact and Eq. (E.11) we can conclude that the two approximations are identical. The same argument can be applied to other cases of equivalency, for instance, to the two-dimensional triangular lattice in which the approximation with a triangle and that with a rhombus[23] leads to the identical results.

III. EXPANSION OF PARTITION FUNCTION

F. Oguchi's Method of Expansion

We shall now compare the partition functions corresponding to various approximations described in the preceding sections with the rigorous ones in order to discuss the nature of these approximations. For this purpose, the expansion of the rigorous partition function presented recently by Oguchi[14] seems to be appropriate. First, we give a short sketch of his method as a preparation of the subsequent discussions.

We characterize the spin on the ith lattice point by $\mu_i(=\pm 1)$, and denote the interaction energy of spin pair (i, k) by $-\mu_i\mu_k\epsilon$. Hence, the spin interactions between parallel or antiparallel pairs are given by $-\epsilon$ or $+\epsilon$, respectively. In the absence of an external magnetic field, the partition function f of an Ising ferromagnet with N spins can be written as

$$f=\sum_{\mu_i=\pm 1}\exp[K\sum_{(i,k)}\mu_i\mu_k], \tag{F.1}$$

with

$$K=\epsilon/kT,$$

where $\sum_{(i,k)}$ is the sum over all spin pairs (i, k) which

[23] The G with a triangle is given by Eq. (G.1) of TCP *I*, and that with a rhombus is

$$G=\{\text{Bond}\}^2/\{\text{Point}\}\{\text{Rhombus}\},$$

or

$$G=\{\text{Triangle}\}^4/\{\text{Point}\}\{\text{Rhombus}\}^3.$$

See T. Watari and M. Kurata, Busseiron-Kenkyu **37**, 89 (1951), in Japanese; R. Kikuchi, unpublished.

are nearest neighbors, and $\sum_{\mu_i=\pm 1}$ represents

$$\sum_{\mu_1=\pm 1}\cdot\sum_{\mu_2=\pm 1}\cdots\sum_{\mu_N=\pm 1}.$$

Equation (F.1) can be transformed into

$$f=(\cosh K)^{\omega N}\sum_{\mu_i=\pm 1}\prod_{(i,k)}(1+\mu_i\mu_k\kappa),$$

with (F.2)

$$\kappa=\tanh K,$$

and expanding the right-hand side of Eq. (F.2) in a power series for κ, we get Oguchi's high temperature expansion of the rigorous partition function,

$$f=2^N(\cosh K)^{\omega N}[1+\sum_n \Omega_n\kappa^n], \qquad (F.3)$$

where Ω_n represents the number of closed figures composed of n bonds as are illustrated in Table II. These closed polygons are the only nonvanishing terms after $\sum_{\mu_i=\pm 1}$ has been performed, and may be simply called a *correlation* polygon, because the effect started at one lattice point returns to the original point after traveling along the closed figure.

On the other hand, writing f in the familiar form

$$f=\sum_c g_c\exp(-E_c/kT), \qquad (F.4)$$

and counting one by one the multiplicity g_c and the total energy E_c of the state c from the lowest value of the energy, we obtain the low temperature expansion of f. For example, in the lowest state, all spins are oriented parallel to one direction, and

$$E_0=-\epsilon\omega N, \quad \text{and} \quad g_0=1.$$

The first higher state is given by the reversal of a single spin, i.e.,

$$E_1-E_0=4\omega\epsilon, \quad \text{and} \quad g_1=N,$$

and so on.

G. Two-Dimensional Square Lattice

Though the rigorous partition function of the two-dimensional square lattice has been obtained by Onsager and Kaufman[24] and others, we adopt here the expansion method of Oguchi which makes our discussion illustrative, and gives a suitable preparation for three-dimensional cases.

In Table II, the correlation polygons of this lattice are given by solid lines and white circles. $\Omega_{n,j}$ gives the number of the jth polygons with n lattice points. The coefficients Ω_n in Eq. (F.3) are connected with them by

$$\Omega_n=\sum_j \Omega_{n,j}. \qquad (G.1)$$

Using this table, one obtains the high temperature expansion as

$$f=2^N(\cosh K)^{2N}\Big[1+N\kappa^4+2N\kappa^6+\Big(\frac{1}{2}N^2+\frac{9}{2}N\Big)\kappa^8+(2N^2+12N)\kappa^{10}+\Big(\frac{1}{6}N^3+\frac{13}{2}N^2+\frac{112}{3}N\Big)\kappa^{12}+\cdots\Big]. \qquad (G.2)$$

In the same table, we give figures in which reversed spins are represented by crosses and are connected by dotted lines. These figures illustrate the states counted in the low temperature expansion, their multiplicities g_c's being related to $g_{c,j}$ by

$$g_c=\sum_j g_{c,j}. \qquad (G.3)$$

Hence, from the table, we see that the low temperature expansion can be written with the same coefficients as in the high temperature expansion,

$$f=H^{2N}\Big[1+NH^{-8}+2NH^{-12}+\Big(\frac{1}{2}N^2+\frac{9}{2}N\Big)H^{-16}+(2N^2+12N)H^{-20}+\Big(\frac{1}{6}N^3+\frac{13}{2}N^2+\frac{112}{3}N\Big)H^{-24}+\cdots\Big]. \qquad (G.4)$$

with

$$H\equiv\exp(\epsilon/kT).$$

As N is sufficiently large, the partition function per lattice point $\lambda=f^{1/N}$ can be simplified as shown in Eqs. (G.5) and (G.8) below, for high and low temperatures, respectively. These are listed together with the expansions of Kramers-Wannier's and of Bethe's approximations for comparison.

The high temperature expansions are as follows:

Rigorous

$$\lambda=2(\cosh K)^2[1+\kappa^4+2\kappa^6+5\kappa^8+14\kappa^{10}+44\kappa^{12}+152\kappa^{14}+\cdots]; \qquad (G.5)^{25}$$

Kramers-Wannier

$$\lambda=2(\cosh K)^2[1+\kappa^4+2\kappa^6+4\kappa^8+8\kappa^{10}+16\kappa^{12}+\cdots]; \qquad (G.6)^{26}$$

[24] L. Onsager, Phys. Rev. **65**, 117 (1944); B. Kaufman, Phys. Rev. **76**, 1232 (1949); G. H. Wannier, Revs. Modern Phys. **17**, 50 (1945).

[25] The coefficients of κ^{14} and H^{-28} of Eqs. (G.5) and (G.8), respectively, are taken from Onsager's paper (reference 24). κ and H in the present paper are connected with κ of Onsager by the relation

$$\kappa(\text{Onsager})=\kappa(1-\kappa^2)/(1+\kappa^2)^2=H^{-2}(1-H^{-4})/(1+H^{-4})^2.$$

It also should be noted that the fact that Eqs. (G.5) and (G.8) have the same coefficients is understood from the dual property of this lattice (see reference 24).

[26] See TCP *I*, Eq. (C3.12),

$$\lambda=2(1-\sinh^2 K)^{-1}.$$

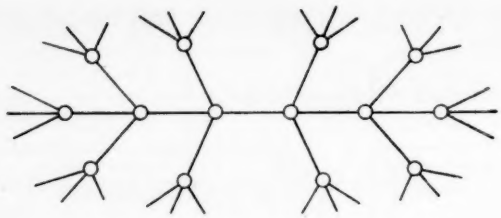

FIG. 7. Bethe lattice, with $2\omega=4$.

Bethe

$$\lambda=2(\cosh K)^2. \tag{G.7}$$

For low temperatures:

Rigorous

$$\lambda=H^2[1+H^{-8}+2H^{-12}+5H^{-16}+14H^{-20}+44H^{-24}+152H^{-28}+\cdots], \tag{G.8}$$[25]

Kramers-Wannier

$$\lambda=H^2[1+H^{-8}+2H^{-12}+5H^{-16}+14H^{-20}+43H^{-24}+\cdots], \tag{G.9}$$[27]

Bethe

$$\lambda=H^2[1+H^{-8}+2H^{-12}+4H^{-16}+8H^{-20}+16H^{-24}+\cdots]. \tag{G.10}$$[28]

Before we discuss the discrepancies between the expansion coefficients given above, let us consider a hypothetical lattice with coordination number 2ω, any part of which has a dendritic build-up schematically shown in Fig. 7. The unique feature of the lattice is that it does not include any closed cells such as triangle, square, etc. The high temperature expansion of the rigorous partition function of this dendritic lattice is obviously

$$f=2^N(\cosh K)^{\omega N}, \tag{G.11}$$

because there are no polygon correlations. In Table III, we give energies and multiplicities of lower energy states of the dendritic lattice for $\omega=2$, from which the low temperature expansion of the rigorous partition function of this lattice is obtained as follows:

$$f=H^{2N}\left[1+NH^{-8}+2NH^{-12}+\left(\frac{1}{2}N^2+\frac{7}{2}N\right)H^{-16}+(2N^2+6N)H^{-20}+\left(\frac{1}{6}N^3+\frac{11}{2}N^2+\frac{31}{3}N\right)H^{-24}+\cdots\right]. \tag{G.12}$$

By the relation $\lambda=f^{1/N}$, Eqs. (G.11) and (G.12) are shown to reduce to Eqs. (G.7) and (G.10) of Bethe's approximation. The similar results are quite generally obtained with any dendritic lattice with any coordination number. Therefore, such a lattice is the one for which Bethe's method gives rigorous results, and might be called the "Bethe lattice."

Now, we are ready to commence our discussion by inspecting the discrepancies between the coefficients of the expansions given above. The comparison of the coefficients leads us to the following conclusions:

(1) The *state* (3, 4),[29] given in Table II, contributes N to the coefficient of H^{-16} of Eq. (G.8), because the lattice has square cells. However, as the Bethe lattice ignores the existence of square cells, there is no such contribution to the corresponding coefficient. Hence, the coefficients of H^{-16} of Eq. (G.12) and (G.10) of Bethe's approximation are underestimated by N and one, respectively.

(2) For the same reason, there are no contributions of the states (4, 6) and (4, 7) to the coefficient of H^{-20} of Bethe's approximation. On the other hand, the states with a figure given in Fig. 8(a), which correspond to the state (3, 4), contribute to this coefficient with overestimated multiplicity of $4N$ in place of the correct

TABLE III. State figures of Bethe lattice.

k	State	$\frac{E_k-E_0}{\varepsilon}$	Multiplicity
1	×	4ω	N
2	×–×	$8\omega-4$	ωN
3	× ×	8ω	$\frac{1}{2}N^2-(\omega+\frac{1}{2})N$
4	×–×–×	$12\omega-8$	$\omega(2\omega-1)N$
5	× ×–×	$12\omega-4$	$\omega N^2-4\omega^2 N$
6	×–×–×–×–×	$16\omega-12$	$\omega(2\omega-1)^2N$
7		$16\omega-12$	$\frac{\omega}{3}(2\omega-1)(2\omega-2)N$
8	× × ×	12ω	$\frac{1}{6}N^3-(\omega+\frac{1}{2})N^2+(2\omega^2+\omega+\frac{1}{3})N$
9	×–× ×–×	$16\omega-8$	$\frac{1}{2}\omega^2N^2-\omega(8\omega^2-4\omega+1)N$
10	× ×–×–×	$16\omega-8$	$\omega(2\omega-1)N^2-\omega(2\omega-1)(6\omega-1)N$
11	×–×–×–×–×–×	$20\omega-16$	$\omega(2\omega-1)^3N$
12		$20\omega-16$	$\omega(2\omega-1)^2(2\omega-2)N$
13		$20\omega-16$	$\frac{2\omega(2\omega-1)(2\omega-2)(2\omega-3)}{4!}N$

[27] See TCP *I*, Eq. (C5.3):

$$\lambda=[H^8+8H^4-11+(H^4-5)^{\frac{1}{2}}(H^4-1)^{\frac{1}{2}}]/(2H^6).$$

[28] $\lambda=(H^4-1)^2/H^2(H^4-2)$.

[29] The *state* (3, 4) means the state for which $c=3$ and $j=4$ in Table II. Similarly the *correlation* (8, 4) means the one for $n=8$ and $j=4$.

multiplicity of N. Hence, we can write

$$(g_4)_{\text{Bethe}}=\sum_{j=1}^{5} g_{4,j}+4g_{3,4}=2N^2+6N,$$

which is exactly the coefficient of H^{-20} of Eq. (G.12).

(3) The discrepancies of the coefficients of the terms higher than H^{-20} can be explained in a similar manner, the details of which are omitted here. However, we add a remark that the states with a figure given in Fig. 8(b), which also correspond to the state (3, 4), contribute to the coefficient of H^{-24} of Bethe's approximation with over-estimated multiplicity of $4N$.

Entirely similar circumstances come out in the case of Kramers-Wannier's approximation. In this approximation, as we have taken into account the existence of square cells, the danger of over-estimation due to such figures as shown in Fig. 8(a) and (b) can be safely avoided. However, in this approximation,[30] we ignore such states and correlations as the state (5, 30) and the correlation (8, 4). Hence, the coefficient of H^{-24} (or κ^8) of Eq. (G.9) [or Eq. (G.6)] is underestimated by one. Exactly in the same way as in the case of Bethe's

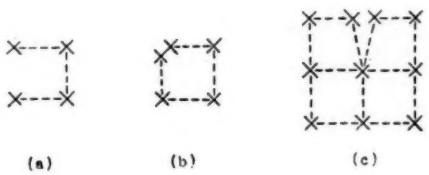

FIG. 8. Examples of states incorrectly counted in Bethe's approximation, (a) and (b), and in Kramers-Wannier's approximation (c).

approximation, the states containing the figure given in Fig. 8(c), which corresponds to the state (5, 30), contribute to the coefficients of higher terms with over-estimated multiplicities.

Summarizing these results and extending them, we may conclude the following rules for a two-dimensional square lattice:

(1) In the expansion of a partition function of the cluster variation method, the contributions to the coefficients from states and correlations having figures open with respect to the basic figure appear always in the correct terms with the proper multiplicities.

(2) The contributions of states and correlations having figures closed with respect to the basic figure appear with overestimated multiplicites in improperly higher terms.

(3) In this method, in order to obtain an improved approximation it is necessary to adopt a basic figure

[30] In the same way as the Bethe lattice was defined, we can consider the "Kramers-Wannier lattice," which has the feature that the lattice does not include any of the figures closed by finite sequence of squares, nevertheless each of the square cells is surrounded by four square cells. The Kramers-Wannier approximation is rigorous when it is applied to this hypothetical lattice.

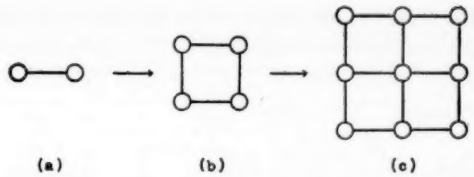

FIG. 9. Basic figures to be successively adopted in two-dimensional square lattice.

closed with respect to the figure which has been used as the basic figure in the preceding approximation.

Besides these rules, we may safely say that the basic figure specified in (3) is also sufficient to improve the approximation for the case of square lattice, though we cannot prove it rigorously. Concerning these rules, we shall make supplementary remarks in Sec. I for the case of face-centered cubic lattice.

These rules give another simple explanation why the center-and-the-first-shell cluster gives the same results as Bethe's, as was discussed in Sec. E. The reason is that such a cluster of radial shape exists in the Bethe lattice, along with the bond which is the basic figure of Bethe's original treatment.

We can also deduce that in the case of the two-dimensional square lattice the approximation is improved each time when the basic figure proceeds one step further as shown in Fig. 9. Using the basic figure shown in Fig. 9(c), we have a low (or high) temperature expansion which is correct up to H^{-28} (or κ^{10}) term.

H. Simple Cubic Lattice

Considerations similar to those above can be easily applied to any other lattices. Here we explain the simple cubic lattice.

The high temperature expansion of the partition function λ can be written as

$$\lambda=2(\cosh K)^3[1+\omega_4\kappa^4+\omega_6\kappa^6+\omega_8\kappa^8+\cdots]. \quad \text{(H.1)}$$

The values of ω's are listed in Table IV for various methods. The rigorous values are obtained from Table V following Oguchi's method.[14]

The discrepancies of ω_6's and ω_8's between the rigorous expansion and the approximate methods can be explained by the rules (1) and (2) in the previous section, because the correlations (6, 3) and (8, 12) given in Table V may disappear from the respective proper terms and appear improperly in higher terms. Thus, ω_6 of the second approximation appears because the coefficient Ω_8 is miscounted as

$$(\Omega_8)_{\text{2nd approx.}}=\sum_{j=1}^{7}\Omega_{8,j}+2\Omega_{8,8}+6\Omega_{6,3}$$
$$=-\frac{9}{2}N^2+\frac{285}{2}N, \quad \text{(H.2)}$$

where the coefficient 2 of $\Omega_{8,8}$ occurs because the corre-

TABLE IV. Values of coefficients ω_i's in the high temperature expansion (H.1) of the partition function for simple cubic lattice.

Method	Cluster	G	ω_4	ω_6	ω_8	Reference
Rigorous			3	22	192	
Third approx.	Cube	$G_1^{(8)}$	3	22	189	a
ter Haar and Martin			3	22	173	b
Second approx.	Square	$G_3^{(4)}$	3	18	147	c

[a] TCP *I*, Eq. (D7.6) and the relation

$$-E/N\epsilon=3K+(4\omega_4-1)K^3+(6\omega_8-8\omega_4+\tfrac{2}{5})K^5+\left(8\omega_8-16\omega_6+\frac{48}{5}\omega_4-4\omega_4{}^2-\frac{17}{105}\right)K^7+\cdots.$$

[b] D. ter Haar and B. Martin, Phys. Rev. **77**, 721 (1950).
[c] TCP *I*, Eq. (D7.3).

lation given in Fig. 10(a) is counted twice as shown in (a′) and (a″), and the coefficient 6 of $\Omega_{6,3}$ is due to counting six times the correlation given in (b) as (b′), (b″), etc. It seems, however, difficult to give any reasonable explanation for ω_8 in ter Haar and Martin's approximation.

The low temperature expansion of this lattice is given by Oguchi[14] as

$$\lambda=H^3[1+H^{-12}+3H^{-20}-3H^{-24}+15H^{-28}-30H^{-32}+101H^{-36}+\cdots]. \quad \text{(H.3)}$$

We can show that the corresponding expansions of the pair (or Bethe), the second and the third approximations are correct up to H^{-28}, H^{-44}, and H^{-56} terms, respectively. Hence, if we use the rigorous high temperature expansion up to κ^8 term, we should also use the low temperature expansion up to H^{-56} term; otherwise, both expansions are treated in different order of approximation. Accordingly, as was pointed out by Oguchi, it seems impossible, due to the poor convergence of the low temperature expansion, to determine the Curie point as the temperature at which both expansions have the same value.

Rules (1), (2), and (3) in the previous section apparently can be applied safely for this case also.

I. Face-Centered Cubic Lattice

In Table VI, correlation figures of face-centered cubic lattice are shown, from which one can calculate the coefficients ω_i's in the high temperature expansion of the partition function,

$$\lambda=2(\cosh K)^6[1+\omega_3\kappa^3+\omega_4\kappa^4+\omega_5\kappa^5+\cdots]. \quad \text{(I.1)}$$

These values are shown in Table VII together with those for several approximations, of which we give some explanation here.

The lattice with N points contains $8N$ triangles. When only qN triangles out of $8N$ have r.d., Eq. (E.5) should be used for the combinatory factor with $p=n=3$ and $\Phi(n,p)_N=\{\text{Triangle}\}_N$,

$$G_q^{(3)}=\frac{X_N{}^{11}}{(N!)^5 Y_N{}^6}\left[\frac{Y_N{}^3 N!}{X_N{}^3\{\text{Triangle}\}_N}\right]^q. \quad \text{(I.2)}$$

Cases for $q=2$, 6, 7, and 8 are shown in Table VII.

In "triangle+square" approximation, r.d. is assured for all of $8N$ triangles and for N squares, and the combinatory factor has the form

$$G_8^{(3)}\cdot[Y_N{}^4 N!/X_N{}^4 Z_N]. \quad \text{(I.3)}^{31}$$

In "tetrahedron+square" approximation, r.d. is attained for all of the tetrahedrons and for N squares, the combinatory factor for it being

$$\frac{Y_N{}^6 N!}{X_N{}^5\{\text{Tetrahedron}\}_N{}^2}\cdot\frac{Y_N{}^4 N!}{X_N{}^4 Z_N}. \quad \text{(I.4)}^{31}$$

Now we are ready to examine the natures of the various approximations given above. The inspection of Table VII reveals that the approximations which fail to give a transition temperature are always associated with the overestimation of ω_n's. By such overestimation

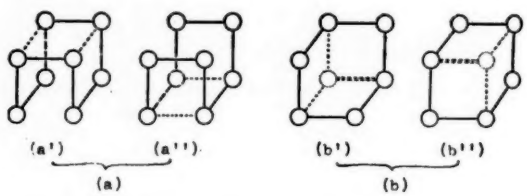

FIG. 10. Correlations incorrectly counted in the second approximation.

$T_t{}^*$ moves too much towards higher temperatures to make the intersection of the higher and the lower temperature expansions of λ possible.

Next we examine the origin of such overestimation of ω_n. By distributing qN triangles over the lattice, each of the bonds is held by $3qN/6N=q/2$ triangles in common. ω_4 (or ω_5) are contributed from configurations in which two (or three) triangles are connected as are shown in the correlation figures $n=4$, $j=1$, 2, and 3 (or $n=5$, $j=1$, 2, and 3). By a simple calculation, these numbers are found to be

$$\omega_4=\Omega_4/N=3q\{(q/2)-1\}/2, \quad \text{(I.5)}$$

and

$$\omega_5=\Omega_5/N=4\omega_4\{(q/2)-1\}/2, \quad \text{(I.6)}$$

in perfect accordance with Table VII. The case for $q=8$ is also interpreted as

$$(\Omega_4)_{q=8}=\sum_{j=1}^{3}\Omega_{4,j}+2\Omega_{4,4}=36N, \quad \text{(I.7a)}$$

[31] The previous G is multiplied by a factor $Y_N{}^4 N!/X_N{}^4 Z_N$ when r.d. is assured for additional N squares. This is analogous to the situation in Eq. (E.5).

TABLE V. Correlation figures of simple cubic lattice.

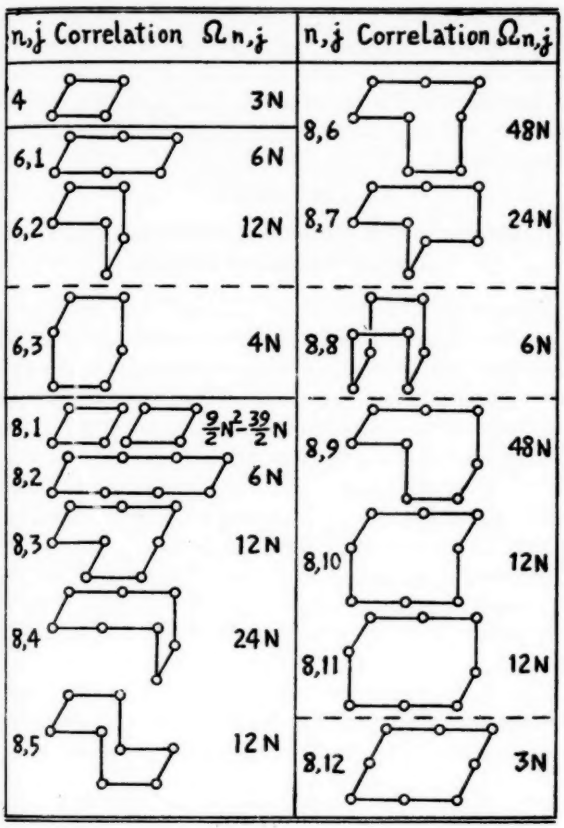

and

$$(\Omega_5)_{q=8}=\sum_{j=1}^{3}\Omega_{5,j}+2\Omega_{5,4}+4\Omega_{4,4}=216N, \qquad \text{(I.7b)}$$

where it should be noted that correlations (4, 4) and (5, 4) are overestimated, whereas (4, 5), (5, 5) are neglected.

When we adopt a tetrahedron as the basic figure, the overestimation due to the correlations (4, 4) and (5, 4) can be avoided, but (4, 5) and (5, 5) are still neglected,

TABLE VI. Correlation figures of face-centered cubic lattice.

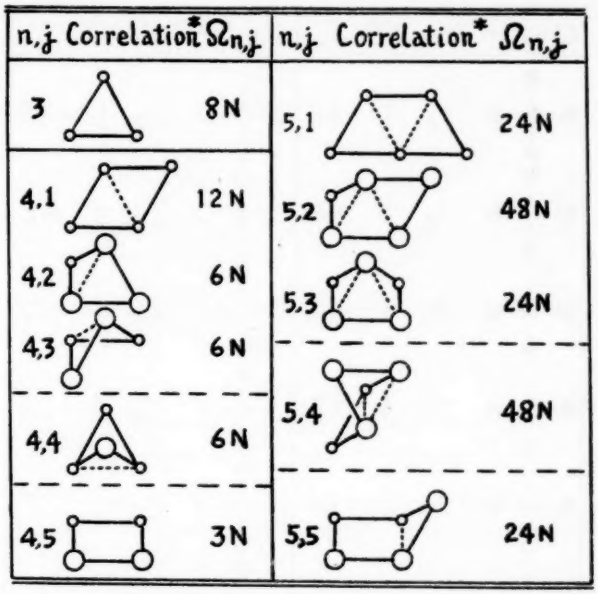

* The points shown with greater circles lie on a lattice plane (111) higher than those with smaller ones (see TCP *I*, Fig. 10).

and we have

$$(\Omega_4)_{\text{tetrahedron}}=\sum_{j=1}^{4}\Omega_{4,j}=30N, \qquad \text{(I.8a)}$$

and

$$(\Omega_5)_{\text{tetrahedron}}=\sum_{j=1}^{4}\Omega_{5,j}=144N. \qquad \text{(I.8b)}$$

When we use an octahedron as the basic figure, we have severe overestimation of ω_4 and ω_5, because not only does the overestimation due to the correlations (4, 4) and (5, 4) again come into play, but also the contribution of the correlations (4, 5) and (5, 5) is newly added.

In the case when we adopt both the tetrahedron and the square as basic figures, it seems as if we could have a better approximation, as we can add the contributions

TABLE VII. Characteristic values of face-centered cubic (Ising) lattice obtained from various approximations.

Basic figure		$(y_2)_{T_t}$	H_t^2	kT_t/ϵ	kT_t^*/ϵ†	c_t/k†	ω_3	ω_4	ω_5	Approx.
Bond		0.22̇7̇	1.2	10.970	···	0.0494	0	0	0	Bethe
Triangle	$q=2$	0.225	1.2018	10.877	···	0.0593	2	0	0	Yang-Li
	6	0.2143	1.2103	10.491	7.645	0.1335	6	18	72	
	7	0.2	1.2206	10.033	9.723	0.4578	7	$\frac{105}{4}$	$\frac{525}{4}$	
	8	imag.	none	none	11.772	···	8	36	216	
Tetrahedron		0.2	1.221	10.025	9.239	0.3355	8	30	144	TCP *I*
Octahedron		imag.	none	none	···	···	8	39	240	
Triangle+Square		imag.	none	none	···	···	8	39	264	
Tetrahedron +Square		imag.	none	none	···	···	8	33	192	
				Correct values of ω_n's			8	33	168	

† T_t^* is the temperature at which the specific heat for the disordered state becomes infinite, and c_t is the specific heat at T_t on the higher temperature side.

TABLE VIII. Probabilities of appearance of (4+1) clusters.

Cluster	Prob.	γ_i^*	ε_i	Cluster	Prob.	γ_i^*	ε_i
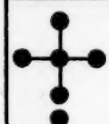	z_1	1	-4ε	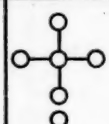	z_{12}	1	-4ε
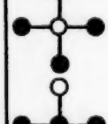	z_2	1	4ε	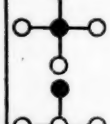	z_{11}	1	4ε
	z_3	4	-2ε	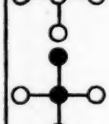	z_{10}	4	-2ε
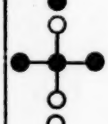	z_4	4	2ε	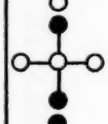	z_9	4	2ε
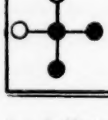	z_5	2	0	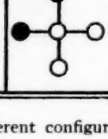	z_8	2	0
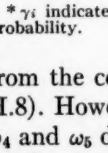	z_6	4	0	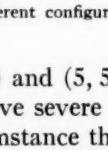	z_7	4	0

* γ_i indicates the number of different configurations having the same probability.

from the correlations (4, 5) and (5, 5) properly to Eq. (I.8). However, we still have severe overestimation of ω_4 and ω_5 due to the circumstance that the correlation (5, 3) is counted not only as a sequence of three triangles but also as a composite of a square and a triangle.

In Sec. G we have listed rules which hold for simple lattices, but for the face-centered cubic lattice some of them must be modified. For instance, the rule (2) in Sec. G does not hold for this lattice, because when we take a triangle as the basic figure, the overestimation of the coefficient due to the correlation $\Omega_{4,4}$ occurs at the term Ω_4, where $\Omega_{4,4}$ should contribute correctly as is seen from the comparison of Eqs. (I.7a) and (I.8a). Concerning the sufficiency for the improved approximation, we may say the following: The basic figure which is adopted in order to have an improved approximation should be the one which is closed with respect to the basic figure of the previous approximation and also which does not cause any overestimation of the expansion coefficients. Though we do not have a definite method of telling which figures give no overestimation, it is generally safe to use a highly symmetric figure. This reasoning made us adopt a tetrahedron in TCP *I*.

The assumption mentioned in TCP *I* to take T_i^*, the temperature for each approximation at which the specific heat for the disordered state becomes infinite, to be lower than the correct value of the transition temperature seems reasonable when there is no risk of any undue overestimation of the coefficient. Hence, the estimate of T_i^* for the simple cubic and the face-centered cubic lattice given in TCP *I* seems legitimate, where, in the latter case, a tetrahedron was adopted as the basic figure.

In conclusion, one of the authors (M.K.) wishes to thank Professor M. Tamura of the Kyoto University for his continued interest and encouragement, and the Ministry of Education of the Japanese Government for a grant-in-aid.

APPENDIX I

J. Derivation of Bethe's Assumption from the Cluster Variation Method

Though it was shown by Takagi[3] that his method gives exactly the same results mathematically as that of Bethe,[2] there was no intuitive explanation why these two methods become identical. The following explanation helps us to understand the relation between them. Takagi used $G_\omega^{(2)}$ as the combinatory factor, but as the $G_{\frac{1}{2}}^{(2\omega+1)}$-approximation, i.e., the "center-and-the-first-shell" approximation, was shown to be equivalent to it in Sec. E, we will start from the latter, and derive the fundamental equations of Bethe. The case of the two-dimensional square lattice will be proved, but the derivation is easily generalized to any other type of lattice.

The probabilities of appearances, z_i's, of $(2\omega+1)$ clusters are given in Table VIII. Using z_i's, the energy E of an assembly with N lattice points is given by

$$E=(N/2)\sum_{i=1}^{12}\gamma_i z_i \epsilon_i. \tag{J.1}$$

In the present case, $\Phi(2\omega+1, 2\omega)_N$ used in Eq. (E.7) is explicitly given by

$$\Phi(5,4)_N=\prod_{i=1}^{12}\{(z_i N)!\}^{\gamma_i}, \tag{J.2}$$

giving the entropy S of the assembly

$$\begin{aligned} S&=k\ln G_{\frac{1}{2}}^{(5)} \\ &=(Nk/2)[3\sum_{i=1}^{2}x_i\ln x_i-\sum_{i=1}^{12}\gamma_i z_i\ln z_i]. \end{aligned} \tag{J.3}$$

It is easily shown that the x_i's and the z_i's are related by the following two independent equations:

$$x_1=z_1+z_2+3z_3+3z_4+z_5+2z_6+2z_7+z_8+z_9+z_{10}, \tag{J.4}$$

$$x_1=z_1+4z_3+2z_5+4z_6+4z_9+z_{11}. \tag{J.5}$$

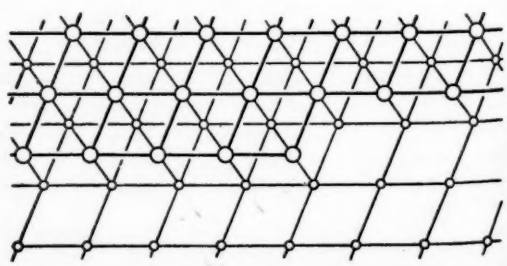

FIG. 11. Lattice plane (110) of body-centered cubic lattice.

Equating these two, one obtains

$$F_1(z_i)\equiv z_2-z_3+3z_4-z_5-2z_6 +2z_7+z_8-3z_9+z_{10}-z_{11}=0. \quad \text{(J.6)}$$

Another restriction for the z_i's is the normalization

$$F_2(z_i)\equiv\sum_{i=1}^{12}\gamma_i z_i-1=0. \quad \text{(J.7)}$$

Taking into consideration the conditions (J.6) and (J.7), the free energy per lattice point μ becomes

$$2\mu=2(E-TS)/N-\eta F_1(z_i)-\lambda F_2(z_i), \quad \text{(J.8)}$$

where η and λ are undetermined multipliers.

Minimizing μ with respect to the z_i's, we have a set of equations

$$\begin{cases} z_1/A=B^4H^4, & z_{12}/A=H^4, \\ z_2/A=B^4H^{-4}C^4, & z_{11}/A=H^{-4}, \\ z_3/A=B^3H^2C^{-1}, & z_{10}/A=BH^2, \\ z_4/A=B^3H^{-2}C^3, & z_9/A=BH^{-2}, \\ z_5/A=B^2C^{-2}, & z_8/A=B^2C^2, \\ z_6/A=B^2C^{-2}, & z_7/A=B^2C^2, \end{cases} \quad \text{(J.9)}$$

where we used abbreviations

$$\begin{cases} A=x_2^3\exp\{2+(\lambda/kT)\}, \\ B=(x_1/x_2)^{\frac{1}{2}}, \\ C=\exp(\eta/4kT), \\ H=\exp(\epsilon/kT). \end{cases} \quad \text{(J.10)}$$

Combining Eqs. (J.5), (J.6), (J.7), and (J.9), it can be shown that

$$C=1. \quad \text{(J.11)}$$

The set of equations (J.9), simplified using (J.11), expresses exactly the assumptions adopted by Bethe,

TABLE IX. Probabilities of appearance of rhombic clusters.

Rhombus	Prob.	γ_i^*	Rhombus	Prob.	γ_i^*
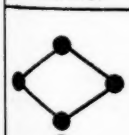	z_1	1	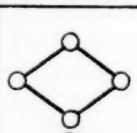	z_9	1
	z_2	2		z_8	2
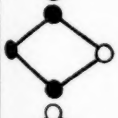	z_3	2		z_7	2
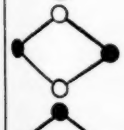	z_4	1	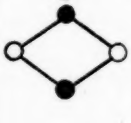	z_6	1
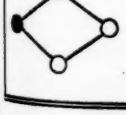	z_5	4			

*γ_i indicates the number of different configurations having the same probability.

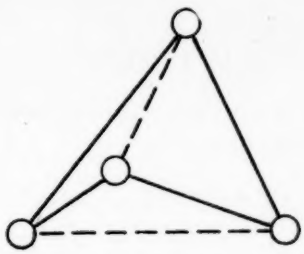

FIG. 12. Correlation neglected in the present approximation. (Dotted lines show spin pairs of the next nearest neighbors.)

which have thus been shown to be derived from the cluster variation method.

APPENDIX II

K. An Improved Treatment for the Body-Centered Cubic Lattice.

In Fig. 11 is illustrated the structure of the body-centered cubic lattice. The lattice points shown with greater circles are on a lattice plane (110) higher than those with smaller ones.

We adopt a rhombus as the basic figure, and define

$$Z_N\equiv\{\text{Rhombus}\}_N. \quad \text{(K.1)}$$

By the pseudo-assembly method, the combinatory factor can be constructed in terms of (two-dimensional) rhombic clusters shown in Table IX as

$$G_6^{(4)}=G_4^{(2)}\cdot[N!Y_N{}^4/X_N{}^4Z_N]^6 =N!{}^3Y_N{}^{20}/X_N{}^{17}Z_N{}^6, \quad \text{(K.2)}$$

from which we have the free energy per lattice point, μ, as

$$\mu=4\epsilon(4y_2-1)+kT[17\sum_{i=1}^{2}x_i\ln x_i -20\sum_{i=1}^{3}\beta_i y_i\ln y_i+6\sum_{i=1}^{9}\gamma_i z_i\ln z_i]. \quad \text{(K.3)}$$

From the above equation, we obtain as a solution of the disordered state

$$\lambda\equiv\exp(-\mu/kT) =8\varphi^4(\varphi+3)^{10}(3\varphi+1)^{10}/(\varphi^2+6\varphi+1)^{14},$$

with

$$H^2=(3\varphi+1)^5/\varphi^2(\varphi+3)^5, \quad \text{(K.4)}$$

and

$$\varphi\equiv z_2/z_4,$$

from which we get

$$\frac{C}{k}=-\frac{8\varphi(\varphi+3)(3\varphi+1)(3\varphi^2+2\varphi+3)}{(\varphi-3)(3\varphi-1)(\varphi^2+6\varphi+1)^2}(\ln H)^2, \quad \text{(K.5)}$$

as the specific heat for the disordered state. The characteristic values of the transition point, become as follows:

$$H_t^2=1.3446, \quad kT_t/\epsilon=6.755, \quad kT_t^*/\epsilon=5.604,$$

and

$$C_t/k=0.1614. \quad \text{(K.6)}$$

These values are to be compared with the results of Bethe's approximation,

$$H_t^2=1.\dot{3}, \quad kT_t/\epsilon=6.952,$$

and

$$C_t/k=0.0811. \quad \text{(K.7)}$$

The high temperature expansion of λ is given by Oguchi as

$$\lambda=2(\cosh K)^4[1+12\kappa^4+148\kappa^6+\cdots]. \quad \text{(K.8)}$$

From Eq. (K.4), we get

$$\lambda=2(\cosh K)^4[1+6\kappa^4+\cdots], \quad \text{(K.9)}$$

which shows a discrepancy already at the coefficient of κ^4. The reason is that we ignored the correlation given in Fig. 12. However, the adoption of this figure as the new basic figure causes other troubles which were avoided in the above approximation.

Although the approximation here given is apparently worse than those already given in the cases of other lattices, it is quite safe to say that the approximation is surely one of the reasonable intermediate approximations, because the danger of undue overestimations of ω_n's is prevented.

THE JOURNAL OF CHEMICAL PHYSICS VOLUME 21, NUMBER 3 MARCH, 1953

Rotation-Vibration Spectra of Diatomic and Simple Polyatomic Molecules with Long Absorbing Paths.

IX. The Spectra of the HCN and DCN Molecules from 2.5μ to 0.5μ*

A. E. Douglas and D. Sharma†
Division of Physics, National Research Council, Ottawa, Canada

(Received October 14, 1952)

The photographic infrared spectrum of HCN has been investigated using a 6-meter concave grating spectrograph and absorption paths up to 600 meters. The near infrared spectra of HCN and DCN have been investigated using a grating infrared spectrometer with a lead sulfide cell as a detector. The interference fringes from a Fabry-Perot etalon have been used as wavelength standards for the recording spectrometer. Twenty-four bands of HCN and six bands of DCN have been measured. From these measurements earlier work has been corrected, and the zero-order frequencies and anharmonic constants have been determined for both HCN and DCN. Perturbations have been found in the vibrational levels of HCN. Corresponding perturbations occur in the B_v values, and it has been shown that even apparently unperturbed B_v values are not linear functions of the vibrational quantum numbers. The B_e values for HCN and DCN were found to be 1.4849 cm^{-1} and 1.2118 cm^{-1}. From these B_e values the C−H and C−N internuclear distances in the equilibrium position have been found to be 1.0657A and 1.1530A, respectively. From the zero-order frequencies the force constants have been determined.

I. INTRODUCTION

THE spectra of HCN and DCN have been investigated by a number of workers. The most extensive study of the ordinary infrared spectrum has been made by Barker and his collaborators.[1,2] The photographic infrared has been studied by Badger and Binder[3] by Herzberg and Spinks,[4] and more extensively by Lindholm.[5] Recently Rank, Ruth, and Vander Sluis[6] have made accurate measurements of two bands in the photographic infrared. In the microwave region one line of the pure rotation spectrum has been observed.[7,8] Though this previous work has established many of the constants of HCN and DCN, the equilibrium internuclear distances, the zero-order frequencies, and consequently the correct force constants are still unknown. The present investigation was undertaken in order to determine some of these constants, to extend our knowledge of the spectrum, and to check the accuracy of previous work.

II. EXPERIMENTAL

The photographic infrared spectrum of HCN was photographed with a 21-ft grating spectrograph giving a dispersion of 2.5A per mm in the first order. A number of the bands at wavelengths shorter than 8000A were photographed in the second order. The error in measurement of the relative positions of the stronger lines of a band should be less than 0.02 cm^{-1}, but the abso-

* Contribution No. 2932 from the National Research Council of Canada.

† National Research Laboratories Postdoctorate Fellow. Now at Allahabad University, Allahabad, India.

[1] A. Adel and E. F. Barker, Phys. Rev. **45**, 277 (1934).
[2] P. F. Bartunek and E. F. Barker, Phys. Rev. **48**, 516 (1935).
[3] R. M. Badger and J. L. Binder, Phys. Rev. **37**, 800 (1931).
[4] G. Herzberg and J. W. T. Spinks, Proc. Roy. Soc. (London) **147**, 434 (1934).
[5] E. Lindholm, Z. Physik **108**, 454 (1938).
[6] Rank, Ruth, and Vander Sluis, Phys. Rev. **86**, 799 (1952).
[7] Nethercot, Klein, and Townes, Phys. Rev. **86**, 798 (1952).
[8] Simmons, Anderson, and Gordy, Phys. Rev. **86**, 1055 (1952).

lute accuracy will be somewhat less. The absorption cell was 5 meters long, and an absorption path up to 600 meters was obtained by using multiple reflection mirrors. The pressure of the gas varied from 1 to 10 cm for the various bands that were photographed. At 10-cm pressure the lines of the bands are considerably broadened, and therefore no higher pressures were used.

Bands at wavelengths longer than 12 000A were recorded with an infrared grating spectrometer using a lead sulphide cell as a detector. This instrument is similar in design and performance to the spectrometer described by Plyler and Gailar.[9] The spectrometer has been placed in a vacuum chamber in order to eliminate the water and carbon dioxide bands.

The greatest difficulty encountered in using the recording infrared spectrometer was that of obtaining sufficiently accurate wavelength measurements. With an instrument that is capable of resolving 0.1 cm^{-1}, it should be possible to measure the wave number of a line with an error of less than 0.02 cm^{-1}. None of the methods commonly used seem to be capable of giving this accuracy. Therefore, we have adopted a method of measurement using interference fringes from a Fabry-Perot interferometer as our wavelength standards. The arrangement is shown in Fig. 1. White light from a Western Union concentrated arc *A* is focused on a pinhole *B* which is at the focal point of the lens *C*. The parallel light from *C* passes through the interferometer *D* and is focused on a small section of the lower half of the entrance slit of the spectrograph by the lens *E*. The interferometer which has quartz spacers can be kept at constant temperature and is enclosed in a vacuum chamber to eliminate the effect of the variation in the index of refraction of air. Light from the interferometer that has passed through the spectrometer falls on a photomultiplier and the intensity is recorded by a pen recorder. A section of a trace from this recorder is shown in Fig. 2. The interference fringes are produced by light in the visible region, but by using the overlapping orders of the grating they appear at the same grating setting as the near infrared spectrum. The recorder chart showing the interference fringes and a

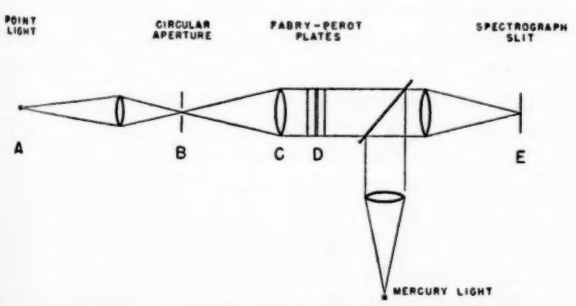

FIG. 1. The optical system of the Fabry Perot interferometer used to produce wavelength standards.

[9] E. K. Plyler and N. Gailar, J. Research Natl. Bur. Standards 47, 248 (1951).

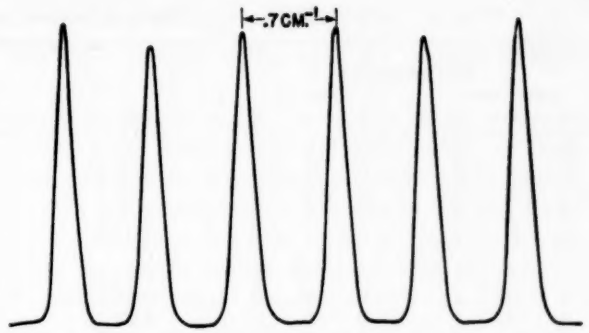

FIG. 2. Interference fringes from a Fabry Perot interferometer recorded by the infrared spectrometer.

chart showing the infrared spectrum can be lined up by fiducial marks on the charts, and the position of the fringes can be transferred to the infrared chart. Since all of the interference fringes are identical it is necessary to find some way of numbering the order of interference of each line. To do this, light from a mercury arc is introduced into the parallel beam of light from the interferometer by means of a narrow mirror across the middle of the beam.

The interferometer can be used in either of two ways. The most accurate method is to calibrate the Fabry Perot spacer by the usual interferometer technique, using some source of monochromatic light such as a Hg^{198} lamp. Once the lengths of the spacers are known, the wavelength of each fringe is determined. The numbering of the fringes can be determined from the known wavelengths of the mercury arc lines that are recorded by the spectrometer. A second method of using the interferometer is to take the mercury lines recorded by the spectrometer as standards and use the interference fringes to produce equal wave number intervals between these mercury lines. This method may not be quite as accurate, but one eliminates the work of calibrating the spacer in the more accurate manner and also eliminates the need for an extremely stable interferometer. In the work described here, the second method of using the interferometer was used. Though the use of an interferometer by no means eliminates all the errors in the measurement of wavelengths, it does provide a convenient method of obtaining accurate wavelength standards which are equally spaced and of equal intensity.

All of the bands photographed in the region from 12 000A to 4500A have been measured and analyzed in detail. For a small region near 9500A only rather poor plates are available, but excluding this region the survey of the photographic infrared spectrum is complete. In the region of the spectrum from 1.2 to 2.5μ no such complete survey was attempted and only those bands that were necessary for our analysis of the spectrum were recorded. For some of these bands, such as the $\nu_2+\nu_3$ band, only the wavelengths of the heads of the *Q* branches have been measured even though it is quite easy to resolve the *P* and *R* branches.

TABLE I. Infrared and Raman bands of HCN.

Band assignment									
Upper state			Lower state			ν cm^{-1} observed	ν cm^{-1} calculated	Obs.-calc.	Comments
v_1	v_2	v_3	v_1	v_2	v_3				
0	1	0	0	0	0	711.7	712.05	−0.35	a
0	2	0	0	0	0	1411.42	1411.89	−0.47	b
1	0	0	0	0	0	2095.5	2096.10	−0.6	Raman line
1	1	0	0	0	0	2804.2	2806.00	−1.8	b
0	0	1	0	0	0	3311.68	3311.50	+0.18	b
0	2^0	1	0	1^1	0	3972.43	3972.14	+0.29	Q branch only measured
0	2^2	1	0	1^1	0	3986.97	3986.66	+0.31	Q branch only measured
0	1	1	0	0	0	4004.25	4003.94	+0.31	Q branch only measured
2	1^1	0	0	0	0	4878.27	4881.95	−3.68	Q branch only measured
1	0	1	0	0	0	5393.77	5390.80	+2.97	Measured with PbS spectrometer
0	0	2	0	0	0	6519.65	6519.34	+0.31	Band origin only measured
1	0	2	0	0	0	8585.56	8581.84	+3.72	Photographic infrared
1	1^1	2	0	0	0	9256.11	9252.54	+3.57	Photographic infrared
0	1^1	3	0	1^1	0	9568.32	9567.90	+0.40	Photographic infrared
0	0	3	0	0	0	9627.02	9626.70	+0.32	Photographic infrared
1	2^0	2	0	0	0	9914.41	9511.03	+3.38	Photographic infrared
1	1^1	3	0	1^1	0	11613.52	11611.45	+2.07	Photographic infrared
1	0	3	0	0	0	11674.47	11672.40	+2.07	Photographic infrared
0	1^1	4	0	1^1	0	12557.31	12558.31	−1.00	Photographic infrared
0	0	4	0	0	0	12635.86	12636.71	−0.85	Photographic infrared
3	0	2	0	0	0	12657.90	12652.84	+5.06	Photographic infrared
2	0	3	0	0	0	13702.30	13700.10	+2.20	Photographic infrared, weak
4	0	2	0	0	0	14653.65	14661.34	−7.69	Photographic infrared
1	0	4	0	0	0	14670.38	14665.61	+4.77	Photographic infrared
0	0	5	0	0	0	15551.92	15552.56	−0.64	Photographic infrared
2	0	4	0	0	0	16667.41	16676.51	−2.3	Photographic infrared, very weak
1	0	5	0	0	0	17551.92	17564.66	−12.74	Photographic infrared
0	0	6	0	0	0	18376.93	18377.40	−0.47	Photographic infrared

[a] See reference 1.
[b] Measured by Shan, Chen, and Bell, Phys. Rev. **75**, 1113 (1949).

III. VIBRATIONAL STRUCTURE OF HCN

The band origins of all the known bands of HCN are listed in Table I. The vibrational energy levels of a linear triatomic molecule are given by the equation:

$$\begin{aligned} G(v_1v_2v_3) = {} & \omega_1(v_1+\tfrac{1}{2})+\omega_2(v_2+1)+\omega_3(v_3+\tfrac{1}{2}) \\ & +x_{11}(v_1+\tfrac{1}{2})^2+x_{22}(v_2+1)^2+x_{33}(v_3+\tfrac{1}{2})^2 \\ & +x_{12}(v_1+\tfrac{1}{2})(v_2+1)+x_{13}(v_1+\tfrac{1}{2})(v_3+\tfrac{1}{2}) \\ & +x_{23}(v_2+1)(v_3+\tfrac{1}{2})+g_2l_2^2+y_{333}(v_3+\tfrac{1}{2})^3. \quad (1) \end{aligned}$$

This is the equation given by Herzberg[10] with the term $y_{333}(v_3+\frac{1}{2})^3$ added. We have found the following constants to represent the observed levels of HCN:

$\omega_1 = 2124.65$ cm^{-1} $x_{11} = -9.0$ $x_{12} = -2.15$ $y_{333} = 0.527$
$\omega_2 = 726.72$ $x_{22} = -2.47$ $x_{13} = -16.8$ $g_2 = 3.63$
$\omega_3 = 3446.19$ $x_{33} = -54.20$ $x_{23} = -19.6$.

With the exception of x_{11} these constants are similar to those given by Adel and Barker.[1] The constant x_{11} in Adel and Barker's work depended upon the value of ν_1 obtained from the Raman work of Kastler[11] and upon their own measurements of the position of the $2\nu_1+\nu_2$ band. Dr. B. Stoicheff, in this laboratory, has photographed the Raman spectrum of HCN gas with a dispersion of 100 cm^{-1} per mm and his plates show the ν_1 frequency excited both by the 4358 and the 4047A mercury lines. From these two Raman lines we have found ν_1 to be at 2095.5 cm^{-1}. The value given by Kastler was 2089 cm^{-1}. Our infrared measurements of the $2\nu_1+\nu_2$ band show it to be at 4878.3 cm^{-1}, and it appears that there is an error in the work of Adel and Barker who give 4992.5 cm^{-1} for this band. The new measurements change the value of x_{11} from +52.0 to a more reasonable value of −9.0 cm^{-1}. This change in x_{11} causes a considerable change in ω_1.

In Table I the positions of the band origins calculated from the constants listed above and the differences between the observed and calculated positions are given. These differences are much greater than the experimental error in the measurements. There are two possible reasons for the failure of Eq. (1) to represent the bands. First, there is the possibility that additional cubic terms may be necessary to represent the bands. It is quite possible that terms such as y_{133}, y_{113}, and y_{111} could contribute ten wave numbers or even more to a vibrational level such as the $4\nu_1+3\nu_3$ level. A second cause for the failure of the equation to represent the band origins lies in the presence of perturbations in the vibrational energy levels, and it appears certain that

[10] G. Herzberg, *Infrared and Raman Spectra of Polyatomic Molecules* (D. Van Nostrand, Company, Inc., New York, 1945).
[11] A. Kastler, Compt. rend. **194**, 858 (1932).

no reasonably simple algebraic equation can be satisfactory. This effect is illustrated in Table II. In this table the wave numbers of the $v_3\nu_3$ and $\nu_1+v_3\nu_3$ series of bands are given together with their first, second, and third differences. For the bands to be represented by a quadratic equation, the second differences should be constant and should be the same for both series. This clearly is not so. The third differences for the $v_3\nu_3$ series are not constant, but the average value was used to determine the constant y_{333}. The $\nu_1+v_3\nu_3$ series is much more irregular than the $v_3\nu_3$ series. Much of this irregularity can be attributed to a perturbation in the $\nu_1+4\nu_3$ band. If the $\nu_1+4\nu_3$ band were at 14662.38 cm^{-1} instead of the observed value of 14670.38 cm^{-1}, then the second differences would become much more nearly equal. Though there does appear to be a perturbation in the $\nu_1+4\nu_3$ band, and possibly in the $4\nu_3$ band, these perturbations cannot readily account for the fact that the second differences of the $v_3\nu_3$ series are considerably different from those of the $\nu_1+v_3\nu_3$ series.

The presence of a perturbation in the position of the $\nu_1+4\nu_3$ band, and possibly a small perturbation in the position of the $4\nu_3$ band, seems to be coupled with the presence of two unexpected bands, namely, the $3\nu_1+2\nu_3$ and $4\nu_1+2\nu_3$ bands. The $\nu_1+2\nu_3$ band of HCN is quite strong but the $2\nu_1+2\nu_3$ band is very weak; thus, one might expect the $3\nu_1+2\nu_3$ and $4\nu_1+2\nu_3$ bands to be extremely weak. Also neither the $3\nu_1+\nu_3$ nor the $4\nu_1+\nu_3$ bands have been found even though they also lie in the photographic infrared where long absorption paths were used. In spite of these considerations, the $3\nu_1+2\nu_3$ and $4\nu_1+2\nu_3$ bands are reasonably strong bands. It is probable that the $3\nu_1+2\nu_3$ and $4\nu_1+2\nu_3$ bands gain their strength by an interaction between their upper states and the upper states of the $4\nu_3$ and $\nu_1+4\nu_3$ bands. This resonance arises from the fact that $3\nu_1$ is almost equal to $2\nu_3$. There is no obvious reason why such an interaction should occur only for the $4\nu_3$ and $\nu_1+4\nu_3$ bands since any band with v_3 greater than two might be expected to show similar effects and be accompanied by a resonance companion. Though the $3\nu_3$ and $\nu_1+2\nu_3$ bands are much stronger than the $4\nu_3$ and $\nu_1+4\nu_3$ bands, no resonance companions are found. It is possible that theoretical calculations would show that these peculiarities are caused by the fact that the anharmonicity makes the resonance particularly close at the $4\nu_3$ and $\nu_1+4\nu_3$ levels.

Since the positions of the bands cannot be represented precisely by Eq. (1), it is impossible to determine accurate constants for this equation. The values of the constants given above are a set that represent the bands without any very large differences between the observed and calculated values. An equally good fit can, however, be obtained with constants significantly different from those given here.

IV. ROTATIONAL STRUCTURE OF HCN

The wave numbers of the lines of the bands of HCN are listed in Table III.

For the stronger bands the rotational constants B_v and D_v were obtained by plotting $\Delta_2F(J)/(J+\frac{1}{2})$ against $(J+\frac{1}{2})^2$. In this way, using the mean value of the lower state combination differences, B_0 was found to be 1.4782 cm^{-1}. A better value of B_0, and the one used in this paper, can be obtained from the $J=0$ to $J=1$ transition found in the microwave region at 88631.55 mc.[7,8] If this value is corrected for the centrifugal stretching constant D and a value of 299 790 km/sec is used for the velocity of light, one obtains $B_0=1.47823$ cm^{-1}. From their precise work, Rank, Ruth, and Vander Sluis found $B_0=1.47829$ cm^{-1}, but the difference between their value and the microwave value given above is not significant to the degree of accuracy obtained in our work.

For the weaker bands, the B value of the upper state was obtained by plotting $R(J-1)+P(J)$ against J^2. This plot gives a line with a slope $2(B'-B'')$ and the $B'-B''$ so obtained was combined with the microwave value of B_0 to give the B_v of the upper state. From the intercept of the same plot the band origins were obtained. The values of B_v are listed in Table V.

The B values of a linear triatomic molecule can be represented by the equation

$$B_{v_1v_2v_3}=B_e-\alpha_1(v_1+\tfrac{1}{2})-\alpha_2(v_2+1)-\alpha_3(v_3+\tfrac{1}{2}). \quad (2)$$

In Table IV the values of the α's and B_e are listed. α_2 is the least accurate of these constants since it could be obtained only from the lower state of the bands oribinating in the $v_2=1$ level or from the $\nu_1+\nu_2+2\nu_3$

TABLE II. Table showing irregularities in series of bands.

v_1	v_2	v_3	ν cm^{-1}	$\Delta\nu$ cm^{-1}	$\Delta^2\nu$ cm^{-1}	$\Delta^3\nu$
0	0	0	0			
				3311.68		
0	0	1	3311.68		103.71	
				3207.97		2.06
0	0	2	6519.65		101.65	
				3106.32		4.17
0	0	3	9627.02		97.48	
				3008.84		4.70
0	0	4	12635.86		92.78	
				2916.06		1.73
0	0	5	15551.92		91.05	
				2825.01		
0	0	6	18376.93			
1	0	0	2095.5			
				3298.27		
1	0	1	5393.77		106.48	
				3191.79		2.60
1	0	2	8585.56		103.88	
				3088.91		10.88
1	0	3	11674.47		93.00	
				2995.91		−21.37
1	0	4	14670.38		114.37	
				2881.54		
1	0	5	17551.92			

TABLE III. Wave numbers of the lines of HCN bands (ν_{vac} cm^{-1}).

	$\nu_1+\nu_3$		$\nu_1+2\nu_3$		$\nu_1+\nu_2+2\nu_3$		
J	$R(J)$	$P(J)$	$R(J)$	$P(J)$	$R(J)$	$Q(J)$	$P(J)^r$
0	5396.72		8588.45		9259.03		
1	99.55	5390.82	91.29	8582.60	61.82		
2	5402.41	87.81	94.06	79.57	64.58	9256.03	9250.08
3	05.19	84.77	96.77	76.48	67.38	55.88	
4	07.94	81.71	99.45	73.38	69.97	55.68	43.89
5	10.68	78.59	8602.00	70.21	72.56	55.42	40.72
6	13.31	75.47	04.54	66.90	75.10	55.12	37.46
7	15.95	72.26	06.99	63.57	77.55	54.80	34.07
8	18.53	69.00	09.40	60.21	79.93	54.45	30.74
9	21.09	65.72	11.75	56.75	82.22	54.03	27.29
10	23.62	62.41	14.01	53.26	84.61	53.56	23.80
11	26.06	59.03	16.19	49.69	86.77	53.07	20.22
12	28.49	55.64	18.37	46.06	88.95	52.51	16.65
13	30.86	52.21	20.47	42.36	91.00	51.94	12.95
14	33.23	48.73	22.44	38.60	93.06	51.27	09.13
15	35.49	45.19	24.43	34.82		50.58	05.37
16	37.75	41.66	26.35	30.94		49.81	01.53
17	39.97	38.06	28.19	26.98		49.05	9197.53
18	42.16	34.59	29.95	22.98			
19	44.29	30.73	31.69	18.94			
20	46.30	27.04	33.32	14.84			
21	48.42		34.91	10.65			
22	50.42		36.41	06.43			
23	52.39		37.88	02.10			
24	54.34		39.29	8497.80			
25			40.63	93.36			
26			41.89				
27			43.12				
28			44.26				
29			45.33				
30			46.41				

	$3\nu_3$		$\nu_1+2\nu_2+2\nu_3$		$\nu_1+3\nu_3$		$\nu_1+\nu_2+3\nu_3-\nu_2$	
J	$R(J)$	$P(J)$	$R(J)$	$P(J)$	$R(J)$	$P(J)$	$R(J)$	$P(J)$
0	9629.92		9917.28		11677.34			
1	32.74	9624.07	19.99	9911.48	80.14	11671.51	11619.20	
2	35.51	21.05	22.95	08.30	82.85	68.47		11607.58
3	38.20	17.95	25.71	05.32	85.47	65.35	24.59	04.16
4	40.83	14.82	28.42	02.21	88.01	62.13	27.09	01.17
5	43.40	11.60	31.10	9899.16	90.48	58.85		11597.90
6	45.91	08.32	33.77	95.87	92.85	55.47	32.01	94.44
7	48.33	04.98	36.38	92.72	95.13	52.03	34.31	91.11
8	50.71	01.56	38.91	89.39	97.33	48.47	36.45	87.55
9	53.03	9598.10	41.39	86.03	99.45	44.86	38.68	83.93
10	55.28	94.56	43.72	82.79	11701.50	41.17	40.60	80.13
11	57.46	90.97	46.12	79.38	03.42	37.38	42.68	76.48
12	59.55	87.32	48.44	75.77	05.29	33.52	44.86	72.60
13	61.60	83.60	50.68	72.32	07.08	29.58	46.34	68.64
14	63.60	79.84	52.97	68.68	08.79	25.55		64.59
15	65.52	75.97	55.08	65.14	10.41	21.43	49.78	60.51
16	67.36	72.06	57.14	61.50	11.93	17.23	51.27	56.34
17	69.17	68.08	59.17	57.57	13.37	12.96	52.72	52.03
18	70.87	64.04	61.27	53.88	14.74	08.59	54.15	47.66
19	72.56	59.93	63.22	50.12	16.03	04.16	55.47	43.23
20	74.14	55.76	65.03		17.22	11599.64	56.73	38.81
21	75.65	51.55	66.75		18.33	95.03		34.20
22	77.12	47.25	68.53		19.36	90.35		
23	78.52	42.88			20.32	85.57		
24	79.85	38.48			21.18	80.73		
25	81.07	33.99			21.93	75.79		
26	82.34	29.53			22.64	70.77		
27	83.45	24.92			23.24	65.70		
28	84.52				23.75	60.51		
29	85.50				24.19	55.28		
30					24.58	49.92		
31					24.91	44.49		
32					25.18			

TABLE III.—*Continued.*

J	$4\nu_3$ R(J)	$4\nu_3$ P(J)	$\nu_2+4\nu_3-\nu_2$ R(J)	$\nu_2+4\nu_3-\nu_2$ P(J)	$3\nu_1+2\nu_3$ R(J)	$3\nu_1+2\nu_3$ P(J)	$2\nu_1+3\nu_3$ R(J)	$2\nu_1+3\nu_3$ P(J)
0	12638.72				12660.62			
1	41.53	12632.91	12562.97		63.49			
2	44.22	29.86	65.69	12551.32				
3	46.82	26.73	68.31	48.16	68.70	12648.68		13693.12
4	49.33	23.52	70.86	44.94		45.41	13715.52	89.78
5	51.76	20.20	73.27	41.66	73.47	42.09	17.83	86.50
6	54.12	16.80	75.68	38.24	75.80		20.10	83.04
7	56.37	13.33		34.78	77.93	35.07	22.29	79.41
8	58.54	09.77	80.14	31.25	79.96	31.42	24.23	75.81
9	60.62	06.10	82.36	27.59		27.65	26.23	72.10
10	62.61	02.39	84.20	23.85	83.77		28.11	68.13
11	64.49	12598.54	86.17	20.12	85.53	19.87	29.75	64.14
12	66.29	94.62	88.04	16.17	87.15	15.80	31.39	
13	68.02	90.63	89.71	12.17	88.71	11.64	32.90	55.84
14	69.65	86.56	91.53	08.12	90.17	07.41	34.31	51.58
15	71.20	82.36	93.06	03.96	91.54	03.07	35.68	47.19
16	72.66	78.14	94.27	12499.72	92.76	12598.54?	36.85	42.74
17	74.04	73.76	96.00	95.42	93.89	94.07?		38.21
18	75.33	69.33	97.38	91.01	94.96			33.39
19	76.52	64.81			95.90			28.76
20	77.61	60.20	99.72	81.99	96.72			23.84
21	78.63	55.50	12601.33		97.51	74.91		
22	79.55	50.74			98.13			
23	80.39	45.87			98.70			
24	81.14	40.91						
25	81.86	35.88						
26	82.37	30.76						
27	82.86	25.56						
28	83.24	20.12						
29		14.88						

J	$\nu_1+4\nu_3$ R(J)	$\nu_1+4\nu_3$ P(J)	$4\nu_1+2\nu_3$ R(J)	$4\nu_1+2\nu_3$ P(J)	$5\nu_3$ R(J)	$5\nu_3$ P(J)	$2\nu_1+4\nu_3$ R(J)	$2\nu_1+4\nu_3$ P(J)
0	14673.24		14656.48		15554.74			
1	76.00	14667.50	59.22	14650.68	57.48	15548.95	16679.6	
2	78.67	64.38	61.83	47.62	60.13	45.92	82.1	
3	81.14	61.23	64.37	44.41	62.62	42.69	84.6	
4	83.52	57.91	66.73	41.13	65.04	39.42	87.0	16661.5
5	85.81	54.50	69.01	37.71	67.33	36.03	89.5	57.9
6	87.94	51.01	71.19	34.20	69.52	32.52	91.2	54.0
7	90.01	47.36	73.24	30.58	71.58	28.89	93.2	50.7
8	91.96	43.61	75.17	26.84	73.53	25.18	95.0	46.7
9	93.77	39.76	76.99	22.99	75.39	21.34	96.8	42.9
10	95.49	35.79	78.67	19.02	77.13	17.39	98.3	38.8
11	97.10	31.68	80.30	14.93	78.76	13.33	99.7	34.6
12	98.59	27.53	81.78	10.75	80.28	09.17	16701.1	30.0
13	99.97	23.23	83.13	06.42	81.68	04.91	02.3	
14	14701.24	18.79	84.40	02.01	82.97	00.50	03.4	
15	02.39	14.29	85.54	14597.51	84.16	15496.01		
16	03.43	09.84	86.55	92.83	85.24	91.41		
17	04.37	04.92	87.44	88.10	86.18	86.69		
18	05.19	00.05	88.24	83.19	87.04	81.88		
19	05.90	14595.14	88.93	78.26	87.77	76.95		
20	06.50	90.08	89.43		88.43	71.88		
21	06.97	84.89			88.94	66.78		
22	07.34	79.62			89.32	61.54		
23	07.65	74.16						
24	07.84							

TABLE III.—*Continued.*

	$\nu_1+5\nu_3$		$6\nu_3$		$3\nu_3$ $HC^{13}N$	
J	$R(J)$	$P(J)$	$R(J)$	$P(J)$	$R(J)$	$P(J)$
0	17553.21		18379.88			
1	55.92	17547.31	82.49	18373.95	9577.28	
2	58.50	44.35	85.10	70.84		9565.85
3	60.88	41.09	87.43	67.61	82.61	62.88
4	63.25	37.80	89.73	64.20	85.21	
5	65.41	34.27	91.86	60.78		56.73
6	67.45	30.72	93.86	57.15	90.26	53.58
7	69.39	26.97	95.75	53.35	92.61	50.29
8	71.20	23.09	97.43	49.50		46.99
9	72.87	19.13	99.06	45.44	97.22	43.66
10	74.39	15.02	18400.60	41.30	99.43	40.24
11	75.81	10.78	01.94	37.00		36.77
12	77.11	06.43	03.09	32.57	9603.69	33.25
13	78.22	01.96	04.17	28.04		
14	79.27	17497.36	05.06	23.30	07.74	25.99
15	80.22	92.57	05.89	18.59	09.69	22.31
16	80.95	87.71	06.59	13.54		18.57
17	81.55	82.74	07.18	08.46	13.36	14.77
18	82.11	77.62		03.09		
19	82.54	72.36		18297.81	16.75	06.88
20	82.84	66.92				
21		61.53			19.28	
22		55.76				9494.67
23		50.09				

	$\nu_1+2\nu_2+\nu_3$	
J	$R(J)$	$P(J)$
0		
1	9574.08	
2	76.86	9562.37
3		59.27
4	82.22	56.10
5	84.81	52.90
6		49.62
7	89.78	46.28
8	92.17	
9		39.42
10	96.65 96.89	35.89
11	98.87 99.08	32.29
12	9600.98 01.28	28.63
13	03.05 03.33	
14		21.15
15	06.98 07.31	17.30
16	08.84 09.20	13.42
17	10.65 11.02	09.45
18	12.40 12.80	05.41
19	14.09	01.35
20	15.69 16.15	9497.18
21	17.23	93.01
22	18.68 19.19	88.69
23		84.35

and $\nu_1+2\nu_2+2\nu_3$ bands. The latter bands are relatively weak, and, as will be discussed later, higher order terms may introduce errors in the values of the α's found from these bands. All the bands originating from the $v_2=1$ level found by us are "hot" bands of the type $\nu_2+\nu_j-\nu_2$ and are overlapped by the much stronger bands originating from the ground state. In the final determination of α_2 the means of all the values of $\Delta_2F(J)$ for the 010 level were used. The sum $\alpha_1+\alpha_3$ was determined by finding $B'-B''$ from the $\nu_1+\nu_3$ and. α_3 was determined from the $3\nu_3$ band and this α_3, when combined with the $\alpha_1+\alpha_3$ already determined, gave α_1.

B_e is given by the expression $B_e=B_0+\frac{1}{2}(\alpha_1+\alpha_3)+\alpha_2$. Since the sum of $\alpha_1+\alpha_3$ was determined from the $\nu_1+\nu_3$ band and α_2 was determined from the "hot" bands, these bands alone were used in the determination of B_e from B_0.

The values of the α's and of B_e given in Table IV have been used to calculate all the values of B_v, and these are listed in Table V. It can be seen that, though the difference between the observed and calculated B values is in many cases within the experimental error (about 0.0002 cm^{-1}), there are some differences much greater than this error. For the two levels $\nu_1+4\nu_3$ and $4\nu_1+2\nu_3$, even though the calculated B values are quite different, the observed B values are nearly the same. There seems little doubt that it is the interaction discussed in the section on the vibrational analysis that also causes these two B values to deviate so far from the expected values. Aside from these two perturbed levels it is possible to make the agreement between observed and calculated B_v values considerably better by introducing a term $\gamma_{33}(v_3+\frac{1}{2})^2$ into Eq. (2). Even with this additional term there are still some B values that cannot

TABLE IV. D_0, B, and α values for HCN and DCN (cm^{-1}).

Molecule	B_0	α_1	α_2	α_3	B_e	D_0
HCN	1.47823	0.00950	−0.0035	0.01079	1.4849±0.0003	2.85×10^{-6}
DCN	1.20776	0.00628	−0.0043	0.01035	1.2118±0.0003	2.1×10^{-6}

be represented within experimental error by the equation.

The failure of Eq. (2) to represent the B values was also noted when we attempted a second method of determining α_2. Suppose we consider any band and the "hot" band (band of the type $\nu_2+\nu_i-\nu_2$) associated with it. Consider the R branches of the two bands and let the subscript c refer to the strong band and h to the hot band

$$R_h(J)=\nu_{0h}+B_h'(J+1)(J+2)-B_h''J(J+1),$$
$$R_c(J)=\nu_{0c}+B_c'(J+1)(J+2)-B_c''J(J+1),$$
$$R_h(J)-R_c(J)=\nu_{0h}-\nu_{0c}+(B_h'-B_c')(J+1)(J+2)-(B_h''-B_c'')J(J+1)$$
$$=\nu_{0h}-\nu_{0c}+2\alpha_2(J+1)$$
$$\text{(if } B_h'-B_c'=B_h''-B_c''=\alpha_2).$$

A similar equation applies to the P branches and by proper numbering the two equations can be combined into one equation linear in J. It can be shown that higher order terms can be neglected except for very high J values. Therefore, if Eq. (2) were valid and the differences of the wave numbers of the corresponding lines in the two bands are plotted against J, the points representing the differences should lie on a straight line of slope $2\alpha_2$. In Fig. 3 these differences are plotted for the $3\nu_3$ and the $\nu_2+3\nu_3-\nu_2$ bands. Though the scatter of points is large, it seems certain that the points do not fall on a straight line. A similar effect has been noted for other bands of HCN and for the $\nu_1+\nu_3$ band of DCN. The failure of the points to lie on a straight line appears to be caused by the fact that $B_h'-B_c'$ does not equal $B_h''-B_c''$ as required by Eq. (2), and as a result the differences between the corresponding lines are a quadratic function of J.

The failure of Eq. (2) to represent the B_v values of all the levels appears therefore to be caused by two separate effects. First, there are the perturbations in B values that accompany an observed vibrational perturbation. Secondly, there are deviations from Eq. (2) that appear to be in no way related to perturbations. It is possible that this second type of deviation from the simple equation could be attributed to higher order terms of the type $\gamma_{ij}(v_i+\frac{1}{2})(v_j+\frac{1}{2})$ that have been neglected. Another possibility is that there are many small perturbations that do not appear obvious from the vibrational analysis, and these small perturbations are sufficient to alter the B values by a measurable amount. Our B values can certainly be represented by Eq. (2) if we add six terms of the type $\gamma_{ij}(v_i+\frac{1}{2})(v_j+\frac{1}{2})$ (except for the B values of the $\nu_1+4\nu_3$ and $4\nu_1+2\nu_2$ levels), but the data are not sufficiently accurate to be sure that the γ's so obtained have any real meaning. It is because of the possibility of the existence of quadratic terms in Eq. (2) that we have determined the α-values used in finding B_e from the ν_2 and the $\nu_1+\nu_3$ levels where the higher order terms can have little effect, rather than using average α-values determined from all the levels.

Only one Q branch of a perpendicular band was resolved, this being the Q branch of the $\nu_1+\nu_2+2\nu_3$ band. In the strong $\nu_2+\nu_3$ perpendicular band B' and B'' are very nearly equal and, even with an instrument capable of resolving 0.1 cm^{-1}, very little of the rotational structure of the Q branch could be seen. All of the other perpendicular bands that we found were weak.

The II-levels of a nonrotating linear molecule are degenerate, but the rotation of the molecule removes this degeneracy giving rise to the so-called l type doubling. There are two energy levels for every J value and two effective B values differing by a constant q. One of the effective B values can be obtained from the Q branch of a perpendicular band and the other from the P and R branches. From the $\nu_1+\nu_2+2\nu_3$ band it was found that the Q branch gave $B=1.4552$ cm^{-1} and the P and R branches gave $B=1.4476$ cm^{-1}. The best method of finding the constant q is to plot the difference between $\Delta_1F(J)$, determined by the Q and R branches, and $\Delta_1F(J)$, determined from the Q and P branches, against $(J+1)^2$. This plot gives a line with a slope $2q$. For the $\nu_1+\nu_2+2\nu_3$ band such a plot showed that $q_{112}=0.00764$ cm^{-1}. The value of q determined for the $v_2=1$ state by microwave measurements is $q_{010}=0.00747$

TABLE V. Observed and calculated values of B_v for HCN

v_1	v_2	v_3	B_{obs}	B_{calc}	Obs.-Calc.
0	0	0	1.47823	1.47823	0.0000
0	1	0	1.4817	1.4817	0.0000
1	0	1	1.4579	1.4579	0.0000
1	0	2	1.4474	1.4471	0.0003
1	1	2	1.4514	1.4507	0.0007
0	0	3	1.4459	1.4459	0.0000
1	2	2	1.4542	1.4542	0.0000
1	0	3	1.4365	1.4364	0.0001
0	0	4	1.4345	1.4351	−0.0006
3	0	2	1.4283	1.4281	0.0002
2	0	3	1.4270	1.4269	−0.0001
1	0	4	1.4225	1.4256	−0.0031
4	0	2	1.4218	1.4186	0.0032
0	0	5	1.4231	1.4243	−0.0012
2	0	4	1.416	1.4161	0.000
1	0	5	1.4142	1.4148	−0.0006
0	0	6	1.4112	1.4135	−0.0023

TABLE VI. Infrared bands of DCN.

Band assignment Upper state v_1	v_2	v_3	Lower state v_1	v_2	v_3	ν cm^{-1}	Comments
0	1	0	0	0	0	568.9	a
0	2	0	0	0	0	1131.5	Perkin-Elmer spectrometer
1	0	0	0	0	0	1928	b
0	0	1	0	0	0	2629.3	a
1	1	1	0	1	0	4510.4	
1	0	1	0	0	0	4523.2	
0	1	2	0	1	0	5188.9	
0	0	2	0	0	0	5220.3	
0	1	2	0	0	0	5758.0	Fine structure not measured

[a] See reference 2.
[b] See reference 13.

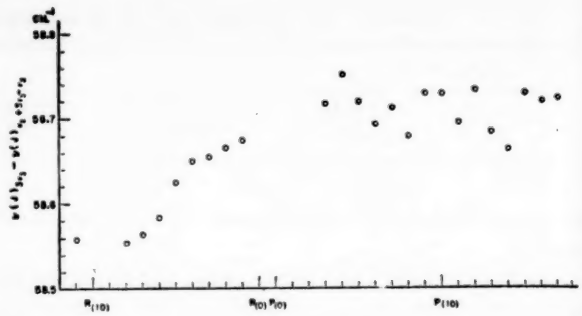

FIG. 3. The wave number differences between the absorption lines of the $3\nu_3$ band and the corresponding lines of the $\nu_2+3\nu_3-\nu_2$ band. The points would lie on a straight line if Eq. (2) were valid.

cm^{-1}.[12] This determination of q therefore removes the discrepancy between the microwave value of q and that calculated by Herzberg[13] from Lindholm's quite inaccurate value of α_2.

The magnitude of the l type doubling can also be found for the $\nu_2+3\nu_3$ level. The $\Pi-\Pi$ band $\nu_2+3\nu_3-\nu_2$ has the $\nu_2+3\nu_3$ level as its upper level and, as is shown in Table III, the lines of the R branch of this band can be resolved into doublets. If q' is the l type doubling constant of the $\nu_2+3\nu_3$ level and q'' is the constant for the ν_2 level then this doublet separation $\Delta R(J)$ can be represented by

$$\Delta R(J)=2q'+(3q'-q'')J+(q'-q'')J^2.$$

Since the doublet separation has been measured and

TABLE VII. Wave numbers of the lines of the DCN bands.

	$\nu_1+\nu_3$		$\nu_1+\nu_2+\nu_3-\nu_2$		$2\nu_3$		$2\nu_3+\nu_2-\nu_2$	
J	$R(J)$	$P(J)$	$R(J)$	$P(J)$	$R(J)$	$P(J)$	$R(J)$	$P(J)$
0	4525.64				5222.70			
1	27.98	4520.83	4515.16		25.04	5217.92	5193.62	
2	30.30	18.37	17.48		27.34	15.45	95.96	5184.02
3	32.58	15.91	19.78		29.59	12.95	98.81	81.52
4	34.83	13.39	22.03		31.82	10.42	5200.54	78.98
5	37.03	10.84	24.26	4497.93	33.96	07.84		
6	39.22	08.26	26.43	95.36	36.09	05.21	04.76	
7	41.37	05.61	28.60	92.73	38.20	02.56	06.89	71.09
8	43.48	02.99	30.74	90.09	40.23	5199.85	08.93	68.41
9	45.56	00.34	32.79	87.40	42.28	97.16	10.94	65.66
10	47.61	4497.61		84.67	44.16	94.31		62.89
11	49.62	94.86		81.92	46.07	91.48	14.90	60.05
12	51.61	92.08		79.15	47.96	88.63	16.82	57.09
13	53.56	89.25	40.86	76.33	49.77	85.72	18.59	
14	55.45	86.39	42.80	73.46	51.59	82.75	20.42	51.53
15	57.34	83.54	44.68	70.62	53.32	79.79	22.24	48.35
16	59.17	80.65	46.53	67.71	55.02	76.73	23.92	45.34
17	61.00	77.70	48.43	64.76	56.69	73.69	25.44	42.28
18	62.78	74.73	50.15	61.80	58.33	70.58		39.21
19	64.52	71.71		58.82	59.90	67.43	28.89	36.03
20	66.21	68.66			61.44	64.22	30.47	32.88
21	67.90	65.61			62.92	60.98		
22	69.53	62.52			64.36	57.83	33.46	
23	71.13	59.37			65.78	54.39	34.93	
24	72.70	56.22			67.16	51.04		
25	74.26	53.02			68.48	47.54		
26	75.74				69.76	44.22		
27					71.00	40.76		
28					72.20	37.21		
29						33.78		
30						30.07		
31						26.43		

[12] R. G. Shulman and C. H. Townes, Phys. Rev. 77, 421 (1950).
[13] G. Herzberg, Revs. Modern Phys. 14, 219 (1942).

since q'' is known to be 0.00747 cm^{-1}, we can solve for q'. This calculation shows that $q_{013}=0.00779$ cm^{-1}.

V. DCN VIBRATIONAL STRUCTURE

The fine structures of the $2\nu_3$, $\nu_1+\nu_3$ and $\nu_1+\nu_2+\nu_3-\nu_2$ bands of DCN have been measured, and the position of the Q head of the $\nu_2+2\nu_3$ band has been determined with the grating spectrometer. The $2\nu_2$ band has been measured by Dr. P. Dyne in this laboratory with a Perkin-Elmer spectrometer. The positions of these bands along with the other known bands of DCN are listed in Table VI. These bands by themselves are insufficient to determine all of the vibrational constants of Eq. (1) for DCN. However, since the values of the ω's are known for HCN, it is possible to calculate values of ω_2 and the product $\omega_1\omega_3$ for DCN. Since the product rule holds rigorously for the zero-order frequencies, the constants of DCN so calculated should be quite accurate. These isotope relationships along with the measured bands are sufficient to determine all the constants of Eq. (1). Since $2\nu_2$ and ν_1 have been measured only with instruments of low dispersion the error in some of the anharmonic constants may be large. The errors in the ω values should, however, be much less than one percent. The constants that we have obtained are

$\omega_1=1953.4$ cm^{-1} $x_{11}=-5.7$ cm^{-1} $x_{12}=+2.9$ cm^{-1}
$\omega_2=579.6$ cm^{-1} $x_{22}=-1.8$ cm^{-1} $x_{13}=-34.0$ cm^{-1}
$\omega_3=2700.25$ cm^{-1} $x_{33}=-19.15$ cm^{-1} $x_{23}=-15.7$ cm^{-1}
$g=+1.35$ cm^{-1}.

VI. DCN ROTATIONAL ANALYSIS

The wave numbers of the lines of the DCN bands are listed in Table VII. From the $\nu_1+\nu_3$ band, B_0 was found to be 1.2079, but the more accurate microwave value of 1.20776 cm^{-1} will be used in this work. From the "hot" bands and from the $\nu_1+\nu_3$ band, B_e was determined in the same way as for HCN. α_3 was determined from the $2\nu_3$ band. The values of the rotational constant are given in Table IV.

VII. DISCUSSION

The perturbations in the vibrational energy levels and in the B_v values of HCN are somewhat surprising since the vibrational frequencies are well separated and are not simple multiples. G. Herzberg and L. Herzberg, in their discussion of the N_2O spectrum,[14] have pointed out that perturbations in the vibrational energy levels of polyatomic molecules are fairly general and suggest that HCN should be an "ideal" molecule and free from these effects. Now that perturbations have been found in the spectrum of HCN it appears that they have been found in the spectrum of every molecule for which the overtone region has been extensively investigated. It follows that if one is to obtain accurate constants for any molecule it is necessary to examine the whole spectrum to determine whether or not any given level is seriously perturbed.

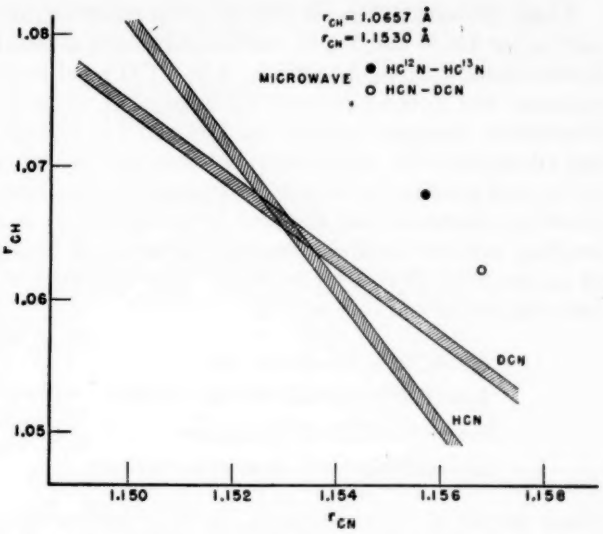

FIG. 4. The graphical determination of the internuclear distances in HCN. The two shaded bands represent the values of the C−H and C−N distances that are consistent with the measured values of B_e for HCN and DCN. The two additional points represent two determinations of the internuclear distances from the microwave values of B_0.

From the values of B_e of HCN and DCN it is possible to determine the equilibrium internuclear distances of these molecules. This calculation leads to

$$r_e(\text{CH})=1.065_7\text{A} \quad \text{and} \quad r_e(\text{CN})=1.1530\text{A}.$$

The largest error in the determination of the internuclear distances arises from the error in α_2. Although there is no very satisfactory way of determining this error, the measurements seem to indicate that there is well over a fifty percent chance that the true value of B_e lies within the ranges indicated in Table IV. The way in which the errors in B_e affect the determination of the internuclear distances can best be visualized by solving the two equations for the internuclear distances graphically as is shown in Fig. 4. In this figure the values of the CH distances that are consistent with the known moments of inertia are plotted against the CN distances for both HCN and DCN. The widths of these shaded strips correspond to the error in the B_e values given in Table IV. The area covered by the two shaded strips in the region where they cross allows one to estimate the error in the determination of the internuclear distances. In order to illustrate the error introduced by using B_0 instead of B_e in the calculation of internuclear distances two points determined from the microwave values of B_0 are shown on the same graph. It is interesting to note that the equiiibrium C−H distance determined here for HCN agrees very closely with the equilibrium C−H distance of 1.0637A in the isoelectronic molecule C_2H_2, determined by Saksena.[15]

[14] G. Herzberg and L. Herzberg, J. Chem. Phys. **18**, 1551 (1950).

[15] B. D. Saksena, J. Chem. Phys. **20**, 95 (1952).

From the zero-order vibrational frequencies ω_1, ω_2, and ω_3 for HCN and DCN, we have obtained a set of force constants k_1, k_2, k_{12}, and k_δ. k_1 is a CH bond force constant and k_2 is a CN bond force constant. k_{12} is an interaction constant between the CH and CN stretching vibrations. The relationship between the constants k_1, k_2, and k_{12} and the zero-order frequencies, has been given by Bartunek and Barker.[2] The constant k_δ is a bending constant and the equation giving k_δ in terms of ω_2 has been given by Herzberg.[10] The constants we have determined in this way are

$$k_1 = 6.292 \times 10^5 \text{ dynes/cm}$$
$$k_2 = 18.583 \times 10^5 \text{ dynes/cm}$$
$$k_{12} = -0.1457 \times 10^5 \text{ dynes/cm}$$
$$k_\delta = 0.2596 \times 10^{-11} \text{ dynes cm/radian.}$$

Since this set of force constants has been derived from zero-order frequencies, it is superior to those sets derived by Bartunek and Barker[2] and by Richardson[16] from the frequencies of the observed bands. From the anharmonic constants and the α values for both HCN and DCN it is possible to derive the constants for a higher order potential function as has already been done by Brooks[17] from less reliable data.

Recently it has been shown by Townes and collaborators[18] that all of the known microwave lines for the various isotopic species of CH_3Cl and CH_3Br could be fitted by a single set of molecular parameters if one assumes that the zero-point vibrations cause the effective C−D bond to be 0.009A shorter than the C−H bond, and the angle between the C−D bond and the molecular axis to be 12′ greater than the corresponding angle for C−H. It was also assumed that the replacement of a hydrogen atom by its heavier isotope changed only the C−H bond distance. It is of interest to see if this method of correcting for the effect of zero-point vibration gives reasonable agreement with the known data for HCN. If one assumes the C−H bond to be 0.009A longer than the C−D bond, then from the microwave lines of HCN and DCN one finds r_0(CH) $=1.083$A, r_0(CD)$=1.074$A, and r_0(CN)$=1.1527$A. If these r_0 distances are compared with the corresponding r_e then one finds that the zero-point vibration causes the CH bond distance to increase by 0.016A, and the CN distance to decrease slightly. In HCN (but not DCN) the CH and the CN vibrations are nearly independent, and one finds that for both of these vibrations the α's are positive, and of the same order of magnitude. It appears, therefore, that in HCN the zero-point vibration tends to increase both the effective CH and CN distances. Thus, the results calculated by assuming the effective C−H bond is 0.009A longer than the CD bond are not in agreement with the observed values of the α's. Also the large change in α_1 that results from the substitution of deuterium for hydrogen tends to show that this substitution does affect the C−N bond distance. It appears, therefore, that the assumptions that lead to a satisfactory representation of the microwave lines of the methyl halides are not valid for the HCN molecule. It is also of interest to note that for the diatomic CH molecule the zero-point vibration lengthens the effective CH bond 0.0103A and the CD bond 0.0075A thus creating a difference of 0.0028A. A difference of about this magnitude would give a more reasonable representation of the data for HCN.

We wish to thank Dr. G. Herzberg for much helpful advice during the course of the work. We also wish to acknowledge the help of Dr. B. Stoicheff and Dr. P. Dyne in the experimental work, and Mrs. K. Innes who carried out a large part of the measurements and calculations.

[16] W. S. Richardson, J. Chem. Phys. **19**, 1213 (1951).
[17] W. Brooks, Trans. Faraday Soc. **47**, 1152 (1951).
[18] Miller, Aamot, Dousmanis, Townes, and Kraitchman, J. Chem. Phys. **20**, 1112 (1952).

On the Radiofrequency Spectrum of the Components of a Sodium Chloride Beam.*† The Dimerization of the Alkali Halides

STEFAN A. OCHS,‡ ROBERT E. COTÉ, AND P. KUSCH
Columbia University, New York, New York

(Received September 17, 1952)

The transitions $\Delta m_I=\pm 1$, $\Delta m_J=0$ for both Na and Cl were studied at high magnetic field in a beam produced by the evaporation of sodium chloride. The observed spectra could not be fully described in terms of the known internal interactions of a diatomic molecule or the interaction of a diatomic molecule with an applied field. It is suggested that the unexplained features of the spectra result from the presence in the beam of molecules of the type $(NaCl)_2$. Similar effects have been observed in sodium fluoride and sodium iodide.

I. INTRODUCTION

THIS paper is concerned primarily with a study by the molecular beam magnetic resonance method[1] of nuclear transitions in a nominal NaCl beam in magnetic fields ranging from 2000 to 16 000 gauss. The research is an outgrowth of a program of investigation of the electric quadrupole and other internal interactions in diatomic molecules. Certain details in the spectra due to the reorientation of the Na and Cl nuclei in what was assumed to be the NaCl molecule cannot be explained in terms of the usual interactions within a diatomic molecule or with an applied magnetic field. There is strong evidence that the beam of sodium chloride, evaporated from a conventional iron oven, contains, in addition to NaCl molecules, one or more other species of molecules which contain Na and Cl.

No direct evidence is available from the spectra alone to lead to an identification of the molecular species, since no statistical theory of the spectrum of a polyatomic molecule, of the form developed by Feld and Lamb for a diatomic molecule,[2] is available. Further, the novel details of the spectrum are themselves second-order effects, and no precise isolation of the spectrum due to the diatomic and polyatomic molecules can be made from presently available data.

II. THEORETICAL CONSIDERATIONS

Transitions of the type $\Delta m_I=\pm 1$, $\Delta m_{I'}=0$, and $\Delta m_J=0$ have been studied in this work in what were assumed to be diatomic sodium chloride molecules. The theory is, therefore, discussed for the special case $I=\frac{3}{2}$. The treatment of Nierenberg and Ramsey[3] is followed. For diatomic molecules in the $^1\Sigma$ state, the frequency for the transition $\Delta m_I=\pm 1$, $\Delta m_J=0$ is

$$\nu(\tfrac{3}{2},\tfrac{1}{2})=\nu_I-cJz+b(3z^2-1)+6b^2z^2(1-z^2)/\nu_I -6bcJz(1-z^2)/\nu_I, \quad (1a)$$

$$\nu(\tfrac{1}{2},-\tfrac{1}{2})=\nu_I-cJz-\tfrac{3}{4}b^2(1-z^2)(9z^2-1)/\nu_I, \quad (1b)$$

$$\nu(-\tfrac{1}{2},-\tfrac{3}{2})=\nu_I-cJz-b(3z^2-1)+6b^2z^2(1-z^2)/\nu_I +6bcJz(1-z^2)/\nu_I, \quad (1c)$$

where the calculation is carried to the first order in c and the second order in b, since in all cases $c\ll b<\nu_I$. Here

$\nu(m_I, m_I-1)$ = frequency of transition $m\leftrightarrow m-1$,
ν_I = Larmor frequency $=|g_I|\mu_0 H/h$,
J = molecular rotational angular momentum,
$z=m_J/J$,
$hb=eqQ/8$, the electric quadrupole interaction energy,
q = gradient of electric field at nucleus,
Q = nuclear quadrupole moment,
$hc=-|g_I|\mu_0 H'$, the $\mathbf{I}\cdot\mathbf{J}$ interaction energy for unit rotational angular momentum, and
H' = magnetic field produced at the nucleus for unit rotational angular momentum.

The beams observed in this experiment were produced at such high temperatures that $J\gg 1$ for practically all molecules. Therefore, in Eqs. (1), terms in $1/J$ have been neglected. The large values of J also allow us to treat z as a continuously varying parameter, ranging from -1 to 1, all possible values of z being equally probable. The molecules in the beam possess all possible values of J according to the function

$$N_J=N_0 J\exp(-\alpha^2 J^2), \quad (2)$$

where $\alpha^2=h^2/8\pi^2 IkT$. The distribution of molecules over J then depends on the moment of inertia I and on the absolute temperature T of the oven in which the beam originates. The most probable value of J is given by $\bar{J}=0.707/\alpha$. At an oven temperature of 1000°K, $\alpha=0.0166$ and $\bar{J}=43$, where the internuclear distance, 2.5×10^{-8} cm, as obtained by electron diffraction experiments on NaCl,[4] is used.

* This research assisted in part by the U. S. Office of Naval Research.

† Submitted by Stefan A. Ochs in partial fulfillment of the requirements for the degree of Doctor of Philosophy in the Faculty of Pure Science, Columbia University, New York, New York.

‡ U. S. Atomic Energy Commission Predoctoral Fellow, now at the R.C.A. Laboratories, Princeton, New Jersey.

[1] Rabi, Millman, Kusch, and Zacharias, Phys. Rev. **55**, 526 (1939).

[2] B. T. Feld and W. E. Lamb, Jr., Phys. Rev. **67**, 15 (1945).

[3] W. A. Nierenberg and N. F. Ramsey, Phys. Rev. **72**, 1075 (1947).

[4] E. S. Rittner, Phys. Rev. **82**, 766 (1951); and private communication.

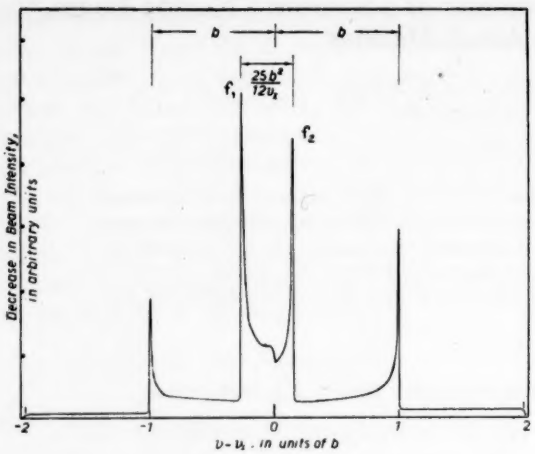

FIG. 1. Line shape calculated for transition $\Delta m_I=\pm 1$, $\Delta m_I \cdot \Delta m_J=0$ of a diatomic molecule in a high magnetic field, for $I=\frac{3}{2}$. The $\mathbf{I}\cdot\mathbf{J}$ interaction has been neglected. hb, the quadrupole interaction energy, is assumed to be $\frac{1}{5}$ of $h\nu_I$, the energy of interaction between the nuclear magnetic moment and the external magnetic field.

At sufficiently high magnetic field the spectrum for a particular value of J consists of a central maximum, contributed by transition (1b) and two symmetrically placed "wings," due to (1a) and (1c). The separation of the wings is substantially independent of field at high fields. The transition probability $P(\frac{1}{2}, -\frac{1}{2})$ is greater by a factor of 4/3 than $P(\frac{3}{2}, \frac{1}{2})$ and $P(-\frac{1}{2}, -\frac{3}{2})$. Hence, the area underneath the central maximum due to (1b), on a graph of intensity *versus* frequency, should be 4/3 of that contributed by either wing. When b^2/ν_I becomes equal to or greater than the resolution width of the apparatus, the central maximum may become asymmetrical in shape and split into two components. A further doubling of one of the components may appear due to the term in hcJ.

Figure 1 is a plot of the line shape corresponding to the transitions of Eqs. (1), when the terms involving c are neglected. The quadrupole interaction energy hb is assumed to be one-fifth of the energy of interaction between the nuclear magnetic moment and the external magnetic field. In the case of sodium chloride this corresponds to a field of about 9000 gauss for the Cl resonance and about 3300 gauss for the Na resonance. The resolution of the apparatus was taken as $b/100$ which for NaCl corresponds to 7 kc/sec for both resonances. The subsidiary maxima of the central pattern occur at $f_1=\nu_I-4/3b^2/\nu_I$ and at $f_2=\nu_I+3/4b^2/\nu_I$, so that the total frequency interval is $25b^2/12\nu_I$; the peak at f_2 occurs for $z=0$ and the peak at f_1 for $z^2=5/9$. The wings have their maximum intensity at the frequencies $\nu_I \pm b$.

If the term in c is included, the peak at f_2 is not affected since $z=0$, but the peak at f_1 is split into two components at $f_1'=f_1-5^{\frac{1}{2}}cJ/3$ and $f_1''=f_1+5^{\frac{1}{2}}cJ/3$. The frequency interval between the components is thus proportional to J and independent of H. The distribution of molecules over J, which falls off rather slowly with increasing and decreasing J values on either side of the most probable value, causes a broadening of the maxima at f_1' and f_1''. If the coefficient c is very small, a small doublet separation will occur; the doublet may then be unresolved and appear as a single well-defined line. If, however, c is large, the nominal doublet separation is highly dependent on J and the contributions of different J values will make the components of the doublet diffuse and possibly unobservable as well defined maxima. Figure 2 shows the line shape calculated for $c\bar{J}=0.18(f_2-f_1)$ and Fig. 3 the line shape for $c\bar{J}=0.62(f_2-f_1)$, where $\bar{J}$ has been taken as 50. The contribution by the wings $(m_I=\frac{3}{2}\leftrightarrow\frac{1}{2}, -\frac{1}{2}\leftrightarrow-\frac{3}{2})$ to the total intensity is substantially constant over the frequency interval considered and has been neglected.

III. EXPERIMENTAL RESULTS

A. Cl Transition in Sodium Chloride

In the molecular beam magnetic resonance method a transition between molecular states is detected by the corresponding decrease in beam intensity at the detector. The deflection, at the detector, of molecules in the beam is proportional to the gyromagnetic ratio of the nucleus which has made a transition. The wings of the Cl resonance can not be studied in any great detail since the integrated intensity in each wing is small as a consequence of the small g value of Cl. In addition, the wing extends over a large frequency range (about $2b$) and the intensity at any frequency is small. It was, however, possible to observe the wings sufficiently well to indicate that, for the Cl^{35} nucleus in NaCl, $b=eqQ/8h$ $=(698\pm 30)$ kc/sec. The spectrum of Cl^{37} could not be observed in detail since the g value is less than that of Cl^{35} and since its natural abundance is low. Nierenberg and Ramsey[3] found by the same method a value of b, for Na in NaCl, of 675 kc/sec, or a quadrupole interaction energy about equal to that of Cl^{35}.

Further detailed study of the central peak for Cl^{35}

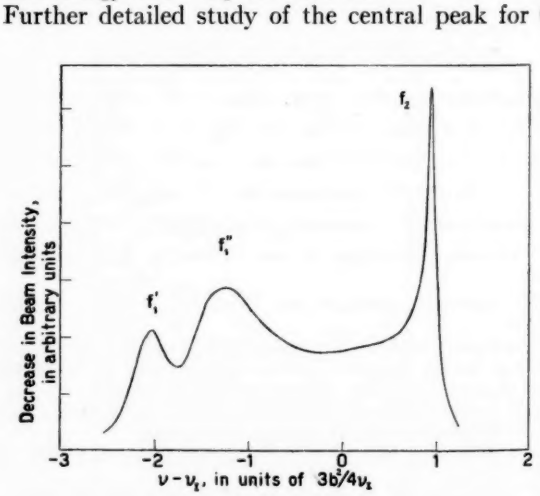

FIG. 2. Central part of line shown in Fig. 1, calculated for the case $c\bar{J}=0.18(f_2-f_1)$, where $\bar{J}=50$.

made it necessary to determine the magnetic field at which the line was observed. Since the g value of Na is about three times as great as that of Cl^{35}, the second-order effects in Eq. (1b) are about one-third as great for Na as for Cl at the same magnetic field. Therefore, the central peak of the Na resonance is sharper than that of the Cl resonance and can serve as an approximate measure of the field. As will be shown later, no simple interpretation of the central maximum of Na can be made in terms of the second-order frequency expression and to calibrate the field we have used, in addition to this peak, the resonance line of Li^7 in LiCl, where the second-order effects are very small because of the small quadrupole interaction of Li^7.

An observation of the central maximum of Cl^{35} in NaCl gave the spectrum shown in Fig. 4(B). The pattern has a similarity to those observed by Nierenberg and Ramsey for the three transitions $m_I=(\frac{3}{2}\leftrightarrow\frac{1}{2})$, $(\frac{1}{2}\leftrightarrow-\frac{1}{2})$, $(-\frac{1}{2}\leftrightarrow-\frac{3}{2})$ at high fields for Na in the sodium halides. However, the central component of the line is asymmetrically placed with respect to the two extreme peaks. The possibility that some new first-order internal interaction has served to disturb the pattern observed by Nierenberg and Ramsey is at once excluded, since the spectrum is extremely field dependent as shown in Fig. 4, where the line shape at four values of the magnetic field is shown. The frequency separation (f_c-f_a) of the extreme components is proportional to $1/H$ to the precision within which it is possible to determine, meaningfully, the center of a line whose width is a significant fraction of (f_c-f_a). The central peak is observed to have the frequency ν_I, at all magnetic fields, to within the uncertainties of measurement. It is also interesting to note that the intensity ratios of the peaks is somewhat variable. This is a crucial point in our interpretation of the spectrum and will be discussed later.

From the discussion in Sec. II it follows that, if the $\mathbf{I}\cdot\mathbf{J}$ interaction is ignored, the central line of the high field pattern should be split into two components (at f_1 and f_2) of frequency separation $25b^2/12\nu_I$ (see Fig. 1). The appearance of three lines in the central pattern now suggests that the peak at f_1 is split by an $\mathbf{I}\cdot\mathbf{J}$ interaction. Three considerations exclude this interpretation

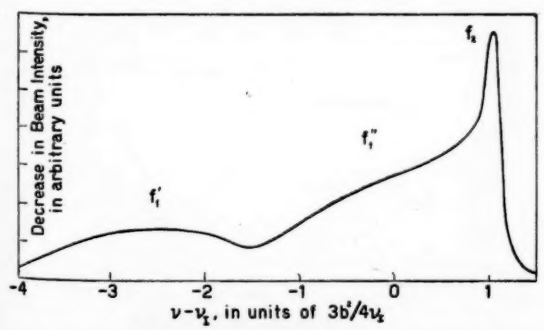

FIG. 3. Central part of line shown in Fig. 1, calculated for the case $c\bar{J}=0.62(f_2-f_1)$, where $\bar{J}=50$.

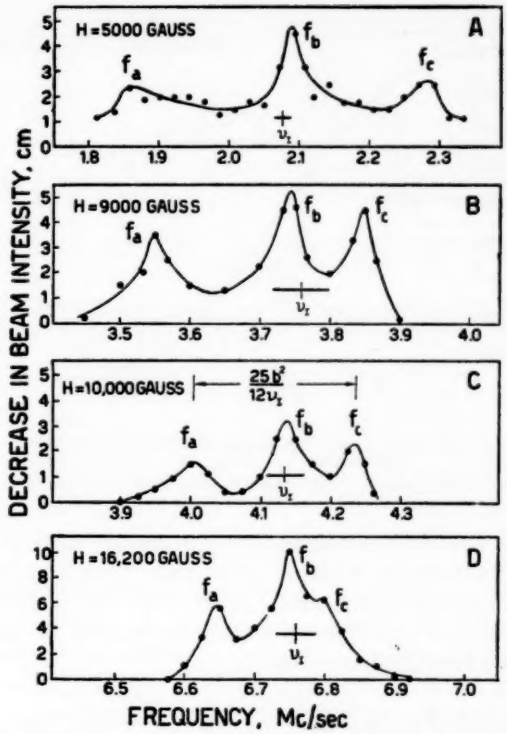

FIG. 4. Central maximum of Cl^{35} resonance observed for sodium chloride beam in different magnetic fields.

(1) An attempt was made to fit the curve of Fig. 4(B) for which $f_a=3.55$ Mc/sec, $f_b=3.74$ Mc/sec, $f_c=3.85$ Mc/sec by an appropriate choice of b and c. The quantity $25b^2/12\nu_I$ is then $f_c-(1/2)(f_a+f_b)=200$ kc/sec and $b=610$ kc/sec. To give the splitting of $2(5^{\frac{1}{2}}c\bar{J}/3)$ between f_a and f_b, it is necessary to assume $c=2.5$ kc/sec. The large value of c broadens the lines f_a and f_b to the point where the maxima have no significance. Figure 3 is the curve calculated for $c=2.5$ kc/sec and $b=610$ kc/sec. It is seen that the calculated curve has no qualitative similarity to the observed curve. In addition, the value of $c=2.5$ kc/sec is extremely high for a nucleus with a g value as small as that of Cl^{35} and implies a magnetic field at the nucleus, owing to the molecular rotation, of six gauss per unit angular momentum. This is much larger than the fields which have been found in other diatomic molecules. (2) The frequency separation of f_a and f_b appears to be proportional to $1/H$, rather than constant, as would be the case if the two peaks were the result of an $\mathbf{I}\cdot\mathbf{J}$ splitting. (3) The frequency separation of f_a and f_c is equal to the predicted value, $25b^2/12\nu_I$, if c is assumed to be negligible. All experimental data of (f_a-f_c) yield for b a value of (714 ± 10) kc/sec. It thus appears that the peaks f_a and f_b can not be described in terms of a doubling of f_1 due to an $\mathbf{I}\cdot\mathbf{J}$ interaction.

An analytic treatment of the frequency of the line in higher order than that given in Eqs. (1), for the purpose of obtaining a more detailed analysis of the intensity maxima, is difficult. To eliminate the possi-

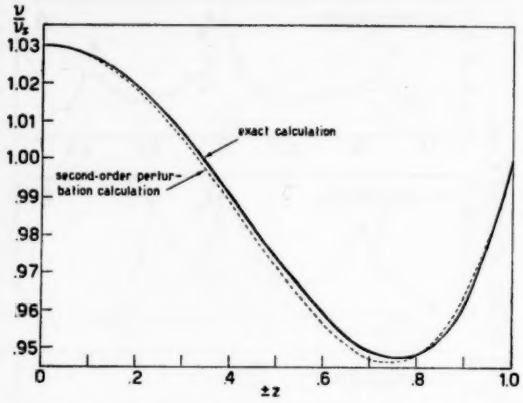

FIG. 5. Frequency corresponding to transition $m_I=\frac{1}{2}\leftrightarrow-\frac{1}{2}$ as function of z, calculated for $I=\frac{3}{2}$, $b/\nu_I=0.2$, $J\gg1$, $m_J\gg1$, $g_I\gg m_J g_J$: (a) exactly, (b) by second-order perturbation theory.

bility that the maximum at f_b is contributed by perturbation terms of higher order than those considered before, an exact numerical calculation was performed. The secular equation for diagonalization of the matrix for the Hamiltonian operator,

$$\mathcal{H}=g_I\mu_0\mathbf{I}\cdot\mathbf{H}+g_J\mu_0\mathbf{J}\cdot\mathbf{H}-\frac{eqQ}{2I(2I-1)(2J+3)(2J-1)}\times\left[3(\mathbf{I}\cdot\mathbf{J})^2+\tfrac{3}{2}(\mathbf{I}\cdot\mathbf{J})-I(I+1)J(J+1)\right], \quad (3)$$

was found. It is a fourth-order equation in the energy W. The roots $W_{\frac{1}{2}}$ and $W_{-\frac{1}{2}}$ (corresponding to $m=\frac{1}{2}$ and $-\frac{1}{2}$, respectively) were calculated numerically for the case

$$I=\tfrac{3}{2},$$
$$x_0=b/\nu_I=0.2,$$
$$J\gg1, \quad g_I\gg m_J g_J.$$

The value of x_0 of 0.2 corresponds to a value of ν_I of 3.5 Mc/sec which is in the lower range of our observations. Figure 5 shows the frequency $\nu=(W_{\frac{1}{2}}-W_{-\frac{1}{2}})/h$, corresponding to the transition $m_I=\frac{1}{2}\leftrightarrow-\frac{1}{2}$, as a function of z, compared to the result obtained by the second-order perturbation method. It is seen that the differences are insignificant and that there is no trace of an additional stationary point at $f=\nu_I$, where the anomalous peak is actually found. Perturbations arising from the other nucleus in the molecule give no contribution to the frequency of any component of the line to at least the second order.

Fabricand, Carlson, Lee, and Rabi[5] have found surprisingly large variations of the quadrupole interaction of Cl in KCl with vibrational quantum number. The value of b for $v=0$ was found to be less than 9 kc/sec, while for $v=1$, 2, and 3 values of 10, 30, and 48 kc/sec, respectively, were obtained. This result suggests the possibility that the Cl transition pattern for NaCl consists of two superposed lines, corresponding to two values of the quadrupole interaction associated with two different sets of vibrational quantum numbers. For instance, if the value of b for molecules in the state $v=0$ is less than 100 kc/sec, while for all higher vibrational states b is very close to 700 kc/sec, the expected pattern would be similar to that actually observed. However, this suggested behavior is beyond the range of behavior observed in similar molecules. It is also to be noted that when such large variations of q with v occur, a large variation of q with J can be anticipated. A large variation of q over a substantially continuous distribution in J would serve to broaden all details of the observed spectrum. Therefore, it appears unlikely that the observed effects can be explained by a variation of b with v and J.

The evidence thus points to the conclusion that the peaks f_a and f_c correspond to the two peaks f_1 and f_2 of the theory. This implies a small value of c, wholly consistent with the small g value of Cl. The observed line f_b is therefore unaccounted for by the theory.

B. Na Transitions in NaCl, NaI, and NaF

The g value of the Na nucleus is almost three times that of the Cl nucleus, so that the central pattern as well as the wings of the Na transition in NaCl could be seen clearly. The shape of the wings is approximately as observed by Nierenberg and Ramsey. The central pattern consists of several more or less well-resolved maxima, as shown in Fig. 6. The variation of intensity

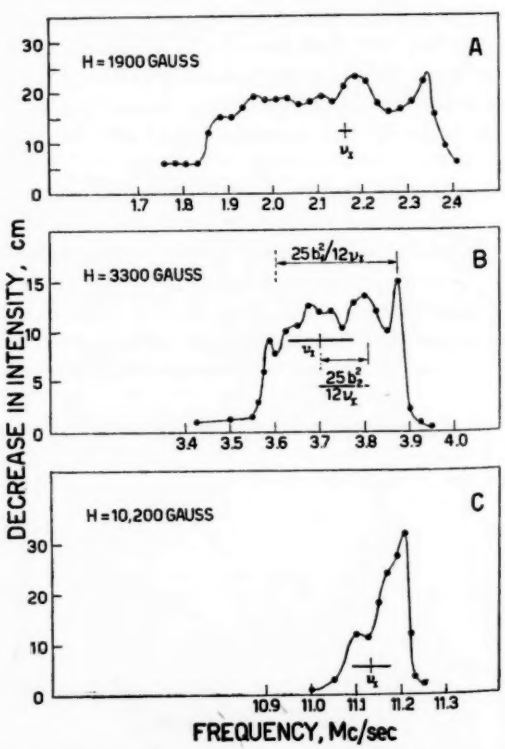

FIG. 6. Central maximum of Na resonance observed for sodium chloride beam in different magnetic fields.

[5] Fabricand, Carlson, Lee, and Rabi, Phys. Rev. 86, 607 (1952).

within the pattern is not much above the noise level of the apparatus, yet certain well-defined features do appear. (1) The total width of the central maximum is proportional to $1/H$. (2) Near the high frequency end two well-resolved peaks are found, and the whole spectrum is reduced to a very low level of intensity within a small frequency interval. (3) There is a less well-resolved small peak near the low frequency end of the pattern, which appears in many cases as a shoulder. (4) Several poorly resolved maxima are located between the peaks mentioned in (2) and (3).

The line shape suggests that it consists of two superimposed patterns, each of the type shown in Fig. 2 (a moderate $\mathbf{I}\cdot\mathbf{J}$ splitting) with the same ν_I but different values of b. If this assumption is made, the sharp peak at the high frequency end of the pattern and the peak at its low frequency end correspond to the lines at f_2 and f_1', respectively, for the larger b, say b_1. The line at f_1'' is not resolved due to the superposition of the contribution of the smaller b, b_2. An estimate of the frequency $(f_1'+f_1'')/2$ from the dip just to the high frequency side of f_1' then allows the determination of $25b_1^2/12\nu_I$ which equals $f_2-(f_1'+f_1'')/2$ and the calculation of the value of b_1. The frequency ν_I is determined from the frequency of the Li^7 resonance in the same field or, less accurately, from the value of the current exciting the magnetic field. In this manner b_1 is estimated to be 665 kc/sec. Moreover, the separations between f_2 and ν_I and between $(f_1'+f_1'')/2$ and ν_I should be in the ratio of 9 to 16. While this ratio was not observed in all cases (Fig. 4(B), for example) it was observed in a sufficient number of cases, especially where the determination of ν_I is good, to lend considerable verification to the analysis. The interval between the wings observed in these experiments gives a value of b of (666 ± 10) kc/sec, in good agreement with the value of 675 kc/sec given by Nierenberg and Ramsey. If the same analysis is applied to that portion of the pattern which appears to correspond to b_2, $f_2-(f_1'+f_1'')/2$ yields an estimate from a large amount of data of a b_2 of 380 kc/sec. No clear indication of a set of wings corresponding to any value of the quadrupole interaction less than 675 kc/sec could be found. Hence, the diatomic theory, which described adequately one contribution to the observed

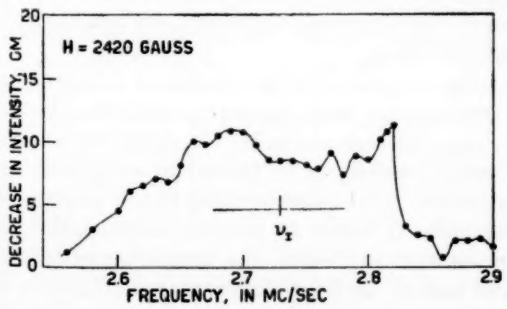

FIG. 7. Central maximum of Na resonance observed for sodium iodide beam at high magnetic field.

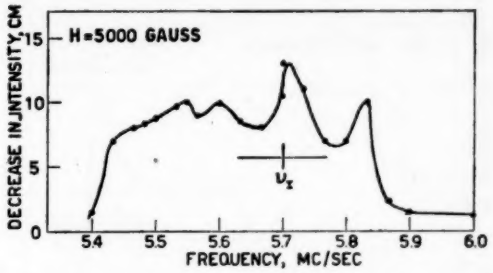

FIG. 8. Central maximum of Na resonance observed for sodium fluoride beam at high magnetic field.

pattern in terms of the larger b value, does not apply to the remaining portion of the pattern.

In order to test the dependence of the line shape on the nature of the halide component of the molecule, the high-field transitions of Na in NaI and NaF were studied also. Figure 7 shows that for Na in NaI a pattern quite similar in structure to that of NaCl is found. The width of the line, but not the structure of its central region, is in approximate agreement with the value of b of 490 kc/sec reported by Nierenberg and Ramsey. The zero field line observed by Coté, Logan, and Kusch[6] can be interpreted in terms of a value of b of 485 kc/sec.

The Na transition in NaF (Fig. 8) shows a relatively high and narrow peak at ν_I. The pattern could be interpreted as consisting of a line of the type shown in Fig. 3 superimposed on a single peak similar to that at f_b in the Cl resonance in NaCl. The width of the pattern yields an approximate value of b consistent with that found to be 1015 kc/sec from a study of the wing at high field.[6] It is to be noted that in the case of NaF, the halogen nucleus has a spin of $\frac{1}{2}$. Thus it can have no quadrupole moment. The theoretical result that the anomalous part of all lines studied in this experiment is not caused by an interaction of the quadrupole moment of the second nucleus, is thus confirmed.

In the case of Na in the alkali halides, therefore, the spectrum appears to consist of the superposition of a spectrum due to the diatomic halide and consistent with other data on the interactions within the molecule, and a spectrum of unknown origin. The analysis for Na is not as clear cut as that for Cl, but it is at once apparent that if the interactions are such as to give a diffuse spectrum over a broad region at the low frequency end, then a single line of high relative intensity should occur at the upper frequency limit of the spectrum as in Figs. 2 and 3.

On a single occasion the spectrum of the Na resonance in NaCl was observed (Fig. 9) to be entirely consistent with the predictions of the theory for a diatomic molecule and the known constants of the NaCl molecule. The experimental curve was repeated as indicated by the crosses and circles in the figure and there is no question about its validity. The exact conditions pre-

[6] Coté, Logan, and Kusch, private communication.

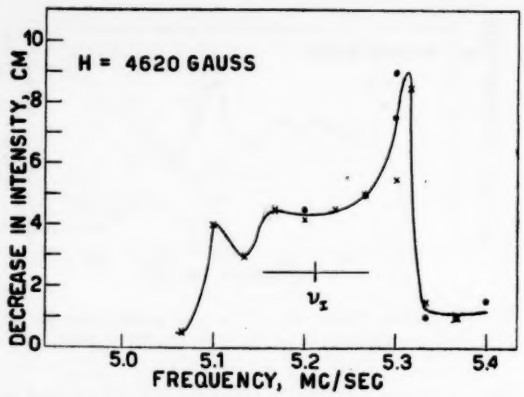

FIG. 9. Central maximum of Na resonance for sodium chloride beam observed on one occasion only. Circles and crosses show two different traversals of maximum. Attempts to reproduce same oven conditions at later times were unsuccessful.

vailing in the oven during the observations are not known, nor has it been possible to repeat the curve on another occasion. The fact that it is possible to produce the indicated spectrum is, however, important in our subsequent analysis. Because of the possibility of residual effects of the type discussed above, it is not possible to interpret the two poorly defined maxima in the low frequency region of the curve, as the doublet due to the $\mathbf{I}\cdot\mathbf{J}$ splitting.

IV. DIMERIZATION

It is clear that the considerations of Sec. II cannot alone explain satisfactorily the spectrum corresponding to the high field transitions in sodium chloride. It is proposed that the molecular beam consists of several components of which one is NaCl. Spectroscopic analysis of the oven charge before vaporization and of the deposit made by the beam after issuing from the slit, has failed to show any appreciable concentration of impurities. Since only the Na component of the beam is actually detected by surface ionization, it appears that all molecules investigated contain Na. Obviously, Cl was also contained by those molecules for which resonances were observed at $g_{Cl}\mu_0 H/h$. Any molecule containing an Na nucleus gives a spectrum centered about $g_{Na}\mu_0 H/h$ and the shape and extent of the spectrum depend on the details of the internal interactions of the molecules. A reasonable assumption is that part of the beam consists of molecules of the form Na_2Cl_2 and higher polymers. According to thermodynamic considerations, dimerization should increase with the pressure in the oven at a fixed temperature and decrease with increasing temperature at a fixed pressure. In the ovens usually employed in molecular beam work [Fig. 10(A)] the pressure can be increased only by an increase in the temperature of the melt and, hence, the temperature of the vapor. The corresponding net change in the composition of the beam can only be determined from detailed thermodynamic considerations from data not available for these molecules. Figure 11 shows a comparison of Na transition patterns for sodium chloride beams issuing from ovens at different temperatures and corresponding pressures. It can be seen that at higher oven temperature and pressure the central region of the pattern is relatively more intense than the outside portions.

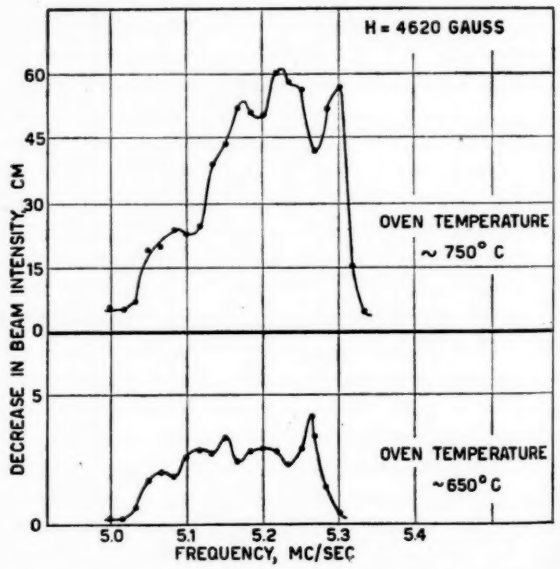

FIG. 11. Comparison of Na resonances at same field for sodium chloride beam originating from oven of design shown in Fig. 10(A), at two different temperatures.

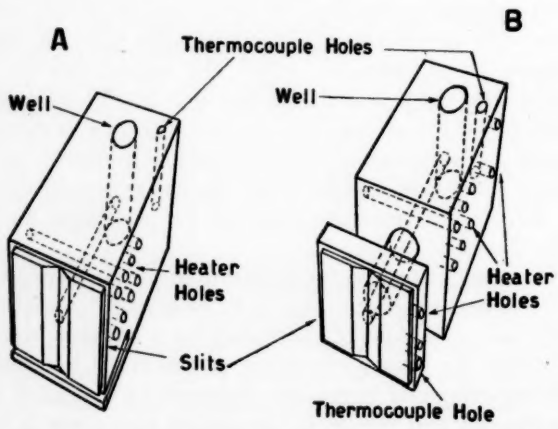

FIG. 10. Sketches of (A) oven employed ordinarily in molecular beam work, (B) special oven built to allow separate heating of well and slit sections.

In order to gain a certain degree of independence in the temperature and pressure conditions inside the oven, a special oven was built [Fig. 10(B)] which allowed the beam molecules to be heated to some temperature different from that corresponding to the vapor pressure of the melt. In order to prevent condensation of the vapor on the oven slits, the temperature of the slit section had to be kept above that of the well at all times. Heat transfer between different parts of the oven, as well as difficulties in the measurement of the tem-

peratures near the well and near the slit, allowed only qualitative comparisons between the temperatures of well and slit for any one run and for different runs. Figure 12 shows the relative intensities of the three maxima found in the central line of the Cl resonance pattern in a field of 9000 gauss and at different combinations of melt and slit temperatures. Figure 13 shows a similar comparison of the shape of the Na line at the same frequency, which corresponds here to a field of 3300 gauss. Although the exact experimental conditions are not clear, there is no doubt that a change of the pressure in the oven affects the intensity of the central portion of the pattern relative to the intensity of its outside regions. For the Cl as well as the Na transitions a higher pressure in the oven increases the intensity of

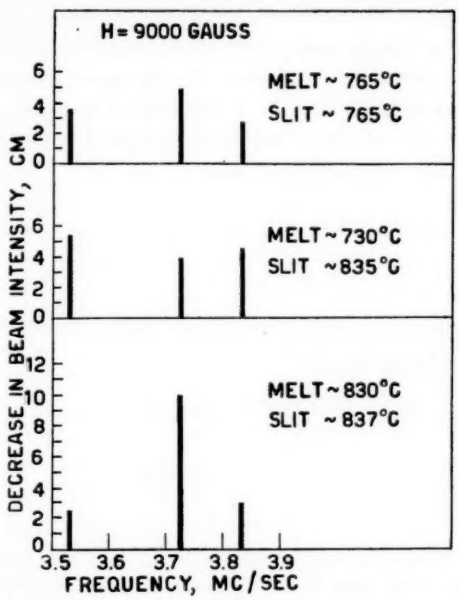

FIG. 12. Graph of relative intensities of the three peaks observed in the central maximum of Cl^{35} resonance of a sodium chloride beam. The magnetic field is constant, but the well and slit temperatures of the oven, of design shown in Fig. 10(B), are different in the three cases.

the center of the line relative to the intensity of its upper and lower frequency ends, while a rise in slit temperatures favors an increased intensity of the outside region relative to the intensity of the central part. In particular, Fig. 9 is to be noted, where a rather complete suppression of the central part of the pattern has occurred due to a fortuitous oven condition.

V. DISCUSSION

The variation in the relative intensities of the various components of the observed spectrum indicates that the complexity of the pattern is caused by the occurrence of several components within the molecular beam. The variation of relative intensity as a function of oven pressure and slit temperature agrees qualitatively with that to be expected for a mixture of monomers and

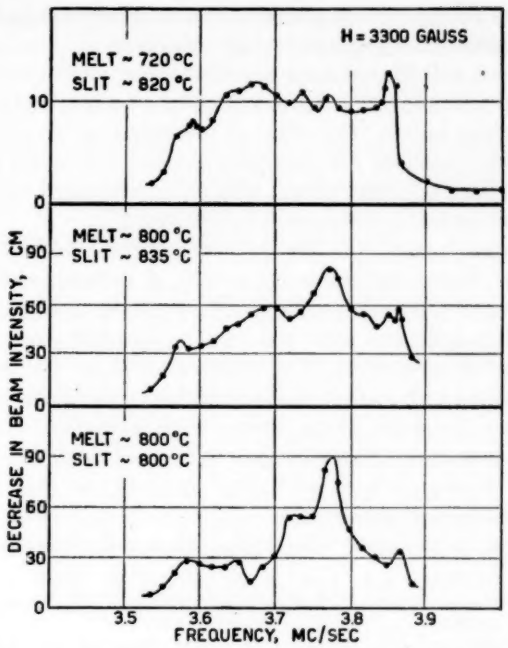

FIG. 13. Central maximum of Na resonance observed for sodium chloride beam at constant magnetic field but for different combinations of well and slit temperatures of oven, of design of Fig. 10B.

dimers under conditions where the two components have a comparable abundance. Although a dimer has resonance lines corresponding to the transition $\Delta m_I = \pm 1$, at frequencies centered about $g_I \mu_0 H/h$, the detailed structure of the spectrum is not known. Polymers, more complex than the dimer, may, of course, be present as well. However, the exact identification of the components and a determination of their concentration as a function of temperature and pressure is a problem in physical chemistry. It should be more amenable to solution by some technique other than the observation of hyperfine structure in molecules.

All three halides here investigated show a substantial fraction of dimerization under the conditions at which a molecular beam is ordinarily obtained. It is not possible to determine the concentration of the various molecular components without detailed knowledge of the nature of the spectra characteristic of each component. A qualitative estimate is that the abundance of the diatomic molecules is between 25 and 75 percent of the total beam. It is somewhat surprising that the percentage dimerization is similar for all three types of beams, but this result may not be unreasonable, since all the beams are produced at similar temperatures (about 1000°K) and pressures (about one mm of mercury). A careful search has been made for atomic sodium in the beam; it is easily identified through its large magnetic moment. No observable component of Na has been found. Atomic or molecular chlorine can not be detected by the techniques employed in this research; however, no chemical effects on the iron oven

and no effects on the pressure in the apparatus due to the evolution of a gas have been observed.

Kusch and Mann[7] have reported the apparent evolution of free iodine in the formation of a molecular beam of lithium iodide. The effect is identified by an objectionable chemical reaction between the iron oven and the iodine. Whether or not this effect is related to the present series of phenomena is uncertain.

Nernst,[8] using the air displacement method of V. Meyer, found the molecular weight of sodium chloride vapor at 1970°C and atmospheric pressure to be about 59. This indicates that the vapor consisted predominantly of monomers. The experiment was, however, performed with sodium chloride in the vapor phase only, whereas the present experiments were carried out essentially in sodium chloride vapor, which, while not necessarily in equilibrium with the liquid phase, was not independent of that phase.

Zimm and Mayer[9] measured the vapor pressure of potassium chloride over its *crystals*, not that of its molten salt, and calculated the entropy of the vapor. Comparison of the experimental value with the entropy of a gaseous mixture of KCl and $(KCl)_2$ allowed the authors to estimate the extent of association in the vapor. It was found that at 800°K less than 2 percent, probably less than 0.3 percent, of the molecules have associated to form dimers.

The extent of the formation of complex molecules for halides other than those studied in this work is unknown. It is clear that any interpretation of the kind of unresolved spectra observed in the molecular beam *magnetic* resonance method must take into account the possibility of contributions to the spectrum by molecules which are not the assumed monomers.

We wish to thank Professor Ralph S. Halford, of the Chemistry Department, for detailed discussion and advice concerning problems in chemical thermodynamics, and Professor T. Ivan Taylor and Mr. John Dunbar, also of the Chemistry Department, for performing the chemical analyses.

[7] P. Kusch and A. K. Mann, Phys. Rev. **76**, 707 (1949).
[8] W. Nernst, Nachr. Kön. Ges. Wiss. Göttingen, Math.-physik. Kl. 75 (1904).
[9] B. H. Zimm and J. E. Mayer, J. Chem. Phys. **12**, 362 (1944).

THE JOURNAL OF CHEMICAL PHYSICS VOLUME 21, NUMBER 3 MARCH, 1953

A Semi-Empirical Theory of the Electronic Spectra and Electronic Structure of Complex Unsaturated Molecules. I.*†

RUDOLPH PARISER, *Jackson Laboratory, E. I. du Pont de Nemours and Company, Wilmington, Delaware*
AND
ROBERT G. PARR, *Department of Chemistry, Carnegie Institute of Technology, Pittsburgh, Pennsylvania*
(Received September 4, 1952)

A semi-empirical theory is outlined which is designed for the correlation and prediction of the wavelengths and intensities of the first main visible or ultraviolet absorption bands and other properties of complex unsaturated molecules, and preliminary application of the theory is made to ethylene and benzene.

The theory is formulated in the language of the purely theoretical method of antisymmetrized products of molecular orbitals (in LCAO approximation), including configuration interaction, but departs from this theory in several essential respects. First, atomic orbital integrals involving the core Hamiltonian are expressed in terms of quantities which may be regarded as semi-empirical. Second, an approximation of zero differential overlap is employed, and an optional uniformly charged sphere representation of atomic π-orbitals is introduced, which greatly simplify the evaluation of electronic repulsion integrals and make applications to complex molecules containing heteroatoms relatively simple. Finally, although the theory starts from the π-electron approximation, in which the unsaturation electrons are treated apart from the rest, provision is included for the adjustment of the σ-electrons to the π-electron distribution in a way which does not complicate the mathematics.

Electronic energy levels in the theory are expressed in terms of ionization potentials of atoms, resonance integrals of bonds, Coulomb repulsion integrals between two π-electrons on the same atom and between two π-electrons on different atoms, and penetration integrals between π-electrons and neutral atoms. Preliminary applications to ethylene and benzene in which only the carbon-carbon resonance integral is treated as an empirical quantity show that the theory can reproduce the results of the purely theoretical method with very little labor. The reasonableness of considering all of the above quantities as semi-empirical is pointed out, however, and it is through a detailed examination and exploitation of this in the second paper of this series that correction for the inadequacies of the π-electron approximation is made and improved agreement with experiment is attained.

1. PREFACE

THIS paper is the first of a series presenting a new semi-empirical theory of the electronic spectra and structure of unsaturated molecules. Papers I and II present the main elements of the theory with primitive examples; later papers will emphasize applications to various molecules and series of molecules. The theory is primarily designed for the prediction of wavelength and intensity of the main visible or near ultraviolet electronic absorption bands of unsaturated organic molecules, but such topics as resonance energy, electron

* Contribution No. 128 from Jackson Laboratory, E. I. du Pont de Nemours and Company, Wilmington, Delaware.
† Presented at the Symposium on Molecular Structure and Spectroscopy, Ohio State University, June 9, 1952.

density, bond order, and dipole moment will receive some attention, and applications to certain saturated and certain inorganic molecules will also be considered.

The theory starts from the so-called π-electron approximation in which the unsaturation, or π, electrons of a molecule are treated apart from the rest, the latter being manifest only in the effective "core" in the field of which the former move. Wave functions for various states of the π-electrons are built from $2p$ atomic orbitals on the individual atoms, and energies of the various states are computed in a prescribed manner. The theory combines the advantages of the conventional semi-empirical LCAO MO method with the advantages of the conventional purely theoretical method of antisymmetrized products of molecular orbitals (in LCAO approximation), including configuration interaction.

The degree to which the semi-empirical LCAO MO method[1] can successfully correlate organic spectra has been examined by several authors.[2] The method is useful, but consideration of configuration interaction is essential for ultimate understanding of band positions and intensities. Configuration interaction is not quantitatively provided for in the conventional method, however, and furthermore, the method does not take proper cognizance of electronic interaction—it makes no distinction between singlet and multiplet states, for example. The present theory may be regarded as a quantitative prescription for inclusion of configuration interaction effects in a semi-empirical LCAO MO theory from which internal inconsistencies have been removed.

The method of antisymmetrized products of molecular orbitals (in LCAO approximation), including configuration interaction, as developed by Goeppert-Mayer and Sklar,[3] Craig,[4] and Roothaan,[5] and as discussed in detail by Mulliken,[6,7] provides a proper theoretical framework for a consistent theory. In its purely theoretical form this method is impractical, however; it lacks the empirical element which one must expect in a genuinely useful theory, and its mathematics is unwieldy—benzene is the most complex molecule on which the method has been fully tested,[8] and the organic chemist may reasonably expect more! The present theory incorporates an empirical element into the antisymmetrized product method. This by itself would not yield a wieldy method, but through the exploitation of a certain approximate property of atomic $2p$ orbitals in molecules a sweeping simplification of the mathematics is achieved which makes applications to complex molecules feasible.

2. THE TOTAL ENERGY OF AN ELECTRONIC STATE

For a molecule containing n π-electrons moving in the field of a core (in C_6H_6, for example, there are 6 π-electrons in the field of a $C_6H_6^{+6}$ core), the Hamiltonian operator will be expressed in the form[3]

$$\mathbf{H}=\mathbf{H}_{\text{core}}+\tfrac{1}{2}\sum_{ij}(e^2/r_{ij}), \tag{1}$$

where e^2/r_{ij} is the electrostatic repulsion between π-electrons i and j, and

$$\mathbf{H}_{\text{core}}=\sum_i \mathbf{H}_{\text{core}}(i), \tag{2}$$

where $\mathbf{H}_{\text{core}}(i)$ is the kinetic energy operator for electron i plus its potential energy operator in the field of the core:

$$\mathbf{H}_{\text{core}}(i)=\mathbf{T}(i)+\mathbf{U}_{\text{core}}(i). \tag{3}$$

Other than π-electrons are evinced only through the terms $\mathbf{U}_{\text{core}}(i)$. This is the so-called *π-electron approximation*.

Wave functions for the n-electron system will be constructed from normalized antisymmetrized product functions of the type

$$\Phi_\Lambda=\frac{1}{\sqrt{n!}}\begin{vmatrix}(\phi_1\alpha)^1 & (\phi_1\beta)^1 & (\phi_2\alpha)^1 & \cdots\\ (\phi_1\alpha)^2 & (\phi_1\beta)^2 & (\phi_2\alpha)^2 & \cdots\\ (\phi_1\alpha)^3 & (\phi_1\beta)^3 & (\phi_2\alpha)^3 & \cdots\\ \cdot & \cdot & \cdot & \cdot\\ \cdot & \cdot & \cdot & \cdot\\ \cdot & \cdot & \cdot & \cdot\end{vmatrix}, \tag{4}$$

where Λ is a running index characterizing the assignment of electrons to particular *molecular orbitals* ϕ_i with spin functions α or β; i.e., Λ is an index indicating the *spin-orbital configuration*.[6] The molecular orbitals (MO) ϕ_i will further be taken to be orthonormal linear combinations of atomic orbitals (AO) χ_p on the several nuclei:

$$\phi_i=\sum_p C_{ip}\chi_p. \tag{5}$$

This is the familiar LCAO *approximation*.

The expectation value for the energy of Φ_Λ, $\int\Phi_\Lambda^*\mathbf{H}\Phi_\Lambda dv$, is given by the formula:[6]

$$E_\Lambda=\sum_i I_i+\tfrac{1}{2}\sum_{ij}(J_{ij}-K_{ij}')$$

$$\text{(sums over occupied MO's in } \Phi_\Lambda), \tag{6}$$

where

$$I_i=\int\phi_i^*(1)\mathbf{H}_{\text{core}}(1)\phi_i(1)dv \tag{7}$$

[1] See, for example, Mulliken, Rieke, and Brown, J. Am. Chem. Soc. **63**, 41 (1941), and R. S. Mulliken and C. A. Rieke, J. Am. Chem. Soc. **63**, 1770 (1941), where the semi-empirical LCAO MO method is described and applied in detail to the phenomenon of hyperconjugation.

[2] See, for example, J. R. Platt, J. Chem. Phys. **18**, 1168 (1950).

[3] M. Goeppert-Mayer and A. L. Sklar, J. Chem. Phys. **6**, 645 (1938).

[4] D. P. Craig, Proc. Roy. Soc. (London) **200**, 474 (1950).

[5] C. C. J. Roothaan, Revs. Modern Phys. **23**, 69 (1951).

[6] R. S. Mulliken, J. chim. phys. **46**, 497 (1949).

[7] R. S. Mulliken, J. chim. phys. **46**, 695 (1949).

[8] Parr, Craig, and Ross, J. Chem. Phys. **18**, 1561 (1950).

is the *core energy* for the MO ϕ_i,

$$J_{ij}=\int \phi_i^*(1)\phi_j^*(2)(e^2/r_{12})\phi_i(1)\phi_j(2)dv \qquad (8)$$

is the *Coulomb integral* between MO's ϕ_i and ϕ_j, and

$$K_{ij}=\int \phi_i^*(1)\phi_j^*(2)(e^2/r_{12})\phi_j(1)\phi_i(2)dv \qquad (9)$$

is the *exchange integral* between ϕ_i and ϕ_j, with $K_{ij}'=K_{ij}$ if ϕ_i and ϕ_j have the same spins in Φ_A, $K_{ij}'=0$ if ϕ_i and ϕ_j have different spins in Φ_A.

Now a single Φ_A may or may not be a good approximation to the total π-electron wave function Ψ_S for an actual electronic state S of the system. In cases for which a single Φ_A suffices, energies may be computed directly from Eq. (6); in cases for which a combination of several Φ_A is needed, a *configuration interaction* calculation needs to be performed by carrying out a linear variational calculation with the Φ_A as starting functions; i.e., by writing

$$\Psi_S=A_1\Phi_1+A_2\Phi_2+\cdots, \qquad (10)$$

determining the energy by solution of a *secular equation*

$$|H_{mn}-S_{mn}E|=0, \qquad (11)$$

and determining the coefficients A_m by solution of the simultaneous equations

$$\sum_m A_m[H_{mn}-S_{mn}E]=0, \quad n=1, 2, \cdots. \qquad (12)$$

The matrix elements,

$$S_{mn}=\int \Phi_m^*\Phi_n dv \qquad (13)$$

and

$$H_{mn}=\int \Phi_m^*\mathbf{H}\Phi_n dv, \qquad (14)$$

required for this calculation are readily derived; in particular, the H_{mn} always turns out to be expressible in terms of integrals which are generalizations of those appearing in Eqs. (7)–(9); namely, *core integrals*,

$$I_{ij}=\int \phi_i^*(1)\mathbf{H}_{\text{core}}(1)\phi_j(1)dv, \qquad (15)$$

and *electronic repulsion integrals*,

$$(ij|kl)=\int \phi_i^*(1)\phi_k^*(2)(e^2/r_{12})\phi_j(1)\phi_l(2)dv. \qquad (16)$$

Once one has chosen starting MO's and decided on the extent of configuration interaction to be taken into account, the determination of electronic energy levels is reduced to the problem of computing core integrals and electronic repulsion integrals. Methods for handling these two types of integrals are described in Secs. 3 and 4. The more subtle problems of choosing the initial MO's and deciding on the extent of configuration interaction are also considered in Sec. 3.

3. CORE INTEGRALS

Since according to Eqs. (5) and (15),

$$I_{ij}=\sum_p\sum_q C_{ip}^*C_{jq}H_{pq}^{\text{core}}, \qquad (17)$$

where

$$H_{pq}^{\text{core}}=\int \chi_p^*(1)\mathbf{H}_{\text{core}}(1)\chi_q(1)dv, \qquad (18)$$

it is sufficient for determination of the core integrals to know the LCAO coefficients C_{ip} and the AO matrix elements H_{pq}^{core}.

To determine the C_{ip}, one *might* set up a semi-empirical procedure of the conventional form,[1,9] using the linear variational method with some effective one-electron Hamiltonian operator $\mathbf{H}_{\text{eff}}(1)$ equal either to $\mathbf{H}_{\text{core}}(1)$ or to a self-consistent operator $\mathbf{F}(1)=\mathbf{H}_{\text{core}}(1)+\mathbf{G}(1)$, where $\mathbf{G}$ includes in the proper way[5] the effect of the other π-electrons on electron 1. One would then obtain simultaneous equations for the coefficients and for one-electron orbital energies of the form

$$\sum_p C_{ip}[H_{pq}^{\text{eff}}-S_{pq}e]=0$$

and

$$|H_{pq}^{\text{eff}}-S_{pq}e|=0, \quad \text{respectively.}$$

If $\mathbf{H}_{\text{eff}}=\mathbf{H}_{\text{core}}$ were used, the roots of the secular equation would be the diagonal elements $I_i\equiv I_{ii}$, and the off-diagonal I_{ij} would be zero; if $\mathbf{H}_{\text{eff}}=\mathbf{F}$ were used, the roots of the secular equation (for a closed-shell ground state) would be the self-consistent field energies.[5] In the former case one could proceed immediately to the use of the formulation of Sec. 2 for determination of total electronic energies, but one would have to be prepared to include a large amount of configuration interaction in order to compensate for the inadequacies of the MO's employed. The MO's used in the self-consistent case would be better, but one would be inextricably tied to a difficult and tedious iterative computational scheme.[10]

The point of view advocated here will be intermediate. Configuration interaction, sufficiently invoked, can correct in effect any error made in the choice of the LCAO coefficients. For this reason, any coefficients C_{ip} may be employed. One may therefore choose the coefficients arbitrarily, subject to the orthonormalization conditions. The closer the chosen MO's are to the

[9] R. G. Parr, J. Chem. Phys. **19**, 799 (1951).

[10] See, for example, R. G. Parr and R. S. Mulliken, J. Chem. Phys. **18**, 1338 (1950), where a self-consistent LCAO MO calculation on butadiene is carried out.

"best" or self-consistent field LCAO MO's, the less configuration interaction will have to be invoked. However, large deviations from self-consistent LCAO MO's brought on by ignorance or dictated by convenience may always be compensated through configuration interaction.

A procedure for obtaining the $H_{pq}{}^{\text{core}}$ will now be outlined. Let

$$\alpha_p \equiv H_{pp}{}^{\text{core}} = \int \chi_p{}^*(1)\mathbf{H}_{\text{core}}(1)\chi_p(1)dv \qquad (19)$$

and[11]

$$\beta_{pq} \equiv H_{pq}{}^{\text{core}} = \int \chi_p{}^*(1)\mathbf{H}_{\text{core}}(1)\chi_q(1)dv \qquad (20)$$

and assume tentatively that

$$\beta_{pq} = 0 \text{ when } p \text{ and } q \text{ are non-neighbors.} \qquad (21)$$

The *resonance integrals* β_{pq} may be shown by theoretical elucidation of H_{core} to depend on the type and length of the bond pq and the atoms p and q, but not sensibly on neighboring bonds or atoms.[12] Accordingly, they may be naturally carried from molecule to molecule and will be treated as basic empirical quantities.

The *Coulomb integrals* α_p, on the other hand, will depend on the bonding to atom p and the neighbors of atom p, and therefore are not appropriate for carry-over from molecule to molecule. They are better expressed in terms of more basic quantities, as follows: According to the argument of Goeppert-Mayer and Sklar,[3] the core Hamiltonian of Eq. (3) may be written as

$$\mathbf{H}_{\text{core}}(1) = \mathbf{T}(1) + \mathbf{U}_p(1) + \sum_{q \neq p} \mathbf{U}_q(1) + \sum_r \mathbf{U}_r{}^*(1), \qquad (22)$$

where the atoms q are charged in the core (e.g., a carbon atom in benzene) and the atoms r are uncharged in the core (e.g., a hydrogen atom in benzene), and where the asterisk connotes a potential which is due to a *neutral* atom. Further,

$$\mathbf{U}_q(1) = \mathbf{U}_q{}^*(1) - \int \chi_q{}^*(2)\chi_q(2)(e^2/r_{12})dv_2. \qquad (23)$$

If, therefore, the AO's χ_p are atomic eigenfunctions in the sense that

$$[\mathbf{T}(1) + \mathbf{U}_p(1)]\chi_p(1) = W_p\chi_p(1), \qquad (24)$$

where W_p is an appropriate *atomic valence state ionization potential*, then Eqs. (19) and (22)–(24) yield

$$\alpha_p = W_p - \sum_{q \neq p} [(pp|qq) + (q:pp)] - \sum_r (r:pp), \qquad (25)$$

where $(pp|qq)$ is the *Coulomb repulsion integral* between χ_p and χ_q [compare Eq. (16)] and $(q:pp)$ and $(r:pp)$ are *Coulomb penetration integrals* between χ_p and *neutral* atoms q and r:

$$(q:pp) = -\int \mathbf{U}_q{}^*(1)\chi_p{}^*(1)\chi_p(1)dv. \qquad (26)$$

Equation (25) will be taken as the fundamental formula for determination of the atomic Coulomb integrals α_p from the empirical atomic ionization potentials W_i.

4. ELECTRONIC REPULSION INTEGRALS

The electronic repulsion integrals of Eq. (16) are of the form

$$(ij|kl) = \int \Omega_{ij}(1)(1/r_{12})\Omega_{kl}(2)dv, \qquad (27)$$

with $\Omega_{ij}(1) = e\phi_i{}^*(1)\phi_j(1)$ and $\Omega_{kl}(2) = e\phi_k{}^*(2)\phi_l(2)$, and can be interpreted as classical electrostatic repulsions between the charge distribution Ω_{ij} and Ω_{kl}. To obtain approximate values for these integrals, one may make the assumption of *formal neglect of differential overlap*,

$$\chi_p{}^*\chi_q \equiv 0 \quad \text{for} \quad p \neq q, \qquad (28)$$

and employ ϕ_i which are orthonormalized accordingly;[13] i.e., make

$$\sum_p C_{ip}{}^* C_{jp} = \delta_{ij}. \qquad (29)$$

One then obtains

$$(ij|kl) = \text{linear combination of integrals over atomic orbitals of the form } (pp|qq). \qquad (30)$$

The problem is thus reduced to the evaluation of a relatively small number of integrals over atomic orbitals, all of them being Coulomb repulsion integrals.

Formulas or tables for the integrals $(pp|qq)$ may be found in the literature.[14] Alternatively, the *uniformly charged sphere approximation* may be employed,[15,16] in

[11] Equation (20) is the *formal* definition of β_{pq} with which one works in conjunction with the formal neglect of overlap of Eq. (28). For theoretical purposes, β_{pq} is better thought of as defined by

$$\beta_{pq} = H_{pq}{}^{\text{core}} - (S_{pq}/2)(H_{pp}{}^{\text{core}} + H_{qq}{}^{\text{core}}), \qquad (20a)$$

which takes more realistic account of the overlap integral

$$S_{pq} = \int \chi_p{}^*(1)\chi_q(1)dv. \quad \text{(See references 1 and 6.)}$$

[12] This may be shown to be true when β_{pq} is defined as in reference 11.

[13] One does not have to *orthogonalize* subject to formal neglect of differential overlap, but this appears to be the most natural and consistent procedure.

[14] Formulas for Coulomb repulsion integrals $(pp|qq)$, for Slater $2p\pi$ AO's, both for $Z_p = Z_q$ and $Z_p \neq Z_q$, are given by C. C. J. Roothaan, J. Chem. Phys. **19**, 1445 (1951). Numerical values for $Z_p \neq Z_q$ are not available in the literature, except for a few special cases. Numerical values for $Z_p = Z_q$ have been given by several authors; the best table now available is that of H. J. Kopineck, Z. Naturforsh. **5a**, 420 (1950).

[15] The uniformly charged sphere approximation seems to have been employed first by G. E. Kimball, who investigated such an approximation for $1s$ orbitals. See G. F. Neumark, Ph.D. thesis, Columbia University, 1951.

[16] For a preliminary discussion of the uniformly charged sphere approximation for $2p\pi$ orbitals, see R. G. Parr, J. Chem. Phys. **20**, 1499 (1952).

TABLE I. Electronic repulsion integrals in ethylene (ev).

Integral	Exact value[a]	Approximate value[b]
J_{11}	13.08	13.09 or 13.58
J_{22}	13.44	
J_{12}	13.01	
K_{12}	4.16	3.84 or 4.50

[a] Reference 18. These values are for Slater $2p\pi$ AO's with effective charge $Z=3.18$.
[b] Values in first column are calculated neglecting differential overlap; values in second column are calculated using uniformly charged sphere approximation. See text and reference 19.

which each $\chi_p^*\chi_p e$ is replaced by a pair of tangent uniformly charged nonconducting spheres of *diameter*

$$R_p=(4.597/Z_p)\times 10^{-8}\text{ cm},^{17} \tag{31}$$

where Z_p is the Slater effective nuclear charge for the $2p\pi$ atomic orbital χ_p, and the integrals $(pp|qq)$ are computed by means of classical electrostatic theory. A pronounced advantage of the uniformly charged sphere model is the relative ease with which heteroatoms may be handled.

5. PRIMITIVE APPLICATIONS TO ETHYLENE AND BENZENE

Tables I–IV give the results of application of the method outlined in Secs. 2–4 to ethylene and benzene. Results obtained by the much more tedious nonempirical antisymmetrized product method using Slater $2p\pi$ AO's are also displayed in the tables.[8,18] The two methods agree within the limits of precision in the nonempirical method. Agreement with experiment is another matter, which will be discussed briefly in Sec. 6 and in detail in paper II of this series.

The two π-electron LCAO MO's in ethylene are determined by symmetry. Neglecting overlap, they are

$$\left.\begin{aligned}\phi_1&=\frac{1}{\sqrt{2}}(\chi_1+\chi_2)\\ \phi_2&=\frac{1}{\sqrt{2}}(\chi_1-\chi_2)\end{aligned}\right\}, \tag{32}$$

where χ_1 and χ_2 are $2p\pi$ AO's on carbons 1 and 2. The electronic repulsion integrals, when differential overlap is neglected, are therefore given by the simple formulas

$$\left.\begin{aligned}2J_{11}=2J_{22}=2J_{12}&=(11|11)+(11|22)\\ 2K_{12}&=(11|11)-(11|22)\end{aligned}\right\}. \tag{33}$$

Table I gives purely theoretical values for these integrals,[18] values computed from Eq. (33) using exact values for the atomic Coulomb integrals $(11|11)$ and $(11|22)$, and values computed from Eq. (33) using uniformly charged sphere values for $(11|11)$ and $(11|22)$.[19]

Table II gives purely theoretical values for the π-electron energy levels of ethylene, values computed ignoring differential overlap, and values computed using the uniformly charged sphere approximation, a value of β being employed in the last two calculations which will make the "states" 1 and 2 have the same splitting as in the first calculation. Here states 1 and 2 arise from assignment of two electrons to the MO's ϕ_1 and ϕ_2, respectively. State N is the result of mixing states 1 and 2

TABLE II. Electronic energy levels of ethylene (ev).

State	Exact LCAO MO energy[a]	Approximate energy[b]	
$1(^1A_{1g})$	0.0	0.0	0.0
$2(^1A_{1g})$	12.5	12.5	12.5
$T(^3B_{1u})$	1.8	2.4	1.8
$V(^1B_{1u})$	10.2	10.1	10.8
Mean of T and V	6.0	6.2	6.2
$N(^1A_{1g})$	−1.3	−1.1	−1.4

[a] Reference 18. These values are for Slater $2p\pi$ AO's with effective charge $Z=3.18$.
[b] Values in first column are calculated neglecting differential overlap; values in second column are calculated using uniformly charged sphere approximation. See text and reference 19. $\beta=-3.125$ ev has been employed in each case.

to give the best approximation to the ground state obtainable from the AO's χ_1 and χ_2. States T and V are the triplet and singlet states arising from assignment of one electron to ϕ_1 and one electron to ϕ_2. The formulas for the energies of these various states have been given elsewhere,[18] and so will not be given here. The quantity α enters all the energies in the same additive way (note that the two carbon atoms in ethylene are equivalent) and, therefore, cancels when excitation energies are computed.

Neglecting overlap, the six π-electron LCAO MO's in benzene, as determined by symmetry, are[3]

$$\phi_l=\frac{1}{\sqrt{6}}\sum_{p=1}^{6}\omega^{lp}\chi_p,\quad l=0,\ \pm1,\ \pm2,\ 3; \tag{34}$$

[17] This value for the diameter forces the integral $(pp|pp)$ to be in agreement with the value computed for Slater $2p\pi$ AO's, $(pp|pp)=0.1957\ (e^2/a_0)Z_p$. (See, for example, R. G. Parr and B. L. Crawford, Jr., J. Chem. Phys. **16**, 1049 (1948).) For the uniformly charged sphere model, with $\chi_p^2 e$ replaced by two tangent uniformly charged spheres each of diameter R_p and carrying charge $e/2$, since the repulsive potential between one such sphere and itself is from classical electrostatics $(12/5R_p)$ for unit charge, $(pp|pp)=(e/2)^2|2(12/5R_p)+2(1/R_p)|=(17/10)\ (e^2/R_p)$. Hence, equating the two expressions for $(pp|pp)$, $R_p=(17/10)(a_0/0.1957Z_p)=(4.597/Z_p)\times 10^{-8}$ cm.

[18] R. G. Parr and B. L. Crawford, Jr., J. Chem. Phys. **16**, 526 (1948).

[19] If one inserts the usual $Z_c=3.18$ in Eq. (31), one finds $R_c=1.45$A, which would cause spheres on neighboring carbon atoms to overlap in ethylene and benzene. The electrostatics can be handled in this case (see reference 15), but it is simpler and in more natural accord with Eq. (28) to contract the spheres enough that neighboring spheres are just tangent, which procedure has been used in computing Tables I–IV and which corresponds to $Z_c=3.40$ in ethylene and $Z_c=3.30$ in benzene.

where $\omega=\exp(2\pi i/6)$ and χ_p is the $2p\pi$ AO on carbon p. Without the formal neglect of differential overlap there are thirty different electronic repulsion integrals in benzene, the values of which cluster in four distinct groups.[20] With the assumption of formal neglect of differential overlap there are only four distinct integrals; namely,

$$\left.\begin{aligned}
6J_{00}=6J_{01} &= \text{etc.}=(11|11)+2(11|22)\\
&\quad +2(11|33)+(11|44)\\
6K_{01}=6K_{12} &= \text{etc.}=(11|11)+(11|22)\\
&\quad -(11|33)-(11|44)\\
6K_{02}=6K_{13} &= \text{etc.}=(11|11)-(11|22)\\
&\quad -(11|33)+(11|44)\\
6K_{03}=6K_{1-2} &= \text{etc.}=(11|11)-2(11|22)\\
&\quad +2(11|33)-(11|44)
\end{aligned}\right\}. \quad (35)$$

TABLE III. Electronic repulsion integrals in benzene (ev).

Integral	Exact value[a]	Approximate value[b]
J_{00} group	8.627, 8.522, 8.495, 8.554, 8.474, 8.517, 8.623, 8.648, 8.787, 8.872; average 8.61	8.56
K_{01} group	2.584, 2.674, 2.867, 2.601, 2.633, 2.772; average 2.69	2.66
K_{02} group	1.304, 1.453, 1.338, 1.367, 1.328, 1.299, 1.302, 1.375, 1.344, 1.362; average 1.35	1.35
K_{03} group	0.934, 1.074, 1.007, 0.993 average 1.00	1.03

[a] Reference 8. These values are for Slater $2p\pi$ AO's with effective charge $Z=3.18$.
[b] Calculated using uniformly charged sphere approximation. See text and reference 19.

In Table III purely theoretical values for these integrals[8] are compared with values computed from Eq. (35) and the uniformly charged sphere approximation.[21]

Table IV gives purely theoretical values for the π-electron energy levels of benzene[8] and values computed using the uniformly charged sphere approximation and a value of β chosen to make the energies of the first excited singlet state equal in the two calculations. Here interaction[22] has been taken into account between all configurations which arise from excitation of an electron from an MO ϕ_1 or ϕ_{-1} to an MO ϕ_2 or ϕ_{-2}. Formulas for the energies again may be found elsewhere,[3] and α again does not enter the excitation energies.

TABLE IV. Electronic energy levels of benzene (ev).

State	Exact LCAO MO energy[a]	Approximate energy[b]
$^1A_{1g}$	0.0	0.0
$^1B_{2u}$	5.9	5.9
$^1B_{1u}$	7.3	7.3
$^1E_{1u}$	9.8	9.9
$^3B_{2u}$	5.8	5.9
$^3B_{1u}$	3.1	3.2
$^3E_{1u}$	4.4	4.5

[a] Reference 8. These values are Slater $2p\pi$ AO's with effective charge $Z=3.18$.
[b] Calculated using uniformly charged sphere approximation, with $\beta=-2.790$ ev. See text and reference 19.

6. DISCUSSION

These results show that the present semi-empirical theory is capable of duplicating the results of the nonempirical antisymmetrized product method in cases where the latter has been applied, and with such a large reduction in labor that applications are now made possible to much more complex molecules than have heretofore been treated by an antisymmetrized product method.

How about agreement with experiment, however? Although the experimental data themselves are not unambigously understood, even in ethylene and benzene, enough is known to make one realize that the nonempirical method is not entirely satisfactory. The present theory, admittedly being semi-empirical, has a flexibility not inherent in the nonempirical method. The possibility of exploiting this flexibility will be investigated in the next paper of this series.

Quantities which enter the expressions for the electronic energy levels of a molecule in the present theory are of four types: (1) atomic ionization potentials, W_p; (2) bond resonance integrals, β_{pq}; (3) Coulomb repulsion integrals, $(pp|qq)$; (4) Coulomb penetration integrals, $(q:pp)$. In the preliminary calculations of Sec. 5 above, only the first two of these types were regarded as empirical. One might well ask whether empirical adjustment of the last two would also be worth while. In the next paper such an adjustment will indeed be carried out, and there will emerge both an improved fit of the theory with experiment and a natural correction for the inadequacies of the π-electron approximation.

[20] See reference 8, especially footnote 9.
[21] Exact (reference 8) values for the atomic Coulomb integrals are $(11|11)=16.93$, $(11|22)=9.03$, $(11|33)=5.67$, $(11|44)=4.97$ ev; uniformly charged sphere approximation values (see footnote 19) are $(11|11)=17.61$, $(11|22)=8.84$, $(11|33)=5.58$, $(11|44)=4.90$ ev.
[22] This interaction can be handled by group theory, but this is a specialized technique not applicable to unsymmetrical molecules. Rather it appears preferable to handle the interaction by the configuration interaction technique of Sec. 2, which is completely general.

Interatomic Electric Quadrupole-Quadrupole Coupling in Salts of Cerium

R. FINKELSTEIN AND A. MENCHER
University of California, Los Angeles, California
(Received July 21, 1952)

We have calculated the magnetic properties of a cerium salt in terms of the one-atom (crystalline field) model at temperatures greater than 1°K. Because the cerium ion is not in an S state, its electronic charge distribution has a quadrupole moment; we have determined the influence of interatomic electric quadrupole-quadrupole interactions on the magnetic moment and optical rotation at very low temperatures. In cerium ethylsulfate this coupling is antiferromagnetic with a characteristic temperature of $\tau=0.01\langle r^2\rangle^4$ degrees, where $\langle r^2\rangle^{\frac{1}{2}}$ is the rms radius of the $4f$ orbit in A. This interaction may be at least partly responsible for a low temperature anomaly found by Becquerel, de Haas, and van den Handel, as well as for the sharp increase in specific heat noticed during adiabatic demagnetization. In other salts τ may be of opposite sign (ferromagnetic case) and possibly much larger (~1°K).

INTRODUCTION

SALTS of the rare earths are characterized by such weak interatomic couplings that their optical and magnetic properties can be understood largely in terms of the one-atom (crystalline field) model. On the other hand, the interatomic couplings, though small, become important whenever the temperature is so low that they are comparable to kT. The calculations to be described are based on the one-atom model at higher temperatures and on the perturbation of this model by an interatomic electric quadrupole-quadrupole coupling at temperatures of about 0.1°K. The numerical calculations are carried out for cerium ethylsulfate ($Ce(C_2H_5SO_4)_3\cdot 9H_2O$).

At the time of this work[1] the following data for the ethylsulfate were available: the optical rotation and magnetic moment over a wide range of temperature and field strengths;[2–4] the crystal structure:[5] C_{3h}; and the ground state of the magnetic ion:[6] $4f\,^2F_{\frac{5}{2}}$. According to the theoretical calculations, the one-atom model, neglecting off-diagonal matrix elements of the trigonal potential, predicted rotations and moments about 10 percent too high over the entire experimental range. It was also shown that the perturbation of the $J=5/2$ level by the $J=7/2$ level could not be responsible for this 10 percent deviation.[7]

The low temperature anomaly of main interest in this note was discovered by Becquerel, de Haas, and van den Handel.[2] They measured the rotation of the plane of polarization as a function of magnetic field strength at temperatures of liquid helium. For the ethylsulfates of Ds, Er, Pr, and Nd they find the law

$$\rho=A\tanh(\mu^*H_a/kT)+BH_a,$$

where H_a is the magnetic field acting on an atom; but for cerium this formula is not obeyed. For cerium also the value of the magnetic moment μ^* indicated by the saturation curves disagrees with the corresponding value μ calculated from the susceptibility-temperature curves (by 14 percent). In addition, the adiabatic demagnetization[8] of cerium ethylsulfate reveals a sharp increase in specific heat near 0.1°K. Following the suggestion of Van Vleck, we have attempted to explain these effects in terms of quadrupole-quadrupole coupling between the electronic charge distributions of different atoms; the results may be expressed in terms of a characteristic temperature $\tau=0.63\times10^{-4}\langle r^2\rangle^4$ degrees where $\langle r^2\rangle$ is the mean square radius of Ce in atomic units. If the entire discrepancy between μ and μ^* is attributed to this effect, $\tau=0.07°$, in approximate agreement with the adiabatic demagnetization experiment, and $\langle r^2\rangle^{\frac{1}{2}}=1.24$A which is possibly permitted by a Fermi-Thomas determination of the radius of the $4f$ orbit in Ce.

We first give a resumé of the results for the one-atom model. This provides a starting point for the discussion of the interatomic coupling.

THE ONE-ATOM MODEL

The ground level $J=5/2$ of the free cerium ion is split by the crystalline field into three levels which, by Kramers' theorem, cannot be further separated in a purely electrostatic field. These three levels will have magnetic moments appropriate to the local crystalline environment, rather than to the free state. In the ethylsulfate the off-diagonal elements of the crystalline potential, which is of trigonal symmetry, obey the selection rules $\Delta M=0, 3, 6$, and therefore the only non-vanishing elements internal to $J=5/2$ connect $M=\pm5/2$ and $M=\mp1/2$. If, however, the mixing of the $\pm5/2$ and $\mp1/2$ states is neglected as a first approximation (equatorial symmetry), then to this accuracy M is a

[1] The calculations reported here were first made in 1940. R. Finkelstein, thesis, Harvard.
[2] Becquerel, de Haas, and van den Handel, Physica **5**, 864 (1938).
[3] R. A. Fereday and E. C. Wiersma, Physica **2**, 575 (1935).
[4] E. C. Wiersma, private communication to J. H. Van Vleck.
[5] J. A. A. Ketelaar, Physica **4**, 619 (1937).
[6] R. J. Lang, Phys. Rev. **49**, 552 (1936).
[7] A recent and more refined theoretical investigation [R. J. Elliott and K. W. H. Stevens Proc. Phys. Soc. (London) **A64**, 932 (1951) and private communication to J. H. Van Vleck] which is based primarily on new paramagnetic resonance data, takes into account the previously neglected off-diagonal trigonal matrix elements (for which $\Delta M=6$) and leads to satisfactory agreement with experiment.
[8] W. J. de Haas and E. C. Wiersma, Physica **2**, 338 (1935).

good quantum number, and the magnetic moments have the values correct for the free ion.

In Figs. 1, 2, and 3 (curves A) the susceptibilities based on this approximation are compared with the experiment.[9] The magneton numbers are computed from the usual formulas

$$n^2=\chi kT/N\beta^2=Z^{-1}\{\sum_{nm}[\sum_{m'}|\mu(nm;nm')|^2+2kT \times\sum_{n'm'}{}'|\mu(nm;n'm')|^2/\delta(nm;n'm')]e^{-W(nm)/kT}\} \quad (1)$$

where

$$Z=\sum e^{-W(nm)/kT},$$

$$(\mu_x\pm i\mu_y)(M;M\mp1)=g[J(J+1)-M(M\mp1)]^{\frac{1}{2}}\beta, \quad (1a)$$

$$\mu_z(M;M)=Mg\beta, \quad (1b)$$

$$g=1+[J(J+1)+S(S+1)-L(L+1)]/2J(J+1).$$

In our case,

$$n_{\parallel}^2=[4.60+0.18e^{-\delta_1/T}+1.65e^{-\delta_2/T}]Z^{-1}, \quad (2a)$$

$$n_{\perp}^2=[1.65e^{-\delta_1/T}+(2T/\delta_2)(0.92)(1-e^{-\delta_2/T}) +[2T/(\delta_2-\delta_1)](1.47)(e^{-\delta_1/T}-e^{-\delta_2/T})]Z^{-1}, \quad (2b)$$

$$Z=1+e^{-\delta_1/T}+e^{-\delta_2/T}$$

with $\delta_1=W(1/2)-W(5/2)$ and $\delta_2=W(3/2)-W(5/2)$. Since the extrapolated value of $n_{\parallel}^2$ at 0° is 3.9, and since $n_{\parallel}$ decreases with increasing temperature, one infers that the lowest level is $M=5/2$; δ_1 and δ_2 are then both positive. The curves (A) are drawn for the choice $\delta_1/k=3°$ and $\delta_2/k=150°$. Equations (2) yield values of $n_{\parallel}^2$ which are ~10 percent too high. Accordingly, all moments have been reduced by the factor 0.901. Curves A are obtained by this procedure, which will be referred to as a flat correction.

A more refined analysis should account for the 10 percent correction and provide more detailed agreement with the experimental curves. For this reason we calculated the possible influence of matrix elements of the crystalline potential connecting the $J=5/2$ ground level with the $J=7/2$ level, which lies 2500 cm^{-1} higher. The results of this calculation, given in the next section, are negative and have no bearing on the rest of this paper.

Perturbation of $J=5/2$ by $J=7/2$

This calculation, which neglects off-diagonal elements of the trigonal field, may be termed the axial approximation; the corresponding Hamiltonian is

$$\mathcal{H}=\mathcal{H}_0+V(z), \quad (3)$$

where $\mathcal{H}_0$ includes the spin-orbit term of the free ion, and $V(z)$ is the crystalline perturbation. In the usual notations $\psi(JM)$ are the RS functions which diagonalize $\mathcal{H}_0$, and the low-lying eigenvalues of $\mathcal{H}_0$ are labelled $4f^2F_{5/2}$ and $4f^2F_{7/2}$. The problem is to find the energy levels and magnetic moments corresponding to $\mathcal{H}$, instead of to $\mathcal{H}_0$.

Let the axial potential in the M_LM_S-representation be

$$(M_L'M_S'|V|M_L''M_S'')=a(M_L')(M_L'M_S'|\delta|M_L''M_S''). \quad (4)$$

Two off-diagonal elements would also have to be included for a field having trigonal symmetry.

In the JM-representation,

$$(J'M'|V|J''M'')=\sum_{M_L'M_S'M_L''M_S''}(J'M'|S^+|M_L'M_S')(M_L'M_S'|V|M_L''M_S'')(M_L''M_S''|S|J''M''), \quad (5)$$

where S is

$$(M_LM_S|S|JM)=(M_S|U_M|J)\delta(M_L+M_S,M) \quad (6)$$

and U_M is

$(M_S\|U_M\|J)=M_S\backslash J$	$l+1/2$	$l-1/2$
$-1/2$	β_M	$-\alpha_M$
$+1/2$	α_M	β_M

$$\alpha_M^2+\beta_M^2=1$$

where

$$\alpha_M^2=(l+1/2+M)/2l+1.$$

Here $l=3$, so $\alpha_M^2=(7/2+M)/7$. By (4), (5), and (6)

$$(JM|V|J'M')=a(M-1/2)(J|U_M|1/2)(1/2|U_M|J')+a(M+1/2)(J|U_M|-1/2)(-1/2|U_M|J'),$$

or

$$(l-1/2\ M|V|l-1/2\ M')=[\beta_M^2a(M-1/2)+\alpha_M^2a(M+1/2)]\delta(M,M'), \quad (7a)$$

$$(l+1/2\ M|V|l+1/2\ M')=[\alpha_M^2a(M-1/2)+\beta_M^2a(M+1/2)]\delta(M,M'), \quad (7b)$$

$$(l-1/2\ M|V|l+1/2\ M')=[\alpha_M\beta_M][a(M-1/2)-a(M+1/2)]\delta(M,M'). \quad (7c)$$

[9] The data shown in these figures have been taken from the following sources: (1) measurements of $\chi_{\parallel}-\chi_{\perp}$ and χ_{mean} at 20°K; and (2) $\chi_{\parallel}-\chi_{\perp}$ over the temperature interval 14°–290° by Fereday and Wiersma (reference 3); (3) optical rotation for a beam parallel to the optic axis over the range 1.37°–290°K by Becquerel et al (reference 2); (4) χ_{mean} at temperatures 1.39°–3.10°K by Wiersma (reference 4). Van Vleck and Hebb have shown the proportionality of the verdet constant, V, and the magnetic susceptibility χ: $V=A\chi+K$. The constant K can be determined from lanthanum ethylsulfate, which is diamagnetic. From (1) and (3) A may be found; then $\chi^{\parallel}$ may be calculated over the whole temperature range; by (2) $\chi_{\perp}$ is then known in the interval 14°–290°; and by (4) at lower temperatures.

The splitting of $J=5/2$ by the crystalline potential is given by (7a) and of $J=7/2$ by (7b). In terms of the parameters $a_0a_1a_2a_3$,

$$\begin{aligned} E(5/2,\pm5/2)&=(6a_3+a_2)/7\\ E(5/2,\pm3/2)&=(5a_2+2a_1)/7\\ E(5/2,\pm1/2)&=(4a_1+3a_0)/7 \end{aligned} \tag{8a}$$

$$\begin{aligned} E(7/2,\pm7/2)&=a_3\\ E(7/2,\pm5/2)&=(a_3+6a_2)/7\\ E(7/2,\pm3/2)&=(5a_1+2a_2)/7\\ E(7/2,\pm1/2)&=(3a_1+4a_0)/7. \end{aligned} \tag{8b}$$

The connections of the parameters a_m with the earlier introduced δ_1 and δ_2 are

$$\begin{aligned} \delta_1&=(4a_1+3a_0-6a_3-a_2)/7,\\ \delta_2&=(3a_2+2a_1-6a_3)/7. \end{aligned} \tag{8c}$$

The magnetic moments are perturbed by the axial field, since V has matrix elements connecting $J=5/2$ and $J=7/2$. The perturbed magnetic moment matrix is

$$\mu=T^{+}\mu^0T=\mu^0+\mu^0T'-T'\mu^0, \tag{9}$$

where

$$T'(l-1/2,\,M;\,l+1/2,\,M')=-V(l-1/2,\,M;\,l+1/2M')/[E(l-1/2,\,M)-E(l+1/2,\,M')]. \tag{9a}$$

The off-diagonal elements of V and of μ^0 which enter into (9) are given by (9a) and (7c), and by

$$\begin{aligned} (l-1/2\;M\,|\,\mu_x\,|\,l+1/2\;M\pm1)&=\mp[(l+1/2\pm M)(l+3/2\pm M)]^{\frac{1}{2}}\beta/2(2l+1),\\ (l-1/2\;M\,|\,\mu_z\,|\,l+1/2\;M)&=[(l+1/2)^2-M^2]^{\frac{1}{2}}\beta/2l+1. \end{aligned} \tag{10}$$

Performing the indicated substitutions, one finds for the fractional perturbations of the magnetic moments

$$\begin{aligned} f_{\parallel}(M)&=\mu_z(l-1/2,\,M;\,l-1/2,\,M)/\mu_z{}^0(l-1/2,\,M;\,l-1/2M)\\ &=1+\{[(l+1/2)^2-M^2]/l(2l+1)M\Delta\}a(M+1/2,\,M-1/2), \end{aligned} \tag{11a}$$

$$\begin{aligned} f_{\perp}(M)&=\mu_z(5/2M;\,5/2M\pm1)/\mu_z{}^0(5/2M;\,5/2M\pm1)\\ &=1\mp\{(l+3/2\pm M)a(M\pm1+1/2,\,M\pm1-1/2)-(l+1/2\mp M)a(M+1/2,\,M-1/2)\}/2l(2l+1)\Delta, \end{aligned} \tag{11b}$$

where $a(M,\,M')\equiv a(M)-a(M')$ and $\Delta=E(7/2\;M')-E(5/2\;M)=2250\ \text{cm}^{-1}$. The dependence of Δ on M and M' is neglected.

Numerically,

$$\begin{aligned} f_{\parallel}(5/2)&=1+5.09\times10^{-5}a_{32} & f_{\perp}(\pm3/2,\,\pm1/2)&=1\mp1.06\times10^{-5}(5a_{21}-3a_{10})\\ f_{\parallel}(3/2)&=1+14.1\times10^{-5}a_{21} & f_{\perp}(\pm5/2,\,\pm3/2)&=1\mp2.11\times10^{-5}(3a_{32}-a_{21})\\ f_{\parallel}(1/2)&=1+50.8\times10^{-5}a_{10} & f_{\perp}(\pm1/2,\,\mp1/2)&=1\mp8.44\times10^{-5}a_{10}. \end{aligned} \tag{12}$$

These equations express the perturbed magnetic moments of all levels in terms of three parameters a_{32}, a_{21}, and a_{10}. Since δ_1 and δ_2 may also be written in terms of the same parameters, it is possible to express all moments in terms of three parameters, say $(\delta_1,\,\delta_2,\,a_1)$.

If one regards δ_1 and δ_2 already found as approximately correct, then one may try to adjust a_1 to give the perturbed moments needed to fit the experimental curves. Curves B, in Figs. 1, 2, 3 were calculated by adjusting the moments in Eqs. (2), for best agreement with the data, as follows:

$$\begin{aligned} \mu_{\parallel}(5/2)^2&=3.69 & \mu_{\perp}(1/2,\,-1/2)^2&=0.72 & \delta_1/k&=7^\circ\\ \mu_{\parallel}(1/2)^2&=0.18 & \mu_{\perp}(5/2,\,3/2)^2&=0.80 & \delta_2/k&=100^\circ.\\ \mu_{\parallel}(3/2)^2&=2.22 & \mu_{\perp}(3/2,\,1/2)^2&=1.50 \end{aligned} \tag{12a}$$

Since even the curves (B) do not fit very well, it appears that the form of the Eqs. (2) as well as the parameters appearing in it, ought to be altered. Furthermore, it was found that these perturbed moments could not be accounted for even approximately in terms of Eqs. (12) by any adjustment of $(\delta_1,\,\delta_2,\,a_1)$—mainly because the experimentally required perturbations of $\mu_{\parallel}(5/2)$ and $\mu_{\perp})1/2,\,-1/2)$ are incompatible with their common dependence on a_1.

One concludes from this calculation that the "10 percent overestimate" cannot be corrected by taking into account the perturbing effect of $J=7/2$. Elliott and Stevens,[7] however, show that a significant improvement may be made by including the off-diagonal trigonal elements for which $\Delta M=6$ and solving the secular equation by exact rather than perturbation methods. Unfortunately this work was done primarily for cerium ethylsulfate diluted with lanthanum, and an equally

precise description has not yet been worked out for the undiluted salt, which is of interest here and has somewhat different properties.[10] We have thought that our earlier results on the axial field might still be of interest as an indication of the errors involved in the simple model which neglects the off-diagonal elements.

THE MANY-ATOM MODEL

We now consider the possible incidence of low temperature anomalies associated with the coupling of magnetic electrons on different cerium ions. To be effective at low temperatures such a coupling must lift the Kramers degeneracy of the lowest level, and that requires the appearance of processes in which the two coupled electrons make simultaneous transitions (i.e., matrix elements off-diagonal in both electrons). Magnetic dipole-dipole coupling is already incorporated into the local field H_a,[11] and electric dipole-dipole couplings are effectively excluded by Laporte's rule. One is therefore led to consider electric quadrupole-quadrupole couplings.

Modification of the Saturation Curves by an Interatomic Potential

Let the Hamiltonian of the crystal in the presence of a magnetic field be

$$H=H_0+Q,$$

where $H_0=\sum_i H_{0i}$ and $Q=\sum_{i<j} q_{ij}$. H_0, including the Zeeman energy, characterizes the one-atom picture, and Q represents an interatomic potential, here the electric quadrupole-quadrupole interaction. The problem is to find the characteristic values of H, denoted by W_n:

$$W_n=E_n+\Delta E_n,$$

where E_n represents the corresponding eit of H_0. Since Q is thought to be small compared to H_0, perturbation theory may be used to determine ΔE_n. The partition function is then

$$Z=\sum_n e^{-W_n/kT}=Z_0(1-\langle\Delta E\rangle/kT),$$

where

$$\langle\Delta E\rangle=[\sum(\Delta E_n)e^{-E_n/kT}]/[\sum e^{-E_n/kT}]. \tag{13}$$

Finally, various macroscopic properties may be determined from Z. For example, the magnetic moment is

$$M=kT\frac{\partial}{\partial H}\ln Z=M_0-\frac{\partial}{\partial H}\langle\Delta E\rangle. \tag{14}$$

It is sufficient to find the contribution to $\langle\Delta E\rangle$ from only the lowest levels; if there is no magnetic field and if $Q=0$, the ground level of the magnetic sublattice containing N ions is 2^N- fold degenerate, and it is enough to determine the 2^N levels into which this is split. Since this degeneracy is not lifted in the first order (ΔE_n is

$$\Delta E_n=-\sum_{n'}\frac{Q(n;n')Q(n';n)}{E(n';n)}, \tag{15}$$

where n designates the energy. Since $Q=\sum_{i>j} q_{ij}$, where q_{ij} depends only on the coordinates of atoms i and j, ΔE_n can be written in terms of two-atom functions. To do this, write the matrix elements of Q between two states of the entire crystal as

$$(n|Q|n')=\sum_{i<j}(m_im_j|q_{ij}|m_i'm_j')\prod_{s\neq i,j}(m_s|\delta|m_s'), \tag{16}$$

where m_s, which labels the states of a single magnetic ion, may assume the values $\pm1/2$, $\pm3/2$, $\pm5/2$. Then

$$\Delta E_n=\sum_{i<j} q_{ij}^{\#}(m_i'm_j'), \tag{17}$$

where

$$q_{ij}^{\#}(m_i'm_j')=-\sum_{m_i''m_j''}\frac{(m_i'm_j'|q_{ij}|m_i''m_j'')(m_i''m_j''|q_{ij}|m_i'm_j')}{E(m_i'')+E(m_j'')-E(m_i')-E(m_j')}, \tag{17a}$$

and the average value of ΔE_n is

$$\langle\Delta E_n\rangle=-\sum_{m_1'\cdots m_N'}[\sum_{i<j} q_{ij}^{\#}(m_i'm_j')]\prod_s\exp(-E(m_s')/kT)\sum_{m_1'\cdots m_N'}\prod_s\exp(-E(m_s')/kT),$$

which is simply

$$\langle\Delta E\rangle=\sum_{i<j}\langle q_{ij}\rangle, \tag{18}$$

[10] One difference is that the order of the 5/2 and 1/2 levels is inverted.
[11] H. A. Kramers, Proc. Amst. Acad. 33, 959 (1930); J. H. Van Vleck, J. Chem. Phys. 5, 320 (1937).

where

$$\langle q_{ij}\rangle=\sum_{m_i'm_j'} q_{ij}^{\#}(m_i'm_j') \exp-(E(m_i')+E(m_j'))/kT/\sum_{m_i'm_j'} \exp-(E(m_i')+E(m_j'))/kT. \tag{18a}$$

These state sums run over only the low-lying levels, i.e., $m_i'=\pm m$ where $m=5/2$. Since it turns out that $q_{ij}{}^{\#}(m_i'm_j')$ depends only on the relative orientation of spins, the notation π (parallel) and α (antiparallel) will be used as follows:

$$\begin{aligned}\pi&=q^{\#}(+m,+m)=q^{\#}(-m,-m),\\ \alpha&=q^{\#}(+m,-m)=q^{\#}(-m,+m).\end{aligned} \tag{19}$$

With this notation,

$$\langle q_{ij}\rangle=[\pi_{ij}\cosh(2mg\beta H/kT)+\alpha_{ij}]/[\cosh(2mg\beta H/kT)+1]. \tag{20}$$

By (14), (18), and (20)

$$M=N\mu[1-(\tau/T)\operatorname{sech}^2\mu H/kT]\tanh\mu H/kT, \tag{21}$$

where τ is a characteristic temperature

$$\tau=(1/Nk)\textstyle\sum_{i<j}(\pi_{ij}-\alpha_{ij}), \tag{21a}$$

and $\mu=gm\beta$. Equation (21) gives the desired result for the magnetic moment, but to use it, one must determine π_{ij} and α_{ij}. The formula (21) is, of course, valid for any interatomic potential, but in the next paragraph a particular choice of q_{ij} will be made.

The Quadrupole-Quadrupole Matrix Elements

Let the significant electronic contribution of two cerium ions A and B to the Coulombic part of the Hamiltonian be e^2/r_{ab}. Let the positions of their $4f$ electrons be denoted by the vectors a_s and b_s ($s=1, 2, 3$) referred to parallel coordinate systems. Then the quadrupole-quadrupole part of e^2/r_{ab} is

$$q_{ab}\doteq\lambda\sum_{s,t,l,m=1}^{3} N_{stlm}a_sa_tb_lb_m, \tag{22}$$

where the tensor N_{stlm} is

$$35n_sn_tn_ln_m-20\delta_{st}n_ln_m+2\delta_{sl}\delta_{tm}-5n_sn_t\delta_{lm}-5\delta_{st}n_ln_m+\delta_{st}\delta_{lm} \tag{22a}$$

in terms of n_s, the unit vector in the direction of the internuclear line AB, again referred to the common coordinate system of A and B. Here

$$\lambda=3e^2/4R^5a_0^5, \tag{22b}$$

where Ra_0 is the distance between the nuclei, located at $a_s=0$ and $b_s=0$; a_0 is the atomic unit of length. One may verify (22) by choosing the z-axis along the line AB: $n_s=(0, 0, 1)$, and noting that the invariant q_{ab} in this simple case reduces to

$$q_{ab}=\lambda[2(a_1b_1+a_2b_2-4a_3b_3)^2+a^2b^2-5a_3{}^2b^2-5a^2b_3{}^2-15a_3{}^2b_3{}^2]. \tag{22c}$$

The matrix elements of q_{ab} are

$$(m_a'm_b'|q_{ab}|m_a''m_b'')=\lambda\sum N_{stlm}(m_a'|a_sa_t|m_a'')(m_b'|b_lb_m|m_b''). \tag{23}$$

If there is axial symmetry,

$$\begin{aligned}(m\pm1|a_sa_t|m)&=\alpha_{st}{}^{\pm}(m\pm1|xz|m),\\ (m\pm2|a_sa_t|m)&=\beta_{st}{}^{\pm}(m\pm2|x^2|m),\end{aligned} \tag{23a}$$

where

$$\begin{aligned}\alpha_{st}{}^{\pm}&=\delta_{s1}\delta_{t3}+\delta_{s3}\delta_{t1}\mp i\delta_{s2}\delta_{t3}\mp i\delta_{s3}\delta_{t2},\\ \beta_{st}{}^{\pm}&=\delta_{s1}\delta_{t1}-\delta_{s2}\delta_{t2}\mp i\delta_{s1}\delta_{t2}\mp i\delta_{s2}\delta_{t1}.\end{aligned}$$

From Eqs. (22a), (23), and (23a) one finds, if $\Delta m_a\cdot\Delta m_b\neq0$,

$$(m_a+\Delta m_a, m_b+\Delta m_b|q_{ab}|m_am_b)=S(\Delta m_a, \Delta m_b)(m_a+\Delta m_a|A|m_a)(m_b+\Delta m_b|B|m_b), \tag{24}$$

where

$$\begin{aligned}(m_a+\Delta m_a|A|m_a)&=\delta(\Delta m_a, \pm1)(m_a\pm1|xz|m_a)+\delta(\Delta m_a, \pm2)(m_a\pm2|x^2|m_a),\\ (m_b+\Delta m_b|B|m_b)&=\delta(\Delta m_b, \pm1)(m_b\pm1|xz|m_b)+\delta(\Delta m_b, \pm2)(m_b\pm2|x^2|m_b),\end{aligned} \tag{24a}$$

$$S(\Delta m_a, \Delta m_b)=\lambda p(\Delta m_a, \Delta m_b)P_4{}^{\Delta m}(\mu)e^{-i(\Delta m)\varphi}. \tag{24b}$$

Here $\Delta m=\Delta m_a+\Delta m_b$, $P_4{}^{\Delta m}$ is an associated Legendre function; μ is the cosine of the angle between the line of

centers AB and the optic axis, and $\|p(\Delta m_a, \Delta m_b)\|$ is the symmetric matrix:

$\Delta m_a \backslash \Delta m_b$	$+1$	-1	$+2$	-2
1	8/3	−32	2/3	−4
−1		8/3	−4	2/3
2			1/3	8
−2				1/3

Matrix elements for which $\Delta m_a \cdot \Delta m_b = 0$ have been dropped since they are of no interest here.

The characteristic temperature τ which enters directly into the expression (21) for the magnetic moment, is by (21a)

$$\tau = (1/2k)\sum_i (\pi - \alpha)_i \zeta_i, \tag{25}$$

where ζ_i is the number of neighbors in the ith shell. (Two neighbors are counted in the same shell if they have the same value of $\pi - \alpha$). Next, combining (25), (19), (17a), and (24) one finds

$$\tau = \frac{9e^4\langle r^2\rangle^4}{32ka_0^2}\left[\frac{T(m_2-m_1, m_2-m_1)\,|(m_2|M|m_1)|^4}{2\delta(m_2, m_1)} + \frac{T(m_3-m_1, m_3-m_1)\,|(m_3|M|m_1)|^4}{2\delta(m_3, m_1)} + \frac{2T(m_2-m_1, m_3-m_1)\,|(m_2|M|m_1)|^2\,|(m_3|M|m_1)|^2}{\delta(m_2, m_1)+\delta(m_3, m_1)}\right], \tag{26}$$

where $\langle r^2\rangle$ = mean square radius of $4f$ shell in units of a_0^2.

$$T(1, 1) = \sum_i 64\{16[P_4^0(\mu)]^2 - (1/9)[P_4^2(\mu)]^2\}_i(\zeta_i/R_i^{10}), \tag{26a}$$

$$T(2, 2) = \sum_i \{64[P_4^0(\mu)]^2 - (1/9)[P_4^4(\mu)]^2\}_i(\zeta_i/R_i^{10}), \tag{26b}$$

$$T(1, 2) = \sum_i 4\{4[P_4^1(\mu)]^2 - (1/9)[P_4^3(\mu)]^2\}_i(\zeta_i/R_i^{10}), \tag{26c}$$

$$\delta(M, M') = W(M) - W(M'), \tag{26d}$$

$$(m_2|M|m_1) = (m_2|xz/r^2|m_1)\delta(m_2-m_1, 1) + (m_2|x^2/r^2|m_1)\delta(m_2-m_1, 2). \tag{26e}$$

In (26) the order of levels is $W(m_3) > W(m_2) > W(m_1)$. The geometry of the crystal is contained only in the $T(i, j)$; these sums converge rapidly since they contain the factor R^{-10}. The matrix elements appearing in (26) may also be given explicitly:

$$(M\pm 2|x^2/r^2|M) = -[(J\pm M+2)(J\pm M+1)(J\mp M)(J\mp M-1)]^{\frac{1}{2}}/8J(J+1), \tag{26f}$$

$$(M|xz/r^2|M\pm 1) = (2M\pm 1)[(J\pm M+1)(J\mp M)]^{\frac{1}{2}}/8J(J+1). \tag{26g}$$

Equation (26) taken with (21) is the desired result for an axial crystal. Before making a numerical application we mention a check of Eqs. (26a)–(26c) which has the advantage of introducing the $P_4^{\Delta m}(\mu)$ in a direct way, and of easy generalization to nonaxial crystals. Take the axis of quantization along the internuclear line so that (22c) is correct. Rewrite (22c) in terms of spherical harmonics:

$$q_{ab} = A\sum_{-2}^{+2} c_m Y_{2m}(a) Y_{2-m}(b), \tag{27}$$

where

$$A = 4\pi e^2 a^2 b^2/5R^5; \quad c_m = c_{-m}; \quad c_0 = 6, \quad c_1 = 4, \quad c_2 = 1, \tag{27a}$$

and $Y_{2m}(a)$ means $Y_{2m}(\theta_a, \varphi_a)$. Note that if $a_s = b_s$ in (27),

$$q(a, a) = A\sum c_m Y_{2m}(a) Y_{2-m}(a) = A[10/(4\pi)^{\frac{1}{2}}]Y_{40}(a).$$

This equation may also be written in the form

$$\sum_{-2}^{+2} c_m D_{m0}^{(2)} D_{-m0}^{(2)} = 6D_{00}^{(4)}, \tag{28}$$

where use has been made of the identities

$$D_{0m}^{(2)} = (4\pi/5)^{\frac{1}{2}} Y_{20}; \quad D_{00}^{(4)} = (4\pi/9)^{\frac{1}{2}} Y_{40}.$$

Equation (28) will be used later.

When the axis of quantization does not coincide with the internuclear line, Eq. (27) becomes

$$q(a, b) = A\sum c_m D_{m\lambda}^{(2)} D_{-m\lambda'}^{(2)} Y_{2\lambda}(a) Y_{2\lambda'}(b),$$

or

$$q(a, b) = \sum A_{\lambda\lambda'} Y_{2\lambda}(a) Y_{2\lambda'}(b), \tag{29}$$

where

$$A_{\lambda\lambda'} = A\sum_{-2}^{+2} c_m D_{m\lambda}^{(2)} D_{-m\lambda'}^{(2)}. \tag{29a}$$

$A_{\lambda\lambda'}$ may be calculated directly from this equation, but the properties of the $D^{(l)}$ are helpful here. One has

$$D_{m\lambda}^{(2)} D_{-m\lambda'}^{(2)} = \sum_{L=0}^{4} S_{Lm-m}{}^* D_{0\lambda+\lambda'}^{(L)} S_{L\lambda\lambda'},$$

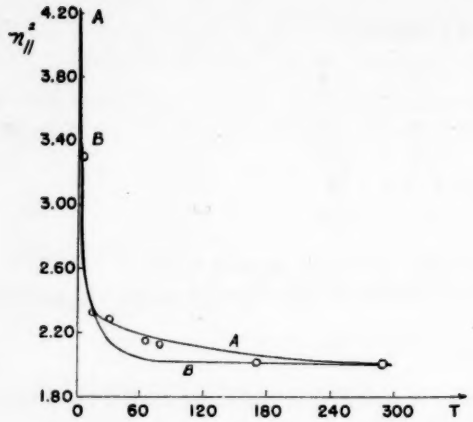

FIG. 1. Field parallel to optic axis. $n^2=\chi kT/N\beta^2=$square of magneton number. $T=$temperature. ○: experimental points. A: flat correction of 0.905 on Eq. (2); $\delta_1/k=3°$; $\delta_2/k=150°$. B: moments corrected individually according to Eqs. (12a).

where the $D^{(L)}$ are irreducible representations. Then

$$A_{\lambda\lambda'}=A\sum_{L=0}^{4} d_L D_{0\lambda+\lambda'}{}^{(L)} S_{L\lambda\lambda'}, \tag{30}$$

where

$$d_L=\sum_{-2}^{+2} S_{Lm-m}{}^{*} c_m.$$

One sees from (30) that $A_{\lambda\lambda'}$ is a linear combination of spherical harmonics $Y_{L,\lambda+\lambda'}$ where $0\leq L\leq 4$. Next one notes that by (30)

$$A_{00}=A\sum_{L=0}^{4} d_L D_{00}{}^{(L)} S_{L00},$$

but according to (29a) and (28)

$$A_{00}=6AD_{00}{}^{(4)}.$$

Hence,

$$6D_{00}{}^{(4)}(\alpha,\beta,\gamma)=\sum_{0}^{4} d_L D_{00}{}^{(L)}(\alpha,\beta,\gamma) S_{L00},$$

or

$$d_L=(6/S_{400})\delta_{L4},$$

and

$$\begin{aligned} A_{\lambda\lambda'}&=6A(S_{4\lambda\lambda'}/S_{400})D_{0\lambda+\lambda'}{}^{(4)} \\ &=6A(S_{4\lambda\lambda'}/S_{400})N_{\lambda+\lambda'}Y_{4,\lambda+\lambda'}. \end{aligned} \tag{31}$$

Here

$$D_{0\lambda+\lambda'}{}^{(4)}=N_{\lambda+\lambda'}Y_{4\lambda+\lambda'},$$

where $N_{\lambda+\lambda'}$ is the proper normalization coefficient. Since the $S_{L\lambda\lambda'}$ are known, Eq. (31) represents a satisfactory determination of the $A_{\lambda\lambda'}$.

The corresponding quadrupole matrix elements now follow from (29). They are

$$\begin{aligned} &(\gamma_a\gamma_b|q_{ab}|\gamma_a'\gamma_b') \\ &\quad=\sum A_{\lambda\lambda'}(\gamma_a|Y_{2\lambda}{}^{(a)}|\gamma_a')(\gamma_b|Y_{2\lambda'}{}^{(b)}|\gamma_b'), \end{aligned} \tag{32}$$

where the γ_a represent crystalline quantum numbers. Equation (32) is general. If the symmetry is axial, (32) reduces to the earlier result (24).

APPLICATION TO CERIUM ETHYLSULFATE

Ketelaar has determined the geometry of this crystal.[5] Using Eqs. (26) and taking into account the first two shells of neighbors ($\zeta_1=2$, $\mu_1=1$; $\zeta_2=6$, $\mu_2=\cos 66°\ 20'$) one obtains the characteristic temperature

$$\begin{aligned} \tau=1.61\ 10^{-3}\langle r^2\rangle^4[&20.4/\theta_2-0.689/\theta_1 \\ &-5.70/(\theta_1+\theta_2)] \end{aligned} \tag{33}$$

where $k\theta_2=\delta(3/2, 5/2)$ and $k\theta_1=\delta(1/2, 5/2)$. The curves ($B$) in Figs. 1, 2, and 3 are based on the choice $\theta_1=7°$ and $\theta_2=100°$. The corresponding τ is $0.826\times 10^{-4}\langle r^2\rangle^4$. Unfortunately, no reliable determination of $\langle r^2\rangle$ has been made. For this reason we adopt the inverse procedure of attempting to calculate $\langle r^2\rangle$ by attributing the low temperature anomaly entirely to qq coupling. To find a satisfactory empirical τ, it is necessary to fit both the

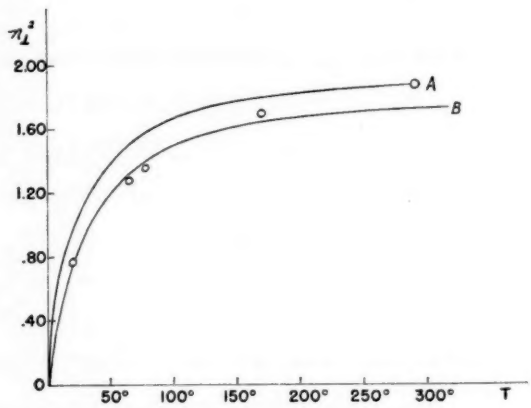

FIG. 2. Field perpendicular to optic axis. Other notation same as for Fig. 1.

$M-H$ and the $\chi-T$ curves. These curves[12] are shown in Figs. 3(C) and 4; they are based on $\theta_1=6.2°$, $\mu(5/2)=1.97$, $\tau=0.070°$, and at helium temperatures on Eq. (21) and $\chi=\chi_0(1-\tau/T)$. That this value of τ will remove the major discrepancy between the MH and the χT-curves may be seen as follows. If one describes the data, as Becquerel and others did, by

$$M=M_\infty \tanh(\mu^*H/kT),$$

then

$$\lim_{H/T\to 0}\left[\frac{d^2M}{d(H/T)^2}\Big/M\right]=2\left(\frac{\mu^*}{k}\right)^2.$$

On the other hand, if

$$M=M_\infty[1-(\tau/T)\operatorname{sech}^2(\mu H/kT)]\tanh(\mu H/kT),$$

[12] The data in Fig. 4 is taken from reference 2. The ratio (optical rotation/magnetic moment), needed to convert Eq. (21) to rotations, is taken from the same paper. Numerically, $M_{11}/\rho_{11}=26.73$ *determined at* $H=0$. It is important that this conversion factor is independent of H.

then

$$\lim_{H/T\to 0}\left[\frac{d^2M}{d(H/T)^2}\Big/M\right]=\frac{1-4\tau/T}{1-\tau/T}2\left(\frac{\mu}{k}\right)^2.$$

Hence, the true moment (μ) is related to the "saturation" moment μ^* by

$$\mu^*=[(1-4\tau/T)/(1-\tau/T)]\mu.$$

The above values of μ, μ^*, and τ satisfy this equation approximately. As a result, the experimental points do not lie more than 3 percent off the theoretical curves 3C and 4. Without this interpretation there is a discrepancy of 14 percent between μ and μ^*.

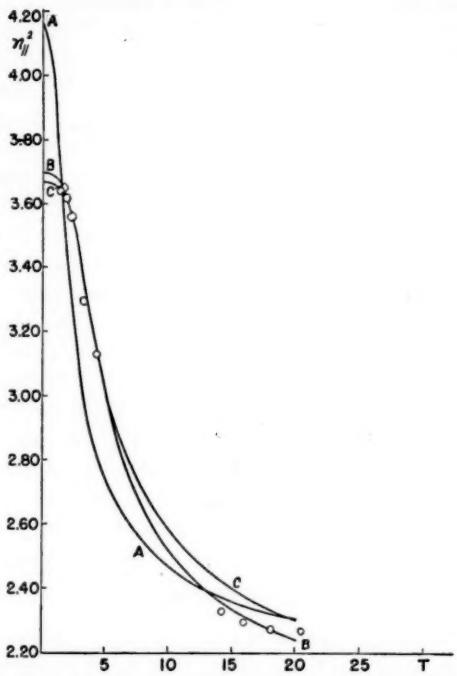

FIG. 3. Field parallel to optic axis. Low temperature measurements only. *A* and *B* same as in Fig. 1. *C*: $\mu_{11}(5/2)=1.97\beta$; $\mu_{11}(1/2)=0.424\beta$; $\delta_1/k=6.2°$ plus quadrupole correction with $\tau=0.07°$K.

To make the preceding analysis more precise the following information is needed: (1) the nonaxial part of the crystalline field, not only because the *qq*-interaction is only a perturbation on the one-atom model, but also because the magnitude of τ is very sensitive to the crystalline spectrum and matrix elements; (2) a theoretical determination of $\langle r^2\rangle$. The value of $\langle r^2\rangle^{\frac{1}{2}}$ corresponding to $\tau=0.07$ is $\langle r^2\rangle^{\frac{1}{2}}=2.35$. A Fermi-Thomas calculation for $Z=58$ yields a value of $\langle r^2\rangle^{\frac{1}{2}}$ somewhat larger than 2.35, but is unreliable because the contraction of the $4f$ orbit, which leads to the formation of the rare earth group, is slightly delayed on this model. On the other hand, the contraction occurs very suddenly, and at $Z=60$ the value of $\langle r^2\rangle^{\frac{1}{2}}$ has already shrunk to 1.45.[13]

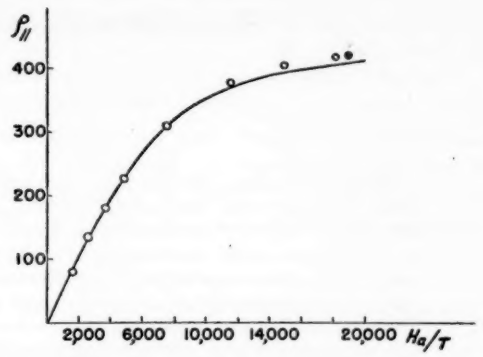

FIG. 4. Optical rotation as function of H_a/T at $T=1.37°$. ⊙: experimental points. Curve according to Eq. (21) with $\tau=0.07°$K; $\mu_{11}(5/2)=1.97\beta$.

We conclude with the following remarks. (1) As Z is increased beyond cerium, the $4f$ radius contracts. It is possible then, especially if the $4f$ radius of cerium is "abnormally" large, that the *qq* interaction, which decreases as r^{-8}, is much more important for cerium than for the other rare earths. (2) The coupling in the ethylsulfate is antiferromagnetic ($\tau>0$), but if the two lower levels were 3° apart (as in the case for example when this salt is diluted with lanthanum), the coupling would be ferromagnetic ($\tau<0$); the sign and magnitude of τ is very sensitive to the spectrum of a single ion. (3) Cooling the ethylsulfate by adiabatic demagnetization[8] reveals a sharp increase in the specific heat at ~0.1°K; that is in agreement with the Curie temperature found here: $\tau=0.07°$K. (4) Situations are quite possible in which the Curie point would be much higher. For example, if the order of the levels 1/2, 3/2 is inverted, then by Eq. (33) τ may easily be as large as 1°K.

We wish to thank J. H. Van Vleck for having suggested this problem and discussed it with us.

[13] We are continuing a Fermi-Thomas investigation of the rare earth group.

The Hydrodynamic Stability of Flame Fronts*

HARVEY EINBINDER
Pupin Physics Laboratory, Columbia University, New York, New York†
(Received April 14, 1952)

The hydrodynamic stability of a plane flame of finite thickness is treated by investigating the temporal behavior of first-order infinitesimal disturbances. This work is a generalization of earlier studies and takes into account the effect of distortion on burning velocity. The general equations of motion for the disturbance in a viscous gas under the influence of gravity are derived and solved. Horizontal and upward propagating plane flames are always unstable and those propagating downward are unstable under most conditions, so their measured transformation velocity under such conditions does not equal the stationary burning velocity. The calculated maximum cell size for downward propagation ($\lambda_{max}=32U_uU_b\times10^{-4}$ cm) and the cell size for a flame propagated by thermal conduction ($\lambda_{thermal}=22k/C_p\rho_uU_u$) are in good agreement with existing experimental observations. The variation of cell size with pressure yields the pressure dependence of the burning velocity. The sudden appearance of cells in slow hydrocarbon flames ($U_u\approx10$ cm/sec) observed at stoichiometric in going from lean to rich mixtures, indicating a corresponding decrease in flame thickness, is advanced as provisional evidence of a shift in the dominant propagation mechanism in these flames—from diffusion by atomic radicals for lean flames to thermal conduction for rich ones.

1. INTRODUCTION

IN the past, the hydrodynamic aspects of combustion have received comparatively little attention. To date, virtually all theoretical work on flame propagation has been concerned with the physico-chemical theory of the burning velocity. These theories, which take into account heat conduction, diffusion, and chemical kinetics, assume laminar flow through an undisturbed plane flame front.[1–3] The complicated and largely unknown nature of the combustion reaction kinetics still constitutes the major obstacle to the satisfactory solution of this problem (see Sec. 4).

Experimental work has shown, however, that only under special conditions, e.g., laminar flow through a small orifice (Bunsen burner), flame propagation proceeds with a velocity uniquely determined by the composition and state parameters of the unburned gas. Under conditions prevailing in the majority of applications, flames propagate into the unburned gas with a velocity which may be one or two times greater than the laminar burning velocity.

Direct evidence of the intrinsic instability of plane flames has been provided by Markstein[4] who observed the spontaneous breakdown of rich hydrocarbon flames into many separate cells in the absence of turbulence in the approach stream. Recently a number of other observations have been reported,[5–7] and an extensive review of the entire field has been given by Markstein.[8]

The observed cells are reminiscent of patterns observed in cellular convection. Consequently, previous studies of flame stability have been based on the temporal behavior of infinitesimal hydrodynamic disturbances, in close analogy to the successful treatment of the stability of cellular convection by Rayleigh[9] and others.[10] In contrast to this fairly complete and satisfactory theory of the hydrodynamic stability of parallel viscous flows, where the velocity field of the undisturbed motion varies only in the direction normal to the streamlines,[11,12] the stability of flame fronts and similar phenomena, e.g., shock waves, which involve velocity gradients along the streamlines, has attracted comparatively little attention.

2. PREVIOUS WORK

The first investigation of the stability of flames was by Darrieus,[13] who treated the flame front as a surface of discontinuity in the undisturbed flow velocity separating two constant velocity regions in a nonviscous gas. Landau[14] later obtained the same results by a more elegant mathematical treatment along the lines of Rayleigh's classic stability studies.

Thermal processes are neglected and the burning velocity is assumed to be a constant independent of the distortion. The hydrodynamic equations are linearized

* Submitted in partial fulfilment of the requirements of the degree of Doctor of Philosophy in the Faculty of Pure Science, Columbia University, New York, New York.

† Present address: Battelle Memorial Institute, Columbus, Ohio.

[1] G. H. Markstein and M. L. Polanyi, Bumblebee Report No. 61 (April, 1947).

[2] C. Tanford, J. Chem. Phys. **15**, 433 (1947); C. Tanford and R. N. Pease, *ibid.*, 861 (1947).

[3] J. O. Hirschfelder and C. F. Curtis, J. Chem. Phys. **11**, 1076 (1949); J. Phys. Colloid Chem. **55**, 774 (1951).

[4] G. H. Markstein, J. Chem. Phys. **17**, 428 (1949); J. Aero. Sci. **18**, (1951).

[5] G. H. Markstein, Cellular Flame Structure and Vibratory Flame Movement in *n*-Butane Mixtures; Fourth Symposium on Combustion, M.I.T. (September, 1952).

[6] Manton, von Elbe, and Lewis, J. Chem. Phys. **20**, 153 (1952).

[7] H. Broida and W. Kane, J. Chem. Phys. **20**, 1043 (1952).

[8] G. H. Markstein, Survey Paper: Instability Phenomena in Combustion Waves; Fourth Symposium on Combustion, M.I.T. (September, 1952).

[9] W. Rayleigh, Phil. Mag. **2**, 533 (1926).

[10] H. Jefferies, Phil. Mag. **2**, 533 (1926); Proc. Roy. Soc. (London) **A118**, 195 (1928); A. R. Low, *ibid.* **A125**, 180 (1929).

[11] L. Synge, Semicent. Pub. Am. Math. Soc. (1938), Vol. 2, p. 227.

[12] C. C. Lin, Quart. Appl. Math. **3**, 117, 218, 277 (1945/1946).

[13] G. Darrieus, Technique Moderne **30**, No. 18 (1938); **31**, Nos. 15, 16 (1939); **33**, Nos. 21, 22 (1941); 6th Internat. Congress of Appl. Mechanics (Paris, 1945).

[14] L. Landau, Acta physicochim. URSS **19**, 77 (1944); see reference 1, pp. 38–42.

by the usual method of introducing first-order infinitesimal disturbances and neglecting all second-order terms. In the unburned and burned gases, the flow velocities, U_u and U_b, and the densities, ρ_u and ρ_b, are taken as constant. With the initial flow velocity along the positive x-axis and the undisturbed flame front as the $y-z$ plane, velocity and pressure disturbances of the form $f(x)\exp(ihy+\delta t)$ are introduced. Thanks to symmetry, only two-dimensional disturbances need be considered. Since by Fourier's theorem any first-order disturbance can be obtained by superposing elementary waves, it is sufficient to investigate the stability for a single arbitrary wave number ($h=2\pi/\lambda$). These disturbances must satisfy the hydrodynamic equations, vanish at infinity, and their normal and tangential velocity and pressure must be continuous passing through the flame front. The parameter δ is now an eigenvalue since only certain values of δ lead to nontrivial solutions which satisfy all these boundary conditions. If any nonvanishing disturbances exist for which the real part of δ is greater than zero, corresponding to undamped solutions, the motion is considered unstable. This first-order treatment only deals with the initial departure from undisturbed flow and cannot yield the final state of the motion, *viz.*, its amplitude and wavelength, where higher order disturbances play a role. As a result, the rate at which the unstable flame front produces vorticity cannot be calculated. Since the initial first-order disturbance consists of a spectrum of wave numbers, it is assumed that the h that is actually observed, which corresponds to the final state of the motion, will be the one that makes δ a maximum ($d\delta/dh=0$), i.e., the wave number with the greatest time amplification.

Darrieus and Landau derive a quadratic equation for δ,

$$(1+1/\epsilon)\alpha^2+2\alpha-(\epsilon-1)=0, \tag{2.1}$$

where $\alpha=\delta/hU_u$ and $\epsilon=U_b/U_u$, which predicts instability for flames under all conditions since $U_b>U_u$ ($T_b>T_u$). As δ is proportional to h, it is a maximum when h is infinite, corresponding to a zero wavelength, but obviously effects have been neglected which must set an upper bound for h, since this result contradicts the implicit assumption that the wavelength of the disturbance is large compared with the thickness of the flame front. Darrieus also pointed out that the unstable flame produces vorticity in the burned gas and gave an interesting diagram illustrating this important phenomenon. This does not contradict Helmholtz's theorem on the conservation of vorticity since it holds only for barotropic fluids $\rho=\rho(P)$,[15] but within the flame due to heat release $\rho=\rho(T)$.

The last advance was made by Markstein[4] who noted that the burning velocity was a function of the curvature of the flame front and would help stabilize it since it increases when the flame is concave to the unburned gas. He added this effect to the earlier stability treatment and found that $h\approx 1/5L$, where $L=k/C_p\rho_u U_u$. Substituting experimental values for L leads to a wavelength of 1.3 cm which is of the same order of magnitude as the observed cell sizes. Since these observations were made for downward propagation, Markstein also included the effect of gravity, which is an additional stabilizing force, and obtained the eigenequation

$$(1+1/\epsilon)\alpha^2+2(1+\kappa\mu)\alpha -(\epsilon-1)(1-\gamma/\epsilon)+2\epsilon\kappa\mu=0, \tag{2.2}$$

where $\kappa\mu=hk/C_p\rho_u U_u$ and $\gamma/\epsilon=g/hU_u^2$.

It is assumed in all these studies that the flame may be treated as a surface of discontinuity in the undisturbed flow velocity. This approximation, adopted on heuristic grounds, can be justified by the general treatment valid for a finite flame. The effect of viscosity is also neglected even though the "viscous thickness," $\eta/\rho_u U_u$, is of the same order of magnitude as the thermal one, $k/C_p\rho_u U_u$, introduced by Markstein. Since he obtains results which agree fairly well with observed cell sizes, it is not surprising that the more rigorous treatment only adds corrections due to the viscous forces, which contrary to expectations have an unstabilizing influence.

3. THE EQUATIONS OF MOTION

Let the flame front of thickness L be parallel to the $y-z$ plane, burning with velocity $-U_u$ in the direction of $-x$. Then initially at time t_0,

$$\begin{gathered} T=T_u \quad (x<0); \quad T=T(x) \quad (0\le x\le L); \\ T=T_b \quad (x<L). \end{gathered} \tag{3.1}$$

From the state and continuity equations,

$$\rho(x)/\rho_u=T_u/T(x); \quad U(x)/U_u=T(x)/T_u. \tag{3.2}$$

Relative to axes fixed in the unburned gas, the flame is propagating to the left with a velocity $-U_u$. With respect to these axes the temperature is a function of time as well as position. To include this effect $T(x)$ must be replaced by $T(x+U_u t)$, i.e.,

$$\begin{gathered} T=T_u \quad (x+U_u t<0); \\ T=T(x+U_u t) \quad (0\le x+U_u t\le L); \\ T=T_b \quad (x+U_u t<L). \end{gathered} \tag{3.3}$$

Likewise, $\rho=\rho(x+U_u t)$ and $U=U(x+U_u t)$.

The effect of a first-order infinitesimal disturbance on the flame front is made up of two parts: the first, a translation of the front due to the added hydrodynamic velocity

$$\int_{t_0}^{t} u\,dt,$$

and the second, a translation in the opposite direction

[15] A. Vazonyi, Quart. Appl. Math. 3, 29 (1945).

due to the increase in burning velocity with distortion

$$\int_{t_0}^{t}(M^{(1)}/\rho)dt,$$

where $M^{(1)}$ is the first-order increase in mass flow. This first-order translation of the flame must be added to the zero-order one, so

$$T=T\left[x+U_u t-\int_{t_0}^{t}(u-M^{(1)}/\rho)dt\right]. \tag{3.4}$$

The term $U_u t$ in the argument can be eliminated by choosing axes fixed in the undisturbed flame front, i.e., axes moving with velocity $-U_u$ with respect to the unburned gas. For these axes

$$\begin{gathered}T=T_u \quad (x-s<0); \quad T=T(x-s) \quad (0\leq x-s\leq L);\\ T=T_b \quad (x-s>L);\end{gathered} \tag{3.5}$$

where

$$s=\int_{t_0}^{t}(u-M^{(1)}/\rho)dt, \tag{3.6}$$

viz., s is the first-order translation of the undisturbed flame front due to the hydrodynamic disturbance. It follows that the total disturbance (zero plus first order) is

$$\begin{gathered}u=U(x-s)+u, \quad v=v, \quad P=P(x-s)+p,\\ \rho=\rho(x-s)+\rho^{(1)}, \quad T=T(x-s)+T^{(1)}.\end{gathered} \tag{3.7}$$

As x is a first-order infinitesimal, the argument $(x-s)$ can be expanded in a Taylor series and terms of higher order than the first neglected. Thus

$$\begin{gathered}u=U(x)-U'(x)s+u; \quad v=v;\\ P=P(x)-P'(x)s+p; \quad \rho=\rho(x)-\rho'(x)s+\rho^{(1)};\\ T=T(x)-T'(x)s+T^{(1)},\end{gathered} \tag{3.8}$$

where the primes stand for derivatives with respect to x.

The general equations of motion are

$$\begin{aligned}\rho\frac{Du_i}{Dt}=&-\frac{\partial P}{\partial x_i}+x_i+\eta\nabla^2 u_i\\ &+\frac{\eta}{3}\frac{\partial}{\partial x_i}\left(\frac{\partial u_i}{\partial x_i}+\frac{\partial u_j}{\partial x_j}\right), \quad \begin{matrix}i,j=1,2\\ i\neq j\end{matrix}\end{aligned} \tag{3.9}$$

$$\frac{\partial\rho}{\partial t}+\nabla\cdot(\rho u)=0, \tag{3.10}$$

where $D/Dt=\partial/\partial t+u_i\partial/\partial x_i+u_j\partial/\partial x_j$ is the Eulerian derivative, and the coefficient of viscosity η is assumed to be constant.

For a flame propagating downward with gravity, $X_1=-\rho g$, the zero-order equations are

$$-\frac{4}{3}\eta\frac{d^2U}{dx^2}+\rho U\frac{dU}{dx}=-\frac{dP}{dx}-\rho g, \tag{3.11}$$

$$U\frac{d\rho}{dx}+\rho\frac{dU}{dx}=0. \tag{3.12}$$

Since it is shown in the appendix that only damped temperature disturbances obey the boundary conditions, they can be neglected, i.e., $T^{(1)}=\rho^{(1)}=0$. The first-order equations are

$$\begin{aligned}\rho\left[\frac{\partial u}{\partial t}-U'\frac{\partial s}{\partial t}+U'u+U\frac{\partial}{\partial x}(u-U's)\right]=&-\frac{\partial}{\partial x}(p-P's)\\ &+g\rho's+\eta\left[\nabla^2 u+\frac{1}{3}\frac{\partial}{\partial x}\left(\frac{\partial u}{\partial x}+\frac{\partial v}{\partial y}\right)\right]\\ &-\eta\left[\nabla^2(U's)+\frac{1}{3}\frac{\partial^2}{\partial x^2}(U's)\right]\end{aligned} \tag{3.13}$$

$$\begin{aligned}\rho\left[\frac{\partial v}{\partial t}+U\frac{\partial v}{\partial x}\right]=&-\frac{\partial}{\partial y}(p-P's)\\ &+\eta\left[\nabla^2 v+\frac{1}{3}\frac{\partial}{\partial y}\left(\frac{\partial u}{\partial x}+\frac{\partial v}{\partial y}\right)-\frac{\partial^2}{\partial y\partial x}(U's)\right].\end{aligned} \tag{3.14}$$

Differentiating Eq. (3.13) by $\partial/\partial y$ and (3.14) by $\partial/\partial x$ and subtracting, the pressure disturbances can be eliminated. Since from (3.6),

$$\frac{\partial s}{\partial t}=u-M^{(1)}/\rho, \tag{3.15}$$

the result is

$$\begin{aligned}&-\frac{\partial}{\partial x}\left[\eta\nabla^2 v-\rho\left(U\frac{\partial v}{\partial x}+\frac{\partial v}{\partial t}\right)\right]\\ &\qquad+\frac{\partial}{\partial y}\left[\eta\nabla^2 u-\rho\left(U\frac{\partial u}{\partial x}+\frac{\partial u}{\partial t}\right)\right]\\ &=\frac{\partial}{\partial y}\left[\eta\nabla^2(U's)-\rho U\frac{\partial}{\partial x}(U's)-g\rho's+U'M^{(1)}\right].\end{aligned} \tag{3.16}$$

The continuity equation yields

$$-\rho\frac{\partial s}{\partial t}+u\frac{\partial\rho}{\partial x}+\rho\left(\frac{\partial u}{\partial x}+\frac{\partial v}{\partial y}\right)-\nabla\cdot(\rho U'+\rho' U)=0, \tag{3.17}$$

and using Eqs. (3.12) and (3.15),

$$U'M^{(1)}+\rho U\left(\frac{\partial u}{\partial x}+\frac{\partial v}{\partial y}\right)=0. \tag{3.18}$$

Because these equations are linear, only disturbances of the form $f(x)\exp(ihy+\delta t)$ need be considered (see Sec. 2). Introducing dimensionless variables,

$$\begin{gathered}\xi=hx; \quad \xi_1=hy; \quad \tau=hU_u t; \quad \alpha=\delta/hU_u;\\ \gamma=g/hU_u^2; \quad \epsilon=U_b/U_u; \quad \epsilon_{1/2}=(\epsilon+1)/2;\\ \kappa\sigma=h\eta/\rho_u U_u; \quad \kappa\mu=hk/C_p\rho_u U_u;\end{gathered} \tag{3.19}$$

$$\mathfrak{A}(\xi)=U(\xi)/U_u; \qquad \rho(\xi)=1/\mathfrak{A}(\xi);$$
$$u/U_u=\phi(\xi)\Gamma(\xi_1,\tau); \qquad v/U_u=\psi(\xi)\Gamma(\xi_1,\tau); \tag{3.20}$$

$$hs=\zeta(\xi)\Gamma(\xi_1,\tau); \quad M^{(1)}/\rho_u U_u=m(\xi)\Gamma(\xi_1,\tau);$$
$$\Gamma(\xi_1,\tau)=\exp(\xi_1+\alpha\tau). \tag{3.21}$$

Equations (3.16) and (3.18) become

$$-\mathfrak{D}[\kappa\sigma\psi''-\psi'-(\alpha/\mathfrak{A}+\kappa\sigma)\psi]$$
$$+i[\kappa\sigma\phi''-\phi'-(\alpha/\mathfrak{A}+\kappa\sigma)\phi]$$
$$=i[(\kappa\sigma\mathfrak{D}^2-\mathfrak{D}-\kappa\sigma)(\mathfrak{A}'\zeta)+\gamma\mathfrak{A}'\zeta/\mathfrak{A}^2+\mathfrak{A}'m, \tag{3.22}$$

$$\psi=i(\phi'-\mathfrak{A}'m)=i(\alpha\zeta'+\mathfrak{A}m'), \tag{3.23}$$

where $\mathfrak{D}=d/d\xi$. Eliminating ψ yields the general disturbance equation

$$-\mathfrak{D}[\kappa\sigma\mathfrak{D}^2-\mathfrak{D}-(\alpha/\mathfrak{A}+\kappa\sigma)](\phi'-\mathfrak{A}'m)$$
$$+[\kappa\sigma\mathfrak{D}^2-\mathfrak{D}-(\alpha/\mathfrak{A}+\kappa\sigma)]\phi$$
$$=(\kappa\sigma\mathfrak{D}^2-\mathfrak{D}-\kappa\sigma)(\mathfrak{A}'\zeta)+\gamma\mathfrak{A}'\zeta/\mathfrak{A}^2+\mathfrak{A}'m. \tag{3.24}$$

To solve this equation the relation between m and ζ must be derived.

4. DEPENDENCE OF BURNING VELOCITY ON DISTORTION

The basic equations for a plane stationary flame front are

$$k\frac{\partial^2 T}{\partial x^2}-C_p\rho U\frac{\partial T}{\partial x}+\sum_j Q_j W_j(T,n_1\cdots n_n)=0, \tag{4.1}$$

$$\rho D_i\frac{\partial^2 n_i}{\partial x^2}-\rho U\frac{\partial n_i}{\partial x}+M_i\sum_j \nu_{ij}W_j(T,n_1\cdots n_n)=0,$$
$$i=1,\cdots n \tag{4.2}$$

where n_i is the concentration of the ith chemical species, Q_j the heat released in the jth reaction, W_j the rate of the jth reaction, ν_{ij} the number of molecules generated in the jth reaction, and M_i the molecular weight of the ith species. The heat conductivity k and the diffusion product ρD_i have been assumed constant; these equations lack generality in other respects as well.[3,16] The mass flow ρU is an eigenvalue of this system of nonlinear equations.

To solve these equations, the quantative values of the $W_j(T,n_1\cdots n_n)$ must be known. But today not even qualitative information is available on the reaction kinetics occurring in flames governed by chain reactions, e.g., hydrocarbons; therefore, the propagation problem for these flames is insoluble. As a result, all existing theories[1–3,16–18] are essentially phenomenological, based on more or less plausible assumptions. They utilize only a single differential equation, the thermal or a diffusion one (the two are equivalent if $\rho D_i=kC_p$[19]) with one or more adjustable constants, hoping in this way to derive a ρU that agrees with experimental data. These theories can only provide qualitative predictions, and in view of the great obstacles present, it is very unlikely that an adequate quantitative theory for these flames will be constructed in the near future.

Such a theory must show how the propagation mechanism is a function of the fuel-air ratio, *viz.*, for a given initial composition which of Eqs. (4.1)–(4.2) play a dominant role in determining the burning velocity, It will now be assumed that for a fixed fuel-air ratio this system of equations can be replaced by a single equivalent equation

$$k_e\frac{d^2T}{dx^2}-C_p\rho U\frac{dT}{dx}+W_eQ_e=0, \tag{4.3}$$

where k_e is an "effective" conduction coefficient and W_eQ_e is an "effective" rate of energy release. The "effective" thickness of the flame, $k_e/C_p\rho U$, is identified with the experimentally determined flame thickness, i.e., the distance through which the temperature varies. For a flame controlled by the diffusion of free radicals, k_e will be much larger than for one controlled by thermal conduction. Since k_e is taken to be a function of the fuel-air ratio, this assumption is far less restrictive than that customarily employed in current theories of flame propagation where k_e is taken as a constant independent of fuel-air ratio. Further, it will be assumed that this zero-ordere quation is independent of the distortion, i.e., there is no redistribution of chemical species within the distorted flame resulting in an altered propagation mechanism. Although such a process appears unlikely for fast flames with their short induction times, it is impossible to give any rigorous justification of this assumption.

Recently Manton, von Elbe, and Lewis,[6] have attributed the hydrodynamic instability of flames to local changes in the concentration of fuel and oxygen molecules caused by differences in their diffusion coefficients, leading to changes in the propagation velocity. While this explanation, which contradicts a basic assumption underlying the treatment presented here, has been supported by the observations of Broida and Kane,[7] it has been criticized by Markstein.[20]

The general equation of heat balance is

$$k_e\nabla^2 T-C_p\rho\frac{DT}{Dt}+W_eQ_e=0, \tag{4.4}$$

while (4.3) is the zero-order equation. Substituting

[16] S. F. Boys and J. Corner, Proc. Roy. Soc. (London) **A197**, 90 (1947).
[17] K. Berchert, Portugal Phys. **3**, 29 (1949); Ann. phys. **5**, 349 (1950).
[18] R. Friedman and E. Burke, J. Aero. Sci. **18**, 239 (1951).
[19] N. Semenov, Prog. Phys. Sci. USSR **24**, 239 (1950).
[20] G. H. Markstein, J. Chem. Phys. **20**, 1051 (1952).

(3.7) into Eq. (4.4) yields the first-order equation

$$k_e\nabla^2(T^{(1)}-T's)-C_p\rho\left[\left(\frac{\partial}{\partial t}+U\frac{\partial}{\partial x}\right)(T^{(1)}-T's)+uT'\right]$$
$$-C_p\rho[\rho^{(1)}U+(\rho U'+\rho'U)s]T'$$
$$+\frac{d}{dT}(W_eQ_e)-(W_eQ_e)'s=0. \quad (4.5)$$

Since $\rho T=$ constant, so $\rho^{(1)}=-(\rho/T)T^{(1)}$, and using Eqs. (3.12) and (3.15), then

$$k_e\nabla^2(T^{(1)}-T's)$$
$$-C_p\rho\left[\frac{\partial T^{(1)}}{\partial t}+U\frac{\partial}{\partial x}(T^{(1)}-T's)+T'\left(\frac{M^{(1)}}{\rho}+\frac{UT^{(1)}}{T}\right)\right]$$
$$+\frac{d}{dT}(W_eQ_e)T^{(1)}-(W_eQ_e)'s=0. \quad (4.6)$$

All terms in s can be removed by differentiating Eq. (4.3), multiplying through by s and subtracting it from this equation. The result is

$$k_e(\nabla^2T^{(1)}-T'\nabla^2s-2T''s')$$
$$=C_p\rho\left[\frac{\partial T^{(1)}}{\partial t}+U\frac{\partial T^{(1)}}{\partial x}+T'\left(\frac{M^{(1)}}{\rho}-Us'-\frac{UT^{(1)}}{T}\right)\right]$$
$$+\frac{d}{dT}(W_eQ_e)T^{(1)}=0. \quad (4.7)$$

Since by definition $M^{(1)}$ is the increase in mass flow through the flame front due to the distortion, it is equated to the terms in s in Eq. (4.7). The temperature disturbances then become independent of the others and can be determined separately (see Appendix). Thus,

$$T'M^{(1)}=-\frac{k_e}{C_p}\left(T's''+2T''s'+T'\frac{\partial^2 s}{\partial y^2}\right)+\rho UT's', \quad (4.8)$$

or introducing the dimensionless variables given by (3.19)

$$m=\kappa\mu[-\zeta''+(1/\kappa\mu-2\mathfrak{A}''/\mathfrak{A}')\zeta'+\zeta]. \quad (4.9)$$

Since $\mathfrak{A}'(\xi)$ is a positive function while $\mathfrak{A}''(\xi)$ is positive and negative in passing through the flame front (mean value$\approx$0), $\mathfrak{A}''/\mathfrak{A}'$ can be neglected in this expression for m. Therefore,

$$m\approx-\kappa\mu\zeta''+\zeta'+\kappa\mu\zeta. \quad (4.10)$$

5. SOLUTION OF THE DISTURBANCE EQUATION

When m is a linear function of ζ (the more general case is briefly discussed in Sec. 7), (3.24) is a fourth-order differential equation which must be solved in the unburned, flame, and burned regions. These solutions when fitted at the two flame surfaces so they satisfy the boundary conditions yield an eighth-order determinantal equation for the eigenvalue α.

In the constant velocity regions ($\mathfrak{A}'=0$) Eq. (3.24) reduces to

$$\mathfrak{D}^2[\kappa\sigma\mathfrak{D}^2-\mathfrak{D}-(\alpha/\mathfrak{A}+\kappa\sigma)]\phi$$
$$-[\kappa\sigma\mathfrak{D}^2-\mathfrak{D}-(\alpha/\mathfrak{A}+\kappa\sigma)]\phi=0, \quad (5.1)$$

or

$$[\kappa\sigma\mathfrak{D}^2-\mathfrak{D}-(\alpha/\mathfrak{A}+\kappa\sigma)](\mathfrak{D}+1)(\mathfrak{D}-1)\phi=0; \quad (5.2)$$

so

$$(\mathfrak{D}-r_1)(\mathfrak{D}-r_2)(\mathfrak{D}+1)(\mathfrak{D}-1)\phi=0, \quad (5.3)$$

where

$$r=\{1\pm[1+4\kappa\sigma(\alpha/\mathfrak{A}+\kappa\sigma)]^{\frac{1}{2}}\}/2\kappa\sigma$$
$$\approx 1/\kappa\sigma+\alpha/\mathfrak{A}+\kappa\sigma;\ -(\alpha/\mathfrak{A}+\kappa\sigma). \quad (5.4)$$

As the disturbances must be bounded at infinity, so

$$\phi_u=F_{u2}e^{\xi}+F_{u1}\exp(1/\kappa\sigma+\alpha+\kappa\sigma)\xi, \quad (5.5)$$

$$\phi_b=F_{b2}e^{-\xi}+F_{b1}\exp[-(\alpha/\epsilon+\kappa\sigma)\xi], \quad (5.6)$$

since $\mathfrak{A}=1$ in the unburned and $\mathfrak{A}=\epsilon$ in the burned gas.

In the flame region ($\mathfrak{A}'\neq0$) Eq. (3.22) may be written as

$$\mathfrak{D}(-\kappa\sigma\mathfrak{D}^2+\mathfrak{D}+\alpha/\mathfrak{A}+\kappa\sigma)(\phi'-\mathfrak{A}'m)=K(\xi,\zeta,m), \quad (5.7)$$

$$K(\xi,\zeta,m)=(\kappa\sigma\mathfrak{D}^2-\mathfrak{D}-\kappa\sigma)(\mathfrak{A}'\zeta)+\gamma\mathfrak{A}'\zeta/\mathfrak{A}^2+\mathfrak{A}'m$$
$$-[\kappa\sigma\mathfrak{D}^2-\mathfrak{D}-(\alpha/\mathfrak{A}+\kappa\sigma)](\alpha\zeta+\mathfrak{A}m)$$
$$\approx(\kappa\sigma\mathfrak{D}^2-\mathfrak{D}-\kappa\sigma)(\mathfrak{A}'\zeta)+\gamma\mathfrak{A}'\zeta/\mathfrak{A}^2$$
$$+\mathfrak{A}'m-\mathfrak{D}(\kappa\sigma\mathfrak{D}-1)(\mathfrak{A}m), \quad (5.8)$$

where terms of order κ^2 are neglected in (5.8) and will be neglected in Eq. (5.10). Successively integrating this equation, then

$$(-\kappa\sigma\mathfrak{D}^2+\mathfrak{D}+\alpha/\mathfrak{A}+\kappa\sigma)(\phi'-\mathfrak{A}'m)$$
$$=F_4+\int_0^{\xi}K(\xi,\zeta,m)d\xi, \quad (5.9)$$

$$(-\kappa\sigma\mathfrak{D}+1)(\phi'-\mathfrak{A}'m)$$
$$=F_3+F_4\xi+\int_0^{\xi}d\xi\int_0^{\xi}K(\xi,\zeta,m)d\xi, \quad (5.10)$$

$$-\kappa\sigma(\phi'-\mathfrak{A}'m)=F_2+F_3\xi+F_4\xi^2/2$$
$$+\int_0^{\xi}d\xi\int_0^{\xi}d\xi\int_0^{\xi}K(\xi,\zeta,m)d\xi$$
$$-\int_0^{\xi}(\alpha\zeta+\mathfrak{A}m)d\xi, \quad (5.11)$$

$$-\kappa\sigma(\alpha\zeta+\epsilon_{1/2}m)=F_1+F_2\xi+F_3\xi^2/2+F_4\xi^3/6$$
$$+\int_0^{\xi}d\xi\int_0^{\xi}d\xi\int_0^{\xi}d\xi\int_0^{\xi}K(\xi,\zeta,m)d\xi$$
$$-\int_0^{\xi}d\xi\int_0^{\xi}(\alpha\xi+\mathfrak{A}m)d\xi. \quad (5.12)$$

These four equations provide the boundary conditions which must be applied at the flame surfaces; the left-hand terms referring to solutions in the burned and unburned gases, and the right to those valid within the flame. As m is taken to be a linear function of $\zeta(m=\kappa\mu\zeta)$, Eq. (5.12) is a linear integral equation of the Volterra type for $\zeta(\xi)$ within the flame which must be substituted into $K(\xi, \zeta, m)$. This equation can be solved by successive approximations. Here it suffices to take the zeroth approximation for $\zeta(\xi)$ given by the inhomogeneous terms, $F_1+F_2\xi+F_3\xi^2/2+F_4\xi^3/6$, i.e., setting the repeated integrals equal to zero. This $\zeta(\xi)$ is then substituted in $K(\xi, \zeta, m)$ which becomes a linear function of the F's, allowing the integrals needed in satisfying the boundary conditions to be explicitly evaluated.

6. SOLUTION FOR DISCONTINUOUS FLAME

Since an infinitely thin flame front ($\xi=0$) leads to an infinite viscous stress normal to the undisturbed plane flame front, this approximation can be made only by going to the discontinuous limit in the solutions for the first-order infinitesimal disturbances of a flame of finite thickness. It would be incorrect to attempt to extend Markstein's treatment to include viscous forces by adding the boundary condition that the tangential stress, $\eta(\partial v/\partial x+\partial u/\partial y)$, be continuous across the flame front, because this neglects the contribution of the component of the zero-order normal stress along the surface of the distorted flame front. When the flame is taken as infinitely thin, the displacement $\zeta(\xi)$ and the mass flow $m(\xi)$ are constant across the flame front. The boundary conditions at the flame surfaces ($\mathfrak{A}'=0$) are given by the left sides of Eqs. (5.9)–(12), *viz.*, the expressions at the right of the colons in Eqs. (6.1)–(4). In the unburned and burned regions the ϕ's and their derivatives in these expressions are obtained from the solutions (5.5) and (5.6), respectively, while within the flame front the left sides of Eqs. (5.9)–(12) are replaced by their corresponding right sides. Neglecting terms of order $(\kappa\sigma)^2$ which are negligible, then

$\xi=(-0)$ (Unburned)

$$(F_{u1}+F_{u2})/\beta_u+F_1=0 \quad : -\kappa\sigma(\alpha\zeta_u+\epsilon_{1/2}mu) \tag{6.1}$$

$$-(\alpha+1+\kappa\sigma)F_{u1}-\kappa\sigma F_{u2}+F_2=0 \quad : -\kappa\sigma\phi_u' \tag{6.2}$$

$$-(\alpha+\kappa\sigma)F_{u1}-\kappa\sigma F_{u2}+F_3=0 \quad : (-\kappa\sigma\mathfrak{D}+1)\phi_u' \tag{6.3}$$

$$(\alpha+1)F_{u2}+F_4=0 \quad : (-\kappa\sigma\mathfrak{D}^2+\mathfrak{D}+\alpha+\kappa\sigma)\phi_u' \tag{6.4}$$

$\xi=(+0)$ (Burned)

$$(F_{b1}+F_{b2})/\beta_b+F_1=0 \quad : -\kappa\sigma(\alpha\zeta_b+\epsilon_{1/2}m_b) \tag{6.5}$$

$$(\kappa\sigma\alpha/\epsilon)F_{b1}+\kappa\sigma F_{b2}+A_3F_1+F_2=0 \quad : -\kappa\sigma\phi_b' \tag{6.6}$$

$$-(\alpha/\epsilon+\kappa\sigma)F_{b1}-(1+\kappa\sigma)F_{b2}+A_2F_1+F_3=0 \quad : (-\kappa\sigma\mathfrak{D}+1)\phi_b' \tag{6.7}$$

$$-(\alpha/\epsilon-1)F_{b2}+A_1F_1+F_4=0 \quad : (-\kappa\sigma\mathfrak{D}^2+\mathfrak{D}+\alpha/\epsilon+\kappa\sigma)\phi_b' \tag{6.8}$$

where

$$\phi_u/\beta_u=-\kappa\sigma(\alpha\zeta_1+\epsilon_{1/2}m_1), \tag{6.9}$$

$$\phi_b/\beta_b=-\kappa\sigma(\alpha\zeta_1+\epsilon_{1/2}m_1), \tag{6.10}$$

and A_i is the ith repeated integral over $K(\xi, \zeta_1, m_1)$. ζ_1 and m_1 arise from the inhomogeneous term F_1.

For a nontrivial solution to exist of this system of linear homogeneous equations, the determinant of its coefficients must vanish, i.e.,

$$\begin{vmatrix} 1/\beta_u & 1/\beta_u & 1 & 0 & 0 & 0 & 0 & 0 \\ -(\alpha+1+\kappa\sigma) & -\kappa\sigma & 0 & 1 & 0 & 0 & 0 & 0 \\ -(\alpha+\kappa\sigma) & 1-\kappa\sigma & 0 & 0 & 1 & 0 & 0 & 0 \\ 0 & \alpha+1 & 0 & 0 & 0 & 1 & 0 & 0 \\ 0 & 0 & 1 & 0 & 0 & 0 & 1/\beta_b & 1/\beta_b \\ 0 & 0 & A_3 & 1 & 0 & 0 & \kappa\sigma\alpha/\epsilon & \kappa\sigma \\ 0 & 0 & A_2 & 0 & 1 & 0 & -(\alpha/\epsilon+\kappa\sigma) & -(1+\kappa\sigma) \\ 0 & 0 & A_1 & 0 & 0 & 1 & 0 & -(\alpha/\epsilon-1) \end{vmatrix} = 0. \tag{6.11}$$

By subtracting rows this determinant can be immediately reduced to fifth order. After removing the degenerate roots $\alpha+1$ and $\alpha/\epsilon-1$, the resulting determinant can be easily evaluated using Chio's rule,[21] yielding

$$\alpha+2-\kappa\sigma+(\beta_b/\beta_u)(\alpha/\epsilon+\kappa\sigma) -2(A_3+\kappa\sigma A_2)/\beta_u+(A_2+A_1)/\beta_u=0. \tag{6.12}$$

Since

$$K(\xi, \zeta_1, m_1)=(\kappa\sigma\mathfrak{D}^2-\mathfrak{D}-\kappa\sigma)\mathfrak{A}'\zeta_1 +\gamma\mathfrak{A}'\zeta_1/\mathfrak{A}^2+\mathfrak{A}'m_1-\mathfrak{D}(\kappa\sigma\mathfrak{D}-1)\mathfrak{A}m_1, \tag{6.13}$$

[21] Whittaker and Robinson, *The Calculus of Observations* (Blackie and Son, London, 1940), p. 71.

then

$$A_1=[(\kappa\sigma\mathfrak{D}-1)\mathfrak{A}'\zeta_1-\kappa\sigma\mathbf{\mathfrak{A}}\zeta_1+\gamma\zeta_1/\mathbf{\mathfrak{A}}+\mathbf{\mathfrak{A}}m_1 -\kappa\sigma\mathfrak{D}\mathfrak{A}m_1+\mathbf{\mathfrak{A}}m_1]_{(-0)}^{(+0)}, \quad (6.14)$$

$$A_2=[\kappa\sigma\mathfrak{A}'\zeta_1-\mathbf{\mathfrak{A}}\zeta_1-\kappa\sigma\mathbf{\mathfrak{A}}m_1]_{(-0)}^{(+0)}, \quad (6.15)$$

$$A_3=[\kappa\sigma A\zeta_1]_{(-0)}^{(+0)}. \quad (6.16)$$

The boldfaced terms make a contribution to their respective A's but not to higher ones, since integrals over them vanish when the limits coalesce. As m has been assumed to be a linear function of ζ, it follows from Eq. (4.10) that

$$m_1=\kappa\mu\zeta_1, \quad (6.17)$$

which is the same relation used by Markstein for the change in burning velocity due to the bending of the flame front by the disturbance. (The effect of the derivative terms in (4.10) will be briefly discussed in Sec. 7.) As $\mathfrak{A}''=\mathfrak{A}'=0$ at the flame surfaces, then

$$\begin{aligned} A_1&=(\epsilon-1)(\gamma/\epsilon+2\kappa\mu-\kappa\sigma)\zeta_1;\\ A_2&=(\epsilon-1)(1+\kappa^2\mu\sigma)\zeta_1;\\ A_3&=(\epsilon-1)\kappa\sigma\zeta_1. \end{aligned} \quad (6.18)$$

From Eq. (5.12) as $\xi\to 0$,

$$\zeta_1=-1/\kappa\sigma(\alpha+\epsilon_{1/2}\kappa\mu). \quad (6.19)$$

Now

$$\phi=(\alpha+\mathfrak{A}\kappa\mu)\zeta, \quad (6.20)$$

so substituting into Eq. (6.9) yields

$$1/\beta_u=-\kappa\sigma(\alpha+\epsilon_{1/2}\kappa\mu)/(\alpha+\kappa\mu). \quad (6.21)$$

Likewise

$$\beta_b/\beta_u=(\alpha+\epsilon\kappa\mu)/(\alpha+\kappa\mu). \quad (6.22)$$

Inserting these results into Eq. (6.12), noting that $A_3+\kappa\sigma A_2=0$, leads to the eigenequation

$$\boxed{(1+1/\epsilon)\alpha^2+2(1+\kappa\mu)\alpha-(\epsilon-1)(1-\gamma/\epsilon) +\epsilon\kappa[2\mu-(1-1/\epsilon)\sigma]=0.} \quad (6.23)$$

When viscosity is neglected ($\kappa\sigma=0$), this reduces to Eq. (2.2) previously derived by Markstein. The quadratic Eq. (6.25) will have a positive root, corresponding to an unstable flow, only if the constant term is negative; i.e., if

$$\Delta=(1-1/\epsilon)(1-\gamma/\epsilon)-\kappa[2\mu-(1-1/\epsilon)\sigma], \quad (6.24)$$

then

$$\left\{\begin{array}{ll}\Delta>0 & \text{unstable}\\ \Delta<0 & \text{stable}\end{array}\right\}. \quad (6.25)$$

Contrary to expectations, viscosity has an unstabilizing influence.

Since $\alpha\ll 1$, the quadratic term in α can be neglected so Eq. (6.23) becomes

$$2(1+\kappa\mu)\delta=U_b h\{(1-1/\epsilon)(1-\gamma/\epsilon) -\kappa[2\mu-(1-1/\epsilon)\sigma]\}. \quad (6.26)$$

The observed wave number is given by $d\delta/dh=0$. As $\gamma=g/hU_u^2$ and κ is proportional to h, the result is

$$\kappa\mu=\frac{1-1/\epsilon}{4[1-(1-1/\epsilon)\sigma/2\mu]}. \quad (6.27)$$

Solving for the wavelength

$$\boxed{\lambda=\frac{8\pi k_e}{C_p\rho_u U_u}\,\frac{[1-(1-1/\epsilon)C_p\eta/2k_e]}{(1-1/\epsilon)}.} \quad (6.28)$$

The coefficient of viscosity η refers to a bulk property of the gas, essentially the N_2 and O_2 present. Only in the case of a thermal flame ($k_e=k$) does k_e refer to the thermal conductivity of the entire gas mixture. In a diffusion flame[22] ($k_e/C_p=\rho D_i$) the propagation velocity is controlled by the diffusion of free radicals present in minute quantities ($\approx 10^{-3}$ mole). Thus in general, k_e will be a function of the fuel-air mixture and the particular hydrocarbon fuel, while η can be taken as a constant independent of the fuel and mixture ratio. Equation (6.29) shows that the cell size is proportional to the equivalent thickness of the flame. As this is a minimum for a thermal flame, it will possess the minimum cell size, provided all the active particles diffuse in the direction of the heat flow. This will be so for hydrocarbon-air flames, but may not be the case when other combustibles are added to the fuel mixture, e.g., H_2. Since diffusion against the heat flow will decrease k_e, in this case k_e may be less than k. For a diatomic gas,[22] $k/C_p\approx 4\eta/3$, so for a thermal flame Eq. (6.28) becomes

$$\boxed{\lambda_{\text{thermal}}=\frac{\pi k}{C_p\rho_u U_u}\,\frac{(5+3/\epsilon)}{(1-1/\epsilon)}.} \quad (6.29)$$

For air[23] (in cgs units) $\rho_u=1.3\times 10^{-3}$, $C_p=0.24$, $k=5.7(\epsilon_{1/2})^{3/4}\times 10^{-5}$. Markstein's[4] experimental conditions, $\epsilon=5$ and $U_u=10$, corresponds to a thermal thickness ($k/C_p\rho_u U_u$) of 0.041 cm, and leads to a wavelength of 0.90 cm which is in good agreement with the minimum observed cell size (0.85, iso-octane). The introduction of viscous forces leads to a 30 percent decrease in the calculated cell size for a thermal flame, i.e., from 1.29 to 0.90 cm. The observed increase in the cell sizes of rich hydrocarbon flames are observed to increase with decreasing molecular weight of the fuel,[4] corresponding to an increase in k_e suggests that the diffusion of active

[22] Kennard, *Kinetic Theory of Gases* (McGraw-Hill Book Company, Inc., New York, 1938), pp. 182, 251.
[23] See reference 20, pp. 157, 198, 252.

radicals plays an increasing role in propagating rich flames of lighter hydrocarbons.

Since $\gamma=\lambda g/2\pi U_u^2$, it is clear from Eqs. (6.24)–(6.25) that a flame propagating downward will become stable for sufficiently long waves. This occurs when $\Delta=0$, but from Eq. (6.27)

$$(1-1/\epsilon)/2=\kappa[2\mu-(1-1/\epsilon)\sigma], \tag{6.30}$$

so substituting into $\Delta=0$, it follows that

$$\gamma/\epsilon=\tfrac{1}{2} \tag{6.31}$$ or $$\boxed{\lambda_{max}=3.2U_uU_b\times10^{-3}\text{ cm.}} \tag{6.32}$$

Note that this maximum cell size is only a function of the initial and final velocities and is independent of the effective thickness of the flame. For $U_u=10$ and $U_b=50$ cm/sec $\lambda_{max}=1.6$ cm, in good agreement with the maximum observed cell sizes (1.65, C_2H_4; 1.6, C_2H_6). It is therefore not surprising that ethane and ethylene cells, whose sizes are approximately λ_{max}, have weak structures (shallow cells) compared with other hydrocarbons. In agreement with Eq. (6.32), whenever U_u is decreased by adding small amounts of N_2 to flame mixtures with shallow cells, the cell structure is destroyed.[8]

From Eq. (6.28) it is evident that λ is not a sensitive function of ϵ (U_b/U_u), so ϵ may be replaced by its approximate value of five in this equation. Since $\eta\approx3k/4C_p$, then

$$\lambda_i=10\pi(L_i+3L_t/10), \tag{6.33}$$

where $L_t=k/C_p\rho_uU_u$ is the thermal flame thickness and $L_i=k_i/C_p\rho_uU_u$. The maximum flame thickness L_{max} which exhibits cell structure is the L_i for which $\lambda_i=\lambda_{max}$. Using Eq. (6.32) it follows that

$$\boxed{L_{max}(\text{cm})=U_uU_b\times10^{-4}+3L_t^{(\text{cm})}/10.} \tag{6.34}$$

Markstein's experimental conditions yield $L_t=0.041$ cm and $L_{max}=0.062$ cm, so $L_{max}/L_t=1.5$. Thus in passing from rich to lean mixtures, the thickness of iso-octane flames increases by at least 1.5 times so the cell structure will be extinguished, while correspondingly smaller increases are required for lighter hydrocarbons.

As might be expected, the addition of He to rich flames increases cell sizes,[4] since this increases their effective thicknesses, and if added in sufficiently large amounts extinguishes cell structure entirely. H_2 added to CH_4 flames at all compositions and to lean mixtures of other hydrocarbons produces small deep cells because H_2 diffuses from the unburned gas in the opposite direction to the heat flow, thus decreasing the k_e of the flame.

Finally the pressure dependence of λ and λ_{max} can be readily derived. If $U_u(P)/U_u(P_0)=(P/P_0)^{-n}$ then Eqs. (6.28) and (6.32) yield

$$\boxed{\lambda(P)/\lambda(P_0)=(P/P_0)^{-1+n}} \tag{6.35}$$

$$\boxed{\lambda_{max}(P)/\lambda_{max}(P_0)=(P/P_0)^{-2n}} \tag{6.36}$$

where in (6.35) it has been assumed that k_e is independent of pressure, i.e., the propagation mechanism is only a function of the initial gas composition. This equation has been combined by Markstein[4] with experimental observations to obtain the pressure dependence of the burning velocity.

From the results of this section it is clear that plane flames propagating horizontally or upward against gravity are always hydrodynamically unstable. As $\lambda_{max}\sim U_uU_b$ and $\lambda\sim1/\rho_uU_u$, it follows that under most conditions hydrocarbon-air flames ($U_u\approx30$ cm/sec) propagating downward will also be unstable. Since in general plane flames are unstable, values reported in the literature for the transformation velocity under such conditions actually include the effect of hydrodynamic disturbances introduced into the flow by the unstable flame as well as the stationary burning velocity—something which has long been known experimentally for flames propagating in pipes.[24] This basic hydrodynamic instability of plane flames helps explain why in a majority of applications plane flames propagate into the unburned gas with a velocity which may be one or two times greater than their stationary burning velocity.

The failure of lean hydrocarbon and methane flames at all compositions to reveal any cell structure indicates that their effective thicknesses $(k_e/C_p\rho_uU_u)$ are so large that $\lambda>\lambda_{max}$, i.e., the propagation of these flames is controlled by the diffusion of free radicals, among which H may be expected to play an important role because of its great diffusivity. This conclusion is supported by the measurement of Anderson and Fein[25] of 0.1 cm for the thickness of a lean propane-air flame ($U_u\approx45$ cm/sec). The sudden appearance of cells, observed precisely as stoichiometric mixtures are reached, would indicate a correspondingly sharp shift to propagation by thermal conduction, or alternately, an inhibition of the radicals effective in propagating lean flames. Such a division into thermal and diffusion flames has already been made on the basis of observed burning velocities.[26] Since general considerations show that $U_u\alpha k_e^{\frac{1}{2}}$, this sudden change in propagation mechanism may be the reason the maximum burning velocity for hydrocarbon flames occurs at a fuel ratio of only 1.1 stoichiometric, i.e., for slightly rich mixtures, a fact which is difficult for existing physico-chemical theories of flame propagation to explain.

The sudden decrease in flame thickness which is predicted in passing from lean to rich mixtures cannot be verified directly since no measurements of thickness exist for the experimental fuel mixtures. Therefore at present, independent confirmation of this postulated shift in propagation mechanism is impossible. Furthermore, this conclusion is based on a simplified stability

[24] Jost, *Explosion and Combustion Processes in Gases* (McGraw-Hill Book Company, Inc., New York, 1946), p. 113.

[25] J. W. Anderson and R. S. Fein, J. Chem. Phys. **17**, 1268 (1949).

[26] E. Bartholome, Naturwiss. **36**, 206 (1949).

treatment and rests on the controversial assumption that the propagation mechanism is independent of the distortion. However, the close agreement between calculated and observed cell sizes adds considerable support to the theory presented here.

Unfortunately to date cell size measurements exist only for slow hydrocarbon flames propagating downward ($U_u \approx 10$ cm/sec, 30 percent N_2 added as a dilutant). Therefore, caution should be exercised before rashly assuming that the conclusions drawn above will also hold for faster flames. It is hoped that additional observations of cell sizes and flame thicknesses will be forthcoming in the near future so these conclusions can be verified and extended.

7. GENERAL TREATMENT

In view of the close agreement between the results of the preceding section and experimental observations and, since from Eq. (6.26)

$$\Delta \sim A_2 + A_1, \tag{7.1}$$

the procedure for a more general treatment will only be sketched very briefly.

In Sec. 6 the flame is treated as infinitely thin, the displacement $\zeta(\xi)$ and mass flow $m(\xi)$ being taken as constant across the flame front. When $m = \kappa\mu\zeta$, the extension to a flame of finite thickness is straightforward. In the determinantal Eq. (6.9), in addition to the A's corresponding to F_1, B's, C's, and D's will now appear arising from $F_2\xi$, $F_3\xi^2/2$, and $F_4\xi^3/6$, respectively; in addition the inhomogeneous terms which contribute unit elements will now yield elements in K, K^2, etc. All this only increases the algebraic complexity of the eigenequation for α.

The use of the complete expression for $m(\xi)$,

$$m = -\kappa\mu\zeta'' + \zeta' + \kappa\mu\zeta, \tag{4.10}$$

introduces new mathematical difficulties in solving the stability problem. When this expression for m is substituted into Eq. (3.24), the resulting differential equation is of sixth order within the flame but only of fourth order in the constant velocity regions, leading to six independent constants within the flame but only four outside it. However, the differential relation (4.10) yields two additional constants which can be used in satisfying the boundary conditions. Since

$$\alpha\zeta + \mathfrak{A}m = \phi = F_j e^{r_j \xi}, \tag{7.2}$$

or

$$\alpha\zeta + \mathfrak{A}(-\kappa\mu\zeta'' + \zeta' + \kappa\mu\zeta) = F_j e^{r_j \xi}, \tag{7.3}$$

then

$$\zeta = \frac{F_j e^{r_j \xi}}{\alpha + \mathfrak{A}(-\kappa\mu r_j^2 + r_j + \kappa\mu)} + F_{m_1} e^{r_{m_1}\xi} + F_{m_2} e^{r_{m_2}\xi}, \tag{7.4}$$

where F_{m_1} and F_{m_2} are solutions of the homogeneous equation

$$-\kappa\mu\zeta'' + \zeta' + (\alpha/\mathfrak{A} + \kappa\mu)\zeta = 0. \tag{7.5}$$

The procedure for deriving solutions in the flame region is the same as in Sec. 5, but now there are six separate boundary conditions instead of the four (5.9)–(12), leading to a twelfth-order determinantal equation for α.

8. CONCLUSION

The importance of the present investigation extends in several directions. First, it demonstrates that a plane flame front is stable only under a very limited set of conditions, i.e., a slow flame ($U_u \lesssim 10$ cm/sec) propagating downward and controlled by the diffusion of free radicals. In general the flame front will be unstable, serving as a primary source of vorticity. Second, the theory permits important conclusions on the nature of the physico-chemical processes occurring within the flame to be drawn from experimental measurements of cell sizes. Since effective conduction (diffusion) coefficients can be calculated from these sizes, it may be possible to evaluate the relative importance of diffusion *vs* thermal processes, on which so many opposing views have been expressed.[27] Stability studies suggest that a sharp change occurs in the dominant propagation mechanism in slow hydrocarbon flames in passing from lean to rich mixtures—from diffusion by free radicals to thermal conduction. Third, the pressure dependence of the burning velocity,[28] which is sorely needed to test proposed theories of propagation, can be determined for flames whose cell sizes can be measured as a function of pressure.

APPENDIX

It will now be proved that all thermal disturbances obeying the boundary conditions are damped and therefore can be neglected.

When m is given by (4.10), the temperature disturbances become independent of the others and can be solved separately. Equation (4.8) becomes

$$k_e \nabla^2 T^{(1)} - C_p \rho \left(\frac{\partial T^{(1)}}{\partial t} + U \frac{\partial T^{(1)}}{\partial x} - \frac{UT'}{T} T^{(1)} \right) - \frac{d}{dT}(W_e Q_e) T^{(1)} = 0. \tag{A.1}$$

Introducing dimensionless variables

$$\xi = x/L; \quad \xi_1 = y/L; \quad \tau = U_u t/L; \quad \alpha = L\delta/U_u; \tag{A.2}$$

$$\epsilon = U_b/U_u; \quad \epsilon_1 = (\epsilon+1)/2; \quad \kappa = hL = hk_e/C_p\rho_u U_u,$$

$$\mathfrak{A}(\xi) = U(\xi)/U_u = T(\xi)/T_u = \rho_u/\rho(\xi), \tag{A.3}$$

$$\omega(\xi) = (L^2/k_e) d(W_e Q_e)/dT, \tag{A.4}$$

$$T^{(1)}/T_u = \theta(\xi) \exp(i\kappa\xi_1 + \alpha\tau), \tag{A.5}$$

[27] G. L. Dugger, J. Am. Chem. Soc. **72**, 5271 (1950); D. M. Simon, *ibid.* **73**, 422 (1951).

[28] P. J. Wheatley and J. W. Linnett, Trans. Faraday Soc. **45**, 1152 (1949); F. H. Garner *et al.*, Nature **164**, 884 (1949); J. W. Linnett *et al.*, *ibid.*, 403 (1949); Badin, Stuart, and Pease, J. Chem. Phys. **17**, 314 (1949).

where the unit of length is the flame thickness L (not $1/h$), then

$$\theta''-\theta'-(\alpha/\mathfrak{A}+\kappa^2-\mathfrak{A}'/\mathfrak{A}-\omega)\theta=0. \quad \text{(A.6)}$$

As θ and θ' must be continuous in passing through the flame front and vanish for $\xi=\pm\infty$, $\theta''<0$ within the flame region. Clearly from Eq. (A.6) this will be the case for α sufficiently large and negative. It will be shown that $\mathfrak{A}'/\mathfrak{A}$ and ω do not assume sufficiently large positive values within the flame for a positive α to exist satisfying the boundary conditions. In the burned and unburned regions Eq. (A.6) reduces to

$$\theta''-\theta'-(\alpha/\mathfrak{A}+\kappa^2)\theta=0, \quad \text{(A.7)}$$

whose solutions are

$$\theta_u=F_u e^{r_u\xi};\quad r_u=\tfrac{1}{2}+c_u;\quad c_u=(\alpha+\kappa^2+\tfrac{1}{4})^{\frac{1}{2}}, \quad \text{(A.8)}$$

$$\theta_b=F_b e^{r_b\xi};\quad r_b=\tfrac{1}{2}-c_b;\quad c_b=(\alpha/\epsilon+\kappa^2+\tfrac{1}{4})^{\frac{1}{2}}. \quad \text{(A.9)}$$

Within the flame Eq. (A.6) will be simplified by replacing its variable coefficients by their average values in the region. Thus,

$$\theta''-\theta'+(\ln\epsilon+\langle\omega\rangle_{Av}-\alpha/\epsilon^{\frac{1}{2}}-\kappa^2)\theta=0, \quad \text{(A.10)}$$

whose solution is

$$\theta_f=F_1 e^{r_1\xi}+F_2 e^{r_2\xi}, \quad \text{(A.11)}$$

$$r_1=\tfrac{1}{2}-iR;\quad r_2=\tfrac{1}{2}+iR;$$
$$R=(\ln\epsilon+\langle\omega\rangle_{Av}-\alpha/\epsilon^{\frac{1}{2}}-\kappa^2-\tfrac{1}{4})^{\frac{1}{2}}. \quad \text{(A.12)}$$

The boundary conditions lead to the determinantal equation

$$\begin{vmatrix} 1 & 1 & 1 & 0 \\ r_u & r_1 & r_2 & 0 \\ 0 & e^{r_1} & e^{r_2} & 1 \\ 0 & r_1 e^{r_1} & r_2 e^{r_2} & r_b \end{vmatrix}=0, \quad \text{(A.13)}$$

$$(r_1-r_u)(r_2-r_b)e^{r_2}-(r_1-r_b)(r_2-r_b)e^{r_1}=0. \quad \text{(A.14)}$$

If r_1 and r_2 are real this can be written as

$$\mathfrak{F}(r_1,r_2)-\mathfrak{F}(r_2,r_1)=0. \quad \text{(A.15)}$$

As $\mathfrak{F}(r_1,r_2)$ is a monotonic function of r, the roots of this equation, apart from $r_1=r_2$, are the zeros of $\mathfrak{F}(r_1,r_2)$, *viz.*, $r_1=r_u$ and $r_2=r_b$. But since all these roots are degenerate, r_1 and r_2 must be complex conjugates, i.e., $\theta''<0$, as previously noted. Then Eq. (A.14) can be written as

$$Z_1Z_2Z_3-Z_1^*Z_2^*Z_3^*=0, \quad \text{(A.16)}$$

or

$$Im(Z_1Z_2Z_3)=0. \quad \text{(A.17)}$$

Using Eqs. (A.8), (A.9), and (A.12) yields

$$Im(c_u+iR)(c_b+iR)(\cos R-i\sin R)=0, \quad \text{(A.18)}$$

or

$$\tan R=-(c_u+c_b)/(R+c_uc_b/R). \quad \text{(A.19)}$$

Since $c_u>0$, $c_b>0$ and $R>0$, the minimum value of R occurs when $\tan R$ lies in the second quadrant, i.e.,

$$\pi/2<R<\pi. \quad \text{(A.20)}$$

Experiments show that the burning velocity of hydrocarbons does not vary strongly with temperature,[29,30] so $\langle\omega\rangle_{Av}\approx 0$. When $\alpha\geq 0$, then $R<(\ln\epsilon+\frac{1}{4})^{\frac{1}{2}}$; if $\epsilon=5$, then $R<1.2$ in contradiction to Eq. (A.20). Therefore α must be negative; only damped temperature disturbances are possible. The primary restriction on this proof is that $\langle\omega\rangle_{Av}<\frac{1}{2}$.

[29] H. Sachase, Z. Physik. Chem. **A180**, 305 (1937).
[30] See reference 22, p. 113.

Note on the Absorption Spectrum of Iodine in Oxygenated Solvents and the Dissociation of Iodine Water

LEONARD I. KATZIN*
Chemistry Division, Argonne National Laboratory, Chicago 80, Illinois
(Received April 4, 1952)

Data are presented on factors in the appearance of the tri-iodide absorption spectrum in solutions of iodine in water and in the alcohols. Some implications of the dissociation of iodine in water for the theory of the iodine-solvent interaction are pointed out.

MOST of the revived attention of the past few years accorded to the phenomenon of the colors of iodine solutions has been given to the spectrum of iodine in the benzenoid hydrocarbons. It is the purpose of this note to call attention to some features of the spectrum of iodine in its "brown" solutions in oxygenated solvents (including water).

The spectrum of iodine dissolved in water or one of the lower alcohols (1–4 carbons) shows three peaks, at about 285 millimicrons, 350–360 millimicrons, and 450–460 millimicrons. Two are the tri-iodide peaks, and the longest-wavelength peak is that of the solvated I_2. With the alcohols it can be shown, as by adding one percent by volume of a concentrated solution of iodine in carbon tetrachloride to the alcohol, that the tri-iodide peaks are present as soon after mixing as the spectrum can be scanned (1–2 minutes). The absorption rises slowly with time, showing that there occurs a reaction between the iodine and the solvent or impurities in it which produces iodide and hence tri-iodide. The initial absorption is so high in comparison with the subsequent rate of alteration that it is not certain all of the tri-iodide is ascribable to reduction products.

More certainty on this point seems justified by behavior such as the following. When a solution of iodine in isopropyl alcohol is diluted, the ratio of the tri-iodide absorption at about 360 millimicrons to the iodine peak at 450 millimicrons increases markedly. This is true for tertiary butyl alcohol, where the tri-iodide absorption is usually very small, as well as for isopropyl alcohol, where it tends to be rather strong. This suggests that there may be a trace of very rapidly reacting impurity in the alcohol and that the amount of tri-iodide formed from this reaction is related to the volume of alcohol with which the iodine has come in contact.

Another type of experiment bearing on the point is the following. Equal portions, one percent by volume, of a stock solution of iodine in carbon tetrachloride were added to samples from five different bottles of isopropyl alcohol. The density for a 1-cm path length at 450 millimicrons was the same for all the samples, 0.40. The density at 360 millimicrons ranged from 0.098 to 0.549. On the basis of this evidence there would seem to be grounds for considering most, if not all, of the tri-iodide absorption found with iodine solutions in the alcohols to be due to reaction and reduction of iodine. Detailed experiments by Batley on ethyl alcohol[1] have led to a similar conclusion.

We have found that under some circumstances formation of tri-iodide can be reversed, which we have not seen reported elsewhere. Addition of carbon tetrachloride to 10 percent by volume to an isopropyl alcohol solution of iodine which shows the tri-iodide spectrum will cause the tri-iodide absorption largely to disappear (see Fig. 1). Thus, an absorption of 0.746 at 360 millimicrons might be reduced to 0.046, and in the case of another alcohol sample, with an equal iodine concentration, from 0.122 to 0.029. The absorption at 450 millimicrons, due to I_2, is not sensibly altered (extinction of the tri-iodide peak is 25–30 times that of the iodine peak). The tri-iodide spectrum may be evoked in an iodine solution in pure tertiary butyl alcohol, in which it is not normally found, by addition of a small portion of an iodide, e.g., tetrabutylammonium iodide. Addition of carbon tetrachloride to 10 percent by volume does not sensibly affect the spectrum. It seems possible that this difference in behavior may be due to a difference between iodide salt and HI, presumably present when reaction with the alcohol is the source.

The origin of the tri-iodide peaks in water is the reaction

$$I^- + I_2 = I_3^-, \tag{1}$$

(ignoring possible hydrations) with the iodide presumably coming from either or both of the reactions

$$I_2 = I^+ + I^-, \tag{2}$$

$$I_2 + H_2O = H^+I^- + IOH, \tag{3}$$

and the question of the possible contribution of reaction (2) being of interest at the moment. The contribution of reaction (3), as well as possible effects of alkali leached from the glass and other side reactions can be eliminated by working in acid solutions. In such an iodine solution, tri-iodide appearing should be due to reactions (1) and (2) alone.

Solutions of cp sublimed iodine were made in perchloric acid of $0.4–10\times10^{-3}M$ concentration, with iodine concentrations varying from $2–10\times10^{-4}M$. Optical densities were measured at 460 millimicrons (the

* With the technical assistance of Miss Elizabeth Gebert.

[1] Alan Batley, Trans. Faraday Soc. **24**, 438 (1928).

iodine peak in water) and at 285 millimicrons (the 350 millimicron tri-iodide peak was too weak). The former serves as a measure of the iodine concentration, with the molar extinction coefficient of 746 given by Awtrey and Connick.[2] The absorption at 285 millimicrons must be corrected for the absorption of the flat 270 millimicron peak of iodine[3] before applying the tri-iodide extinction coefficient of 40 000. Our measurements have indicated this correction to be 16 percent of the absorption at 460 millimicrons. The free iodide concentration is calculated from these values through the equilibrium constant[3] for reaction (1) of 1.40×10^{-3}. With reaction (2) as the sole source of iodide, the concentration of I^+ should equal the sum of the I^- and I_3^- concentrations, and the constant for reaction (2) may be calculated. Of ten such solutions, 5 gave values for the dissociation constant of reaction (2) of $0.52\text{–}0.62\times10^{-8}$, 3 others ranged up to 1.2×10^{-8}, and the rest were higher.

By an electrometric procedure which assumes all iodide in an iodine solution has arisen from dissociation of iodine (as our method of calculation does also), Murray[4] obtained a value of 1×10^{-8} for the same constant. In a most recent paper Bell and Gelles,[5] however, making use of an electrometric technique which should be independent of an initial iodide content of the iodine, obtain the value 1.2×10^{-11} for the equilibrium constant. They were also able to demonstrate electrometrically the presence of variable small amounts of iodide in different iodine samples. Experiments of our own, in which successive dilutions of the same stock iodine solution gave successively larger values of the iodine dissociation equilibrium constant can be ascribed in part to the presence of some small amount of stable iodide in even the solutions with the smallest apparent dissociation constants. The spectrophotometric determination of the dissociation constant, accepting the value of Bell and Gelles, in an iodide-free sample of iodine would be impossible, because of the large background of the 270 millimicron peak of the iodine itself.

The amount of I^+ which forms by this dissociation is small, but it achieves importance in relation to the theoretical explanations of the absorption spectrum of iodine in water.[6] According to Mulliken's explanation, the dissociation of iodine in water involves an electron transfer from oxygen to one of the iodine atoms, the other remaining essentially a free radical associated

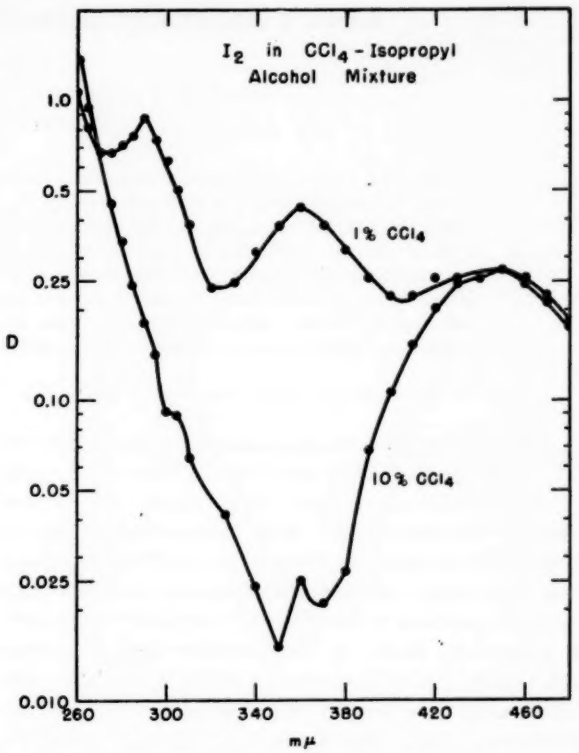

FIG. 1. Effect of carbon tetrachloride on the tri-iodide absorption peaks of a solution of iodine in isopropyl alcohol.

with the now electron-deficient oxygen. The existence of (undoubtedly hydrated) I^+ deduced from the dissociation constant for reaction (2) obtained by Bell and Gelles indicates that theory must also allow for electron transfer between the two iodine atoms. The existence of the non-iodide member of the pair as Mulliken's[6] $(H_2O)^+\cdot I$ to a significant concentration, when inspection shows the formulation to be rearrangeable to $H^+\cdot OH\cdot I$, containing two free radicals, seems unlikely.

Another point in the picture which perhaps merits reconsideration is that of the configuration of the iodine-oxygenated solvent complexes. Mulliken[6] has excluded any but the essentially triangular arrangement of the oxygen and the two iodine atoms. Trihalide complexes like I_3^-, which one would expect to be rather comparable, tend strongly toward a linear[7] structure rather than the planar one which would correspond to the iodine-solvent picture.

Spectral measurements were made with the Beckmann DU spectrophotometer and hydrogen light source.

[2] A. D. Awtrey and R. E. Connick, J. Am. Chem. Soc. **73**, 1842 (1951).
[3] G. Jones and B. B. Kaplan, J. Am. Chem. Soc. **50**, 1845 (1928).
[4] H. D. Murray, J. Chem. Soc. **1925**, 882.
[5] R. P. Bell and E. Gelles, J. Chem. Soc., 2734 (1951).
[6] R. S. Mulliken, J. Am. Chem. Soc. **72**, 600 (1950).
[7] R. W. G. Wyckoff, *Crystal Structures* (Interscience Publishers, Inc., New York, 1948), Vol. 1, Chap. VI.

Electric Resistivity of Interstitial Compounds of Graphite

S. MROZOWSKI
Department of Physics, University of Buffalo, Buffalo, New York
(Received August 25, 1952)

Assuming that the formation of interstitial compounds is accompanied by creation of excess holes in the otherwise full band of graphite, it is shown that a linear energy-momentum relation at the Brillouin zone corners is incapable of explaining the decrease of the electric resistance with oxidation. It appears that for a more general model the decrease in relative resistance should be independent of temperature for large oxidations if suitable corrections for the initial conditions are made. Data for polycrystalline graphite corrected for the existence of an energy gap and of excess holes in the untreated material give curves which converge for higher oxidation with the curve for natural graphite. Discussion of the low temperature properties of graphite leads to the conclusion that large graphite crystals possess slightly overlapping zones.

WHEN foreign ions are introduced between the graphitic layers or into the intercrystalline voids in polycrystalline graphite, compounds are formed which, in the last decade, have attracted considerable attention. It is believed that foreign negative ions chase a corresponding number of electrons out from the π-band of graphite (unsaturation electrons), thus forming conducting holes in the otherwise full resonance band. It seems that the decrease of the electric resistance of the compound along graphitic planes with increasing ion concentration is mainly due to this variation in the number of carriers, the counterbalancing effect of scattering of the electronic current by the introduced ions being of lesser importance. Thus, a study of the electronic properties of such compounds as a function of the ion concentration should be a valuable tool in probing into the structure of Brillouin zones in graphite. Recently, Hennig[1] performed a number of interesting experiments with graphite bisulfate. Among other things he has shown that the temperature coefficient of resistivity for polycrystalline graphite gradually changes from negative to positive as the substance is transformed into an interstitial compound, the resistivity decreasing continuously with the increase in amount of treatment. E. Kmetko has confirmed and extended Hennig's work and is reporting his results in a forthcoming paper. It is the author's intent to illustrate at this time how cautious one has to be with the interpretation of results of such work. A number of possible pitfalls will be discussed below.

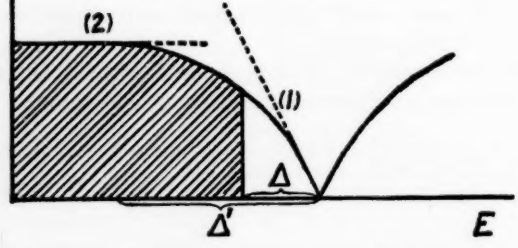

FIG. 1. Density of electronic states in graphite according to the plane model of Wallace: (1) $E\sim k$, (2) $E\sim k^2$. Δ is the depression of the Fermi level for the treated graphite.

It seems straightforward, at first, that the resistivity of graphite should decrease when electrons are removed from the full band. After all the transformation goes from that of an intrinsic semiconductor with a zero energy gap to a hole conductor of a semimetallic type with an increasing number of carriers. A more careful consideration shows, however, that in general this is not necessarily true: For a plane model of a semiconductor with a zero gap and with a linear relation between the energy E of electrons and holes and their k vectors in the neighborhood of Brillouin zone corners ($E\sim k$), such as has been treated by Wallace,[2] the scattering probability $1/\tau_e$ by the lattice vibrations is a function of the energy[3]: $1/\tau_e=\alpha_1\cdot T\cdot|E|$. The scattering probability is proportional to the energy of the electron, since the number of states the electron can be scattered into is for such a plane model proportional to $|E|$. For the same reason the scattering probability by the boundaries of microcrystals and by lattice defects will be $1/\tau_B=\beta_1\cdot|E|$, α_1 and β_1 being constants determined by the corresponding interactions (β_1 is inversely proportional to the average distance of scattering centers, that is, defects and boundaries). The total probability is

$$1/\tau=1/\tau_e+1/\tau_B=|E|\cdot(\alpha_1 T+\beta_1). \quad (1)$$

The mean free time τ thus obtained has to be substituted into the equation for the conductivity derived by Wallace [his Eq. (3.12) but with τ left under the

[1] G. Hennig, J. Chem. Phys. **19**, 922 (1951); see also McDonnell, Pink, and Ubbelohde, J. Chem. Soc. **1**, 191 (1951).

[2] R. P. Wallace, Phys. Rev. **71**, 622 (1947).

[3] This relation for a two-dimensional model is derived analogously to the formula for the probability of the tri-dimensional scattering, such as given in W. Shockley [*Electrons and Holes in Semi-Conductors* (D. Van Nostrand Company, Inc., New York, 1950), Eq. (29) on p. 493]. The direct proportionality of the interaction matrix element to the temperature holds, according to F. Seitz [Phys. Rev. **73**, 549 (1948)], all the way down to very low temperatures, down to about 1°K (especially for graphite, where electrons have such a small effective mass).

integral sign],

$$\sigma = -A\int_{-\infty}^{+\infty} \tau \cdot |E| \cdot \frac{\partial f_0}{\partial E} \cdot dE, \quad \text{with} \quad A = 8\pi e^2/h^2 c. \quad (2)$$

The resistivity of graphite is, therefore,

$$\rho_0 = a_1 \cdot T + b_1, \quad (3)$$

with a_1 and b_1 independent of temperature T, in best agreement with the experimental findings for large graphite crystals in general, and for polycrystalline graphite at high temperatures. For the latter one the presence of a negative temperature coefficient at lower temperatures remains unexplained in this model.

Surprisingly the resistivity turns out to be independent of the position of the Fermi level, that is, of the number of missing electrons from the filled band: Denote the depression of the Fermi level below the top of the full band by Δ. The Fermi distribution is

$$f_0(E) = 1/1 + \exp(E - \Delta/kT). \quad (4)$$

It is easy to see that the value of the integral (2), with τ given by (1), is independent of Δ. This independence of resistivity on the number of conducting excess holes is a peculiar consequence of the linear relation between the energy and momentum of electrons. It can be interpreted that in the elementary formula $\rho = (m/N)_{\text{eff}}/e^2\tau$ it is just the energy dependence of the scattering probability which counterbalances the variation of $(m/N)_{\text{eff}}$.

A decrease of the resistivity with depression Δ is obtained, however, for any plane model for which $E \sim k^n$, where $n > 1$. For instance, for a parabolic relationship $E \sim k^2$ the total scattering probability is independent of the energy of the electrons[3]

$$1/\tau = \alpha_2 T + \beta_2. \quad (5)$$

Thus, τ can be taken out in (2) from under the integral sign, and the conductivity turns out to be

$$\sigma = -A\tau(\Delta - 2kT \ln[1 + e^{\Delta/kT}]). \quad (6)$$

(See Hennig,[1] page 929). For a large depression $\Delta \gg kT$, consequently,

$$\rho_\Delta = 1/\Delta \cdot (a_2 T + b_2). \quad (7)$$

Actually for a graphite crystal the energy-momentum relationship is more complicated, as was already pointed out by Wallace.[2] For a plane model we might take the number of electronic states to follow a curve like that in Fig. 1 with a gradual change from a linear into a parabolic relationship [see Wallace, Eq. (2.14) and his Fig. 6]. In such a case formula (3) has to be used for the initial resistivity ρ_0 and for the treated graphite, when Δ is large, formula (7). Therefore,

$$\rho/\rho_0 \sim 1/\Delta \quad \text{for} \quad \Delta > \Delta'. \quad (8)$$

The dependence of ρ on Δ could be calculated with a given energy-momentum relationship for intermediate values of Δ. It is, however, questionable if such a calculation would be worthwhile: In the process of formation of the interstitial compounds the ions invade graphitic layers in groups, the penetration by one atom breaking the path for others. The curve as a function of Δ represents rather the statistics of invasions and not a continuous and gradual shift of the Fermi level. After all, if the latter were true, the curve ρ/ρ_0 would start out horizontal for small Δ's ($E \sim k$), contrary to observation (see, however, the discussion of the diamagnetism below).

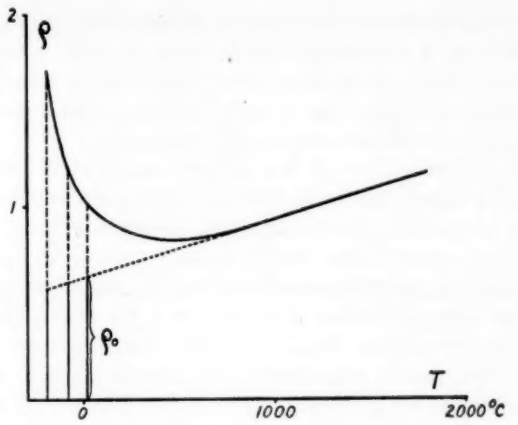

FIG. 2. Temperature dependence of electric resistivity ρ of the untreated polycrystalline graphite.

If the scattering by the foreign ions is negligible, the curve ρ/ρ_0 should be independent of temperature: The interaction coefficients α_1, β_1 and α_2, β_2 being, respectively, proportional to each other, the temperature dependence cancels out from the ratio (8). This is not found to be true for polycrystalline graphite (see Fig. 8 of Hennig[1]). The disagreement is not real, however, and is due to an inappropriate way of plotting the data. As was shown by the author[4] the character of the temperature dependence of the resistivity of an untreated polycrystalline graphite (see Fig. 2) is explained by the presence of a small but finite energy gap $\Delta\epsilon$ between the filled and empty energy bands. A small concentration of excess holes due to peripheral acceptors (free carbon valencies) is present. A detailed discussion of the character of the temperature dependence and a quantitative formula in terms of the width of the gap and of the concentration of excess holes is given in the paper mentioned.[4] Here it will be sufficient to point out that the linear portion in Fig. 2 corresponds to temperatures for which $kT > \Delta\epsilon$ (existence of the gap is immaterial and the number of acceptors is negligible), and the left part of the curve with a negative temperature coefficient corresponds to a decrease of resistance caused by an increasing activation of electrons over the energy gap.

When so many electrons are removed from such a material by formation of an interstitial compound that $\Delta \gg kT$, the existence of the gap loses its importance

[4] S. Mrozowski, Phys. Rev. 85, 609 (1952); Errata, Phys. Rev. 86, 1056 (1952).

and the substance becomes a semimetallic conductor similar to a compound made from a large graphite crystal. Thus, the change from a negative to a positive temperature coefficient of resistivity becomes a natural consequence of the existence of the gap.

If the resistivity of the treated material is plotted relative to the resistivity which this material would have in an untreated state if it did not possess an energy gap nor any excess holes, then, in such a plot, all curves should coincide with the curve for the graphite crystal in the range of higher Δ's [Eq. (8)]. By extrapolating the linear relation Fig. 2 to lower temperatures, such corrected initial resistivities are obtained; and using these values for ρ_0, Hennig's curves for $+25°C$, $-129°C$, and $-200°C$ were replotted in form of Fig. 3. Hennig's curve for natural graphite (his Fig. 4) is also included in Fig. 3. All these curves merge for higher depressions Δ, as expected. For the lower values of Δ the spread is due to the differences in initial conditions (at $\Delta=0$).

This case is an excellent illustration of the fact that different ρ/ρ_0 curves are obtained if no correction for the difference in initial conditions is made. After all, the resistivity of the untreated material ρ_0 is much more susceptible to the presence of small amounts of excess electrons or holes (due to impurities or to difference in crystalline structure) than that of the treated one. Strictly speaking, the curves should be shifted in plotting to the left or right by an amount corresponding to the number of excess holes or electrons. This shift Δ_0 is in most cases of polycrystalline graphites small (not so for baked carbons. See the forthcoming paper by Kmetko). However, the change in ρ_0 is large, since the concentration of activated electrons and holes is also small.

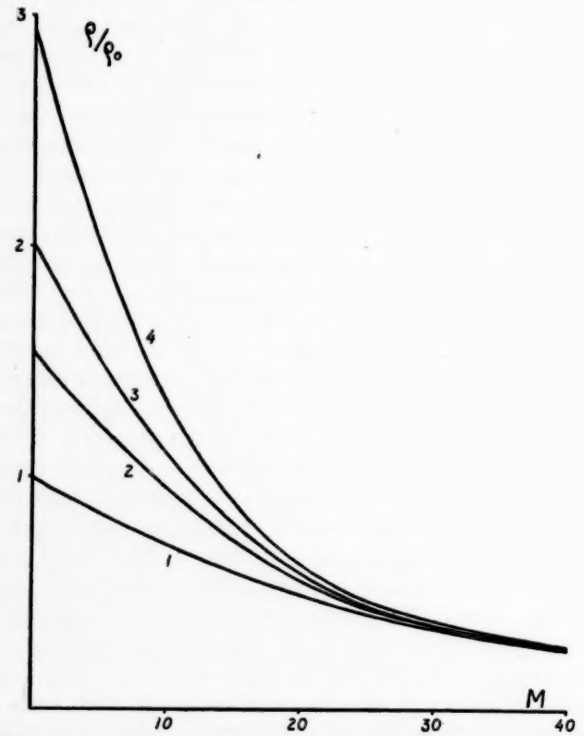

FIG. 3. Relative resistivities ρ/ρ_0 for bisulfate compounds of natural (1) and polycrystalline graphite (2 — +25°C, 3 — −129°C, 4 — −200°C) as a function of oxidation M (in 10^{-4} equiv/g atom). The extrapolated values from Fig. 2 are used for the initial resistivities ρ_0.

Another illustration of the same source of difficulties are the theoretical curves published by Hennig.[1] Hennig has obtained a system of predicted curves discordant with the experimental ones (his Fig. 8). The disagreement can be traced to the cancellation of τ in the formula for R/R_t of Hennig (reference 1, page 929), which cancellation is equivalent to the assumption of a definite parabolic relationship between E and k through the whole range up to the top of the Brillouin zone corners [use of Eq. (6) for $\Delta=0$]. Such a relationship is definitely out of question, since it corresponds to $N(E)$ = const [see Fig. 1 and also Eq. (9) below]. In lack of a better assumption at the time, Wallace[2] took out τ from under the integral. It was clear to him, however, that this is an approximation and that τ is a function of energy of the electrons (see the discussion of the temperature dependence of the mean free path, reference 2, page 620). As was shown previously (reference 4, footnote 15), Wallace's assumption did not affect his final conclusions. In general, however, such a procedure will lead to incorrect results. For graphite compounds the average energy of electrons varies with Δ in wide limits and so does the scattering probability $1/\tau$ (except in case of a parabolic relation). Even if Wallace's procedure is used, the τ's being different cannot be canceled out from the ratio R/R_t.

It would seem best, therefore, to use for the ρ/ρ_0 curves a plot in which the curves overlap in the region of higher Δ's. In general, this is not easy to do, since usually there are two unknowns: the magnitude of the horizontal shift Δ_0 and the correction for ρ_0 (in Fig. 3 Δ_0 was negligible and ρ_0 could be evaluated from Fig. 2!). Moreover, the hyperbolic relationship, Eq. (7), should break down for higher Δ's again. In graphite the inflection point ($\partial^2 E/\partial k^2=0$) is located not far below the top of the band, and at this point all distinction between hole and electron conduction becomes meaningless. When Δ becomes larger than the depth of the inflection point, the resistivity should start to rise. It would seem attractive to explain the increase of resistance observed by Hennig above 0.014 equivalent for graphite bisulfate compounds and by Grisdale, Pfister, and Van Roosbroeck[5] above 0.045 equivalent for borocarbon compounds by such an effect. The increase, however, is too steep to be due exclusively to this factor: Large amounts of a foreign substance might seriously disturb the whole polycrystalline structure and be responsible for the observed increase.

Another way of probing into the zone structure of graphite is to study its diamagnetism. It is clear that

[5] Grisdale, Pfister, and Van Roosbroeck, Bell System Tech. J. 30, 271 (1951).

the linear energy-momentum relation is incompatible with the existence at lower temperatures of a large approximately-temperature-independent diamagnetic susceptibility.[6] Thus, the linear distribution, Fig. 1, cannot hold up to the Brillouin zone corners (thus, the curves ρ/ρ_0 do not start out exactly horizontal for small Δ's after all, as stated before). Wallace's treatment of a tri-dimensional lattice[2] gives a density of electronic states such as presented approximately in Fig. 4a. Such a model, however, leads to a steep rise of electric resistivity at low temperatures ($1/\tau \to \beta_2$ and the mean free path $\lambda \to 0$ for $T \to 0°K$) which is not observed experimentally for large graphite crystals. Substituting, for instance, (5) into (6) and taking $\Delta=0$, one finds

$$\rho = a + (b/T). \tag{9}$$

In fact, any model with $n>1$ is objectionable for the same reason. In order to satisfy at the same time the two conditions: approximately constant diamagnetic susceptibility, and linear increase of resistance with temperature in the low temperature range, a slight overlapping of the energy bands has to be assumed (Fig. 4b). Thus, an untreated large graphite crystal is probably a semimetal similar to bismuth and not a semiconductor with a zero gap. Wallace's results led him to the conclusion that the energy bands just touch (reference 2, pages 630–631). According to a recent more extensive analysis by Polder, splitting, touching, or overlap are possible: Touching, therefore, would be highly accidental. Polder's conclusion is that a slight overlap is most likely to occur in graphite.

It may be interesting to note that the plane model with a parabolic energy-momentum relation gives diamagnetic susceptibility χ independent of Δ. In fact, for larger Δ's ($\Delta \gg kT$) an exact cancellation takes place between N_{eff} and T_g in the formula $\chi = -N_{\text{eff}}\mu^2\alpha_1\alpha_2/2kT_g$, where μ, α_1 and α_2 are constants and T_g is the degeneracy temperature[7]

$$\left(kT_g = \Delta \quad \text{and} \quad N_{\text{eff}} = \int_{-\infty}^{+\infty} N(E)\cdot f(E)dE \sim \Delta\right).$$

In order to have a decrease of the susceptibility with chemical treatment, as observed in experiments,[8] the exponent n must be smaller than 2 ($\chi \sim \Delta^{1-(2/n)}$).

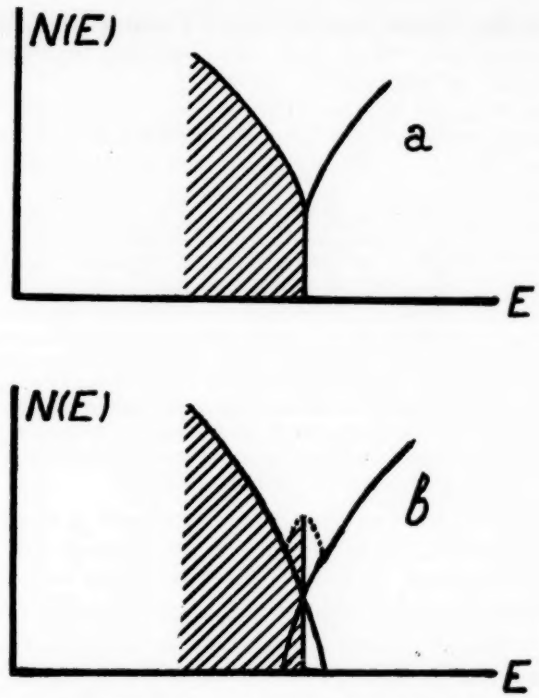

FIG. 4. Density of electronic states in graphite: (a) according to calculations by Wallace (tri-dimensional); (b) as obtained from interpretation of low temperature properties of graphite.

The foregoing shows that no single model with a simple energy-momentum relation is capable of explaining even qualitatively all the properties of graphite and its compounds. The best fit for the temperature dependence of resistivity is obtained with $n=1$, but for the resistivity *versus* oxidation, n must be definitely greater than 1, possibly close to 2. A combination of the two (Fig. 1) seems to explain satisfactorily all the results for the resistivity. On the other hand, both values, $n=1$ and $n=2$, have to be excluded when the magnetic susceptibility is considered. Thus a more complicated behavior has to be assumed in the neighborhood of the zone corners, such as given in Fig. 4b. The main reason for the failure of the simple models is probably the fact that in case of compounds (and more so for baked carbons) experimental probing is done to a considerable depth below the Brillouin zone corners. Thus, the energy-momentum surfaces have to be considered in all their details; it can be expected that theoretical approach will be successful only if the calculations are performed with few approximations.

The author is indebted to Dr. D. Polder (Bristol) for information on results of his work prior to publication.

[6] The author was fully aware of this difficulty when the modified Ganguli-Krishnan theory was proposed (see reference 4). This was not stressed at that time, however, in order not to complicate the discussion.

[7] W. Ganguli and K. S. Krishnan, Proc. Roy. Soc. (London) 117, 168 (1941).

[8] M. Goldsmith, J. Chem. Phys. 18, 523 (1950); see also McDonnell, Pink, and Ubbelohde, reference 1.

On the Molecular-Orbital Theory of Conjugated Organic Compounds with Application to the Perturbed Benzene Ring*

PER-OLOV LÖWDIN
Department of Physics, Duke University, Durham, North Carolina†
(Received August 13, 1952)

The electronic structure of a molecular system is investigated by using the idea of molecular orbitals. The behavior of the separate molecular orbitals and the orbital energies under the influence of the substitution of one or more heteroatoms, considered as perturbations, is examined. A series of quantities, separate charge orders, bond orders, and mutabilities are introduced, giving information about some characteristic physical and chemical properties of the compound. The perturbation scheme is carried out explicitly to the second order in the energies and to the first order in the orbitals, and special attention is paid to the treatment of degenerate levels. The overlapping problem is fully discussed. The basic results are independent of any empirical parameters, and they may be used either in the naïve semi-empirical theory or in a more elaborate theoretical approach based on an antisymmetrized molecular wave function.

As an example, numerical applications are carried out in detail on benzene. Separate charge orders, bond orders, and mutabilities are tabulated, and orbital energies for a perturbed benzene ring with one or two heteroatoms are explicitly given.

INTRODUCTION

THE molecular orbital theory for treating properties of molecules, developed by Lennard-Jones, Hund, and Mulliken, was first applied to the aromatic organic compounds by Hückel[1] in his investigation of the mobile electrons of the benzene ring. Hückel[2] was also interested in the problem of the change of the electronic structure caused by the introduction in the ring of a heteroatom or a substituent, which he considered as perturbations. However, Hückel's mathematical results concerning the directing power of such a perturbation were given their correct chemical interpretation first by Wheland and Pauling,[3] who further developed the theory.

The whole approach had a *semi-empirical* character, since the fundamental integrals were considered as adjustable parameters which had to be found from observed data, and the whole theory was, therefore, essentially a device for correlating one set of experimental data with another. This naïve molecular theory has been successful in treating the ground state of the aromatic molecules and conjugated systems in general, describing the connection between such quantities as electron affinities, resonance energies, ionization energies, dipole moments, bond lengths, etc., and explaining the fundamental chemical law of alternating polarity.[4]

A general theory of the electronic structure of conjugated systems based on these ideas has later been developed by Coulson and Longuet-Higgins.[5] By introducing the new and useful concepts of total charge orders, bond orders, and mutual polarizabilities of all the mobile electrons, they could obtain valuable information particularly about such properties of the molecule as are independent of the adjustable parameters. Their theory was still based on the "naïve" assumption that the total energy of the mobile electrons could be derived simply by summing the orbital energies of all occupied orbitals,[6] and the basic quantities mentioned above could then be obtained as the first and second derivatives of this energy with respect to the perturbation integrals.

Although the naïve theory has been remarkably successful in treating the ground state of the conjugated compounds, it has usually failed when one has tried to extend it to the excited states. There are also other strong indications that a more exact theory would be desirable. It is well known that a better theoretical approach can be based on an antisymmetrized molecular wave function, which is approximated by a determinant or a sum of determinants constructed from molecular spin orbitals. We note that, in this case, the molecular orbitals and the orbital energies play still a fundamental role,[7] but that the sum of the orbital energies involved has lost its simple physical meaning. This implies that it is probably just as important to investigate the separate orbital energies and their derivatives with respect to the perturbation integrals as it was to consider the "total" quantities, obtained by simply summing the contributions from all the mobile electrons.

The purpose of this paper is therefore to give a theory

* Work supported by the U. S. Office of Naval Research under Contract N6ori-107, Task Order I, with Duke University.
† Permanent address: Institute of Mechanics and Mathematical Physics, University of Uppsala, Uppsala, Sweden.
[1] E. Hückel, Z. Physik **70**, 204 (1931).
[2] E. Hückel, Z. Physik **72**, 310 (1931); **76**, 628 (1932).
[3] G. W. Wheland and L. Pauling, J. Am. Chem. Soc. **57**, 2091 (1939). See also G. W. Wheland, J. Am. Chem. Soc. **64**, 902 (1942), and H. C. Longuet-Higgins and C. A. Coulson, Trans. Faraday Soc. **43**, 87 (1947).
[4] A survey of the development of the theory, treating mostly bond lengths but also other properties, has recently been given by J. Lennard-Jones, Proc. Roy. Soc. (London) **A207**, 75 (1951), where also a list of references may be found.
[5] C. A. Coulson and H. C. Longuet-Higgins, Proc. Roy. Soc. (London) **A191**, 39; **192**, 16 (1947); **193**, 447, 456; **195**, 188 (1948).
[6] Compare V. Fock, Z. Physik **61**, 126 (1930); see also R. G. Parr, J. Chem. Phys. **19**, 799 (1951).
[7] Compare also the band theory of crystals.

of the mobile electrons of a conjugated system, which is a generalization of the ideas introduced by Coulson and Longuet-Higgins, but where, instead of the naïve total energy and its derivatives, we will investigate the behavior of the separate molecular orbitals and orbital energies under the influence of a perturbation caused by the substitution in the system of one or more heteroatoms. We will define a series of quantities, separate charge orders, bond orders, and mutabilities, which can be derived from the orbital energies in the same way as the total quantities could be derived from the previous "total energy." In this case, particular attention has to be paid to the treatment of the *degenerate* levels, i.e., the molecular orbitals having the same orbital energy, and, for this purpose, we will use a special perturbation scheme which was recently described by the author. The perturbation treatment will be carried out explicitly to the second order in the energies and to the first order in the orbitals.

The results obtained are independent of all adjustable parameters, and we note that they can be used in the naïve semi-empirical theory as well as in a more elaborate theory based on an antisymmetrized molecular wave function. In this paper, we will consider only the problem of calculating the separate molecular orbitals and orbital energies by using perturbation theory, and the question, how these orbitals should be properly combined in order to correspond to the various molecular states, will be treated in a later publication.[8]

As an example of the theory, numerical applications will be carried out in detail on the perturbed benzene ring. Separate charge orders, bond orders, and mutabilities will be tabulated, and the orbital energies for a ring perturbed by one or two heteroatoms will be explicitly given.

PART I. ON THE GENERAL MOLECULAR-ORBITAL THEORY OF CONJUGATED SYSTEMS

1. The Effective Hamiltonian and the Secular Equation; The Overlapping Problem

The molecular orbital method for treating properties of molecules is essentially based on the idea of the existence of an *effective Hamiltonian* H_{eff}, which is a one-electron operator working on the space-coordinates, $\mathbf{x}=(x_1, x_2, x_3)$, of a single electron. The physical meaning of H_{eff} is simple: it is the quantum-mechanical equivalent to the energy of a single electron moving in the potential field of the nuclear framework and of all the other electrons. The molecular orbitals $\psi(\mathbf{x})$ and the orbital energies ϵ are then given as the eigenfunctions and the eigenvalues of the Schrödinger equation

$$H_{eff}\psi=\epsilon\psi. \tag{1}$$

The idea that the behavior of each electron in a many-electron system is approximately regulated by an effective Hamiltonian goes back to Hartree, who developed it for the atomic case. Later this idea was refined by Slater, Fock, and Dirac, showing that the effective Hamiltonian could be derived from the ordinary Hamiltonian for the total many-electron system by using the variational principle and forms of the total wave function approximated by simple products or antisymmetrized products of one-electron wave functions. In this paper we will confine ourselves to considering only closed-shell ground states, but, even in this simple case, the mathematical expression for H_{eff} is rather complicated: H_{eff} is the sum of the operator for the kinetic energy of the electron and the operator for the potential energy of the electron in the Coulomb field of the nuclei and of all electrons belonging to the system, minus the exchange operator for the electron in the field of all electrons. The effect of the exchange operator is essentially that it subtracts the interaction between the electron in a particular orbital and itself from the Coulomb potential.[9] A more detailed discussion of this subject for the molecular case will be given in another paper. Here it is sufficient that the operator H_{eff} exists and that it is the *same* for all orbitals. The last fact means also that, in the theoretical part, it is not necessary to distinguish between the different types of the orbitals.[10]

Because of the difficulty of treating the eigenvalue problem (1) exactly, we will here use the approximate MO–LCAO approach,[11] where the molecular orbitals (MO) are formed by linear combinations of the atomic orbitals (AO) associated with the molecule under consideration. These atomic orbitals ϕ_μ $(\mu=1, 2, \cdots, n)$ are here assumed to be real and normalized. Atomic orbitals belonging to the same atom are further orthogonal, and for different atoms they are overlapping with *overlap integrals* $S_{\mu\nu}$ defined by

$$S_{\mu\nu}=\int \phi_\mu\phi_\nu d\tau-\delta_{\mu\nu}. \tag{2}$$

The overlap integrals form together a matrix $\mathbf{S}$, which is real and symmetric, $S_{\mu\nu}=S_{\nu\mu}$. The fundamental quantities in the theory are the matrix elements of H_{eff} with respect to these AO:

$$H_{\mu\nu}=\int \phi_\mu H_{eff}\phi_\nu d\tau. \tag{3}$$

The quantities $H_{\mu\mu}=\alpha_\mu$ and $H_{\mu\nu}=\beta_{\mu\nu}(\mu\neq\nu)$ are in the literature usually called the Coulomb and exchange integrals, respectively, but this description is not a particularly happy one, since, among other things, H_{eff}

[8] P. O. Löwdin, "On the basis of the molecular orbital theory of molecules" (to be published).

[9] See, for instance, J. C. Slater, Phys. Rev. **81**, 385 (1951).

[10] Compare P. A. M. Dirac, Proc. Cambridge Phil. Soc. **26**, 376 (1930). See also F. Seitz, *Modern Theory of Solids* (McGraw-Hill Book Company, Inc., New York, 1940), p. 245.

[11] The names and abbreviations used here are mainly those introduced by Mulliken.

contains also the kinetic energy operator in addition to the electrostatic parts.

In a large part of the literature, the overlap integrals (2) have simply been neglected, but a number of authors has shown that they are in reality of fundamental importance. Here we will treat the non-orthogonality problem by using the simple scheme previously developed by the author.[12] In addition to the ordinary AO ϕ_μ, we will introduce a set of orthonormalized atomic orbitals (ON–AO) φ_μ ($\mu=1, 2, \cdots, n$), given by the matrix formula

$$\varphi=\phi(1+S)^{-\frac{1}{2}} \tag{4}$$

or

$$\varphi_\mu=\phi_\mu-\tfrac{1}{2}\sum_\alpha \phi_\alpha S_{\alpha\mu}+\tfrac{3}{8}\sum_{\alpha\beta}\phi_\alpha S_{\alpha\beta}S_{\beta\mu}-\cdots. \tag{5}$$

It is easily shown that $\int \varphi_\mu\varphi_\nu d\tau=\delta_{\mu\nu}$. The ordinary AO ϕ_μ are *localized*, whereas the ON–AO φ_μ are only semi-localized; the latter orbitals have further a many-orbital character, which sometimes will lead to important physical consequences.[13] In addition to (3), we will also introduce the matrix elements

$$H_{\mu\nu}'=\int \varphi_\mu H_{\text{eff}}\varphi_\nu d\tau, \tag{6}$$

and between $\mathbf{H}'$ and $\mathbf{H}$ there is then the matrix relation

$$\mathbf{H}'=(1+S)^{-\frac{1}{2}}\mathbf{H}(1+S)^{-\frac{1}{2}}. \tag{7}$$

We have previously pointed out an interesting difference between $\mathbf{H}'$ and $\mathbf{H}$. The matrix $\mathbf{H}'$ has the fundamental property that its nondiagonal elements are invariant against an arbitrary change k of the zero-point of H_{eff}, whereas the diagonal elements all undergo the same change k. This does not apply to $\mathbf{H}$, which means that $\mathbf{H}'$ (but not $\mathbf{H}$) may have a simple physical interpretation. Following a suggestion of Chirgwin and Coulson, we will call the elements $H_{\mu\mu}'=\alpha_\mu'$ and $H_{\mu\nu}'=\beta_{\mu\nu}'(\mu\neq\nu)$ the *charge affinity* of the ON–AO μ and the *bond affinity* of the bond $\mu-\nu$, respectively. A purely theoretical evaluation of the elements of $\mathbf{H}'$ and $\mathbf{H}$ is a rather complicated mathematical problem,[14] and in the naïve theory they have, therefore, usually been determined by fitting some derived quantities to observed data. However, it may be emphasized that, due to the invariance condition pointed out above and the necessity of taking the overlap into consideration in almost all cases, it is in reality only the matrix $\mathbf{H}'$ which should be used for this fitting process.

In the following treatment, we will characterize a molecular orbital by an *upper* index j, k, $\cdots$, and an atomic orbital by a *lower* index μ, ν, $\cdots$. In the MO–LCAO approach, the molecular orbitals ψ^j are formed by linear combination of the given AO or of the ON–AO:

$$\psi^j=\sum_\mu \varphi_\mu C_\mu{}^j. \tag{8}$$

In order to determine the values of the complex or real coefficients $C_\mu{}^j$, which correspond to the best approximation of the eigenfunctions of H_{eff}, we will use the variation principle:

$$\epsilon^j=\int \psi^{j*}H_{\text{eff}}\psi^j d\tau=\text{extreme value}, \tag{9}$$

$$\int \psi^{j*}\psi^j d\tau=1, \tag{10}$$

which leads to the linear equation system

$$\sum_{\nu=1}^{n}(H_{\mu\nu}'-\epsilon^j\delta_{\mu\nu})C_\nu{}^j=0, \quad \mu=1, 2\cdots n \tag{11}$$

where the quantities ϵ^j are the best approximations for the orbital energies, which can be obtained by this approach. The energies are determined by the condition

$$\det\{H_{\mu\nu}'-\epsilon\delta_{\mu\nu}\}=0, \tag{12}$$

and when this secular equation is solved, the coefficients can be found from (11). Due to the Hermitean property of H_{eff}, two MO belonging to two different values of ϵ are always orthogonal to each other. If m solutions of (12) appear to be equal, the corresponding level is degenerate, and, in this case, there exist m linearly independent solutions of (11), which may be chosen orthogonal to each other. In this way, the set of MO forms an orthonormalized system, and, since the relation (8)

$$\psi=\varphi\mathbf{C} \tag{13}$$

represents a transformation between two orthonormalized systems, the matrix $\mathbf{C}$ of the coefficients must be a *unitary* matrix:

$$\mathbf{C}^\dagger\mathbf{C}=\mathbf{C}\mathbf{C}^\dagger=\mathbf{1}. \tag{14}$$

Here we have used the notation that, if $\mathbf{A}$ is an arbitrary matrix, $\mathbf{A}^\dagger$ denotes its Hermitean adjoint matrix defined by $A_{\mu\nu}{}^\dagger=A_{\nu\mu}{}^*$.

2. Charge and Bond Orders for Individual Orbitals

In their general theory of conjugated systems, Coulson and Longuet-Higgins introduced the useful concepts of charge and bond orders of the *total* system of mobile electrons. Here we will further develop this idea by investigating the contribution to these quantities from the separate orbitals involved. In fact, separate bond orders have been treated previously by Coulson,[15] and the importance of separate charge orders has been stressed recently by Lennard-Jones[16] and by Fukui,

[12] P. O. Löwdin, Arkiv Mat. Astron. Fysik **35A**, 9 (1947); *A Theoretical Investigation into Some Properties of Ionic Crystals* (thesis) (Almqvist & Wiksell, Uppsala, Sweden, 1948); J. Chem. Phys. **18**, 365 (1950). Compare also B. H. Chirgwin and C. A. Coulson, Proc. Roy. Soc. (London) **A201**, 196 (1950).

[13] For instance, the *many-body forces* in ionic crystals; see reference 12.

[14] For a more detailed study, see reference 8.

[15] C. A. Coulson, Proc. Roy. Soc. (London) **A169**, 413 (1939).

[16] J. Lennard-Jones, see reference 4.

Yonezawa, and Shingu.[17] Let us therefore in greater detail consider the quantities

$$q_\mu{}^j = C_\mu{}^{j*} C_\mu{}^j, \quad p_{\mu\nu}{}^j = \tfrac{1}{2}(C_\mu{}^{j*} C_\nu{}^j + C_\nu{}^{j*} C_\mu{}^j). \tag{15}$$

According to (8), the quantity $|C_\mu{}^j|^2$ measures the fraction of the time the electron in the MO ψ^j spends in the ON–AO φ_μ, or more approximately "at the atom μ," and $q_\mu{}^j$ will therefore be called the *charge order at atom μ of the orbital j*. Following Coulson,[15] the quantity $p_{\mu\nu}{}^j$ $(\mu \neq \nu)$ will be interpreted as the *bond order of the bond $\mu-\nu$ of the orbital j*. The total charge order q_μ and the total bond order $p_{\mu\nu}$ of a complex of electrons are then found by summing over the orbitals involved:

$$q_\mu = \sum_j q_\mu{}^j, \quad p_{\mu\nu} = \sum_j p_{\mu\nu}{}^j, \tag{16}$$

giving the quantities investigated by Coulson and Longuet-Higgins.

By using (11) and its conjugate complex relation,

$$\sum_\nu H_{\mu\nu}' C_\nu{}^j = \epsilon^j C_\mu{}^j, \quad \sum_\nu H_{\mu\nu}' C_\nu{}^{j*} = \epsilon^j C_\mu{}^{j*},$$

and multiplying the first with $C_\mu{}^{j*}$ and the second with $C_\mu{}^j$, we obtain a formula for the connection between the separate charge and bond orders:

$$\sum_{\nu \neq \mu} H_{\mu\nu}' p_{\mu\nu}{}^j = (\epsilon^j - H_{\mu\mu}') q_\mu{}^j. \tag{17}$$

A similar simple relation for the total quantities does not exist.

We note that there is also a close connection between the quantities (15) and the orbital energies. From (9), (8), and (6), it follows

$$\epsilon^j = \sum_{\mu\nu} C_\mu{}^{j*} H_{\mu\nu}' C_\nu{}^j. \tag{18}$$

Let us first consider a *nondegenerate* level, and let us assume that each element $H_{\mu\nu}'$ obtains an independent symmetric variation $dH_{\mu\nu}' = dH_{\nu\mu}'$. According to (11) and (12), both the orbital energy ϵ^j and the coefficients $C_\mu{}^j$ are then changed by infinitesimal quantities, and, by taking the derivative of (18) with respect to $H_{\mu\nu}'$ and by using (11) and the normalization condition, we obtain for every nondegenerate level j:

$$q_\mu{}^j = \frac{\partial \epsilon^j}{\partial H_{\mu\mu}'}, \quad p_{\mu\nu}{}^j = -\frac{1}{2}\frac{\partial \epsilon^j}{\partial H_{\mu\nu}'}, \quad (\mu \neq \nu). \tag{19}$$

From (18) we get by a second derivation

$$\begin{aligned}
&\frac{\partial q_\mu{}^j}{\partial H_{\kappa\kappa}'} = \frac{\partial^2 \epsilon^j}{\partial H_{\kappa\kappa}' \partial H_{\mu\mu}'} = \frac{\partial q_\kappa{}^j}{\partial H_{\mu\mu}'}; \\
&\frac{\partial q_\mu{}^j}{\partial H_{\kappa\lambda}'} = \frac{\partial^2 \epsilon^j}{\partial H_{\kappa\lambda}' \partial H_{\mu\mu}'} = 2\frac{\partial p_{\kappa\lambda}{}^j}{\partial H_{\mu\mu}'}; \\
&\frac{\partial p_{\mu\nu}{}^j}{\partial H_{\kappa\lambda}'} = -\frac{1}{2}\frac{\partial^2 \epsilon^j}{\partial H_{\kappa\lambda}' \partial H_{\mu\nu}'} = \frac{\partial p_{\kappa\lambda}{}^j}{\partial H_{\mu\nu}'}.
\end{aligned} \tag{20}$$

[17] Fukui, Yonezawa, and Shingu, J. Chem. Phys. **20**, 722 (1952).

This gives the following three reciprocity theorems: For a given nondegenerate level j, the change of the charge order of an atom μ with respect to the change of the charge affinity of the atom κ equals the change of the charge order of the atom κ with respect to a change of the charge affinity of the atom μ; the change of the charge order of an atom μ with respect to a change of the bond affinity of the bond $\kappa-\lambda$ is twice the change of the bond order of the bond $\kappa-\lambda$ with respect to the change of the charge affinity of the atom μ; and, finally, the change of the bond order of the bond $\mu-\nu$ with respect to a change of the bond affinity of the bond $\kappa-\lambda$ equals the change of the bond order of the bond $\kappa-\lambda$ with respect to a change of the bond affinity of the bond $\mu-\nu$.

The corresponding theorems for the total quantities were first stated by Coulson and Longuet-Higgins.[5]

The treatment of a *degenerate* energy level ϵ^j is somewhat more complicated due to the ambiguity in the choice of the eigenfunctions. Let m^J be the order of the degeneracy, and let further (J) denote the class of all molecular orbitals associated with the eigenvalue ϵ^j. In order to describe this class, we will use an orthonormalized set of m^J orbitals j', j'', j''', $\cdots$ etc., which is determined except for a unitary transformation. We note that, for each orbital of this set, the quantities $q_\mu{}^j$ and $p_{\mu\nu}{}^j$ formally exist according to (15), but that they cannot have any direct physical interpretation, since they are not invariant against unitary transformations within the class (J). However, by summing once over the contributions from all indices j', j'', j''', $\cdots$, we get quantities

$$\begin{aligned}
q_\mu{}^J &= \sum_j^{(J)} q_\mu{}^j = \sum_j^{(J)} C_\mu{}^j C^\dagger{}^j{}_\mu, \\
p_{\mu\nu}{}^J &= \sum_j^{(J)} p_{\mu\nu}{}^j = \frac{1}{2}\sum_j^{(J)} (C_\mu{}^j C^\dagger{}^j{}_\nu + C_\nu{}^j C^\dagger{}^j{}_\mu),
\end{aligned} \tag{21}$$

which have the desired invariance property and consequently are independent of the particular reference set. These quantities $q_\mu{}^J$ and $p_{\mu\nu}{}^J$ will be called the *total charge orders* and the *total bond orders* of the degenerate level J, respectively. By treating the energy sum

$$\epsilon^J = \sum_j^{(J)} \epsilon^j = m^J \epsilon^j \tag{22}$$

in the same way as (18), we then easily obtain

$$q_\mu{}^J = \frac{\partial \epsilon^J}{\partial H_{\mu\mu}'}, \quad p_{\mu\nu}{}^J = -\frac{1}{2}\frac{\partial \epsilon^J}{\partial H_{\mu\nu}'}, \quad (\mu \neq \nu). \tag{23}$$

The treatment of a real degeneracy usually does not render any serious difficulty. The problem is instead to find the eventual splitting of a degenerate level under the influence of a perturbation.

In this connection, a few words may be said about the use of *complex* coefficients $C_\mu{}^i$ in forming the molecular orbitals. The effective Hamiltonian H_{eff} is always Hermitean, but, in most molecular applications, it is also *real*. The absence of the imaginary unit i in H_{eff} means that all its eigenfunctions can be represented in a real form. For a nondegenerate level, it is usually simplest to use the real description, since a complex factor is entirely without importance and vanishes automatically in forming, e.g., the quantities (15). For a degenerate level, it may sometimes be feasible to consider a complex description[18] of the class (J), but even in such a case the complex reference set can be derived from a real reference set by a unitary transformation. This implies that the sum,

$$\sum_j^{(J)} C_\mu{}^j C_\nu{}^{j*} = \sum_j^{(J)} C_\mu{}^j C^\dagger{}_{j\nu}, \tag{24}$$

is always *real*, since it is real for a real reference set and it is further invariant against unitary transformations within the class (J); see Eq. (60). We have, therefore,

$$\sum_j^{(J)} C_\nu{}^j C_\mu{}^{j*} = (\sum_j^{(J)} C_\mu{}^j C_\nu{}^{j*})^* = \sum_j^{(J)} C_\mu{}^j C_\nu{}^{j*}, \tag{25}$$

and the symmetrization in the second of the relations (21) is therefore in reality unnecessary.

Finally, we observe that the quantities (15) are only special elements of a more general matrix

$$d_{\mu\nu}{}^{jk} = \tfrac{1}{2}(C_\mu{}^{j*} C_\nu{}^k + C_\nu{}^{j*} C_\mu{}^k), \tag{26}$$

which will be called the *complete charge and bond order matrix* with respect to pairs of individual orbitals. This matrix fulfills the symmetry relations

$$d_{\mu\nu}{}^{jk} = d_{\nu\mu}{}^{jk}, \quad d_{\mu\nu}{}^{kj} = (d_{\mu\nu}{}^{jk})^*. \tag{27}$$

According to (15) and (26), we have further

$$q_\mu{}^j = d_{\mu\mu}{}^{jj}, \quad p_{\mu\nu}{}^j = d_{\mu\nu}{}^{jj}, \quad (\mu \neq \nu), \tag{28}$$

which means that the separate charge and bond orders are particular elements of the matrix $\mathbf{d}^{jk}$ for $j=k$.

The quantities (15) and (26) are useful both in the "naïve" MO-theory and in a more elaborate theoretical treatment of a molecular system. In the semi-empirical theory, the *total charge orders* were used already by Wheland and Pauling[3] for investigating the chemical reactivities of the various atoms of a conjugated system, and recently some authors[4,17] have stressed the special importance for this problem of the charge orders of the *frontier* electrons, i.e., the electrons occupying the orbital with the highest energy. All these treatments have been based on a semi-empirical assumption concerning the connection between the charge orders and the reactivities. For this connection the relations (19) may be of fundamental importance. Following Coulson and Longuet-Higgins,[5] we wish to emphasize that it is probable that a closer examination of the connection between the (total and frontier) orbital energies and the reaction energies would give a deeper theoretical understanding of the substitution process, since the charge order for an atom in a specific position gives just the rate of the change of the orbital energy which depends on the change of the charge affinity due to the approach of a substituent.

Sometimes the separate charge and bond orders or the total quantities may be evaluated by special simple rules,[19] and in such cases the corresponding orbital energies may be found by using the relations (19) in a reverse way. Longuet-Higgins[19] has used this reverse process for treating some energy problems in heteroaromatic compounds.

In the semi-empirical theory, the *total bond orders* have been used by Coulson and Longuet-Higgins[5] for determining the bond lengths and the force constants in conjugated systems.

We note that, independent of the interpretation of the separate or total charge and bond orders in the semi-empirical theory, the quantities $d_{\mu\nu}{}^{jk}$ given by (26) are of essential importance also in a more elaborate theoretical approach, since they are very useful for the simplification and systematization of the mathematical expressions involved.[20]

3. Perturbation Theory

Here we will investigate how the separate orbitals, orbital energies, charge orders, and bond orders are affected by the substitution in a given molecule of one or more atoms or groups, which may be considered as perturbations. Let us characterize quantities belonging to the original system by the index zero:

$$\psi^{j(0)} = \sum_\mu \varphi_\mu{}^{(0)} C_\mu{}^{j(0)}, \quad H_{\mu\nu}{}'^{(0)} = \int \varphi_\mu{}^{(0)} H_{\text{eff}}{}^{(0)} \varphi_\nu{}^{(0)} d\tau, \tag{29}$$

whereas for quantities associated with the new molecule we will use the ordinary notations:

$$\psi^j = \sum_\mu \varphi_\mu C_\mu{}^j, \quad H_{\mu\nu}{}' = \int \varphi_\mu H_{\text{eff}} \varphi_\nu d\tau. \tag{30}$$

Both the effective Hamiltonian, the atomic orbitals, the overlapping conditions, and the molecular orbitals may be changed by the substitution, but, if the two molecules under consideration are related closely enough, it is possible to treat these changes by means of perturbation theory. For this purpose we will introduce

[18] See, for instance, the treatment of benzene in Part II.

[19] H. C. Longuet-Higgings, J. Chem. Phys. **18**, 265, 275, 283 (1950).

[20] See P. O. Löwdin, J. Chem. Phys. **19**, 1570, 1579 (1951), and reference 8.

the *perturbation integrals*

$$V_{\mu\nu}=H_{\mu\nu}'-H_{\mu\nu}'^{(0)}, \tag{31}$$

i.e., the changes in charge and bond affinities, which may be expressed as fractions of the integrals $H_{\mu\nu}'^{(0)}$. We observe that a perturbation treatment based on (31) goes beyond the conventional perturbation theory, which would consider only the operator $H_{\text{eff}}-H_{\text{eff}}^{(0)}$ as a perturbation.

According to (11) and (14), our fundamental problem is to solve the matrix equations

$$\mathbf{H'C}=\mathbf{C\varepsilon}, \quad \mathbf{C}^\dagger\mathbf{C}=\mathbf{CC}^\dagger=\mathbf{1}, \tag{32}$$

where $\boldsymbol{\varepsilon}$ is the diagonal matrix formed from the unknown eigenvalues ϵ^j. This means that we have to find a unitary matrix $\mathbf{C}$ which transforms $\mathbf{H'}$ into diagonal form:

$$\mathbf{C}^\dagger\mathbf{H'C}=\text{diagonal matrix}, \tag{33}$$

and the orbital energies are then determined by the diagonal row of the right-hand side matrix. For the original "unperturbed" molecule, we obtain in the same way

$$\mathbf{H}'^{(0)}\mathbf{C}^{(0)}=\mathbf{C}^{(0)}\boldsymbol{\varepsilon}^{(0)}, \quad \mathbf{C}^{(0)\dagger}\mathbf{C}^{(0)}=\mathbf{C}^{(0)}\mathbf{C}^{(0)\dagger}=\mathbf{1}. \tag{34}$$

The definition (31) gives the matrix relation

$$\mathbf{H'}=\mathbf{H}'^{(0)}+\mathbf{V}, \tag{35}$$

where $\mathbf{V}$ is the matrix of the elements $V_{\mu\nu}$. By introducing the notations

$$\mathbf{C}=\mathbf{C}^{(0)}\mathbf{X}, \quad \mathbf{v}=\mathbf{C}^{(0)\dagger}\mathbf{V}\mathbf{C}^{(0)}, \tag{36}$$

and by multiplying (32) to the left by $\mathbf{C}^{(0)\dagger}$, we obtain the following perturbation equation in the MO-space:

$$(\boldsymbol{\varepsilon}^{(0)}+\mathbf{v})\mathbf{X}=\mathbf{X}\boldsymbol{\varepsilon}, \quad \mathbf{X}^\dagger\mathbf{X}=\mathbf{X}\mathbf{X}^\dagger=\mathbf{1}. \tag{37}$$

This equation can now be solved by ordinary perturbation theory. For the treatment of a degenerate level we will use the simple scheme the author[21] recently developed by generalizing an idea given by Gora.[22] This scheme was particularly meant for applications to quantum chemistry.

Simplification of the Matrix Elements used in the Perturbation Scheme

For the sake of simplicity, let us treat here also a non-degenerate level as the simplest case of a degeneracy with $m^J=1$. Let us then consider an arbitrary index j, which belongs to a degenerate class (J) of the unperturbed molecule. In order to solve the eigenvalue problem (37) by perturbation theory explicitly to the first and second orders in the eigenfunctions and eigenvalues, respectively, we will introduce the quantities

$$(j\alpha)=\epsilon^{j(0)}-\epsilon^{\alpha(0)}, \tag{38}$$

$$U^{jk}=\epsilon^{j(0)}\delta^{jk}+v^{jk}+\sum_{\alpha\neq(J)}\frac{v^{j\alpha}v^{\alpha k}}{(j\alpha)}, \tag{39}$$

where, in the last term, we sum only over $\alpha\neq(J)$, i.e., we omit all terms for which $(j\alpha)=0$. According to reference 21, the eigenvalues of the class (J) of the perturbed molecule are then given by the m^J roots of the algebraic equation:

$$\begin{vmatrix} U^{j'j'}-\epsilon; & U^{j'j''}; & U^{j'j'''}; & \cdots \\ U^{j''j'}; & U^{j''j''}-\epsilon; & U^{j''j'''}; & \cdots \\ U^{j'''j'}; & U^{j'''j''}; & U^{j'''j'''}-\epsilon; & \cdots \\ \cdots & \cdots & \cdots & \cdots \end{vmatrix}=0. \tag{40}$$

The problem of the splitting of the levels in the class (J) is therefore solved by finding the eigenvalues of a submatrix $\mathbf{U}_{\text{sub}}$ of order m^J. Let further $\mathbf{X}_{\text{sub}}$ be the unitary matrix of order m^J, which transforms $\mathbf{U}_{\text{sub}}$ into diagonal form. According to reference 21, the coefficients X^{ki} in general are then given by

$$X^{ki}=\begin{cases} X_{\text{sub}}{}^{ki}, & k \text{ in } (J) \\ \dfrac{1}{(jk)}\displaystyle\sum_{\alpha=(J)} v^{k\alpha}X_{\text{sub}}{}^{\alpha i}, & k\neq(J) \end{cases} \tag{41}$$

and the perturbation problem is solved.

We are here particularly interested in the simplification of the explicit forms of the matrix elements in the relations (39)–(41). The perturbation matrix $\mathbf{V}$ in (31) is symmetric, $V_{\mu\nu}=V_{\nu\mu}$, and by using this property and (26), the perturbation matrix $\mathbf{v}$ in (36) takes the form

$$v^{jk}=\sum_{\mu\nu}C^{\dagger j}{}_{\mu}{}^{(0)}V_{\mu\nu}C_{\nu}{}^{k(0)}=\sum_{\mu\nu}V_{\mu\nu}d_{\mu\nu}{}^{jk(0)}, \tag{42}$$

which implies that the complete charge and bond order matrix $\mathbf{d}^{(0)}$ is of essential importance in the perturbation scheme. In the following we will omit the index zero on the matrix $\mathbf{d}$, if there is no possibility of misunderstanding.

For the second-order term in U^{jk} in (39), we obtain in the same way by a symmetrization

$$\begin{aligned}\sum_{\alpha\neq(J)}\frac{v^{j\alpha}v^{\alpha k}}{(j\alpha)}&=\sum_{\alpha\neq(J)}\sum_{\mu\nu\kappa\lambda}V_{\mu\nu}V_{\kappa\lambda}\frac{d_{\mu\nu}{}^{j\alpha}d_{\kappa\lambda}{}^{\alpha k}}{(j\alpha)}\\ &=\tfrac{1}{2}\sum_{\mu\nu\kappa\lambda}\sum_{\alpha\neq(J)}V_{\mu\nu}V_{\kappa\lambda}\frac{d_{\mu\nu}{}^{j\alpha}d_{\kappa\lambda}{}^{\alpha k}+d_{\kappa\lambda}{}^{j\alpha}d_{\mu\nu}{}^{\alpha k}}{(j\alpha)}\\ &=\tfrac{1}{2}\sum_{\mu\nu\kappa\lambda}V_{\mu\nu}V_{\kappa\lambda}\pi_{\mu\nu,\kappa\lambda}{}^{jk},\end{aligned} \tag{43}$$

[21] P. O. Löwdin, J. Chem. Phys. **19**, 1396 (1951). The author's attention has been drawn to the existence of three recently published papers, which were not available to us during the preparation of our manuscript and which we therefore would like to refer to here, namely: S. Sueoka, J. Phys. Soc. (Japan) **4**, 361 (1949); M. H. L. Pryce, Proc. Phys. Soc. (London) **A63**, 25 (1950); M. Lax, Phys. Rev. **79**, 200 A (1950). Sueoka treating the interaction between two diagonal subsystems, and Pryce and Lax investigating the degeneracy problem have obtained results similar to those given in our paper. In all these independent works, the methods of derivation are closely related to the simple idea introduced by Gora, reference 22.

[22] E. Gora, Z. Physik **120**, 121 (1942–43).

where we have introduced the notation

$$\pi_{\mu\nu,\kappa\lambda}{}^{jk}=\sum_{\alpha\neq(J)}\frac{d_{\mu\nu}{}^{j\alpha}d_{\kappa\lambda}{}^{\alpha k}+d_{\kappa\lambda}{}^{j\alpha}d_{\mu\nu}{}^{\alpha k}}{(j\alpha)}. \tag{44}$$

The quantities π fulfill the following symmetry relations:

$$\begin{gathered}\pi_{\mu\nu,\kappa\lambda}{}^{jk}=\pi_{\nu\mu,\kappa\lambda}{}^{jk},\quad \pi_{\mu\nu,\kappa\lambda}{}^{jk}=\pi_{\kappa\lambda,\mu\nu}{}^{jk},\\ \pi_{\mu\nu,\kappa\lambda}{}^{kj}=(\pi_{\mu\nu,\kappa\lambda}{}^{jk})^{*},\end{gathered} \tag{45}$$

and, as we shall see later, they are closely related to the mutual polarizabilities introduced by Coulson and Longuet-Higgins.[5] Using a name proposed by Lennard-Jones[4] for quantities of this type, we will call the matrix $\boldsymbol{\pi}$ the *complete mutability matrix*.

By using (42) and (43), the fundamental matrix element U^{jk} given by (39) can now be written in the form

$$U^{jk}=\epsilon^{j(0)}\delta^{jk}+\sum_{\mu\nu}V_{\mu\nu}d_{\mu\nu}{}^{jk(0)}+\tfrac{1}{2}\sum_{\mu\nu\kappa\lambda}V_{\mu\nu}V_{\kappa\lambda}\pi_{\mu\nu,\kappa\lambda}{}^{jk(0)}, \tag{46}$$

where it is expressed directly in the perturbations $V_{\mu\nu}$ of the charge and bond affinities.

In the case of a *real* effective Hamiltonian H_{eff}, it is convenient to introduce also the auxiliary quantities

$$\Omega_{\mu\nu}{}^{j}=\sum_{\alpha\neq(J)}\frac{C_{\mu}{}^{\alpha}C_{\nu}{}^{\alpha*}}{(j\alpha)} \tag{47}$$

for the evaluation of the mutabilities π and the coefficients in the eigenfunctions. According to (25), we have the symmetry relation

$$\Omega_{\mu\nu}{}^{j}=\sum_{\alpha\neq(J)}\frac{d_{\mu\nu}{}^{\alpha\alpha}}{(j\alpha)}=\Omega_{\nu\mu}{}^{j}, \tag{48}$$

and, by using (44), (26), (47), and (48), we obtain the formula

$$\pi_{\mu\nu,\kappa\lambda}{}^{jk}=\tfrac{1}{2}(d_{\mu\kappa}{}^{jk}\Omega_{\nu\lambda}{}^{j}+d_{\mu\lambda}{}^{jk}\Omega_{\nu\kappa}{}^{j}+d_{\nu\kappa}{}^{jk}\Omega_{\mu\lambda}{}^{j}+d_{\nu\lambda}{}^{jk}\Omega_{\mu\kappa}{}^{j}), \tag{49}$$

giving a simple way of calculating the mutabilities.

Now it remains to compute the coefficients $C_{\mu}{}^{j}$ used in (30) for forming the MO of the perturbed molecule. According to (36) and (41), we obtain

$$C_{\mu}{}^{j}=\sum_{k}C_{\mu}{}^{k(0)}X^{kj}=\sum_{k=(J)}C_{\mu}{}^{k(0)}X_{\text{sub}}{}^{kj}+\sum_{k\neq(J)}C_{\mu}{}^{k(0)}\frac{1}{(jk)}\sum_{\alpha=(J)}v^{k\alpha}X_{\text{sub}}{}^{\alpha j}. \tag{50}$$

Changing the names of the summation indices k and α in the last term, and using (42), (26), (47), and (48), we can derive the formula

$$\begin{cases}C_{\mu}{}^{j}=\sum_{k=(J)}T_{\mu}{}^{k(0)}X_{\text{sub}}{}^{kj},\\ T_{\mu}{}^{k(0)}=C_{\mu}{}^{k(0)}+\tfrac{1}{2}\sum_{\kappa\lambda}V_{\kappa\lambda}(\Omega_{\mu\kappa}{}^{j}C_{\lambda}{}^{k}+\Omega_{\mu\lambda}{}^{j}C_{\kappa}{}^{k})^{(0)}.\end{cases} \tag{51}$$

(i) *The Nondegenerate Case.* Let us investigate in greater detail a level j which is nondegenerate in the original molecule, i.e., $m^{J}=1$. According to (40), the fundamental secular equation takes the form

$$U^{jj}-\epsilon=0, \tag{52}$$

and (46) gives then the following expression for the orbital energy in the perturbed molecule:

$$\epsilon^{j}=\epsilon^{j(0)}+\sum_{\mu\nu}V_{\mu\nu}d_{\mu\nu}{}^{jj}+\tfrac{1}{2}\sum_{\mu\nu\kappa\lambda}V_{\mu\nu}V_{\kappa\lambda}\pi_{\mu\nu,\kappa\lambda}{}^{jj}. \tag{53}$$

The unitary matrix $\mathbf{X}_{\text{sub}}$ has a single element $X_{\text{sub}}{}^{jj}=1$, and formula (51) gives therefore for the coefficients in the perturbed MO

$$C_{\mu}{}^{j}=C_{\mu}{}^{j(0)}+\tfrac{1}{2}\sum_{\kappa\lambda}V_{\kappa\lambda}(\Omega_{\mu\kappa}{}^{j}C_{\lambda}{}^{j}+\Omega_{\mu\lambda}{}^{j}C_{\kappa}{}^{j})^{(0)}. \tag{54}$$

The separate charge and bond orders may be derived from the orbital energy by using (19), and we obtain

$$\begin{aligned}q_{\mu}{}^{j}&=q_{\mu}{}^{j(0)}+\sum_{\kappa\lambda}V_{\kappa\lambda}\pi_{\mu\mu,\kappa\lambda}{}^{jj(0)},\\ p_{\mu\nu}{}^{j}&=p_{\mu\nu}{}^{j(0)}+\sum_{\kappa\lambda}V_{\kappa\lambda}\pi_{\mu\nu,\kappa\lambda}{}^{jj(0)}.\end{aligned} \tag{55}$$

Hence it is possible to find the orbital energy, the form of the MO, and the separate charge and bond orders for the perturbed molecule, if the quantities $\mathbf{d}$ and $\boldsymbol{\pi}$ are tabulated for the original compound. By another differentiation of (55), we get

$$\begin{aligned}\pi_{\mu\mu,\kappa\kappa}{}^{jj}&=\frac{\partial q_{\mu}{}^{j}}{\partial V_{\kappa\kappa}}=\frac{\partial^{2}\epsilon^{j}}{\partial V_{\mu\mu}\partial V_{\kappa\kappa}},\\ \pi_{\mu\mu,\kappa\lambda}{}^{jj}&=\frac{1}{2}\frac{\partial q_{\mu}{}^{j}}{\partial V_{\kappa\lambda}}=\frac{\partial p_{\kappa\lambda}{}^{j}}{\partial V_{\mu\mu}}=\frac{1}{2}\frac{\partial^{2}\epsilon^{j}}{\partial V_{\mu\mu}\partial V_{\kappa\lambda}},\quad(\kappa\neq\lambda),\\ \pi_{\mu\nu,\kappa\lambda}{}^{jj}&=\frac{1}{2}\frac{\partial p_{\mu\nu}{}^{j}}{\partial V_{\kappa\lambda}}=\frac{1}{4}\frac{\partial^{2}\epsilon^{j}}{\partial V_{\mu\nu}\partial V_{\kappa\lambda}},\quad(\mu\neq\nu,\ \kappa\neq\lambda),\end{aligned} \tag{56}$$

showing that, for a nondegenerate level, the mutabilities are the second derivatives of the orbital energy with respect to the charge and bond affinities. Combining (17) and (56), we obtain then easily a series of connection formulas for the separate mutabilities.

(ii) *The Degenerate Case.* Let us now go back to the degenerate case with $m^{J}\geq 2$. In order to describe the degenerate class (J) of the unperturbed molecule, we will use a particular orthonormalized set $j', j'', j''', \ldots$ of MO belonging to (J) as a fixed reference set. The

matrices $d_{\mu\nu}{}^{jk}$ and $\pi_{\mu\nu,\kappa\lambda}{}^{jk}$ exist formally according to (26) and (44) for each pair (j, k) of orbitals of this set, but we note that these quantities cannot have any direct physical meaning, since they are not invariant against a unitary transformation of the reference system. We may consider $d_{\mu\nu}{}^{jk}$ and $\pi_{\mu\nu,\kappa\lambda}{}^{jk}$ as the first and second derivatives, respectively, of the matrix elements U^{jk}, defined by (46), with respect to the perturbation integrals, but even these relations have only formal meaning.

In this connection it is of interest to consider the transformations of the quantities $d_{\mu\nu}{}^{jk}$, $\Omega_{\mu\nu}{}^{j}$, $\pi_{\mu\nu,\kappa\lambda}{}^{jk}$, U^{jk}, etc., under a unitary transformation of the reference set, which may be of the form $\bar{C}=\mathbf{CD}$, or

$$\bar{C}_{\mu}{}^{j}=\sum_{\alpha=(J)} C_{\mu}{}^{\alpha}D^{\alpha j}, \tag{57}$$

where $\mathbf{D}$ is an arbitrary unitary matrix of order m^J:

$$\mathbf{D}^{\dagger}\mathbf{D}=\mathbf{D}\mathbf{D}^{\dagger}=\mathbf{1}. \tag{58}$$

Combining (26) and (57), we obtain

$$\bar{d}_{\mu\nu}{}^{jk}=\sum_{\alpha,\beta=(J)} D^{\dagger j\alpha}d_{\mu\nu}{}^{\alpha\beta}D^{\beta k}. \tag{59}$$

For the total quantities (21), obtained by summing once over the contributions from all indices j', j'', j''', $\cdots$ associated with the class (J), we get

$$\bar{d}_{\mu\nu}{}^{JJ}=\sum_{j=(J)}\bar{d}_{\mu\nu}{}^{jj}=\sum_{\alpha,\beta=(J)} d_{\mu\nu}{}^{\alpha\beta}\sum_{j=(J)} D^{\beta j}D^{\dagger j\alpha}$$

$$=\sum_{\alpha,\beta=(J)} d_{\mu\nu}{}^{\alpha\beta}\delta^{\alpha\beta}=\sum_{\alpha=(J)} d_{\mu\nu}{}^{\alpha\alpha}=d_{\mu\nu}{}^{JJ}, \tag{60}$$

where we have utilized the unitary property (58) of $\mathbf{D}$. This gives a detailed proof of the invariance theorem stated in connection with (21).

In forming the quantities $\Omega_{\mu\nu}{}^{j}$ by means of (48), we sum only over complete classes of eventually degenerate levels, and according to (60), they are therefore invariant:

$$\Omega_{\mu\nu}{}^{j,\mathrm{tr}}=\Omega_{\mu\nu}{}^{j}, \tag{61}$$

and they are further the same for all indices j belonging to the same degenerate class. By using (49), (59), and (61), we get for the mutabilities

$$\bar{\pi}_{\mu\nu,\kappa\lambda}{}^{jk}=\sum_{\alpha,\beta=(J)} D^{\dagger j\alpha}\pi_{\mu\nu,\kappa\lambda}{}^{\alpha\beta}D^{\beta k}. \tag{62}$$

If we define the *total mutabilities* of the class (J) by by summing once over all indices j', j'', j''', $\cdots$:

$$\pi_{\mu\nu,\kappa\lambda}{}^{JJ}=\sum_{j=(J)}\pi_{\mu\nu,\kappa\lambda}{}^{jj}, \tag{63}$$

we obtain again a quantity which can be shown to be invariant in the same way as (60). All these quantities are, of course, associated with the unperturbed molecule, but, for the sake of simplicity, we have omitted the upper index zero.

Let us now consider the quantities in the perturbation scheme. According to (59) and (62), the elements U^{jk} of the fundamental matrix (46) have the transformation property

$$\bar{U}^{jk}=\sum_{\alpha,\beta=(J)} D^{\dagger j\alpha}U^{\alpha\beta}D^{\beta k}. \tag{64}$$

Hence, the matrix $\bar{U}$ undergoes only a unitary transformation, which implies that its eigenvalues are invariant. According to (60), the sum of the diagonal elements of $\bar{U}$ is another invariant.

Let us assume that the degeneracy is completely removed by the perturbation under consideration. If $\mathbf{X}_{\mathrm{sub}}$ and $\bar{\mathbf{X}}_{\mathrm{sub}}$ are the unitary matrices of order m^J which transform $\mathbf{U}$ and $\bar{U}$, respectively, to diagonal form, then we have the relation

$$\bar{\mathbf{X}}_{\mathrm{sub}}=\mathbf{D}^{\dagger}\mathbf{X}, \tag{65}$$

for we have the matrix equations

$$\bar{\mathbf{X}}_{\mathrm{sub}}{}^{\dagger}\bar{U}\bar{\mathbf{X}}_{\mathrm{sub}}=\mathbf{X}_{\mathrm{sub}}{}^{\dagger}\mathbf{D}\cdot\mathbf{D}^{\dagger}\mathbf{U}\mathbf{D}\cdot\mathbf{D}^{\dagger}\mathbf{X}_{\mathrm{sub}}$$
$$=\mathbf{X}_{\mathrm{sub}}{}^{\dagger}\mathbf{U}\mathbf{X}_{\mathrm{sub}}=\text{diagonal matrix}. \tag{66}$$

The matrix $\mathbf{T}$, defined by (51), has the transformation property $\bar{T}=\mathbf{TD}$. Using this relation and (65), we find that also the coefficients of the perturbed MO given by (51) are invariant, for

$$\bar{C}=\bar{T}\bar{\mathbf{X}}_{\mathrm{sub}}=\mathbf{TD}\cdot\mathbf{D}^{\dagger}\mathbf{X}_{\mathrm{sub}}=\mathbf{T}\mathbf{X}_{\mathrm{sub}}=\mathbf{C}. \tag{67}$$

This means that the eigenvalues and the eigenfunctions are completely independent of the particular choice of reference set used for describing the degenerate class of the unperturbed molecule.

If the degenerate class (J) is split up in the perturbed molecule, we can determine the separate charge and bond orders of the perturbed orbitals according to (51) and the definitions (15), but, in such a case, the algebraic equation (40) has first to be solved.

There is one information about the perturbed molecule which can be obtained without solving (40) explicitly, namely the properties of the total quantities associated with the class (J) as a whole. By applying the coefficient theorem for the sum of the roots of an algebraic equation to (40), and by using (60) and (63), we get

$$\epsilon^J=\sum_{j=(J)}\epsilon^j=\sum_{j=(J)} U^{jj}=m^J\epsilon^{J(0)}$$
$$+\sum_{\mu\nu} V_{\mu\nu}d_{\mu\nu}{}^{JJ(0)}+\tfrac{1}{2}\sum_{\mu\nu,\kappa\lambda} V_{\mu\nu}V_{\kappa\lambda}\pi_{\mu\nu,\kappa\lambda}{}^{JJ(0)}, \tag{68}$$

a result which is independent of the splitting of the class (J). Hence we obtain for the *total charge and bond orders* associated with the class (J) in the perturbed molecule

$$q_{\mu}{}^{J}=\frac{\partial\epsilon^J}{\partial V_{\mu\mu}}=q_{\mu}{}^{J(0)}+\sum_{\kappa\lambda} V_{\kappa\lambda}\pi_{\mu\mu,\kappa\lambda}{}^{JJ(0)},$$
$$p_{\mu\nu}{}^{J}=\frac{1}{2}\frac{\partial\epsilon^J}{\partial V_{\mu\nu}}=p_{\mu\nu}{}^{J(0)}+\sum_{\kappa\lambda} V_{\kappa\lambda}\pi_{\mu\nu,\kappa\lambda}{}^{JJ(0)},\quad(\mu\neq\nu), \tag{69}$$

TABLE I.

Notation used here	Notation used by Coulson and Longuet-Higgins	
$\pi_{\mu\mu,\,\kappa\kappa}^{\rm tot}$	$\pi_{\mu,\kappa}$	
$\pi_{\mu\mu,\,\kappa\lambda}^{\rm tot}$	$\pi_{\kappa\lambda,\,\mu}=\frac{1}{2}\pi_{\mu,\,\kappa\lambda}$	$(\kappa\neq\lambda)$
$\pi_{\mu\nu,\,\kappa\lambda}^{\rm tot}$	$\frac{1}{2}\pi_{\mu\nu,\,\kappa\lambda}$	$(\mu\neq\nu,\ \kappa\neq\lambda)$

showing that the total mutabilities $\pi_{\mu\nu,\,\kappa\lambda}^{JJ(0)}$ may be considered as the second derivatives of the sum ϵ^J of the orbital energies of class (J), with respect to the perturbation integrals $V_{\mu\nu}$.

In this connection, we may also say a few words about the total quantities associated with a complex of electrons, obtained by summing over all occupied orbitals:

$$\epsilon^{\rm tot}=\sum_j \epsilon^j,\quad q_\mu^{\rm tot}=\sum_j q_\mu^j,\quad p_{\mu\nu}^{\rm tot}=\sum_j p_{\mu\nu}^j,$$
$$d_{\mu\nu}^{\rm tot}=\sum_j d_{\mu\nu}^{jj},\quad \pi_{\mu\nu,\,\kappa\lambda}^{\rm tot}=\sum_j \pi_{\mu\nu,\,\kappa\lambda}^{jj}. \tag{70}$$

By summing over all classes involved in the system, we obtain from (68) and (70),

$$\epsilon^{\rm tot}=\epsilon^{\rm tot(0)}+\sum_{\mu\nu} V_{\mu\nu}d_{\mu\nu}^{\rm tot(0)}+\tfrac{1}{2}\sum_{\mu\nu\kappa\lambda} V_{\mu\nu}V_{\kappa\lambda}\pi_{\mu\nu,\,\kappa\lambda}^{\rm tot(0)}. \tag{71}$$

For the total charge and bond orders, we get further

$$q_\mu^{\rm tot}=\frac{\partial\epsilon^{\rm tot}}{\partial V_{\mu\mu}}=q_\mu^{\rm tot(0)}+\sum_{\kappa\lambda} V_{\kappa\lambda}\pi_{\mu\mu,\,\kappa\lambda}^{\rm tot(0)},$$
$$p_{\mu\nu}^{\rm tot}=-\frac{1}{2}\frac{\partial\epsilon^{\rm tot}}{\partial V_{\mu\nu}}=p_{\mu\nu}^{\rm tot(0)}+\sum_{\kappa\lambda} V_{\kappa\lambda}\pi_{\mu\nu,\,\kappa\lambda}^{\rm tot(0)}, \tag{72}$$

and, for the total mutabilities, we finally obtain

$$\pi_{\mu\mu,\,\kappa\kappa}^{\rm tot}=\frac{\partial q_\mu^{\rm tot}}{\partial V_{\kappa\kappa}}=\frac{\partial^2\epsilon^{\rm tot}}{\partial V_{\mu\mu}\partial V_{\kappa\kappa}},$$
$$\pi_{\mu\mu,\,\kappa\lambda}^{\rm tot}=-\frac{1}{2}\frac{\partial q_\mu^{\rm tot}}{\partial V_{\kappa\lambda}}=\frac{\partial p_{\kappa\lambda}^{\rm tot}}{\partial V_{\mu\mu}}=-\frac{1}{2}\frac{\partial^2\epsilon^{\rm tot}}{\partial V_{\mu\mu}\partial V_{\kappa\lambda}},\quad (\kappa\neq\lambda) \tag{73}$$
$$\pi_{\mu\nu,\,\kappa\lambda}^{\rm tot}=-\frac{1}{2}\frac{\partial p_{\mu\nu}^{\rm tot}}{\partial V_{\kappa\lambda}}=-\frac{1}{4}\frac{\partial^2\epsilon^{\rm tot}}{\partial V_{\mu\nu}\partial V_{\kappa\lambda}},\quad (\mu\neq\nu,\ \kappa\neq\lambda).$$

All these total quantities have previously been investigated by Coulson and Longuet-Higgins,[5] who introduced the name *mutual polarizabilities* for the derivatives of the charge and bond orders. Since this term is used in another meaning also in the theory of dielectrics, we have here instead used the name *mutabilities* proposed by Lennard-Jones.[4] We note that, in order to maintain the symmetry relations (45), which for the total quantities take the form

$$\pi_{\mu\nu,\,\kappa\lambda}^{\rm tot}=\pi_{\nu\mu,\,\kappa\lambda}^{\rm tot},\quad \pi_{\mu\nu,\,\kappa\lambda}^{\rm tot}=\pi_{\kappa\lambda,\,\mu\nu}^{\rm tot}, \tag{74}$$

and which are of essential importance for the simplicity of our formulas, we have changed also the notations slightly. Consequently, for quantities $\pi_{\mu\nu,\,\kappa\lambda}$ having the last pair of indices corresponding to a bond, a factor $\frac{1}{2}$ in the treatment in reference 5 is here included in the symbol itself; see also Table I for comparison.

Treatment of a Doubly Degenerate Level

The solution of the secular equation (40) is simple in the case of a doubly degenerate level, $m^J=2$, and, since this type of degeneracy is also of particular importance in the theory of conjugated systems, we will treat it in somewhat greater detail here. This example may be instructive for the study of the higher degeneracies, too.

(a) *Real reference set.* We may use either a real or a complex description of the degenerate class (J), and we will begin with the real case. The matrix U^{ik}, defined by (39), is Hermitean, $U^{ki}=U^{ik*}$, and, for a purely real representation, it is therefore also symmetric:

$$U^{ki}=U^{ik}. \tag{75}$$

For the sake of simplicity, let us denote the reference orbitals of the class by the upper indices 1 and 2. The submatrix $\mathbf{U}$ associated with the class has the form

$$\mathbf{U}_{\rm sub}=\begin{pmatrix} U^{11} & U^{12} \\ U^{21} & U^{22}\end{pmatrix}, \tag{76}$$

and, according to (40), its eigenvalues are given by

$$\epsilon=\tfrac{1}{2}\{(U^{11}+U^{22})\pm[(U^{11}-U^{22})^2+4U^{12}U^{21}]^{\frac{1}{2}}\}. \tag{77}$$

The unitary matrix $\mathbf{X}$, which transforms $\mathbf{U}$ to diagonal form, is found by solving the equation system $\mathbf{UX}=\mathbf{X}\boldsymbol{\epsilon}$ for the known eigenvalues. By introducing the angle φ given by

$$\operatorname{tg}\varphi=\frac{(U^{11}-U^{22})-[(U^{11}-U^{22})^2+4U^{12}U^{21}]^{\frac{1}{2}}}{2U^{12}}, \tag{78}$$

the solution may be expressed in the form

$$\mathbf{X}_{\rm sub}=\begin{pmatrix} \cos\varphi & \sin\varphi \\ -\sin\varphi & \cos\varphi\end{pmatrix}, \tag{79}$$

and the coefficients C_μ^i of the perturbed MO can then be calculated according to (51). A still simpler formula for φ is given below.

(b) *Complex reference set.* We shall discuss a complex description of the doubly degenerate class, which is so chosen that the two reference orbitals for the unperturbed molecule are *conjugate complex* functions. By using this property and the ordinary definitions, it is easily shown that the charge orders, the bond orders, and the mutabilities for $j=k$ are the same for both unperturbed orbitals. Since the diagonal elements of the matrix $\bar{U}_{\rm sub}$ for the perturbed molecule are also the

same, the eigenvalues of $\bar{U}_{sub}$ are now given by

$$\epsilon=\bar{U}^{11}\pm|\bar{U}^{12}|. \tag{80}$$

If the angle φ is defined as half the argument of the complex quantity U^{12}, the matrix $\bar{U}_{sub}$ is further transformed to diagonal form by the unitary matrix

$$\bar{X}_{sub}=\frac{1}{\sqrt{2}}\begin{pmatrix} e^{i\varphi} & -ie^{i\varphi} \\ e^{-i\varphi} & ie^{-i\varphi} \end{pmatrix}, \tag{81}$$

and the coefficients $C_\mu{}^i$ of the perturbed MO can then be calculated according to (51).

Finally, we will investigate the connection between the real and complex descriptions. For the unperturbed molecule, our complex conjugate reference set may be obtained from an arbitrary real set by a unitary transformation (57) with the transformation matrix

$$\mathbf{D}=\frac{1}{\sqrt{2}}\begin{pmatrix} 1 & 1 \\ i & -i \end{pmatrix}. \tag{82}$$

According to (64), we then obtain $\bar{U}_{sub}=\mathbf{D}^\dagger\mathbf{U}_{sub}\mathbf{D}$, or

$$\bar{U}_{sub}=\begin{pmatrix} \bar{U}^{11} & \bar{U}^{12} \\ \bar{U}^{21} & \bar{U}^{22} \end{pmatrix}$$

$$=\frac{1}{2}\begin{pmatrix} U^{11}+U^{22}; & U^{11}-U^{22}-2iU^{12} \\ U^{11}-U^{22}+2iU^{12}; & U^{11}+U^{22} \end{pmatrix}. \tag{83}$$

A comparison between (77) and (80) based on (83) shows at once that the eigenvalues are the same. The angle φ is in the complex case defined by

$$\text{tg}\,2\varphi=I\{U^{12}\}/Re\{U^{12}\}=-2U^{12}/(U^{11}-U^{22}), \tag{84}$$

which implies that it is identical with the angle φ in the real case, since (84) can be derived from (78). Finally, for the matrix (81), we have $\bar{X}_{sub}=D^\dagger X_{sub}$ in agreement with (65).

4. Hybridization between Atomic Orbitals of 2*s* and 2*p* Types

The MO–LCAO theory of molecules is essentially based on the assumption that it is possible to make a convenient choice of atomic orbitals for the atoms constituting the molecule under consideration, and we will therefore discuss this problem in greater detail. In investigating the simplest conjugated compounds we are particularly interested in the AO of the atoms of the elements belonging to the second row of the periodic system. In the ground state of these elements, the two electrons occupying the 1*s*-orbital do not take part in bond formation, so we have to consider only the outer electrons distributed over the four orbitals 2*s*, 2*px*, 2*py*, and 2*pz*, having about the same energy. These AO are given by the formulas

$$\phi_{2s}=\frac{1}{(4\pi)^{\frac{1}{2}}}\frac{f_{2s}(r)}{r}, \qquad \phi_{2px}=\left(\frac{3}{4\pi}\right)^{\frac{1}{2}}\frac{f_{2p}(r)}{r^2}x,$$

$$\phi_{2py}=\left(\frac{3}{4\pi}\right)^{\frac{1}{2}}\frac{f_{2p}(r)}{r^2}y, \quad \phi_{2pz}=\left(\frac{3}{4\pi}\right)^{\frac{1}{2}}\frac{f_{2p}(r)}{r^2}z, \tag{85}$$

where $f_{2s}(r)$ and $f_{2p}(r)$ are the radial wave functions, which may be of Slater or Hartree-Fock type. The *p*-orbitals are direction dependent, and we introduce the notation $2p\xi$ for a $2p$-orbital in the direction of the ξ-axis, where ξ also may be the distance to a plane through the origin perpendicular to this axis. If the quantities $\cos\gamma_{\xi x}$, $\cos\gamma_{\xi y}$, and $\cos\gamma_{\xi z}$ are the direction cosines for the ξ-axis, then we have

$$\phi_{2p\xi}=\left(\frac{3}{4\pi}\right)^{\frac{1}{2}}\frac{f_{2p}(r)}{r^2}\xi,$$

$$\xi=x\cos\gamma_{\xi x}+y\cos\gamma_{\xi y}+z\cos\gamma_{\xi z}. \tag{86}$$

Such a $2p\xi$-orbital is antisymmetric with respect to the plane $\xi=0$, and it has therefore the same extension along the positive and negative directions of the ξ-axis.

As was first pointed out by Pauling[23] and Slater,[24] an orbital of the form

$$h=a\phi_{2s}+(1-a^2)^{\frac{1}{2}}\cdot\phi_{2p\xi}, \tag{87}$$

with $a>0$, has its largest extension in the direction of the ξ-axis, and it may therefore be convenient for the description of a *directed valency*. The mixing of *s*- and *p*-orbitals is called a hybridization, and the orbital h in (87) is called a *hybrid* with its direction along the positive ξ-axis.

The theory of hybridization has been treated by several authors,[25] and here we only wish to stress the simplicity of the mathematics involved, if the theory is presented in matrix form. From the four AO given by (85), we can by linear combinations form four linearly independent hybrids h_1, h_2, h_3, and h_4, and we may write the hybridization in the form $\mathbf{h}=\boldsymbol{\phi}\mathbf{Y}$, or

$$h_k=\sum_\alpha \phi_\alpha Y_{\alpha k}, \tag{88}$$

where the transformation matrix has the form

$$\mathbf{Y}=\begin{bmatrix} a_1 & a_2 & a_3 & a_4 \\ a_{x1} & a_{x2} & a_{x3} & a_{x4} \\ a_{y1} & a_{y2} & a_{y3} & a_{y4} \\ a_{z1} & a_{z2} & a_{z3} & a_{z4} \end{bmatrix}. \tag{89}$$

Here we restrict $\mathbf{Y}$ to having only real elements. The quantity $a_k{}^2$ gives the amount of *s*-character in the

[23] L. Pauling, Proc. Nat. Acad. Sci. U. S. **14**, 359 (1928); J. Am. Chem. Soc. **53**, 1367 (1931).

[24] J. C. Slater, Phys. Rev. **37**, 481 (1931).

[25] See, for instance, C. A. Coulson, Proc. Roy. Soc. (Edinburgh) **61**, 115 (1941).

hybrid h_k. According to Pauling,[26] the approximate bond strength of the hybrid h_k is given by the expression $a_k+(3-3a_k^2)^{\frac{1}{2}}$, but we are not going to use this property here. The given set (85) is orthonormalized, and, if we impose on the hybrids the fundamental condition that they should be orthonormalized, too, the hybridization matrix $\mathbf{Y}$ must be a unitary matrix, $\mathbf{Y}^\dagger\mathbf{Y}=\mathbf{Y}\mathbf{Y}^\dagger=1$, or

$$\sum_\alpha Y_{\alpha k}Y_{\alpha l}=\sum_\alpha Y_{k\alpha}Y_{l\alpha}=\delta_{kl}. \tag{90}$$

A comparison between Eqs. (86)–(89) shows further that the largest extension of the hybrid h_k is along a k-axis having the direction cosines

$$\cos\gamma_{xk}=\frac{a_{xk}}{(1-a_k^2)^{\frac{1}{2}}},\quad \cos\gamma_{yk}=\frac{a_{yk}}{(1-a_k^2)^{\frac{1}{2}}},$$

$$\cos\gamma_{zk}=\frac{a_{zk}}{(1-a_k^2)^{\frac{1}{2}}}. \tag{91}$$

By using this relation and the orthogonality condition $a_{xk}a_{xl}+a_{yk}a_{yl}+a_{zk}a_{zl}=-a_ka_l$, contained in (90), we can then derive the following basic formula for the angle γ_{kl} between the axes of two hybrids, h_k and h_l:

$$\alpha_{kl}=\cos\gamma_{kl}=-\frac{a_ka_l}{\{(1-a_k)^2(1-a_l^2)\}^{\frac{1}{2}}}. \tag{92}$$

The general problem of the evaluation of the appropriate matrix $\mathbf{Y}$ for a particular atom in a molecule is very important, but the principle of "maximum overlapping," stated by Pauling and by Slater for this purpose, has not yet been fully theoretically proven.[27] Recently, Mulliken[28] has investigated the connection between the overlap integrals and the amounts of s-character of the bonding hybrids in a diatomic molecule, but the corresponding bond energies are still treated only by means of a semi-empirical formula.

We note that the simple formula (92) will sometimes give useful informations about the form of the matrix $\mathbf{Y}$, for instance, when the amounts of s-character of the four hybrids h_k have been found in some other way. By using the four quantities a_1, a_2, a_3, a_4, fulfilling the condition $\sum a_k^2=1$ contained in (90), formula (92) gives the angles between the axes of the hybrids. Utilizing these angles for fixing four axes in the space, determined except for a rigid rotation, we can then evaluate the remaining part of the elements of $\mathbf{Y}$ from the known direction cosines by using (91):

$$a_{xk}=(1-a_k^2)^{\frac{1}{2}}\cos\gamma_{xk},\quad a_{yk}=(1-a_k^2)^{\frac{1}{2}}\cos\gamma_{yk},$$
$$a_{zk}=(1-a_k^2)^{\frac{1}{2}}\cos\gamma_{zk}. \tag{93}$$

This gives a very simple method for constructing, e.g., the conventional matrices $\mathbf{Y}$ for the basic digonal, trigonal, and tetragonal hybridizations[25] associated with the following sets of s-coefficients: $a_k=(1/2^{\frac{1}{2}}, 1/2^{\frac{1}{2}}, 0, 0)$, $a_k=(1/3^{\frac{1}{2}}, 1/3^{\frac{1}{2}}, 1/3^{\frac{1}{2}}, 0)$, and $a_k=(1/2, 1/2, 1/2, 1/2)$, respectively.

We note that also the reverse process may be useful, i.e., the calculation of the amount of s-character and the construction of the explicit forms of the hybrids from, for instance, experimentally known bond angles. For this purpose, let us introduce a quantity κ_k, the *characteristic s-number* of the hybrid h_k, by

$$\kappa_k=\frac{a_k}{(1-a_k^2)^{\frac{1}{2}}},\quad a_k=\frac{\kappa_k}{(1+\kappa_k^2)^{\frac{1}{2}}}. \tag{94}$$

The basic formula (92) may then be written in the form

$$\alpha_{kl}=-\kappa_k\kappa_l. \tag{95}$$

Because of the product form and the condition $\sum a_k^2=\sum\kappa_k^2/(1+\kappa_k)^2=1$, only *three* of the six elements α_{kl} are independent in the general case. Let us first consider the case that the directions of the three hybrids h_1, h_2, and h_3 are known, and that the angles between them all are *different* from 90°. The characteristic s-numbers κ_1, κ_2, κ_3 can then be determined from the three known direction cosines α_{12}, α_{23}, α_{31}, according to (95), which gives

$$\omega=(-\alpha_{12}\alpha_{23}\alpha_{31})^{\frac{1}{2}},$$
$$\kappa_1=-\frac{\omega}{\alpha_{23}},\quad \kappa_2=-\frac{\omega}{\alpha_{31}},\quad \kappa_3=-\frac{\omega}{\alpha_{12}}. \tag{96}$$

The coefficients a_1, a_2, and a_3 are then found from (94), and a_4 is computed from the condition $\sum a_k^2=1$. Finally the other elements of $\mathbf{Y}$ are calculated according to (93).

As an example of this procedure, we shall discuss the molecules in which we are particularly interested here, namely the *conjugated systems*, i.e., the organic compounds having alternating single and double bonds in the conventional structure formulas. By using x-ray and electron diffraction technique, one has found experimentally that the conjugated systems are almost completely coplanar and that the bond angles in the plane are 120°. This indicates strongly that the bonds associated with these "trivalent" carbon atoms or their equivalents are formed by three coplanar hybrids h_1, h_2, and h_3 with the angles 120° between them, whereas the

[26] L. Pauling, *Nature of the Chemical Bond* (Cornell University Press, Ithaca, New York, 1940), p. 85.
[27] Compare A. Maccoll, Trans. Faraday Soc. **46**, 359 (1950) and W. Moffitt, Proc. Roy. Soc. (London) **A202**, 534, 548 (1950).
[28] R. S. Mulliken, J. Chem. Phys. **19**, 900 (1951); R. S. Mulliken, J. Am. Chem. Soc. **72**, 4493 (1950).

type of the fourth hybrid is not known from the beginning.

However, utilizing the three angles of 120° and formulas (96) and (94), we obtain:

$$\alpha_{12}=\alpha_{23}=\alpha_{31}=\cos 120°=-\tfrac{1}{2}, \quad \omega=1/2\sqrt{2},$$
$$\kappa_1=\kappa_2=\kappa_3=1/\sqrt{2}, \tag{97}$$
$$a_1=a_2=a_3=1/\sqrt{3}; \quad a_4=0.$$

If our basic assumption of the orthonormality of the hybrids is true, the fourth orbital h_4 must therefore be a pure $2p$-orbital which is perpendicular to the (h_1, h_2, h_3)-plane.

Let us put our coordinate system with the xy-plane in the molecular plane of the conjugated system. The three hybrids in this plane are usually called σ-orbitals and are denoted by σ_1, σ_2, σ_3, and the fourth hybrid is called a π-orbital. By fixing the directions of these orbitals according to Fig. 1 and by using (93), we obtain for the matrix $\mathbf{Y}$:

$$\mathbf{Y}=\begin{pmatrix} \frac{1}{\sqrt{3}} & \frac{1}{\sqrt{3}} & \frac{1}{\sqrt{3}} & 0 \\ \sqrt{2}/\sqrt{3} & -\frac{1}{(6)^{\frac{1}{2}}} & -\frac{1}{(6)^{\frac{1}{2}}} & 0 \\ 0 & \frac{1}{\sqrt{2}} & -\frac{1}{\sqrt{2}} & 0 \\ 0 & 0 & 0 & 1 \end{pmatrix}. \tag{98}$$

Of the four outer electrons of a normal carbon atom in the "trivalent" state, three electrons are placed in the orbitals σ_1, σ_2, and σ_3, forming *single bonds* together with other similar electrons with opposite spin from the neighboring atoms, and the fourth electron is placed in the π-orbital contributing to a *partial double bond* according to the MO-theory. Here we are particularly interested in these π-electrons.

In the MO–LCAO theory developed in this paper, we have up till now taken *all* bonding electrons into account in forming the matrices $\mathbf{S}$, $\mathbf{H}$, and $\mathbf{H}'$ for the molecule under consideration. However, the σ-orbitals and the π-orbitals are of a different symmetry type, since the former are symmetric and the latter antisymmetric with respect to the molecular plane. For the overlap matrix $S_{\mu\nu}$ as well as for the energy matrix $H_{\mu\nu}$ and $H_{\mu\nu}'$, based on a Hartree-Fock-Dirac effective Hamiltonian for the ground state, this implies that all *mixed* elements with $(\mu\nu)=(\pi\sigma)$ will vanish identically. All these matrices will therefore exactly split into a

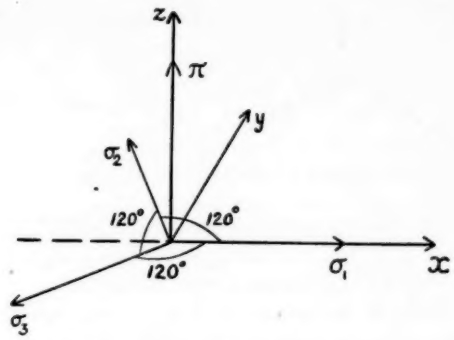

FIG. 1. Trigonal hybridization in a conjugated system.

π-part and a σ-part:

$$\mathbf{S}=\begin{pmatrix} \mathbf{S}_\pi & 0 \\ 0 & \mathbf{S}_\sigma \end{pmatrix}, \quad \mathbf{H}=\begin{pmatrix} \mathbf{H}_\pi & 0 \\ 0 & \mathbf{H}_\sigma \end{pmatrix},$$
$$\mathbf{H}'=\begin{pmatrix} \mathbf{H}_\pi' & 0 \\ 0 & \mathbf{H}_\sigma' \end{pmatrix}. \tag{99}$$

This result does not mean that the treatment of the π-electrons can be entirely separated from the treatment of the σ-electrons since both types are involved in the mathematical expression for the effective Hamiltonian causing a rather complicated interaction of the Coulomb and the exchange type. However, if the elements of $\mathbf{H}'$ in some way have been evaluated, then the questions of finding the eigenvalues and the eigenfunctions of $\mathbf{H}_\pi'$ and $\mathbf{H}_\sigma'$ may be considered as independent problems. A more detailed study of the possibility of separating the treatments of the π- and σ-electrons has recently been given by Altmann.[29]

Before concluding this section, we will go back to the general hybridization problem, where it remains to investigate the special case when the three hybrids h_1, h_2, and h_3 with known directions form angles, of which at least one is 90°. In this case the solution (96) breaks down, and the problem must be reexamined.

Let us consider the case of $\alpha_{12}=0$. According to (95), at least one of the relations $\alpha_{13}=0$ or $\alpha_{23}=0$ must hold, and if, e.g., the former is true, we conclude that $\kappa_1=0$ i.e., that the hybrid h_1 is a pure $2p$-orbital, and that the remaining orbitals h_2, h_3, and h_4 all have their directions in the plane perpendicular to h_1. More information is then needed for solving the problem, and we will therefore consider the triple α_{23}, α_{34}, and α_{42}, which usually determines the values of κ_2, κ_3, and κ_4, in a way analogous to (96). However, also this solution breaks down if, e.g., $\alpha_{23}=0$. In this case, at least one of the relations $\alpha_{24}=0$ or $\alpha_{34}=0$ must be true, and if the former holds, we conclude that $\kappa_2=0$, i.e., that h_2 is a pure $2p$-orbital, and that the remaining orbitals h_3 and h_4 must have their directions along the line perpendicu-

[29] S. L. Altmann, Proc. Roy. Soc. (London) **A210**, 327, 343 (1952). See also Coulson, March, and Altman, Proc. Nat. Acad. Sci. U. S. **38**, 372 (1952).

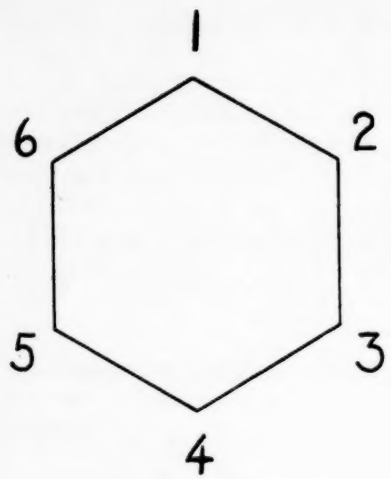

FIG. 2. Numbering of the carbon atoms in a benzene ring.

lar to the (h_1, h_2)-plane. We observe that it is impossible to determine the amount of s-character in these orbitals from the angular dependence, but that we have $a_3^2+a_4^2=1$. The acetylene molecule C_2H_2 is an example of a hybridization of this type.

PART II. APPLICATIONS OF THE MOLECULAR ORBITAL THEORY TO THE PERTURBED BENZENE RING

5. Properties of the π-Orbitals of the Unperturbed Benzene Molecule

Here we will apply the MO-theory developed in Part I to the treatment of the benzene molecule, C_6H_6, which represents the simplest example of a conjugated system of the ring type. According to the general theorem proven in the previous section in connection with the formula (99), the fundamental matrices **S**, **H**, and **H′** for *all* bonding electrons exactly split into two parts, a π-part and a σ-part. In this paper we are going to discuss only the former, i.e., the matrices $\mathbf{S}_\pi$, $\mathbf{H}_\pi$, and $\mathbf{H}_\pi'$ of order six, which are associated with the six π-orbitals of the ring. We will number the atoms and the π-AO according to Fig. 2.

The benzene problem is essentially simplified by the high symmetry D_{6h} of the molecule. The π-problem may be considered as having a special form of *cyclic symmetry* of order N, for $N=6$.[30] Treating first the general case, a matrix **A** is said to be a cyclic matrix of order N, if it fulfills the conditions

$$A_{\mu,\nu}=A_{0,\nu-\mu}=A_p, \quad (p=\nu-\mu); \quad A_{p+N}=A_N. \tag{100}$$

Such a matrix is a linear form of the more general crystal matrix, and it is easily proven[31] that the matrix **A** is transformed into diagonal form by the unitary matrix

$$C_\mu{}^j=\frac{1}{N^{\frac{1}{2}}}e^{2\pi i\mu j/N}, \quad j=0, 1, \cdots, N-1. \tag{101}$$

[30] The case of $N=3$ occurs, for example, in a treatment of borazole by C. C. J. Roothaan and R. S. Mulliken, J. Chem. Phys. **16**, 118 (1948).

[31] See F. Bloch, Z. Physik **52**, 555 (1929).

The eigenvalues of **A** are the diagonal elements of the matrix $\mathbf{a}=\mathbf{C}^\dagger\mathbf{A}\mathbf{C}$:

$$a^j=(\mathbf{C}^\dagger\mathbf{A}\mathbf{C})^{jj}=\sum_{p=0}^{N-1}A_p\exp(2\pi ipj/N). \tag{102}$$

By using the same unitary transformation, it is also easy to calculate any matrix **F**, which is a function of **A**, $\mathbf{F}=F(\mathbf{A})$, for we obtain

$$\mathbf{F}=\mathbf{C}F(\mathbf{C}^\dagger\mathbf{A}\mathbf{C})\mathbf{C}^\dagger=\mathbf{C}F(\mathbf{a})\mathbf{C}^\dagger, \tag{103}$$

and

$$\mathbf{F}_{\mu\nu}=\frac{1}{N}\sum_{j=0}^{N-1}F(a^j)\exp\{2\pi i(\mu-\nu)j/N\}. \tag{104}$$

The product of two cyclic matrices, **A** and **B**, of order N is further another cyclic matrix of the same order, and we have

$$(\mathbf{AB})_p=\sum_{\alpha=0}^{N-1}A_\alpha B_{p-\alpha}. \tag{105}$$

Let us now consider the case of the π-electrons of benzene, i.e., $N=6$. The fundamental matrices **H** and **S** are both cyclic matrices of order 6, and we introduce the customary notations:

$$\begin{aligned}H_{\mu\nu}&=(\alpha, \beta_1, \beta_2, \beta_3, \beta_2, \beta_1)_{\text{cyclic}},\\ S_{\mu\nu}&=(0, S_1, S_2, S_3, S_2, S_1)_{\text{cyclic}}.\end{aligned} \tag{106}$$

By using (105), it is easily shown that the matrices **S** and **H** commute, $\mathbf{SH}=\mathbf{HS}$, and the matrix **H′** given by (7) is therefore simplified to the form

$$\mathbf{H}'=\mathbf{H}(1+\mathbf{S})^{-1}. \tag{107}$$

Since **H′** is another cyclic matrix of order 6, it is also transformed to diagonal form by the unitary transformation (101) with $N=6$, and we obtain the *orbital energies*

$$\epsilon^j=\frac{\alpha+2\beta_1\cos\pi j/3+2\beta_2\cos 2\pi j/3+\beta_3\cos\pi j}{1+2S_1\cos\pi j/3+2S_2\cos 2\pi j/3+S_3\cos\pi j}, \tag{108}$$

where $j=0, 1, \cdots 5$, or $j=0, \pm1, \pm2, 3$. We note that the levels $j=0$ and $j=3$ are nondegenerate, whereas the levels $j=\pm1$ and $j=\pm2$ are doubly degenerate. By using the diagonal matrix $\mathbf{s}=\mathbf{C}^\dagger\mathbf{S}\mathbf{C}$ with elements given by (102), formula (108) is easily derived from (107) by means of the matrix relation

$$\mathbf{C}^\dagger\mathbf{H}'\mathbf{C}=\mathbf{C}^\dagger\mathbf{H}(1+\mathbf{S})^{-1}\mathbf{C}=\mathbf{C}^\dagger\mathbf{H}\mathbf{C}\cdot(1+\mathbf{s})^{-1}. \tag{109}$$

Introducing the quantities $\gamma_k=\beta_k-\alpha S_k$ $(k=1, 2, 3)$, which are invariant[32] against an arbitrary change of the zero-point of the effective Hamiltonian, we can finally write the orbital energies in the form

$$\epsilon^j=\alpha+(2\gamma_1\cos\pi j/3+2\gamma_2\cos 2\pi j/3+\gamma_3\cos\pi j)/(1+s_j). \tag{110}$$

[32] P. O. Löwdin, J. Chem. Phys. **18**, 365 (1950); see p. 368.

According to (101) for $N=6$, the coefficients C in the molecular orbitals are given by

$$C_\mu{}^j=\frac{1}{6^{\frac{1}{2}}}e^{\pi i\mu j/3}, \tag{111}$$

and the MO themselves have therefore the form

$$\psi^j=\frac{1}{6^{\frac{1}{2}}}\sum_{\mu=1}^{6}\varphi_\mu e^{\pi i\mu j/3}, \tag{112}$$

where φ_μ are the orthonormalized π-AO. By using the matrix relation

$$\psi=\varphi\mathbf{C}=\phi(1+\mathbf{S})^{-\frac{1}{2}}\mathbf{C}=\phi\mathbf{C}(1+\mathbf{s})^{-\frac{1}{2}}, \tag{113}$$

the MO can also be expressed in the form

$$\psi^j=(6+6s^j)^{-\frac{1}{2}}\sum_{\mu=1}^{6}\phi_\mu e^{\pi i\mu j/3}, \tag{114}$$

where ϕ_μ are the given AO of the $2pz$-type defined in (85).

Here we have used a conjugate complex description of the degenerate levels, but we note that the most general *real* representation of the coefficients C may be written in the form

$$C_\mu{}^j=\frac{1}{6^{\frac{1}{2}}}\cos\pi\mu j/3,\quad j=0,3$$
$$C_\mu{}^{j'}=\frac{1}{\sqrt{3}}\cos(\alpha+\pi\mu j/3),\quad C_\mu{}^{j''}=\frac{1}{\sqrt{3}}\sin(\alpha+\pi\mu j/3),\quad j=1,2 \tag{115}$$

where α is an arbitrary real angle.

In order to prepare the treatment of the *perturbed* benzene molecule according to Sec. 3, we will now evaluate the fundamental quantities $d_{\mu\nu}{}^{jk}$, $\Omega_{\mu\nu}{}^j$, and $\pi_{\mu\nu,\kappa\lambda}{}^{jk}$ for the unperturbed molecule. According to (26) and (111), we obtain, in the conjugate complex description,

$$d_{\mu\nu}{}^{jk}=\tfrac{1}{6}\exp\pi i(k-j)(\mu+\nu)/6\cdot\cos\pi(k+j)(\mu-\nu)/6, \tag{116}$$

which gives for the separate charge and bond orders

$$q_\mu{}^j=\tfrac{1}{6},\quad p_{\mu\nu}{}^j=\tfrac{1}{6}\cos\pi(\mu-\nu)j/3. \tag{117}$$

By using (48) and (111), we get further for $p=\nu-\mu$:

$$\Omega_{\mu\nu}{}^j=\Omega_{0,\nu-\mu}{}^j=\Omega_p{}^j=\tfrac{1}{6}\sum_{\alpha\neq(J)}\frac{\cos\pi p\alpha/3}{\epsilon^j-\epsilon^\alpha}, \tag{118}$$

where the denominators may be taken from (108) or (110). We note that, for each $j=0$, 1, 2, and 3, there are only four independent elements $\Omega_p{}^j$. The mutabilities are then determined by the general formula (49):

$$\pi_{\mu\nu,\kappa\lambda}{}^{jk}=\frac{1}{2}(d_{\mu\kappa}{}^{jk}\Omega_{\nu-\lambda}{}^j+d_{\mu\lambda}{}^{jk}\Omega_{\nu-\kappa}{}^j+d_{\nu\kappa}{}^{jk}\Omega_{\mu-\lambda}{}^j+d_{\nu\lambda}{}^{jk}\Omega_{\mu-\kappa}{}^j), \tag{119}$$

which for $j=k$ gives

$$\pi_{\mu\nu,\kappa\lambda}{}^{jj}=\frac{1}{12}\{\Omega_{\mu-\kappa}{}^j\cos\pi(\nu-\lambda)/3+\Omega_{\mu-\lambda}{}^j\cos\pi(\nu-\kappa)/3+\Omega_{\nu-\kappa}{}^j\cos\pi(\mu-\lambda)/3+\Omega_{\nu-\lambda}{}^j\cos\pi(\mu-\kappa)/3\}. \tag{120}$$

All the quantities fundamental for a second-order perturbation theory are then evaluated, and the results in Sec. 3 can be directly applied to computing the properties of the perturbed ring. All these results are of a general nature and may be taken over also in a more elaborate MO-theory of the perturbed benzene molecule.

6. The "Nearest Neighbor" Approximation in the Naïve Molecular Orbital Theory

In addition to the general theory given in the previous section, we will now consider in greater detail the "nearest neighbor" approximation in the naïve MO-theory of the perturbed benzene ring. This type of approximation, which is sometimes also called the "tight-binding" approximation, seems to have been first introduced by Bloch[31] in the band theory of metals. It is based on the assumption that, in the matrices $\mathbf{S}$ and $\mathbf{H}$ with respect to the given AO, only the elements associated with the same or adjacent atoms are of importance, whereas elements associated with a pair of higher neighborhood may be neglected. This approximation is characterized by a high simplicity, but it is certainly not very accurate.

The fundamental matrices (106) are in this approximation of the simple form

$$\mathbf{H}=(\alpha,\beta,0,0,0,\beta)_{\text{cyclic}}$$
$$\mathbf{S}=(0,S,0,0,0,S)_{\text{cyclic}}. \tag{121}$$

For S we will use the values $S=0$ (overlap neglected) and $S=0.25$, and further we will use the quantity $\gamma=\beta-\alpha S$. We note that it is easy to evaluate any given function of the matrix $\mathbf{S}$ according to formula (104), and, as examples, we give the matrices

$$(1+\mathbf{S})^{-1}=(1.1555;\ -0.3111;\ 0.0888;\ -0.0444;\ 0.0888;\ -0.3111)_{\text{cyclic}},$$
$$(1+\mathbf{S})^{-\frac{1}{2}}=(1.0548;\ -0.1430;\ 0.0303;\ -0.0129;\ 0.0303;\ -0.1430)_{\text{cyclic}}, \tag{122}$$

for $S=0.25$, which may be useful in treating a molecule having about the same overlapping scheme as benzene.

We observe that the "nearest neighbor" approximation is explicitly based on an assumption concerning the extension of the given AO, which means that it cannot be generalized with the same degree of accuracy to matrices with respect to the ON-AO, which usually have much larger extensions. The matrix $\mathbf{H}'$, evaluated

TABLE II.

j	$S=0$	$S=0.25$
0	$\alpha+2\beta$	$\alpha+1.3333\gamma$
±1	$\alpha+\beta$	$\alpha+0.8\gamma$
±2	$\alpha-\beta$	$\alpha-1.3333\gamma$
3	$\alpha-2\beta$	$\alpha-4\gamma$

(124)

from (107), (121), and (122), has also the form

$$\mathbf{H}'=(\alpha-0.6222\gamma;\ 1.2444\gamma;\ -0.3555\gamma;\ 0.1777\gamma;\ -0.3555\gamma;\ 1.2444\gamma)_{\text{cyclic}}, \quad (123)$$

showing also interaction between ON–AO of higher neighborhood. The matrix (123) was first given in another way by Chirgwin and Coulson.[12]

According to (108) and (110), we obtain the values for the orbital energies ϵ^j of the unperturbed molecule, which are listed in Table II. Hence, the symmetry around the point $\epsilon=\alpha$ is disturbed by the inclusion of the overlap. The matrix $\mathbf{d}$ is given by (116), and, by using (118) and (124), we obtain the values of the quantities $\Omega_p{}^j$ which are presented in Table III. The mutabilities $\pi_{\mu\nu,\kappa\lambda}{}^{jj}$ can then be evaluated by means of (120), and the results for $S=0$ are given in Table IV. As we will see later, the alternating signs in the series of total atom-atom mutabilities for the ground state will render an explanation of the chemical law of "alternating polarity" for benzene. The total atom-bond mutabilities are zero, in agreement with a general theorem given by Coulson and Longuet-Higgins.[5]

In Table V, we have presented a comparison between the values of the separate mutabilities $\pi_{\mu\nu,\kappa\lambda}{}^{jj}$ for $S=0$ and $S=0.25$. The series of total atom-atom mutabilities was first given for $S=0.25$ by Chirgwin and Coulson,[12] who remarked that, except for the change in unit from $1/\beta$ to $1/\gamma$, these total quantities are only slightly affected by the inclusion of the overlap. However, even if this is true for the total mutabilities, the table shows that the *separate* mutabilities are rather strongly changed when going over from $S=0$ to $S=0.25$. This means that if, for instance, the *frontier* electrons turn out to have particular importance, then the overlap must be included from the very beginning, particularly when treating heteromolecules. Finally, we note that there are a series of simple identities and check relations for the mutabilities, which may be derived by considering such perturbations as leave the orbital energies unchanged.

TABLE III(a). The quantities $\Omega_p{}^j$ in units of $1/72\beta$ for $S=0$.

j \ p	0	1	2	3
0	35	5	−13	−19
1	4	−22	−14	−4
2	−4	−22	14	−4
3	−35	5	13	−19

TABLE III(b). The quantities $\Omega_p{}^j$ in units of $1/576\gamma$ for $S=0.25$.

j \ p	0	1	2	3
0	450	126	−198	−306
1	−70	−245	−205	−110
2	−90	−117	45	18
3	−130	−2	38	−50

Charge and Bond Orders of the Perturbed Benzene Ring—the Directing Power of a Perturbation

For the sake of simplicity, let us first consider the case of overlap neglected, $S=0$. Let further the perturbations $V_{\mu\nu}$, defined by (31), be given as fractions of the quantity β:

$$V_{\mu\mu}=\delta_\mu\beta, \quad V_{\mu\nu}=\vartheta_{\mu\nu}\beta \quad (\mu\neq\nu). \quad (125)$$

According to the general formula (72) and Table IV, we obtain for the *total charge orders* q_μ associated with the ground state,

$$q_1=1+(43\delta_1-17\delta_2+\delta_3-11\delta_4+\delta_5-17\delta_6)/108,$$
$$q_2=1+(43\delta_2-17\delta_3+\delta_4-11\delta_5+\delta_6-17\delta_1)/108,$$
$$\cdots \text{ and cyclic.} \quad (126)$$

A special case of these formulas was first given by Wheland and Pauling,[3] and the coefficients in general may be found in Coulson and Longuet-Higgins.[5] Since all atom-bond mutabilities are zero, all the charge orders are independent of the perturbations $\vartheta_{\mu\nu}$ of the bond affinities.

As was mentioned previously in Sec. 2, the total charge orders were first utilized by Wheland and Pauling for investigating the "directing power" of a perturbation, and here we will add a few remarks concerning this problem for the perturbed benzene ring. Since a cationoid reagent is always electron-seeking, it seems natural to assume that a substitution of such a reagent will take place preferentially at that carbon atom of the ring, which has the largest negative charge.[33] The atom-atom mutabilities of Table IV show now that, for $\delta_\mu>0$, there will be a large increase of the electron density at the place μ of the perturbation and that the perturbation will cause also a slight increase of the density at the *meta*-position and comparatively large decreases at the *ortho-* and *para*-positions (*meta*-directing power). For $\delta_\mu<0$, the conditions will be changed (*ortho-para*-directing power).

The alternating signs in the row for the total atom-atom mutabilities seem therefore to give an explanation of the chemical law of *alternating polarity* for the perturbed ring. The same law holds probably in general for all conjugated systems, and here it may therefore be of some interest to test explicitly for benzene the validity of the idea mentioned previously by Lennard-Jones[4] and by Fukui, Yonezawa, and Shingu[17] that the

[33] See reference 26, p. 149.

TABLE IV. Separate mutabilities $\pi_{\mu\nu,\kappa\lambda}{}^{ij}$ in units of $1/216\beta$ for $S=0$.

Indexes j	Atom-atom 11,11	11,22	11,33	11,44	Atom-bond 11,12	11,23	11,34	Bond-bond 12,12	12,23	12,34	12,45
0	35	5	−13	−19	20	−4	−16	20	8	−10	−16
±1	4	−11	7	4	−10	2	8	−3.5	−9.5	8.5	5.5
±2	−4	11	−7	−4	−10	2	8	3.5	9.5	−8.5	−5.5
3	−35	−5	13	19	20	−4	−16	−20	−8	10	16
total[a]	86	−34	2	−22	0	0	0	26	−22	14	−10

[a] Total = twice the sum of the contributions from the orbitals 0 and ±1, associated with the ground state.

alternating character should depend mainly on the properties of the highest occupied orbital in the ground state. In Table IV, we can find the contributions to the total atom-atom mutabilities from the different occupied orbitals, and the phenomenon of the alternating signs is here due to the combined effect of the lowest orbital and the next two higher orbitals.[33a] The particular importance of the frontier electrons may be true for more complicated conjugated compounds, but Table IV shows that it is not valid for the simple case of benzene.

The simple theory of directing power by Wheland and Pauling was slightly complicated by the observation that most *ortho-para*-directing perturbations also activate the ring in comparison to benzene, and that most *meta*-directing perturbations deactivate the ring. In order to obtain even this effect, Wheland and Pauling[3] assumed that each perturbation A, in addition to the perturbation δ_A in its own position, causes also smaller perturbations $\delta_A' = \kappa\delta_A$ in the positions of the adjacent atoms. According to (126), this activation condition is fulfilled and the nature of the directing power is preserved, if κ satisfies the inequality, $1/28 < \kappa < 1/4$. Wheland and Pauling proposed the reasonable value $\kappa = 1/10$, but, following Nordheim and Sponer,[34] we will here use the value $\kappa = 1/8$. Still other values are in use.[35]

We can now treat the question of the different reactivities of the carbon atoms in a perturbed benzene ring by formula (126), where for δ_μ ($\mu = 1, 2, \cdots, 6$) we take the values obtained by summing the contributions from the perturbations $A, B, \cdots$ introduced in the ring.

By using the general formula (72) and Table IV, we obtain further, for the *total bond orders* $p_{\mu\nu}$ associated with the ground state,

$$\begin{aligned} p_{12} &= \tfrac{2}{3} + (13\vartheta_{12} - 11\vartheta_{23} + 7\vartheta_{34} \\ &\qquad - 5\vartheta_{45} + 7\vartheta_{56} - 11\vartheta_{61})/108, \\ p_{23} &= \tfrac{2}{3} + (13\vartheta_{23} - 11\vartheta_{34} + 7\vartheta_{45} \\ &\qquad - 5\vartheta_{56} + 7\vartheta_{61} - 11\vartheta_{12})/108, \\ &\cdots \text{ and cyclic.} \end{aligned} \tag{127}$$

After computing these bond orders, the *bond lengths* may be found according to the semi-empirical scheme described by Coulson and Longuet-Higgins. We note that even (127) gives rise to properties of alternating character. Since all total bond-atom mutabilities are zero, the total bond orders are entirely independent of the perturbations δ_μ in the charge affinities. This implies that, since the quantities $\vartheta_{\mu\nu}$ usually may be considered as rather small, the bond orders and hence the

TABLE V. Comparison between separate mutabilities $\pi_{\mu\nu,\kappa\lambda}{}^{ij}$ in units of $1/\beta$ for $S=0$, and in units of $1/\gamma$ for $S=0.25$.

j	S	Atom-atom 11,11	11,22	11,33	11,44	Atom-bond 11,12	11,23	11,34	Bond-bond 12,12	12,23	12,34	12,45
0	0	0.16204	0.02315	−0.06019	−0.08796	0.09259	−0.01852	−0.07407	0.09259	0.03704	−0.04630	−0.07407
	0.25	0.26042	0.07292	−0.11458	−0.17708	0.16667	−0.02083	−0.14583	0.16667	0.07292	−0.08333	−0.14583
±1	0	0.01852	−0.05093	0.03241	0.01852	−0.04630	0.00926	0.03704	−0.01620	−0.04398	0.03935	0.02546
	0.25	−0.04051	−0.07089	0.05932	0.06366	−0.08102	0.00579	0.07523	−0.05570	−0.06004	0.05715	0.06149
±2	0	−0.01852	0.05093	−0.03241	−0.01852	−0.04630	0.00926	0.03704	0.01620	0.04398	−0.03935	−0.02546
	0.25	−0.05208	0.03385	−0.01302	0.01042	−0.02083	0.01042	0.01042	−0.00911	0.02995	−0.02474	−0.00130
3	0	−0.16204	−0.02315	0.06019	0.08796	0.09259	−0.01852	−0.07407	−0.09259	−0.03704	0.04630	0.07407
	0.25	−0.07523	0.00116	0.02199	0.02894	0.03704	−0.01157	−0.02546	−0.03704	−0.01273	0.01852	0.02546
total[a]												
	0	0.39814	−0.15740	0.00926	−0.10186	0	0	0	0.12038	−0.10186	0.06482	−0.04630
	0.25	0.35880	−0.13774	0.00810	−0.09954	0.00926	−0.01852	0.00926	0.11054	−0.09432	0.06192	−0.04572

[a] The total quantities are referred to the ground state.

[33a] *Note added in proof:* Compare also H. H. Greenwood, J. Chem. Phys. **20**, 1653L (1952).

[34] G. P. Nordheim and H. Sponer, J. Chem. Phys. **20**, 285 (1952).

[35] H. H. Jaffé, J. Chem. Phys. **20**, 279, 778 (1952) has used the large value $\kappa = 1/3$ together with the assumption that even higher neighbors are affected according to a geometrical progression in κ.

TABLE VI. Dipole moments of some heterocyclics containing nitrogen in Debye units ($=10^{-18}$ esu). $\delta_N=0.6$.

Compound	Calculated π-moment	Calculated σ-moment	Dipole moment calculated	Dipole moment observed[a]
Pyridine	1.51	0.85	2.36	2.22
Pyridazine	2.60	1.48	4.08	3.94
Pyrimidine	1.51	0.85	2.36	2.42
Pyrazine	0	0	0	0

[a] The observed data are taken from Wesson's compilation: L. G. Wesson, *Tables of Electric Dipole Moments* (Massachusetts Institute of Technology, 1948).

bond lengths are only slightly affected by perturbations of the ring. This is in agreement with experience.

We have here investigated only the case $S=0$, but the corresponding formulas for $S=0.25$ are easily written up by using (72) and Table V. We note that, in the latter case, the perturbations $V_{\mu\nu}$, defined by (31), must be given as fractions of the quantity γ:

$$V_{\mu\mu}=\delta_\mu\gamma, \quad V_{\mu\nu}=\vartheta_{\mu\nu}\gamma \quad (\mu\neq\nu). \tag{128}$$

When overlap is included, there is a slight complication of the theory depending on the fact that the charge orders q_μ are strictly speaking associated with the ON–AO φ_μ, and these orbitals are only semilocalized on the atoms μ.[36] However, since the whole naïve MO-theory is in all events very crude, we believe that the quantities q_μ and $p_{\mu\nu}$ may be used and "interpreted" in the semi-empirical theory in the same way as before.

In this connection, we observe that, since the advantage of the naïve theory is just its simplicity, it is in general impossible to improve the theory within its own frame. An essential improvement can first be obtained by studying a much more elaborate theory, based on antisymmetrized molecular wave functions, but, also in this case, many of the quantities treated here will still be useful.

Calculation of Dipole Moments of the Perturbed Benzene Ring[37]

We shall now investigate the contributions from the π-electrons to the dipole moment of the perturbed benzene ring. Since the total charge of the π-electrons is different from zero, it is convenient to use the symmetry center of the ring as fixed reference point and origin of the coordinate system.

Let us first consider the simple case $S=0$. In the naïve MO-theory, the total π-electron charges at the various atoms are given by the quantities eq_μ determined by (126). Since these relations are linear in the first-order approximation, it is sufficient to consider only one of the perturbations δ_μ. According to (127), the bond lengths are only slightly affected by the perturbations introduced in the ring, and we will therefore use a constant bond length a equal to the benzene value ($a=1.40\times10^{-8}$ cm) and a hexagonal form of the ring. From (126), it is then easily shown that each perturbation gives rise to a vector contribution to the π-moment of the magnitude $ea\delta_\mu/3$ esu with the direction from the center to the atom μ. Using the value $e=4.80\times10^{-10}$ esu, this gives a vector contribution of

$$2.24\ \delta_\mu \text{ Debye units} \tag{129}$$

for each perturbation. However, each heteroatom or group A introduced in a specific position in the ring causes, in addition to δ_A, also smaller perturbations $\delta_A'=\delta_A/8$ in the adjacent positions, and the resulting vector contribution from A is therefore

$$2.52\ \delta_A \text{ Debye units.} \tag{130}$$

Thus we have found theoretically that the ordinary *vector addition rule* for calculating dipole moments holds even for the contributions from the *mobile* π-electrons of the perturbed benzene ring. In order to find the total dipole moment of the molecule, we have then only to add the contribution from the σ-electrons with respect to the center, determined by the vector rule from the bond moments.

As examples, we will consider perturbed benzene rings containing nitrogen or methyl-groups. If in pyridine, C_5H_5N, the value $\delta_N=2$, recommended by Wheland and Pauling[3] is used, formula (130) gives a π-moment of 5.04 D; a more exact solution of the secular equation gives 4.48 D. Both these values are much too high to be in agreement with the observed data, and thus δ_N and then the whole δ-scale must be essentially reduced in value in order to correspond to the correct dipole moments. We have found a value of $\delta_N=0.6$ more reasonable, and in Table VI we have summarized our results for pyridine and the diazines in comparison to the experimental values. Our δ_N-value is supported by a recent paper by Orgel *et al.*,[38] where it is shown by solving the secular equation that a value of $\delta_N=1.0$ gives π-moments which are too high by a factor 1.6.

We will further investigate some benzene derivatives containing a methyl group. Neglecting hyperconjugation, the influence of the methyl group is treated as only causing a perturbation δ_{CH_3} at the carbon atom of the ring, where it is attached. From chemical observations, it is a well-known fact that nitrogen in pyridine is meta-directing, whereas the methyl group in toluene is ortho-paradirecting; the former corresponds to a positive value of δ_N and the latter to a negative value of δ_{CH_3}. By using the value $\delta_{CH_3}=-0.10$, we have obtained the results for toluene, the xylenes, and the picolines listed in Table VII.

In this investigation, two adjustable parameters give values of the dipole moments of eleven molecules in good

[36] See also R. McWeeny, J. Chem. Phys. **19**, 1614 L (1951) with errata in J. Chem. Phys. **20**, 920 L (1952).

[37] For a preliminary report of the results in this section, see P. O. Löwdin, J. Chem. Phys. **19**, 1323 L (1951).

[38] Orgel, Cottrell, Dick, and Sutton, Trans. Faraday Soc. **47**, 113 (1951).

agreement with experience. The naïve MO-theory gives us here a device for correlating the observed chemical properties of directing power with the values of the dipole moments. We note particularly the increase of the dipole moment from pyridine to γ-picoline, which is associated with the difference in sign between δ_N and δ_{CH_3}, i.e., with the difference in directing power.

Here we have discussed only the naïve MO-theory in the simple case when overlap is neglected ($S=0$), but now we will derive also a more exact expression for the dipole moment of the π-electrons. For this purpose we will consider the *bonding-overlapping* matrix **R** introduced in reference 20, p. 1572, by the formula

$$\mathbf{R}=(\mathbf{1}+\mathbf{S})^{-\frac{1}{2}}\mathbf{d}^{\mathrm{tot}}(\mathbf{1}+\mathbf{S})^{-\frac{1}{2}}, \tag{131}$$

or

$$R_{\mu\nu}=\sum_{\alpha\beta}(\mathbf{1}+\mathbf{S})_{\mu\alpha}{}^{-\frac{1}{2}}d_{\alpha\beta}{}^{\mathrm{tot}}(\mathbf{1}+\mathbf{S})_{\beta\nu}{}^{-\frac{1}{2}}. \tag{132}$$

We describe the system of π-electrons in the ground state by an antisymmetrized molecular wave function, Ψ, which is approximated by a determinant of molecular spin-orbitals (MSO) formed by taking the product of the MO ψ^j and the ordinary spin functions. The π-moment is then

$$\mathbf{D}_\pi=e\int\Psi^*\mathbf{x}\Psi(d\tau). \tag{133}$$

This expression, can be simplified in the following way by using (131):

$$\begin{aligned}
\mathbf{D}_\pi&=2e\sum_j^{\mathrm{occ}}\int\psi^{j*}\mathbf{x}\psi^j d\tau\\
&=2e\sum_j^{\mathrm{occ}}\sum_{\mu\nu}C^{\dagger j}{}_\mu\int\varphi_\mu\mathbf{x}\varphi_\nu d\tau\cdot C_\nu{}^j\\
&=2e\sum_j^{\mathrm{occ}}\sum_{\mu\nu}d_{\nu\mu}{}^{jj}\int\varphi_\mu\mathbf{x}\varphi_\nu d\tau\\
&=e\sum_{\mu\nu}d_{\nu\mu}{}^{\mathrm{tot}}\int\varphi_\mu\mathbf{x}\varphi_\nu d\tau\\
&=e\sum_{\mu\nu,\alpha\beta}d_{\nu\mu}{}^{\mathrm{tot}}(\mathbf{1}+\mathbf{S})_{\mu\alpha}{}^{-\frac{1}{2}}\int\phi_\alpha\mathbf{x}\phi_\beta d\tau(\mathbf{1}+\mathbf{S})_{\beta\nu}{}^{-\frac{1}{2}}\\
&=e\sum_{\alpha\beta}\{\sum_{\mu\nu}(\mathbf{1}+\mathbf{S})_{\beta\nu}{}^{-\frac{1}{2}}d_{\nu\mu}{}^{\mathrm{tot}}(\mathbf{1}+\mathbf{S})_{\mu\alpha}{}^{-\frac{1}{2}}\}\int\phi_\alpha\mathbf{x}\phi_\beta d\tau\\
&=e\sum_{\alpha\beta}R_{\beta\alpha}\int\phi_\alpha\mathbf{x}\phi_\beta d\tau,
\end{aligned} \tag{134}$$

which gives the formula

$$\mathbf{D}_\pi=e\sum_{\mu\nu}R_{\nu\mu}\int\phi_\mu\mathbf{x}\phi_\nu d\tau. \tag{135}$$

TABLE VII. Dipole moments of some benzene derivatives containing nitrogen and methyl, in Debye units. $\delta_N=0.6$ and $\delta_{CH_3}=-0.1$.

Compound	Dipole moments calculated	Dipole moments observed[a]	Compound	Dipole moments calculated	Dipole moments observed[a]
Toluene	0.25	0.37			
o-xylene	0.44	0.52	α-picoline	2.49	1.72
m-xylene	0.25	0.37	β-picoline	2.25	2.30
p-xylene	0	0	γ-picoline	2.61	2.57

[a] See reference a, Table VI.

In order to compute the π-moment, we have therefore to calculate the total charge and bond orders, q_μ and $p_{\mu\nu}$, which form the elements of the matrix $d_{\mu\nu}{}^{\mathrm{tot}}$, and after inclusion of the overlap matrix **S** according to (131), we can then find the π-moments if the integrals $\int\phi_\mu\mathbf{x}\phi_\nu d\tau$ are known. We note that the quantities q_μ and $p_{\mu\nu}$ still play a fundamental role, but that more information about the molecule is needed here than in the naïve theory.

Calculation of Orbital Energies for the Perturbed Benzene Ring

The orbital energies are of particular importance for investigating various properties of the molecule as a whole. We observe that the orbital energies cannot be directly used for evaluating excitation energies, since, for this purpose, they have to be completed with information about the separate "repulsion integrals," but that they give the *ionization energies* of the perturbed molecule according to Koopmans' theorem[39] with a high degree of accuracy.[40]

The orbital energies ϵ^j for the perturbed benzene ring can easily be obtained to the second order by means of the perturbation scheme developed in Sec. 3. According to Eqs. (52) and (80), we obtain for the nondegenerate and the doubly degenerate levels, respectively:

$$\begin{aligned}
&\epsilon^j=U^{jj}, && j=0,\,3,\\
&\epsilon^j=U^{jj}\pm|U^{jj'}|, && j=\pm1,\,\pm2.
\end{aligned} \tag{136}$$

where the elements U^{jk} are given by (46). As an example we will tabulate the orbital energies for the sim-

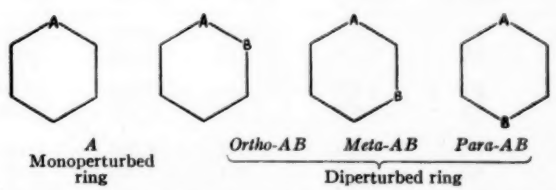

FIG. 3. Types of perturbations introduced in the ring. In addition to the perturbations δ_A and δ_B in the positions of *A* and *B*, respectively, there are also smaller perturbations $\delta_A'=\delta_A/8$ and $\delta_B'=\delta_B/8$ in the adjacent positions.

[39] T. Koopmans, Physica **1**, 104 (1934). See also C. C. J. Roothaan, Revs. Modern Phys. **23**, 69 (1951).

[40] See the discussion given by Mulliken in R. S. Mulliken, J. chim. phys. **46**, 497 (1949).

ple cases of a ring containing one or two perturbations, A and B, according to Fig. 3.

For the sake of simplicity, only the case of perturbed charge affinities for $S=0$ will be treated explicitly, i.e.,

$$V_{\mu\mu}=\delta_\mu\beta, \quad V_{\mu\nu}=0 \quad (\mu\neq\nu). \tag{137}$$

The more general problem can be solved in the same way without any difficulties. The actual matrix elements U^{ii} and $U^{ij'}$ $(j'=-j)$ have now the form

$$\begin{aligned} U^{ii}&=\epsilon^{i(0)}+\frac{\beta}{6}\sum_\mu \delta_\mu+\frac{\beta^2}{2}\sum_{\mu\kappa}\delta_\mu\delta_\kappa\pi_{\mu\mu,\kappa\kappa}{}^{ii}, \\ U^{ij'}&=-\frac{\beta}{6}\sum_\mu \delta_\mu e^{-2\pi i\mu j/3}+\frac{\beta^2}{6}\sum_{\mu\nu}\delta_\mu\delta_\kappa\Omega_{\mu-\kappa}{}^j e^{-\pi i(\mu+\kappa)j/3}, \end{aligned} \tag{138}$$

and, for the real and imaginary parts of $U^{ij'}$, we get specifically

$$\begin{aligned} Re\{U^{ij'}\}&=-\frac{\beta}{6}\sum_\mu \delta_\mu\cos 2\pi\mu j/3 \\ &\quad+\frac{\beta^2}{6}\sum_{\mu\kappa}\delta_\mu\delta_\kappa\Omega_{\mu-\kappa}{}^j\cos\pi(\mu+\kappa)j/3, \\ I\{U^{ij'}\}&=-\frac{\beta}{6}\sum_\mu \delta_\mu\sin 2\pi\mu j/3 \\ &\quad-\frac{\beta^2}{6}\sum_{\mu\kappa}\delta_\mu\delta_\kappa\Omega_{\mu-\kappa}{}^j\sin\pi(\mu+\kappa)j/3, \end{aligned} \tag{139}$$

TABLE VIII. Orbital energies for a monoperturbed ring for $S=0$ and $\delta_A'=\delta_A/8$: $\epsilon^j=\alpha+\beta(\tau^j+c_A{}^j\delta_A+c_{AA}{}^j\delta_A{}^2)$.

j	τ^j	$c_A{}^j$	$c_{AA}{}^j$
0	2	0.20833	0.08840
1′	1	0.35417	−0.00731
1″	1	0.06250	0.00195
2′	−1	0.35417	0.00731
2″	−1	0.06250	−0.00195
3	−2	0.20833	−0.08840

TABLE IX. Comparison between values of the orbital energies[a] for a monoperturbed ring, obtained by means of perturbation theory (PT) or by solving the secular equation (SE): $\delta_A=0.5$, 1, 1.5, and 2.

j	Method	$\delta_A=0.5$	$\delta_A=1$	$\delta_A=1.5$	$\delta_A=2$
0	PT	2.126	2.297	2.511	2.770
	SE	2.130	2.322	2.584	2.907
1′	PT	1.175	1.347	1.515	1.679
	SE	1.172	1.319	1.431	1.510
1″	PT	1.031	1.064	1.098	1.133
	SE	1.031	1.064	1.098	1.133
2′	PT	−0.821	−0.639	−0.452	−0.262
	SE	−0.824	−0.659	−0.512	−0.383
2″	PT	−0.969	−0.939	−0.911	−0.883
	SE	−0.969	−0.939	−0.911	−0.883
3	PT	−1.918	−1.880	−1.886	−1.937
	SE	−1.915	−1.857	−1.816	−1.785

[a] $(\epsilon-\alpha)/\beta$.

and thereafter the angle 2φ in (84), which determines the coefficients in the perturbed MO.

The results for a monoperturbed benzene ring are given in Table VIII, and, in Table IX, we have given a comparison between the energies obtained according to second-order perturbation theory (PT) and the energies obtained by solving the secular equation (SE). In the last table, only the quantities $(\epsilon-\alpha)/\beta$ are listed. We note that the perturbation theory shows excellent agreement with the SE-values in the region $\delta_A=0.5$, and that the accuracy is sufficient for most purposes in the naïve theory also around the point $\delta_A=1$.

In Table X we have finally listed the orbital energies for a diperturbed benzene ring with $S=0$ and $\delta_A'=\delta_A/8$, $\delta_B'=\delta_B/8$. The energies are here expressed in the form:

$$\begin{aligned} &\epsilon^j=\alpha+\beta x^j, \\ &x^j=\tau^j+c_A{}^j\delta_A+c_B{}^j\delta_B+\bar{c}^j\delta \\ &\quad+c_{AA}{}^j\delta_A{}^2+c_{AB}{}^j\delta_A\delta_B+c_{BB}{}^j\delta_B{}^2 \\ &\quad+(\bar{c}_{AA}{}^j\delta_A{}^3+\bar{c}_{AB}{}^j\delta_A{}^2\delta_B+\bar{c}_{BA}{}^j\delta_A\delta_B{}^2+\bar{c}_{BB}{}^j\delta_B{}^3)/\delta, \\ &\delta=(\delta_A{}^2-\delta_A\delta_B+\delta_B{}^2)^{\frac{1}{2}}. \end{aligned} \tag{140}$$

The results given in Tables VIII and X will be utilized in subsequent papers.

A discussion of the *symmetry properties* of the mono- and diperturbed benzene ring has recently been given by Nordheim and Sponer,[34] who have also investigated the molecular orbitals and the orbital energies of some compounds of these types by solving the secular equations.

7. Concluding Remarks

The general second-order perturbation theory for perturbed conjugated systems, developed in the first part of this paper, seems to have a sufficient accuracy for most applications in the semi-empirical theory. If the basic MO-properties of, e.g., a parent hydrocarbon are known, it is possible to derive the corresponding properties of a heterocompound, obtained by replacing one or more carbon atoms by heteroatoms or groups, in a rather simple way without the laborious solution of higher order secular equations with different elements.

For small perturbations $(\delta<1)$, the same perturbation scheme may be used also in a more elaborate MO-theory, and, for larger perturbations, one has the possibility of improving the accuracy by the inclusion of terms of the third and higher orders.

In the second part of the paper, the theory has been applied to the perturbed benzene ring having six π-orbitals, and a number of useful "benzene constants" have been tabulated. We note that, by splitting the secular equation in a way recently described by the author,[21] it is possible to transform problems concerning substituted benzenes having seven, eight, or more π-orbitals, into a form where they are closely related to the

TABLE X. Orbital energies for a diperturbed benzene ring with $S=0$, $\delta_A'=\delta_A/8$, and $\delta_B'=\delta_B/8$, according to formula (140).

Compound	j	r	$c_{A^j}=c_{B^j}$	$\bar{c}^j$	$c_{AA^j}=c_{BB^j}$	c_{AB^j}	$\bar{c}_{AA^j}=\bar{c}_{BB^j}$	$\bar{c}_{AB^j}=\bar{c}_{BA^j}$
Ortho-AB	0	2	0.20833	...	0.08840	0.04832	...	...
	1′	1	0.20833	0.14583	−0.00268	−0.04029	−0.00463	−0.05165
	1″	1	0.20833	−0.14583	−0.00268	−0.04029	0.00463	0.05165
	2′	−1	0.20833	0.14583	0.00268	0.04029	0.00463	0.05165
	2″	−1	0.20833	−0.14583	0.00268	0.04029	−0.00463	−0.05165
	3	−2	0.20833	...	−0.08840	−0.04832	...	...
Meta-AB	0	2	0.20833	...	0.08840	−0.07668	...	...
	1′	1	0.20833	0.14583	−0.00268	0.02611	−0.00463	0.04210
	1″	1	0.20833	−0.14583	−0.00268	0.02611	0.00463	−0.04210
	2′	−1	0.20833	0.14583	0.00268	−0.02611	0.00463	−0.04210
	2″	−1	0.20833	−0.14583	0.00268	−0.02611	−0.00463	0.04210
	3	−2	0.20833	...	−0.08840	0.07668	...	...
Para-AB	0	2	0.20833	...	0.08840	−0.12008	...	...
	1′	1	0.35417	...	−0.00731	0.07133	...	...
	1″	1	0.06250	...	0.00195	−0.00390	...	...
	2′	−1	0.35417	...	0.00731	−0.07133	...	...
	2″	−1	0.06250	...	−0.00195	0.00390	...	...
	3	−2	0.20833	...	−0.08840	−0.12008	...	...

benzene problem treated here, and where the same "benzene constants" may again be useful.

ACKNOWLEDGMENTS

This work was performed as a part of the research program concerning the properties of polyatomic molecules being carried out at Duke University under the general direction of Professor Hertha Sponer, and the author would like to express his sincere gratitude to her for many inspiring and fruitful discussions about the aromatic molecules and for many valuable suggestions.

Finally I should like to thank Professor Walter M. Nielsen, Professor Hertha Sponer, and their colleagues at the Department of Physics for the great hospitality I enjoyed during my stay in Durham, North Carolina.

The Absorption Spectrum of Cyclopropane in the Vacuum Ultraviolet. Note on the Absorption Spectrum of Methyl Cyclopropane†

PAUL WAGNER* AND A. B. F. DUNCAN
Department of Chemistry, University of Rochester, Rochester, New York

(Received August 29, 1952)

The spectrum of cyclopropane has been investigated from 600A to 2200A with high dispersion. Three very broad electronic transitions with apparent maxima at 1594, 1449, and 1202A were found. A strong continuous absorption begins at 1123A, and no resolved transitions could be observed at shorter wavelengths. A very weak band system consisting of twelve bands was found between 1889 and 1816A. It is concluded that the electronic transitions arise from excitation of an electron from a bonding molecular orbital localized principally in the carbon ring. The weak transition is interpreted as a forbidden transition. A tentative analysis of the bands in this transition is given. A note on the absorption spectrum of methyl cyclopropane is included.

INTRODUCTION

SEVERAL discussions of the normal state of cyclopropane have appeared.[1–6] These treatments have attempted a correlation of the somewhat unusual chemical properties of the molecule with the ground-state electronic configuration. Coulson and Moffitt[5] have discussed the bonding nature of the molecular orbitals, approximately localized in the ring, with the view that the bonds are strained. The present paper does not attempt to discuss these points further.

The three carbon atoms in cyclopropane are located at the vertices of an equilateral triangle, and the hydrogen atoms lie in planes perpendicular to the plane of the ring through the twofold axes. This geometrical structure (point group D_{3h}) has been verified by electron diffraction[7] and by the analysis of infrared[8] and Raman[9] spectra.

A former study of the ultraviolet spectrum of cyclopropane in the gas and liquid phases has been made by Ashdown, Harris, and Armstrong[10] with a quartz spectrograph. They showed that the absorption spectrum of the vapor in an absorbing path of one meter (pressure unspecified), and the absorption spectrum of the liquid in a path length of 1.5 cm began at 1950A and was continuous to at least 1860A. Unpublished work in this laboratory[11] with a Cario and Schmitt-Ott vacuum spectrograph showed six weak bands between 53 350 cm^{-1} (1874A) and 54 750 cm^{-1}. The present work was done with an approximate reciprocal dispersion 4.14 A/mm over a wide pressure range.

EXPERIMENTAL DETAILS

Materials

Cyclopropane of stated 99.5 percent purity (from Ohio Chemical Company) was used. An infrared spectrogram of this material was identical with that reported[8] for the pure material. This test is not expected to show traces of impurities, which are critically important in view of the fact that we have found one very weak electronic transition. Further discussion of trace impurities will be made in connection with this weak absorption. Some samples[11] were purified further by passage through bromine water to remove unsaturated compounds, then through 10 percent KOH solution and dried. This treatment was followed by fractionation in vacuum.

To determine the extent of possible photodecomposition or isomerization during the course of an exposure, the following experiment was carried out. The spectrograph was filled with cyclopropane to a pressure of 4 mm Hg, and illuminated for four hours. This pressure was about the same as that used in photographing the cyclopropane, but the exposure time was about ten times as long as the normal exposure. An infrared spectrogram of the irradiated sample was identical with the starting material. This was taken as evidence that photochemical reactions probably did not interfere with the observations.

Equipment

The ultraviolet spectrum was photographed with a four-inch, 120 000-line, two-meter radius of curvature grating, mounted at about normal incidence in a vacuum spectrograph. The reciprocal dispersion in the first order was about 4.14A/mm. The slit width was 0.09 mm. The Lyman continuum[12] was used as a source for the region 550–1750A and a hydrogen discharge for the region 1650–2225A. The absorbing gas at a definite pressure was contained in the spectrograph, which served as an absorbing column about 4 meters long. In some experiments at high pressures, the discharge was separated from the spectrograph by a lithium fluoride window, which transmitted above 1300A. Eastman III-0 U.V. sensitized plates and Eastman SWR plates were used.

EXPERIMENTAL RESULTS

Cyclopropane was investigated in a pressure range from 0.002 mm to 100 mm. Wavelength measurements

† This work was supported in part under Contract N6onr-241, Task Order X, with the U. S. Office of Naval Research, United States Navy.

* Part of a dissertation presented to the Faculty of the Graduate School of the University of Rochester in partial fulfillment of the requirements for the degree of Doctor of Philosophy.

[1] T. M. Sugden, Nature **160**, 367 (1947).
[2] A. D. Walsh, Nature **159**, 164 (1947).
[3] R. Robinson, Nature **159**, 400 (1947).
[4] C. A. Coulson and W. E. Moffitt, J. Chem. Phys. **15**, 151 (1947).
[5] C. A. Coulson and W. E. Moffitt, Phil. Mag. **40**, 1 (1949).
[6] A. D. Walsh, Trans. Faraday Soc. **45**, 179 (1949).
[7] L. Pauling and L. O. Brockway, J. Am. Chem. Soc. **59**, 1223 (1937).
[8] G. Herzberg, *Infrared and Raman Spectra of Polyatomic Molecules* (D. Van Nostrand Company, Inc., New York, 1945), p. 352.
[9] J. W. Linnett, J. Chem. Phys. **6**, 692 (1938).
[10] Ashdown, Harris, and Armstrong, J. Am. Chem. Soc. **58**, 850 (1936).
[11] Observations by Ta-Kong Liu.
[12] R. E. Worley, Rev. Sci. Instr. **13**, 67 (1942).

of the sharpest bands were made with a conventional precision comparator. The error did not exceed 15 cm^{-1}. The intensity maxima of the broad transitions and of the weakest sharp bands were determined from microphotometer tracings.

At low pressures, three regions of continuous absorption, with maxima at 62 728 cm^{-1}, 68 989 cm^{-1}, and 83 150 cm^{-1} were found. Because of the large frequency separations, it is evident that these are separate electronic transitions. All of these transitions appeared first at about 0.005 mm. In view of their high intensity, they are probably allowed transitions, and will be referred to as such in the subsequent description and discussion. The allowed transitions broaden symmetrically with pressure, until at a pressure of 0.020 mm the transitions merge. At even lower pressures, about 0.003 mm, continuous absorption begins at 89 000 cm^{-1} and extents to higher frequencies, but no transitions can be resolved. Careful examination of all these spectra have revealed no associated vibrational structure.

At pressures of about 2 mm (four-meter column) there appear twelve weak but fairly sharp bands in the region 52 930–55 065 cm^{-1} (see Fig. 1). These bands are believed to belong to one electronic transition which has an estimated integrated intensity of about 10^{-4} the intensity of the other electronic transitions. This band system will be referred to as the forbidden transition, for reasons which will be discussed later. The shortest wavelength members to this system are partly obscured by the neighboring allowed transition at 62 728 cm^{-1}. As the pressure is increased, the latter transition extends progressively to lower frequencies and obscures the sharp bands of the forbidden transition, but the sharp bands appear to be affected only slightly by pressure. At 20-mm pressure, the sharp bands cannot be seen, and the long wavelength limit of the 62 728 cm^{-1} transition extends to 52 900 cm^{-1}. This limit corresponds to the observation of Ashdown, Harris, and Armstrong[10] that continuous absorption appears below 1860A.

The possibility must be considered that the forbidden transition originated from an impurity present in the commercial sample of cyclopropane, which was not removed or changed in concentration on subsequent purification. We have no information on the method of preparation, but it may be supposed that a conventional preparation from 1,3 dichloropropane (b.p. 120°C) and Zn dust was used. It appears doubtful that any appreciable amount of high boiling material could have been left in the samples which were washed and dried. Traces of propylene might be expected in the original material, and they might not have been removed with treatment with bromine. It is known that propylene absorbs in the same general region of the weak bands, and although published description[13] of the propylene spectrum made it appear improbable that the weak bands were due to this molecule, the absorption spectrum of propylene at low pressures was rephotographed. A few weak and very diffuse (200–300 cm^{-1} wide) bands appeared at 0.02–0.03 mm pressure, which bore no resemblance whatever to the weak bands of cyclopropane. Furthermore, at this pressure of propylene, total absorption occurs at higher frequencies where cyclopropane is transparent. While an unknown impurity in cyclopropane cannot be excluded as a source of the weak bands, it appears fairly certain that the impurity is not propylene.

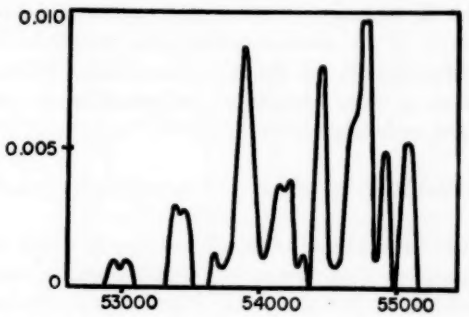

FIG. 1. Structure of the 52 273 cm^{-1} transition in cyclopropane vapor. Ordinate: absorption coefficient in cm^{-1}. Abscissa: frequency in cm^{-1}.

DISCUSSION

The geometrical structure of cyclopropane conforms to the symmetry point group D_{3h}. The molecular orbitals of this molecule have been discussed by Coulson and Moffitt,[5] and their discussion is taken as a basis for the present interpretation of the observed electronic transitions.

If the 1*s* hydrogen and carbon atomic orbitals are neglected, as well as six other carbon orbitals for the C−H bonds, the electronic configuration of the closed shell ground state ($^1A_1'$) may be formulated as $(a_1')^2(e')^4$, where (a_1') and (e') are molecular orbitals constructed from suitably hybridized carbon functions. While no detailed computations of energies have been made, it is probable that the doubly degenerate (e') orbital has a higher energy than the (a_1') orbital, and it will be assumed that the absorption spectra at lowest frequency occur when an electron is excited from the (e') orbital. The forms of some of the possible excited molecular molecular orbitals are given also by Coulson and Moffitt. These are antibonding orbitals orthogonal to (a_1') and (e') and are designated here as $(\bar{a}_2')$ and $(\bar{e}')$. The relative energies of these orbitals are not known either, but the same types of excited electronic states will result if the electron goes to an $(\bar{a}_2')$ or to an $(\bar{e}')$ orbital, since the configurations $(a_1')^2(e')^3(\bar{a}_2')$ and $(a_1')^2(e')^3(\bar{e})$ give the same types of excited states A_1', A_2', and E'. The same excited states result when an electron is excited from the (a_1') orbital. Furthermore,

[13] W. C. Price and W. T. Tutte, Proc. Roy. Soc. (London) **A174**, 207 (1940).

the same types of excited states result from the excitation of two electrons simultaneously from either orbital or one from each orbital.

With the restriction that the upper states are A_1', A_2', or E', selection rules allow electronic transitions only to E' states, with the dipole moment changing in the plane of the molecule. But this restriction follows from the neglect of the C−H orbitals. If these are included, a more complete configuration in terms of localized molecular orbitals is

$$(a_1')^2_{CH}(a_2'')^2_{CH}(e')^4_{CH}(e'')^4_{CH}(a_1')^2_{CC}(e')^4_{CC},\ {}^1A_1'.$$

It might be supposed that all the C−H orbitals are of lower energy than the C−C orbitals which have been treated above, but this is far from certain. If the C−H orbitals are considered, there will be additional excited orbitals of species $(\bar{a}_2)$ and $(\bar{e})$. Excitation to these orbitals result in additional excited states, among which are those of species A_2''. Transitions from the ground state to A_2'' states are allowed with the dipole moment moving perpendicular to the ring. The preceding conclusions are summarized as follows. In general, the excited states will be of species A_1', A_2', E', A_2'', and E'', but states of the latter two species occur only by excitation from C−H orbitals. If the C−H orbitals are neglected only excited states of species A_1', A_2', and E' remain, with transitions to E' states allowed and transitions to A_1' and A_2' states forbidden.

It appears probable that the strong electronic transitions at 62 728, 68 989, and 83 150 cm^{-1} are allowed transitions, and with a treatment restricted to C−C orbitals, they must have a symmetry of species E'.

The weak transition 52 930–55 065 cm^{-1}, which is about 10^{-4} as intense as the other transitions is believed to be forbidden by the electronic selection rules. From the preceding argument, the upper state must be of species A_1' or A_2' if it is a singlet state.‡ Since the energies of these states are not known, there is no basis for a decision between the two for the upper state for the longest wavelength transition. Transition to either state may be allowed, if a vibration of the proper symmetry species is excited in the upper or lower electronic states. Vibrations of species a_1' or e' allow transitions to an upper state A_2' and vibrations a_2' and e' allow transitions to an A_1' upper state from the ground state. The a_1 vibration (ν_4) is described[14] as CH_2 twisting;[8] there are two a_2' vibrations (ν_6 and ν_7), CH stretching and CH_2 rocking; there are four e' vibrations (ν_8, ν_9, ν_{10}, ν_{11}), described as CH stretching, CH_2 deformation, CH_2 bending and ring deformation, respectively. It is probable that the electronic transition is allowed by a vibration which offers the greatest perturbation, and since it has been assumed that the electronic excitation is localized in the ring, the ring deformation frequency ν_{11} (e') should be most effective. However, this does not help in a decision about the upper state, since an e' vibration allows both the transitions $A_1'\rightarrow A_1'$ and $A_1'\rightarrow A_2'$.

An attempted analysis of the vibrational structure of the forbidden transition leads to many difficulties, some of which may be mentioned. The twelve bands are very close together, and the vibrational frequencies are all too large, even when allowance is made for some lowering of the normal state values in the excited state, to be consistent with an origin near the intense bands. An interpretation which involved the excitation of vibrations in the lower state leads to the objection that the Boltzmann factors for the vibrational intensities are far too small to allow observation of the transitions at room temperature. It is possible that the observed band structure corresponds to two intermingled transitions, but this does not lead to a convincing explanation.

The preferred tentative interpretation is summarized in Table I. The double maxima of the bands ($\nu_0+\nu_{11}$) and ($\nu_0+\nu_9$) are taken to be P and R branches of vibrational transitions. The separations of the maxima are consistent with those observed in the infrared spectrum. The vibrations which appear in the upper state are of species e', which allow the transition, and of a_1', which appears in combination. Each of the e' vibrations has an upper state value about 20 percent lower than the normal state value, while the a_1' frequency has a slightly higher value in the upper than in the lower electronic state. Some of the less convincing aspects of the assignment are the facts that the most intense transitions are assigned either to combinations or to

TABLE I. Electronic transitions in cyclopropane.

A. Structure of the 52 273 cm^{-1} transition

Frequency (cm^{-1})	Tentative assignment
(52 273)	ν_0
52 930 }	$\nu_0+\nu_{11}$
53 031 }	
53 654	$\nu_0+2\nu_{11}$
54 295	$\nu_0+3\nu_{11}$
54 148	$\nu_0+\nu_{11}+\nu_9$
53 888	$\nu_0+\nu_{11}+\nu_{10}$
54 210	$\nu_0+\nu_{11}+\nu_8$
55 065	$\nu_0+\nu_{11}+2\nu_9$
54 741	$\nu_0+\nu_{11}+2\nu_{10}$
54 782	$\nu_0+2\nu_{11}+\nu_9$
54 888	$\nu_0+2\nu_{11}+\nu_8$
53 392 }	$\nu_0+\nu_9$
53 442 }	
54 435	$\nu_0+2\nu_9$

B. Relative integrated intensities of electronic transitions

Frequency (cm^{-1})	Relative intensity
52 273	1
62 728	9.2×10^4
68 989	4.1×10^4
83 150	14.9×10^4

‡ That the weak transition might be to a triplet state $^3E'$ (which is allowed by symmetry) was suggested to us by the reviewer of this paper. There is no direct evidence for or against this possibility. The difficulties of interpretation which are discussed in the following paragraph are not simplified in any way by an upper state of this type.

[14] The notation of reference 8 is used.

overtones, and the numerical agreement of the assignments $(\nu_0+\nu_{11}+2\nu_9)$, $(\nu_0+2\nu_{11}+\nu_9)$, with $(\nu_0+\nu_{11})$, $(\nu_0+2\nu_9)$, $(\nu_0+2\nu_{11})$ is not good. In view of these difficulties, this assignment should be regarded as tentative.

Attempts were made to observe the forbidden electronic transition (tentatively assigned at 52 273 cm^{-1}). High pressure photographs were searched for an indication of absorption at this frequency. It was thought that the transition might be present, but too narrow to observe with the available resolution, and argon at 700-mm pressure was added to cyclopropane at 6 mm in an attempt to broaden the band, but nothing was observed. Attempts were made (see following note) to find the corresponding spectrum and pure electronic transition in methyl cyclopropane. None of these attempts was successful in producing evidence for the origin of the forbidden electronic transition in cyclopropane. It may be suggested that the spectrum of partly deuterated cyclopropane might be of interest in this connection.

The ionization potential of cyclopropane has been measured[15] by an electron impact method. The value reported is 10.14 ± 0.05 ev (81 804 cm^{-1}). There are not enough resolved transitions observed in the present work to fit into a Rydberg series. The fact that there is a region of transmission at approximately 87 500 to 89 000 cm^{-1} does not in itself refute an ionization potential as low as 81 804 cm^{-1}, since the continuous absorption beginning at 89 000 cm^{-1} may be associated with a higher ionization potential.

NOTE ON THE VACUUM ULTRAVIOLET ABSORPTION SPECTRUM OF METHYL CYCLOPROPANE

When a pure electronic transition is forbidden because of symmetry restrictions, it is sometimes possible to observe it in a derivative of the molecule which has a lower symmetry. It was hoped that the absorption spectrum of a derivative of cyclopropane would show the counterpart of the forbidden transition in cyclopropane, and in particular the origin of the transition. It is to be expected that the frequency of the origin of the transition of the substituted compound would be shifted in frequency from the predicted origin of the parent substance. To preserve the similar features of vibrational transitions, the derivative should be as similar as possible to the parent substance. Methyl cyclopropane was the available derivative which was most similar to cyclopropane. A partly deuterated cyclopropane would have been better.

The ultraviolet spectrum of methyl cyclopropane has not been reported previously. The infrared[16] and Raman spectra[17] have been studied, but no analysis has been published.

Methyl cyclopropane was prepared by a zinc dust reduction of 1,3 dibromobutane in 85 percent ethyl alcohol. The product was purified by washing with a saturated solution of bromine water, followed by washing with 20 percent KOH solution. The sample was dried over solid KOH and P_2O_5, and freed from air in a vacuum apparatus before use. An infrared spectrogram of the material was identical with the reported infrared spectrum[16] obtained from samples which had been prepared by two different methods. In the present work the spectrum was photographed from 1625 to 2400A in a vacuum spectrograph with a 60 000 line, one-meter radius of curvature grating. The spectrograph served as an absorbing column about two meters long. The reciprocal dispersion was 8.32 A/mm.

The spectrum was photographed in a pressure range from 0.040 to 19 mm. At the lowest pressures, only continuous absorption was observed. At 0.5 mm, two narrow bands appeared at 49 468 and 48 383 cm^{-1}. As the pressure was increased, the low frequency limit of the absorption decreased until at a pressure of 19 mm, the limit was at 48 190 cm^{-1}.

Since the symmetry of this molecule corresponds to the point group C_1, all transitions will be allowed. At this stage there does not appear to be any simple relation between methyl cyclopropane and cyclopropane. It is felt that any interpretation of the spectrum which has been observed should be deferred until a more thorough investigation.

[15] F. H. Field and E. A. Hinkle, J. Chem. Phys. **18**, 1122 (1950).

[16] F. E. Condon and D. E. Smith, J. Am. Chem. Soc. **69**, 965 (1947).

[17] R. Lespicau, M. Bourguell, and R. Wakeman, Bull. Soc. Chim. **51**, 400 (1932).

Some Heavy Water Rotational Absorption Lines*

C. K. JEN, D. R. BIANCO, AND J. T. MASSEY
Applied Physics Laboratory, The Johns Hopkins University, Silver Spring, Maryland
(Received August 20, 1952)

Three new heavy water rotational absorption lines have been observed in the microwave region. One of these lines and another line previously observed by McAfee have been identified as HDO lines by a study of the variation of their intensities with isotopic molecular concentration. By interpreting their Stark structure, the two HDO lines are assigned as follows: HDO: $8_{-1}\rightarrow 8_0$ at 24 884.85 Mc/sec and HDO: $6_{-2}\rightarrow 7_{-6}$ at 26 880.47 Mc/sec. In addition, results on the Zeeman spectra of the two identified HDO lines are presented.

I. INTRODUCTION

VARIOUS studies have been made on the rotational spectra of water molecules in the microwave region. King, Hainer, and Cross[1] made a notable contribution in calculating the expected transition frequencies and their line intensities. Strandberg and his collaborators[2] studied the known $5_{-1}-6_{-5}$ H_2O line and observed four HDO lines. McAfee[3] found a new line in a heavy water sample. More recently, Beard and Bianco[4] observed two D_2O lines.

The present work was initially stimulated by the need of finding additional heavy water lines for the purpose of studying their rotational magnetic moments.[5] Three new lines have actually been observed. One of the new lines and the line found by McAfee were chosen to be the subject of a detailed study for identification of their isotopic molecular origin, quantum number assignment by the Stark structure and rotational g-factors by the Zeeman effect.

II. EXPERIMENTAL

For all the work reported herein except for the Zeeman studies, the microwave spectrometer used contains a Hughes-Wilson absorption cell made of a 10-foot section of X-band wave guide. The Stark potential is either a square wave voltage at 100 kc/sec or an adjustable dc voltage modulated with a small sinusoidal voltage at 100 kc/sec. The electric field strength inside the wave guide is calibrated by the Stark splitting of the $O^{16}C^{12}S^{32}$ $J=1\rightarrow 2$ line while assuming the dipole moment of this molecule to be 0.7085 ± 0.004 Debye unit as given by Shulman and Townes.[6]

For the Zeeman splitting, a cavity spectrometer in conjunction with a microwave source frequency modulated at 100 kc/sec was used.[7]

All frequency measurements were made using a frequency standard continuously monitored against WWV transmission.

For simplicity, the present study of the isotopic species of the water molecule is limited to H_2O, HDO, and D_2O, where O stands for O^{16}. It would naturally be desirable to use three samples, each pure in one species. We have used ordinary distilled water as representing a pure H_2O sample and the Atomic Energy Commission deuterium oxide (99.8 percent) as representing a pure D_2O sample. For HDO, however, the best available sample is one which is only 50 percent pure in HDO in the equilibrium mixture of initially equal amounts of pure H_2O and D_2O. All the samples described are in the liquid phase. Only the vapor of a given sample is let into the Stark cell for the microwave absorption. In so doing, we are assuming the isotopic concentration for a given species in the vapor phase is the same as that in the liquid phase, if the cell is not otherwise contaminated.

TABLE I. Observed frequencies and intensities of four heavy water lines.

Line	Frequency (Mc/sec)	Intensity
A	24 884.85±0.1	medium
B	26 880.47±0.1 (first observed by McAfee)	medium
C	30 182.57±0.1	weak
D	30 778.62±0.1	weak

III. OBSERVATION OF NEW WATER LINES

Searching for new water lines was mostly done by using the intermediate sample (50 percent HDO, 25 percent H_2O, and 25 percent D_2O). This sample affords the chance of observing a line belonging to any isotopic species. The frequency range searched was between 21 300 and 30 800 Mc/sec. Other than confirming a line already observed by McAfee, we found three new lines. The zero-field frequencies of these lines were determined as shown in Table I.

* The work described in this paper was supported by the Bureau of Ordnance, U. S. Navy, under Contract NOrd 7386.
[1] King, Hainer, and Cross, Phys. Rev. **71**, 433 (1947).
[2] M. W. P. Strandberg, M. I. T. RLE Report No. 85 (1948); Golden, Wentink, Hillger, and Strandberg, Phys. Rev. **73**, 92 (1948).
[3] K. B. McAfee, Harvard thesis (1950). We are indebted to Dr. McAfee for communicating his results to us.
[4] C. I. Beard and D. R. Bianco, J. Chem. Phys. **20**, 1488 (1952).
[5] C. K. Jen, Phys. Rev. **81**, 197 (1951).
[6] R. G. Shulman and C. H. Townes, Phys. Rev. **77**, 500 (1950).
[7] C. K. Jen, Phys. Rev. **76**, 1494 (1949).

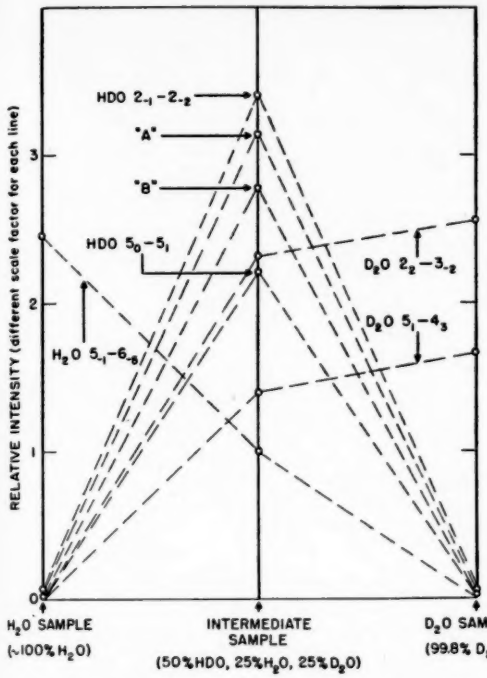
HDO 2₋₁ − 2₋₂
"A"
"B"
HDO 5₀ − 5₁
H₂O 5₋₁ − 6₋₆
D₂O 2₂ − 3₋₂
D₂O 5₁ − 4₃
RELATIVE INTENSITY (different scale factor for each line)
H₂O SAMPLE (~100% H₂O)
INTERMEDIATE SAMPLE (50% HDO, 25% H₂O, 25% D₂O)
D₂O SAMPLE (99.8% D₂O)

FIG. 1. Relative intensities of water molecule absorption lines as functions of isotopic molecular concentrations.

IV. IDENTIFICATION OF THE ISOTOPIC MOLECULAR SPECIES OF A LINE BY CONCENTRATION VARIATION

If the effect of intensity saturation is negligible and the line widths due to the isotopic molecules are essentially the same, the peak intensity of a given absorption line should be very nearly proportional to the concentration of that isotopic molecular species to which the line belongs; hence, the most direct method of determining the isotopic molecular species of a line is to correlate its intensity variation with the change in concentration of one of the isotopic molecules. It is true that quite often the isotopic species of a line as well as its quantum number assignment for the transition can be defined through a single procedure by securing a very close fit between the experimental and theoretical Stark structure, but there is no assurance that the close fitting obtained might not be accidental. It is conceivable that an error of this kind can be made.

Using the three samples mentioned in Sec. II, we have performed a "concentration test" for the lines *A* and *B* and five other known lines consisting of one H_2O line, two HDO lines, and two D_2O lines. The lines *C* and *D* listed above were not included, because their intensities are deemed to be not large enough to render the results conclusive.

One serious difficulty encountered in the concentration test comes from the contamination by H_2O in the absorption cell and/or in the sample tube. The contamination in the cell depends very much on its history. As it is common experience that water molecules adhere strongly to surfaces, there is always a potential source of contamination even though the cell is apparently clean as judged from a good vacuum condition before a new sample is introduced.[8] To counteract this situation, we used the well-known technique of continuously flushing the cell for a very long period with the sample that is to be studied. As to the contamination in the sample tube, the H_2O sample and the intermediate sample (50 percent HDO) naturally offered no trouble, but the D_2O sample can be easily contaminated by H_2O if special precautions are not taken. For this reason, we found it was necessary to provide for breaking the seal of an Atomic Energy Commission D_2O sample tube under vacuum and to introduce the sample through an intermediate enclosure so as to avoid possible reverse contamination from the cell.

The results of a concentration test are plotted in Fig. 1. No attempt was made to measure the intensity of a line in absolute units, but it was felt that large changes in the peak values of spectral lines have a definite significance, provided all experimental conditions are kept constant. It is seen that all the known lines have their largest intensities coincident with the highest concentration of their respective molecular species. The intensities of the two D_2O lines at the intermediate concentration are much higher than what the supposed concentration (25 percent) of D_2O might indicate. This is probably due to an imperfect experimental condition. Nevertheless, the evidence confirms their identification as D_2O lines. Finally, the unknown

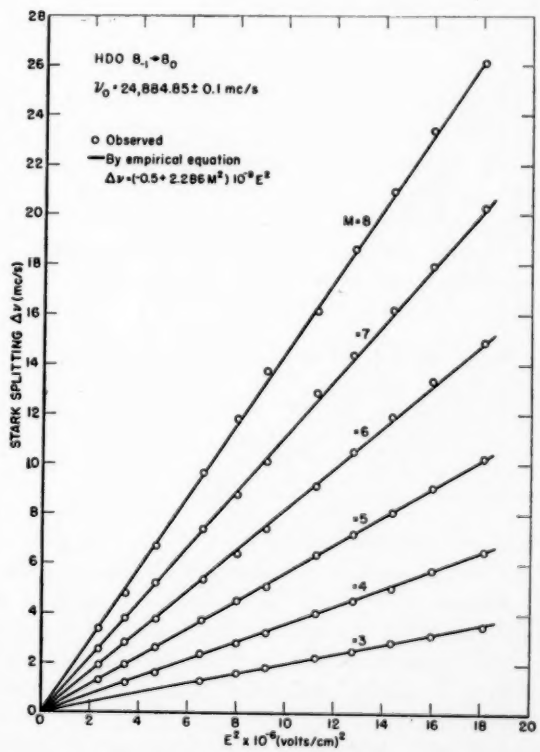

FIG. 2. Observed Stark splitting for HDO $8_{-1}\rightarrow 8_0$ line.

[8] Fuson, Randall, and Dennison, Phys. Rev. **56**, 982 (1939).

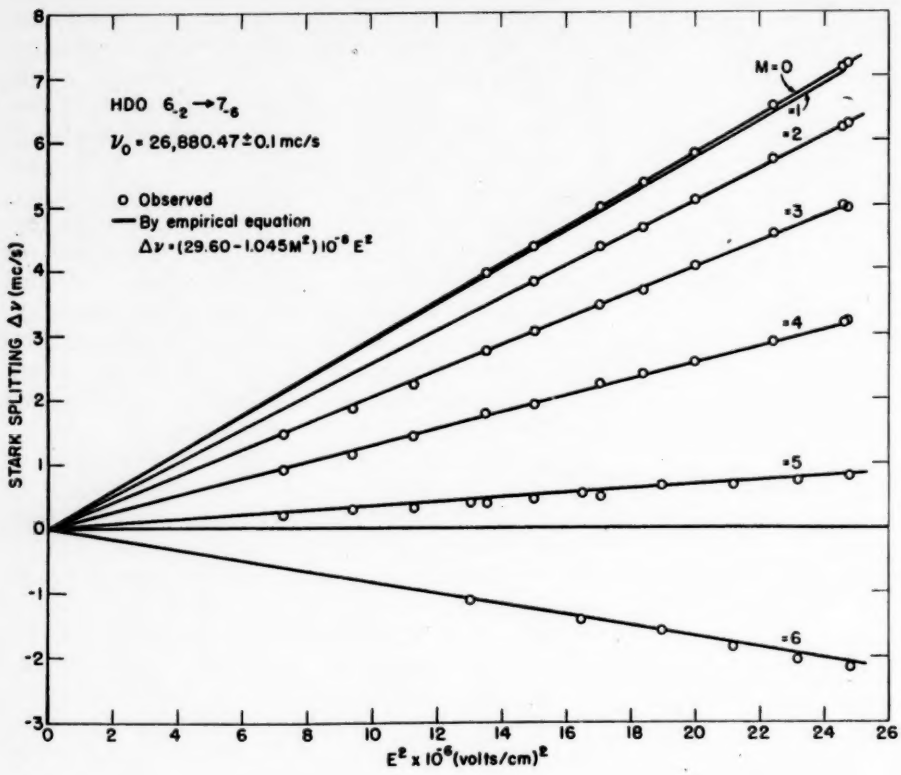

FIG. 3. Observed Stark splitting for HDO $6_{-2} \rightarrow 7_{-6}$ line.

lines A and B (labeled in Fig. 1 as "A" and "B," respectively) must be interpreted from the evidence as being caused by the HDO molecules.

V. STARK SPECTRA

Data for the Stark spectra of line A are plotted in Fig. 2, line B in Fig. 3, lines C and D in Fig. 4. Since the Stark splittings are in all cases proportional to the electric field strength (E) squared, we are dealing throughout with a second-order Stark effect.

The experimental results are accurately representable by the following empirical equations (representing $\Delta M = 0$ transitions):

$$\text{Line } A: \ \Delta\nu = (-0.5 + 2.286M^2) \times 10^{-8}E^2, \quad (1)$$

$$\text{Line } B: \ \Delta\nu = (29.60 - 1.045M^2) \times 10^{-8}E^2, \quad (2)$$

$$\text{Line } C: \ \Delta\nu = 33.9 \times 10^{-8}E^2, \quad (3)$$

$$\text{Line } D: \ \Delta\nu = 33.6 \times 10^{-8}E^2, \quad (4)$$

where $\Delta\nu$ is in Mc/sec, E in v/cm and $|M| = 0, 1, 2, \cdots$. In Eq. (1) the maximum value for $|M|$ is 8, because such an assumption is necessary for the best fit of the experimental data. In Eq. (2) the maximum value for $|M|$ is 6, because an $|M|_{\max} = 7$ component was not detected although its intensity should be strong enough to be observed if it were present.

For the interpretation of the experimental results, we have made calculations using the results of King, Hainer, and Cross[1] (hereafter referred to as KHC) for the term values and line strengths and Golden and Wilson's theory[9] for the perturbation calculations on the Stark effect.

Since the lines C and D have not been identified in their isotopic molecular species and their Stark components are not resolved, we have made no serious attempt for their quantum number assignment. We shall limit our present discussion to the lines A and B, which are to be taken as HDO lines as a result of the concentration test.

Using the KHC nomenclature, the following parameters† have been used for the HDO molecule: $(a+c)/2 = 14.923$ cm^{-1}, $(a-c)/2 = 8.453$ cm^{-1}, $\kappa = -0.700$, $\delta = 20° 38'$. With the help of these constants and the KHC tables, Golden and Wilson's equations can be evaluated with only the value for the electric dipole moment yet to be determined.

It turns out that the theoretical and experimental results can be readily brought to good agreement for the A line. The Stark structure for this line clearly indicates that it is a $\Delta J = 0$ transition and $M_{\max} = 8$. There is only one probable $J = 8_{-1} \rightarrow 8_0$ transition listed

[9] S. Golden and E. B. Wilson, Jr., J. Chem. Phys. **16**, 669 (1948).

† The parameters κ and δ were directly taken from the KHC paper (reference 1), while those for $(a+c)/2$ and $(a-c)/2$ were deduced from the tabulated term values in the same reference. By a private communication, Dr. R. M. Hainer kindly informed the authors, after the present paper had been completed, that the parameters actually used in the KHC paper were $a = 23.377$ cm^{-1}, $c = 6.381$ cm^{-1}, and $\kappa = -0.6847$ to be compared with our present values $a = 23.376$ cm^{-1}, $c = 6.470$ cm^{-1}, and $\kappa = -0.700$.

by KHC for HDO in this frequency range. Calculation has confirmed this supposition with the following result:

$$\Delta\nu=(-0.502+2.286M^2)\times10^{-8}E^2, \quad (5)$$

where the value of μ (dipole moment) is assumed to be 1.75 Debye units.[10] The agreement between Eq. (5) and Eq. (1) is very satisfactory.

The calculated results for the B line, on the other hand, are much less gratifying. Based on the experimental information concerning the Stark structure and intensity distribution, line B is definitely a $\Delta J=1$ transition. Furthermore, since the maximum M is 6 by observation, this means that the transition must be $J=6-7$. The calculated results for all the $6-7$ transitions listed by KHC are as follows (using $\mu=1.75$ d.u.):

$$\text{HDO: } 6_{-2}\rightarrow7_{-6}\Delta\nu=(32.11-0.928M^2)10^{-8}E^2, \quad (6)$$

$$7_{-7}\rightarrow6_{-2}\Delta\nu=(41.09-0.531M^2)10^{-8}E^2, \quad (7)$$

$$6_{-2}\rightarrow7_{-2}\Delta\nu=(84.41-30.43M^2)10^{-8}E^2, \quad (8)$$

$$6_0\rightarrow7_{-5}\Delta\nu=(0.61-0.940M^2)10^{-8}E^2. \quad (9)$$

The above results were obtained under the following conditions. The energy difference between the two levels, as given by KHC, in each assumed transition varies between 0.02 and 2.55 cm^{-1}. The observed frequency corresponds to an energy difference of roughly 0.897 cm^{-1}. Within the limits of accuracy of KHC's calculations, particularly in view of their neglect of centrifugal distortion effects, any one of the four sets should be considered as a possible transition. In dealing with each case individually, we assume that the energy difference in the set temporarily treated as a possibility coincides exactly with that corresponding to the observed frequency. In calculating the Stark effect, the largest contribution to the Stark energy of one level is mostly caused by the interaction with the other level of the assumed microwave transition. This is exactly what happened with the HDO $8_{-1}\rightarrow8_0$ line that we have just assigned. On the other hand, it happens sometimes that one of the energy levels in the supposed transition has a "near-degeneracy" with one or more other energy levels which may exert strong perturbing effects.[11] Under these conditions the small energy differences for these levels listed by KHC are not believed to be accurate enough for this kind of strong perturbation calculation. It so happens, unfortunately, that each one of the above four possible transitions has at least one near-degeneracy which requires special consideration. These cases will be discussed below.

First, we take up the case of $6_{-2}\rightarrow7_{-6}$ possible transition. The 7_{-7} level is near-degenerate to the 6_{-2} level. A straightforward calculation using the KHC value for $W^0(6_{-2})-W^0(7_{-7})=1.31$ cm^{-1} gives the result $\Delta\nu=(23.89-0.760M^2)10^{-8}E^2$. This is to be compared with the experimental determination $\Delta\nu=(29.60-1.045M^2)10^{-8}E^2$ as given in Eq. (2). It is clear we need to make up the deficiency (roughly 20 percent) in the calculated contribution by a stronger perturbation. A partial solution to the problem is obtained by arbitrarily adjusting the degree of near-degeneracy so as to secure the closest fit with the experimental result. Since we have only one adjustable parameter, it is not possible to fit the two Stark coefficients at the same time. We have assumed $W^0(6_{-2})-W^0(7_{-7})=-0.016$ cm^{-1} to give a compromise fit for both coefficients with the result as expressed in Eq. (6).

A similar situation exists for the second possible transition $7_{-7}\rightarrow6_{-2}$, in which the level 6_{-2} is perturbed by the level 7_{-6}. A straightforward calculation using the KHC result $W^0(7_{-6})-W^0(6_{-2})=0.02$ cm^{-1} gives $\Delta\nu=(-543.9+11.41M^2)10^{-8}E^2$ which is radically wrong both in magnitude and in sign. Again, to bring the result to closer agreement with observation, we have arbitrarily assumed $W^0(7_{-6})-W^0(6_{-2})=0.27$ cm^{-1} giving the net result as expressed in Eq. (7).

In the third and fourth possible transitions, $6_2\rightarrow7_{-2}$ and $6_0\rightarrow7_{-5}$, the near-degenerate level in each case has the same J-value as the principal level that is being perturbed. Such a perturbation, according to Golden

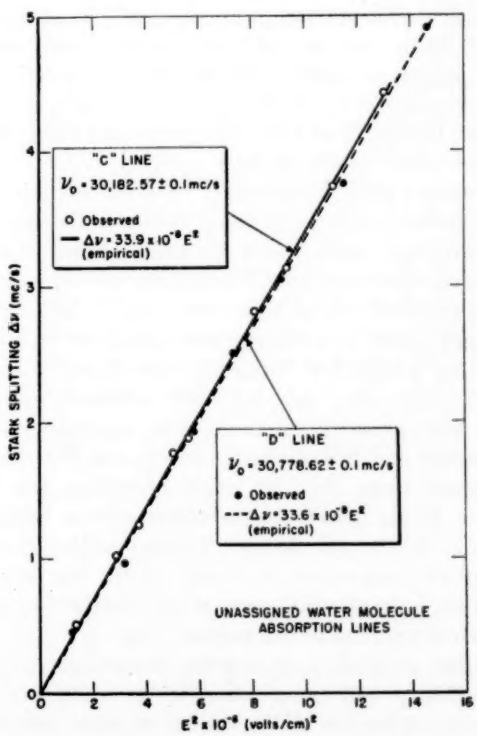

FIG. 4. Observed Stark splitting for unassigned water molecule absorption lines "C" and "D."

[10] The value of μ(HDO) determined here depends upon the calibration of field strength in the Stark cell. Had we used Strandberg's value $\mu(O^{16}C^{12}S^{32})=0.732$ instead of Shulman and Towne's value $\mu(O^{16}C^{12}S^{32})=0.7085$, we would have got μ(HDO) $=1.87$ in fair agreement with Strandberg's result (see reference 2).

[11] Calculation has shown that the nearly degenerate levels considered in this paper are still sufficiently far apart that Golden and Wilson's formulation for the degenerate levels gives the same result as that derived from the nondegenerate case.

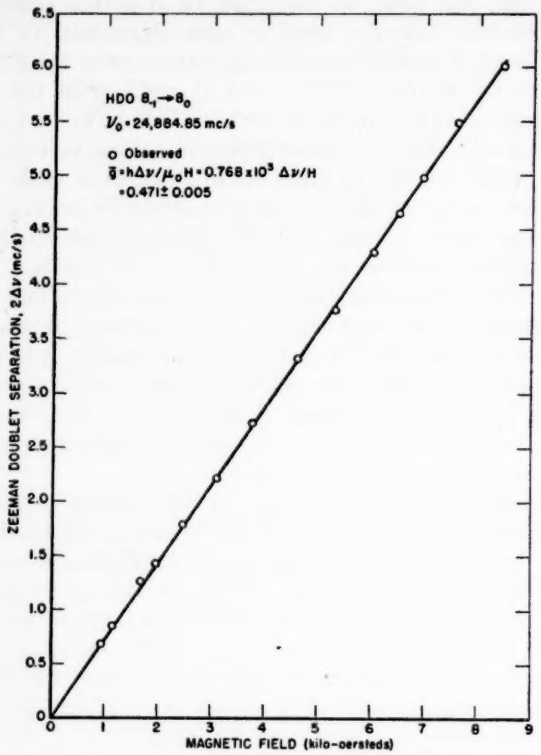
HDO $8_{-1}\rightarrow 8_0$
ν_0 = 24,884.85 mc/s
o Observed
$\bar{g} = h\Delta\nu/\mu_0 H = 0.768 \times 10^3\ \Delta\nu/H$
= 0.471 ± 0.005
ZEEMAN DOUBLET SEPARATION, $2\Delta\nu$ (mc/s)
MAGNETIC FIELD (kilo-oersteds)

FIG. 5. Observed Zeeman splitting for HDO $8_{-1}\rightarrow 8_0$ line.

and Wilson's theory, can only affect the Stark coefficient in the M^2 term. Therefore, no adjustment of the amount of near-degeneracy of the same J-value level can change the Stark coefficient independent of M^2. Equations (8) and (9) show that the M^2-independent coefficients in both cases are so widely different from observation that an adjustment of near-degeneracy will serve no useful purpose. Hence, these two cases were calculated directly from the KHC tabulated term values.

It seems quite reasonable to conclude that the $6_{-2}\rightarrow 7_{-6}$ transition gives much better agreement with the Stark data than the other three transitions, as a comparison between Eq. (2) and Eqs. (6)–(9) will show. The agreement might have been much better, if we could get access to more accurate term values and line strengths (preferably including centrifugal distortion effects) than what are currently available from the KHC rigid rotor calculations. The inaccuracy of the term values and line strengths affects not just the near-degenerate cases but all cases involving the intermediate levels whose perturbation effects figure significantly in the calculation. These considerations are particularly important in cases where the supposed transition is weak and some of the perturbing transitions are strong, as in the present case.

Another possibility of securing better agreement between theory and observation is by using a slightly different κ-value for HDO, similar to what Strandberg has done.[2] With a new value of κ there would be correspondingly new values for δ, term values and line strengths. A re-evaluation of the Stark coefficients based upon a given value of κ can be carried out for lines A and B. The new value for κ should be such that, together with adjustment of the value for the dipole moment μ, theory and observation of the Stark coefficients agree best for both lines A and B. As this procedure is laborious and does not in any way eliminate uncertainties associated with near-degeneracies, we do not feel that it is advantageous to resort to this measure.

The supposition of a $6_{-2}\rightarrow 7_{-6}$ transition for line B can be considered as plausible also from the intensity considerations. The calculated absorption coefficient for line A (HDO $8_{-1}\rightarrow 8_0$) is 22.2×10^{-6} cm^{-1} while that for line B is 52.3×10^{-6} cm^{-1}.[12] Experimentally line A and line B had roughly the same apparent intensity. But the apparent intensity of a spectral line, when Stark modulation is used, often depends upon the degree of resolution between the Stark components. In general, the smaller the Stark effect, the lower is the apparent intensity, when the same modulation voltage is used. Since line B has a much smaller Stark effect than that of line A, it is not surprising to find that line B is not as strong as the calculated intensity might indicate.

VI. ZEEMAN SPECTRA

The results for the Zeeman splitting of the lines A and B are given, respectively, in Figs. 5 and 6. The transitions observed are of the σ-type ($\Delta M = \pm 1$). It is

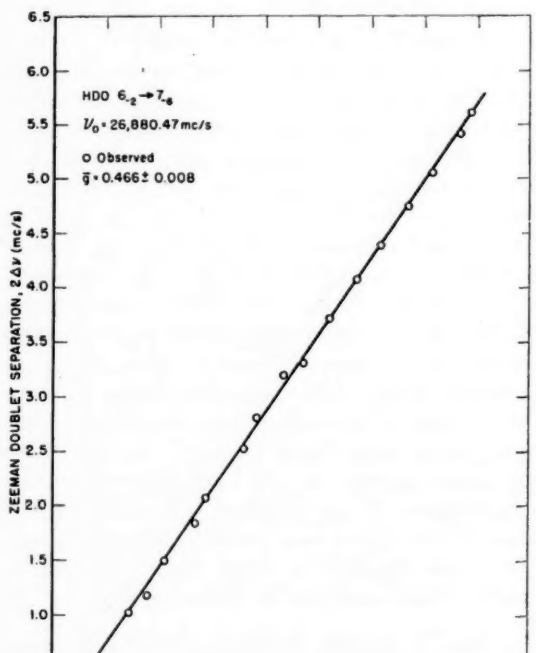

FIG. 6. Observed Zeeman splitting for HDO $6_{-2}\rightarrow 7_{-6}$ line.

[12] These values for the absorption coefficient are those given by KHC corrected by the square of the ratio of frequencies.

noted that experimentally only a doublet-like splitting is observed for both lines A and B. The fact that the doublet character is not appreciably lost even at high magnetic fields means that the g-factors for the transition energy levels do not differ drastically. The g-factors derived from lines A and B are, respectively, 0.471 and 0.466. These values do not differ appreciably from the g-factors previously determined for the other HDO lines.[5] Thus the Zeeman data for the lines A and B are not in disagreement with the supposition that they are HDO lines.

The authors wish to express their appreciation to Mr. J. W. B. Barghausen for his valuable assistance in the experimental work.

THE JOURNAL OF CHEMICAL PHYSICS VOLUME 21, NUMBER 3 MARCH, 1953

The Thermal Decomposition of Nitromethane*†

LOUIS J. HILLENBRAND, JR., AND MARY L. KILPATRICK
Department of Chemistry, Illinois Institute of Technology, Chicago, Illinois

(Received October 14, 1952)

A study of the thermal decomposition of nitromethane was made by the flow method, with nitrogen as carrier gas, the reaction being followed by polarographic analysis of the effluent from the furnace for nitromethane. When carefully dried nitrogen was used the rate of disappearance of nitromethane became erratic; it was, however, found possible to obtain reproducible results by passing wet nitrogen through the unit before the kinetic run. The decomposition follows the first-order law, and over the range 420–480°C is represented by the equation $k=2.7\times10^{13}\exp(-50\,000/RT)$ sec^{-1}. At 420°, k is in good agreement with the value obtained by Cottrell, Graham, and Reid by the static method, but at higher temperatures the observed rate is lower than that computed from their equation. Although the energy of activation is close to that required to break the C—N bond, the high initial yield of formaldehyde obtained in the flow-method experiments suggests that the rate is in part determined by an intramolecular rearrangement.

INTRODUCTION

WHEN this work was begun, there was in the literature only one paper on the thermal decomposition of nitromethane vapor, that by Taylor and Vesselovsky,[1] who measured the increase of pressure as the reaction proceeded at constant volume. They got a final increase of 130 percent, and calculated first-order velocity constants from the times necessary to attain $\frac{1}{4}$ and $\frac{1}{2}$ of the final increase. The specific rate calculated from the half-life was usually smaller than that calculated from the quarter-life, but they concluded that the decomposition was a homogeneous first-order reaction, with an energy of activation of about 61 kcal.

Since reactions between the products of decomposition complicate the measurement of rate by the static method, we decided to undertake a study of the reaction by the flow method, using an inert gas as carrier, and analyzing the gas effluent from the furnace for nitromethane. This work, of which a preliminary report has already been published,[2] was nearly complete when there appeared a note by Cottrell and Reid,[3] then a paper by Cottrell, Graham, and Reid,[4] describing their work on the reaction.

Like Taylor and Vesselovsky, Cottrell, Graham, and Reid used the static method. Like them, they got an over-all increase in pressure of 130 percent and found the reaction to be largely homogeneous. Cottrell and co-workers computed the specific rate from the initial slope of the pressure-time curve, i.e.,

$$k=(dp/dt)_0/1.3p_0;$$

however, the individual curves followed the first-order law over much of their length, and the specific rate calculated by Guggenheim's method was close to that calculated from the initial slope except at the highest pressures. They found the specific rate to be independent of nitromethane pressure at pressures above 200 mm, but below that to drop off with decreasing pressure; to be unaffected by the addition of nitric oxide; and over the range of temperature investigated (380–430°C) to be given by the equation

$$k=10^{14.6}\exp(-53\,600/RT)\ \text{sec}^{-1}. \quad (1)$$

Since the energy of activation is close to $\Delta H_{298}°$ for the reaction

$$CH_3NO_2\rightarrow CH_3+NO_2, \quad (2)$$

as calculated from the heats of formation, they suggested that the initial and rate-determining step is the fission of the C—N bond, and that this is followed by a series of radical reactions in a nonchain mechanism. The higher energy of activation obtained by Taylor and Vesselovsky they attributed to the fact that the earlier workers in most experiments employed pressures below 200 mm.

* Work done under contract with the U. S. Office of Naval Research, Research Contract N7onr-329, Task Order III.

† Abstracted from the dissertation of Louis J. Hillenbrand, Jr., presented May 15, 1952, to the Faculty of the Graduate School of Illinois Institute of Technology in partial fulfilment of the requirements for the degree of Doctor of Philosophy.

[1] H. A. Taylor and V. V. Vesselovsky, J. Phys. Chem. **39**, 1095 (1935).

[2] L. J. Hillenbrand, Jr., and M. L. Kilpatrick, J. Chem. Phys. **19**, 381 (1951).

[3] T. L. Cottrell and T. J. Reid, J. Chem. Phys. **18**, 1036 (1950).

[4] Cottrell, Graham, and Reid, Trans. Faraday Soc. **47**, 584 (1951).

EXPERIMENTAL PART

Our kinetic experiments fall into two groups. In the earlier runs, a stream of nitrogen, saturated with nitromethane at 31°C at atmospheric pressure, passed through the furnace at reaction temperature. The mole fraction of nitromethane in the stream entering the furnace under these conditions was 0.06. It was planned to obtain higher concentrations of nitromethane by raising the temperature of the saturator; however, it proved difficult to achieve saturation at temperatures much above room temperature, and in the later experiments the "saturation technique" was replaced by the "injection technique" in which nitromethane was injected into the nitrogen stream from a motor-driven syringe, and vaporized.

The effluent from the furnace was passed through traps kept at −78°C, where the undecomposed nitromethane condensed, together with any products nonvolatile at this temperature. The nitromethane in the condensate was determined by polarographic analysis.[5]

The procedure followed below is to describe at the start those features common to both groups of experiments, and then give the special features for each group, in turn, together with the results obtained.

Nitromethane

Two lots were used. The first was a commercial product which was put through a distilling column; the fraction retained boiled at 100.0–100.9°C at 750 mm and had an index of refraction of 1.3793 at 26°. The second was a special sample kindly provided by the Commercial Solvents Corporation. It was used without further processing. Its specifications are as follows: Water (by Karl Fischer) = 0.05 percent. Acidity (as acetic acid) = 0.007 percent. Aldehydes and ketones (as acetone) = 0.23 percent. Nitrogen (micro Dumas) = 22.84 percent. Theoretical N, corrected for the above = 22.88 percent. Theoretical N for CH_3NO_2 = 22.95 percent. No difference in rate of decomposition was found between the two lots.

Furnace

The furnace consisted of three sections, 4, 8, and 12 inches long, respectively. The free space between the ceramic holders and the coils of the heaters was filled with alundum cement to increase the heat capacity, and the transite end plates were removed from the inside ends of the sections of furnace so as to bring the heaters closer together. To reduce the drop in temperature at the junctions between the sections, the glass reactor was placed in an aluminum tube which (except for the necessary tolerances) eliminated the free space between the glass tube and the heaters; after installation of the aluminum tube, the drop in temperature at the junctions was less than 1°C.

[5] Miller, Arnold, and Astle, J. Am. Chem. Soc. **70**, 3971 (1948).

The three heating units of the furnace were operated by three Celectray Indicating Potentiometer Controllers made by the C. J. Tagliabue Corporation. The thermocouples for the controllers were placed between the glass reactor and the aluminum tube, each at the center of its section of furnace.

Reactor

The reactor was a 16 mm o.d. Pyrex glass tube packed with smooth $\frac{1}{8}$-inch Pyrex beads and having an axial thermocouple well. The free volume was 0.747 cc per cm of length.

The temperature profile of the reactor consisted of a 17.5-inch length constant within ±1°, together with a 2.5-inch length at the inlet end and a 3.0-inch length at the outlet end where the temperature rose to, or fell from, control temperature. The end lengths were converted to equivalent lengths at control temperature in the manner described below.

The end lengths were divided into short increments ΔL^* whose temperature was taken as a constant. For a first-order reaction, and for no change in the number of molecules per unit mass of gas, the equivalent increment of length at control temperature, ΔL, is given by

$$\Delta L = \left[\frac{k_t}{k_c}\cdot\frac{T_c}{T_t}\right]\Delta L^*, \tag{3}$$

where T_t and T_c are the local and control temperatures (°K) and k_t and k_c are the corresponding values of the specific rate of decomposition of nitromethane. The ratio of specific rates was computed from the equation

$$\ln\frac{k_t}{k_c} = -\frac{50\,600}{R}\left[\frac{T_c - T_t}{T_t T_c}\right]. \tag{4}$$

The effective free volume of the reactor, at all temperatures, was found to be 40.2±0.6 cc.

Thermocouples

The thermocouples were of No. 30 gauge iron and constantan wire. The three used to operate the controllers have already been mentioned. The other two, which were placed in the axial well of the reactor, were used to determine the temperature profile. The first of the two indicating thermocouples was read on the dial of the Celectray, the second on a Leeds and Northrup portable precision potentiometer. Both indicating thermocouples were calibrated against a platinum resistance thermometer with Bureau of Standards certificate; in making the calibration, the reactor was removed from the furnace and replaced by a Pyrex tube of the same diameter, with an opening at the top for the thermometer, and one at the bottom for the thermocouple, thermometer and thermocouple meeting in the middle of the center section of the furnace. In addition

the second indicating thermocouple was calibrated at frequent intervals at the freezing point of zinc.

Contact Time

In evaluating the time which the gas spends in the reactor, it is necessary to allow for the increase in velocity of flow accompanying reaction in the case of a reaction of the type $A \rightarrow \nu B$ where $\nu > 1$. The theory of this effect has been treated by Hulburt[6] and by Brinkley.[7] If the reactor is in the form of a cylindrical tube within which reaction occurs in a homogeneous fluid flowing isothermally with negligible pressure drop, and if the composition, density, and velocity of the fluid are uniform over any cross section of the reactor, the ratio of the true to the apparent contact time is given for the case of a first-order reaction by the equation[7]

$$\frac{\theta}{\theta^*} = \frac{\ln \eta_L}{(1+\beta)\ln \eta_L + \beta(1-\eta_L)}, \tag{5}$$

where η_L = fraction of the reference constituent (here nitromethane) remaining after passage through tube of length L, and β = relative increase in volume, per unit mass of gas, for complete reaction.

Cottrell, Graham, and Reid obtained for ν values from 2.3 to 2.4 by analysis of the products at various stages of the reaction, and from the final increase in pressure both they and Taylor and Vesselovsky obtained 2.3. With nitromethane present at low concentration in a stream of inert gas, θ/θ^* is quite insensitive to small changes in ν. The value 2.4 was employed in the present investigation for the computation of β and θ/θ^*. The contact time t_c was obtained from Eq. (10) or (13).

The Polarographic Analysis for Nitromethane

We found, as had previously been reported,[5] that in acid solution nitromethane yields a well-defined wave whose height is proportional to the concentration. Our measurements were made on a Model XX Sargent polarograph. The solution analyzed was $0.01M$ in hydrochloric acid and $0.2M$ in potassium chloride in all cases. Our routine, when kinetic runs were made, was to accumulate a number of samples, determine the calibration factor (moles nitromethane per liter, per mm wave height) by means of the standard solution, then analyze the unknowns.

The standard solution, *ca* $0.001M$, was prepared by dissolving nitromethane in distilled water. It was put into ten Pyrex bottles, very little air space being left over the solution, and the bottles tightly closed. One of the bottles was used per week, each bottle being opened only two or three times. The standard solution proved to be stable over the period it lasted.

[6] H. M. Hulburt, Ind. Eng. Chem. **36**, 1012 (1944).
[7] S. R. Brinkley, Jr., Ind. Eng. Chem. **40**, 303 (1948).

Gas Analysis

The products not condensing in the trap at $-78°$ were collected with the carrier in a gas burette over saturated sodium chloride solution. Except in the experiments where ethanol was used in the trap, a portion of the gas collected was displaced into a sample tube and analyzed in a standard Fisher gas analysis unit for oxides of carbon, hydrogen, and methane. The low concentration of the product gases made accurate measurement of the individual components difficult.

EXPERIMENTS BY THE SATURATION TECHNIQUE

A stream of tank nitrogen was passed over copper turnings at 300°, to remove oxygen, and through a capillary flowmeter, and then was saturated with nitromethane. The saturator, which was immersed in a thermostat regulated to $31.0 \pm 0.05°$, consisted of four towers packed with glass beads, the first three, but not the fourth, being filled with nitromethane to a depth of six inches. From the saturator the gas passed to the reactor, from there to two traps in a dry ice-acetone bath, and finally to the gas burette. Between reactor and traps there was a three-way stopcock permitting passage of the gas stream to the traps, or to the atmosphere. To prevent condensation of nitromethane, the tubes leading from the saturator to the reactor and from the reactor to the traps were heated through a wrapping of Nichrome wire.

To carry out an experiment, the traps, placed in the dry ice-acetone bath, were flushed with nitrogen which had passed through the heated reactor; after the flushing, the stream was vented to the atmosphere and the traps shut off. The nitrogen stream was next diverted to the saturator, and the flow adjusted to the desired rate. When a volume of gas equal to at least ten times the free volume of the reactor had passed, the experiment was started by diverting the stream to the traps and gas burette. The experiment was stopped by venting the stream to the atmosphere when *ca* 700 cc of gas had collected in the burette.

At the end of the experiment the traps were removed from the bath, and before the frosting of ice which formed upon their outer surface upon removal had entirely melted, they were rinsed out with a measured volume of HCl-KCl solution for polarographic analysis. Although two traps were used, in series, no condensate was visible in the second. As the traps warmed from -78 to $0°$ the brown fumes of NO_2 were frequently seen, and occasionally there was visible a drop or two of a blue liquid which gave off NO_2 on warming, and which was judged to be N_2O_3.

The partial pressure of nitromethane in the inlet stream was found by carrying out a set of runs with the reactor at 300°, where decomposition was negligible. The nitromethane was collected in the trap in the usual manner, and the nitrogen in the gas burette. The result of the runs, which were carried out at rates of gas flow

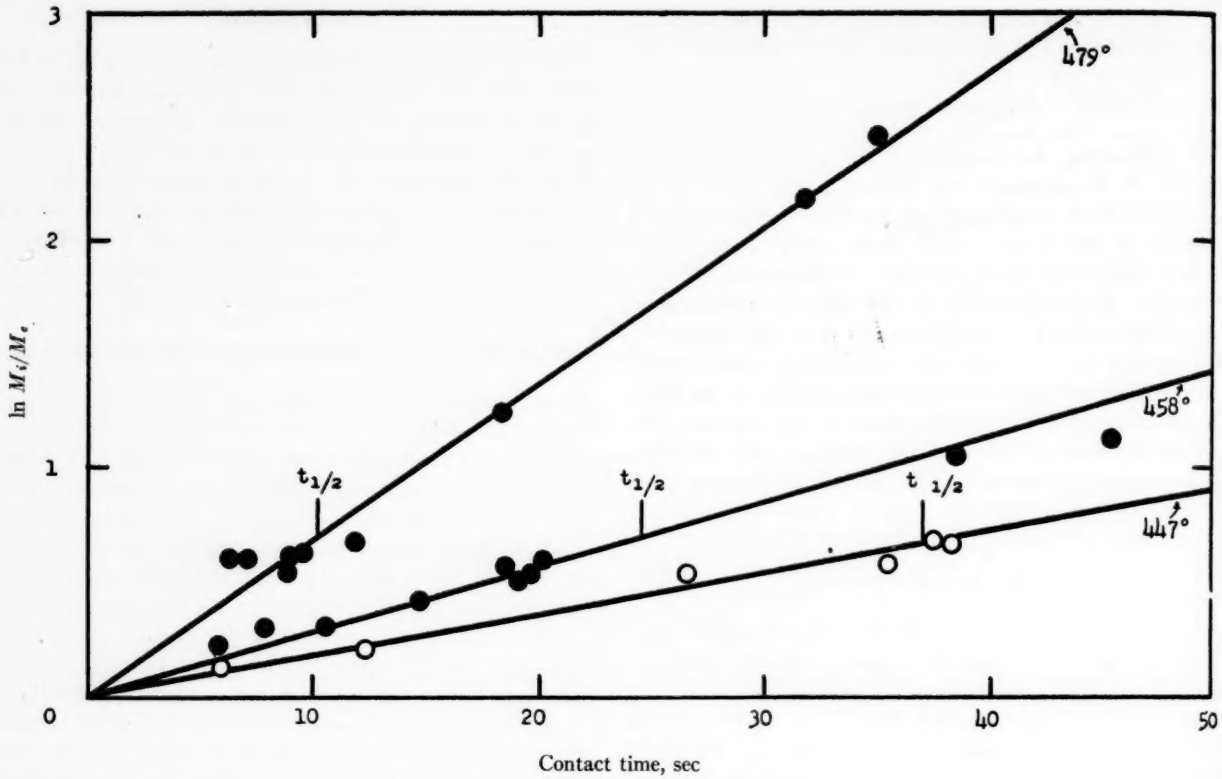

FIG. 1. Results with the saturation technique.

from 29 to 110 cc/min, was 47.0±0.7 mm, with no trend. This may be compared with 49.1 mm, the vapor pressure given by Hodge[8] for this temperature.

The rate of flow of nitrogen was not obtained from the flowmeter reading because of fluctuation of the flowmeter with passage of gas through the saturator; instead, it was computed from the volume of gas collected. Here it was necessary to make a small correction for the presence of products of decomposition, and in making the correction it was assumed that 1.7 moles of permanent gas are produced per mole of nitromethane decomposed.

The quantities necessary for the calculation of the specific rate were evaluated by means of the equations below. The various rates of flow of gas were calculated at the temperature of the saturator (31.0°C) and at existing atmospheric pressure:

$$R_P=(M_i-M_e)(1.7)\bar{V}_B/t=\text{rate of flow of product gases,} \quad (6)$$

$$R_{N_2}=R_T-R_P=\text{rate of flow of carrier,} \quad (7)$$

$$R_{NM}=P_{NM}R_{N_2}/(P-P_{NM})=\text{rate of inflow of } CH_3NO_2, \quad (8)$$

$$M_i=R_{NM}t/\bar{V}_B=\text{moles } CH_3NO_2 \text{ entering furnace,} \quad (9)$$

$$t_c=\{60V_f/(R_{N_2}+R_{NM})\}\cdot\{T_B/T_F\}\theta/\theta^*=\text{contact time, sec,} \quad (10)$$

$$k=(1/t_c)\ln(M_i/M_e)=\text{specific rate, sec}^{-1}, \quad (11)$$

where P = barometric pressure, corrected, P_{NM} = partial pressure of CH_3NO_2, $\bar{V}_B$ = volume of 1 mole of ideal gas at 31.0°C and pressure P, t = time of run = time of collection of products, min, M_e = moles CH_3NO_2 found in trap, R_T = total rate of flow from traps, gaseous products and carrier, V_f = effective free volume of reactor, θ/θ^* = correction factor from Eq. (5), T_B = temperature (absolute) of saturator, and T_F = temperature (absolute) of reactor.

Experiments were carried out at 446.8, 458.3, and 478.7°C, the mole fraction of nitromethane in the inlet stream being 0.06 in all cases. The results are shown in Fig. 1, where the slope of each line is the average of the values obtained for k in the individual experiments. Within the accuracy of the measurements the disappearance of nitromethane follows the first-order law.

During the course of the experiments a red, resinous deposit was observed to accumulate slowly in the outlet tube leading from the reactor to the traps; the reactor itself, however, remained clean. A sample of resin scraped from the outlet tube at this time analyzed as follows:

C, 33.50; H, 6.21; N, 34.43; O, 25.86 weight percent.

EXPERIMENTS BY THE INJECTION TECHNIQUE

The Injector

In the experiments carried out by this technique, nitromethane was injected into the nitrogen stream (see Fig. 2) from a Luer tuberculin syringe, the plunger

[8] E. B. Hodge, Ind. Eng. Chem. 32, 748 (1940).

of which was driven in at a known and constant rate by means of gears operated by a synchronous Telechron motor with a shaft speed of one revolution per minute. The 2-inch No. 25 stainless steel needle attached to the syringe extended into the tube of the unit through a self-sealing rubber ampoule cap.‡ The tip of the needle touched a ball of Pyrex glass wool, heated to 104°C by radiant heat from two small globars located outside the tube. The gears and motor are not shown in the figure. The rate of ejection of nitromethane from the syringe was varied by changing the drive gear or by changing the size (cross section) of the syringe. Except for the fact that the globars were located outside the tube in which vaporization occurred, the apparatus was similar to that used by Robertson and co-workers[9] and by Lingane.[10]

Syringes of $\frac{1}{4}$ and 1 cc capacity were calibrated first by measuring the rate of ejection of mercury, to test the constancy of the cross section of the barrel, then that of nitromethane. The liquid ejected was caught in a small vial and weighed. Comparison of the rates of ejection gave a measure of the apparent reduction of the cross section with nitromethane in the syringe, due to its ability to wet the channel between the plunger and the barrel. It was found that the rate of ejection of nitromethane could be represented by an equation of the form

$$D=AT-B, \tag{12}$$

where D is the discharge, in moles/min, T is the number of teeth on the drive gear, A is the "perfect" discharge per tooth, and B is the vaporization loss. The method of least squares, applied to the discharge from the 1 cc syringe, yielded

$$D=9.155\times10^{-6}T-1.82\times10^{-6},$$

and to that from the $\frac{1}{4}$ cc syringe,

$$D=4.740\times10^{-6}T-3.16\times10^{-6},$$

the average deviation of the observed from the calculated discharge being 0.3 percent for the 1 cc and 0.6 percent for the $\frac{1}{4}$ cc syringe.

The completeness of vaporization of nitromethane was tested in a series of experiments carried out with the furnace at 300°. At the end of the collection the cold trap containing the condensate was sealed at both ends with a torch. After coming to room temperature the trap was weighed, then it was opened, cleaned, and weighed again; the difference in weight, corrected for losses in opening (0.0003 g), and for buoyancy, gave the weight of nitromethane collected. Satisfactory agreement was found, at all rates of ejection, between the weight of nitromethane collected and that calculated from the calibration of the syringe.

Purification of Nitrogen

The nitrogen used in the injection technique experiments passed through: (1) a tube filled with cupric oxide, heated in a furnace to *ca* 550°, to oxidize hydrocarbons; (2) a tube filled with Ascarite, to remove CO_2; (3) a tube of Drierite; (4) a long tube filled with copper deposited on silica gel, heated to *ca* 300°, to remove oxygen; and (5) a long tube filled with glass beads coated with P_2O_5.

The Flowmeter

The flowmeter, which was filled with dibutyl phthalate, was enclosed in a box kept at 29.5±2°. It was calibrated directly in terms of moles of nitrogen passing per minute.

Analysis for Formaldehyde

During the first series of runs carried out using the injector formaldehyde was detected, by odor, in an experiment where the traps were allowed to come to room temperature. Thereafter it was tested for routinely, analysis for the carbonyl group being made with

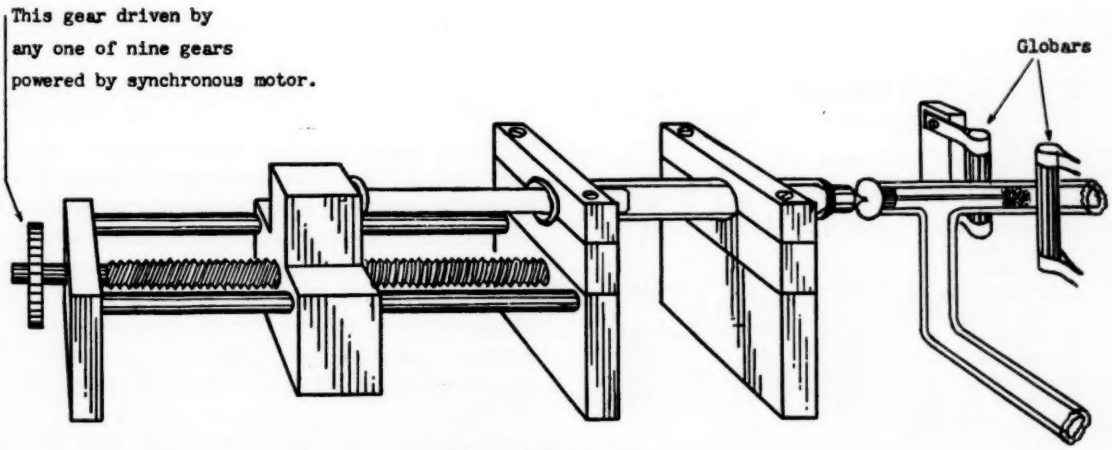

FIG. 2. The injector.

‡ The ampoule caps were kindly donated by Eli Lilly and Company.

[9] Robertson, Bigg, Puck, and Miller, J. Exptl. Med. **75**, 593 (1942).

[10] J. J. Lingane, Anal. Chem. **20**, 285 (1948).

TABLE I. Effect of pretreatment of unit with oxygen on specific rate.

Run	Pretreatment[a] with	hrs	F_{NM}	t_c sec	k at 444.8°C sec^{-1}
99–120			0.06 to 0.18	4 to 53	0.0178±0.0034[b]
121–126			0.06, 0.18	6 to 38	0.037 to 0.31
127			0.18	38	0.12
128	Air	48	0.18	10	0.041
129			0.18	39	0.035
130	O_2	15	0.18	39	0.030
131			0.18	23	0.027
132	O_2	64	0.18	23	0.022
133			0.18	23	0.020
134–142			0.06, 0.18	5 to 41	0.014 to 0.039

[a] A blank space signifies that only N_2 passed between runs.
[b] Two experiments at low t_c's omitted from average.

hydroxylamine reagent according to the directions of Trozzolo and Lieber.[11] Although the reaction between acetone and hydroxylamine occurs at once, that between hydroxylamine and the product in the trap was found to occur slowly. The same slowness of reaction was observed in a test made on an alcoholic solution of formaldehyde prepared by passing nitrogen through 40 percent formalin solution and then into ethanol; it may be due to a slow depolymerization prior to reaction with hydroxylamine.[12] Nitromethane was shown not to interfere in the analysis for formaldehyde.

In some cases, analysis for formaldehyde was made on the contents of the trap in a run duplicating that in which analysis was made for nitromethane. In others, the two empty traps were replaced by a single trap of 180 cc capacity, in which was put 50 ml of 95 percent ethanol, and which was chilled as before. At the end of the run one aliquot of the alcoholic solution was diluted with aqueous HCl-KCl for polarographic analysis for nitromethane, another with ethanol for analysis for formaldehyde. It was demonstrated that ethanol and formaldehyde did not interfere in the analysis for nitromethane. If a single trap containing ethanol replaced the two empty traps, an equivalent head of water was used in the vent to the atmosphere.

TABLE II. Various tests to determine cause of erraticalness in specific rate.

Run	Conditions	F_{NM}	t_c, sec	k at 472.6°C sec^{-1}
143–153	Normal run	0.06, 0.18	4 to 37	0.10 to 0.48
155	Outlet tube not heated	0.18	10	0.15
156	Outlet tube not heated	0.18	10	0.14
157	Normal run	0.18	10	0.059
158–168	Increased heat on outlet tube	0.06, 0.18	4 to 21	0.062 to 0.19
169	Normal run	0.18	21	0.088
173	CH_3NO_2 saturated with H_2O at 25°	0.18	21	0.089
174	Carrier is air	0.18	20	0.150
175	Normal run	0.18	21	0.070
176	Normal run	0.18	21	0.070
177	Carrier is N_2 saturated with H_2O at 29°	0.18	21	0.072

[11] A. M. Trozzolo and E. Lieber, Anal. Chem. **22**, 764 (1950).
[12] R. Sautery, Compt. rend. **220**, 595 (1945).

The Kinetic Experiments

The procedure for carrying out a kinetic run was similar to that already described. The rates of inflow of nitrogen and nitromethane in moles per minute, R_{N_2}' and R_{NM}', were obtained from the calibrations of flowmeter and syringe, respectively, and the total flow at reactor conditions in cc/min, R, from their sum by means of the gas law. The contact time was calculated from the equation

$$t_c = 60(V_f/R)(\theta/\theta^*). \tag{13}$$

The first series of experiments was carried out at 444.8°, at mole fractions of nitromethane of 0.06, 0.12, and 0.18. There was no effect of change in concentration, and the average value of the specific rate (0.0178±0.0034 sec^{-1}) is in reasonable agreement with that obtained by the saturation technique at 446.8° (0.0190±0.0019 sec^{-1}).

After about twenty runs, however, the results became high, and erratic (compare with runs 121–127 in Table I). Since nitromethane as a fuel is deficient in oxygen, which causes a reducing atmosphere to prevail during the decomposition, it was decided to try pretreating the unit with oxygen; after run 127 air was passed through the unit for 48 hours, after which it was flushed out thoroughly with dry, oxygen-free nitrogen, and run 128 performed. In run 128 k was less than half that in run 127. It will be seen that after each pretreatment with oxygen or air the rate fell, but that the results did not continue to be reproducible (runs 134–142).

After run 133 the reactor was examined and found to be as clean as when it was originally packed. Visible condensation of resinous material began in the outlet tube at the edge of the furnace. A sample of resin scraped from the outlet tube at this time analyzed as follows:

C, 45.47; H, 5.84; N, 31.44; O, 17.25 weight percent.

The resin began to soften at *ca* 115°, but was still not very fluid at 146°. The melt contained many bubbles. From the cleanness of the reactor it appears that the resinous products are not formed at reaction temperature, but are formed via condensation or addition reactions occurring in the cooler outlet tube. The high values obtained for the rate of disappearance of nitromethane could be accounted for by participation of nitromethane in one or more of these secondary reactions.

The furnace was next set at 472.6° with the expectation that the discrepancies would be exaggerated at the higher temperature. The first results obtained are shown in Table II. In a normal run the carrier was dry nitro-

TABLE III. The decomposition of nitromethane in nitrogen with the injection technique at 472.6°C. Effect of pretreatment with wet nitrogen

Products collected in ethanol P=740–750 mm θ/θ^*=0.85–1.00

Run	Pretreatment Wet N_2 hr	Pretreatment Dry N_2 hr	R'_{NM} ×10⁴	R'_{N_2} ×10⁴	F_{NM}	t min	M_i ×10⁴	M_e ×10⁴	Moles HCHO ×10⁴	t_o sec	k sec⁻¹
178		1.5	2.911	13.26	0.18	14.00	40.75	10.0	6.4	21.5	0.0652
179[a]	20	2	10.968	49.97	0.18	3.50	38.39	22.82	5.0	6.05	0.0857
180			6.573	29.94	0.18	6.00	39.44	23.20	5.6	10.1	0.0525
181[a]	1.5	0.5	3.381	52.97	0.06	6.30	21.30	12.72	3.8	6.75	0.0763
182			5.656	88.61	0.06	4.20	23.76	16.41	3.3	4.06	0.0908
183[a]	30	3.5	1.630	7.43	0.18	21.20	34.56	3.79	4.0	37.1	0.0596
184	3	2	0.8216	12.87	0.06	25.00	20.54	2.36	3.0	26.95	0.0801
185[a]	14	1	0.6794	10.64	0.06	31.50	21.40	2.09	2.8	32.6	0.0715
186[a]	13.5	2.5	1.355	6.17	0.18	28.00	37.94	2.32	5.0	44.0	0.0634
187			1.630	7.43	0.18	30.00	48.90	4.50	5.5	37.0	0.0644
188[a]	17	1	0.8216	12.87	0.06	30.00	24.65	4.25	4.2	29.0	0.0606

Average, excepting 179 and 182, 0.0642±0.0051

[a] Outlet tube cleaned.

gen, and the outlet tube was heated, the temperature in the gas stream rising from *ca* 100° above the trap to *ca* 200° close to the furnace. In runs 143–153 k varied by a factor of five and tended to become higher as more runs were made. In runs 155 and 156 no heat was applied to the outlet tube; here collection of products was begun as soon as injection was started, then after a measured interval of time injection was stopped, and nitrogen was allowed to flow through the unit and into the trap to carry all the nitromethane down from the outlet tube into the trap. The unit was flushed with nitrogen for an hour between runs 156 and 157. Although runs 155, 156, and 157 indicated that increasing the temperature of the outlet tube causes a decrease in k, raising the temperature from 100° to 200° did not suffice to yield reproducible results (runs 158–169). The next runs proved more significant. After introducing a small amount of water (run 173) and carrying out a run with air as carrier (run 174), where carbon and hydrogen would be converted to CO_2 and H_2O, there were obtained three results in excellent agreement, even though in one run (177) the carrier gas was saturated with water vapor, and in the other two (175, 176) it was carefully dried. It thus appeared that treatment of the unit with water vapor might inhibit the secondary reactions involving nitromethane.

In all of the experiments listed in Table III, with the exception of 178, 180, 182, and 187, the unit was flushed out for a considerable time before the run with nitrogen which, after leaving the purifying train and flowmeter, passed through *ca* 2 inches of water in a bubbler tube packed with glass beads; the bubbler tube was located in a by-pass between the flowmeter and syringe. The unit was then flushed out for at least one-half hour with dry nitrogen before the run was started. The carrier gas used during the run was always dry nitrogen. The outlet tube was heated in all runs. The measurements, which extend over more than 90 percent of the reaction, conform to the first-order law within the experimental error, and k is in reasonable agreement with the value obtained by the saturation technique at 478.7°. The good reproducibility of k in the experiments carried out by the saturation technique thus appears to have been due to the fact that water vapor was not removed from the carrier gas.

Similar sets of experiments were carried out at 443.1 and 420.0° (see Fig. 3). The unit was pretreated with moist nitrogen, as in the experiments of Table III, and k showed no tendency to increase as more experiments were performed.

After the adoption of the water-vapor treatment, the alcoholic solution of nitromethane and its decomposition products in the trap was always water-white. The film which collected on the wall of the outlet tube during these runs was small and white, and it never

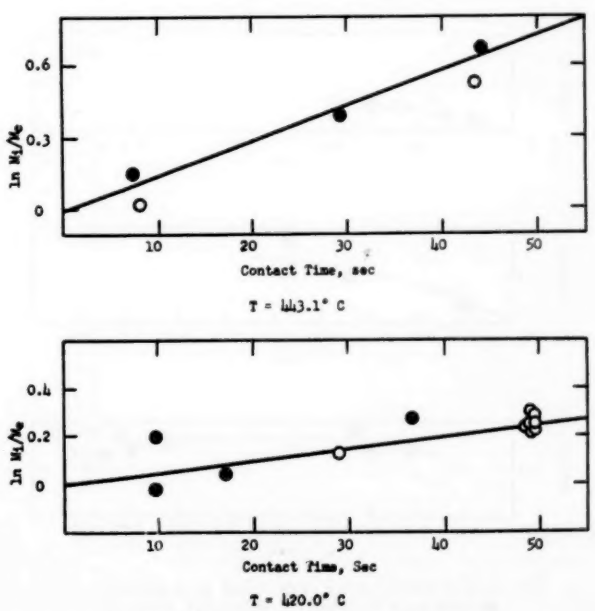

FIG. 3. Results with the injection technique at 443.1 and 420.0°C. Unit pretreated with wet nitrogen. ● Mole fraction CH_2NO_2=0.06. ○ 0.18.

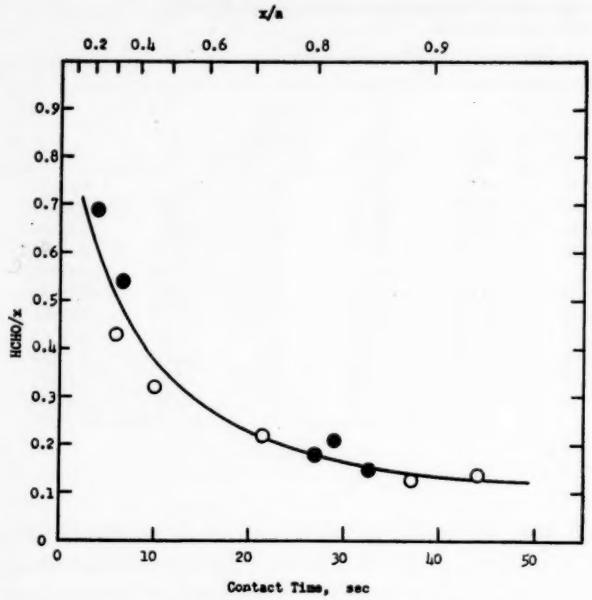

FIG. 4. The variation in yield of formaldehyde at 472.6°C with time of reaction. ● 0.06 mole fraction. ○ 0.18 mole fraction.

turned yellow overnight as in the experiments carried out before adoption of the treatment.

Tests with ferric chloride solution were frequently made on the material in the trap, but no red coloration was obtained, either before or after adoption of the water-vapor treatment. Formaldoxine, formhydroxamic acid, and methazonic acid, which have been mentioned as intermediate products of decomposition in the gas phase,[1] or in solution,[13,14] give a red color with ferric chloride.

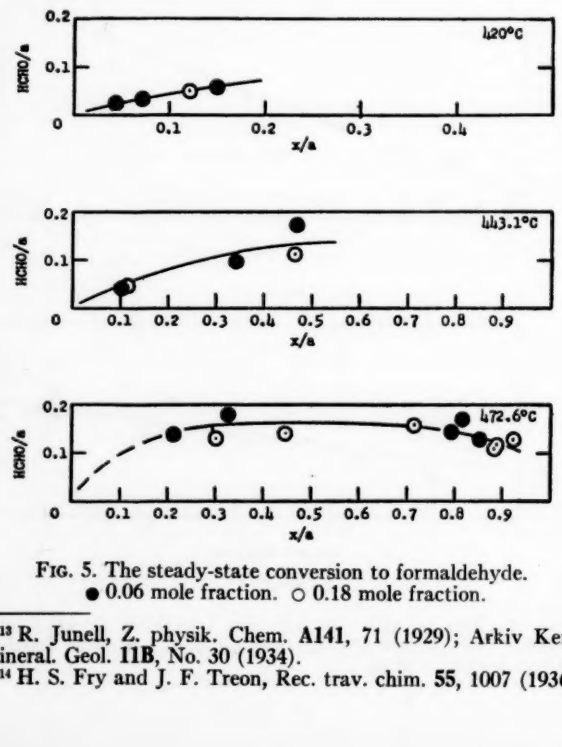

FIG. 5. The steady-state conversion to formaldehyde. ● 0.06 mole fraction. ○ 0.18 mole fraction.

[13] R. Junell, Z. physik. Chem. **A141**, 71 (1929); Arkiv Kemi Mineral. Geol. **11B**, No. 30 (1934).
[14] H. S. Fry and J. F. Treon, Rec. trav. chim. **55**, 1007 (1936).

The Yields of Formaldehyde and of Methane

Figure 4 shows the results of the analysis for formaldehyde in the experiments at 472.6°. As ordinate there is plotted the ratio moles formaldehyde found over moles nitromethane decomposed, the value of x (the moles decomposed) being calculated from the specific rate. The scale at the top of the figure gives the extent of reaction, x/a, where a is the number of moles of nitromethane introduced. At 443.1 and 420.1° the curves showing the yield of formaldehyde as a function of x/a are less steep and would cut the axis of ordinates at about 0.5, or a little above.

Several aspects of Fig. 4 are of interest. First, the relatively small scatter of the points suggests that condensation of formaldehyde in the outlet tube of the reactor is of minor importance; second, the values of $HCHO/x$ are independent of the initial concentration of nitromethane; and third, the steep slope indicates that the yield of formaldehyde in the early stages of the reaction is high.

On the other hand, Fig. 5 shows that over a large portion of the reaction the number of moles of formaldehyde recovered per mole nitromethane charged, $HCHO/a$, is constant. Thus, at 472.6° the formaldehyde found amounts to about 14 percent of the nitromethane charged for reaction times corresponding to 20 to 90 percent decomposition.

TABLE IV. The rate of decomposition of nitromethane at 420°C.

Investigators	Method	Initial pressure, mm Hg nitromethane	nitrogen	k sec^{-1}
Cottrell, Graham, and Reid	static	200 to 400	0	0.0049_5[a]
Taylor and Vesselovsky	static	27 to 198	0	0.0034[b]
Present	flow	45 and 135	700, 610	0.0048

[a] Calculated from Eq. (1).
[b] Calculated from the average value of the quarter-life.

The yield of methane, CH_4/x, is shown in Fig. 6 plotted as a function of the extent of decomposition. Although the reproducibility is poor, the yield appears to be independent of the extent of decomposition. Cottrell, Graham, and Reid obtained a yield of methane about twice as large as that shown in Fig. 6, and constant over a large part of the reaction.

COMPARISON OF RESULTS BY THE STATIC AND FLOW METHODS

A direct comparison of the rate of decomposition as determined by the two methods can be made at 420°C, which lies within the range of temperature of the measurements of Cottrell, Graham, and Reid, and at which both Taylor and Vesselovsky, and the authors, carried out experiments; the comparison is shown in Table IV. The low value of Taylor and Vesselovsky has been explained by Cottrell, Graham, and Reid as due to

decrease in k with decrease in nitromethane pressure, at pressures below 200 mm. The difference between the first and third values of k in the table is well within the error of the measurements.

The indications are, however, that at higher temperatures the agreement would be less good. Our results are summarized in Table V, and in Fig. 7 they are shown plotted according to the Arrhenius equation

$$\ln k = \ln A - \frac{E_A}{R}\left(\frac{1}{T}\right). \tag{14}$$

The dashed line in Fig. 7 represents Eq. (1). The solid line was drawn by inspection; it represents the equation

$$\ln k = 31.36 - 50\,600/RT. \tag{15}$$

If the value of ln A from (15) is used, together with the experimental values of k, to compute E_A by (14), there are obtained for the seven temperatures of Table V the following: 50.5, 50.6, 50.5, 50.5, 50.7, 50.5, 50.8, with an average of 50.6 kcal. The residuals of ln k computed by (15) showed no trend, and 50.6 was taken as a working value of E_A.

TABLE V. Summary of velocity constants.

Temperature °C ±1.0°	Technique[a]	k in sec^{-1}
420.0	I	0.0048±0.0009
443.1	I	0.0151±0.0024
444.8	I	0.0178±0.0034
446.8	S	0.0190±0.0019
458.3	S	0.0288±0.0015
472.6	I	0.0642±0.0051
478.7	S	0.0700±0.0056

[a] I = Injection; S = Saturation.

To determine the best value of E_A we employed Deming's[15] method for exponential equations. Since one normal equation was found to be very nearly a multiple of the other, it was necessary to be satisfied with an approximate solution. A weight of N_i was assigned to the average value of k at temperature T_i, N_i being the number of determinations used in calculating the average; however, at 478.7°, a weight of $0.5N_i$ was assigned because here the factor 1.7 in Eq. (6) becomes significant in the calculation of k for the experiments carried out with the saturation technique and the factor is not accurately known. We obtained $E_A = 50.00$ with standard error 0.58 kcal/mole, and $A = 2.70\times10^{13}$ with standard error 1.35×10^{13} sec^{-1}. In computing the standard errors unit weight was assigned to the mean value of k obtained from the largest set of observations. It cannot be said, however, that E_A and A are known with the accuracy indicated, as only the random errors have been considered.

[15] W. E. Deming, *Statistical Adjustment of Data* (John Wiley and Sons, Inc., New York, 1943).

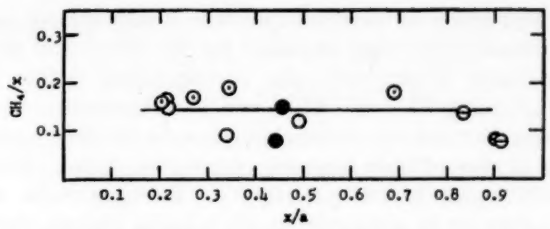

FIG. 6. The yield of methane. ⊙ 458.3°C, saturation technique. ● 478.7°C, saturation technique. ○ 443.1°C, injection technique. ⊖ 472.6°C, injection technique. (In the lower right-hand corner, the pair of circles, the left one should be solid.)

DISCUSSION

Because they found E_A to be close to $\Delta H_{298}°$ for the reaction

$$CH_3NO_2(g) \rightarrow CH_3(g) + NO_2(g)$$

viz., 52.3 kcal/mole, as calculated from the heats of formation:

$$\Delta H^0_f(CH_3NO_2) = -12.2,^{16}$$
$$\Delta H^0_f(CH_3) = 32.0,^{17}$$
$$\Delta H^0_f(NO_2) = 8.1^{17} \text{ kcal/mole.}$$

Cottrell, Graham, and Reid suggested that the rate-determining step in the thermal decomposition is the fission of the C−N bond. On the other hand, in a sub-

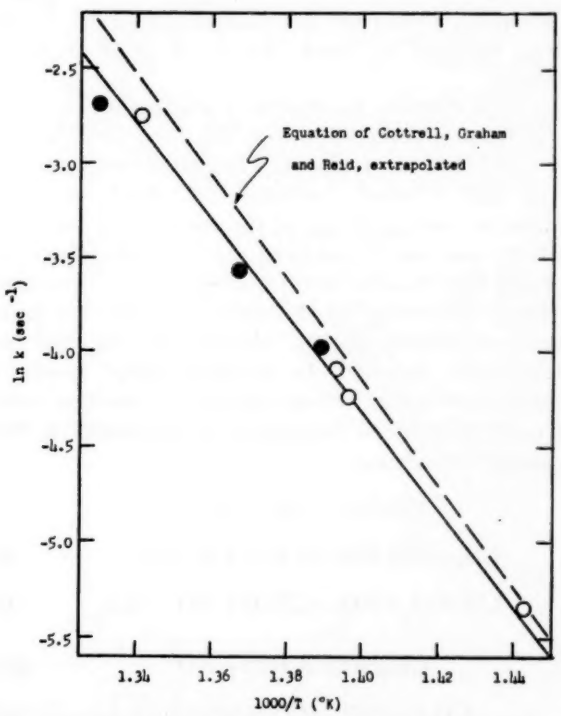

FIG. 7. The Arrhenius equation for the thermal decomposition of nitromethane. ● saturation technique. ○ injection technique.

[16] D. E. Holcomb and C. L. Dorsey, Ind. Eng. Chem. 41, 2788 (1949).

[17] "Tables of Selected Values of Chemical Thermodynamic Properties," National Bureau of Standards, Washington, D. C., 1949.

sequent study of the decomposition of nitroethane and 1-nitropropane[18] they obtained for E_A 47±2 and 49.6 kcal/mole, respectively, the corresponding values of $\Delta H_{298°}$ being 57.6 and 55.9, and in consequence, concluded that the rate-determining step in the decomposition of these higher homologs cannot be fission of the C−N bond, and is probably an intramolecular rearrangement to a complex which splits to give an olefin and nitrous acid.

The flow-method value of E_A for nitromethane thus lies between the static-method values of E_A for nitromethane and the higher homologs, and appears to be *ca* 2 kcal less than the energy required to break the C−N bond. However, if the heats of formation selected by Szwarc,[19]

$$\Delta H^0_f(CH_3)=31\pm1,$$
$$\Delta H^0_f(NO_2)=7.4 \text{ kcal/mole},$$

are employed, one finds $\Delta H_{298°}=50.6$. At the higher temperatures of the kinetic study ΔH would be somewhat less; lacking a knowledge of the heat capacities, one can make a rough estimate of them by means of the theorem of equipartition of energy and calculate the lower limit of ΔH at the average temperature of 723°K; one finds for the lower limit of $\Delta H_{723°}$ either 50.6 or 48.9 kcal/mole, depending on the value chosen for $\Delta H_{298°}$. The flow-method value of E_A thus appears to be equal, within the uncertainties involved, to the energy required to break the C−N bond in nitromethane.

The next question to consider is whether fission of the C−N bond is compatible with the observed products and could lead to a scheme compatible with the observed rate. Cottrell, Graham, and Reid made gas analyses at various stages of the reaction by the usual methods, and also by infrared spectroscopy. The main products they found to be nitric oxide, carbon monoxide, methane, and water; some carbon dioxide, and small amounts of ethane, ethylene, nitrous oxide, and nitrogen dioxide were detected. In addition, there formed a small deposit of dark-colored solid in the reaction vessel and connecting tubes. To account for the products, they suggested the scheme

$$CH_3NO_2\rightarrow CH_3+NO_2 \quad \text{(i)}$$
$$CH_3+CH_3NO_2\rightarrow CH_4+CH_2NO_2 \quad \text{(ii)}$$
$$CH_2NO_2+NO_2\rightarrow CH_2O+NO+NO_2 \quad \text{(iii)}$$

or

$$CH_2NO_2\rightarrow CH_2O+NO \quad \text{(iiia)}$$
$$CH_2O+NO_2\rightarrow CO+NO+H_2O, \text{ etc.}, \quad \text{(iv)}$$

and to some extent

$$CH_3+CH_3\rightarrow C_2H_6. \quad \text{(v)}$$

They took $k_2\simeq10^{-3}Z\exp(-9000/RT)$ from a consideration of analogous reactions; as a lower limit for k_4 they took $10^9\exp(-19\,000/RT)$ (mole/l)$^{-1}$ sec^{-1};[20] k_5 they took as 10^{11} in the same units. The energy of activation of (iii) or (iiia) they considered to be small. If (v) can be neglected, the specific rate k would be $2k_1$, and since the velocity coefficients of reactions (ii)–(iv) as chosen are very much larger than k, the over-all reaction would be

$$CH_3NO_2\rightarrow 0.5CH_4+NO+0.5CO+0.5H_2O.$$

Cottrell, Graham, and Reid calculated that at 700°K, and $[CH_3NO_2]=8\times10^{-3}$ mole/l,

$$\frac{[NO_2]}{[CH_3NO_2]}=\frac{[CH_2O]}{[CH_3NO_2]}=\left\{\frac{k_1/k_4}{[CH_3NO_2]}\right\}^{\frac{1}{2}}<0.025,$$

in agreement with the fact that only a trace of nitrogen dioxide was detected, and no formaldehyde; but since the scheme requires yields of 0.5 for methane and carbon monoxide, while for each they obtained only 0.3, they judged it to be an oversimplification.

On turning to the flow-method experiments one encounters a number of difficulties. The high initial yield of formaldehyde suggests either that formaldehyde is produced as a first product after an intramolecular rearrangement, as proposed by Hirschlaff and Norrish[21] in their study of the photolysis of nitromethane, or that in addition to (i)–(v) the reactions

$$CH_3NO_2+NO_2\rightarrow CH_2NO_2+HNO_2 \quad \text{(vi)}$$
$$2HNO_2\rightarrow H_2O+NO+NO_2 \quad \text{(vii)}$$

may be occurring. It is also possible that (vi) is insignificant, and that a rearrangement and the split into radicals, both contribute. Harnsberger[22] studied the reaction of nitrogen dioxide with methane over the range 250–350°C and found the primary product to be nitromethane, which in turn reacted with nitrogen dioxide to give formaldehyde and carbon dioxide. He concluded that both processes were homogeneous and that for the former

$$\left(\frac{-d[NO_2]}{dt}\right)_a=k_a[NO_2][CH_4],$$

and for the latter

$$\left(\frac{-d[NO_2]}{dt}\right)_b=k_b[NO_2][CH_3NO_2],$$

where

$$k_b=ca\ 10k_a$$
$$=10\{10^6\exp(-21\,000/RT)\}\ (\text{mole/l})^{-1}\text{ sec}^{-1}.$$

[18] Cottrell, Graham, and Reid, Trans. Faraday Soc. **47**, 1089 (1951).
[19] M. Szwarc, Chem. Revs. **47**, 75 (1950).
[20] F. H. Pollard and R. M. H. Wyatt, Trans. Faraday Soc. **45**, 760, 767 (1949); **46**, 281 (1950).
[21] E. Hirschlaff and R. G. W. Norrish, J. Chem. Soc. **1936**, 1580.
[22] H. F. Harnsberger, dissertation, University of California, 1951.

In the experiments carried out by the flow method formaldehyde was present in appreciable quantities, while in those carried out by the static method no formaldehyde was found. It is desirable, therefore, to re-examine the information on reaction (iv). Pollard and Wyatt[20] found k_4 to be $10^{7.1}\exp(-15\,100/RT)$ $(\text{mole/l})^{-1}$ sec^{-1} for temperatures below 160°C, and $10^{9}\exp(-19\,000/RT)$ from 160 to 180°; above 180°, they found the reaction to be explosive when certain pressures of the reactants were exceeded, and they considered the explosions to be thermal.

We shall now attempt to show the magnitude of the effect of reaction (vi) in the flow-method experiments, using the data of Pollard and Wyatt and of Harnsberger. The estimated values of k_4 and k_6, in $(\text{moles/l})^{-1}$ sec^{-1}, are:

At 472.6°C	At 443.1°C
$k_4=6\times10^{2}$ or 3.5×10^{3}	$k_4=4\times10^{2}$ or 2×10^{3}
$k_6=8$	$k_6=4$,

and the corresponding values of k (observed) are 6×10^{-2} and 1.5×10^{-2} sec^{-1}. The steady state for $[CH_2O]$ shown in Fig. 5 is reached when the rate of destruction of formaldehyde via (iv) equals the rate of formation, assumed to occur via (i), (ii), (iii) and via (vi), (iii). As the temperature is lowered, k_1 and k_6 decrease more rapidly than k_4, causing the accumulation of formaldehyde to be slower, and in consequence the rate of destruction will not equal the rate of formation until a greater portion of the nitromethane has disappeared. This is in accord with the observation that the steady state is reached at approximately $(3/4)[CH_3NO_2]_0$ at 472.6° and $(1/2)[CH_3NO_2]_0$ at 443.1°. Neglecting (v), which is justified by the high initial yield of formaldehyde, and obtaining $[NO_2]$ from the relationship

$$[CH_2O]=f([CH_3NO_2]_0)$$
$$=[CH_3NO_2]\{k_1+k_6[NO_2]\}/k_4[NO_2]$$

the specific rate after attainment of the steady state would be

$$k=k_1(2+k_6[CH_3NO_2]/\{k_4[CH_2O]-k_6[CH_3NO_2]\}).$$

Putting in

$$[CH_2O]=0.14[CH_3NO_2]_0,$$
$$[CH_3NO_2]=0.75[CH_3NO_2]_0,$$

and the velocity coefficients k_4 and k_6 given above, the calculated value of k upon attainment of the steady state at 472.6° is $k_1\{2.00+0.08\}$ or $k_1\{2.00+0.01\}$ depending on the value chosen for k_4, and from then on $k\rightarrow2k_1$ since $[CH_2O]$ is nearly constant and $[CH_3NO_2]\rightarrow0$. Thus, the effect of (vi) after attainment of the steady state would not be expected to exceed a few percent. In the early part of the reaction several high values of k were obtained (see Table III); however, it is here that the effect of experimental error is most serious, and a more exact method of following the reaction is needed in order to decide whether or not the initial rate is indeed higher than that prevailing later on. That the initial specific rate is much higher is unlikely from the work of Cottrell, Graham, and Reid, and of Taylor and Vesselovsky, as well as from ours.

Since it is unlikely that (vi) makes more than a small contribution, the problem of the high initial yield of formaldehyde remains. At 472.6° the yield extrapolated to zero time appears to be well over 0.5, and at 443.1 and 420.0° to be *ca* 0.5, or a little above. If the decomposition occurs via the scheme of Cottrell, Graham, and Reid, the maximum yield is 0.5, which is obtained when all the methyl radicals react with nitromethane to form methane and CH_2NO_2, and none combine to form ethane. A formaldehyde yield of 0.5 thus requires a methane yield of 0.5, whereas Cottrell, Graham, and Reid obtained 0.3, and we about half that. The most probable explanation seems to be that the rate is in part determined by an intramolecular rearrangement.

ACKNOWLEDGMENT

We wish to express our gratitude to the Office of Naval Research for support of this work. We also wish to thank Mr. L. D. Simmons, statistician in the Research Laboratories of the United Gas Corporation, Shreveport, Louisiana, for his help with the determination of the parameters of the Arrhenius equation.

A $(K+2)$nd Order Formula for Asymmetry Doublets in Rotational Spectra*

DANIEL KIVELSON
Mallinckrodt Chemical Laboratory, Harvard University, Cambridge, Massachusetts
(Received October 9, 1952)

Higher order perturbation theory is used to derive a formula for K type doubling of the energy levels of a rigid asymmetric rotor. The result is

$$\Delta W=\Delta W_0[1+\{A+BJ(J+1)+CJ^2(J+1)^2\}\beta^2],$$

where ΔW_0 is the Wang[2] Kth-order result for the splitting of the energy levels, β is an asymmetry parameter, and A, B, C are independent of the structural parameters and of the quantum number J. A, B, C, have been tabulated for all values of K up to $K=14$.

INTRODUCTION

ROTATIONAL energy levels of symmetric rotors, specified by the rotational quantum numbers J and K, are doubly degenerate in the quantum number K, $(K>0)$. In asymmetric rotors this degeneracy is removed, giving rise to the phenomenon of K doubling or asymmetry doubling. In the asymmetric rotor, K is taken as the quantum number of the limiting symmetric rotor.[1] An approximate formula for asymmetry splitting has been given by Wang.[2]

$$\Delta W_0=\tfrac{1}{2}(a-c)\binom{J+K}{K}\binom{J}{K}K^2 16(\beta/8)^K/(1-\beta). \quad (1)$$

a and c are reciprocal moments of inertia, $a\geqslant c$, and β is an asymmetry parameter defined below. This formula[3] is easy to use so that the observation of asymmetry doublets is a great aid in the analysis of rotational spectra.

The Wang formula is not accurate enough to calculate direct transitions between members of a doublet, such as sometimes give rise to absorption lines in the microwave region. However, it is often suitable for calculating the splitting of two absorption lines which would merge in the symmetric rotor limit. The purpose of the present paper is to derive a correction term to the Wang formula. This should serve a double purpose: it will provide a more accurate, though more complicated splitting formula, and it will allow an estimate of the accuracy of the Wang formula in any particular case, provided, of course, that the perturbation series converges. In obtaining the desired result it will be helpful to rederive the Wang formula.

WANG FORMULA

The theory of the asymmetric rotor has been discussed in detail by KHC. Their notation will be used whenever possible. They have written the rotational Hamiltonian for an asymmetric rotor as

$$\mathbf{H}=J(J+1)\tfrac{1}{2}(a+c)+\tfrac{1}{2}(a-c)\mathbf{E}, \quad (2)$$

where $\mathbf{E}$ is the reduced energy matrix. The reduced energy matrix expressed in the Wang symmetric rotor basis[2] can be factored into four submatrices, $\mathbf{E}^+$, $\mathbf{E}^-$, $\mathbf{O}^+$, $\mathbf{O}^-$, each of a different symmetry species.[1] In the region where a splitting formula is meaningful it is useful to use the I^r or III^r representation of KHC. Then $\mathbf{E}^+$ and $\mathbf{E}^-$ are submatrices that yield the energy levels for even K, while $\mathbf{O}^+$ and $\mathbf{O}^-$ yield the energy levels for odd K.[4] Doublet splitting arises from the differences between the corresponding eigenvalues of $\mathbf{E}^+$ and $\mathbf{E}^-$ or between those of $\mathbf{O}^+$ and $\mathbf{O}^-$.

A perturbation technique will be used in solving this problem. The general Hamiltonian may be written in the form

$$\mathbf{H}=\mathbf{H}^{(0)}+\mathbf{H}^{(1)}, \quad (3)$$

where $\mathbf{H}^{(0)}$ is the Hamiltonian of the symmetric rotor and $\mathbf{H}^{(1)}$ is the perturbing operator which arises because of the asymmetry. The successive perturbations for the energies W may be written as[5]

$$\begin{aligned}
&W_{a'}{}^{(0)}=H_{a'a'}{}^{(0)},\\
&W_{a'}{}^{(1)}=H_{a'a'}{}^{(1)},\\
&W_{a'}{}^{(K)}=\sum_{a_1\cdots a_r,\neq a'} H_{a'a_1}{}^{(i)}\mathcal{H}_{a_1a_2}{}^{(j)}\\
&\qquad\times\cdots\mathcal{H}_{a_{r-1}a_r}{}^{(l)}H_{a_ra'}{}^{(m)}\\
&\qquad\times[(W_{a'}{}^{(0)}-W_{a_1}{}^{(0)})(W_{a'}{}^{(0)}-W_{a_2}{}^{(0)})\\
&\qquad\times\cdots(W_{a'}{}^{(0)}-W_{a_{r-1}}{}^{(0)})(W_{a'}{}^{(0)}-W_{a_r}{}^{(0)})]^{-1},
\end{aligned} \quad (4)$$

where $i+j+\cdots+l+m=K>1$, $(i, j, \cdots, m\geqslant 1)$, and $\mathcal{H}_{a_{n-1}a_1}{}^{(j)}=H_{a_{n-1}a_n}{}^{(j)}-W_{a'}{}^{(j)}\delta_{a_{n-1}a_n}$. In the case under

* The research reported in this paper was made possible by support extended Harvard University by the U. S. Office of Naval Research under ONR Contract N5ori-76, Task Order V.

[1] King, Hainer, and Cross, J. Chem. Phys. **11**, 27 (1943). Referred to as KHC.

[2] S. C. Wang, Phys. Rev. **34**, 243 (1929).

[3] $\binom{J+K}{K}\binom{J}{K}K^2/J(J+1)$ is tabulated in Hainer, Cross, and King, J. Chem. Phys. **17**, 826 (1949).

[4] The energy levels are designated by KHC by the two quantum numbers $K_{-1}K_1$. The K used above refers to K_{-1} for a nearly prolate top. A doublet is formed in this case between two levels with the same K_{-1} but different K_1. The rules for K_{-1} and K_1 are interchanged for a nearly oblate top.

[5] R. Karplus, Ph.D. thesis, Harvard University (1949).

consideration $\mathbf{H}^{(0)}$ has only diagonal elements,[6] $(K|\mathbf{H}^{(0)}|K)=(G-F)K^2$, where G and F are dimensionless asymmetry constants defined by KHC. $\mathbf{H}^{(1)}$ has only $(K|K\pm2)$ elements when K is even. For odd K, $\mathbf{H}^{(1)}$ has $(K|K\pm2)$ elements; furthermore, it has a $(1|1)$ element equal to $\pm H\frac{1}{2}J(J+1)$, the sign indicating whether the energy matrix $\mathbf{O}^+$ or $\mathbf{O}^-$ is used. The form of the off-diagonal elements and the definition of the dimensionless parameter H are given by KHC.[7]

From KHC it is seen that $\mathbf{E}^+$ and $\mathbf{E}^-$ are identical except for the E_{02} element which is zero in $\mathbf{E}^-$. Thus the Kth eigenvalues of these two matrices differ from each other only in the Kth order. The only Kth-order term which is different for the two is the one that includes E_{02}. Thus using Eq. (4) one has

$$\begin{aligned}\Delta W_0&=\tfrac{1}{2}(a-c)[(E^+)_K{}^{(K)}-(E^-)_K{}^{(K)}]\\&=\tfrac{1}{2}(a-c)[E_{K:K-2}E_{K-2:K-4}\cdots E_{20}E_{02}\cdots E_{K-2:K}]\\&\times[(E_{K:K}-E_{K-2:K-2})^2\cdots(E_{KK}-E_{22})^2\\&\qquad\times(E_{KK}-E_{00})]^{-1},\quad(5)\end{aligned}$$

where $E_{02}=E_{02}{}^+$ and $(E^+)_K{}^{(K)}$ is the Kth-order contribution to the Kth eigenvalue of $\mathbf{E}^+$. If the explicit values of these elements as given by KHC are inserted, the resulting formula is the Wang formula.

For odd K's it is seen from KHC that $\mathbf{O}^+$ and $\mathbf{O}^-$ are identical except for the $(1|1)$ elements. Here again the Kth eigenvalues of the two matrices will differ only in Kth order and the only Kth-order term which will contribute to the difference is the one that includes $\mathcal{H}_{11}{}^{(1)}=\pm HJ(J+1)(1-\delta_{1K})/2$. For $K\geqslant3$ the difference of the Kth-order contributions to the Kth eigenvalues is[8]

$$\begin{aligned}\Delta W_0&=\tfrac{1}{2}(a-c)[(O^+)_K{}^{(K)}-(O^-)_K{}^{(K)}]\\&=\tfrac{1}{2}(a-c)[O_{K:K-2}O_{K-2:K-4}\cdots O_{31}O_{13}\cdots O_{K-2:K}]\\&\times HJ(J+1)[(O_{KK}-O_{K-2:K-2})\cdots(O_{KK}-O_{33})\\&\qquad\times(O_{KK}-O_{11})]^{-2}.\quad(6)\end{aligned}$$

If the explicit values of these elements are inserted, this equation yields the Wang formula.

HIGHER ORDER FORMULAS: EVEN K

The $(K+2)$nd perturbation yields the next contribution to the splitting formula. The case of even K is discussed first. It is seen that $(\mathcal{H}^+)_{a''a'''}{}^{(K')}-(\mathcal{H}^-)_{a''a'''}{}^{(K')}=-\Delta W_0\delta_{a''a'''}$ if $K'=K$, and is equal to zero if $K'<K$.[9] Thus terms with numerators of the form $E_{K:K\pm2}\mathcal{H}_{K\pm2:K\pm2}{}^{(K)}E_{K\pm2:K}$ will contribute to the splitting in $(K+2)$nd order. Furthermore, there will be terms of the form

$$\Delta W_0E_{M:M-2}E_{M-2:M}/(E_{KK}-E_{MM})(E_{KK}-E_{M-2:M-2}),$$

where M takes on all even values between 2 and $K-2$. Each of these terms comes in twice except for the one in which $M=2$, which enters only once. Finally there will be a $(K+2)$nd contribution to the splitting consisting of terms with numerators of the form $E_{K:K-2}\cdots E_{KM}\mathcal{H}_{MM}{}^{(2)}E_{M:M-2}\cdots E_{K-2:K}$, where M takes on all even values between 0 and $K-2$. Putting in the expression for $\mathcal{H}_{MM}{}^{(2)}$ and remembering Eq. (5), these terms take on the form

$$\begin{aligned}-\Delta W_0[&E_{K:K-2}{}^2/(E_{KK}-E_{K-2:K-2})(E_{KK}-E_{MM})\\&+E_{K:K+2}{}^2/(E_{KK}-E_{K+2:K+2})(E_{KK}-E_{MM})].\end{aligned}$$

Each of the above comes in twice except for the one for which $M=0$ which enters once. After inserting the explicit values of these elements as given by KHC, one gets the following splitting formula for even K, $(K\geqslant4)$

$$\begin{aligned}\Delta W&=\tfrac{1}{2}(a-c)[(E^+)_K{}^{(K+2)}-(E^-)_K{}^{(K+2)}]\\&=\Delta W_0[1+\{2\sum_1^{(K-2)/2}f(J,2n-1)/\\&\quad(K^2-4n^2)[K^2-(2n-2)^2]\\&\quad-2\sum_{n=1}^{(K-2)/2}f(J,K-1)/[K^2-(K-2)^2](K^2-4n^2)\\&\quad-f(J,K-1)/K^2[K^2-(K-2)^2]\\&\quad-2\sum_{n=1}^{(K-2)/2}f(J,K+1)/[K^2-(K+2)^2](K^2-4n^2)\\&\quad-f(J,K+1)/[K^2-(K+2)^2]K^2\\&\quad-f(J,K-1)/[K^2-(K-2)^2]^2\\&\qquad-f(J,K+1)/[K^2-(K+2)^2]^2\}\beta^2].\quad(7)\end{aligned}$$

β is an asymmetry parameter[10] given by

$$\beta=\pm H/(G-F),\quad(8)$$

where the plus and minus signs apply to the I^r and III^r representations, respectively, and $f(J,n)$ is defined as

$$f(J,n)=\tfrac{1}{4}[J(J+1)-n(n+1)][J(J+1)-n(n-1)],$$

where $f(J,K+1)$ equals zero if $K=J$ or $J-1$. For $K=2$ some of the terms must be omitted. The result is

$$\Delta W=\Delta W_0[1+\{-2f(J,1)+(2/9)f(J,3)\}\beta^2/16].\quad(7a)$$

[6] Since for doublet splitting $\Delta J=0$, it follows from Eq. (2) that $\mathbf{H}$ and $\mathbf{E}$ may be considered equivalent to within a factor of $\frac{1}{2}(a-c)$. Also the submatrices $\mathbf{E}^\pm$ and $\mathbf{O}^\pm$ are considered to be interchangeable with $\mathbf{H}$ except for this factor. Furthermore, the submatrices used here differ slightly from those given by KHC. The ones here are equal to those of KHC minus $FJ(J+1)$. Since $\Delta J=0$, the two forms yield the same result for doublet splittings.

[7] The asymmetry parameter H should not be confused with the Hamiltonian $\mathbf{H}$.

[8] For $K=1$, ordinary first-order perturbation theory may be used. Thus $\Delta W_0=HJ(J+1)\frac{1}{2}(a-c)$.

[9] $(\mathcal{H}^\pm)_{a''a'''}{}^{K'}=-\frac{1}{2}(a-c)(E^\pm)_K{}^{(K')}\delta_{a''a'''}$ or the analogous expression in $\mathbf{O}^\pm$.

[10] For the I^r representation (nearly prolate top), $\beta=-(b-c)/(2a-b-c)$. For nearly oblate top, (III^r representation), $\beta=+(a-b)/(2c-b-a)$.

TABLE I. Values of the coefficients of Eq. (10) when $J>K+1$. For $K=1$, $B=0.031250$. $B=0$ for all other values of K.

K	A	$C\times10^4$
0	0.000000	0.000000
1	−0.046875	−39.062500
2	0.250000	−277.777778
3	0.562500	−48.828125
4	0.875000	−16.666667
5	1.187500	−7.595486
6	1.500000	−4.081633
7	1.812500	−2.441406
8	2.125000	−1.574704
9	2.437500	−1.074219
10	2.750000	−0.765228
11	3.062500	−0.564236
12	3.375000	−0.427894
13	3.687500	−0.332164
14	4.000000	−0.262985

TABLE II. Values of the coefficients of Eq. (10) when $J=K$ or $K+1$.

K	A	B	$C\times10^4$
0	0.000000	0.000000	0.00000
1	0.000000	0.000000	0.00000
2	0.000000	0.062500	−312.50000
3	−0.140625	0.093750	−78.12500
4	−0.468750	0.111979	−39.06250
5	−1.000000	0.125000	−24.95660
6	−1.745833	0.135243	−17.88194
7	−2.715625	0.143750	−13.67188
8	−3.917411	0.151060	−10.89941
9	−5.358259	0.157490	−8.94872
10	−7.044494	0.163242	−7.51075
11	−8.981847	0.168452	−6.41328
12	−11.175553	0.173221	−5.55277
13	−13.630440	0.177620	−4.86328
14	−16.351003	0.181705	−4.30088

HIGHER ORDER FORMULAS: ODD K

Levels designated by odd K's are treated in an analogous fashion. Terms with numerators of the form $O_{K:K\pm2}\mathcal{H}_{K\pm2:K\pm2}{}^{(K)}O_{K\pm2:K}$ will contribute to the $(K+2)$nd order splitting formula. There will also be terms of the form

$$2\Delta W_0 O_{M:M-2}O_{M-2:M}/(O_{KK}-O_{M:M})(O_{KK}-O_{M-2:M-2}),$$

where M takes on all odd integral values between 3 and $K-2$, and terms of the form $2\Delta W_0\mathcal{H}_{MM}{}^{(2)}/(O_{KK}-O_{MM})$, where M ranges over the odd integers between 1 and $K-2$. In addition there is a term of the form $\Delta W_0[\mathcal{H}_{11}{}^{(1)}]^2/(O_{KK}-O_{11})^2$. The splitting formula for odd K, $(K\geqslant5)$, is

$$\begin{aligned}\Delta W_0&=\tfrac{1}{2}(a-c)[(0^+)_K{}^{(K+2)}-(0^-)_K{}^{(K+2)}]\\
&=\Delta W_0[1+\{2\sum_{n=2}^{(K-1)/2}f(J,2n-2)/\\
&\quad[K^2-(2n-1)^2][K^2-(2n-3)^2]\\
&\quad-2\sum_{n=1}^{(K-1)/2}f(J,K-1)/\\
&\quad[K^2-(K-2)^2][K^2-(2n-1)^2]\\
&\quad-2\sum_{n=1}^{(K-1)/2}f(J,K+1)/\\
&\quad[K^2-(K+2)^2][K^2-(2n-1)^2]\\
&\quad-f(J,K-1)/[K^2-(K-2)^2]^2\\
&\quad-f(J,K+1)/[K^2-(K+2)^2]^2\\
&\quad+\tfrac{1}{4}J^2(J+1)^2/(K^2-1)^2\}\beta^2].\end{aligned}\tag{9}$$

For $K=3$ the splitting formula is

$$\Delta W=\Delta W_0[1+\{-f(J,2)3/64+3f(J,4)/256+\tfrac{1}{4}J^2(J+1)^2/64\}\beta^2],\tag{9a}$$

while for $K=1$ it is

$$\Delta W=\Delta W_0[1-\beta^2 f(J,2)/64].\tag{9b}$$

RESULTS

Equations (6) and (9) can be rewritten in the following form:

$$\Delta W=\Delta W_0[1+\{A+BJ(J+1)+CJ^2(J+1)^2\}\beta^2].\tag{10}$$

For $J>K+1>2$, B is equal to zero and A and C are given by the following relations (see Table I):

$$A=0.25000+0.31250(K-2),\tag{11}$$

$$C=-(1/16)(K+2)/(K+1)^2(K-1)^2.\tag{12}$$

For $J=K$ or $K+1$, the terms

$$(1/32)(K+2)[\tfrac{1}{2}K-(K+1)\textstyle\sum(1/n)]\tag{13}$$

$$-0.03125+(1/16)(K+1)K^{-1}\textstyle\sum(1/n)\tag{14}$$

$$(1/64)(K+1)^{-1}[(K+1)^{-1}-2K^{-1}\textstyle\sum(1/n)],\tag{15}$$

where the sums are from 1 to $K-1$, must be added to the previous values of A, B, C, respectively (see Table II). To facilitate the use of the correction term, these functions have been tabulated up to $K=14$.

The range of asymmetry over which the Wang formula is applicable is discussed by Hainer, Cross, and King.[3] The formula given here is valid over the same region.

The author takes great pleasure in acknowledging the valuable suggestions of Professor E. Bright Wilson, Jr.

Theory of the Stark Effect of Asymmetric Rotator with Hyperfine Structure*

MASATAKA MIZUSHIMA†
Department of Physics, Duke University, Durham, North Carolina
(Received September 26, 1952)

The Stark effect of asymmetric rotator is calculated, including the effect of hyperfine structure, for weak and stronger field cases. The result includes the Stark effect of symmetric rotator and linear rotator as special cases.

I. INTRODUCTION

THE theory of the Stark effect of asymmetric rotator was published by Golden and Wilson.[1] Their result can be expressed as

$$W_{J\tau M}=\sum_{g=1}^{3}(W_g)_{J\tau M}, \tag{1}$$

where

$$(W_g)_{J\tau M}=\mu_g^2\mathfrak{F}^2\Big\{\frac{J^2-M^2}{J(4J^2-1)}\sum_{\tau'}\frac{\lambda_g(J\tau,J-1\tau')}{E_{J\tau}-E_{J-1\tau'}}$$
$$+\frac{M^2}{J(J+1)(2J+1)}\sum_{\tau'}\frac{\lambda_g(J\tau,J\tau')}{E_{J\tau}-E_{J\tau'}}$$
$$+\frac{(J+1)^2-M^2}{(J+1)(2J+1)(2J+3)}\sum_{\tau'}\frac{\lambda_g(J\tau,J+1\tau')}{E_{J\tau}-E_{J+1\tau'}}\Big\}. \tag{1a}$$

In this formula W is the Stark energy, g denotes one of the three principal moment of inertia, and μ_g is the dipole moment along gth axis, $\mathfrak{F}$ is the strength of external electric field, $E_{J\tau}$ is the energy of J,τ level without the effect of external field, and $\lambda_g(J\tau,J'\tau')$ is the function defined by Golden and Wilson,[1] the numerical value of which is tabulated by Cross, Hainer, and King.[2] Golden and Wilson discussed the case of accidental degeneracy of rotational levels, but since such a case was never found actually, the above second-order formula will be enough in discussing experimental results.

In the Stark effect of rotational spectra, however, the effect of hyperfine structure is often large and must be taken into account.

The theory of Stark effect in the rotational spectra of the molecule with hyperfine structure was first worked out by Fano[3] on linear rotator and then by Low and Townes[4] on symmetric rotator. In this paper we shall extend their theory to the case of an asymmetric rotator.

II. WEAK FIELD CASE

When the perturbation caused by the external electric field is smaller than the separation among hfs, the Stark energy can be calculated by means of the second-order perturbation theory in J, τ, I, F, M system, where I is the nuclear spin (when there is more than one nucleus to be taken into account I can be interpreted in this section as the absolute value of $\sum_i \mathbf{I}_i$, where $\mathbf{I}_i$ is the spin vector of ith nucleus) and F is the absolute value of $\mathbf{J}+\mathbf{I}$.

Denoting the angle between gth axis and external field by α_g, the Stark energy is expressed as

$$\sum_g (W_g)_{J\tau IFM}=\sum_g\sum_{J'\tau'F'}\times\frac{(J\tau IFM|\cos\alpha_g|J'\tau'IF'M)^2}{E_{J\tau IF}-E_{J'\tau'IF'}}\mu_g^2\mathfrak{F}^2. \tag{2}$$

The matrix element of $\cos\alpha_g$ can be obtained, using Racah's method,[5] as follows:

$$(J\tau IFM|\cos\alpha_g|J'\tau'IF'M)^2=(2F+1)(2F'+1)\{(J\tau||\cos\alpha_g||J'\tau')\times W(JFJ'F';I1)V(FF'1;-MM0)\}^2, \tag{3}$$

where

$$(J\tau||\cos\alpha_g||J'\tau')^2=\{(J\tau m|\cos\alpha_g|J'\tau'm)/V(JJ'1;-mm0)\}^2. \tag{3a}$$

In this formula W and V are the functions defined by Racah,[5] and m is the component of J along the direction of external field.

Using the function λ_g which appeared in formula (1), we obtain

$$(J\tau m|\cos\alpha_g|J\tau'm)^2=m^2\lambda_g(J\tau,J\tau')/J(J+1)(2J+1)$$
$$(J\tau m|\cos\alpha_g|J-1\tau'm)^2=(J^2-m^2)\lambda_g(J\tau,J-1\tau')/J(4J^2-1)\equiv\Phi(J\tau\tau'),$$
$$(J\tau m|\cos\alpha_g|J+1\tau'm)^2=\Phi(J+1\tau'\tau), \tag{4}$$

and all the other matrix elements are zero.

Calculating W and V functions, we obtain the following formula for the Stark energy of asymmetric rotator

* The research reported in this paper has been sponsored by the Geophysics Research Directorate of the Air Force Cambridge Research Center, Air Research and Development Command, under Contract No. AF19(604)-258.
† On leave from Department of Physics, Faculty of Science, University of Tokyo, Tokyo, Japan.
[1] S. Golden and E. B. Wilson, Jr., J. Chem. Phys. **16**, 669 (1948).
[2] Cross, Hainer, and King, J. Chem. Phys. **12**, 210 (1944).
[3] U. Fano, J. Research Natl. Bur. Standards **40**, 215 (1948).
[4] W. Low and C. H. Townes, Phys. Rev. **76**, 1295 (1949).
[5] G. Racah, Phys. Rev. **62**, 438 (1942).

in the case of weak field:

$$(W_g)_{J\tau IFM}=\mu_g{}^2\mathfrak{F}^2\Big\{f_1(JIFM)\sum_{\tau'}\frac{\lambda_g(J\tau J+1\tau')}{E_{J\tau F}-E_{J+1\tau' F}}+f_2(JIFM)\sum_{\tau'}\frac{\lambda_g(J\tau J+1\tau')}{E_{J\tau F}-E_{J+1\tau' F+1}}$$
$$+f_3(JIFM)\sum_{\tau'}\frac{\lambda_g(J\tau J+1\tau')}{E_{J\tau F}-E_{J+1\tau' F-1}}+f_4(JIFM)\sum_{\tau'}\frac{\lambda_g(J\tau J\tau')}{E_{J\tau F}-E_{J\tau' F+1}}$$
$$+f_5(JIFM)\sum_{\tau'\neq\tau}\frac{\lambda_g(J\tau J\tau')}{E_{J\tau F}-E_{J\tau' F}}+f_4(JIF-1M)\sum_{\tau'}\frac{\lambda_g(J\tau J\tau')}{E_{J\tau F}-E_{J\tau' F-1}}$$
$$+f_1(J-1IFM)\sum_{\tau'}\frac{\lambda_g(J\tau J-1\tau')}{E_{J\tau F}-E_{J-1\tau' F}}+f_2(J-1IF-1M)\sum_{\tau'}\frac{\lambda_g(J\tau J-1\tau')}{E_{J\tau F}-E_{J-1\tau' F-1}}$$
$$+f_3(J-1IF+1M)\sum_{\tau'}\frac{\lambda_g(J\tau J-1\tau')}{E_{J\tau F}-E_{J-1\tau' F+1}},\quad(5)$$

where

$$f_1(JIFM)=\frac{M^2(J+I+F+2)(I+F-J)(I+J+1-F)(F+J+1-I)}{4F^2(F+1)^2(2J+3)(2J+1)(J+1)},$$
$$f_2(JIFM)=\frac{(J+I+F+3)(J+I+F+2)(J-I+F+2)(J-I+F+1)\{(F+1)^2-M^2\}}{4(F+1)^2(2F+3)(2F+1)(2J+3)(2J+1)(J+1)},$$
$$f_3(JIFM)=\frac{(I+F-J)(I+F-J-1)(I+J-F+2)(I+J-F+1)(F^2-M^2)}{4F^2(2F-1)(2F+1)(2J+3)(2J+1)(J+1)},$$
$$f_4(JIFM)=\frac{(I+J+F+2)(I+J-F)(I+F-J+1)(J+F-I+1)\{(F+1)^2-M^2\}}{4J(J+1)(2J+1)(F+1)^2(2F+3)(2F+1)},$$
$$f_5(JIFM)=\frac{M^2\{J(J+1)+F(F+1)-I(I+1)\}^2}{4J(J+1)(2J+1)F^2(F+1)^2}.\quad(6)$$

Noting that the formulas for symmetric rotator, corresponding to our formulas (4), are

$$(JKm|\cos\alpha_g|JKm)^2=\{Km/J(J+1)\}^2,$$
$$(JKm|\cos\alpha_g|J+1Km)^2=\{(J+1)^2-K^2\}\{(J+1)^2-m^2\}/J^2(4J^2-1),$$
$$(JKm|\cos\alpha_g|J-1Km)^2=(J^2-K^2)(J^2-m^2)/J^2(4J^2-1),\quad(4')$$

we can easily see that the second-order Stark energy of symmetric rotator in the weak field case can be obtained if we put

$$\sum_{\tau'}\frac{\lambda(J\tau,J+1\tau')}{E_{J\tau F}-E_{J+1\tau' F'}}\rightarrow\frac{(J+1)^2-K^2}{(J+1)(E_{JKF}-E_{J+1KF'})},$$
$$\sum_{\tau'}\frac{\lambda(J\tau,J\tau')}{E_{J\tau F}-E_{J\tau' F'}}\rightarrow\frac{(2J+1)K^2}{J(J+1)(E_{JKF}-E_{JKF'})},\quad(7)$$

in formula (5) and neglect the f_5 term. The f_5 term goes up to the first-order Stark energy in this case, and the corresponding formula is obtained by Low and Townes.[4] If we put K to be zero in this formula, we shall obtain the formula for the linear molecule.

In many cases the approximation

$$E_{J\tau F}-E_{J'\tau' F'}\doteqdot E_{J\tau}-E_{J'\tau'}\quad(8)$$

is valid. In these cases our formula (5) is much simplified and can be reduced to formula (1) if only we put $\langle m^2\rangle$ instead of M^2 there, where $\langle m^2\rangle$ is the average value of m^2, which is

$$\langle m^2\rangle=(JIFM|m^2|JIFM)=\frac{\{3M^2-F(F+1)\}\{3D(D-1)-4J(J+1)F(F+1)\}}{6F(F+1)(2F-1)(2F+3)}+\frac{J(J+1)}{3},\quad(9)$$

where

$$D=F(F+1)+J(J+1)-I(I+1).^{3,4}$$

Since $\langle m^2\rangle$ is equal to M^2 (or m^2) when $I=0$, we see our result include Golden and Wilson's result under the assumption (8).

If we make displacement (7) in the formula thus obtained, we obtain Low and Townes' result.[4] In their paper, however, there are misprints, and the formula which we obtain should be (their formula at the bottom of page 1296, reference 4)

$$(W^{(2)})_{JKIFM}=\frac{-\mu^2\mathfrak{F}^2}{B}\frac{3\langle m^2\rangle-J(J+1)}{(J+1)(2J)(2J+3)(2J-1)}$$
$$+\frac{\mu^2\mathfrak{F}^2}{B}K^2\frac{\langle m^2\rangle\{(2J+3)(J+1)^3-J^3(2J-1)\}-3J^2(J+1)^2(2J+1)}{2(2J-1)(2J+1)J^3(J+1)^3(2J+3)}. \quad (10)$$

Again putting $K=0$, we obtain Fano's result for a linear molecule.[3]

III. STRONGER FIELD CASE

When the external field becomes stronger and the perturbation caused by the field is comparable to the coupling constant between the nuclear quadrupole moment and molecular rotation, the JIF scheme no longer holds, and one must calculate the energy in the $JIm m_I$ scheme, where m_I is the magnetic quantum number of nuclear spin.

The Hamiltonian to be considered is

$$H=H_r+H_Q+\sum_g \mu_g\mathfrak{F}\cos\alpha_g, \quad (11)$$

where H_r is the rotational energy, and

$$H_Q=eQ\langle\partial^2V/\partial Z^2\rangle_{Av}\{3(\mathbf{I}\cdot\mathbf{J})^2+(3/2)(\mathbf{I}\cdot\mathbf{J})-I^2J^2\}/2I(2I-1)J(2J-1) \quad (12)$$

is the coupling between nuclear quadrupole moment Q and molecular rotation, where V is the electric field caused by all changes within the molecule except that of the nucleus under consideration (at the place of that nucleus) Z is the direction of external field, and $\langle\ \rangle_{Av}$ means a quantum-mechanical average.

By means of the argument similar to that of Fano,[3] one can easily obtain the following secular equation:

$$|eQ\langle\partial^2V/\partial Z^2\rangle_J(JIm m_I|\,3(\mathbf{I}\cdot\mathbf{J})^2+(3/2)(\mathbf{I}\cdot\mathbf{J})-I^2J^2|\,JIm'm_I')\cdot\{2I(2I-1)J(2J-1)\}^{-1}+(W_{J\tau I=0m}-E)\delta_{mm'}\delta_{m_Im_I'}|=0, \quad (13)$$

where $W_{J\tau I=0m}$ is obtained by putting M to be m in formula (1). This secular equation will be easily factorized corresponding to each value of $m+m_I=M$, since the matrix element of H_Q between different M is zero.

The matrix element of $3(\mathbf{I}\cdot\mathbf{J})^2+(3/2)(\mathbf{I}\cdot\mathbf{J})-I^2J^2$ is given by Kellogg *et al.*,[6] and the explicit expression of $\langle\partial^2V/\partial Z^2\rangle_{Av}$ in the case of asymmetric rotator is given by Bragg and Golden.[7]

The theory for the case of more than one nucleus will easily be obtained.

IV. INTENSITY

The relative intensity of the various components is almost the same as that of the symmetric rotator for which Low and Townes[4] give the following result:

(a) Weak field case,

$$\Delta F=0 \quad I_M=PM^2,$$
$$\Delta F=\pm1 \quad I_M=Q(F^2-M^2),$$

where P and Q are parameters independent of M, and F is the larger of the two levels.

(b) Extremely strong field case,

$$\Delta J=0 \quad I_m=Rm^2,$$
$$\Delta J=\pm1 \quad I_m=S(J^2-m^2),$$

where R and S are parameters independent of m, and J is the larger of the two levels.

The intermediate case between these two is rather complicated but can be obtain when the secular equation (13) is solved and the wave function for each state is obtained.

The author wishes to thank Professor W. Gordy for his suggestions and interest in this work.

[6] Kellogg, Rabi, Ramsey, and Zacharias, Phys. Rev. **57**, 677 (1940).

[7] J. K. Bragg, Phys. Rev. **74**, 533 (1948); J. K. Bragg and S. Golden, Phys. Rev. **75**, 735 (1948).

Infrared Spectra and Structure of Uranyl and Transuranium (*V*) and (*VI*) Ions in Aqueous Perchloric Acid Solution*

LLEWELLYN H. JONES AND ROBERT A. PENNEMAN
Los Alamos Scientific Laboratory, University of California, Los Alamos, New Mexico

(Received September 2, 1952)

Infrared spectra of aqueous solutions of U(*VI*), Np(*VI*), Pu(*VI*), and Am(*VI*) show conclusively that these ions exist as symmetrical and linear, or nearly linear, XO_2^{++}. The spectra of Np(*V*) and Am(*V*) show that they are probably XO_2^{+} ions. Force constants and estimated distances are given for the X−O bonds. For the XO_2^{++} series, the X−O force constant is expressed as a parabolic function of atomic number, with the maximum occurring at NpO_2^{++}. This is contrary to behavior expected if there were a regular contraction in ionic radii for the series XO_2^{++}.

IT has been established by fluorescence[1] and infrared[2] spectra of uranyl salts, and by Raman[3] spectra of aqueous uranyl solutions that the uranyl ion has three vibrational frequencies: a symmetric stretching frequency at 860–880 cm^{-1}, an asymmetric stretching frequency at 930–960 cm^{-1}, and a bending frequency at 199–210 cm^{-1}. These results indicate that the uranyl ion has a linear or very nearly linear, triatomic structure, UO_2^{++}. Studies by Crandall[3] have shown that two uranyl oxygens exchange only very slowly with solvent water, and thus are tightly bonded. X-ray data of Fankuchen[4] demonstrates indirectly that the UO_2^{++} group in sodium uranyl acetate is linear. Zachariasen[5] has reported that in calcium uranyl dioxide there is a linear UO_2 group having U−O bond distances of 1.91±0.10A. With the above information as a basis, we accept as a fact that the uranyl ion is linear, symmetrical UO_2^{++}.

TABLE I. Observed vibrational frequencies, calculated force constants, and estimated bond distances for XO_2^{++} and XO_2^{+} ions.

Species and conc.	(ν_3) max	k_{X-O}, megadynes/cm Observed	k_{X-O}, megadynes/cm Calc. by Eq. 3	R_{X-O}, A[a] from Eq. 2
1 f $UO_2(ClO_4)_2$ 4 f $HClO_4$	965±1	0.775±0.002	0.775	1.90_{35}
2.5 f $UO_2(ClO_4)_2$[b] 1 f $HClO_4$				
1 f $NpO_2(ClO_4)_2$ 4 f $HClO_4$	969±1	0.781±0.002	0.782	1.90_{20}
2.5 f $PuO_2(ClO_4)_2$ 3 f $HClO_4$	962±1	0.771±0.002	0.769	1.90_{45}
1.5 f $AmO_2(ClO_4)_2$[b] 4 f $NaClO_4$ 3.5 f $HClO_4$	939±1	0.735±0.002	0.736	1.91_{30}
0.5 f $AmO_2(ClO_4)_2$ 3 f $HClO_4$				
1 f NpO_2ClO_4 1.4 f $HClO_4$	824±4	0.565±0.006		1.96_{30}
1.5 f AmO_2ClO_4 4 f $NaClO_4$	832±2	0.577±0.003		1.95_{85}

[a] There is an uncertainty of about 0.05A in the use of this extrapolation of Badger's rule. However, though the actual bond distances may be considerably different from those reported in Table I, the relative values are believed to be accurate to 0.001A for the (*VI*) ions, and accurate to 0.003A for the (*V*) ions. It is encouraging that the U−O bond distance agrees so well with the value 1.91±0.10A reported by Zachariasen (see reference 5) for $Ca(UO_2)O_2$.
[b] Where two solutions are given, b identifies the one shown in Fig. 1.

Several investigators[6] have interpreted certain fine structure in the visible absorption spectra of aqueous solutions of uranyl and transuranium (*V*) and (*VI*) ions as arising from transitions to successive vibrational levels (corresponding to the symmetrical stretching frequency) in an excited electronic state of XO_2^{++} and XO_2^{+} ions. This fine structure has been presented as evidence that the U(*VI*), Np(*VI*), Pu(*VI*), and Np(*V*) ions do indeed have the structure O−X−O. This indirect evidence is certainly not conclusive. However, from the infrared spectra of these ions, if they all exist as XO_2^{++} and XO_2^{+}, one should observe absorption due to the O−X−O asymmetric stretching frequency and, thus, conclusively prove the structural similarity of these ions.

EXPERIMENTAL

In this laboratory, the infrared spectra of aqueous solutions of uranyl and transuranium (*V*) and (*VI*) ions have been observed for the first time. The technique which led to successful results with aqueous solutions was the use of extremely short path lengths (about 5 microns) of concentrated solutions ($\gtrsim$0.5 f in metal ion). A small drop (about 3 microliters) of solution was pressed between optically flat, silver chloride windows. The window assembly was gasketed between the plates of the usual cell holder, and surrounded on the sides by Lucite, which effectively prevented the escape of alpha-activity. The spectra were recorded on a Perkin-

* This work was sponsored by the U. S. Atomic Energy Commission.

[1] G. H. Dieke and A. B. F. Duncan, "Spectroscopic Properties of Uranium Compounds," *National Nuclear Energy Series*, III-2 (McGraw-Hill Book Company, Inc., New York, 1949).
[2] J. Lecomte and R. Freyman, Bull. soc. chim. France **8**, 622 (1941); G. K. T. Conn and C. K. Wu, Trans. Faraday Soc. **34**, 1483 (1938).
[3] B. S. Santyanarayana, Proc. Ind. Acad. Sci. **15A**, 414 (1942); H. W. Crandall, J. Chem. Phys. **17**, 602 (1949); G. K. T. Conn and C. K. Wu, Trans. Faraday Soc. **34**, 1483 (1938).
[4] I. Fankuchen, Z. Krist. **91**, 473 (1935).
[5] W. H. Zachariasen, Acta Cryst. **1**, 281 (1948).
[6] R. Sjoblom and J. C. Hindman, J. Am. Chem. Soc. **73**, 1744 (1951); M. Kasha, J. Chem. Phys. **17**, 349 (1949); R. H. Betts and B. G. Harvey, J. Chem. Phys. **16**, 1089 (1948).

Elmer Model 12-C spectrometer, using the spectrum of NH_3 (g) as a wavelength calibration before and after each run.

Of the four elements, U^{238}, Np^{237}, Pu^{239}, Am^{241}, uranium was studied the most thoroughly; the results are representative of numerous uranium runs. For the three remaining elements, each result was obtained from at least two different preparations from different stock materials. Stock Np(V) perchlorate was used, and Np(VI) was prepared using ozone as the oxidant. Plutonium (VI) perchlorate was prepared by evaporating an aqueous solution of Pu(IV) nitrate and $HClO_4$ to dryness with a stream of ozone. Americium(V) was prepared by ozone oxidation of Am(III) in either Na_2CO_3 or K_2CO_3; after dissolution of the thoroughly washed precipitate in $HClO_4$, a portion was oxidized to Am(VI) with ozone.[7]

RESULTS AND DISCUSSION

Some of the results are shown in Fig. 1.

The existence and similarity of the vibrational frequencies ν_3 of the U(VI), Np(VI), Pu(VI), and Am(VI) ions are conclusive proof of their similarity in structure. Thus, they are all linear, or nearly linear, XO_2^{++} ions.

The Np(V) and Am(V) ions exhibit similar vibrational frequencies, considerably lower than the XO_2^{++} ions. The latter fact is expected, as the oxygen atoms should be less tightly bonded to the central atom which has one less positive charge. Figure 1 shows that the XO_2^+ absorption bands are much broader than those of XO_2^{++}. The bending frequency for XO_2^+ is probably considerably lower than that for XO_2^{++}, and of the order of kT_{298}. This leads to thermal excitation of a large proportion of the ions to excited states of the bending vibration, thus broadening the absorption maximum. Since the Np(V)–(VI) potential is hydrogen ion independent,[8] unhydrated Np(V) ions are represented by one of the three structures: NpO_2^+, $NpO(OH)_2^+$, or $Np(OH)_4^+$. Each of these three ions forms a hydrogen-ion independent couple with NpO_2^{++}. All of these involve the same number of covalent bonds, but NpO_2^+ seems the most likely of the three, as it allows more space for water molecules of hydration. Thus, though it is not conclusive, it appears that Np(V) is NpO_2^+ in aqueous solution. The similarity of the Am(V) absorption to that of NpO_2^+ is sufficient evidence to establish that it exists as AmO_2^+ and that the Am(V)–(VI) potential should be hydrogen ion independent. Although the XO_2^+ ion is probably linear, at present there is no experimental evidence for this.

In Table I are given the measured frequencies for the various ions investigated. In this table are also given force constants for the various X—O bonds, assuming linearity of the ions, and the potential function:

$$2V = k_{X-O}(\Delta R_1^2 + \Delta R_2^2) + k'(R_0 + \Delta R_1 + \Delta R_2)^{-n} + k_\alpha(\Delta\alpha)^2. \quad (1)$$

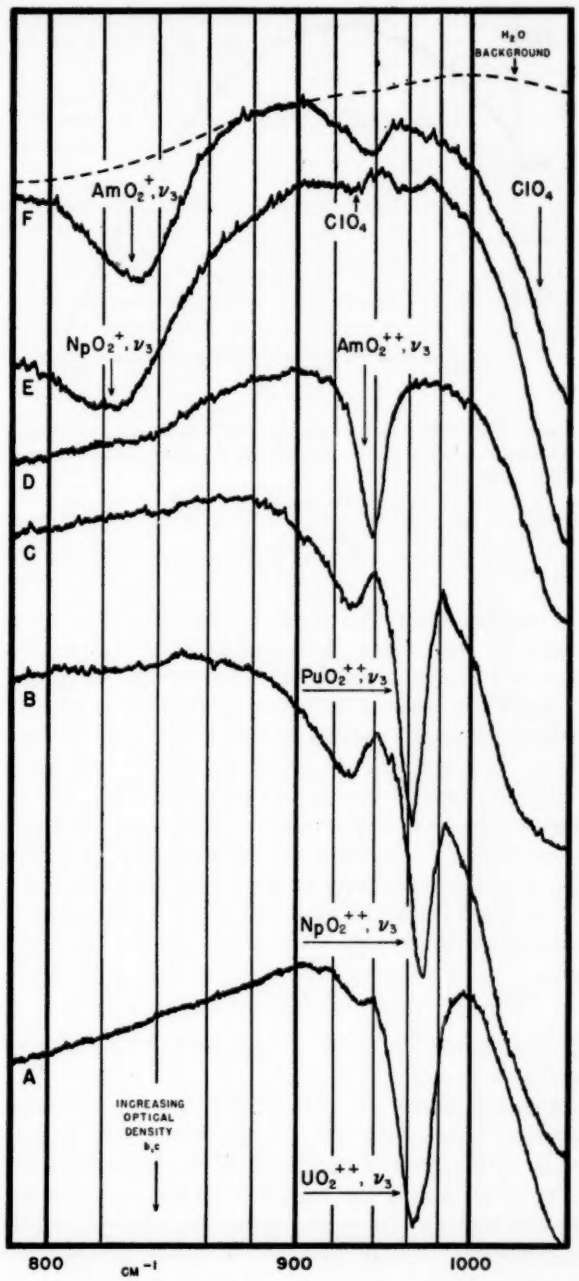

FIG. 1. Infrared absorption owing to the asymmetric stretching vibration of XO_2^{++} and XO_2^+ ions. (a) Path lengths of solution were of the order of 5 microns. (b) The molar absorption coefficients, at the maximum of absorption, are not yet known accurately as there is an uncertainty in the path length. They are of the order of 500 cm^{-1} $moles^{-1}$ liters for XO_2^{++} and 300 cm^{-1} $moles^{-1}$ liters for XO_2^+ (optical density being expressed as $\log_{10}I_0/I$). (c) The optical density scale is displaced for each spectrum. (d) The concentrations of solutions used to obtain the above spectra are given in Table I. (e) In curve F, the band at ~940 cm^{-1} is no doubt from Am(VI) formed by Am(V) disproportionation.

[7] T. K. Keenan and S. E. Stephanou, unpublished Los Alamos work.

[8] Magnussen, Hindman, and LaChapelle, *The Transuranium Elements* (McGraw-Hill Book Company, Inc., New York, 1949), p. 1059.

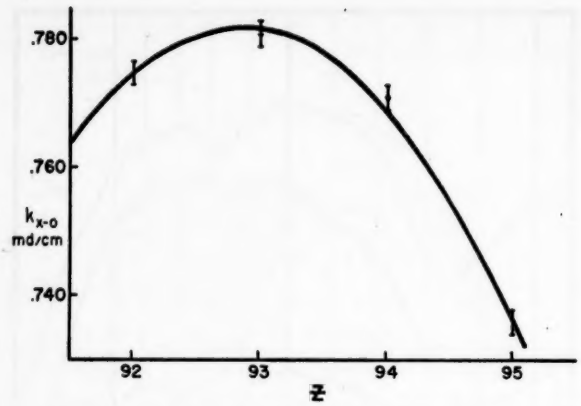

FIG. 2. Plot of X−O force constant in XO_2^{++} ions as a function of atomic number of X. *I*=experimental points. Smooth curve is plot of equation,

$k_{X-O}=k_{U-O}[Z_X/Z_U]^2-0.010(Z_X-Z_U)^2$
$k_{U-O}=0.775$ megadynes/cm.
$Z_X=92, 93, 94, 95$ for U, Np, Pu, Am, respectively.

The second term represents repulsion of the oxygen atoms for each other. Adel and Dennison[9] found that for CO_2 a repulsive potential between the two oxygens should be included. For the asymmetric stretching frequency $\Delta R_1+\Delta R_2=0$ and $\Delta\alpha=0$, so the last two terms of Eq. (1) do not enter in. Of course, UO_2^{++} may require a different type of interaction term than CO_2, but this term will be small and no doubt constant for the XO_2^{++} series, and will contribute only a small constant correction at most to the force constants given in Table I.

The bond distances were estimated from these force constants with the use of an extrapolation of Badger's[10] rule:

$$r_{X-O}=(\beta_{ij}/(k_{X-O})^{\frac{1}{3}})+d_{ij}. \quad (2)$$

The extrapolation leads to $\beta_{1,6}=0.49$A (megadynes/cm)$^{\frac{1}{3}}$ and $d_{1,6}=1.37$A.

Although there is a marked similarity in the absorption spectra of all the XO_2^{++} ions, there are small differences which require explanation. Zachariasen,[11] from x-ray data, found for $NaXO_2(C_2H_3O_2)_3$ crystals that the cell constant decreases in the order X=U, Np, Pu, suggesting a regular decrease in X−O distance from U−O to Pu−O. However, in aqueous solution, this is not the case if the bond distance is a monotonic function of the force constant for the X−O bond in these ions. From the infrared spectra of these solutions, the Np−O distance appears to be shorter than that of U−O, but the Pu−O distance appears longer than, and the Am−O distance considerably longer than, that of U−O. The regular decrease in cell constant mentioned above does not necessarily signify a decrease in X−O bond distance, but may be a reflection of a decrease in other interatomic distances.

Table I shows that the X−O force constant in XO_2^{++} is greatest for NpO_2^{++} and smallest for AmO_2^{++}. A plot of X−O force constant *versus* atomic number of X for XO_2^{++} ions can be fitted by an equation of the form

$$k_{X-O}=k_{U-O}[Z_X/Z_U]^2-\beta(Z_X-Z_U)^2 \quad (3)$$
$\beta=0.010$
Z_X=atomic number of X
X=U, Np, Pu, and Am.

This plot is shown in Fig. 2 along with the experimental points.

Qualitatively we can say that the change in force constant with atomic number, as expressed in Eq. (3), is a reflection of at least two opposing effects. The increase in nuclear charge tends to increase the X−O force constant, while the additional electrons weaken the X−O bond. A further effect may be a difference in interaction of the solvent molecules with the XO_2^{++} ions. This effect should also be dependent on Z_X.

It should be pointed out that, although the broad Np(*V*) and Am(*V*) maxima are difficult to determine precisely, the Am(*V*) frequency is higher than that of Np(*V*), apparently reversing the situation observed for Am(*VI*) and Np(*VI*). By a change in constants, one could fit the XO_2^+ ions to a similar parabolic function with a change in maximum. However, until PuO_2^+ and possibly UO_2^+ can be determined, there is no justification for doing this.

It will be noted in Table I that the solutions studied are of different concentrations. This was due to the difficulty in preparing some of the solutions on a microliter scale. However, for uranyl perchlorate, as long as the perchloric acid concentration is greater than 1 formal, the UO_2^{++} frequency is the same for solutions in the concentration range 0.25–2.5 formal. Thus, the comparison of XO_2^{++} frequencies at different concentrations is justified.

[9] A. Adel and D. M. Dennison, Phys. Rev. **44**, 99 (1933).
[10] R. M. Badger, J. Chem. Phys. **3**, 710 (1935).
[11] W. H. Zachariasen, Phys. Rev. **73**, 1104 (1948). A. F. Wells, *Structural Inorganic Chemistry* (Oxford University Press, London, 1950), second edition, p. 661.

The Asymmetric Rotor. XI. Hydrogen Sulfide Absorption in the Regions 8700 cm^{-1} and 11 000 cm^{-1}*

K. Keith Innes,† Paul C. Cross, and Edward J. Bair
Department of Chemistry and Chemical Engineering, University of Washington, Seattle, Washington

(Received July 1, 1952)

By the use of a 21-foot grating spectrograph and absorbing paths of up to 350 feet, sixty lines in the region from 10 870 cm^{-1} to 11 100 cm^{-1} have been measured and analyzed as the rotational structure of an A-type band. It may be identified as the lower component of the resonating pair $(n_\sigma, n_\pi, n_\delta) = (131), (311)$.

Most of the more than eighty hydrogen sulfide absorption lines measured between 8560 and 8830 cm^{-1} have been assigned to an A-type band identified as the lower component of the (121), (301) resonating pair. Several additional lines definitely not due to water appear to indicate the existence of a superimposed B-type band having about the same upper state parameters, presumably the lower component of the pair (211), (031). In cm^{-1},

$\nu_0 = 8697.3 \quad A^* = 10.29 \quad B^* = 8.75 \quad C^* = 4.48$
$\nu_0 = 11008.78 \quad A^* = 10.197 \quad B^* = 8.559 \quad C^* = 4.411.$

INTRODUCTION

BAND centers resulting from earlier analyses have recently been used to evaluate the complete quadratic expression for the unperturbed vibrational energies of hydrogen sulfide and the Darling and Dennison interaction parameter, γ.[1] With this expression and some empirically observed trends in the combination and overtone bands it is possible to predict the most likely regions of previously unobserved absorption, namely, that by the perpendicular type resonating pairs (121), (301) and (131), (311) in the regions 8700–8900 cm^{-1} and 11 000–11 200 cm^{-1}, respectively.

EXPERIMENTAL

Commercial hydrogen sulfide was frozen in a liquid air trap and redistilled to a pressure of 57 cm into the

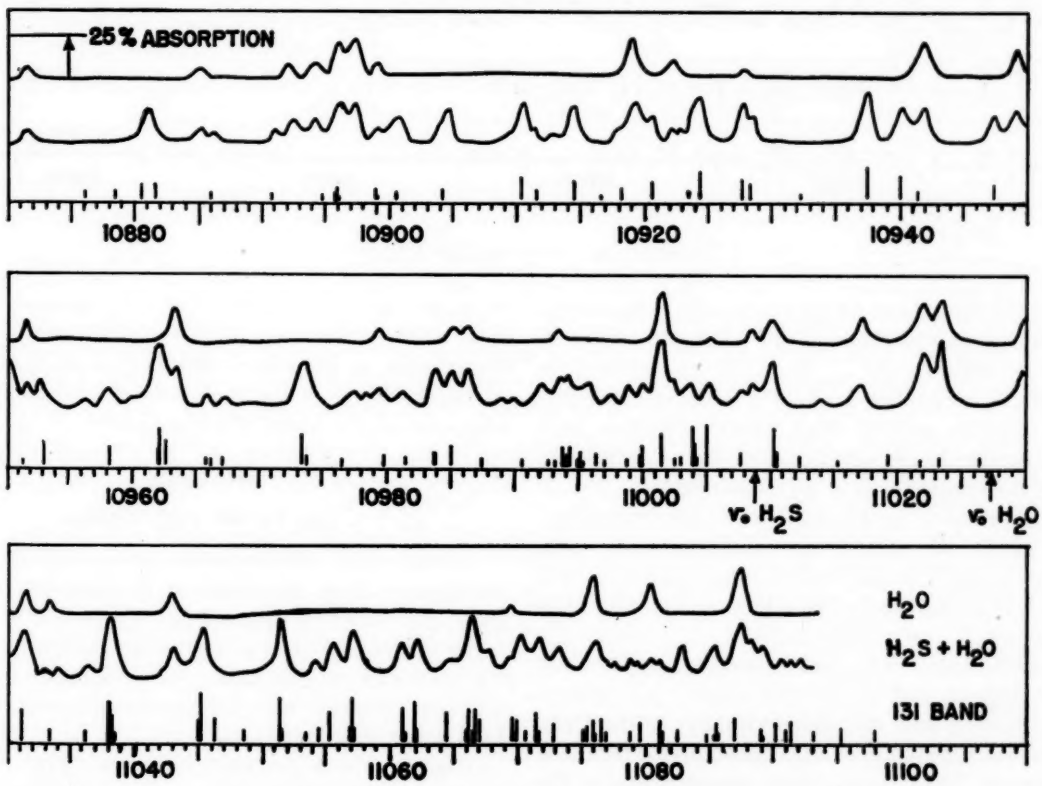

FIG. 1. The spectrum of hydrogen sulfide 10 870–11 100 cm^{-1}.

* This work was supported in part by the U. S. Office of Naval Research under Contract N8onr 52010, and in part by a grant from the Research Corporation. It is based on a portion of a thesis presented by K. K. Innes in partial fulfillment of the requirements for the degree of Doctor of Philosophy at the University of Washington.

† Now at the Division of Physics, National Research Council, Ottawa, Canada.

[1] Allen, Cross, and King, J. Chem. Phys. 18, 1412 (1950).

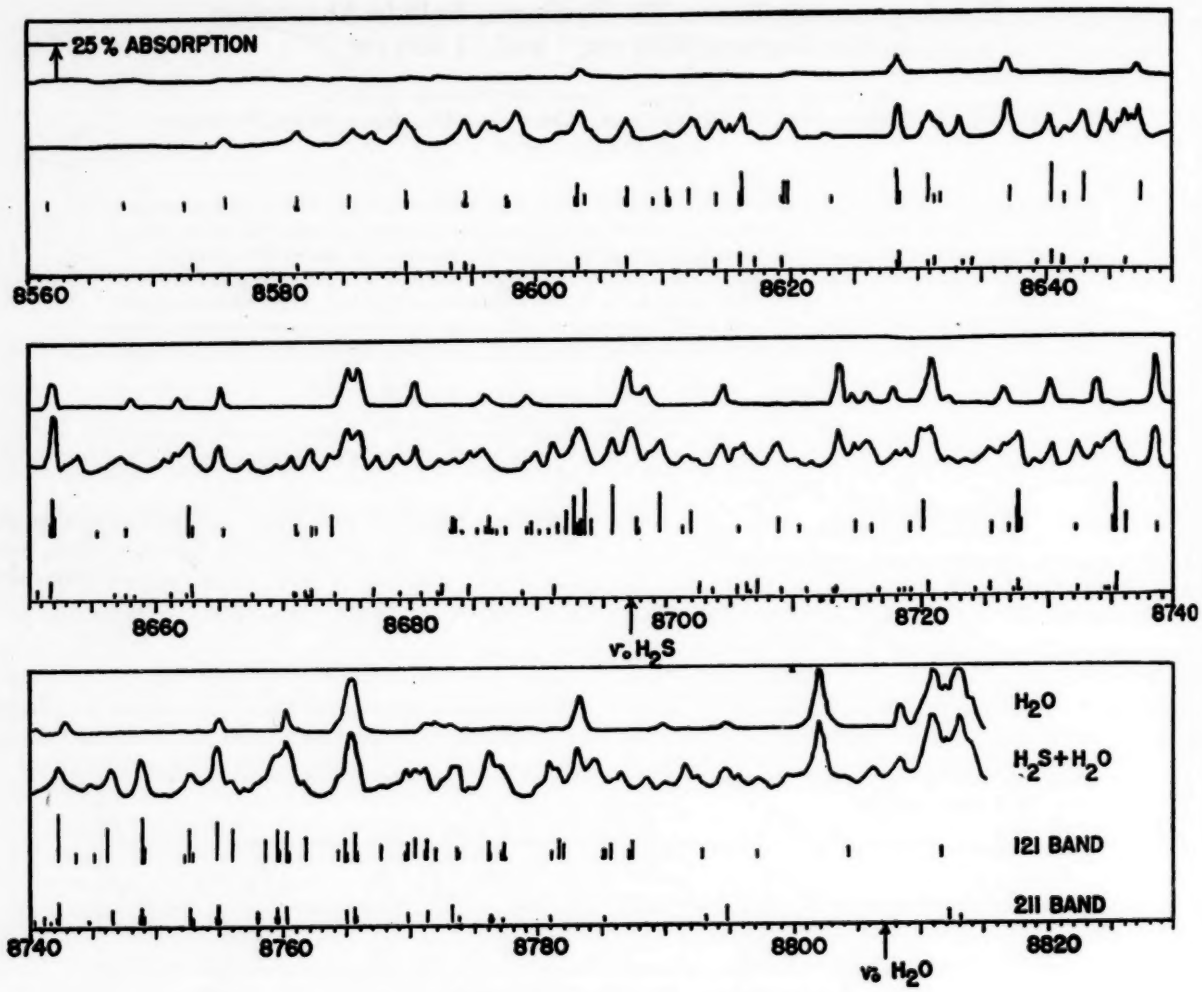

FIG. 2. The spectrum of hydrogen sulfide 8560–8830 cm^{-1}.

evacuated absorption cell which employed the Bernstein and Herzberg[2] modification of the multiple reflection technique of White.[3]

The spectra were taken in the first order of a twenty-one foot concave grating with 15 000 lines per inch mounted in the Eagle arrangement in a mechanism providing automatic focus at all wavelengths.[4]

The photographic plates used were hypersensitized Kodak I–M, IV–M, and I–Z. Overlapping orders were eliminated using Wratten filters; No. 26 at 0.9μ and No. 70 at 1.15μ. Third-order iron lines were employed as standards.

The experimental data and calculated spectra are plotted in Figs. 1 and 2. The line widths and experimental intensities were estimated visually. In the 1.15μ region, use was also made of a photoconductor record of the absorption. These figures show a comparison of the absorption in the regions 0.9μ and 1.15μ, due to 42 feet of atmosphere with the absorption due to 280 feet of hydrogen sulfide plus 42 feet of atmosphere. Of the 105 lines observed between 10 870 and 11 100 cm^{-1}, thirty were found on the water reference plates. Similarly, 50 of the 150 lines in the region 8560 to 8530 cm^{-1} were observed on the water reference plates.

ANALYSIS

The 11 000 cm^{-1} region

Excited state inertial constants were estimated on the assumption that the observed A-type structure arose from the lower component of the resonating pair of levels (131), (311) and using the linear expansions of the moments of inertia in terms of the vibrational quantum numbers[5] together with the averaging process described by Darling and Dennison.[6]

The ground state energies were taken from the analysis of the 9911 cm^{-1} region[7] and the final values of the parameters of the upper state were obtained by the method of least squares.[7]

[2] H. J. Bernstein and G. Herzberg, J. Chem. Phys. **16**, 30 (1948).
[3] J. U. White, J. Opt. Soc. Am. **32**, 285 (1942).
[4] Bair, Cross, Dawson, Wilson, and Wise, to be described later.
[5] H. C. Allen thesis, University of Washington (1951).
[6] B. T. Darling and D. M. Dennison, Phys. Rev. **57**, 128 (1940).
[7] P. C. Cross, Phys. Rev. **47**, 7 (1935).

The calculated spectrum in Fig. 1 was derived from the constants listed in Table I. This spectrum, together with the known absorption by water vapor, provides a satisfactory explanation for the observed absorption.

The 8700 cm^{-1} region

An analysis similar to the one above, with assignment of the absorption to the lower component of the pair (121), (301), accounted for somewhat more than half of the observed lines not obviously due to water. A number of the remaining lines could not be fitted by either this A-type H_2S band or by the water band of this region, even assuming an unreasonably large amount of water in the sample.

The possibility of the superposition of a B-type band assignable to the lower component of the pair (211), (031) was then considered. The fit of the spectrum shown in Fig. 2 was obtained with the A-type and B-type bands exactly superposed at 8697.3 cm^{-1} and with the same inertial constants, as shown in Table I. About fifteen lines not accounted for by the A-type band or the water band were consistent with calculated transitions of the B-type band. A few of the readings recorded as lines are not satisfactorily explained by assignment to either of these hydrogen sulfide bands or to water absorption. However, in attempting to plot absorption peaks from such a complicated absorption pattern, it is not unreasonable to expect a few spurious readings, and these are not believed to detract appreciably from the correctness of the more salient features of the analysis. Also, our calculated spectrum does not include many weak lines nor any transitions involving levels with $J>12$.

TABLE I. Observed excited state parameters (cm^{-1}).

	(121)	(131)
ν_0	8697.3	11 008.78
A	10.29	10.197
B	8.75	8.559
C	4.48	4.411

Because of the coincidence of the strongest P and R-branch lines of the bands in the 8700 cm^{-1} region, the analysis of the B-type band is not as conclusive as is that of the two A-type bands reported here. There are, however, regions of support for its presence, *e.g.*, a study of Fig. 2 shows that several transitions of the B-type band are needed to explain the collections of lines in the vicinity of 8680 cm^{-1} and 8705 cm^{-1}. It was the absorption in these regions that first called attention to the possibility of the presence of two bands.

Excited Electronic States and Molecular Vibrations of Thiophosgene

JULES DUCHESNE
Institut d'Astrophysique, University of Liège, Cointe-Sclessin, Belgium

(Received December 29, 1952)

The most general vibration potential function of the lower excited electronic state of thiophosgene is computed and interpreted in terms of theory. It is shown that the π^* antibonding orbital is not far from being localized in the CS bond and that the sulfur lone pair electrons play a great part in the angular rigidity of the molecule. A general rule for the behavior of the sign of the cross terms is formulated.

A preliminary study of the next excited state is undertaken and a correlation between some properties of the molecular orbitals of both states is made.

THE potential function governing the molecular vibrations of polyatomic molecules in the ground state is now sufficiently well interpreted[1] to make possible the extension of the study to the excited electronic states. The work of Garforth, Ingold, and Poole[2] on benzene already revealed the potentialities of this field. More recently, Delsemme and Duchesne confirmed this in their study of difluorobenzene.[3] However, these authors made use of a limited force field without cross terms, and it is the aim of the present paper to demonstrate the importance of these for a more complete knowledge of the properties of the molecular orbitals.

The longest wavelength absorption system of $CSCl_2$ occurs in the region 5710A–3990A and is composed of a great number of sharp bands. Among the vibrations associated with the electronic excited state, two were assigned with certainty by Henri and Duchesne[4] to species A_1 of the point group C_{2v}. One of them, which refers to the CS stretching (ν_1), was shown to have a frequency of 914 cm^{-1}, while the other, related to the ClCCl bending (ν_3), had a frequency of 240 cm^{-1}. The most general form of potential energy describing the normal modes has been written as[5]

$$2U=f_1\Delta l_1^2+f_2\sum_2^3\Delta l_i^2+f_\theta l_2^2\Delta\theta^2+f_\phi l_2^2\Delta\phi^2+2f\Delta l_2\Delta l_3$$
$$+2\gamma_c l_2\Delta l_1\Delta\theta+2f_c\sum_2^3\Delta l_1\Delta l_i$$
$$+2g_c' l_2\sum_2^3\Delta l_i\Delta\phi+2g_c'' l_2\sum_2^3\Delta l_i\Delta\theta.$$

In this expression, l_1 and l_i are, respectively, the CS and CCl bond distances, whereas θ and ϕ are the ClCCl and ClCS bond angles, at the equilibrium position. The values of the force constants, expressed in 10^5 dynes/cm units, found for A_1 in the ground state are

$$f_1=6.75 \qquad f_c=0.335,$$
$$f_2'(\equiv f_2+f)=4.18 \qquad \gamma_c=-0.516,$$
$$\Gamma(\equiv 2f_\theta+f_\phi/2)=0.97, \quad g_1(\equiv 2g_c'-4g_c'')=-1.2.$$

A first attempt has now been made to calculate the corresponding main force constants f_1, f_2', and Γ of the upper level, using the two observed frequencies. As the excited CCl vibration (ν_2) was not identified in the spectrum of the earlier work,[4] frequencies have been considered within the range 600–400 cm^{-1}. As the observed value in the normal state is 497 cm^{-1},[4,6] the limits adopted are certainly quite safe. Furthermore, if the angle θ is modified with respect to its normal state value of 116°,[7] there is no noticeable influence on the final results. In spite of having taken these factors into account, no real values have been obtained for the force constants. There can, therefore, be no doubt as to the great part played by the interaction forces in the excited state. In order to introduce them into the equations, the assumption is made that they do not change in sign on going from the ground to the upper state, and uniformly decrease by 40 percent. Then, using $f_c=0.2$, $\gamma_c=-0.31$, $g_1=-0.8$, with $\theta=116°$, it may be deduced that $f_1=3.93$, $f_2'=3.71$, and $\Gamma=0.68$. This solution is obtained by selecting $\nu_2=450$ cm^{-1}, whereas the upper limit of ν_2 beyond which imaginary numbers are found is 470 cm^{-1}. Smaller values than 450 cm^{-1} do not significantly modify f_1 or Γ, but have a decreasing effect on f_2'. Although these cannot be definitely ruled out, they are less probable on account of the nonappearance of the ν_2 vibration in the excited state which indicates a slight change in frequency with respect to the ground state. A negative sign was necessarily chosen for g_1 in both the excited and ground states, in order to avoid imaginary solutions. This fact had not been recognized by the author in earlier publications concerned with the ground state.[5] This analysis reveals that the CS and CCl force constants are very differently affected.

The interpretation of this fact obviously depends

[1] Coulson, Duchesne, and Manneback, *V. Henri Mém. Vol.* (Desoer, Liège, 1948), p. 33; J. Duchesne, Mém. acad. roy. Belg. **26**, 1 (1952).
[2] Garforth, Ingold, and Poole, J. Chem. Soc. 491 (1948).
[3] A. Delsemme and J. Duchesne, Compt. rend. (Paris) **234**, 612 (1952).
[4] V. Henri and J. Duchesne, Nature, **143**, 28 (1939); Bull. soc. roy. sci. Liège **1**, 19 (1939).
[5] J. Duchesne, Physica, **8**, 525 (1941); Mém. soc. roy. sci. Liège **1**, 429 (1943); *V. Henri Mem. Vol.* (Desoer, Liège, 1948), p. 47.
[6] H. W. Thompson, J. Chem. Phys. **6**, 748 (1938).
[7] Brockway, Beach, and Pauling, J. Am. Chem. Soc. **57**, 2693 (1935).

upon the nature of the electronic transition. This is presumably a space symmetry-forbidden one $A_1 \rightarrow A_2$ resulting from the excitation of a nonbonding 3 p_S electron to an antibonding π orbital. Mulliken's and McMurry's views obtained from their extensive study of carbonyl compounds[8] support this interpretation. The multiplicity of A_2 remains an open question; the analysis of certain features of the high resolution spectrum and preliminary experiments now performed relative to the photochemical formation of the well-known dimer, studied earlier by several authors,[9] do not permit as yet a definite settling of this problem. The transition is designated as $n \rightarrow \pi^*$ according to a notation of Kasha.[10] As the CCl force constant is only slightly affected as compared with the CS one, it follows that the π^* orbital is not far from being localized in the CS bond. It will be impossible to give the exact degree of delocalization until the ν_2 frequency is more precisely known. One is, however, led to the conclusion that the CS and Cl bonds, in the ground state itself, are conjugated to only a small extent. The value of Γ is nearly independent of ν_2. Thus, there is no doubt that it is considerably reduced in the upper level. The change which it undergoes is even of the same order of magnitude as that of f_1. Therefore, this effect shows definitely that the trigonal hybridization at the carbon atom is far from maintaining by itself the angular rigidity of the system. We are here confronted with a very significant case which provides us with a direct check of the great part played by the nonbonding electrons in the determination of the valence angles.

[8] R. S. Mulliken, J. Chem. Phys. **3**, 564 (1935); H. L. McMurry, ibid. **9**, 231 (1941).

[9] A. Schönberg and A. Stephenson, Ber. **66**, 567 (1933); Delépine, Labro, and Lange, Bull. soc. chim. France **2**, 1969 (1935).

[10] M. Kasha, Disc. Faraday Soc. **9**, 14 (1950).

It is to be pointed out that the invariability of the sign of the cross terms is strongly indicated not only by the spectrum of thiophosgene and the satisfactory results of the present interpretation, but also more definitely by the spectra of certain other molecules which will be dealt with in another paper. The following general rule may therefore be formulated: *in electronic states that are derived from the normal state by transitions of the type $n \rightarrow \pi^*$ or $\pi \rightarrow \pi^*$, the cross terms for the planar vibrations of molecular systems have an invariant sign.*

The next band system composed of about one hundred broad and rather diffuse bands lies in the ultraviolet region between the limits 3200A–2800A. One of the upper state frequencies, first observed by Henri,[11] is 400 cm^{-1}. The present analysis shows that it is the main excited vibration and that it corresponds to the CCl motion ν_2. If the transition is an allowed one such as $^1A_1 \rightarrow {}^1B_2$, it should arise from the excitation of an n electron to an antibonding σ^* orbital. This assignment is obtained by analogy with what occurs in the carbonyl compounds.[8] It would then appear that the B_2 electronic state gives rise to a lower symmetrical CCl frequency than the A_2 state. As a consequence, *the σ^* orbital is presumed to have a greater antibonding power on the CCl bond than the π^* orbital.*

In conclusion, it is hoped that the valence theory of the excited electronic states may considerably benefit from the development of the present method. A full account of this investigation will be published later.

The author would like to express his thanks for the cooperation of Mr. Yvan Ottelet in the computational part of this work.

[11] V. Henri, *Structure des molécules* (Hermann, Paris, 1925), p. 90.

The Energies of Strained Carbonium Ions

J. L. FRANKLIN AND F. H. FIELD
Technical and Research Division, Humble Oil and Refining Company, Baytown, Texas
(Received January 5, 1953)

The appearance potentials of two sterically hindered nonplanar carbonium ions (from bicyclo [2.2.1] heptyl bromide and bicyclo [2.2.2] octyl bromide) are found to be higher than the appearance potential of an analogous planar carbonium ion. From these results it is inferred that in general the appearance potentials of unhindered ions correspond to the formation of the ions in essentially equilibrium configurations.

THE mechanism of ionization and dissociation under electron impact appears to be as follows: first an electron is ejected, which results in the formation of the parent ion; and second, if the energy is sufficiently great, the ion, after several vibrations, decomposes into characteristic fragments each in a configuration of minimum energy. The principal reasons for this are (1) bond strengths calculated from electron impact measurements agree quite closely with those determined by other means, and (2) in most instances the heats of formation of a fragment ion calculated from appearance potentials of the ion as produced from a variety of compounds agree within experimental accuracy. Table I illustrates this point with data on the *t*-butyl ion.

However, more direct evidence supporting the postulated mechanism is obviously desirable. On the basis of this mechanism, if an ion could be hindered sterically from achieving the configuration of maximum stability, its appearance potential under electron impact should be greater than that of an unhindered ion of the same general type. Since the charged carbon atom in an alkyl carbonium ion is in the sp^2 state of hybridization, the configuration involving planar bonds to the charged carbon is the most stable. It is clear that such planarity cannot readily be achieved in the bicyclic ions with structures

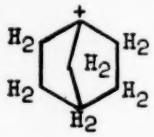

and

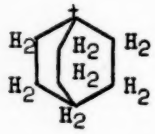

and thus a comparison of the appearance potentials of these ions with that of the unhindered *t*-butyl ion would provide a means of testing the postulated mechanism.

TABLE I. Heat of formation of the *t*-butyl ion.

Compound	$\Delta H_f(t\text{-}C_4H_9^+)$ (kcal/mole)
t-butyl chloride	165[a]
neopentane	166[b]
2,2 dimethylbutane	166[b]
2,2,3 trimethylbutane	170[b]
2,2,3,3 tetramethylbutane	169[b]

[a] D. P. Stevenson and J. A. Hipple, J. Am. Chem. Soc. **64**, 2766 (1942).
[b] D. P. Stevenson, Disc. Faraday Soc. **10**, 35 (1951).

We have measured the appearance potentials of these ions as produced by electron impact from the corresponding bromides (bicyclo [2.2.1] heptyl bromide, bicyclo [2.2.2] octyl bromide, and *t*-butyl bromide) and also the ionization potentials of the cyclic bromides. The results are given in Table II. The measurements were made with a Westinghouse Type LV mass spectrometer using the vanishing current method and techniques as previously described.[1]

The strain (deviation from planarity) in the ions decreases in the order bicyclo [2.2.1] heptyl > bicyclo [2.2.2] octyl > *t*-butyl, and consequently the proposed mechanism of ionization would lead one to expect the energies and appearance potentials of the ions to decrease in the same order. However, it is seen from Table II that such is not the case.

We believe that the deviation from the expected order is due to peculiarities specific to the ionization and dissociation of the *t*-butyl bromide. Two points are of significance. First, Morrison and Nicholson[2] detected no parent ion in the mass spectrum of *t*-butyl bromide, a finding confirmed by work in this laboratory. Second, the energy of the *t*-butyl bromide molecule-ion is greater than the energy of a *t*-butyl ion and a bromine atom. It is, of course, impossible to measure the ionization potential of *t*-butyl bromide, but it is seen from Table III (taken from Morrison and Nicholson) that the ionization potentials of alkyl bromides are rather insensitive to chain branching, and one would estimate the potential energy curve of the *t*-butyl bromide molecule-ion to be 10.0–10.3 ev above that for the molecule. On the other hand, the difference in energy between *t*-butyl ion plus the bromine atom and the *t*-butyl bromide molecule is $167+27-(-28)=222$ kcal/mole $=9.6$ ev.[3]

From these facts we conclude that the potential energy curve of the *t*-butyl bromide molecule-ion is repulsive, and in the ionization and dissociation of *t*-butyl bromide the transition to this repulsive curve under the initial electron impact is followed immediately by decomposition of the molecule-ion into fragments

[1] F. H. Field, J. Chem. Phys. **20**, 1734 (1952).
[2] J. D. Morrison and A. J. C. Nicholson, J. Chem. Phys. **20**, 1021 (1952).
[3] 167 kcal/mole $=\Delta H_f(t\text{-}C_4H_9^+)$, average of values given in Table I; 27 kcal/mole $=\Delta H_f(Br\cdot)$; -28 kcal/mole $=\Delta H_f(t\text{-}C_4H_9Br)$, estimated using Franklin's method of group equivalents, J. L. Franklin, Ind. Eng. Chem. **41**, 1070 (1949).

having considerable excess energy. This view is supported by the fact that the observed appearance potential of the *t*-butyl ion is quite close to the estimated "ionization potential" of *t*-butyl bromide.

Thus, it is not proper to compare the appearance potentials of the bicyclic ions with the measured value of the appearance potential of the *t*-butyl ion from *t*-butyl bromide. However, a comparison with the calculated appearance potential should be valid,[4] in which case the order of decrease of the appearance potentials is in accord with the order predicted by the theory, i.e., bicyclo (2.2.1) heptyl (10.66 ev)>bicyclo (2.2.2) octyl (9.98 ev)>*t*-butyl (~9.6 ev). It should perhaps be mentioned that the high values of the appearance potentials of the two cyclic ions cannot be due to repulsive potential energy curves in the molecule-ions, for both bicyclic bromides give parent ions of appreciable intensity, and further, as can be seen from Table II, the ionization potentials of the molecules are lower than the corresponding appearance potentials. It is also quite interesting that the relative rates of hydrolysis of the bromides are just what would be predicted from the appearance potentials: bicyclo (2.2.1) heptyl bromide very slow, bicyclo (2.2.2) octyl bromide intermediate, and *t*-butyl bromide very fast.[5] From these results we infer that in general (barring exceptional cases such as that of *t*-butyl bromide) the appearance potentials of unhindered ions correspond to the formation of the ions in essentially equilibrium configurations.

TABLE II. Ionization and appearance potentials.

Ion	Appearance potential (ev)	Ionization potential
Bicyclo [2.2.1] heptyl	10.65, 10.67; Av=10.66	
Bicyclo [2.2.2] octyl	9.93, 10.03; Av= 9.98	
t-Butyl	10.29, 10.43; Av=10.36	
Bicyclo [2.2.1] heptyl bromide		9.79, 9.81, 10.11; Av=9.90
Bicyclo [2.2.2] octyl bromide		9.71, 9.81; Av=9.76

TABLE III. Effect of chain branching on ionization potential of alkyl bromides.

	n-Pr	*i*-Pr	*n*-Bu	*i*-Bu	Sec-Bu
I.P. (ev)	10.29	10.11	10.12	10.24	10.15

It is, of course, quite possible to reverse the argument given above. Thus, if one accepts the premise that the energies measured by electron impact in a mass spectrometer correspond to the formation of the fragments in their ground states, then the relatively high appearance potentials of the necessarily nonplanar bicyclic ions constitute evidence that the planar configuration of an ionized carbon atom in an sp^2 state of hybridization is of lowest energy.

We wish to express our appreciation to Professor W. E. Doering for the gift of samples of the two bicyclic bromides and to Mr. R. K. Saunders for helping with the measurements.

[4] The key quantity in the calculated appearance potential is the value of $\Delta H_f(t\text{-}C_4H_9^+)$, which is taken from Table I. It must be mentioned that all the compounds listed in Table I give parent ions of very small or vanishing intensities, and it might be argued that the value of *ca.* 167 kcal/mole found for $\Delta H_f(t\text{-}C_4H_9^+)$ therefore contains some excess energy as a result of the presence in the molecule-ions of repulsive potential energy curves. We are inclined to doubt this, however, for the value of $D(t\text{-}C_4H_9\text{-}H)$ which results from $\Delta H_f(t\text{-}C_4H_9^+)$ (89 kcal/mole, reference b, Table I) is in good agreement with a value [86? kcal/mole, M. Szwarc, Chem. Revs. **47**, 75 (1950)] obtained by another method. Furthermore, the appearance potentials of the *t*-butyl ions formed from paraffin hydrocarbons (reference b, Table I) are about the same as the values of the ionization potentials of the compounds as estimated from the known ionization potentials of the normal paraffins. It would appear that the small parent-ion intensities of the compounds listed in Table I are due to the presence in the molecule-ions of essentially horizontal potential energy curves.

[5] Private communication from Professor W. E. Doering.

On the Presence of Free Sodium in Sodium Chloride Crystals Containing Color Centers and Color Center Precursors

MICHAEL HACSKAYLO AND DUMAS OTTERSON
National Advisory Committee for Aeronautics, Lewis Flight Propulsion Laboratory, Cleveland, Ohio
(Received October 6, 1952)

The presence of "free sodium" in NaCl crystals containing color centers and color center precursors, as indicated by the results of Hacskaylo and Groetzinger, has been confirmed by the use of a more precise method of chemical analysis. The present measurements were carried out by dissolving the crystals in question in a solution containing an indicator, *p*-nitrophenol, and determining the resulting change in the optical density of the solution at a wavelength of 415 mμ. The ratio of the number of "free sodium" atoms to vacancy pairs was about one for crystals which had been subjected to electrolysis and about one-tenth for crystals irradiated with x-rays, independent of whether these crystals had been first subjected to electrolysis.

IN an investigation concerning the properties of NaCl crystals which had been subjected to electrolysis without becoming discolored, Hacskaylo and Groetzinger[1] (in a paper to be designated as HG in the sequel) reported the existence of a metastable state characterized by a high sensitivity for the formation of nonpermanent color centers and a susceptibility for the formation of permanent color centers upon irradiation with x-rays. Crystals in this state were consequently said to contain color center precursors. In the course of their studies, they compared a number of properties of crystals in the metastable state with those of normal crystals and crystals in which color centers had been induced in various fashions, and found evidence that such crystals differ in their chemical properties. More specifically, when a crystal containing either precursors or color centers was dissolved (after the removal of the surface layers) in distilled water, the hydrogen ion concentration of the resulting solution appeared to be somewhat less than that of a solution of the same concentration prepared from an untreated crystal. The simplest interpretation of this result is that the treated crystals contained a quantity of sodium slightly in excess of the stoichiometric amount. There are a number of arguments against such a viewpoint, especially in the case of crystals which were subjected only to x-irradiation. The difference in the *p*H of a solution of a treated and untreated crystal indicates a change in the chemistry of the crystal which can be expressed in terms of numbers of equivalent "free" sodium atoms. In view of the fact that the authors of HG did not consider this effect as definitely established, it was decided to carry out a more quantitative investigation of the chemical properties of such crystals.

Aside from the question of whether a change in *p*H can occur without a change in the stoichiometric ratio, a matter to which we will return later, we believed that there were two possible sources of error in the work reported in HG. In the first place, there is the possibility that in the case of irradiated samples an oxidation reaction took place between the crystal and the surrounding atmosphere under the influence of the x-rays. To exclude this possibility we performed some of our irradiations in a dried helium atmosphere but found that this did not affect the results. Secondly, the *p*H measurements reported in HG were made with a glass electrode and were not very reproducible—possibly because of the sodium ion effect. Therefore, we decided to determine the equivalent free sodium in the crystals by the following method, based on the use of the indicator *p*-nitrophenol which was chosen because its region of maximum sensitivity lies in the vicinity of *p*H 6.5, close to the value of our solutions.

An aqueous indicator solution was prepared containing 0.2 g/l of *p*-nitrophenol and 0.1 g/ml of sodium chloride. (It was found that the use of solutions with this content of sodium chloride improved the reproducibility of the results without adversely affecting the sensitivity of the method.) The optical density at a wavelength of 415 mμ of an aliquot of this solution was measured by the use of a model B Beckmann spectrophotometer. To determine the excess sodium in a sample of treated crystal, the crystal was first weighed and dissolved in 10 ml of the indicator solution. The optical density of the resulting solution at 415 mμ was then determined. The nominal amount of free sodium present in the treated crystal is proportional to the change in optical density. (Actually, of course, part of the change in optical density is the result of the effect of dissolved sodium chloride upon the activities of the other ions in the solution.) In order to obtain the factor of proportionality, a series of calibrating experiments was carried out in which known amounts of sodium hydroxide were added to aliquots of the indicator solution, and the resulting change in optical density measured. (Each free sodium atom present in a crystal is, of course, converted to a molecule of sodium hydroxide when the crystal is dissolved.) The values obtained for the factor over the range of concentration of interest all agreed to within about 10 percent. As a further check, the optical absorption coefficient of *p*-nitrophenol in the dissociated state was determined. Then, by using the value for the dissociation constant of *p*-nitrophenol given by Kolthoff

[1] M. Hacskaylo and G. Groetzinger, Phys. Rev. 87, 789 (1952).

and Laitinen,[2] it was possible to calculate the change in optical density to be expected when a known amount of sodium hydroxide was added to the indicator solution. The calculated values thus obtained agreed to within 10 percent with those obtained by direct measurement.

In order that it be possible to infer the quantity of free sodium present in a crystal from the results of our measurement, it is necessary to know the change of optical density resulting when an untreated crystal is dissolved in the indicator solution. Weighed samples of normal crystal were, therefore, dissolved in 10 ml of indicator solution and a change in optical density corresponding to $(1.5\pm0.2)\times10^{17}$ free sodium atoms per cm^3 of dissolved crystal was found. This quantity was subtracted from the results for treated crystals which consequently are reported as net atoms of free sodium per cm^3. Table I gives the value of this quantity for crystals which had been subjected to various treatments. The terminology employed to designate the state of the crystal is the same as that used in HG.

The number of vacancy pairs present per cm^3 of the treated crystal in excess of those present in a normal crystal (measured by the method based on the change of density of the crystals as described in HG) is also given in Table I. The number of excess vacancies is presumably a rough measure of the departure from equilibrium as far as effects concerning color centers and color center precursors are concerned, and the ratio between number of free sodium atoms and number of vacancy pairs is therefore given in Table I. It is seen that crystals which have been subjected to electrolysis show a number of free sodium atoms somewhat exceeding the number of vacancy pairs, independent of whether color centers or color center precursors result from the electrolysis. When either normal crystals or those which have undergone electrolysis are subjected to x-irradiation, there is an apparent production of "free sodium atoms" in an amount equal to ten or twenty percent of the number of vacancy pairs. The measurements of the amount of free sodium are considerably more precise than those given in HG but serve to verify the existence of the effects reported there.

In order to determine whether the coloration produced during irradiation is associated with an irreversible chemical change, some crystals which had been subject to irradiation were annealed to remove the coloration by keeping them at a temperature of 300° to 400°C for five minutes in a dried helium atmosphere. No free sodium could be detected in such crystals. It is evident that whatever change occurs in the chemical properties during irradiation is reversible.

[2] I. M. Kolthoff and H. A. Laitinen, *pH and Electrotitrations* (John Wiley and Sons, Inc. New York, 1944), second edition, p. 43.

TABLE I. Amount of free sodium and its relation to the number of vacancies for various states of NaCl crystals.

Color	Uncolored	Nonpermanently colored	Permanently and nonpermanently colored		Permanently colored
Condition	Metastable state	Irradiated in normal state	Irradiated in metastable state	Irradiated after colored by electrolysis	Colored by electrolysis
Net free Na atoms/$cm^3\times10^{-17}$	3.2 ± 0.9	3.2 ± 0.8	7.5 ± 3.0	11 ± 2.0	7.5 ± 2.0
Vacancy pairs/$cm^3\times10^{-17}$	2.5	27	65	58	3.2
Ratio of free Na atoms to vacancy pairs	1.3	0.1	0.1	0.2	2.0*

* This value would be reduced to 1 if it were assumed that only Cl^- vacancies were formed within the crystal.

A crystal subjected to electrolysis undergoes a certain amount of decomposition with the production of sodium in the elementary form at the surface. It is, therefore, not surprising that there results a deviation from the stoichiometric ratio in the interior. Ordinarily, the presence of excess sodium seems to be associated with the existence of permanent color centers whereas these are not found in crystals in the metastable state; but the formation of such color centers in a crystal containing excess sodium may depend upon the conditions under which this is introduced into the crystal. It is more difficult to understand why excess sodium should occur in a crystal colored by irradiation. There are two mechanisms which might account for the chemical behavior of these crystals. Both of these are based on the assumption that some of the free electrons trapped in vacancies to form color centers are originally produced as a consequence of the neutralization of chloride ions so that there exist in a colored crystal a certain number of free chlorine atoms. If some of these atoms were to escape by diffusion, the crystal would indeed contain a true excess of sodium. This possibility has, however, to be excluded because it would lead to permanent color centers, or at least to a chemical effect even in the case of a crystal from which the color centers (produced by irradiation) had been bleached out. On the other hand, even if the free chlorine atoms were to fail to escape the crystal, the apparent excess of sodium could still be explained on the following basis. Chemically, such a chlorine atom would not really belong to the sodium chloride crystal, and, consequently, might dissolve independently as free chlorine when the crystal is dissolved. Therefore, during this process, the crystal would behave as though there were an excess of free sodium present.

We are indebted to Dr. P. Schwed and Dr. G. Groetzinger for valuable discussions.

Polarized Fluorescence of Molecules of Some Single Organic Crystals

S. C. GANGULY AND N. K. CHOUDHURY
Bangabasi College Research Laboratory, Calcutta, India

(Received August 11, 1952)

The polarized fluorescence of single crystals of pyrene, phenanthrene, and benzil have been studied. It has been observed that, whether the incident light is polarized or not, the fluorescent light is polarized in all three cases. From the study of the intensity of fluorescence light the directions of oscillators, and so the favored condition of excitation of fluorescence with particular reference to the crystal structure, have been determined, and an attempt has been made to find the orientation of the molecules with reference to the crystal axis where the structure is not known.

I. INTRODUCTION

ALTHOUGH the study of luminescence has made considerable progress during recent years, the study of polarized fluorescence of solids,[1] particularly of organic crystals, has not drawn much attention.

In a recent communication[2] we have shown that from the study of crystal fluorescence, particularly from the study of polarizations of the fluorescence, it is possible to find out the unique direction of oscillators with reference to crystallographic axes.

Again, from x-ray and other studies, if the orientation of the molecules are known, the relation between the molecular plane and the incident electric vector on the one hand and the intensity and the direction of electric vector of fluorescence light on the other can be established; thus, the favored condition of excitation of fluorescence of solids will be known to us.

Conversely, when the molecular orientations are not known to us, the study of anisotropy of fluorescence in different directions will give much useful information regarding the directions of oscillators and so of molecular orientations.

Since the method employed in the x-ray analysis of the crystal structure is a tedious one, it will be extremely useful if from optical study we get any information regarding molecular orientation.

It is known[3] that the benzene molecule has a striking optical anisotropy, so we can reasonably expect polarization of the fluorescence of aromatic organic substances. So from the study of the polarization of the fluorescent spectrum in different directions, we can get informations regarding the orientation of the molecule inside a crystal. Studies on fluorescence in the vapor state or in solution in which fluorescing molecules are oriented at random do not give us the same information regarding the directional properties of fluorescence of molecules.

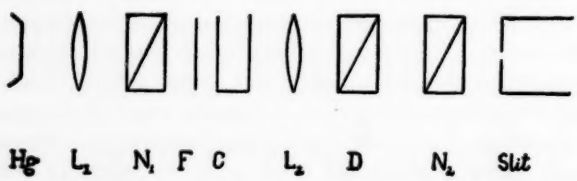

FIG. 1. Hg = mercury arc, L_1 = lens, N_1 = polarizing Nicol, F = filter, C = substance, D = double-image prism, and N_2 = analyzing Nicol.

II. EXPERIMENTAL

The crystals were generally grown out of solutions in the usual solvents. The experimental methods adopted for the measurement of anisotropy of fluorescence was essentially the same as that described in the previous paper.[2]

The general plan of the experiments was to excite the fluorescence by the radiations (usually 3650 group) of an Hg arc incident normally on the crystal flake, either unpolarized or polarized with the electric vector along a or b or c axis if possible, and to study the fluorescence in the forward direction for its polarization and intensity. A sketch of the experimental arrangement used is given in Fig. 1. The light from the Hg arc is focused with the help of a lens L on a square aperture A having its sides vertical and horizontal, respectively. Between the arc and aperture is placed a filter to isolate the exciting radiations and a Nicol N to polarize the light; C is the crystal flake mounted just behind the aperture with its plane normal to the path of the light.

The fluorescent light in the forward direction is allowed to pass through a double image prism D, so oriented as to separate the images vertically; a Nicol N_2 and lens L_2 are placed between the spectrograph (Adam Hilger) slit and double image prism. Two images of the aperture A resulting from fluorescent light form on the slit one above the other, the polarization of which is determined by rotating the Nicol N_2 so as to make the two images of the fluorescence bands appearing in the spectrograms equal.

If it is observed that all the fluorescence bands are equally polarized and in the visible region, the spectrographs can be dispensed with altogether.

[1] P. Pringsheim, *Handbuch der Physik* Bd. 21, (1929).
[2] S. C. Ganguly and N. K. Choudhury, J. Chem. Phys. **19**, 617 (1951).
[3] C. V. Raman and K. S. Krishnan, Proc. Roy. Soc. (London) **113A**, 574 (1927).

FIG. 2. The fluorescence spectra of the benzil crystal excited by the 3650 group of mercury lines.

III. RESULTS

Pyrene

A quantitative x-ray analysis of the crystal has been made by Robertson and others.[4] The crystal is monoclinic prismatic in the space group $C_{2h}(^5P2_1/a)$. Its unit cell has a dimension $a=13.60$, $b=9.24$, $c=8.37$, and $\beta=100.2$, and it contains 4 molecules of $C_{16}H_{10}$. The molecule has a plane structure, and it consists of a regular hexagon as shown in the figure. Pyrene crystals absorb radiations extending up to 4000A and fluoresce radiations extending from 4000A to 5600A.

Phenanthrene

The crystalline structure of phenanthrene was studied by the x-ray method by Basak.[5] The crystal belongs to the space group $C_2^2-P2_1$ in the monoclinic crystal class. The number of molecules in the unit cell is 2, and the unit cell has a dimension $a=8.57$, $b=6.11$, $c=9.47$A, and $\beta=82°\ 30'$. Phenanthrene crystals absorb radiation extending up to 3900A and fluoresce radiations extending up to 4900A.

TABLE I.

Crystal	Symmetry axis vertical	a axis vertical	Face normal to the path of light	Ratio of intensity from graph	Angle between the oscillator direction and symmetry axis
1 Pyrene	b component stronger	b component stronger	001	0.63	38°.5
2 Phenanthrene	b component stronger	b component stronger[a]	001	0.44	33°.5
3 Benzil	a component stronger	a component stronger	$10\bar{1}0$	2.9	60°

Benzil

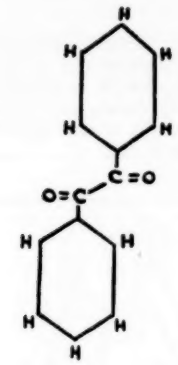

The chemical formula is $C_6H_5CO\cdot COC_6H_5$. Benzil crystallizes from ether, and it belongs to the trigonal trapezohedral class with axial angle 78° 13′. It[6] is built upon a hexagonal lattice, and the unit cell contains 3 molecules which are disposed spirally. The molecule of benzil has a diad axis, and the space group is D_3^4 or D_3^6. The axial lengths calculated for the cell are $a=8.42$A and $c=13.75$A. Benzil crystal absorbs radiations extending up to 4900A from ultraviolet and fluoresce from 4900A to 5900A (Figs. 2 and 3).

The pyrene and phenanthrene crystals were mounted with the b axis vertical, and the crystal benzil was mounted with the c axis vertical. The light with electric vector vertical was incident normally on the c face of phenanthrene and pyrene and on the $10\bar{1}0$ face of benzil. The fluorescent light after passage through the double image prism (suitably oriented to separate the two principal vibrations) was allowed to fall on the

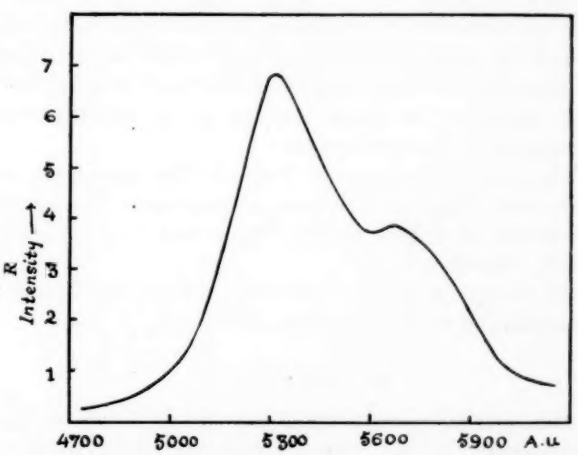

FIG. 3. The intensity curve of the fluorescence spectrum of the benzil crystal.

[4] J. Robertson, J. Chem. Soc. **1947**, 358.
[5] B. S. Basak, Ind. J. Phys. **24**, 309 (1950); H. Mark and J. Henstenberg, Z. Kristallogr. **70**, 287 (1929).
[6] N. C. B. Allen, Phil. Mag. **3**, 1037 (1927); K. Banerjee and N. L. Sinha, Ind. J. Phys. **11**, 409 (1937).

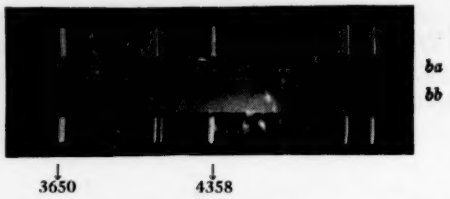

FIG. 4. The fluorescence spectra of the pyrene crystal: *bb* represents the component of fluorescence radiation that is vibrating along the *b* axis when the electric vector of incident light is along the same direction; *ba* represents the component of fluorescence radiation vibrating along the *a* axis when the electric vector of incident light is along the *b* axis.

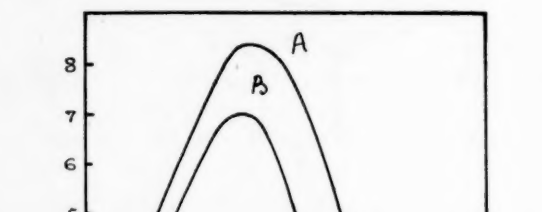

FIG. 5. *A* represents the intensity curve of the fluorescence spectra of pyrene that is vibrating along the *b* axis when the electric vector of incident light is along *b*; *B* represents the same curve vibrating along the *a* axis, when the electric vector of incident light is along *b*

slit of the spectrograph. The two spectra were unequal in intensity. Applying the relation $\rho = \tan^2\phi$, where ρ = ratio of two intensity of any individual band, ϕ = angle between the *b* axis (or *c* axis in case of benzil) and the direction of oscillators in the *c* face (*a* face in benzil), ϕ is determined. The same result is confirmed by rotating the analyzing Nicol from one of its extinction direction in either way so as to equalize the intensities of the two images.

The results are given in Table I. The anisotropy of fluorescence spectra of pyrene, phenanthrene, and benzil are shown in Figs. 4 and 5, Figs. 6 and 7, and Figs. 8 and 9, respectively.

All the spectrograms were taken with a E498 quartz spectrograph of Adam Hilger, Ltd.

IV. DISCUSSION

Measurements were made on the intensity of the fluorescence in the forward direction with incident light vibrations (electric vector) along the *b* axis of the crystal (pyrene and phenanthrene) and again with the light vibrations along *a*. In benzil they were along *c* and *a*. In both cases, the fluorescence spectra of pyrene and phenanthrene along the *b* axis are found to be stronger than those along *a* axis. The fluorescence spectra of benzil along the *a* axis are found to be stronger than those along the *c* axis, whether the electric vector of the incident light is along *c* or along *a*. In other words, the *b* vibrations are predominant in the fluorescent light of phenanthrene and pyrene, not only when the exciting light vector is along the same direction—a result normally to be expected—but also when the exciting light vector is along *a* which is perpendicular to *b*—a very striking result. The same is also true for benzil. Here the *a* vibrations are predominant in the fluorescence of benzil, even when the exciting light vector is along *c* which is perpendicular to *a*. Now, since the polarization of fluorescence is found to be independent of incident light vector, we should expect the same polarization with incident unpolarized light also. Removing the Nicol N_1 in the experimental arrangement we measured the polarization of fluorescence in the forward direction again. The ratio of intensities of the *a* and the *b* vibrations and also of the *c* and *a* (benzil) vibrations were found to be the same as before. The coefficient of absorption of *b* and *a* vibrations are not the same, and loss due to reflection at the

FIG. 6. The fluorescence spectra of phenanthrene crystal. *bb* represents the component of fluorescent radiation that is vibrating along the *b* axis when the exciting light vibrations are along the same direction; *ba* represents the component of fluorescent radiation that is vibrating along the *a* axis when the exciting light vibrations are along the *b* axis.

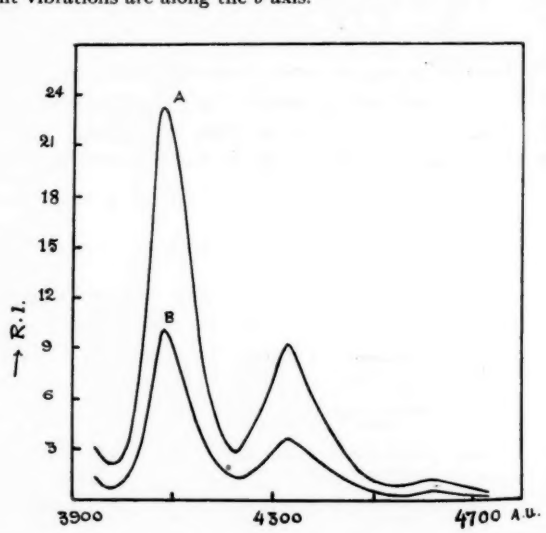

FIG. 7. *A* represents the intensity curve of the fluorescence spectra of phenanthrene that is vibrating along the *b* axis when the electric vector of exciting light is in the same direction; *B* represents the same curve along the *a* axis when the electric vector of incident light is along the *b* axis.

back surface, is also different for the two directions. Corrections for these differences are to be considered in each measurement.

The result that the ratio of the two intensities (along b and a or c and a) is independent of the incident light vector is significant. It shows that in the (001) plane of pyrene and phenanthrene, and in the $10\bar{1}0$ plane of benzil there are two unique directions, and these two directions are on either side of the b (or c) axis and make equal angles with it. It should be mentioned here that although the ratio remains the same, the intensity of the individual fluorescence component is not independent of the direction of the incident electric vector. It is maximum when the electric vector of the incident light is along the unique directions which make ϕ with b axis on either side of it. In benzil the unique directions make ϕ with c axis. The electric vector of the fluorescence radiation will also be in the same unique direction. The ratio of the intensity of the fluorescence radiations along the b and a directions or along the c and a directions depends on the inclination of the above directions to the a axis.

Now, from x-ray study, the angles obtained between the molecular plane and the b axis in the c face of pyrene and phenanthrene agree fairly well with the angles between unique directions of oscillators with the b axis as obtained from our measurement. We can conclude therefrom that along the various directions lying in the (001) plane, along which the electric vector may be incident, there is a particular direction for the maximum excitation of fluorescence and also that, when the incident electric vector is in the plane of the molecule, the fluorescence light is maximum. Again from the polarization measurement of benzil, we find that electric vector of the fluorescent light of benzil makes an angle 60° with the c axis in the $(10\bar{1}0)$ face. So the molecular plane makes an angle of 60° with the c axis in that face. The results obtained can be summarized as follows:

(1) Independently of whether the crystal is mounted with the b axis vertical or with the a axis vertical, the b vibrations (a for benzil) are stronger than the a vibrations (c for benzil).

(2) The ratio of the two intensities of fluorescent light is independent of the incident light.

FIG. 8. The fluorescence spectra of the benzil crystal. *cc* represents the component of fluorescent radiation that is vibrating along the *c* axis when the exciting light vibrations are along the same direction; *ca* represents the component of fluorescent radiation that is vibrating along the *a* axis when the electric vector of incident light is along *c*.

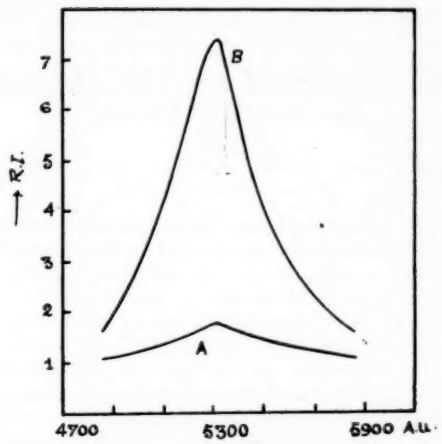

FIG. 9. *A* represents the intensity curve of *cc*, and *B* represents the intensity curve of *ca* of the fluorescence spectra of benzil.

(3) Therefore, $I_a/I_b = \tan^2\phi$. The crystals have unique direction of oscillators, which lie in the molecular plane.

(4) Therefore, maximum excitation would have been obtained if the incident light had been polarized at an angle ϕ to the b axis, that is, if the incident electric vector is in the molecular plane.

The authors offer their sincere thanks to Principal P. K. Bose, Bangabasi College, for giving facilities for work, to the Government of West Bengal for giving a research grant, and to Professor K. Banerjee of the Indian Association for the Cultivation of Science for allowing them to use the microphotometer for intensity measurement.

Letters to the Editor

THIS section will accept reports of new work, provided these are terse and contain few figures, and especially few half-tone cuts. The Editorial Board will not hold itself responsible for opinions expressed by the correspondents. Contributions to this section should not exceed 600 words in length and must reach the office of the Editor not later than the 15th of the second month preceding that of the issue in which the Letter is to appear. No proof will be sent to the authors. A publication charge of $10.00 per Letter is made which, when honored, will entitle the Institution to 100 free reprints.

Ultrasonic Absorption in Liquid Mixtures and Structural Effects*

D. SETTE†
Department of Physics, Catholic University of America, Washington, D. C.
(Received January 15, 1953)

AN interesting kind of binary liquid mixtures is formed by the systems which present a maximum in the ultrasonic absorption coefficient at an intermediate concentration. Most of these systems have water as a component;[1] some others are formed by nitrobenzene and alcohols,[2] and recently we have found the same behavior in the ethyl ether-ethyl alcohol and nitrobenzene-*n*-hexane mixtures. In these two last cases the maximum appears at mole fractions of about 0.30 alcohol and 0.41 nitrobenzene.

A satisfactory explanation of this behavior has not yet been presented, but it is usually believed that it is to be found in the presence of structural effects.

In order to obtain more data on the subject, we have examined the temperature dependence of the ultrasonic absorption coefficient in some of these systems. Only mixtures having a composition corresponding to maximum absorption have been studied in the following binary systems: water-*n*-propyl alcohol, nitrobenzene-ethyl alcohol, and nitrobenzene *n*-hexane. In these three cases the absorption coefficient decreases when the temperature increases, as happens in liquids presenting structural dissipative phenomena.

The frequency dependence of the absorption coefficient in the water-*n*-propyl alcohol and nitrobenzene-*n*-hexane mixtures has also been studied in the range 7–36 Mc/sec, and it has been found that the maximum absorption coefficient decreases when the frequency increases in both cases.

These results confirm the structural nature of the dissipative effects observed in this class of mixtures and indicate that if they are due to relaxation phenomena, the relaxation frequencies are inside the range accessible to experiment, at least for some mixtures. At present it is not possible to see if the structural effects in the different mixtures are of the same origin or not. Such a conclusion can only be drawn after having explained the phenomena in each system. Some investigators[3] have suggested a relaxation mechanism based on the formation of a compound in solution as an explanation of the maximum absorption in some mixtures, but this hypothesis is not confirmed by other indications.

It is very interesting to examine the cases of the nitrobenzene-*n*-hexane mixtures, where it is possible to determine the origin of the additional losses which produce a maximum in the absorption. The mixture for which the ultrasonic absorption is maximum in this system is also the one for which the solubility curve shows a maximum. Moreover, the consolute temperature (19.2°C) is not far from the range in which the experiments were made (21–40°C). It seems therefore evident that the particular phenomena present in the critical region are the origin of the dissipative effect observed. A high ultrasonic absorption has also been observed by Chynoweth and Schneider in the critical regions of one and two component systems.[4]

The critical phenomena essentially consist in the fact that the solution is no more a homogeneous phase; clusters of different compositions and sizes are present. The sizes of these clusters are of the order of magnitude of the wavelength of visible light or smaller[5] so that no sound dissipation for scattering has to be considered.

There are, however, two other ways in which the presence of clusters can produce an increase of absorption in addition to the normal classical absorption. The first is due to the fact that when density fluctuations are present in a liquid the losses produced by viscosity increase.[6] It is possible to show the validity of the following relation for the dependence of the new absorption coefficient for viscosity (α_v) upon the frequency

$$\frac{\alpha_v}{\nu^2}=A+\frac{B}{\nu^2}, \tag{1}$$

where A and B are two constants depending on the properties of the liquid and the density fluctuations in it. Moreover, A is the sum of two terms of which the first represents the losses in a normal homogeneous liquid and the second is due to the presence of density fluctuations. Equation (1) shows that as consequence of the presence of clusters the parameter α_v/ν^2 is not only increased but it also becomes frequency dependent. It decreases with increasing frequency.

The second way in which the presence of clusters can produce ultrasonic absorption is through relaxation phenomena. The clusters of different composition and sizes are in fact in equilibrium among themselves and with the mother phase, and the sound waves can perturb these equilibria, giving rise to relaxation phenomena. Owing to the large variety of sizes and compositions of the clusters, a very broad distribution of relaxation times is to be expected. This means that the parameter α/ν^2 due to these relaxation phenomena will decrease with frequency in a very wide range.

It seems, therefore, difficult to separate the contribution of the two kinds of phenomena to the observed absorption. In order to make this distinction, it is necessary to have an evaluation of the constants A and B based on other information. Data on these calculations as well as the particulars of the related experiments will be reported later.

* Supported by the U. S. Office of Naval Research.
† From the Instituto di Ultracustica, Rome, Italy. At present at the Catholic University of America.
[1] F. H. Willis, J. Acoust. Soc. Am. **19**, 242 (1947); C. J. Burton, J. Acoust. Soc. Am. **20**, 186 (1948).
[2] D. Sette, J. Acoust. Soc. Am. **23**, 359 (1951).
[3] J. M. M. Pinkerton, *Colloquium Ultrasonore* (Trillingen-Brussel, 1951), p. 117.
[4] A. G. Chynoweth and W. G. Schneider, J. Chem. Phys. **19**, 1566 (1951); **20**, 1777 (1952).
[5] R. S. Krishman, Proc. Indian Acad. Sci. **1A**, 211, 915 (1935); **2A**, 221 (1935); **5A**, 577 (1937); **9A**, 303 (1939); C. Fuchtbauer, Z. Phys. Chem. **48**, 549 (1904).
[6] R. Lucas, J. phys. et radium **8**, 41 (1937).

The Ozone Band at 1110 cm^{-1}*

J. N. HOWARD AND J. H. SHAW
Department of Physics and Astronomy, Ohio State University, Columbus, Ohio
(Received December 31, 1952)

THERE has been considerable discussion[1–3] concerning the shape of the ozone molecule since sufficient data from the infrared absorption spectrum of ozone are not yet available to prove unambiguously whether the molecule is acute- or obtuse-angled. Electron diffraction[4] and microwave absorption studies[5] both indicate an obtuse-angled molecule.

Recently a weak band of ozone was discovered at 1110 cm^{-1}.[6] Badger and Wilson[7] have shown that neither this band nor any of the other known infrared bands can be a difference band, which strongly suggests that the 705, 1040, and 1110 cm^{-1} bands are the fundamentals. Such an assignment is consistent with an obtuse-angled molecule.

Further evidence that the 1110 cm^{-1} band is a fundamental may be inferred from work recently carried out at this laboratory.[8]

Measurements of the infrared solar spectrum have shown an improved resolution of the 1040 cm^{-1} atmospheric ozone band. In addition, a series of weak lines occur in the region near 1110 cm^{-1} which are probably due to ozone. Because of overlapping by absorptions of carbon dioxide, nitrous oxide, and water vapor, and the weakness of these lines, no conclusions can be drawn regarding their structure. However, investigations of the structure of the 1040 cm^{-1} band show that there is a very strong convergence of the lines on the high frequency side. So strong a convergence as observed here is unusual in infrared spectra, particularly in fundamental bands. When it occurs, it is usually due to a Coriolis resonance interaction of the fundamental frequency with another nearby fundamental frequency. The ozone bands at 1040 and 1110 cm^{-1} lie very close together and, on the assumption that the 1040 cm^{-1} band is ν_3 and the 1110 cm^{-1} band is ν_1, such an interaction between rotation and oscillation may be expected to occur. This effect has been discussed by Nielsen,[9] who has shown that when such an interaction occurs there is a strong convergence of the spacings between rotation lines of the two perturbing bands on the sides that are adjacent to each other. Since the convergence of the 1040 cm^{-1} band is on the high frequency side, the other fundamental frequency band involved in the perturbation should be at a somewhat higher frequency, for example, 1110 cm^{-1}, as is observed. Thus far, it has been impossible to obtain sufficiently good measurements on the 1110 cm^{-1} band to determine whether or not it shows a similar convergence.

* Supported in part by a contract between the Geophysics Research Division of the Air Force Cambridge Research Center and the Ohio State University Research Foundation.

[1] H. S. Gutowsky and E. M. Petersen, J. Chem. Phys. **18**, 564 (1950).
[2] M. K. Wilson and R. A. Ogg, J. Chem. Phys. **18**, 766 (1950).
[3] Klein, Cleveland, and Meister, J. Chem. Phys. **19**, 1068 (1951).
[4] W. Shand and R. A. Spurr, J. Am. Chem. Soc. **65**, 179 (1943).
[5] R. H. Hughes, Phys. Rev. **85**, 717 (1952).
[6] M. K. Wilson and R. M. Badger, J. Chem. Phys. **16**, 741 (1948).
[7] R. M. Badger and M. K. Wilson, J. Chem. Phys. **18**, 998 (1950).
[8] Shaw, Oxholm, and Claassen, Astrophys. J. (to be published).
[9] H. H. Nielsen, J. Chem. Phys. **5**, 818 (1937).

On the Application of the Cell Method to r-mer Liquids

I. PRIGOGINE, N. TRAPPENIERS,* AND V. MATHOT†
Faculty of Sciences, University of Brussels, Brussels, Belgium
(Received December 30, 1952)

THE cell theory of liquids, originated by Lennard-Jones and Devonshire,[1] applies to molecules with approximately spherical symmetry only. The authors have attempted to extend its use also to r-mer molecules, in order to secure a firm base for the study of r-mer solutions.

The r-mer is pictured as an assembly of r point centers, linked together by elastic valence forces. Each center "s" interacts with the centers "j" of neighboring molecules according to a $L-J$ potential law,

$$\varphi_{sj}=\varphi_0\left[\left(\frac{r_0}{r_{sj}}\right)^{12}-2\left(\frac{r_0}{r_{sj}}\right)^{6}\right]. \tag{1}$$

It is further assumed that the N molecules of the liquid can be arranged on a quasi-crystalline lattice so that the r point centers of each molecule occupy r neighboring sites. In general this will be true if r_0 is of the same order as the distance between two neighboring centers of the molecule.

In order to obtain the cell partition function of a molecule, each of the r point centers is located by its distance r_s from the corresponding lattice point. The molecular potential energy, for an arbitrary location of the r point centers, is written down by taking account of the two types of interactions which do occur.

1. It is assumed that the potential energy of each point center, resulting from interactions with neighboring molecules, can be smeared into a spherically symmetrical field $\omega^s(r_s)$, according to the well-known $L-J$ method. The $L-J$ mean field, however, is approximated by a much more simple harmonic field,

$$\omega(r_s)=\frac{\omega_{(0)}{}^s}{(a-\sigma)^2}r_s{}^2, \tag{2}$$

a being the distance between first neighbor sites, σ the distance for which in Eq. (1) $\varphi_{sj}=0$; $\omega_{(0)}{}^s$ is the equilibrium potential energy when the point center is on its lattice site.

2. The intramolecular forces, arising from the deformation of the molecule, also give rise to an harmonic potential: $\omega^i(r_1\cdots r_r)$.

Assuming that all displacements are small, the total molecular potential energy,

$$\sum_{s=1}^{r}\omega^s(r_s)+\omega^i(r_1\cdots r_r),$$

can be written as a quadratic form, which in turn is reduced to a sum of squares by an orthogonal transformation. The molecule may thus be represented by an assembly of $3r$ linear harmonic oscillators. Accordingly, the cell partition function ψ takes the form

$$\psi=\prod_{i}^{3r}\left(\frac{kT}{h\nu_i}\right), \tag{3}$$

ν_i being the frequency of the harmonic oscillator i.

In the case of the unbranched homogeneous open chain r-mer it was found that the translational and rotational degrees of freedom give rise to a sixfold degenerate frequency,

$$\nu=\frac{1}{2\pi}\left[\frac{2\omega_{(0)}{}^s}{m(a-\sigma)^2}\right]^{\frac{1}{2}}, \tag{4}$$

where m is the mass per center. The $(r-1)$ stretching and the $(r-2)$ bending modes, with spectroscopic frequencies $\nu_i{}^0$, are perturbed by the intermolecular forces, the resultant frequencies being of the form $\nu_i{}^{01}=(\nu_i{}^{02}+\nu^2)^{\frac{1}{2}}$. In as far as $\nu_i{}^0>200$ cm^{-1}, the perturbation is small and the $(2r-3)$ corresponding factors may be absorbed into the internal partition function $Z_0(T)$. To each of the $(r-3)$ twisting modes there also corresponds a frequency ν, at least if there is free rotation around the valence bond connecting two successive point centers.

The complete partition function for the r-mer liquid reads

$$Z^{1/N}=Z_0{}^{1/N}(T)g\left(\frac{kT}{h\nu}\right)^{r+2}\exp(-Nr\omega_{(0)}{}^s/kT),$$

with

$$\omega_{(0)}{}^s=\frac{\varphi_0}{2}\left[\left(\frac{v_0}{v}\right)^4\sum_k z_k\left(\frac{a}{r_k}\right)^{12}-2\left(\frac{v_0}{v}\right)\sum_k z_k\left(\frac{a}{r_k}\right)^6\right]q/r \tag{5}$$

g is the combinatory factor and ν is defined by Eq. (4). v defines the volume per point center, i.e., $v=V/rN$, V being the total volume. Also $v=\gamma a^3$ and the characteristic volume, $v_0=\gamma r_0{}^3$, γ being a geometrical factor. The number q is defined by $q=r-(2/z)(r-1)$, where z denotes the number of first neighbors. The Σ_k are the lattice sums. Equation (5) is valid for $r\geqslant 2$.

From Eq. (5) a reduced equation of state, expressing a principle of corresponding states for the r-mer liquid, is obtained,

$$\frac{P^xV^x}{T^x}=(1-V^{x-\frac{1}{3}}2^{-1/6})-6(V^{x-2}-1)(V^{x-2}-2)^{-1}+T^{x-1}(V^{x-4}-V^{x-2}), \tag{6}$$

where the reduced variables are defined by

$$T^x=\frac{kT(1+r/3)}{2zq\varphi_0};\quad V^x=\frac{V}{rNv_0};\quad P^x=P\frac{rv_0}{2zq\varphi_0}.$$

These relations may be useful for a comparative study of characteristic thermodynamic properties in an homologous series of r-mers, i.e., the hydrocarbon series. Future results will appear in *The Transactions of the Faraday Society*.

A direct comparison with the experiment is not possible as the parameters r_0 and φ_0 are not available for any r-mer. However, the mutual consistency of the equations has been tested by calculating, for a given r-mer, the parameter φ_0 in two different ways: firstly, by using density data and the equation of state (6); secondly,

TABLE I.

	r	φ_0 ergs 10^{-16} from (7)	from (5)	from 2° virial coef.
argon	1	130	···	165
methane	1	181	···	206
propane	2	225	···	···
pentane	3	200	166	···

from the heat of vaporization and the theoretical vapor pressure curve,

$$\lg P = \text{Cst.} - \frac{zq\varphi_0 4.25}{2kT}, \tag{7}$$

which is obtained by equating the chemical potential of the liquid to that of the perfect gas. Table I gives a few results for the series: methane, propane, pentane. Following Van der Waals[2] and Tompa,[3] these molecules were taken respectively as mono-, di-, and trimer, in order to obtain a regular lattice. Sufficient density data are not available for methane and propane; argon has also been included as an example of a monomer.

The agreement is satisfactory. The table also shows that each element of the r-mer is approximately equivalent to a methane group.

* Chargé de Recherches du Fonds National Belge de la Recherche Scientifique.
† Chercheur Qualifié du Fonds National Belge de la Recherche Scientifique.

[1] J. E. Lennard-Jones and A. F. Devonshire, Proc. Roy. Soc. (London) **A163**, 53 (1937); **A165**, 1 (1938).
[2] Van der Waals and Hermans, Rec. Trav. chim. Pays-Bas **68**, 181 (1949).
[3] Tompa, Trans. Faraday Soc. **45**, 107 (1949). The definition adopted here is intermediate between those proposed by these two authors.

On the Statistical Theory of r-mer Solutions

I. PRIGOGINE, V. MATHOT,* AND N. TRAPPENIERS†
Faculty of Sciences, University of Brussels, Brussels, Belgium
(Received December 30, 1952)

UP to the present, the theories of r-mer solutions have been concerned solely with the computation ot the combinatory factor. Making use of the results already obtained for the pure r-mer liquid, the authors have tried to put forward a more general treatment for r-mer solutions which, in addition to the well-known combinatory effects, will take account also of the changes in the partition functions of the components, as brought about by mixing.

For the sake of clarity the case of a monomer—r-mer mixture has been treated. "a" denotes the monomer point center while "b" denotes one of the r point centers which make up the r-mer molecule. Our basic assumption[1] is modified so that now both monomer and r-mer molecules can be arranged on a quasi-crystalline lattice. This will generally be true if the characteristic distances r_0 of the $L-J$ potential for the three types of interactions: $a-a$, $b-b$, and $a-b$ are the same and equal to the distance between two neighboring point centers of the r-mer molecule; however, no limitations are placed on the characteristic energies $\varphi_0{}^{aa}$, $\varphi_0{}^{bb}$ and $\varphi_0{}^{ab}$. Consider a mixture of N_a monomers and N_b r-mers, with $N=N_a+N_b$.

The partition function of the mixture is given by

$$\psi = g\psi_a{}^{N_a}\psi_b{}^{N_b}\exp[-1/kT(N_a\omega_{(0)}{}^a + rN_b\omega_{(0)}{}^b)], \tag{1}$$

where ψ_a and ψ_b denote the cell partition functions, g is the value of the combinatory factor which minimizes the free energy, $\omega_{(0)}{}^a$ and $\omega_{(0)}{}^b$ are the potential energies of centers "a" and "b" on their respective lattice sites.

Cell partition functions ψ_a and ψ_b, as given in reference (1), have to be modified in order to take account of the changes in the environment of each center, as produced by mixing. To that purpose only interactions between first neighbors are considered and the parameter N_{ab}, defining the total number of first-neighbor pairs, $a-b$ is introduced. The number of $a-b$ and $a-a$ pairs which originate from a given center "a" are then defined, respectively, by the relations $z^{ab}=N_ab/N_a$ and $z^{aa}=z-(N_ab/N_a)$, while $z^{ba}=N_ab/rN_b$ and $z^{bb}=qz/r-(N_ab/rN_b)$ give the number of $b-a$ and $b-b$ pairs, originating from a point center "b." It is thereby assumed that the end effects of the r-mer are evenly distributed over the whole molecule; $qz=rz-2r+2$ gives the total number of first-neighbor pairs to the r-mer molecule.

The partition function for the mixture now reads,

$$Z^{1/N} = Z_0{}^{1/N}(T)g\left(\frac{kT}{h\nu_a}\right)^{3x_a}\left(\frac{kT}{h\nu_b}\right)^{(r+3)x_b} \cdot\exp\left[-1/kT\left(\frac{\varphi_0{}^{aa}}{2}zx_a+\frac{\varphi_0{}^{bb}}{2}qzx_b+x_{ab}w\right)(\alpha^2-2\alpha)\right], \tag{2}$$

where the characteristic frequencies ν_a and ν_b are given by

$$\nu_a=\frac{1}{2\pi}\left[\frac{(\alpha^2-2\alpha)(z^{aa}\varphi_0{}^{aa}+z^{ab}\varphi_0{}^{ab})}{m_a(a-\sigma)^2}\right]^{\frac{1}{2}};$$
$$\nu_b=\frac{1}{2\pi}\left[\frac{(\alpha^2-2\alpha)(z^{bb}\varphi_0{}^{bb}+z^{ba}\varphi_0{}^{ab})}{m_b(a-\sigma)^2}\right]^{\frac{1}{2}}, \tag{3}$$

with $\alpha=(v_0/v)^2$. $x_a=N_a/N$; $x_b=N_b/N$; $x_{ab}=N_{ab}/N$, define the mole fractions ($N=N_a+N_b$); $w=\varphi_0{}^{ab}-(\varphi_0{}^{aa}+\varphi_0{}^{bb})/2$, denotes a "characteristic interchange energy." The meaning of the other symbols is the same as in reference (1).

x_{ab}, or rather its value which minimizes the free energy, and the corresponding combinatory factor g are computed, either by assuming random mixing (zeroth approximation), $x_{ab}{}^0=z(x_aqx_b/x_a+qx_b)$, or by Guggenheim's quasi-crystalline formula (first approximation); in the latter case $x_{ab}{}^1$ is conveniently written in the form of a series expansion:[2]

$$x_{ab}{}^1=x_{ab}{}^0+2\frac{x_a{}^2x_b{}^2}{(x_a+qx_b)^3}\frac{zw}{kT}(\alpha^2-2\alpha)+\cdots.$$

Thermodynamic excess properties are readily calculated from Eq. (2). The excess entropy of mixing is given by $S^e=S_{\text{I}}{}^e+S_{\text{II}}{}^e+S_{\text{III}}{}^e$, where $S_{\text{I}}{}^e$ denotes the combinatory excess entropy of the older theories and

$$\frac{S_{\text{II}}{}^e}{Nk}=3x_a\ln\frac{\alpha^{-1/6}-2^{-1/6}}{\alpha_a{}^{-1/6}-2^{-1/6}}+(3+r)x_b\ln\frac{\alpha^{-1/6}-2^{-1/6}}{\alpha_b{}^{-1/6}-2^{-1/6}}, \tag{4}$$

$$\frac{S_{\text{III}}{}^e}{Nk}=-\tfrac{3}{2}x_a\ln\frac{(z^{aa}\varphi_0{}^{aa}+z^{ab}\varphi_0{}^{ab})(2\alpha-\alpha^2)}{z\varphi_0{}^{aa}(2\alpha_a-\alpha_a{}^2)} -\frac{r+3}{2}x_b\ln\frac{(z^{bb}\varphi_0{}^{bb}+z^{ba}\varphi_0{}^{ab})(2\alpha-\alpha^2)}{z\varphi_0{}^{bb}(2\alpha_b-\alpha_b{}^2)} \tag{5}$$

define two new terms, related directly to the changes of the frequencies on mixing. The excess internal energy turns out to be

$$-\frac{E^e}{NkT}=-1/kT(\alpha^2-2\alpha)(x_az\varphi_0{}^{aa}/2+qx_bz\varphi_0{}^{bb}/2+x_{ab}w) +1/kT(\alpha_a{}^2-2\alpha_a)x_az\varphi_0{}^{aa}/2+1/kT(\alpha_b{}^2-2\alpha_b)qxbz\varphi_0{}^{bb}/2.$$

The excess volume of mixing is obtained by a series expansion of the equation of state,

$$\frac{v^e}{v_0}=R_1(T^*-x_aT_a{}^*-x_bT_b{}^*), \tag{6}$$

R_1 is a constant which depends on the expansion; the reduced temperatures are defined by

$$T^*=kT\frac{(1+r/3)}{4(x_az\varphi_0{}^{aa}/2+q^{xb}z\varphi_0{}^{bb}/2+x_{ab}w)};$$
$$T_a{}^*=\frac{kT}{2z\varphi_0{}^{aa}};\quad T_b{}^*=\frac{kT(1+r/3)}{2zq\varphi_0{}^{bb}}.$$

In order to assess the magnitude of these various effects numerical values have been calculated for an equimolal carbon-monoxide–propane mixture, maintained at 90.6°K, the triple point temperature of methane. Following reference (1) propane is

treated as a dimer composed of two methane groups; CO is a monomer. Interaction constants,[3] calculated from second-virial coefficient data, have been used. It was found that

$$\frac{v^e}{v_0}=-0.016;\quad \frac{S_I^e}{Nk}=0.051;\quad \frac{S_{II}^e}{Nk}=-0.041;$$

$$\frac{S_{III}^e}{Nk}=0.01;\quad \frac{E^e}{NkT}=0.04.$$

For this case there is, thus, contraction on mixing; the new entropy effects are roughly of the same order ot magnitude as the combinatory term but of opposite sign.

The present treatment extends to r-mer solutions which are the previous work by Prigogine and co-workers[4] for mixtures of spherical molecules. A full report on this and the work described in reference (1) will appear in the *Transactions of the Faraday Society*.

* Chercheur Qualifié du Fonds National Belge de la Recherche Scientifique.

† Chargé de Recherches du Fonds National Belge de la Recherche Scientifique.

[1] Prigogine, Trappeniers, and Mathot, J. Chem. Phys. **21**, 559 (1953).

[2] See E. A. Guggenheim, *Mixtures* (Clarendon Press, Oxford, 1952), pp. 196, 221.

[3] R. J. Lunbeck, Thesis, Amsterdam (1951).

[4] I. Prigogine and G. Garikian, Physica **16**, 239 (1950); I. Prigogine and V. Mathot, J. Chem. Phys. **20**, 49 (1952).

Application of the Cell Model to the Statistical Thermodynamics of Solutions. Volume Change of Mixing in Solutions of Molecules Slightly Different in Size

I. PRIGOGINE AND A. BELLEMANS
Faculty of Sciences, University of Brussels, Brussels, Belgium
(Received December 30, 1952)

IN preceding papers of this series,[1–6] the cell method of the liquid state has been applied to the statistical theory of solutions. Assumptions made were that (a) the molecules are spherical in shape and nonpolar, (b) their radii are equal, and (c) there is random mixing. This last condition has been recently discussed by Salsbury and Kirkwood[7] and by L. Saroléa,[5] and it has been shown that the order-disorder effects are generally small. We shall neglect them in this paper.

Condition (b), on the contrary, is much more restrictive. We shall limit our discussion to the volume change on mixing. In our preceding paper,[2] we found that the excess volume was given by (when limiting to terms of the second order)

$$v_e/(r^*)^3=1.64x_Ax_B[-2\theta+\delta^2+4\theta^2x_Ax_B+4\delta\theta x_B]kT/\Lambda_{AA}, \quad (1)$$

where r^* is the abscissa of the minimum of the potential energy curve between two molecules, and δ and θ are given by[2]

$$\delta=(\Lambda_{BB}-\Lambda_{AA})/\Lambda_{AA}=(\Lambda_{AB}-1/2\Lambda_{AA}-1/2\Lambda_{BB})/\Lambda_{AA}. \quad (2)$$

In the case of dispersion forces, to which we shall limit here, we have[2]

$$\theta=-\delta^2/8,\quad v_e/(r^*)^3=-1.23x_Ax_B\delta^2kT/\Lambda_{AA}. \quad (3)$$

So our preceding calculations predicted a volume contraction in this case. This has been verified for systems like cyclohexane-neopentane, benzene-neopentane, and carbon tetrachloride-neopentane.[3] However, most of the systems experimentally studied, with nonpolar forces, show an expansion on mixing. In these mixtures, condition (b) is not satisfied. The intermolecular energy between two molecules of kind i and j, at a distance a, is now of the form

$$\epsilon_{ij}=\epsilon_{ij}^*\left[\left(\frac{r_{ij}^*}{a}\right)^{12}-2\left(\frac{r_{ij}^*}{a}\right)^{6}\right], \quad (4)$$

with

$$r_{BB}^*\neq r_{AA}^* \quad \text{and} \quad 2r_{AB}^*=r_{AA}^*+r_{BB}^*. \quad (5)$$

To take account of this, we introduced two characteristic distances a_A and a_B, which are the mean distances of the first neighbors of a molecule A and a molecule B. The partition function of the solution can easily be written, assuming that there is random mixing, and the free energy of mixing is (for the smoothed potential model)[2]

$$\frac{F_m}{NkT}=x_A\log x_A+x_B\log x_B+x_A\frac{\omega_A(0)-\omega_{AA}(0)}{2kT}$$

$$+x_B\frac{\omega_B(0)-\omega_{BB}(0)}{2kT}-x_A\log(\psi_A/\psi_{AA})-x_B\log(\psi_B/\psi_{BB}), \quad (6)$$

where $\omega_A(0)$ and $\omega_B(0)$ are the potential energies of A and B at the center of their cells in the mixture, $\omega_{AA}(0)$ and $\omega_{BB}(0)$ the potential of A and B pure, ψ_A and ψ_B the free volumes of A and B in the mixture, and ψ_{AA} and ψ_{BB} the free volumes of A and B pure. We have (c and d being geometrical constants)

$$\omega_A(0)=z\epsilon_{AA}^*x_A\left[c\left(\frac{r_{AA}^*}{a_A}\right)^{12}-d\left(\frac{r_{AA}^*}{a_A}\right)^{6}\right]$$

$$+z\epsilon_{AB}^*x_B\left[c\left(\frac{r_{AB}^*}{a_A}\right)^{12}-d\left(\frac{r_{AB}^*}{a_A}\right)^{6}\right] \quad (7)$$

$$=\Lambda_{AA}x_A(c\alpha_A^2-d\alpha_A)+\Lambda_{AB}x_B(c\lambda^2\alpha_A^2-d\lambda\alpha_A), \quad (8)$$

with $\alpha_A=(r_{AA}^*/a_A)^6$ and $\lambda=(r_{AB}^*/r_{AA}^*)^6$;

$$\omega_B(0)=\Lambda_{BB}x_B(c\alpha_B^2-d\alpha_B)+\Lambda_{AB}x_A(c\mu^2\alpha_B^2-d\mu\alpha_B), \quad (9)$$

with $\alpha_B=(r_{BB}^*/a_B)^6$ and $\mu=(r_{AB}^*/r_{BB}^*)^6$;

$$\psi_A=\gamma(r_{AA}^*)^3\alpha_A^{-\frac{1}{2}}[1-(x_A+x_B\lambda^{1/6})(\alpha_A/2)^{1/6}]^3; \quad (10)$$

$$\psi_B=\gamma(r_{BB}^*)^3\alpha_B^{-\frac{1}{2}}[1-(x_B+x_A\mu^{1/6})(\alpha_B/2)^{1/6}]^3 \quad (11)$$

(γ is a geometrical constant). $\omega_{AA}(0)$, $\omega_{BB}(0)$, ψ_{AA}, and ψ_{BB} are the same as in reference 2. The volume of the mixture is

$$v=\gamma[x_A(r_{AA}^*)^3\alpha_A^{-\frac{1}{2}}+x_B(r_{BB}^*)^3\alpha_B^{-\frac{1}{2}}]. \quad (12)$$

The free energy and the volume depend on two variables α_A and α_B. One of them can be eliminated by minimizing the free energy with respect to it, at constant volume. But, for condensed systems, we can put $p=0$ in the equation of state and in this case, each type of cells A and B obey a particular equation of state given by the partial derivatives

$$\frac{\partial F}{\partial\alpha_A}=0,\quad \frac{\partial F}{\partial\alpha_B}=0. \quad (13)$$

The excess volume is now, for dispersion forces,

$$\frac{v_e}{\gamma(r_{AB}^*)^3\left(\frac{2c}{d}\right)^{\frac{1}{2}}}=x_Ax_B[(4.125\rho^2+0.75\rho\delta)$$

$$+2.22(-10.4\rho^2+0.227\rho\delta-0.50\delta^2)kT/\Lambda_{AA}], \quad (14)$$

with

$$\rho=(r_{BB}^*-r_{AA}^*)/r_{AA}^*.$$

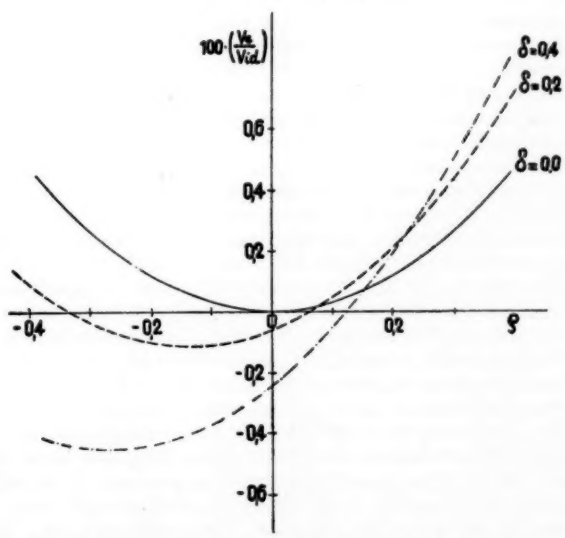

FIG. 1. Excess volume in function of ρ for various values of δ.

Relation (14) reduces nearly to (3) when $\rho=0$, but the present expression is more correct, even for $\rho=0$, because the artificial condition of equality of size of the cells A and B has been removed. (In deriving (14), we admitted that $\rho \leqslant 0.08$). Relation (14) has been plotted on Fig. 1, in function of ρ and for various values of $\delta(x_A=x_B=\frac{1}{2}$ and $kT/\Lambda_{AA}=0.0545)$. For $\rho/\delta>0$, there is a very narrow domain of contraction, soon replaced by an expansion. On the contrary, for $\rho/\delta<0$, there is a wide domain of contraction. It must be noticed that, even for nondispersion forces, the effect, due to the difference of size of the molecules, appears in terms of the second order (ρ^2 and $\rho\delta$). We give some comparison with experiment in Table I. The values of ρ and δ were roughly estimated from vapor pressure, heat of vaporization, densities and critical constants, and are very inaccurate. So, too much importance should not be accorded to the absolute value of v_e.

TABLE I. Parameters ρ and δ have been roughly estimated from vapor pressure, heat of vaporization, densities and critical constants, and are very inaccurate. So, too much importance should not be accorded to the absolute value of v_e.

	$100\, v_e/v_{\text{ideal}}$ for $x_A=0.5$ Calculated	Observed	Temperature
Neopentane—Carbon tetrachloride[a]	−0.20 to −0.35	−0.47	0°C
Neopentane—cyclohexane[a]	−0.15 to −0.25	−0.98(?)	0°C
Neopentane—benzene[a]	−0.10 to −0.25	−0.48	0°C
Carbon tetrachloride—benzene[b]	+0.10 to +0.20	+0.03	25°C
Cyclohexane—benzene[b]	+0.20 to +0.35	+0.65	30°C
Cyclohexane—carbon tetrachloride[b]	+0.05 to +0.15	+0.16	25°C

[a] See reference 3.
[b] Scatchard, Wood, and Mochel, J. Phys. Chem. **43**, 119 (1939); J. Am. Chem. Soc. **62**, 712 (1940).

mated from vapor pressure and densities. Quantitative agreement for mixtures containing benzene is bad, probably on account of noncentral forces.

Detailed calculations on this model will be published in the *Transactions of the Faraday Society.*

[1] I. Prigogine and G. Garikian, Physica **16**, 239 (1950).
[2] I. Prigogine and V. Mathot, J. Chem. Phys. **20**, 49 (1952).
[3] V. Mathot and A. Desmyter, J. Chem. Phys. (to be published).
[4] J. Nasielski, J. Chem. Phys. **21**, 184 (1953).
[5] I. Saroléa, J. Chem. Phys. **21**, 182 (1953).
[6] A. Bellemans, J. Chem. Phys. **21**, 369 (1953).
[7] Z. W. Salsburg and J. G. Kirkwood, J. Chem. Phys. **20**, 1538 (1952).

The Dielectric Constants of Water-Ethyl Acetate Mixtures*

A. P. ALTSHULLER†
Department of Chemistry, University of Cincinnati, Cincinnati, Ohio
(Received January 6, 1953)

IT is necessary that data on the dielectric constants of solvent nonelectrolyte (nonsolvent molecule) mixtures be available for the application of the various electrostatic[1,2] theories to the calculation of the activity coefficients of nonelectrolytes in electrolyte solutions. It is the purpose of the present investigation to provide such information for the system water-ethyl acetate in the temperature range from 20° to 40° at 5° intervals.

A resonance type dielectric constant apparatus was employed for the dielectric constant measurements. Resonance was detected with an oscilloscope by determining when zero phase angle occurred. The frequency employed was 4×10^4 cycles/second. The water used was distilled water which was passed through a cation-anion exchange column. The water obtained had a specific conductance of from 1.3 to 2.0×10^{-6} ohm^{-1} cm^{-1}.

It was decided that the dielectric constants of the mixtures could be most accurately calculated by use of Wyman's dielectric constants for water at various temperatures[3] as standards.

The ethyl-acetate water mixtures were measured at various concentrations up to saturation. The data were treated by the method of least squares and a linear relationship was found between the electrical capacity and the concentration of the ethyl acetate. The capacity of the saturated solution could then be found by use of the solubilities of ethyl acetate in water.[4] The dielectric constants could then be readily calculated. The probable error in the dielectric constants is estimated to be ±0.05 to 0.1 units.

TABLE I.

Temp. °C	D_s	D	$S\times10^9$	$S'\times10^9$	$R\times10^9$
20	75.2	5.1	2.59	2.95	2.42
25	73.5	5.0	2.71	3.09	2.45
30	71.8	4.9	2.83	3.23	2.48
35	70.3	4.7	2.92	3.32	2.50
40	68.8	4.4	2.94	3.33	2.51

The results of the measurements are presented in Table I where the quantity D_s is the dielectric constant of water saturated with ethyl acetate, and ΔD is the dielectric constant lowering resulting from saturation of the water with ethyl acetate. The quantities S and S' are equal to $\ln f/\Sigma c_i z_i^2 b_i^{-1}$ in the Debye-MacAulay equation[1,2] and the equation proposed by the author.[2] The quantity R appears in the Debye equation.[1,2]

Albright[5] found a ΔD of 5.2 units at 25° which agrees fairly well with the 5.0 units reported in the present investigation. De Voto[6] found a molar dielectric constant depression dD/dc of 5 units at 25° for methyl acetate compared with a $dD/dc=5.5$ units for ethyl acetate.

Since the quantities S, S' and R contain all of the temperature dependent variables, D, ΔD, and T, it is seen that at least for the ethyl acetate-water-electrolyte system the theoretically calculated activity coefficients increase with increasing temperature, or more precisely $d\ln f/dT=+$quantity. A more detailed application of these results will be published elsewhere.

The author wishes to offer his appreciation to Dr. H. E. Everson for his interest, encouragement, and advice and to Dr. P. Berghausen for his valuable assistance in modifying the dielectric constant apparatus employed.

* This research was supported in part by a grant from the American Academy of Arts and Sciences.
† Present address: National Advisory Committee for Aeronautics, Lewis Flight Propulsion Laboratory, Cleveland, Ohio.
[1] F. A. Long and W. F. McDevit, Chem. Revs. **51**, 119 (1952).
[2] A. P. Altshuller and H. E. Everson, J. Phys. Colloid Chem. **55**, 1368 (1951).
[3] J. Wyman, Phys. Rev. **35**, 623 (1931).
[4] A. P. Altshuller and H. E. Everson, J. Am. Chem. Soc. **75** (to be published).
[5] P. S. Albright and J. W. Williams, Trans. Faraday Soc. **33**, 247 (1937).
[6] G. De Voto, Chem. Ber. **67**, 1985 (1934).

On the Miescher-Baer Emission Bands in the Far Ultraviolet Region*

YOSHIO TANAKA†
Department of Physics, University of Chicago, Chicago 37, Illinois
(Received December 23, 1952)

WHILE studying a high current discharge (of He+enriched $N^{15}O$ or ordinary NO), Miescher and Baer[1] found a new system of bands in the region from 1368 to 1680A. These bands are single headed and degraded toward the red. The vibrational frequency of the lower state is close to the frequency of the $X^1\Sigma_g^+$ state of the N_2 molecule as well as to that of the $A^2\Sigma^+$ state of the NO molecule. They did not find any alternation of intensity in the rotational structure, nor did they observe the heads of N_2^{15} isotope bands. Hence, they were unable to decide whether this system arose from the N_2 or the NO molecule.

With a view to determine experimentally the origin of these bands, we tried a high current discharge of NO, (He+NO), N_2 and (He+N_2), each with and without a condenser. The 84-cm normal incidence vacuum spectrograph was used.

We could not observe the bands in the condensed discharge of any of the above-mentioned gases, nor in the uncondensed discharges of N_2 and (He+N_2). We can, however, observe them in the uncondensed discharge of either pure NO or, much stronger, in the case of (He+NO). The results of the measurements are shown in Table I together with those of Miescher and Baer. In the

TABLE I.

v',	v''	ν obs. (cm^{-1}) present	I	ν (cm^{-1}) Miescher and Baer
0,	6	59513.9	1	59517
0,	5	61702.5	2	61704
0,	4	63908.8	4	63910
0,	3	66149.4	6	66161
0,	2	68431.3	6	68437
1,	2	69988.3	5	69999
0,	2	70745.4	5	70751
1,	1	72307.6	6	72310
6,	4	72585.8	1	
0,	0	73083.9	3	73087
2,	1	73819.8	3	
7,	4	73874.9	1	
1,	0	74642.5	5	
2,	0	76158.0	5	
6,	2	77121.8	1	
3,	0	77636.1	6	
5,	1	78134.2	1	
7, 9,	2 3	78361.9	4	$\omega_e' = 1599.6$ cm^{-1}
4,	0	79072.0	6	
6,	1	79455.9	4	$\omega_e'\chi_e' = 20.6$ cm^{-1}
5,	0?	80488.1	1	
9,	2	80645.2	2	$\omega_e'' = 2366.5$ cm^{-1}
7,	1	80690.1	1	
6,	0	81768.8	3	$\omega_e''\chi_e'' = 14.6$ cm^{-1}
8,	1	81887.3	0	
7,	0	83042.0	2	
8,	0	84209.8	2	
9,	0	85284.9	1	
10,	0	86214.3	1	

present work, the system has been greatly extended towards shorter wavelengths, down to about 1200A. Some of the bands come close to and are confused with the Lyman-Birge-Hopfield bands of N_2, which appear quite strong in the region below 1500A. We can, nevertheless, discriminate between them by comparison with the picture of the pure N_2 spectrum because, as observed by Miescher and Baer, this new system has no intensity alternation in the rotational structure.

It seems probable that this system is due to NO or NO^+ rather than N_2. The reasons for this conclusion are the following. First of all, no intensity alternation is observed. Secondly, as pointed out by Miescher and Baer, there are no corresponding isotope bands of N_2^{15} observed. This new system appears only in the silent discharge of (He+NO) or NO and are not observed in the N_2 or (He+N_2) spectra. If we assume that the lower state of this system is $A^2\Sigma^+$ of NO, then the upper state is about 14.54 ev above the $v=0$ level of the ground state ($X^2\Pi$) of NO. Tanaka[2] has found several progressions of absorption bands in this region but none fit with the upper state of the present bands.

There is the possibility that this system is due to the NO^+ ion. As Mulliken[3] has pointed out, the ground state of NO^+ is $^1\Sigma^+$, having the electron configuration $(kk)\sigma^2\sigma^2\pi^4\sigma^2$, and both the dissociation energy and the vibration frequency of this state will be larger than that of the ground state of NO because the outermost antibonding electron $v\pi$ of the NO is missing in NO^+. We may then also expect a $^1\Pi$ excited state in NO^+ analogous to the upper state of the L−B−H bands of N_2 which falls at about 8.55 ev from the ground state ($^1\Sigma_g^+$). The (0,0) band of the new system is 9.06 ev, and both the ω_e' and ω_e'' values of this system agree closely with those of the $^1\Pi_g - {}^1\Sigma_g^+$ system of N_2. Therefore, it seems quite probable that this system is due to transitions from the upper $^1\Pi$ state to the ground $^1\Sigma^+$ state of NO^+. Experimentally, this system appears far stronger in the case of (He+NO) compared with pure NO. This also seems to support the idea suggested above.

In conclusion the author wishes to express his sincere gratitude to Professor R. S. Mulliken and Professor J. R. Platt for their cooperation in this work, and to Mr. Schagrin for his assistance in the laboratory.

* This work was assisted by the U. S. Office of Naval Research under Task Order IX of Contract N6ori-20 with The University of Chicago.

† Present address Geophysics Research Division, Air Force Cambridge Research Center, 230 Albany Street, Cambridge 39, Massachusetts.

[1] R. Miescher and P. Baer, Nature **169**, 581 (1952).
[2] Y. Tanaka, Sci. Pap. I.P.C.R. (Tokyo) **39**, 456 (1942).
[3] R. S. Mulliken, Revs. Modern Phys. **4**, 73 (1932).

The Microwave Spectrum and General Properties of Ethylene Imine*

W. S. WILCOX, K. C. BRANNOCK, W. DEMORE, AND J. H. GOLDSTEIN
Department of Chemistry, Emory University, Emory University, Georgia
(Received December 23, 1952)

THE chemistry of ethylene imine, the simplest heterocyclic compound containing nitrogen, is quite unlike that of pyrrole, whose behavior is aromatic in character.[1] The reactions of ethylene imine which do not involve opening the ring are chiefly those of a secondary amine. Pyrrole, on the other hand, gives many reactions analogous to those of the phenols. The hydrogen attached to the nitrogen of pyrrole is distinctly acidic. Part of the interest in ethylene imine has been based upon a number of attempts to resolve certain of its derivatives into optically active enantiamorphs with the optical asymmetry residing in the nitrogen atom. No such attempt has been successful.

The microwave spectrum of ethylene imine has been investigated in a Stark effect spectrograph. A preliminary study of this spectrum yields some information of interest about the molecule and the configuration of its nitrogen bonds and affords some comparisons with results obtained from a study of the pyrrole spectrum.[2]

In Table I are given the frequencies and the observed and theoretical relative intensities of the ethylene imine lines. The error in measurement of the relative intensities of a pair of lines ranges from about 10 percent for lines fairly near each other to perhaps 20 percent for lines separated by several thousand Mc.

TABLE I. Ethylene imine spectrum.

Line	Frequency Mc/sec	Obs. rel. intensity	Calc. rel. intensity No spin factor	Calc. rel. intensity With spin factor
$0_{00}\rightarrow 1_{11}$	36 130.92 ±0.2	1.00	1.00	1.00
$3_{22}\rightarrow 3_{30}$	35 334.4 ±0.5	0.52	[a]	[b]
$3_{22}\rightarrow 3_{21}$	30 494.62 ±0.1	1.26	1.36	1.36
$2_{12}\rightarrow 2_{21}$	28 058.34 ±0.1	0.93	0.83	0.50
$2_{02}\rightarrow 2_{11}$	23 634.41 ±0.1	0.93	1.14	1.14
$3_{12}\rightarrow 3_{21}$	22 262.34 ±0.1	1.82	2.11	1.27

[a] Depends upon magnitude of component of dipole moment in "c" inertial axis as compared to component in "b" axis.
[b] Not allowed for coplanar model.

As in the case of pyrrole, if the three nitrogen bonds of ethylene imine were coplanar, the molecule would possess a twofold axis of symmetry passing through the nitrogen atom. Two pairs of protons would be exchanged on rotation through 180 degrees about this axis, and nuclear spin statistical weight factors of 10 for levels symmetric in the nuclei and 6 for antisymmetric levels would have to be included in the computation of the relative intensities of the rotational absorption lines.[3] Inspection of Table I shows that the observed relative intensities are in much better agreement with the noncoplanar model, and that one line appears which would not be allowed for the coplanar model. The $3_{22}\rightarrow 3_{30}$ transition is allowed because of the presence of a component of the dipole moment parallel to the axis of greatest moment of inertia, which is nearly perpendicular to the plane of the ring. This component of the dipole moment vanishes for the coplanar model. Thus it may be concluded that the N−H bond of ethylene imine, unlike that of pyrrole, does not lie in the plane of the ring.

The lines listed in Table I were identified by observation of their characteristic Stark effect patterns and by calculation of the frequencies. The $J=0\rightarrow 1$ line was found to increase in intensity by

TABLE II. Ethylene imine rotational constants.

a	22 741.8$_5$ Mc/sec
b	21 198.2$_0$
c	13 389.0$_7$
κ	0.6699

a factor of 4 on cooling the wave guide to the temperature of dry ice. The theoretical intensity ratio is about 3.6 to 1.

Table II gives the rotational constants calculated from the two $J=2$ lines and the $0\rightarrow1$ line. These constants fit the remaining frequencies with a mean error of about 0.7 Mc.

Quantitative Stark effect measurements and observations of the quadrupolar hyperfine structure of some of the lines have been made. These data are being analyzed, and a full report will be made at an early date.

* This work was supported by the U. S. Office of Ordnance Research.

[1] See, for example, R. C. Elderfield, *Heterocyclic Compounds* (John Wiley and Sons, Inc., New York, 1950), Vol. I, Chapters II and VI.
[2] W. S. Wilcox and J. H. Goldstein, J. Chem. Phys. **20**, 1656 (1952).
[3] G. Herzberg, *Infra-Red and Raman Spectra* (D. Van Nostrand Company, Inc., New York, 1945), p. 53.

Applications of Large Digital Computers to Calculations of Microwave Spectroscopy

B. L. Hicks, T. E. Turner, and W. W. Widule
Ballistic Research Laboratories, Aberdeen Proving Ground, Maryland
(Received December 23, 1952)

We wish to report the progress that has been made using the EDVAC and the ORDVAC at the Ballistic Research Laboratories for the computation of two problems of interest in microwave spectroscopy. The first of these problems is the improvement of existing asymmetric rotor energy level tables[1,2] by increasing the accuracy of the computed eigenvalues, determining eigenvalues for smaller intervals of κ, and extending the table to higher values of J. The second problem is the determination of the rotational constants of an asymmetric top molecule from its structural parameters.

The rigid asymmetric rotor eigenvalues were calculated on the EDVAC for $J=0$ (1) 12 and for $\kappa=0.00$ (0.01) 1.00 and are accurate to seven decimals up to $J=5$ and to six decimals thereafter, although in effect several more decimals than this were carried. Mr. George Reitwiesner of the Ballistic Research Laboratories' Computing Laboratory coded the calculation of the four energy submatrices[1] and their eigenvalues on the EDVAC, using Jacobi's diagonalization method.[3] This computation required sixty hours of machine time, and we plan to repeat the whole computation for checking purposes. We are now making small changes in the coding so that the transformation matrices, which diagonalize the energy submatrices, will be printed out for $J=0$ (1) 12 and for $\kappa=0.0$ (0.1) 1.0. These transformation matrices will be useful in calculations of transition probabilities.

We do not plan to publish the data for $J\leqq12$ nor to extend the calculation of eigenvalues above $J=12$ until several matters have been considered, namely: (1) checking, form and size of table to be presented; (2) accuracy of various interpolation and asymptotic techniques that have been devised;[4,5] (3) incidence of centrifugal distortion, which causes the eigenvalues of the rigid rotor to be only an approximation, though a very useful one; (4) number of transformation matrices needed; (5) usefulness of calculating directly the rotational terms of a nonrigid rotor[6] by the numerical diagonalization process.

The calculation of the rotational constants a, b, c, and the derived constants $(a\pm c)/2$ and κ was coded for 1200 models of the ethylenimine molecule. This first calculation was set up as a "practice" problem in coding for the ORDVAC and required about six hours including printing time. We have now generalized this code so that the same set of six constants can be calculated for any set of models of any molecule and of its various isotopic species. Features of this general coding are: (1) all the values of the parameters to be used in a calculation of a set of models are first stored in the ORDVAC memory; (2) a set of indices on an input tape defines each model desired; (3) calculations for one model are completed and printed out before going on to the next model defined by the next set of indices; (4) the greater part of the coding remains the same no matter what molecule it is whose rotational constants are being computed, for the only changes necessary in going from one molecule to another are in the calculation of the coordinates of each atom from the structural parameters. This code has been used to calculate 224 more models of ethylenimine including each of the isotopic species containing one heavy atom.[7] With appropriate changes in masses and structural parameters, the rotational constants for ethylene oxide and sulfide, for example, could be calculated without altering the code at all.

We should like to express our appreciation for several helpful discussions with Professor E. Bright Wilson, Dr. Gilbert W. King, and Professor C. H. Townes.

[1] King, Hainer, and Cross, J. Chem. Phys. **11**, 27 (1943).
[2] E. E. Witmer, "Tabulation of a Function for Calculating the Rotational Energy Levels of a Rigid Polyatomic Molecule," University of Pennsylvania (1950).
[3] Suggested for application to large computers by H. H. Goldstine, The Institute for Advanced Study, Princeton, New Jersey.
[4] Hainer, Cross, and King, J. Chem. Phys. **17**, 826 (1949).
[5] S. Golden, J. Chem. Phys. **16**, 78 (1948).
[6] D. Kwelson and E. Bright Wilson, Jr., J. Chem. Phys. **20**, 1575 (1952).
[7] Turner, Fiora, Kendrick, and Hicks, J. Chem. Phys. **21**, 564 (1953).

Preliminary Analysis of the Microwave Spectrum of Ethylenimine

T. E. Turner, Verna C. Fiora, W. M. Kendrick, and B. L. Hicks
Ballistic Research Laboratories, Aberdeen Proving Ground, Maryland
(Received December 23, 1952)

The pure rotational spectrum of C_2H_4NH has been observed and analyzed in the microwave region (see Table I). Seven assigned Q branch transitions in the 35 000 mc/s region and several observed unassigned transitions are not listed. The spectrum was examined using a Stark effect modulation spectrometer with an oscillographic display. Stark effect identification aided in making the assignments even though the Stark patterns were not completely resolved for the high J transitions. Theoretical relative intensities were in agreement with the observed values. Hyperfine splitting (≈1 mc/s) which decreased rapidly with increasing J was observed for the low J transitions. These patterns were comparable with those to be expected from nuclear quadrupole interaction.

By making the best fit to the observed spectrum with greater weight being given to the low J transitions, it was determined that

Table I. Assignments in the spectrum of ethylenimine.

Transition	Observed	Theoretical	Observed rel. int.
$2_{0,2}\rightarrow2_{1,1}$	23 634.5 ±0.5 mc/s	23 633.6 mc/s	w.
	23 632.9		
$3_{1,2}\rightarrow3_{2,1}$	22 262.1	22 262.2	m.
	22 261.2		
$4_{2,2}\rightarrow4_{3,1}$	21 360.5	21 361.3	s.
$5_{3,2}\rightarrow5_{4,1}$	21 473.9	21 475.7	s.
$5_{4,1}\rightarrow5_{5,0}$	24 682.4	24 681.7	m.
$6_{4,2}\rightarrow6_{5,1}$	23 025.5	23 028.4	v.s.
$7_{5,2}\rightarrow7_{6,1}$	26 329.2	26 320.2	v.s.
$5_{4,1}\rightarrow5_{5,1}$	22 671.9	22 670.5	v.w.
$8_{6,2}\rightarrow8_{7,2}$	25 732.7	25 743.6	w.
$0_{00}\rightarrow1_{1,1}$	36 130±30		m.

$a-c=9352\pm1$ mc/s and $\kappa=+0.6700\pm0.0002$. The theoretical spectrum (see Table I) uncorrected for centrifugal distortion or hyperfine splitting was calculated using these rotational parameters. The transition $0_{0,0}\rightarrow1_{1,1}$, having a frequency equal to $a+c$, was measured at 36 130±30 mc/s. This transition was identified by its Stark pattern, relative intensity, and by its occurrence in a region predicted from the calculation of several molecular models.[1] From these data the effective moments of inertia for the most abundant isotopic species were determined as

$$I_a=(36.89\pm0.03)\times10^{-40}\text{ g cm}^2,$$
$$I_b=(39.57\pm0.03)\times10^{-40}\text{ g cm}^2,$$
$$I_c=(62.65\pm0.07)\times10^{-40}\text{ g cm}^2.$$

Two very weak transitions, $5_{4,1}\rightarrow 5_{5,1}$ and $8_{6,2}\rightarrow 8_{7,2}$ which are allowed by *c* axis transition rules, were observed whereas all the other assigned transitions are allowed by *b* axis transition rules. This indicates that the electric dipole moment has a component along the *c* axis as well as one along the *b* axis and thus supports the evidence that the imine H does not lie in the plane of the C_2N triangle.

Tentative structural data are given in Table II. The C−C, C−N distances and the C_2NH angle were fitted to the measured moments of inertia with the help of the ORDVAC calculations.[1]

TABLE II. Determined and assumed structural data for ethylenimine.

C−C distance	1.480A	determined
C−N distance	1.488A	determined
C_2NH angle	112°	determined
C−H distance	1.082A	assumed
HCH angle	116° 41′	assumed
H_2CC angle	159° 25′	assumed
H−H distance	1.00A	assumed

The HCH, H_2CC angles, and the C−H distance were assumed to be equal to those of ethylene oxide[2] and the N−H distance was taken as the sum of the Pauling radii. The three structural parameters determined in this manner are, of course, subject to change depending on the validity of the assumptions made. We plan to make a more definite structure determination from a study of deuterated and other isotopic species.

The eigenvalues used in the initial stages of this analysis were obtained by making Gregory Newton interpolations in the King, Hainer, and Cross table.[3] It was found that the eigenvalues obtained in this manner were not accurate enough for most of the transitions involved. The final analysis was made using the asymmetric rotor eigenvalue table recently computed by the EDVAC.[1]

[1] Hicks, Turner, and Widule, J. Chem. Phys. **21**, 564 (1953).
[2] Cunningham, Boyd, Meyers, Gwinn, and LeVan, J. Chem. Phys. **19**, 676 (1951).
[3] King, Hainer, and Cross, J. Chem. Phys. **11**, 27 (1943).

The Molecular Structure of Carbon Tetrafluoride*

C. W. W. HOFFMAN AND R. L. LIVINGSTON
Department of Chemistry, Purdue University, West Lafayette, Indiana
(Received January 1, 1953)

THE length of the C−F bond in CF_4 reported in the literature[1] is 1.36±0.02A; this is based on electron diffraction investigations which were carried out prior to 1936. A comparison of this result with more recent data on other fluoromethanes suggested that this distance might be in error.

In CH_3F, the C−F distance has been given as 1.39A by electron diffraction[2] and 1.385A by microwave and infrared spectroscopy.[3] In CH_2F_2, this distance is very nearly 1.36A; three electron diffraction investigations[4] and one microwave study[5] have given this value although interpretation of the infrared spectrum[6] of this compound gave C−F=1.32A. Spectroscopic results[7] on CHF_3 give C−F=1.335A if the ∠FCF is assumed to be 108°; two electron diffraction investigations[8] gave C−F=1.34 and 1.35A. It is thus reasonably definite that the C−F distance decreases as one replaces H atoms by F in the series CH_3F, CH_2F_2, CHF_3 and the value of 1.36A in CF_4 seems anomalous. This suggested the reinvestigation of the interatomic distances in CF_4 which is the subject of this letter.

Electron diffraction photographs of CF_4 were prepared using a sample which was provided by Dr. W. H. Pearlson of the Minnesota Mining and Manufacturing Company; infrared analysis of the sample indicated a purity of at least 99 percent. A camera distance of 107.61 mm was used and the electron wavelength, which varied slightly from one photograph to another, was always near 0.0594A. The photographs were measured visually, and the resulting s_0 values for the maxima and minima are given in Table I.

The observed *s* values (s_0) are compared in Table I with those obtained from a curve calculated from a rigid tetrahedral model of CF_4 in which the C−F distance was set at 1.32A. In computing the average of the s_{calc}/s_{obs} ratios, the ratios for the first few peaks have been omitted (since visual measurements of these are usually not reliable), and the ratio for the fourth maximum is not included since the observers felt that measurements on this peak were not

TABLE I. Quantitative electron diffraction data for carbon tetrafluoride.

Max	Min	s_0	s_{calc}/s_0
1		(3.81)	
	2	(5.17)	
2		(6.56)	
	3	8.15	0.988
3		9.60	1.006
	4	10.98	0.999
4		(12.44)	
	5	13.86	0.987
5		15.34	0.997
	6	16.89	1.002
6		18.36	0.996
	7	19.57	0.994
7		20.98	0.997
	8	22.49	1.002
8		24.09	1.003
	9	25.51	1.004
9		26.88	0.996
	10	28.29	0.995
10		29.70	1.003
			Ave 0.998
			Mean deviation 0.004

reliable. The C−F distance in CF_4, as determined by this investigation, is then $1.32\times 0.998=1.31_7$A. This is appreciably shorter than the value of 1.36A previously reported for CF_4 and falls in line with the distances in the other fluoromethanes. It should be remarked that this distance does not depend upon the assumption of a rigid model; the same result is obtained from models which allow the fluorine atoms large amplitudes of vibration.

The authors wish to thank Professor H. J. Yearian of the Purdue Physics Department for the use of his diffraction apparatus and Dr. W. H. Pearlson for providing the sample of CF_4.

* From the M.S. thesis of C. W. W. Hoffman, Department of Chemistry, Purdue University.
[1] L. O. Brockway, Revs. Modern Phys. **8**, 231 (1936).
[2] V. Schomaker and D. P. Stevenson, J. Am. Chem. Soc. **63**, 37 (1941).
[3] Gilliam, Edwards, and Gordy, Phys. Rev. **75**, 1014 (1949).
[4] L. O. Brockway, J. Chem. Phys. **41**, 185 (1937); Walter C. Hamilton and Kenneth Hedberg, J. Am. Chem. Soc. **74**, 5529 (1952); R. L. Livingston and C. R. Rice, unpublished.
[5] David R. Lide, Jr., J. Am. Chem. Soc. **74**, 3548 (1952).
[6] H. B. Stewart and H. H. Nielsen, Phys. Rev. **75**, 640 (1949).
[7] H. J. Bernstein and G. Herzberg, J. Chem. Phys. **16**, 30 (1948) (infrared), and reference (3) (microwave).
[8] See tabulation by P. W. Allen and L. S. Sutton, Acta Cryst. **3**, 46 (1950).

Investigation of Proton Magnetic Resonance Line Width of Sorbed Water

T. M. SHAW AND R. H. ELSKEN
Western Regional Research Laboratory, Albany, California*
(Received January 6, 1953)

MEASUREMENTS of the proton magnetic resonance absorption for hygroscopic substances have been reported.[1] The resonance was shown to consist of a narrow line attributed to protons in the sorbed water superimposed on a broad line (~25–40 kc wide) due to protons in the solid absorbent. A small increase in the width of the narrow line was observed when the water content was reduced to approximately 10 percent, but the change was largely obscured by effects on the line width of inhomogeneities in the field of the permanent magnet. Substitution of a larger permanent magnet for the one used previously has resulted in a substantial improvement in the uniformity of the applied magnetic

field, and an investigation has been made of the dependence of the line width on the water content.

The proton resonance was recorded by means of a radio-frequency (rf) spectrometer.[2] A magnetic field of 6380 gauss was provided by a permanent magnet with 6-inch diameter poles and 1¾-inch gap. Samples were contained in 1 cm o.d. Pyrex tubes. The rf probe containing the sample was designed to be immersed in a constant-temperature bath between the poles of the magnet. The rf magnetic field was held at a level of approximately 0.01 gauss to minimize saturation effects. The portion of the magnetic field occupied by the sample was found to be uniform to within 0.05 gauss. The modulation was set by trial at a value less than the width of the narrow line in order to reduce modulation broadening to a negligible amount.

Line width measurements for starch and egg albumin at 27°C are summarized in Tables I and II. In these measurements the water content n was varied over a range from about 6 to 17 g water per 100 g dry solids. Interpretation of water sorption isotherms for these materials in terms of the Brunauer, Emmett, and Teller theory[3-5] shows the moisture range investigated here does not include the range of n from zero to n_1 where water is presumed to be sorbed onto primary absorption sites in the solid. At the highest water contents investigated the line width $\delta\nu$ is still several times larger than the minimum value set by magnet inhomogeneities. As n is decreased $\delta\nu$ increases; the rate of increase with decreasing n becoming very large as n approaches the value n_1.

TABLE I. Summary of line width measurements for starch.

Water content, n (g water/100 g dry solid)	Line width,[a] $\delta\nu$ (kc)
6.3	2.3
8.2	1.3
10.2	1.0
13.2	0.60
15.7	0.45

[a] A correction of 0.10 kc has been subtracted from the observed values to allow for magnet inhomogeneities.

TABLE II. Summary of line width measurements for egg albumin.

Water content, n (g water/100 g dry solid)	Line width, $\delta\nu$[a] (kc)	E_{vap} (kcal/M)	τ_c sec	$(\delta\nu/\tau_c)$ sec^{-2}
7.1	1.7	11.08	1.86×10^{-5}	0.92×10^{8}
7.8	1.7	10.98	1.58×10^{-5}	1.08×10^{8}
9.8	1.1	10.72	1.02×10^{-5}	1.08×10^{8}
10.7	1.05	10.64	0.896×10^{-5}	1.17×10^{8}
12.3	0.80	10.51	0.724×10^{-5}	1.10×10^{8}
14.2	0.65	10.42	0.610×10^{-5}	1.07×10^{8}
14.4	0.52	10.40	0.600×10^{-5}	0.87×10^{8}
15.8	0.55	10.36	0.563×10^{-5}	0.98×10^{8}
16.8	0.50	10.33	0.534×10^{-5}	0.94×10^{8}
			Mean	$=1.03\pm0.10\times10^{8}$

[a] A correction of 0.10 kc has been subtracted from the observed values to allow for magnet inhomogeneities.

The theory of Bloembergen, Purcell, and Pound[6] shows that $\delta\nu$ may be expressed in terms of the correlation time τ_c defined as the time during which the molecular arrangement about a given nucleus persists.

The experimental results for water sorbed by egg albumin can be represented by the equations

$$\delta\nu = C\tau_c \tag{1}$$

and

$$\tfrac{3}{2}\tau_c = \tfrac{3}{2}\tau_0 \exp(E_{vap}/RT) = (h/kT)\exp(E_{vap}/RT). \tag{2}$$

Here C is a constant, E_{vap} is the energy of vaporization of the sorbed water, and τ_c is assumed to be the average time during which a sorbed water molecule remains in the same equilibrium position. It is apparent that Eq. (2) assumes a process of evaporation and condensation to account for the apparent motion of the sorbed water. At 27°C the time $\tau_0 = h/kT$ is about 10^{-13} second.

As shown in Table II, comparison of τ_c calculated from experimental values of E_{vap}, according to Eq. (2), with the experimental values of $\delta\nu$ shows that over the range of water content investigated here C in Eq. (1) is a constant equal to $1.03\pm0.10\times10^{8}$ sec^{-2}. The constancy of C probably results from the small range of variation of $\delta\nu$. The magnitude of C found for egg albumin agrees with an estimate of $\sim5\times10^{8}$ based on the ratio of the theoretical values of $\delta\nu$ and τ_c for water at the mid-point of the relation connecting line width and correlation time.

The applicability of Eqs. (1) and (2) to the experimental results for starch has not been tested because sorption data suitable for the calculation of E_{vap} are not available. However, a preliminary investigation of the variation of $\delta\nu$ with water content for textile fibers has yielded values for C which agree with the value found for egg albumin to within 10 percent. This agreement is considered to be within the limits of error for $\delta\nu$ and E_{vap}.

* Bureau of Agricultural and Industrial Chemistry, Agricultural Research Administration, U. S. Department of Agriculture.

[1] T. M. Shaw and R. H. Elsken, J. Chem. Phys. **18**, 1113 (1950); T. M. Shaw and K. J. Palmer, Phys. Rev. **83**, 213 (1951).
[2] R. V. Pound and W. D. Knight, Rev. Sci. Instr. **21**, 219 (1950).
[3] Brunauer, Emmett, and Teller, J. Am. Chem. Soc. **60**, 309 (1938).
[4] T. M. Shaw, J. Chem. Phys. **12**, 391 (1944).
[5] A. D. McLaren and J. W. Rowen, J. Polymer Sci. **7**, 299 (1951).
[6] Bloembergen, Purcell, and Pound, Phys. Rev. **73**, 679 (1948).

Ionic Hydration and Stokes' Law

ARTHUR L. LEVY
Department of Chemistry, Rensselaer Polytechnic Institute, Troy, New York
(Received January 5, 1953)

HOW to calculate theoretically the number of water molecules surrounding an ion is a difficult problem, and the attempts already made show a wide range of disagreement for the various ions. There are two recent papers by H. Mukherjee[1] which are of interest, since they calculate hydration numbers close to those obtained experimentally by transference methods and also because they use kinetic theory and a modified Stokes' law for the velocity of a particle moving in a viscous medium.

Mukherjee points out that Stokes' law must be modified to take into account the fact that the solvent cannot be continuous with respect to the ions in solution, since the intermolecular separation in the solvent is not negligibly small compared to the size of the ions. Using Millikan's modification of the Stokes' formula, he arrives at an expression for ionic mobility, involving two terms whose values are not known directly; the mean intermolecular separation of the solvent and the radius of the particle.

The first term is calculated by using the known mobility of the hydrogen ion, which is assumed to be hydrated by one water molecule, and taking the radius of this hydrated ion to be essentially that of the water molecule, since the latter is much larger than the proton. The radius of the water molecule is found using the Eötvös relationship between surface tension, temperature, density, and average of the molecular weights of associated and unassociated water molecules,[2] and is calculated to be 2.06×10^{-8} cm.

With this value Mukherjee compares the mobility or the equivalent conductance of the ion with that of the hydrogen ion

TABLE I. Hydration numbers.

Ion	Experimental	Mukherjee	This note
Li^+	14	15.9	13.3
Na^+	8.4	10.8	9.9
K^+	5.4	6.2	6.7
C_s^+	4.7	5.5	4.2
Cl^-	4	5.6	5.0

and calculates the radius of the hydrated ion. Then the hydration number is defined as

$$n' = \frac{a'^3 - a_0'^3}{a_0^3},$$

where a_0' is the radius of the unhydrated ion obtained from x-ray data, a_s is the radius of the solvent molecule, and a_x' the radius of the hydrated ion.

The constant in the Eötvös formula is obtained by putting in the appropriate values from the literature of the quantities involved. It is supposed to be a universal constant independent of the nature of the liquid. In practice, however, it is not at all constant. As Adam states, "It can only be said that experiment has proved the Eötvös Law absolutely unreliable. It is now abundantly clear that there is no 'constant' of Eötvös."[2] Therefore, Mukherjee's use of the so-called "universal Eötvös" constant to calculate an apparent molecular weight of water molecules is not justifiable. Furthermore, it is unnecessary. The Bernal and Fowler[3] theory of the structure of water suggests that it has a quasi-crystalline structure and is not associated. They give a value for the radius of water molecules as 1.38A as compared to Mukherjee's value of 2.06.

The Table compares the hydration numbers obtained experimentally by the transference method of Washburn and Millard[4] with those calculated using Mukherjee's water radius and the Bernal-Fowler radius. It can be seen that it is not necessary to use the associated theory of water structure to calculate hydration numbers which agree with these experimental values. If anything, the numbers calculated using the Bernal-Fowler radius, are in better agreement with experiment.

Since a modified Stokes' Law seemed to have some success in determining hydration numbers, it was thought that this modification would be useful in the Onsager-Fuoss theory of diffusion of electrolytes.[5] While this theory has been extremely successful in accounting for diffusion coefficients of electrolytes in aqueous solutions, the work of Harned[6] and co-workers has shown that various electrolytes deviate from the theory. The largest deviation was found for calcium chloride.

Thus, in the theory where Stokes' formula was used in calculating the decrease in velocity of an ion due to electrophoresis, the modified form was substituted, and the appropriate calculations then made. It was found, however, that the difference in the diffusion coefficients was too small to be significant. It seems that there is no difference between the usual form of Stokes' law and Millikan's modification of it as far as electrolytic diffusion is concerned.

[1] H. Mukherjee, Indian J. Phys. **23**, 503 (1949); **24**, 137 (1950).
[2] N. A. Adam, *The Physics and Chemistry of Surfaces* (Oxford University Press, London, 1941), third edition, pp. 158–160.
[3] J. D. Bernal and R. H. Fowler, J. Chem. Phys. **1**, 515 (1933).
[4] E. W. Washburn and E. B. Millard, J. Am. Chem. Soc. **37**, 694 (1915).
[5] L. Onsager and R. M. Fuoss, J. Phys. Chem. **36**, 2270 (1932).
[6] For most recent contributions see H. S. Harned and R. M. Hudson, J. Am. Chem. Soc. **73**, 5083 (1951).

Some Additional Remarks on a Hypothesis Concerning the Critical State

JOHAN VAN DRANEN
Laboratory for Analytical Chemistry, University of Amsterdam, Amsterdam, Netherlands
(Received January 6, 1953)

THE liquid state is stable between the triple point and the critical point. With respect to the critical point we have recently[1] enunciated the hypothesis that the critical state is the result of the fact that at the critical temperature the average kinetic energy is equal to the average (negative) potential energy. To test this hypothesis we shall now give a somewhat more refined calculation of the potential energy.

The following symbols are used: U_c', the van der Waals part of the potential energy or the internal energy of gas imperfection (the index c denotes value at the critical point); P_cV_c, the external part of the potential energy; $U_c = U_c' + P_cV_c$, the total potential energy; $K_c = (3/2)RT_c$, the kinetic energy; $E_c = U_c' + K_c$, the internal energy; $W_c = U_c + K_c$, the total energy or heat content of the substance.

TABLE I. The van der Waals part of the potential energy. U' *versus* T. (cal./mol).[a]

	150°C	75°C	0°C	T_c	T_c (theor. c.)
Argon	−409	−426	−455	−526	−510
Nitrogen	−333	−345	−373	−455	−445
Methane	−565	−582	−621	−677	−660

[a] The volume is at each temperature equal to the critical volume.

In reference 1 we have given, as stated there, a rather crude "whole number" calculation of the van der Waals part of the potential energy U_c' (in reference 1 U' is used without index). We include also the small, but by no means negligible, term P_cV_c.

Furthermore we shall try to give a more accurate value for U_c', using the values for the internal energy of gas imperfection obtained by Michels and co-workers directly from their experimental PVT data.[2] The difficulty is, however, that these values were obtained for temperatures between 0°C and 150°C. We must therefore extrapolate the values for U' at these temperatures to T_c. The density is, of course, the same for each temperature, namely, the critical density. The dependence of U' from the temperature is too strong to claim much accuracy for this procedure, and therefore we can only give very preliminary conclusions.

Using the modern statistical theories of liquids, Hirschfelder and co-workers[3] and Kirkwood and co-workers[4] have made extensive theoretical calculations of the thermodynamical properties of compressed gases and liquids. The general trend of U' as a function of the temperature is given somewhat better by the calculations of Hirschfelder (reference 3, Table XVIII and XIX; reference 4, Table X), notwithstanding the fact that the procedure of Kirkwood is the more exact one. In addition, we give therefore in Table I the value for U_c' obtained by drawing the theoretical curve for the temperature dependence of U' (reference 3, Table XI) through the experimental value for U' at 0°C (Table I, column T_c theor. c.)

We have calculated the various energies for three substances: argon ($T_c = 150.7$°K; critical density 298 Amagat units), nitrogen ($T_c = 126$°K; critical density 249 Amagat units), and methane ($T_c = 191$°K; critical density 225 Amagat units). The results are given in Tables I and II.

From the values obtained for W_c (Table II) the conclusion can be drawn that there is some evidence that the physical cause for the critical point is the fact that at this point the potential energy is equal to the kinetic energy. From a pictorial point of view we can say that as long as the kinetic energy is smaller than the (negative) potential energy a liquid, in equilibrium with its vapor, is bound in its own characteristic volume.

If true this hypothesis holds, of course, not only for molecules with van der Waals interaction, but also for other liquids. For mercury the critical conditions are not known with any accuracy, but accepting the values $T_c = 1900$°K, $V_c = 44$ cc, and $P_c = 300$ atmos we obtain for U_c' the value −6000 cal./mol. This is a reasonable value in view of the experimental sublimation energy of about 16 000 cal./mol.

We hope to publish an account on the properties of systems with total energy equal to zero. This problem is, for this case, connected with the question if there is a critical region or a critical

TABLE II. The various contributions to the total energy W_c (cal./mol).

	U_c'	P_cV_c	U_c	K_c	W_c
Argon	−526	+87	−439	+449	+10
Nitrogen	−455	+73	−382	+375	−7
Methane	−677	+108	−569	+569	0

point; this question, for the first time treated in Mayer's theory of condensation,[5] requires the calculation of the minimum energy necessary to form a meniscus.

[1] J. van Dranen, J. Chem. Phys. **20**, 1175 (1952).
[2] Argon: Michels, Lunbeck, and Wolkers, Physica **15**, 689 (1949); Nitrogen: Michels, Wouters, and de Boer, Physica **7**, 585 (1936); Methane: A. Michels and G. W. Nederbracht, Physica **7**, 569 (1936).
[3] Wentorf, Buehler, Hirschfelder, and Curtiss, J. Chem. Phys. **18**, 1484 (1950).
[4] Kirkwood, Lewinson, and Alder, J. Chem. Phys. **20**, 930 (1952); J. Chem. Phys. **20**, 930 (1952).
[5] J. E. Mayer and M. G. Mayer, *Statistical Mechanics* (John Wiley and Sons, Inc., New York, 1940), Chapters 12–14.

The Spectrum of an Argon-Nitrogen Mixture Excited in an High Voltage Arc*

R. W. Nicholls
Department of Physics, University of Western Ontario, London, Canada
(Received January 12, 1953)

ATTENTION has been directed[1–4] to the many afterglow effects which are obtained by exciting the filling (A:N_2::99.5 percent:0.5 percent at 600-mm pressure) of commercial lamp bulbs by various means, e.g., Teslacoil, rf power-oscillator, etc.

Recently, experiments have been made upon a 200-watt lamp whose filament had been destroyed. A neon-sign transformer was used for excitation. A high tension arc was struck between the filament support leads, which acted as electrodes. Potentials used were in the range 1000–2000 volts rms, and currents were in the range 0–30 milliamps rms. The arc took the form of a central ribbon-like region of luminosity between the electrodes. Its curvature diminished with increasing current. Above this main arc was a flame-like afterglow, presumably swept from the main arc by thermal convection. Its color was yellow-brown, and it was reminiscent of active nitrogen. The electrical characteristics of the whole discharge (rms current as ordinate and rms voltage as abscissa) was Z shaped. The present spectroscopic observations were made at low current values (0–5 ma) on the lowest limb of the Z shaped characteristic.

Spectra of the arc ribbon and the afterglow above it were photographed between λλ3500 and 9000A on Kodak IN plates. The only recorded bands were the following:

N_2 *first positive system:* (10), (21), (32), (20), (31), [(42), (53) faint]
N_2 *second positive system:* (01), (02), (03), (04), (13), (14), (15)

This unusual spectrum shows that processes taking place in the arc cause vibrational excitation of low quantum number levels of the $C^3\pi_u$ and $B^3\pi_g$ states of N_2. Indirect excitation mechanisms of two steps[6–8] probably set up this vibrational excitation as follows:

The energetic electrons in the arc may be thought predominantly to excite levels of the singlet states $a^1\pi_g$, $a'^1\Sigma_u^-$, and w. All of these states are metastable towards downward radiative transitions.

Further, collisional de-excitation of levels of these states is improbable, in view of the high percentage of argon filling the bulb, except for levels near the 11.5 electron volt first excited state of argon.

The high gas pressure in the source will ensure that each of the high energy electrons which perform the primary excitation, rapidly becomes part of a copious body of slow electrons, which, it is suggested, are responsible for the multiplicity change necessary to excite the triplet levels C and B from the singlet levels a, a', and w by collision. This is the second part of the indirect excitation mechanism.

Therefore, it may be supposed that molecules initially excited to low vibrational levels of the $a^1\pi_g$ state, of long lifetime, will in secondary collisions with slow electrons, populate the adjacent low vibrational levels of $B^3\pi_g$. Radiation from these levels will give rise to the observed first positive bands. It is further proposed that some of the levels of the metastable $a'^1\Sigma_u^-$ and w states whose absolute energy placing is unknown,[9] are in fact adjacent to the $C^3\pi_u$ levels. Slow electron collisions with molecules in the singlet states could then readily cause the intercombination transitions which would populate the triplet levels. Further, collision between metastable molecules in a' and w levels, near to and higher than 11.5 electron volts, and argon atoms would result in radiationless de-excitation of these levels. Thus, one would expect that any a' or w levels suitable for transfer to $C^3\pi$ ($v'=2$, 3, 4) levels would be preferentially depopulated by collision with argon atoms whose gas kinetic collision frequency can be shown to be of the order of 10^9 per sec. Also, if any $C^3\pi$ ($v'=2$, 3, 4) levels were populated by a direct process from the ground $X^1\Sigma_g^+$ state, though there would be competition in the depopulation of these levels by radiation and second kind collision with argon atoms, some radiation of bands originating on these levels would nevertheless result. This is because by no means all of the gas kinetic collisions are certain to produce a de-excitation.

The fact that the observed spectrum shows only those bands of the second positive system which originate on the $v'=0$, 1 levels is, therefore, evidence of an indirect excitation mechanism and also of the probable rough position of the $a'^1\Sigma_u^-$ and w states of the N_2 molecule.

Experimental work on this source continues.

* This work has been performed as part of a project supported by The Geophysics Research Division of The U. S. Air Force under contract AF 19(122)-470.
[1] C. Kenty, Phys. Rev. **89**, 000 (1953).
[2] R. S. Mackay, Am. J. Phys. **18**, 319 (1950).
[3] Jenkins and Botwell, Nature **163**, 401 (1949).
[4] N. D. Sayers and K. G. Emeleus, Proc. Phys. Soc. (London) **A65**, 219 (1952).
[5] R. W. Nicholls, Nature **162**, 231 (1948).
[6] R. W. Nicholls, Nature **167**, 31 (1951).
[7] R. W. Nicholls, J. Chem. Phys. **20**, 1040 (1952).
[8] W. B. Kunkel, Bull. Am. Phys. Soc. **27**, 12 (1952).
[9] G. Herzberg, *Spectra of Diatomic Molecules* (1950), second edition, p. 449.

An Improvement in the π-Electron Approximation in LCAO MO Theory

Rudolph Pariser
Jackson Laboratory, E. I. du Pont de Nemours and Company, Wilmington, Delaware
(Received January 12, 1953)

AS is usual in the π-electron approximation for complex unsaturated molecules, the total electronic energy is divided into two noninteracting parts: (1) the energy of the π-electrons, and (2) the energy of all other, or σ-electrons. The energy of the σ-electrons is consequently assumed to remain constant and independent of the charge distribution of the π-electrons. This is undoubtedly an unrealistic assumption. As is argued below, the effect of the σ-electrons can be approximately taken into account without any additional complication to the mathematics of the π-electron approximation, by changing the value of primarily one Coulomb repulsion integral.

The zero of energy is chosen to be the energy of the "core," which is obtained by removing the π-electrons from the molecule while holding the atoms in their original equilibrium positions. The σ-electrons are defined to have the energy which they would have in their valence state in a hypothetical molecule, where each atom is neutral with respect to π-electron polarization.

One now assumes that the energy of the σ-electrons is not affected in non-ionic valence bond resonance structures, but that it is affected in ionic resonance structures and particularly the energy of those σ-electrons which "belong" to the atom carrying a formal + or − sign. The occurrence of ionic structures in a neutral molecule in the LCAO MO treatment is determined by the occurrence of the Coulomb repulsion integral,

$$(11|11)=\int \chi_a(1)\chi_a(2)\frac{e^2}{r_{12}}\chi_a(1)\chi_a(2)dv_1dv_2. \quad (1)$$

The occurrence of this integral, giving the repulsive energy of two π-electrons on atom "a," implies that some other atom is deficient of its π-electron. The accompanying change of the σ-electron

energy may thus conveniently be included by modifying the value of (11|11).

To estimate (11|11) for carbon, consider two neutral infinitely separated C atoms in their sp^2 valence states. By the π-electron approximation, their combined energy is expressed as $2W_p$, where W_p is the ionization potential of the $2p\pi$ electron. Now form the ions C^+ and C^- by ionizing one π-electron and placing it in the $2p\pi$ orbital of the other atom. The energy of the ions is, by the same theory, $2W_p+(11|11)$, so that the energy of forming the ion pair is just (11|11). Experimentally this energy is given by the valence state ionization potential I of neutral carbon minus its electron affinity A. Thus,

$$(11|11)=I-A. \tag{2}$$

According to Mulliken,[1] $I=11.22$ ev and $A=0.69$ ev, making $(11|11)=10.53$ ev.

However, theoretical calculations for carbon using Slater orbitals give $(11|11)=16.93$ ev[2]. By Eq. (2), this implies an ionization potential of about 16 ev or a high negative electron affinity of about -6 ev, which values are inconsistent with the basic assumption that a carbon atom in a molecule behaves essentially as a free carbon atom in its valence state. Moffitt[3] has called attention to this basic discrepancy by showing that the usual MO theory does not give the correct assymptotic energies, as molecules are dissociated into atoms and ions. He has employed a method of correction (using ionization potentials and electron affinities) which is basically related to the method advocated above. As Moffitt points out, the discrepancy in the present case is due chiefly to the failure to consider the change in σ-electron energy when forming C^+ and C^- from 2C.

The question arises whether other interelectronic Coulomb repulsion integrals should also be modified in the π-electron approximation. The repulsion between two π-electrons on different atoms would be affected by the presence of a formal minus charge on one or both of the atoms. This effect, as well as correlation of the two π-electrons, would tend to lower the effective value of all Coulomb repulsion integrals with respect to values computed theoretically from Slater orbitals. The magnitude of the lowering is difficult to estimate precisely, but the correction should be considerably less than for (11|11).

Detailed application of these ideas will be made in subsequent publications.

[1] R. S. Mulliken, J. Chem. Phys. **2**, 782 (1934).
[2] R. G. Parr and B. L. Crawford, Jr., J. Chem. Phys. **16**, 526 (1948).
[3] W. Moffitt, Proc. Roy. Soc. (London) **A210**, 224 (1951).

Calculation of the Concentration of Atomic Hydrogen at a Cathode

J. O'M. Bockris and Roger Parsons
Imperial College of Science, London, England, and University College, Dundee, Scotland

(Received December 1, 1952)

In a note with the above title, Salzburg and Schuldiner[1] have criticized the equation[2–4]

$$i=2F(kT/h)10^{-18}x^2\exp[-\Delta G^{\ddagger}/RT], \tag{1}$$

as dimensionally incorrect and lacking a probability factor. (Here i is the current density, F is the Faraday, kT/h is the fraction of the surface covered with atomic hydrogen, and $\Delta G^{\ddagger}$ is the electrochemical free energy of activation at a given electrode potential.)

The exponential factor in (1) is an expression for the equilibrium constant relating to the formation of an activated complex from the reactants [see Eqs. IV 156 and 157, p. 195 of reference (5)]. Consequently this factor must have the dimensions of this equilibrium constant. This fact is usually obscured by the omission of the dimensional factor of unity from rate process equations of this type (strictly, the exponential itself is dimensionless). The situation may be clarified by the following simple argument.[6] The Van't Hoff isotherm,

$$\Delta G=-RT\ln K+RT\,\Sigma_i n_i \ln c_i \tag{2}$$

gives

$$K=\Pi_i(c_i)^{n_i}\exp[-\Delta G/RT], \tag{3}$$

where c_i is the concentration of the ith species, n_i is the number of molecules of the ith species participating in the reaction (n_i is positive for products, negative for reactants), ΔG is the free energy change in the reaction, and K is the equilibrium constant which can, at once, be seen to have the dimensions of concentration raised to the $\Sigma_i n_i$th power. Under standard conditions all the c_i's have their standard values c_i^0 and $\Delta G=\Delta G^0$, but all the c_i^0s are unity in the concentration units defined by the choice of standard state. Thus (3) becomes

$$K=\Pi_i(c_i^0)^{n_i}\exp[-\Delta G^0/RT], \tag{4}$$

which is usually abbreviated

$$K=\exp[-\Delta G^0/RT], \tag{5}$$

because $\Pi_i(c_i^0)^{n_i}=1$. However, if the abbreviation (5) is used, it must always be borne in mind that the exponential factor has implicit dimensions (concentration)$^{\Sigma n_i}$. While these dimensions are clearly independent of the definition of the standard state, the magnitude of ΔG^0 and hence of K is determined by the choice of standard states for reactants and products; or, for the activation process, by the choice of standard states for reactants and activated complex. (The term dimension is used in a loose way by Salzburg and Schuldiner to denote the magnitude as well as the physical dimension of a quantity.) The clear definition of the standard states which we have given [reference (2), p. 920, 3 lines below Eq. (37)] leads to "dimensions" mole^{-1} cm^2 for the exponential term. Since $10^{-18}x^2$ has the "dimensions" mole^2 cm^{-4} and $2F(kT/h)$ is in amp mole^{-1}, the correct "dimensions" of (1) can easily be verified.

The apparent absence of a probability term in (1) is due to the fact that this is contained within the entropy of activation which, of course, forms one of the components of the standard free energy of activation, ΔG^0.

We wish to reiterate the fact that the $\Delta G^{\ddagger}$ used in (1) is the standard electrochemical *free* energy of formation of the activated complex from the reactants, since Salzburg and Schuldiner in their Eq. (3) have apparently confused this quantity with the difference in zero point energies between the initial and activated states which is often extracted from the partition function ratio in this formulation. An equilibrium constant may be expressed in terms of the standard free energy change (as we have done) or in terms of the ratio of the partition functions of reactants and products [reference (5), p. 15], but not both simultaneously as Salzburg and Schuldiner have done in their Eq. (3), which, though attributed to reference (5), is not to be found there.

With regard to the mechanism of hydrogen evolution at platinum electrodes, we merely summarize the relevant part of the view which we have already published[4,7] by stating that the occurrence of a limiting current at a current density of the order of 10 amp cm^{-2} in pure acid solutions may most easily be explained by assuming that the surface is approaching saturation by adsorbed hydrogen at this current density, an assumption which leads to a value of $\Delta G_0^{\ddagger}$ of near to zero for a standard state of mole cm^{-2}. The further increase of current which occurs at higher potentials must then be due to the occurrence of a desorption mechanism alternative to the surface combination of atoms. It appears most likely that this is the electrochemical mechanism. We consider the argument based on experimental evidence as more reliable than its purely theoretical arguments, although the latter provide some corroboration.

[1] H. W. Salzberg and S. Schuldiner, J. Chem. Phys. **20**, 1495 (1952).
[2] Parsons and Bockris, Trans. Faraday Soc. **47**, 914 (1951).
[3] Bockris and Azzam, Trans. Faraday Soc. **48**, 145 (1952).
[4] Bockris and Potter, J. Electrochem. Soc. **99**, 169 (1952).
[5] Glasstone, Laidler, and Eyring, *Theory of Rate Processes* (McGraw Hill Book Company, Inc., New York, 1941).
[6] Ives, private communication.
[7] Parsons, J. chim. phys. **49**, C82 (1952); Azzam, thesis, University of London (1949), 374–397.

The Phase Transformation of Cobalt as Observed on Single Crystals*

VICTOR J. KEHRER AND HENRY LEIDHEISER, JR.
Virginia Institute for Scientific Research, Richmond, Virginia
(Received December 22, 1952)

AS part of a general study of the surface properties of metal single crystals we are carrying out experiments with single crystals of cobalt. The current great interest in phase transformations prompts us to report some preliminary results.

A cobalt crystal[1] was machined in the form of a sphere, $\frac{5}{16}$ in. in diameter, with a small shaft for handling, $\frac{1}{8}$ in. in diameter and $\frac{1}{2}$ in. in length. The strained layer resulting from the machining operation was removed by deep etching, and the sphere was electrolytically polished in 42.5 percent by volume orthophosphoric acid.[2] The sphere was oxidized in air in separate experiments both below and above 420°C, at which point the low temperature hexagonal close-packed form is converted to the high temperature face-centered cubic form.[3] As shown in Fig. 1 at 350–400°C the

FIG. 1. The interference color pattern formed on a single crystal of cobalt with a hexagonal close-packed structure during oxidation in air at 350–400°C. Photograph taken normal to (0001) plane.

oxidation pattern[4] which formed on the surface was indicative of a hexagonal close-packed structure while at 450–500°C the symmetry of the pattern was indicative of a face-centered cubic structure. Etching of the cobalt crystal at room temperature after the formation of a face-centered cubic pattern at 450–500°C, always resulted in an etch pattern with hexagonal close-packed symmetry. The experiments at 350–400°C and at 450–500°C were repeated several times and the sharpness and perfection of the patterns increased each time the experiments were repeated.

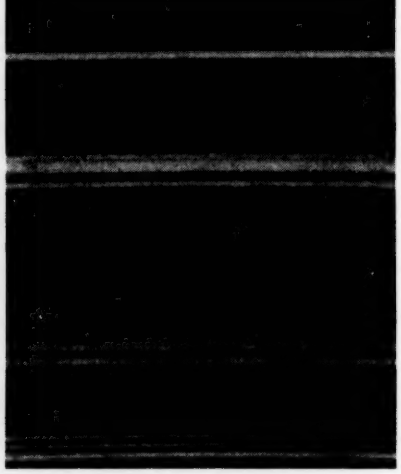

FIG. 2. Photomicrograph of parallel bands formed on a single crystal of cobalt during oxidation. ×600. Curvature of bands is a consequence of the spherical shape of the specimen.

Cobalt crystals were thus passed repeatedly through the transformation point without recrystallization into small grains.

Several interesting observations were made. First, in every experiment the same set of (111) planes in the face-centered cubic structure corresponded to the (0001) planes in the hexagonal form. In other words, although the (0001) planes presumably had a choice of taking the place of any one of 4 sets of (111) planes, they always chose the same set of (111) planes. Second, in all experiments there existed on the surface a system of parallel bands 80–90° from the (0001) pole position such as those shown in the photomicrograph in Fig. 2. The bands ran concentrically around the sphere and had a geometry such that they could be attributed to the intersection of (0001) planes with the surface. The most interesting feature of these bands was that neighboring bands had different activities as indicated by the different interference colors in the bands. In the region in which these bands were concentrated x-ray back reflection photographs showed a multiplicity of each of the Laue spots. This multiplicity may be attributed to a mosaic type of structure with each of the blocks having an orientation only slightly different from its neighbors. The origin of these bands is as yet unknown. They may have been formed by slipping of parts of the crystal along (0001) planes during the machining operation, or more likely they may have been a secondary effect of the shearing process proposed to account for this transformation.[5] Third, in view of the interpretations of the crystal structure of cobalt[6] it is of interest to point out that chemically cobalt in bulk behaves as a face-centered cubic metal above approximately 420°C and as a hexagonal close-packed metal below approximately 420°C.

* The results reported herein were obtained during the course of research being carried out for The Texas Company.

[1] Kindly furnished by Dr. Allan Gwathmey of the University of Virginia, who obtained it from Dr. Freed of Columbia University.

[2] W. C. Elmore, Phys. Rev. **53**, 757 (1938).

[3] *Metals Handbook* (The American Society for Metals, 1948), eighth edition, p. 1136.

[4] A spherical single crystal is unique in that all crystal faces are present on the surface. In the case of face-centered cubic metals the (100) face occurs 6 times, the (111) face 8 times, the (110) face 12 times, and the minor faces either 24 or 48 times. The oxidation of cobalt results in the formation of interference color films on the surface. Since the various crystal faces oxidize at different rates, a range of colors is obtained. The repetition of results on each octant of the surface gives rise to a pattern, from which the crystal faces may be identified.

[5] A. R. Troiano and A. B. Greninger, *Metals Handbook* (The American Society for Metals, 1948), eighth edition, pp. 263–6.

[6] O. S. Edwards, J. Inst. Metals **69**, 177 (1943); O. S. Edwards, Proc. Roy. Soc. (London) **A180**, 268 (1942); Edwards, Lipson, and Wilson, Nature **148**, 165 (1941).

The Out-of-Plane Deformation Frequency of the NH Group in the Peptide Link

H. K. KESSLER AND G. B. B. M. SUTHERLAND
Physics Department, University of Michigan, Ann Arbor, Michigan
(Received January 12, 1953)

A CHARACTERISTIC feature of the infrared spectra of proteins is a diffuse absorption band extending from about 800 cm^{-1} to beyond 650 cm^{-1} with an ill-defined maximum near 700 cm^{-1}. A similar band is present in Nylon, in synthetic polypeptides, and in the spectra of *N*-mono-substituted amides. Clearly this band is due to some fundamental frequency of the peptide group.

We have found that partial deuteration of the NH bonds in all of these compounds causes a marked decrease in the intensity of this band. In the case of *N*-methyl formamide almost complete deuteration was accomplished, causing the band to disappear entirely and a new band to appear with its maximum absorption near 530 cm^{-1}. This reduction in frequency by a factor of 1.36 on deuteration is exactly what would be expected for a pure NH deformation vibration free from interaction with other motions.

The dichroism of this band was studied in Nylon which had been oriented by stretching. It was found that the intensity of absorption was greatest with the electric vector of the incident radiation perpendicular to the direction of stretch. Since the NH bonds in stretched Nylon are known to be predominantly perpendicular to

the direction of stretch,[1] this proves that the NH deformation vibration responsible for the 700 cm^{-1} band must be that in which the motion of the hydrogen atom is perpendicular to the plane of the peptide group.

The behavior of this band in solutions of *N*-mono-substituted amides in carbon disulfide is of considerable interest. As dilution progressively increases, the molar absorption decreases very markedly and, in fact, parallels closely that of the NH stretching frequency near 3300 cm^{-1}. Thus the width and diffuseness of the 700 cm^{-1} absorption is presumably due to hydrogen bonding. Whereas the wide band near 3300 cm^{-1}, due to the NH stretching frequency, is replaced by a narrow band at 3450 cm^{-1}, when hydrogen bonding is destroyed, we have not yet found the corresponding unbonded frequency in the case of the 700 cm^{-1} band. It would be expected in the longer wavelength region, and work is in progress to locate it. The resemblance of the 700 cm^{-1} frequency in the peptide link to the analogous OH deformation frequency in the alcohols is very striking.[2]

It should be added that the 700 cm^{-1} out of plane NH deformation frequency has also been identified in the lactams (γ-butyrolactam, δ-valero-lactum, and ε-caprolactam), where it exhibits the same behavior on dilution and deuteration as that described above for the *N*-mono-substituted amides.

This work (which will be described in full elsewhere) was supported in part by the Rockefeller Foundation.

[1] C. W. Bunn and E. V. Garner, Proc. Roy. Soc. (London) **A189**, 39 (1947).
[2] A. V. Stuart and G. B. B. M. Sutherland, J. Chem. Phys. **20**, 1977 (1952).

Erratum: Preliminary Analysis of the Pure-Rotational Spectrum of Methyl Amine

[J. Chem. Phys. **20**, 1812 (1952)]

DAVID R. LIDE, JR.
Mallinckrodt Chemical Laboratory, Harvard University, Cambridge, Massachusetts

THE following figure should have been included with this letter:

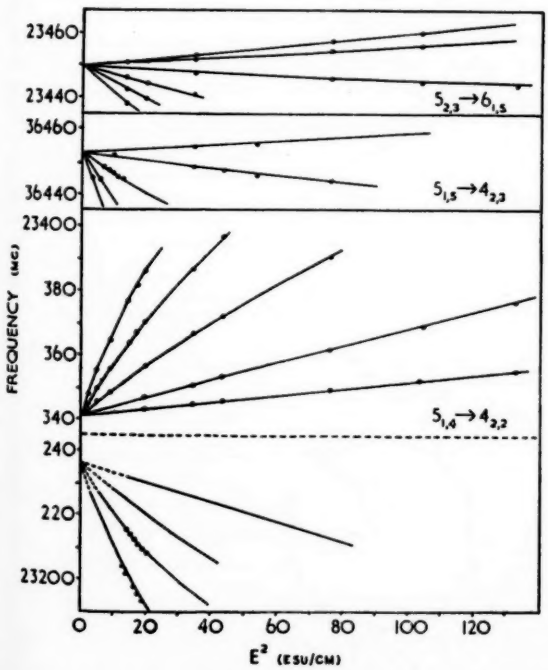

FIG. 1. Stark effects in methyl amine. The curves are predicted Stark shifts; circles are experimental points.

On the Nature of the Hydrogen Bridge

R. T. SANDERSON
Department of Chemistry, State University of Iowa, Iowa City, Iowa
(Received December 22, 1952)

IN diborane B_2H_6 and related "electron-deficient" compounds, it is now fairly well accepted that two atoms each having an otherwise vacant orbital can be held together by a bridge of two hydrogen atoms, mutually shared, or that two alkyl groups can sometimes bring about a similar bridging. However, the nature of this bonding is not understood.[1,2] The interesting observation is reported here that such bonds occur only when the hydrogen atoms have partial negative charge.

The basis for determining the nature of the charge on hydrogen is the postulate that atoms adjust to equal electronegativity in a molecule.[3] The relative charge on combined hydrogen is taken as the difference between its electronegativity in the compound and its electronegativity in the elementary state

$$\Delta SR_H = SR_m - 3.55,$$

ΔSR_H is the electronegativity change made by hydrogen in combining, SR_m is the electronegativity of the molecule of hydrogen compound, determined as the geometric mean stability ratio of all the atoms of the molecule before combination,[3] and 3.55 is the electronegativity of elementary hydrogen. ΔSR_H values for a number of hydrogen compounds, real and hypothetical, are given in Table I.

TABLE I. Relative partial charge on combined hydrogen (hypothetical compounds in brackets).

Compound	ΔSR_H	Compound	ΔSR_H
$MeBF_2$	0.43	Al_2Et_6	−0.03
$[BHCl_2]$	0.40	$B_2H_2Me_4$	−0.03
$C_2H_4O_2BH$	0.25	$B_2H_3Me_3$	−0.05
$[BH_2F]$	0.23	B_2H_5Cl	−0.06
$(MeO)_2BH$	0.21	$B_2H_4Me_2$	−0.08
$(EtO)_2BH$	0.16	Ga_2H_6	−0.08
Me_2BF	0.14	B_2H_5Br	−0.09
$(PrO)_2BH$	0.14	Al_2Me_6	−0.11
$[BH_2OH]$	0.11	B_2H_5Me	−0.12
$[BH_2Cl]$	0.10	$Al_2H_2Me_4$	−0.16
$[MeOBH_2]$	0.10	B_2H_5I	−0.16
$[(C_6H_5)_2BH]$	0.08	B_2H_6	−0.19
$C_6H_5BH_2$	0.04	B_4H_{10}	−0.22
$GaMe_3$	0.03	B_5H_{11}	−0.24
$[B_2H_5F]$	0.01	B_5H_9	−0.28
$[BH_2Br]$	0.01	B_6H_{10}	−0.28
$AlPr_3$	0.00	$B_{10}H_{14}$	−0.31
BMe_3	−0.01	$(AlH_3)_x$	−0.49
$[B_2H_5OH]$	−0.03		

Although it is frequently assumed that dissociation to the monomer is a prerequisite to the disproportionation so commonly observed, as in halo- and alkyldiboranes, it should be recognized that other mechanisms are possible. For example, two dimer molecules might form two new molecules by switching bridges.

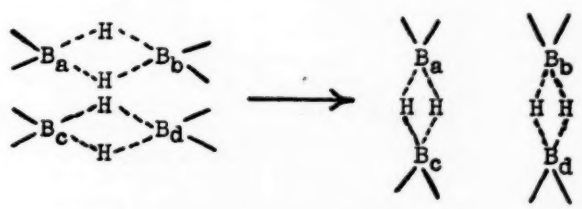

If alkyl groups containing negative hydrogen may form bridges also, then similar switching involving alkyl groups as well as, or in place of, hydrogen atoms might occur, accounting for disproportionation in methyldiboranes, for example. Therefore, although thermal stability of bridge bonds and rates of disproportionation probably have some relationship, it is not necessarily direct. However, it is of interest that in the very similar compounds, the monohalodiboranes, fluorodiborane is unknown and the rate of

disproportionation is greatest for chlorodiborane and least for iododiborane,[4] which is consistent with the magnitude of negative charge on the hydrogen. Another factor influencing disproportionation in the monomers would be the existence of adjacent like charges. For example, the hypothetical molecule BH_2Cl would contain hydrogen of partial positive charge attached to boron of like charge, which would increase the tendency toward formation of the more stable BCl_3 and $BH_3(B_2H_6)$.

[1] K. S. Pitzer, J. Am. Chem. Soc. **67**, 1126 (1945).
[2] R. E. Rundle, J. Chem. Phys. **17**, 671 (1949).
[3] R. T. Sanderson, Science **114**, 670 (1951); J. Am. Chem. Soc. **74**, 272 (1952); J. Chem. Ed. **29**, 539 (1952).
[4] A. Stock, *Hydrides of Boron and Silicon* (Cornell University Press, Ithaca, New York, 1933).

Erratum: A Note on Rotational Line Strengths in Slightly Asymmetric Rotors

[J. Chem. Phys. **20**, 1761 (1952)]

DAVID R. LIDE, JR.
Mallinckrodt Chemical Laboratory, Harvard University, Cambridge, Massachusetts

THE last sentence in the caption to Table III should read "γ is the parity $J+K+K_1$ in the b case and of $J+K+K_1+1$ in the c case."

A Mnemonic Device for Molecular Orbital Energies

ARTHUR A. FROST AND BORIS MUSULIN
Department of Chemistry, Northwestern University, Evanston, Illinois
(Received January 1, 1953)

JAFFÉ[1] has recently pointed out the correlation between free electron wave functions and the coefficients in a molecular orbital expressed as a linear combination of atomic orbitals (LCAO–MO). The relationship is exact for both ring and open chain compounds under the usual simplifying assumptions of identical orbitals on all atoms, equal Coulombic and equal exchange integrals, and neglect of all overlap integrals and exchange integrals from other than near neighbors. This result is contained explicitly in algebraic, but not graphical, form in Hückel's[2] papers of 1931 and 1932. Hückel's formulas are

Rings of n Atoms

Wave functions:

$$\chi^{(k)}=\frac{1}{\sqrt{n}}\sum_{f=0}^{n-1}\epsilon_n^{fk}\psi_f \tag{1}$$

with

$$\epsilon_n=e^{2\pi i/n}.$$

Energy levels:

$$\eta^{(k)}=-2\beta\cos\frac{2\pi k}{n},$$

$$k=0,\pm1,\pm2\cdots \quad \pm\frac{n-1}{2} \text{ for } n \text{ odd}, \quad +\frac{n}{2} \text{ for } n \text{ even}. \tag{2}$$

Open Chains of n Atoms

Wave functions:

$$\chi^{(l)}=\frac{1}{\sqrt{N_l}}\sum_{f=1}^{n}\sin\left(\pi\frac{l+1}{n+1}f\right)\psi_f. \tag{3}$$

Energy levels:

$$\eta^{(l)}=-2\beta\cos\left(\pi\frac{l+1}{n+1}\right) \tag{4}$$

$$l=0,1,2,\cdots n-1.$$

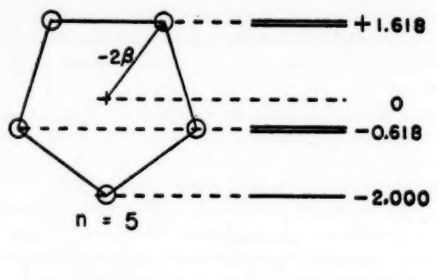

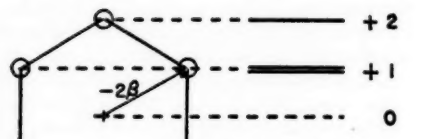

FIG. 1. Projection scheme for construction of energy level diagram of ring compounds. Resonance energies, unit: $-\beta$.

In these formulas the χ's are MO wave functions, ψ_f is an AO on atom f. The η's are negative resonance energies, i.e. the energies disregarding Coulombic energies. β is the exchange integral (usually negative). k and l are quantum numbers. The pre-summation factors in (1) and (3) are for normalization.

It is obvious from (3) that the correlation with free electron should exist for open chains. For rings the complex functions in (1) may be combined in pairs, corresponding to degenerate levels, to form sine and cosine functions also.

Just as it is convenient to have Jaffé's graphical representation of LCAO coefficients, so it is also useful to have a graphical representation of energy levels. The following construction of the energy level diagram for ring and open chain molecules follows directly from Eqs. (2) and (4), respectively.

For *ring* compounds make a diagram of the ring with one of the n atoms at its lowest point. See Fig. 1 for $n=5$ and 6, respectively. Now project each atom horizontally. This automatically constructs the energy level diagram for the given ring, including double degeneracies where they occur, and gives the correct energy scale if the radius of the ring is taken as 2β, the center corre-

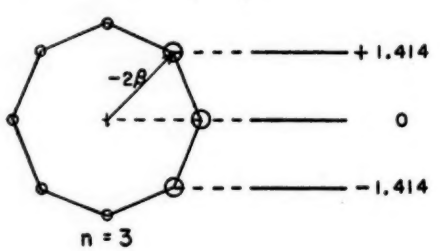

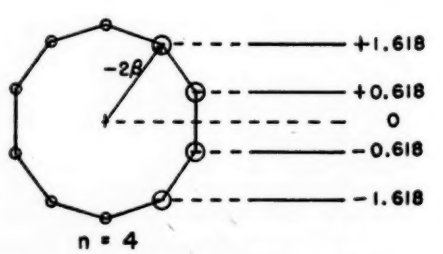

FIG. 2. Projection diagram for energy levels of open chain compounds. Resonance energy, unit: $-\beta$.

sponding to zero resonance energy. It should not be construed from this construction that the several energy levels are associated with particular atoms. It is just a curious mathematical coincidence that this scheme works.

For *open chain* compounds of n atoms add $n+2$ fictitious atoms and construct a ring of $2n+2$ atoms just as was done above for n atoms. Now, considering the n atoms of the open chain represented by the n positions on one side of the ring between the lowest and the highest, project horizontally to obtain the relative positions of the n nondegenerate energy levels. See Fig. 2 for the cases of $n=3$ and $n=4$. Here again, if the radius of the circumscribed circle is 2β and the projected center is taken as zero, the resonance energies are correct on an absolute basis.

It should be noted that this scheme does not require the geometrical structure of the molecule to be the same as the geometrical figure used in the construction. In particular, open chains may be zigzag.

A research grant from the National Science Foundation in support of this work is hereby acknowledged.

[1] H. H. Jaffé, J. Chem. Phys. **20**, 1646 (1952).
[2] E. Hückel, Z. Physik **70**, 204 (1931); **76**, 628 (1932).

On the Molecular Evaporation of Group IVB Elements

RICHARD E. HONIG
Radio Corporation of America Laboratories, Princeton, New Jersey
(Received December 22, 1952)

IN the course of an investigation of the impurities in germanium (1), some Group IVB elements were evaporated in a mass spectrometer. Mass spectral data, obtained with 45-volt electrons, showed for germanium not only the expected singly- and multiply-charged atomic ions, but also moderate concentrations of ionic clusters containing as many as seven atoms. Similarly, ionic clusters containing up to five atoms were observed in the evaporation of tin, while lead gave rise to diatomic ions.

A detailed description of the Dempster-type 180° mass spectrometer will be found elsewhere.[1] To obtain spectra covering masses 1 to 650 at a single setting of ion accelerating potential, a magnetic field scan was employed which minimized so-called mass discrimination. Indirectly heated crucibles made of alumina, silica, or carbon were used in the evaporation of germanium. Tin and lead were evaporated from a silica crucible.

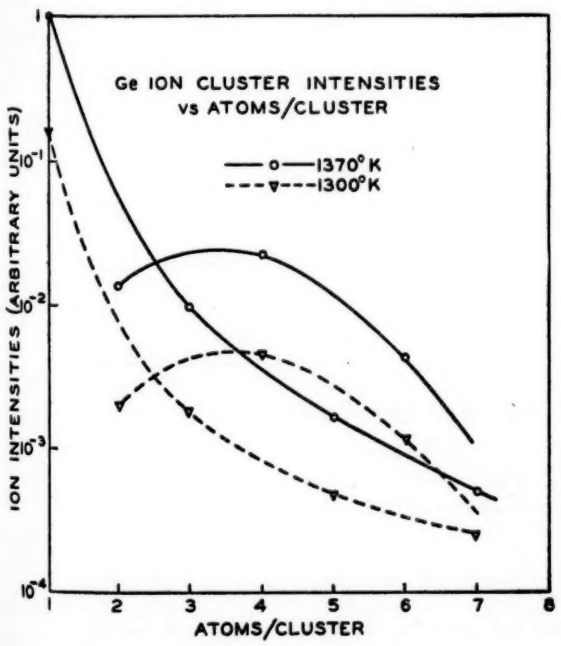

FIG. 1.

Evaporation of the elements under study was first detected at vapor pressures of about 5×10^{-8} mm Hg. Clusters were recorded at pressures ranging from about 5×10^{-6} to 5×10^{-4} mm Hg. Positive identification of these clusters was made not only by their location on the mass scale, but also by their isotopic distributions which, whenever possible, were checked against computed values. Although the instrumental resolving power was limited to about one part in 200, cluster intensities were measured quite reliably up to mass 400, because, for all clusters in question, the isotopic combinations yielded predominantly peaks with even mass numbers. The total intensity of a given cluster, summed over all possible isotopic combinations, was computed from the intensity of the strongest peak.

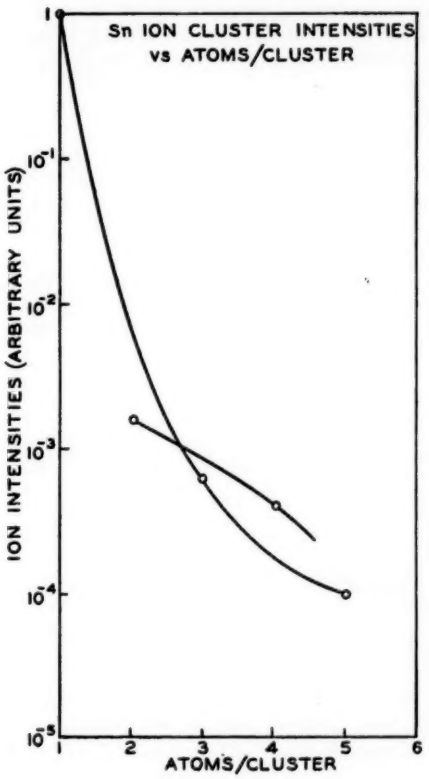

FIG. 2.

The evaporation of liquid germanium from an alumina crucible produced the data shown in Fig. 1, which is a semilogarithmic plot of total cluster intensities *vs* the number of atoms per cluster, at two different source temperatures (1300 and 1370°K). While clusters containing seven atoms were recorded in small concentrations, no eight-atomic molecules could be detected. If they exist, their intensity must be at least ten times smaller than the Ge_7^+ intensity. It will be noted that smooth curves can be drawn through the odd-numbered points, while the even-numbered ones cannot be fitted. Comparison of the two sets of curves, taken at pressures differing by a factor of six, shows no significant difference in patterns. From this, one may conclude that cluster formation cannot be caused by a combination of particles in the gas phase (which would result in patterns proportional to pressure), but must take place during the evaporation process itself. Similar results were obtained for the evaporation of germanium from silica and carbon crucibles.

Unfortunately, the proportions in which the different molecular species of germanium evaporate cannot be determined directly from the ion cluster intensities observed, because neither fragmentation patterns nor ionization cross sections are known for each individual cluster. The distribution of "parent" ions might be ascertained, at a considerable loss of intensity, by adjusting the ionizing energy to a value sufficient for ionization but too low for the production of fragment ions, but there is no way in which individual cross sections can be measured. Nevertheless, it may be estimated that the fraction of liquid germanium evaporating in molecular form (containing from two to seven atoms) amounts to roughly 20 percent, and Ge_4 and Ge_6 may well be preferred forms. If these results are applied to the recent determination of the vapor pressure of germanium,[2] it appears that all pressure values should be lowered by perhaps as much as 10 percent.

Figure 2 presents some data typical of the evaporation of liquid tin at about 1200°K from a silica crucible. The plot is similar to the germanium cluster curves, except that in this case the fraction representing molecular evaporation is much smaller (less than one percent). Again, the even-numbered clusters observed (Sn_2^+, Sn_4^+) do not fall in line with the odd-numbered ones. Because of mass range limitations, clusters beyond Sn_5^+ could not be investigated. These results are in qualitative agreement with Brewer's statement[3] that in the evaporation of tin the atomic species is more important than Sn_2 or Sn_4.

The evaporation of liquid lead from a silica crucible, at about 800°K, produced the diatomic ion in very low concentrations. The intensity ratio observed ($Pb_2^+/Pb^+=3\times10^{-5}$) agrees, in order of magnitude, with a rough estimate of the relative vapor pressures based on the heats of sublimation of Pb and Pb_2 (the latter quantity computed from Gaydon's[4] spectroscopic data).

[1] R. E. Honig, article in preparation.
[2] A. W. Searcy, J. Am. Chem. Soc. **74**, 4789 (1952).
[3] L. Brewer, *The Chemistry and Metallurgy of Miscellaneous Materials* (McGraw-Hill Book Company, Inc., New York, 1950), p. 31.
[4] A. G. Gaydon, *Dissociation Energies* (Chapman and Hall, Ltd., London, 1947), p. 212.

Announcement

The following meetings will be held in France, at the University of Paris (Sorbonne) in the summer of 1953.

24th–26th June:
A Colloquium sponsored by the Rockefeller Foundation and organized by the French National Bureau of Scientific Research (CNRS) on: "Water molecules in crystals and solids studied by electromagnetic waves (from x-rays to wavelengths in the radiofrequency range)."
Active participation restricted to 20 invited persons.
Secretary: Dr. A. Kastler, Laboratoire de Physique, ENS, 24 rue Lhomond, Paris 5e.

29th June–3rd July:
General International Meeting on Molecular Spectroscopy (from x-rays to wavelengths in radiofrequency range).
Secretary: Dr. J. Lecomte, Laboratoire des Recherches Physiques, Sorbonne, 1 rue Victor Cousin, Paris 5e.

6th–10th July:
Symposium organized by the Société francaise de Chimie physique, on "Recent Advances in Studies of Molecular Structure."
Secretary: Dr. M. Magat, Laboratoire de Chimie physique, 11 rue Pierre Curie, Paris 5e.